CONF-9210121--

Proceedings of the

WORKSHOP ON THE PRODUCTION AND USE OF INTENSE RADIOACTIVE BEAMS AT THE ISOSPIN LABORATORY

JOINT INSTITUTE FOR HEAVY ION RESEARCH
OAK RIDGE, TENNESSEE

October 7-10, 1992

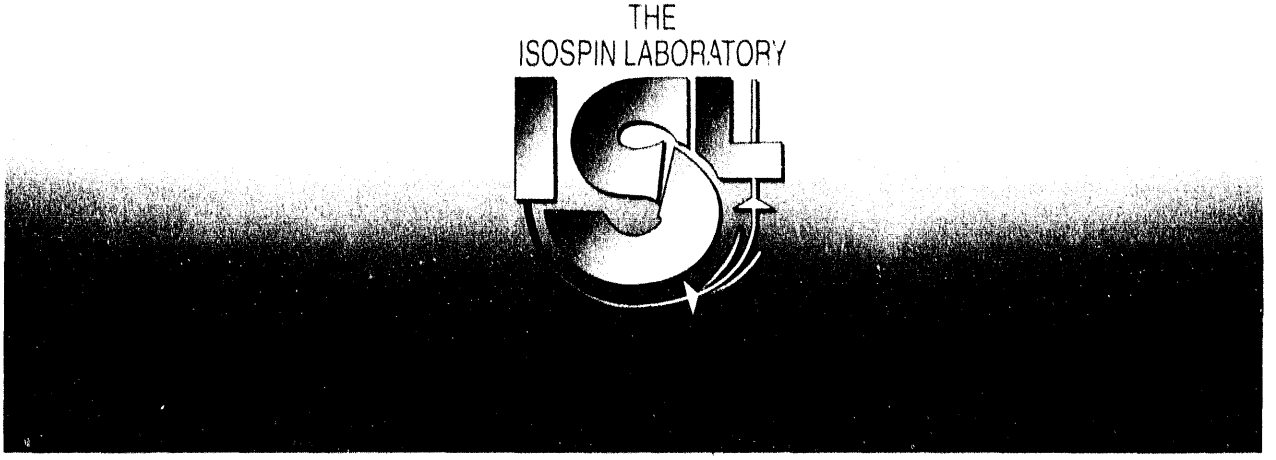

Contributing editor and writer: ***Fred M. O'Hara***

Production editor: ***Lorna Perkins, Oak Ridge Institute for Science and Education***

DISCLAIMER

Oak Ridge National Laboratory is managed by Martin Marietta Energy Systems, Inc. for the U.S. Department of Energy under contract DE-AC05-84OR21400.

This document describes activities performed under contract number DE-AC05-76OR00033 between the U.S. Department of Energy and Oak Ridge Associated Universities.

CONF-9210121 --

Proceedings of the
WORKSHOP ON THE PRODUCTION AND USE OF INTENSE RADIOACTIVE BEAMS AT THE ISOSPIN LABORATORY

edited by Jerry D. Garrett, Physics Division, Oak Ridge National Laboratory, Oak Ridge, Tennessee

JOINT INSTITUTE FOR HEAVY ION RESEARCH
OAK RIDGE, TENNESSEE

October 7-10, 1992

THE ISOSPIN LABORATORY

Workshop sponsored by:

Georgia Institute of Technology
Joint Institute for Heavy Ion Research
Lawrence Berkeley Laboratory
Los Alamos National Laboratory
Louisiana State University
Mississippi State University
Oak Ridge Institute for Science and Education
Oak Ridge National Laboratory
Simon Fraser University
Tennessee Technological University
University of Maryland
University of Notre Dame
University of Tennessee
Vanderbilt University

Table of Contents

Preface

These proceedings report the deliberations of a 3 1/2 day workshop on the Production and Use of Intense Radioactive Ion Beams at the Isospin Laboratory, which was held at the Joint Institute for Heavy Ion Research in Oak Ridge, Tennessee, October 7-10, 1992. Although the stated purpose of the workshop was to consider a variety of technical problems associated with the construction of a broad mass-range, intense I(sotope) S(eparator) O(n) L(ine) Radioactive Beam Facility in North America and the experimental equipment needed for such a facility, the 125 participants included some 20 from outside the United States and Canada. Such a sizable international participation is indicative of the universal interest in research with radioactive ion beams. (Indeed, astrophysics is an important research topic for radioactive beams!)

From its inception by the North American Steering Committee for the IsoSpin Laboratory, the purpose of this workshop was not to duplicate the programs of other recent radioactive ion beam workshops or international conferences that have focused on the scientific concepts which radioactive beams can, and in fact already are, addressing. Instead, the intent was to address the technical problems associated with the construction of the next generation ISOL facility and to initiate a discussion of the type of experimental equipment that should be developed for such a facility. We have tried to bring together in Oak Ridge the world's experts in radioactive targets/ion sources, light- and heavy-ion accelerators, and detection systems. After 1 1/2 days of overview presentations, the participants divided into three discussion groups (Experiments with Radioactive Beams, Target Ion Sources and Mass Separation, and Accelerators—Primary and Secondary) for 1 1/2 days of detailed discussions of the most pertinent issues. The final session was devoted to reports from each of the discussion groups and a general discussion of where to go from here. An outgrowth of these discussions was the establishment of working groups to coordinate future technical developments associated with the pertinent issues. For further information on these working groups the reader is referred to Section V: Concluding Remarks by R. Casten in these proceedings.

The proceedings include the text of all the overview presentations, reports from each discussion group, as well as contributions from those participants who chose to provide the text of their presentations in the discussion groups and the Concluding Remarks.

It indeed was a pleasure for Oak Ridge National Laboratory (ORNL), Oak Ridge Institute for Science and Education (ORISE) (formerly Oak Ridge Associated Universities), and the Joint Institute for Heavy Ion Research (JIHIR) at Oak Ridge to host this workshop. Not only is it always a pleasure to extend our southern hospitality to

guests, but the timing of this workshop also afforded us the special opportunity to discuss our plans for the forthcoming Oak Ridge Radioactive Ion Beam (RIB) Facility with distinguished colleagues from throughout the world.

The workshop was sponsored by the Georgia Institute of Technology, the Joint Institute of Heavy Ion Research in Oak Ridge, Lawrence Berkeley Laboratory, Los Alamos National Laboratory, Louisiana State University, Mississippi State University, Oak Ridge Institute for Science and Education, Oak Ridge National Laboratory, Simon Fraser University, Tennessee Technological University, the University of Maryland, the University of Notre Dame, the University of Tennessee, and Vanderbilt University. The members of the ISL and Local Organizing Committees are given in Appendix C. Special thanks go to the coordinators of the various discussion groups, John D'Auria, Michael Nitschke, Dave Vieira, and Michael Wiescher, who not only organized the programs for the various discussion groups, the backbone of the workshop, but also prepared the discussion group reports. Jody Heath (ORNL), the conference secretary; Jackie Smith (JIHIR); and Carlene Stewart (ORISE) assisted in various aspects of the local organization of the workshop. Fred M. O'Hara assisted in the preparation and editing of the discussion reports, and Lorna Perkins (ORISE) served as the production editor for the proceedings.

Jerry D. Garrett
Oak Ridge National Laboratory
Oak Ridge, Tennessee
May 1993

Section I
Experiments with Radioactive Beams

D. J. Vieira and M. Wiescher, Coordinators

Section I
Invited Papers

Prototypical Experiments in Nuclear Astrophysics

A.E. CHAMPAGNE
Department of Physics and Astronomy, University of North Carolina at Chapel Hill, Chapel Hill, North Carolina 27599, USA
and
Triangle Universities Nuclear Laboratory, Duke University, Durham, North Carolina 27706, USA

1. Introduction

During explosive nucleosynthesis, temperatures are on the order of (0.2 - 1.5) x 10^9 K and average densities can be 10^3 - 10^6 g/cm^3. Under these extreme conditions, nuclear reactions will proceed on timescales of ns - min (though more typically sec - min). Thus any nuclei produced with comparable half lives will become targets for subsequent nuclear reactions. Measurements of at least some of these reactions are desirable, both from an astrophysical and from a nucleosynthetic perspective: Cataclysmic binaries are powered by these reactions and so a knowledge of their rates is crucial to an understanding of the outburst mechanism. We are also interested in elemental abundances, particularly of spectroscopic tracers such as ^{22}Na, ^{26}Al and ^{44}Ti. In type II supernovae, these reactions are incidental to the outburst, but again nucleosynthesis can provide clues as to the physical conditions during an explosion.

To be very general, these reactions will have both large cross sections and small cross sections. The former reactions are important for energy generation and in principle they can be measured directly with radioactive beams. The latter reactions limit power output and play a role in the production of the trace elements which could be used as spectroscopic probes. Here direct measurements are probably impractical, but nuclear spectroscopy, involving both stable and radioactive beams, can provide the desired information.

The quantity that we are ultimately interested in is the thermonuclear reaction rate

$$\langle \sigma v \rangle = \left(\frac{8}{\pi\mu}\right)^{1/2} (kT)^{-3/2} \int \sigma(E)\, E \exp(-E/kT)\, dE. \qquad 1.$$

Most of the reactions of interest involve resonances and their cross sections may be expressed in the usual Breit-Wigner form:

$$\sigma(E) = \pi \lambda^2 \omega \frac{\Gamma_a \Gamma_b}{(E - E_r)^2 + \Gamma^2/4}. \qquad 2.$$

For narrow resonances ($\Gamma << E_r$), eqn. 1 may be approximated by

$$\langle\sigma v\rangle = (2\pi/\mu kT)^{3/2}\, \hbar^2\, \omega\gamma \exp(-E_r/kT),\ \omega\gamma = \frac{(2J_f + 1)}{(2J_i + 1)(2J_t + 1)}\,\frac{\Gamma_a \Gamma_b}{\Gamma}. \qquad 3.$$

In a direct measurement, the resonance strength $\omega\gamma$ can be obtained from the thick-target yield:

$$\omega\gamma = \text{YIELD} \cdot \frac{\varepsilon_{lab}}{2\pi^2 \lambda^2}\,\frac{M_1 + M_2}{M_2} \qquad 4.$$

where ε_{lab} is the energy loss evaluated in the laboratory frame. The indirect approach involves individual measurements of the resonance parameters. The experimental requirements for both direct and indirect measurements relevant to astrophysics will be discussed in the following sections. Specific examples will be taken from explosive hydrogen burning (where there are some estimated cross sections), but the techniques have more general applicability.

2. Direct Measurements of Charged-Particle Reactions

2.1 GENERAL CONSIDERATIONS

Figure 1 shows the most effective energies for (p,γ) reactions at a stellar temperature of 0.8 x 10^9 K. In general, direct measurements will involve beam energies of 0.2 - 2 MeV/amu, which restricts us in most cases to fairly light nuclei with their comparatively low Coulomb barriers.

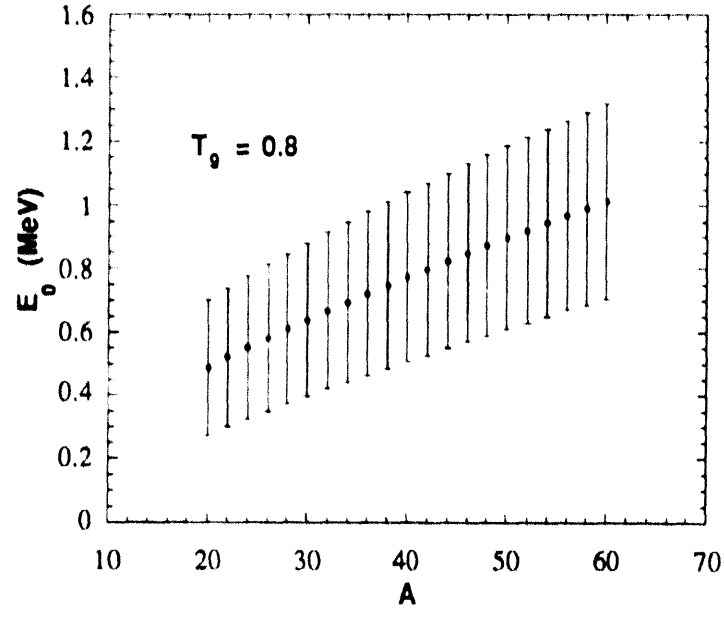

Fig. 1. Range of effective energies versus mass for T_9 = 0.8.

Predicted count rates for three interesting reactions are shown in table 1. These rates assume a 5 $\mu g/cm^2$ gas target and 100% detection efficiency. Although this latter assumption is certainly

Table 1: Examples of Direct Measurements

	E_{cm} (keV)	E_{lab} (MeV)	σ_{res} (mb)	$\omega\gamma$ (meV)	COUNT RATE (counts/ hour/pnA)
$^{4}He(^{15}O,^{19}Ne)\gamma$ (ref.[1])	504	2.39	0.32	0.014	0.064
	850	4.04	>163	>10	>19
	1020	4.85	94	4.5(25)	6.6
	1070	5.08	440	198(51)	273
	1183	5.62	157	113(17)	124
$^{1}H(^{17}F,^{18}Ne)\gamma$	597	10.75	1.9×10^{-3}	3.7	125
	639	11.50	2.9×10^{-3}	17	185
$^{1}H(^{19}Ne,^{20}Na)\gamma$ (ref.[2])	447	8.94	650	90	3860

optimistic, it is clear that the majority of these resonances have measurable yields. From these and other rate estimates, a figure of merit emerges: If $\omega\gamma > 1$ meV, then it is reasonable to attempt a direct measurement. Several resonances could be measured during a week-long run, but 3-4 additional weeks will probably be required to develop each experiment. Weaker resonances will be difficult to measure. The standard procedure for studying weak resonances is to simply run for a longer period of time. However, this approach is impractical for radioactive beams, both from the standpoint of scheduling pressure and because scattered beam makes radioactive-beam measurements inherently noisy. In other words, these experiments may suffer from such low signal-to-noise that doubling or even tripling the run time will not help. Therefore, for $\omega\gamma < 1$ meV we will most likely have to resort to nuclear spectroscopy.

Because each experiment represents a time-consuming development project, it is important to try to determine at the outset whether a direct or indirect approach is appropriate. Thus selected nuclear-structure measurements with stable and radioactive beams must be considered as part of the development process.

2.2 TARGETS

Most of the reactions of interest will involve hydrogen or helium targets. Helium requires the use of either extended or jet-type gas targets[3]. Hydrogen, targets can be produced in both gaseous and solid form. Any target will have to be thin enough so that the beam can be transported away from detectors. Although solid targets (such as CH_2 or other plastics) are inexpensive and easy to

construct, the reaction yield will be lower using these targets than from a gas target because of the lower density of hydrogen over a thickness corresponding to the resonance width. For example, in the $^{1}H(^{19}Ne,^{20}Na)\gamma$ reaction, the yield from a CH_2 target will only be about 40% of that from pure hydrogen. Also, the heavy constituents in a solid target will add to the radioactive background produced by scattered beam. As compared to a target of pure hydrogen, a solid target will have a higher cross section for scattering and will scatter the beam over a wider angular range. Thus the background will be larger and spread over a greater area. Nonetheless, solid targets have been used successfully in the recent measurement of the $^{13}N(p,\gamma)^{14}O$ reaction at Louvain-la-Neuve[4]. Gas targets are not immune from problems associated with scattered beam because pump nozzles and collimators near the target will serve as thick scatterers or absorbers. In addition, these targets are costly and complicated. As a result, it is probably wise to design initial measurements with solid targets.

2.3 DETECTION TECHNIQUES

2.3.1 Recoil separators

Although the cross sections for explosive nucleosynthesis are large on the scale of those normally encountered in nuclear astrophysics, expected count rates are still low enough to place a premium on detector efficiency. An obvious signature of the desired reaction would be detection of the appropriate recoil nucleus. This can be accomplished with high efficiency because of the extreme inverse kinematics of these reactions. For example, recoiling ^{19}Ne from the $^{4}He(^{15}O,^{19}Ne)\gamma$ reaction will be found within a 1.4° cone. For (p,γ) reactions, the kinematic focusing is more severe [$\theta_{1/2} = 0.25°$ in the case of the $^{1}H(^{19}Ne,^{20}Na)\gamma$ reaction]. Therefore, recoil detection can be efficient even for a device with modest angular acceptance. In this case, the overall efficiency would be limited primarily by charge-state selection, but even this restriction might be overcome in selected cases (for instance, by using a gas-filled dipole magnet). However, clean separation of recoils from the beam is complicated by the fact that they have almost identical momenta. Since optical elements which simply disperse in momentum will not provide adequate separation, some form of velocity selection (e.g. a Wien filter) is also required. The recoil detector itself will present a challenge because it must be capable of measuring Z and A for low-energy ($E \leq$ 2 MeV/amu) heavy ions.

2.3.2 Prompt or delayed activity

If the recoil product is itself short-lived, but lives long enough to be transported away from the vicinity of the target, then its beta decay or beta-delayed activity could be measured under "clean" conditions. This technique obviates the need for a recoil detector since the decay is quite specific to the final nucleus. As an example, ^{20}Na recoils could be detected through the beta-delayed alpha particles ($E_\alpha = 2.69$ MeV) which accompany 16% of the decays.

2.3.3 Decay products

Gamma rays or light particles are also reaction-specific and thus offer an independent means of detecting the reaction of interest. However, when designing suitable detectors, attention must be paid to the fact that they will be operating in a high-background environment. For illustration, consider again the $^{1}H(^{19}Ne,^{20}Na)\gamma$ reaction: If a beam current of 1 pnA is used and one of every 10^5 projectiles are scattered near the target then a background composed primarily of pairs of 0.511-MeV gamma rays will reach an equilibrium rate of 6.25×10^4/sec after about 2 min of bombardment. If the target is viewed by a 12.7 cm x 12.7 cm NaI detector at a distance of 4-5 cm, then the detected background rate will be about 1.2×10^4/sec versus the foreground rate of ≈ 1/sec. Although the energy of this background is well-defined, pileup could spread this background out to higher energies. In contrast, if this detector were replaced with a 7.6 cm x 7.6 cm detector at r = 16 - 20 cm, then the background rate would be reduced to 600 - 800/sec. The need for high detection efficiency necessitates a large number of these detectors. Further background reduction may be gained by using such a detector array in coincidence with a recoil separator.

2.3.4 Conclusions

A general-purpose spectrometer for direct resonance measurements is shown in fig. 2. It is not

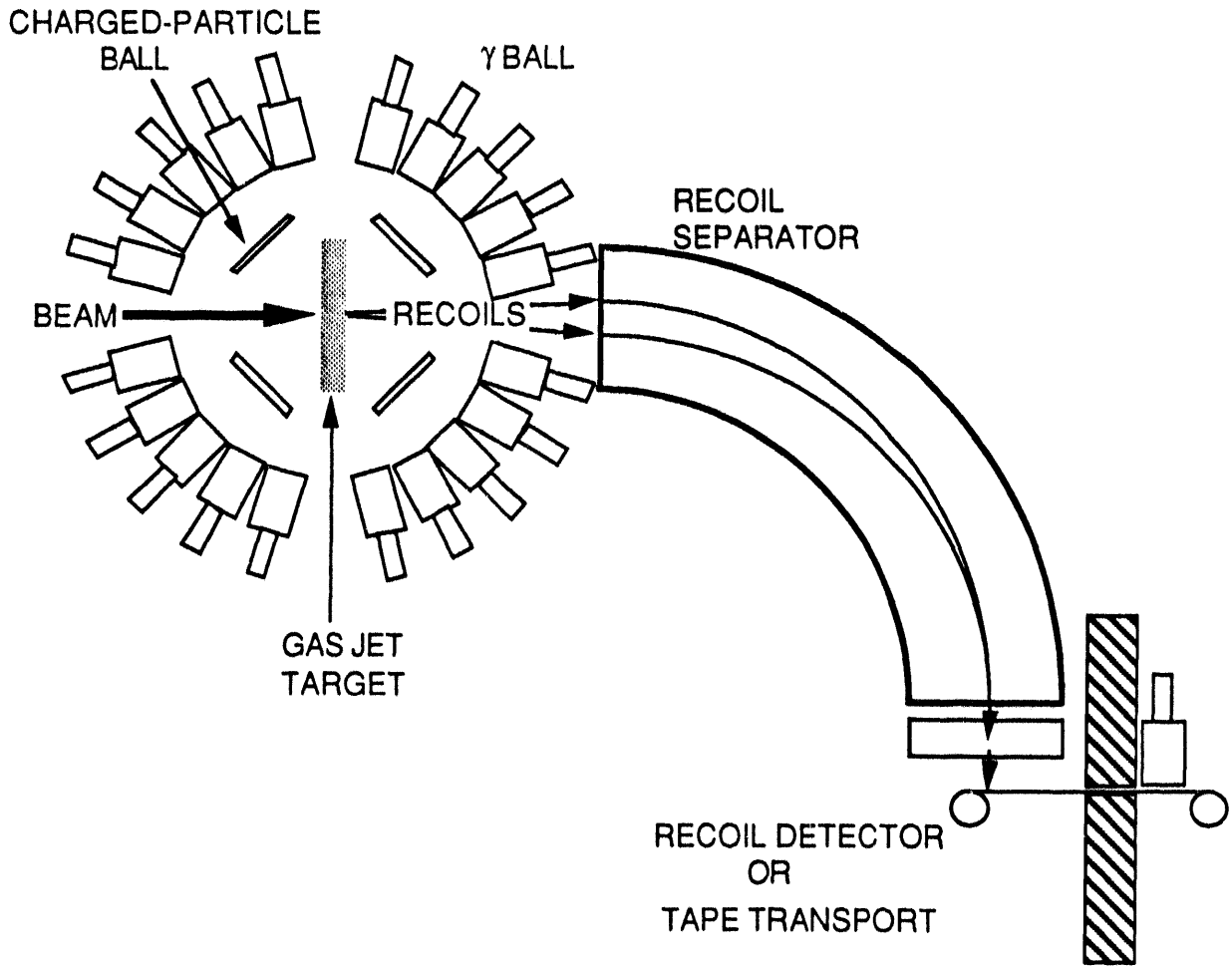

Fig. 2 Prototype nuclear-astrophysics spectrometer

meant to represent an actual device, but merely summarizes the different techniques which may be employed. Clearly real hardware will evolve with the experimental program. However, because each experiment will present unique challenges, it is important that the system be flexible enough to be re-configured as warranted. For some experiments, detection of gamma rays or recoils in singles may be sufficient. Others may require a coincidence condition to reduce backgrounds. Since the recoils are readily accessible, it is probably advantageous to consider recoil detection as the basis for most measurements.

3. Indirect Measurements

A typical resonance located at center-of-mass energies appropriate to explosive nucleosynthesis can have a particle width in the range of eV to keV and a gamma width of 0.01 - 1 eV. However, there are cases where one or the other of these widths is suppressed. If $\omega\gamma < 1$ meV, then a direct measurement of the resonance strength is probably not possible. Nevertheless, resonance parameters can still be obtained via spectroscopy of the compound nucleus. This technique has been used successfully with stable beams for nuclei near stability, but for nuclei further from stability, it can be difficult to populate the compound nucleus with a reasonable cross section. Radioactive beams can permit these nuclei to be studied in more detail. In particular, proton- or neutron-stripping reactions will populate states corresponding to proton- or neutron-capture resonances. Measurements of their decay widths then determine the resonance strength. For weak resonances, we are faced with having to measure the weakest of these decay branches because, for example, if $\Gamma_p << \Gamma_\gamma$ then $\omega\gamma \approx \Gamma_p$ (and similarly, if $\Gamma_\gamma << \Gamma_p$ then $\omega\gamma \approx \Gamma_\gamma$). In principle, Γ_p can be extracted in a straightforward manner from stripping data. However, measurements of Γ_γ are likely to be more difficult.

3.1 MEASUREMENTS OF STRIPPING REACTIONS

The $^1H(^{39}Ca,^{40}Sc)\gamma$ reaction is an example of a reaction that is astrophysically interesting, but is dominated by very weak resonances. Predicted count rates for this reaction are shown in table 2.

Table 2. Resonances in the $^1H(^{39}Ca,^{40}Sc)\gamma$ Reaction

E_{cm} (keV)	Γ_p (meV)	$\omega\gamma$ (meV)	COUNT RATE (counts/hour/pnA)
242	1.1×10^{-5}	7.1×10^{-6}	7×10^{-4}
360	2.8×10^{-3}	3.9×10^{-3}	0.25

Clearly this is a case where $\Gamma_p << \Gamma_\gamma$. As an alternative to a direct measurement, it is possible to populate the same states with the $^3He(^{39}Ca,^{40}Sc)^2H$ reaction. Here the proton width can be obtained from the proton spectroscopic factor via the familiar procedure:

$$\Gamma_p = 2\,\gamma_p^2\,P_l(E) = 2\,C^2S\,\gamma_{sp}^2\,P_l(E) \qquad 5.$$

$$= 0.45\,\frac{(2J_i+1)(2J_t+1)}{(2J_f+1)}\left[\frac{\sigma_{exp}}{\sigma_{DWBA}}\right]\gamma_{sp}^2\,P_l(E) \qquad 6.$$

where γ_p^2 is the reduced width, $P_l(E)$ is the penetrability, C^2 is an isospin Clebsch-Gordan coefficient, S is the spectroscopic factor, and γ_{sp}^2 is the (calculated) single-particle reduced width. For this and similar measurements, the beam energy will have to be above the Coulomb barrier and high enough so that the direct component of the cross section is enhanced relative to compound-nuclear and multistep channels. These requirements imply E ≥ 5 MeV/amu, but E = 20-25 MeV/amu may be more typical. Detection schemes can be similar to those described above except that in this case it is necessary to measure kinematics as well as yields.

If E_{39} = 400 MeV in the present example, then the recoiling ^{40}Sc will emerge in a 6.4° forward cone with E_{40} = 359 - 394 MeV. The total cross section will be on the order of several b, thus recoil detection would again seem to be an efficient approach. However, now it is also necessary to measure momentum (or energy) and angle (to correct for $dp/d\theta$) in order to determine the population of individual excited states in the recoiling nucleus. A number of factors combine to complicate this task: Although momentum can be measured precisely with a magnetic spectrometer, the beam and recoils will have similar momenta and so once again separation will be difficult. Also, since the beam is more rigid than the recoils, scattered beam will present a troublesome background. Finally, even if the recoils can be detected cleanly, the angular divergence of the beam will limit the resolution of the measurement (if $\theta_{beam} = \pm 0.5°$, $\Delta E_x \approx 2$ MeV). As a consequence, it is probably necessary to measure the residual deuterons, or recoil-deuteron coincidences. Although the spectroscopic factor can be extracted from a spectrum of deuterons alone, a measurement of θ_{recoil}, p_{recoil} and θ_d completely determines the reaction kinematics (including the effect of beam divergence) and permits the recoils to be measured with higher resolution. A schematic of this approach is shown in fig. 3. The outgoing deuterons will have 40 times the angular spread of the recoils (i.e. θ_d = 180° - 52° for θ_{recoil} = 0° - 3.2°) and so a measurement of θ_d can be carried out with a fairly simple detector (e.g. a Si microstrip). Because of the large cross sections involved, this type of measurement can be performed over the course of a few days.

Although what has been described above appears promising as a means to determine Γ_p, it may not be particularly useful for cases where Γ_γ is the quantity of interest. A triple-coincidence (recoil-d-γ) measurement is a possibility, but in most cases will prove to be impractical because of low count rate.

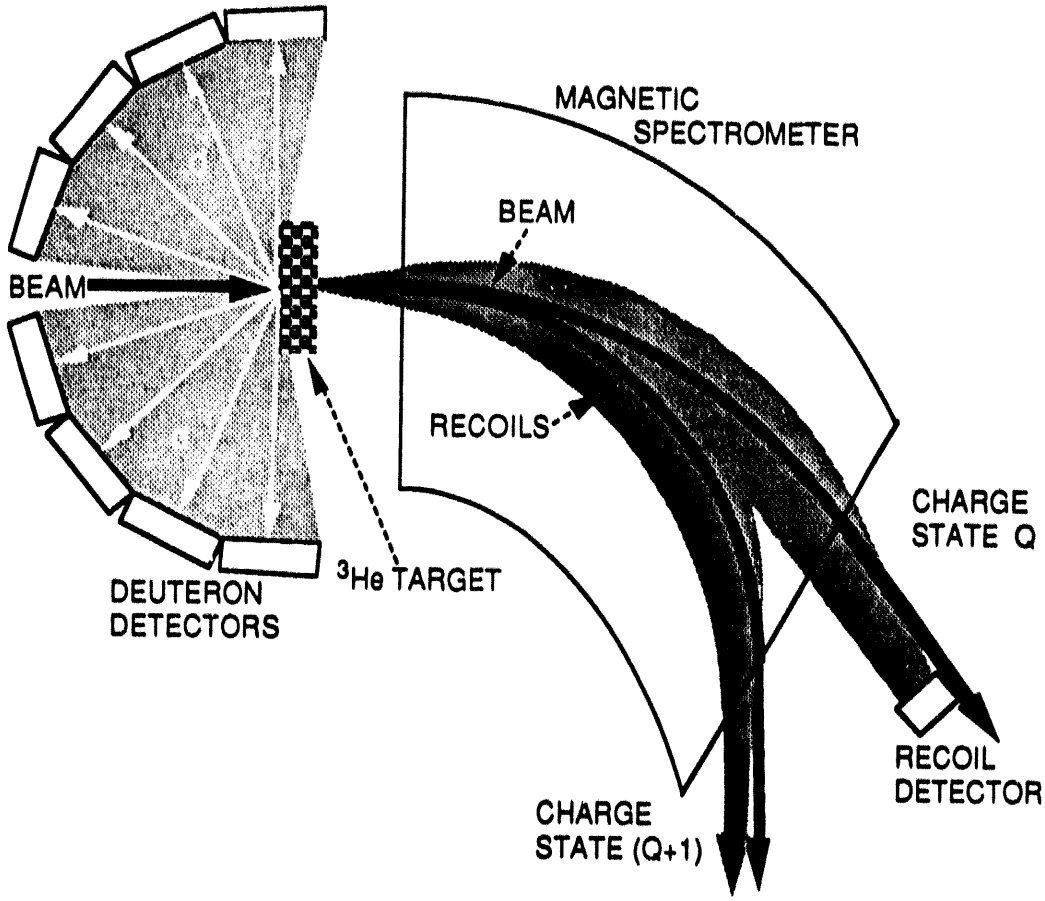

Fig. 3. Schematic of a deuteron-recoil coincidence measurement

3.2 COULOMB BREAKUP

Coulomb breakup (in which a projectile is photodissociated in the Coulomb field of the target) has been proposed[5] as another way of studying the inverse radiative-capture process. Because the density of virtual photons supplied by a high-Z target (such as lead) can be quite large, the breakup yield can be enhanced relative to capture. Although this approach has been applied successfully to measurements[6,7] of Γ_γ in the breakup of ^{14}O, systematic problems limit its usefulness. In general, it is difficult to obtain an accurate radiative-capture cross section from breakup because Coulomb post-acceleration will perturb the relative kinematics of fragments with differing charge-to-mass ratios (since the center-of-mass energies of interest can be as low as 200 keV, this effect is important, even though breakup occurs "far" from the target). However, Γ_γ can be extracted by comparing the observed yield with a calculation of Coulomb breakup. Nonetheless, this technique is useful only for those few cases involving an E1 decay directly to the ground state. For more complicated decays, additional gamma-ray spectroscopy must be performed to correct for unobserved branches in the breakup results. Finally, breakup measurements require high beam

energies (E ≈ 100 MeV/amu) in order to ensure that strong excitations can be neglected relative to pure Coulomb excitation. It is difficult to satisfy this requirement with a facility that must also produce intense low-energy beams for resonance measurements.

4. Other Data Needs

4.1 ADVANCED STAGES OF HYDROGEN BURNING

Reactions occurring in the A ≥ 40 nuclei with sufficiently high Q values will populate regions of high level density in the compound nucleus. Here resonances may be broad and/or overlapping and the cross section can take on a statistical character. Although we can attempt to measure these reactions, it should be simpler to measure excitation energies and spins in order to constrain a statistical-model calculation. These calculations have been shown to accurately reproduce existing data. In addition, it is necessary to measure masses and half lives, particularly for nuclei near the proton drip line. Such measurements should also be performed for heavy (p-process) nuclei. These experiments are conceptually identical to those contemplated for nuclear-structure studies and would presumably share the same equipment.

4.2 NEUTRON-RICH NUCLEOSYNTHESIS

4.2.1 Reactions involving light nuclei

In inhomogeneous big-bang models, a number of potentially interesting neutron-capture reactions can occur involving light nuclei. Because typical half lives are on the order of seconds, a direct neutron-capture measurement using a radioactive target would be challenging. However, a neutron-stripping reaction such as (d,p) can be used in the same manner as was described in sec. 3 for proton stripping. Since it is expected that $\Gamma_\gamma << \Gamma_n$ for these reactions, a triple-coincidence (recoil-p-γ) measurement is required.

4.2.2 Reactions involving heavy nuclei

Neutron-capture reactions on heavy nuclei can be categorized according to whether they are slow compared to beta decay (s-process) or rapid (r-process). The s-process, which runs close to the line of stability, is comparatively well-studied. However, very detailed information concerning the stellar environment during the s-process can be obtained by studying branch points where the rates for neutron capture and beta decay are comparable. These nuclei live long enough ($T_{1/2}$ = months to years) so that a radioactive target can be produced and exposed to an off-line neutron source.

The r-process can run as much as 20 mass units beyond the most neutron-rich stable nuclei. During equilibrium, the reaction flow is governed by the neutron separation energy, S_n. In essence, the experimental approach here is similar to that for statistical cross sections in hydrogen burning. Near closed shells, the r-process flow comes close enough to stability to permit a direct measurement of S_n. In transitional regions, we require systematics for masses and half lives to construct a realistic mass formula and calculate S_n. Again the experimental techniques involved are similar to those used for general nuclear-structure measurements.

5. Conclusions

5.1 TARGETS AND DETECTORS

In principle, a gas jet would be the best choice for a target because of its combination of high count rate and low background. However, existing designs would cause severe backgrounds arising from scattering off of collimators and other hardware. Solid targets will prove useful for selected experiments, but a suitable gas-jet target should be developed.

Because experiments for nuclear astrophysics involve extreme inverse kinematics, a recoil separator immediately suggests itself as the basis for a detection system. This device will need to have a beam-rejection factor of at least 10^{10}. Although beam and recoils will have similar momenta, their velocities will differ by 5-20% and so this objective can be met with a reasonably simple velocity filter. The actual detection scheme will be determined by the requirements of a particular experiment. However, detectors located near the target will have to be multi-element arrays in order that the background rate in an individual detector is manageable.

5.2 BEAM REQUIREMENTS

General parameters for astrophysics measurements with radioactive beams are listed in table 3.

Table 3. Radioactive-Beam parameters

Beam Energy:	0.2 - 25 MeV/amu
Energy Resolution:	0.5 - 1% for $E \leq 2$ MeV/amu
	0.1 - 10% at higher energies
Energy Calibration:	±1 keV for $E \leq 2$ MeV/amu
Beam Current:	10^{10}/s
Normalized Emittance:	approximately 2π mm-mr
Isobaric Purity:	better than 10^{-4}

The low end of the energy range is required for resonance studies whereas the upper end is appropriate for spectroscopy. For resonance measurements, the energy resolution need not be drastically better than the target width (if the target is thick compared to the width of the resonance). The resolution listed for higher energies was arrived at by assuming that the beam will contribute about 20 keV to the total energy resolution. If recoil energies are measured, then $\Delta E = 0.1\%$ is needed. On the other hand, if the measurement is based upon detecting the residual particles, then the resolution requirement may be relaxed to as much as 10%. The specification for energy calibration is based on the fact that our expected yields are too low to permit "resonance hunting". Although many resonances will be more narrow than ±1 keV, the targets will be several keV thick. Consequently, if the beam energy can be set to an accuracy of ±1 keV, then we are assured of hitting the resonance energy somewhere within the target. Beam current is an obvious

limitation on our projected count rates. The figure given in table 3 was chosen as a realistic goal for the best beams. However, since the beam must be delivered to the target cleanly to minimize scattering, tandem-quality emittance is desirable. Finally, many of the resonances of interest have strengths of only a few meV while resonances in isobaric reactions can be 10^3 - 10^4 times stronger. Therefore, the level of isobaric contamination can be no more than 10^{-4} of the beam of interest.

5.3 INITIAL BEAMS

The selection of interesting beams is clearly determined by astrophysical considerations which will continue to evolve. The present list is summarized in table 4.

Table 4. Initial Beams

Inhomogeneous Big Bang:	^{8}Li, ^{16,17}N, ^{19}O, ^{20,21}F...
Explosive Hydrogen Burning:	^{14,15}O, ^{17,18}F, ^{18,19}Ne, ^{20,22}Na, $^{21\text{-}23}$Mg, $^{24\text{-}26}$Al, ^{26,27}Si, ^{30,31}S, ^{39}Ca.... plus selected beams in the Fe region
s-Process:	selected targets of e.g. ^{90}Sr, ^{95}Nb, ^{106}Ru, ^{137}Cs, ^{155}Eu, etc. (ref.[8])
r-Process:	selected neutron-rich beams such as those listed above for big-bang studies

All of these astrophysical processes involve sequences of reactions or reaction cycles. As a result, a measurement at one step of a reaction path can alter our view of which of the subsequent reactions is important to study. In the interest of efficiency, it is best to start with several key measurements early in the reaction network and then re-evaluate the network as new results are obtained. For example, since the ^{8}Li(α,n)^{11}B reaction appears to regulate the flow to heavier masses during an inhomogeneous big bang, a ^{8}Li beam should be developed before some of the other light, neutron-rich beams. A similar situation exists for studies of the hot CNO cycles and the rp-process. The beams listed between oxygen and sulfur would permit us to study reactions up through the early stages of the rp-process. Since most explosions do not progress beyond this point, these measurements would be of more immediate observational interest than measurements in the iron region. However, this list can be expected to undergo major changes as our understanding of these processes improves.

It is a pleasure to acknowledge the help of M.S. Smith, P.V. Magnus, J. Görres, B. Sherrill, M. Wiescher, P.D. Parker and R.N. Boyd in discussions leading to the preparation of this article.

References

1. P.V. Magnus *et al.*, *Nucl. Phys.* **A506** (1990) 332.

2. R. Sherr, private communication.

3. Noble-gas targets can be produced via ion implantation. However, in order to achieve a target density that would be useful for our purposes, a thick backing is required. It does not appear likely that a transmission target can be implanted with enough helium to be useful.

4. P. Decrock *et al.*, *Phys. Rev. Lett.* **67** (1991) 808.

5. G. Bauer, C.A. Bertulani and H. Rebel, *Nucl. Phys.* **A458** (1986) 188.

6. T. Motobayashi *et al.*, *Phys. Lett.* **B264** (1991) 259.

7. J. Kiener *et al.*, *Proc. 2nd Int .Conf. on Radioactive Nuclear Beams*, Th. Delbar, ed., (Adam Hilger 1992) 311.

8. F. Käppeler, private communication.

HIGH-SPIN NUCLEAR STRUCTURE STUDIES WITH RADIOACTIVE ION BEAMS

Cyrus Baktash

Physics Division, Oak Ridge National Laboratory, Oak Ridge, TN 37831-6371

1. Introduction

Two important developments in the sixties, namely the advent of heavy-ion accelerators and fabrication of Ge detectors, opened the way for the experimental studies of nuclear properties at high angular momentum. Addition of a new degree of freedom, namely spin, made it possible to observe such fascinating phenomena as occurrences and coexistence of a variety of novel shapes, rise, fall and occasionally rebirth of nuclear collectivity, and disappearance of pairing correlations. Today, with the promise of development of radioactive ion beams (RIB) and construction of the third-generation Ge-detection systems (GAMMASPHERE and EUROBALL), we are poised to explore new and equally fascinating phenomena that have been hitherto inaccessible. With the addition of yet another dimension, namely the isospin, we will be able to observe and verify predictions for exotic shapes as varied as rigid triaxiality, hyperdeformation and triaxial-octupole shapes, or to investigate the T=0 pairing correlations. In this paper, we shall review, separately for neutron-deficient and neutron-rich nuclei, these and a few other new high-spin physics opportunities that may be realized with RIB. Following this discussion, we shall present a list of the beam species, intensities and energies that are needed to fulfill these goals. The paper will conclude with a description of the experimental techniques and instrumentations that are required for these studies.

2. High-Spin Physics in the Neutron-Deficient Nuclei

The medium-heavy RIB with $Z \geq 32$ and $T_z \leq 1$ will allow access to the self-conjugate and mirror nuclei up to ^{100}Sn, and those bordering or beyond the proton- drip line above the N, Z=50 magic numbers. According to the theoretical models, some of the richest

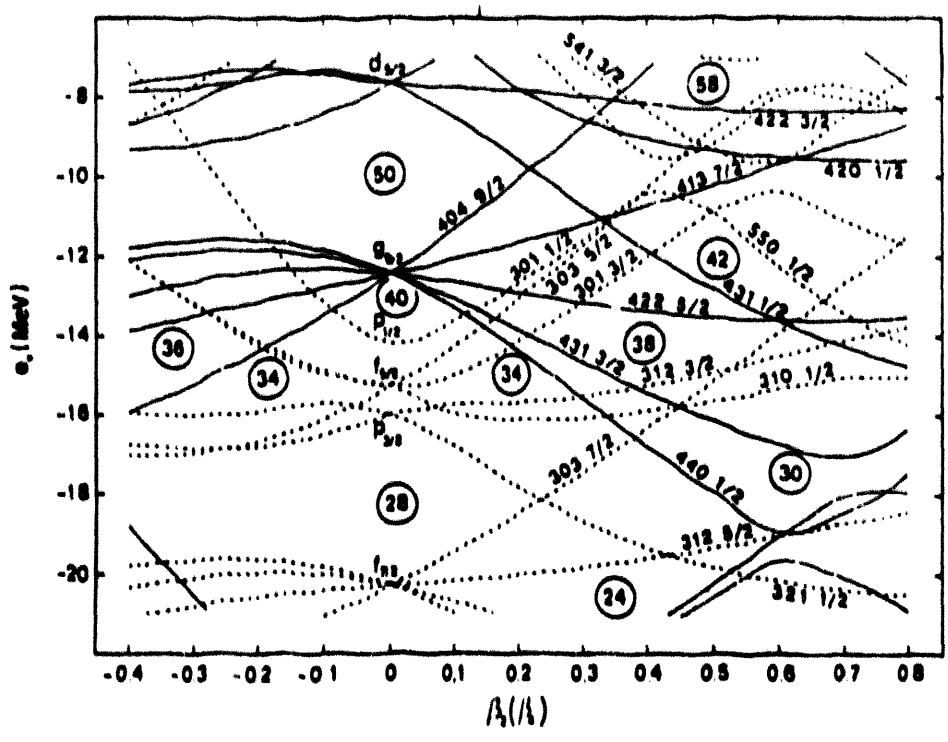

Fig. 1 Nilsson single-particle levels in the A=80 mass region as functions of the quadrupole deformation β_2, calculated using the Woods-Saxon potential. Some particle numbers corresponding to large shell gaps are shown in circles (adopted from Ref. 1).

examples of shape coexistence and shape transition are expected to exist among these nuclei. This is because of the fact that (a) the single-particle energy levels show large gaps corresponding to oblate, spherical, prolate and superelongated shapes for the particle numbers below 50 (see Fig. 1), and (b) these shell structures are reinforced when protons and neutrons simultaneously occupy these levels. Consequently, one encounters a variety of nuclear shapes that change rapidly with N, Z, and angular momentum.[1] As such, these nuclei provide the best testing ground for the microscopic models.

With stable beams, studies of the even-mass, self-conjugate nuclei have been recently extended to ^{84}Mo, using (H.I., 2n) fusion-evaporation reactions near the Coulomb barrier.[2] The yields of the two-neutron evaporation reactions that are used to produce these self-conjugate nuclei are at the limit of our present experimental capabilities. This is because of the fact that (a) charged-particle emission is by far the dominant evaporation mode in proton-rich compound systems, and (b) fusion cross sections are very small near the Coulomb barrier. For example, the experimental cross section for the ^{28}Si(^{58}Ni,2n)^{84}Mo reaction is reported to be less than 10μb.[2] Thus, identification of these

nuclei has required a combination of a recoil mass separator (RMS) and a relatively large array of Ge detectors. The resulting spectroscopic information has been limited, so far, to a few gamma rays which are assumed to de-excite the lowest states in these nuclei. Because of the rising Coulomb barrier, the cross section for the (H.I., 2n) reactions become vanishingly small as we approach ^{100}Sn. Moreover, production of very proton-rich nuclei with stable beams suffers from a second, and fundamentally more serious, problem: near-barrier fusion reactions populate compound nuclei with small angular momentum. Thus, studies of high-spin physics in these nuclei will not be possible with the stable beams, even if the detection sensitivity is enhanced by two-three orders of magnitude using the GAMMASPHERE and the third-generation RMS.

In contrast, the use of proton-rich RIB removes or mitigates many of these obstacles. First, many of the self-conjugate nuclei can be reached via the (RIB, xp yα) reactions, which involve only charged-particle emission. As a result, the expected cross sections are enhanced by nearly an order of magnitude each time the T_z (≡(N-Z)/2) of the beam is reduced by 1/2. This is illustrated in Fig. 2, which compares the yields for the emission of neutron and proton from ^{90}Ru(T_z=1) nucleus, leading to the isobars ^{89}Ru(T_z=1/2) and ^{89}Tc(T_z=3/2), respectively. The yields, calculated using the PACE code[3], correspond to the decay of 10^4 compound nuclei ^{92}Pd(T_z=0) and ^{94}Pd(T_z=1) which are produced in reactions of, respectively, ^{52}Fe(T_z=0) and ^{54}Fe(T_z=1) beams on a ^{40}Ca target, as shown in Figs. 2a and 2b. The numbers give the peak yields for neutron emission (left arrows) and proton emission (down arrow), and illustrate the particle-decay pathways as the T_z is changed due to particle evaporation. Because of the differences in the proton and neutron binding energies, the peak yields occur at different excitation energies. (To get the actual cross sections, the yields should be normalized to 10^4 and multiplied by the geometric cross sections at the corresponding bombarding energies. This is sometimes quite small, as the peak yields occur at sub-barrier energies for some reactions.) Several lessons may be drawn from these calculations:

(1) In Fig. 2a, the proton-to-neutron yield ratios decrease steadily from 9900:1=9900 in ^{92}Pd(T_z=0), to only 4800/640=7 in ^{89}Tc(T_z=3/2), as the T_z increases from 0 to 3/2. These numbers illustrate the predominance of proton emission from the heavy proton-rich nuclei. For comparison, the peak yields for α emission from ^{90}Ru and ^{89}Tc are also shown by diagonal double arrows in Fig. 2a. They indicate the following order of preference for particle emission from proton-rich systems: protons first, alphas second and neutrons last.

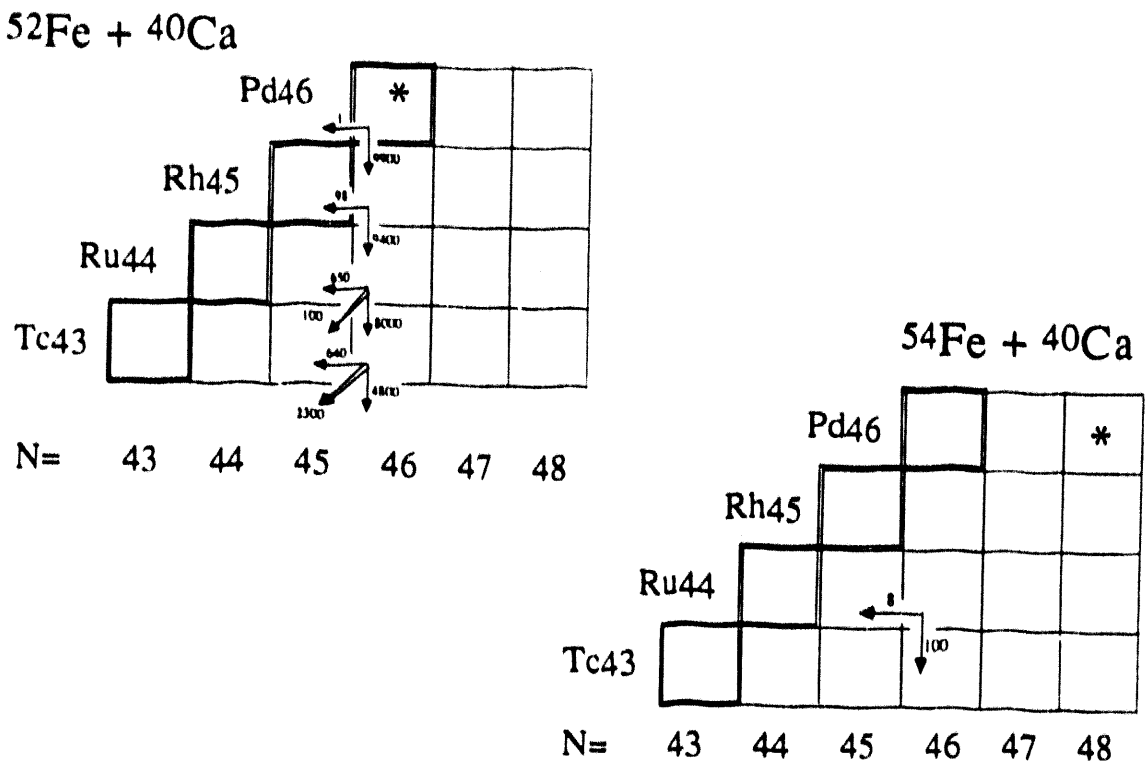

Fig. 2. Monte Carlo predictions of the peak yields for the emission of proton (down arrow), neutron (left arrow) and alpha (diagonal double arrow) from the decay of 10^4 compound nuclei shown by (*). The top and bottom panels correspond to the reactions of (a) $^{52}Fe(T_z=0)$, and (b) $^{54}Fe(T_z=1)$ beams on a ^{40}Ca target, respectively. See the text for details.

(2) A comparison of the yields given in Figs. 2a and 2b illustrates the importance of having neutron-deficient beams for the production of neutron-deficient residual nuclei. Although the proton-to-neutron *yield ratios* are the same (nearly 13) in both reactions, the absolute peak yield for the production of ^{89}Ru increases from 8 to 650 in going from the $^{54}Fe(T_z=1)$ beam to $^{52}Fe(T_z=0)$, respectively. That is, the peak yield for the (2p n) channel is nearly two orders of magnitude larger than that of the (2p 3n) channel. This simply reflects the fact that the phase space gets larger, and becomes more biased toward the larger T_z values, as the T_z of the compound system is increased. Figure 3 illustrates the variety of the self-conjugate nuclei that may be produced with large cross sections using a neutron-deficient RIB, such as $^{30}S(T_z=-1)$. Experimentally, the smaller phase spaces, and the larger partial cross sections for neutron-deficient residual nuclei that result from the use of neutron-deficient radioactive ion beams translate to less demand on the selectivity

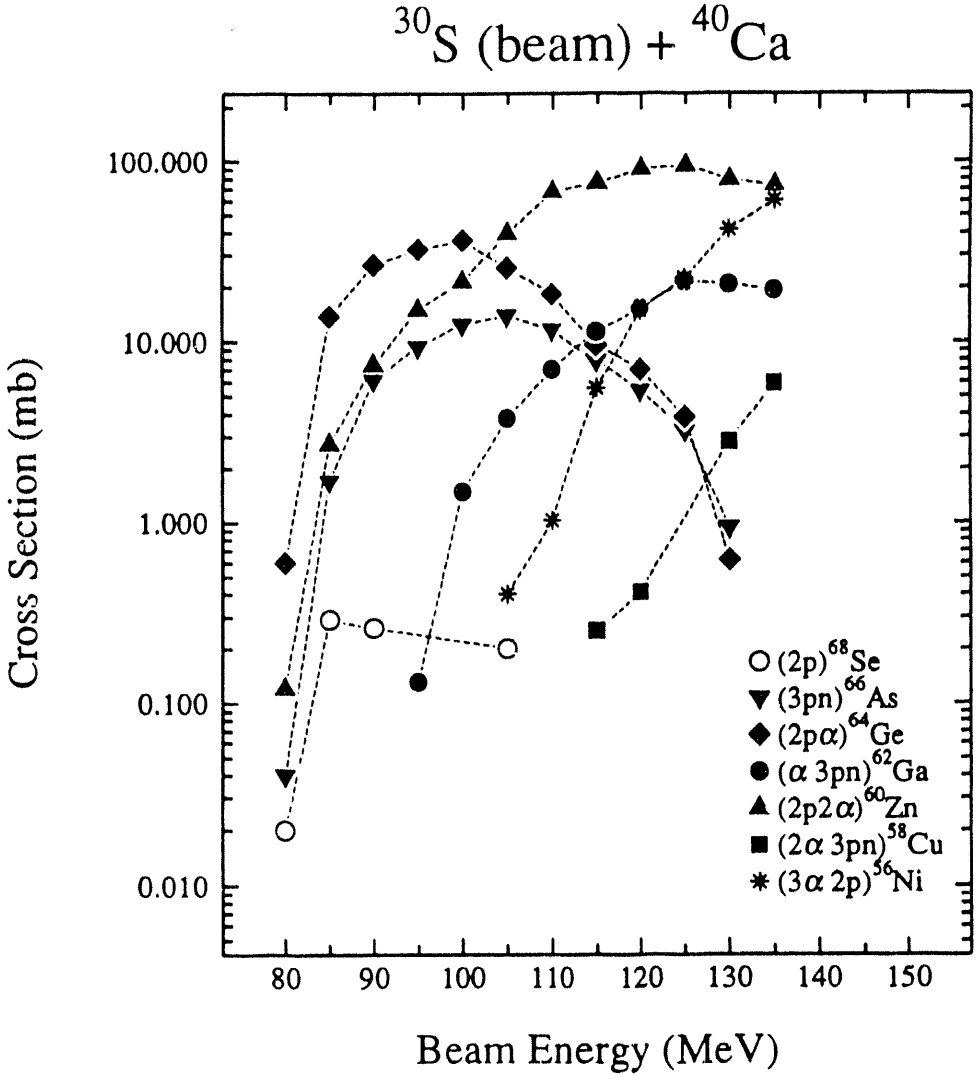

Fig. 3. Predicted excitation functions for the production of several self-conjugate nuclei using the ^{30}S + ^{40}Ca reaction. The evaporated particles are indicated in parenthesis.

and efficiency of the experimental detection systems. Also, since many of the exit channels of interest may be produced via pure charged-particle emission, channel selection may be easily and efficiently effected by the use of 4π charge-particle detector systems, such as the Washington University Dwarf Ball.[4]

The second advantage of RIB lies in the fact that the experimental studies of the heavy, nearly self-conjugate, odd-Z nuclei becomes possible. This is crucial for the studies of the heavy mirror nuclei, and the T=0 pairing correlations, thought to be important in the N=Z nuclei (see Sec. 2.3).

Finally, insofar as the high spin physics is concerned, the biggest advantage offered by RIB is that many proton-rich nuclei of interest (including those which are already accessible via (H.I., 2n) with stable beams) may be produced at high angular momentum. In the following subsections, we shall briefly describe a few of the new physics opportunities that will be opened up with proton-rich radioactive ion beams.

2.1 Superdeformed and Hyperdeformed Shapes

Superelongated shapes result from a delicate balance between the microscopic shell effects and pairing interactions on the one hand, and the macroscopic rotating liquid drop energy, including the Coulomb force, on the other. Due to the strong dependence of the liquid drop energy on the proton and neutron number, the details of this balance vary greatly from light to heavy nuclei. In heavy nuclei near ^{208}Pb, superelongated shapes are stabilized due to both the shell, and the large macroscopic liquid drop (fissility and Coulomb repulsion) effects. The low-spin, superdeformed (SD) fission isomers observed in the actinides are prime examples of this cooperative phenomenon. In contrast, SD shapes are, by and large, stabilized by the shell effects in the very light nuclei. In the intermediate region, where the liquid drop terms dominate, superdeformation and hyperdeformation (HD) is stabilized only at high spins. Therefore, identification of the superelongated structures in different mass regions would provide valuable insight into the question of the competition between the microscopic and macroscopic effects.

So far, a variety of SD bands have been identified at high spins in the A=150 and 190 mass regions.[5,6] However, except for a weak SD ridge structure in ^{82}Sr [Ref. 7], experimental searches for the predicted SD shapes in the A=80 region have not yet met with success. This is because of the difficulty encountered in populating the high spin states ($I \geq 40\ \hbar$) in ^{82}Sr and the neighboring nuclei, at which the SD structures are predicted to become yrast. Calculations by Ragnarsson indicate that SD shapes in the neutron-deficient nuclei ^{60}Zn and ^{88}Ru become yrast at spins $22\hbar$ and $36\hbar$, respectively.[8] Neutron-deficient RIB with a T_z=-1 may be used to populate these states with a significant cross sections (see, e.g., Fig. 3).

Several calculations have predicted the onset of hyperdeformed nuclear states (with the major to minor axis ratio of 3:1) at very high spins in some medium-mass and rare-earth nuclei.[9-11] Unfortunately, in the candidate nuclei which may be accessed using stable beams, fission is the dominant decay mode at the spin values where the hyperdeformed states are predicted to become yrast. With the aid of RIB, one could investigate such neutron-deficient nuclei as ^{118}Ba, for which the predicted[12] critical angular momentum is about 60 $\hbar$, well below the limit set by fission. (The large gap corresponding to hyperdeformation at Z=56 may be seen in the single-particle energies shown in Fig. 4.)

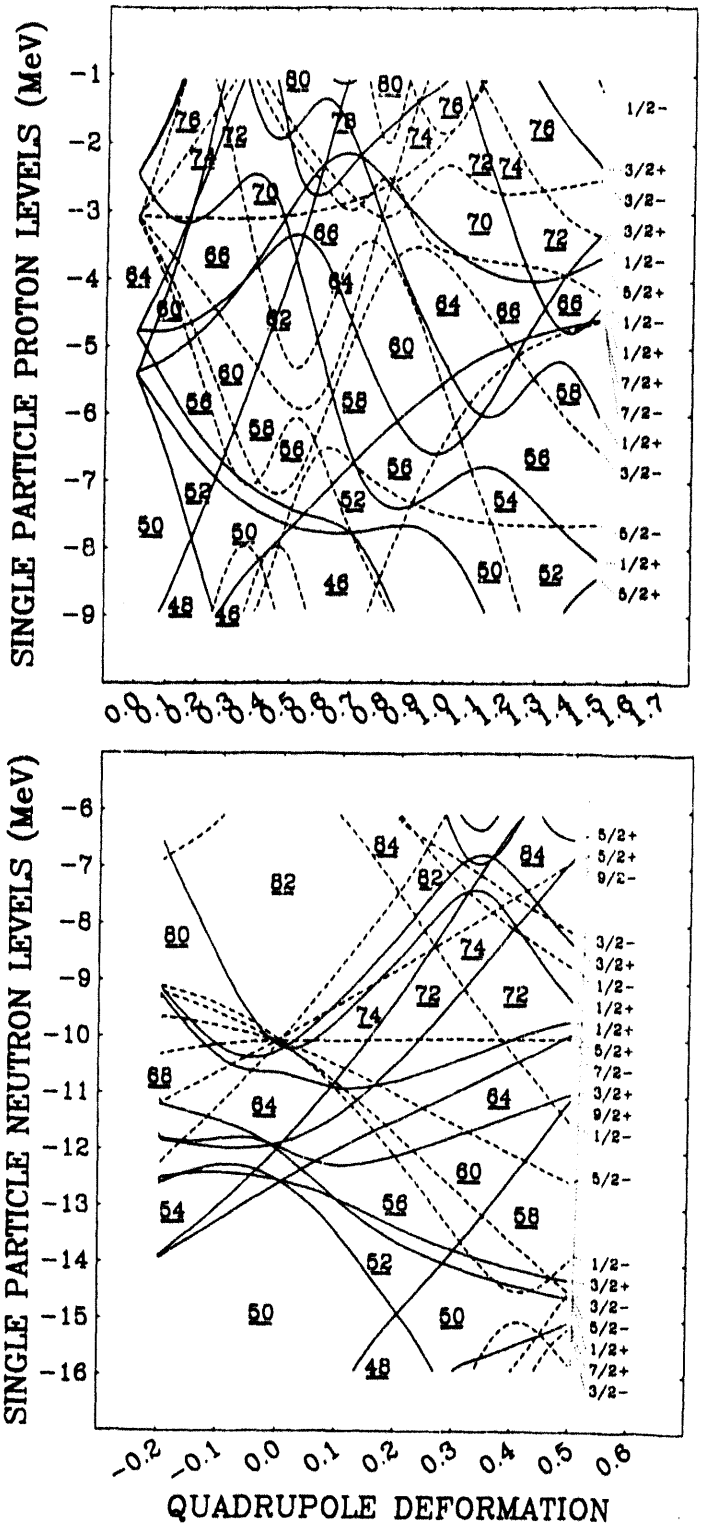

Fig. 4. Plots of single-particle energies of proton (top) and neutron (bottom) as functions of the quadrupole deformation. They are calculated using Woods-Saxon potentials.[20]

2.2 Rigid Triaxial and Octupole Shapes

Despite the fact that *dynamical* triaxiality and octupole deformation[13] has been observed in many nuclei, convincing evidence for the presence of *rigid* triaxial or octupole shapes has not yet emerged. Interestingly, rigid triaxiality is either absent or is rarely predicted in many nuclear models. Therefore, it is very interesting to verify the existence of deep triaxial minima when they appear in the calculated potential energy surfaces. A distinctive feature of the medium-mass nuclei is the relative abundance of rigid triaxial and octupole minima in the calculated potential energy surfaces. Recent calculations[14] predict deep triaxial minima in the self-conjugate ^{44}Ti and ^{72}Kr nuclei. Similarly, nuclei near ^{64}Ge(N=Z=32) and ^{112}Ba(N=Z=56) are among the best candidates for octupole deformation.[15,16] In fact, the predicted hyperdeformed minima in the potential energy surfaces of the neutron deficient Ba nuclei are also accompanied by softness toward β_3 deformation.[12]

In addition to the Y_{30}, the non-axial octupole operators proportional to Y_{31}, Y_{32}, and Y_{33} may also produce a minimum in the potential energy surfaces.[17] The effect of these operators is most visible in nearly self-conjugate nuclei where proton and neutron shell effects arising from these terms add coherently. With neutron-deficient RIB, detailed spectroscopy of these nuclei becomes feasible, thus making it possible to explore such exotic deformations as triaxial-octupole, or hyperdeformed-octupole shapes.

2.3 Proton-Neutron Interaction

It is well known that the long-range quadrupole component of the T=0 proton-neutron interaction plays an important role in the evolution of collectivity and deformation (see Ref. 18 for a recent review of this subject). However, much less is known about the short-range p-n interaction, which acts primarily among the strongly overlapping states with identical principal and orbital quantum numbers. Since the neutron-proton T=0 pairing depends strongly on the neutron excess, the self conjugate nuclei provide the best systems to study this interaction. (The T=0 pairing is dominant over, comparable with, or negligible compared to the T=1 like-particle pairing for T_Z=0, 1, or >1, respectively.[18]) Since the Coriolis force breaks more easily the T=1 pairing interaction that acts on the time-reversed orbitals, the T=1 pairing is expected to be destroyed at lower spins as compared to the T=0 pairing. Survival of the T=0 pairing at high spins is expected to lead to such observable effects as the shift in the crossing frequencies, or mixing between the proton and neutron s-bands built on the $g_{9/2}$ orbitals in the A=80 mass region. For example, by comparing the energy spectra of an N=Z core and its three neighboring (N, Z+1), (N+1, Z), and (N+1, Z+1) nuclei, the p-n interaction strength can be accurately

established empirically. Such high-spin studies of the self-conjugate and mirror nuclei would require neutron-deficient radioactive ion beams.

Although the self-conjugate nuclei become proton unbound above ^{100}Sn, similar studies of the strongly attractive p-n interaction among the high-j intruder orbitals would be still possible. For example, for many well-deformed bands built on the high-j intruder orbitals in odd-N(Z) nuclei, the expected band crossing based on the aligned protons (neutrons) has not been observed. A possible explanation is that the aligned high-j protons and neutrons have a large spatial overlap that leads to a strong p-n interaction, causing a shift in the band crossing frequencies.[19] Since the correct strength of such p-n interactions is not known empirically, we cannot at present appraise the validity of these arguments. With the availability of RIB, one may systematically explore the p-n interaction among identical high-j orbitals based on the $f_{7/2}$, $h_{9/2}$, $h_{11/2}$, and $i_{13/2}$ orbitals in very neutron-deficient nuclei with Z≈ 60 and 80 (see, e.g., Fig. 4).

3. High-Spin Physics in the Neutron-Rich Nuclei

The high-spin states in the neutron-rich nuclei may be populated using Coulomb excitation, heavy-ion transfer, fusion-evaporation, and quasi-elastic reactions. These reactions are by and large complementary, and probe different structures in nuclei.

3.1 Coulomb Excitation

Coulomb excitation provides a powerful method for the investigation of the collectivity and deformation of the yrast and near yrast structures in nuclei. With RIB, Coulomb excitation of the projectile on a series of targets, ranging from ^{40}Ca to ^{208}Pb , would be the method of choice. In this way, one could determine hundreds of diagonal and non-diagonal electromagnetic matrix elements that connect the near-yrast states.[21] These matrix elements would provide a very stringent test of the nuclear structure models. The advantage of Coulomb excitation lies in the fact that it selectively excites the ground state band and the vibrational bands that are coupled to it via strong matrix elements. Thus, one is able to obtain useful information about the structure of these bands with only modest beam intensities, starting with about 10^6 pps.[22,23]

3.2 Heavy-ion Transfer Studies

Heavy-ion transfer reactions provide a unique tool to preferentially populate states that are not easily accessible by other means.[24] For example, one may selectively populate the

aligned non-yrast bands built on the intruder high-j orbitals using odd-A beams in which the intrinsic and orbital spins are anti aligned.[25] An intriguing possibility is the use of such reactions with neutron-rich odd-N radioactive beams to populate the predicted superdeformed[26] and hyperdeformed[11] shapes in the neutron-rich Hg-Ra nuclei via transfer reactions. Because these reactions populate "cold" high spin states,[27] they would minimize the background due to fission, which is usually a major problem in the studies of the high-Z systems.

With the neutron- and proton-rich RIB, one obtains large Q-values for the transfer of a single nucleon with odd-A beams, and one or more pairs with even-even beams. For example, neutron stripping (proton pick up) reactions of very neutron-rich odd-N(Z) RIB with neutron-rich stable targets will result in neutron-rich residual systems. (Naturally, the analog reactions of proton-rich odd-A beams on proton-rich targets will result in a proton-rich residual system.) Comparison of the one- and two-nucleon transfer cross sections would provide valuable information about the strength of pairing correlation at high spins in nuclei.

However, perhaps one of the most interesting transfer studies will be those involving reactions of very neutron-rich RIB with very neutron-deficient targets. To equilibrate their N/Z ratios, the two reaction partners will undergo transfer of multiple pairs of neutrons. This may be a qualitatively different physics than the simple single-pair transfer feasible with stable beams.

3.3 Fusion-Evaporation Reactions

Fusion of neutron-rich targets and radioactive beams results in the formation of neutron-rich compound systems that de-excite by pure neutron evaporation. Therefore, these reactions will not in general form very neutron-rich residual systems, far beyond what is already accessible via one- and two-neutron radiative capture reactions. However, their significance is that they would provide high-spin nuclear structure information that is complimentary to the (n, γ) reactions, which provide nearly complete spectroscopic information about the low-spin states in neutron-rich nuclei (see, e.g., the contribution of I. Ahmad and M. P. Carpenter at this workshop).

In the very heavy systems, neutron-rich beams are needed to explore the predictions for the existence of superdeformed[26] and hyperdeformed[11] structures in the neutron-rich Hg-Ra nuclei that cannot be accessed by stable beams. Since the fission barrier is higher for the neutron-rich isotopes of the same element, the neutron-rich beams would allow the investigation of superelongated shapes in the Pb region at higher spins, where yet higher-lying intruder orbitals may become active.

3.4 Quasi-Elastic Reactions

At beam energies of about 1.5 to 2 times the Coulomb barrier energy, the dominant reaction mechanism becomes quasi-elastic collisions that include the incomplete fusion, massive transfer, and Deep-Inelastic Reactions (DIC).[28] The Pittsburgh group has recently demonstrated the utility of these reactions for high-spin spectroscopic studies with a beam of 10MeV/nucleon of ^{20}Ne beam on a ^{170}Er target.[29] Using neutron-rich radioactive beams, these reactions can result in the high-spin population of neutron-rich residual nuclei. A large array of charged-particle detectors, and third-generation Ge detector systems would be needed to fully realize the potentials of these reactions for nuclear spectroscopy. Needless to say, these reactions would also provide valuable insight into the mechanisms that govern the charge- and mass-equilibration processes.

4. Summary of the Required Beams

Realization of the high-spin nuclear structure program outlined above would require a variety of odd- and even-Z radioactive beams at the extremes of T_Z. Unfortunately, the intensities of the most neutron-rich and proton-rich radioactive ion beams fall almost exponentially as the neutron excess increases and decreases, respectively. (See, e.g., a typical ISL beam-intensity profile for the Ge isotopes shown in Fig. 5.) Therefore, the breadth of the high-spin physics programs at the future RIB facilities would depend directly on the tails of the intensity distributions of the produced radioactive ion beams. For the neutron-rich radioactive ion beams, this implies the need for an actinide target. Shown in the inset of Fig. 5 is a sketch of the required beam energies and the approximate intensity thresholds, in particles per second (pps), above which various reactions reach their threshold of detection sensitivity. The needed beam energies are, generally speaking, about 5MeV/nucleon, with the exception of the incomplete fusion and deep inelastic collision reactions that require somewhat higher beam energies. To realize the full scope of this program, radioactive ion beams of varying Z, both odd and even, are needed.

5. Experimental Techniques and Instrumentation

Any discussion of a new facility should include not only the accelerator system(s) used to produce the beams of interest, but also the detector systems. Since the experimental count rate depends directly on the efficiency and selectivity of the detection system, it may

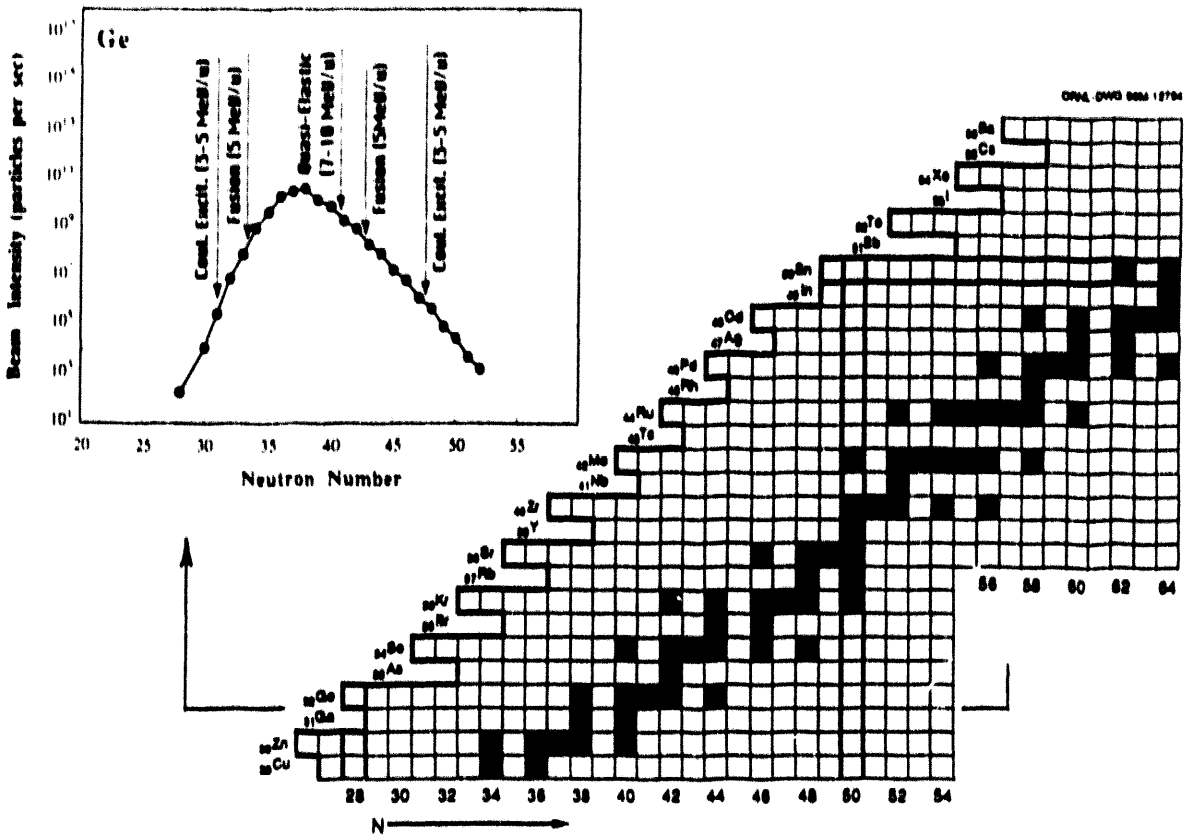

Fig. 5. A sketch of the profile of the approximate beam intensities and energies needed for the high-spin physics program. Indicated for both the neutron-deficient and neutron-rich Ge isotopes are the minimum beam intensities, above which various reactions reach their threshold of detection sensitivity. A wide range of elements, both odd- and even-Z, will be needed for a broad high-spin physics program.

be sometimes more practical or economical to enhance the detection capabilities than to increase the beam intensities. This is particularly relevant for the high-spin physics studies with RIB which, as mentioned above, utilizes the extreme tails of the intensity distribution.

Although, in general, the detector requirements for the studies of the n-rich and n-deficient nuclei are different, both share the need for a powerful high-resolution gamma-detection system, such as the third-generation GAMMASPHERE and EUROGAM detectors currently under construction. These detectors have a total photo-peak efficiency of $N \varepsilon \Omega \approx 0.1$ for ^{60}Co lines (N is the number of the Ge detectors in the system, and ε and Ω are the photo-peak efficiency and solid angle of each detector, respectively). However, in many applications, the most forward quadrant of these detectors will be subjected to a large background count rate due to the gamma- and beta-decay of the elastically and inelastically scattered radioactive beams. For example, Rutherford

scattering of 1 pna of a rare-earth beam on 1 mg/cm^2 of ^{208}Pb target would deposit about 10^6 particles/sec on the forward quadrant of the target chamber, which is to be compared with about 10^5 events/sec for the yield of a typical fusion-evaporation reaction. Considering the fact that the background activity persists for several half lives (typically several minutes or more), the singles count rate in the Ge detectors will be dominated by the background activity due to the forward-scattered radioactive beams. In this respect, a high granularity Ge array is desirable. A high granularity Ge detector system is also desirable to minimize the effects of Doppler broadening which deteriorates the energy resolution of the gamma-ray spectra (see the discussion below).

In situations where, due to the low beam intensity, the particle and gamma detectors have not reached their singles count-rate limit, the background count rate may be reduced by pulsing and bunching the beam. For high-spin studies, demanding events with high-gamma multiplicity will also serve to suppress the background radioactivity which has low gamma multiplicity. Similarly, gamma-recoil and gamma-particle coincidence requirement would suppress the background significantly.

In the case of intense radioactive beams, a simple, although inefficient, solution would be to remove the Ge and other ancillary detectors from the most forward angles (e.g., $\theta \leq 45^\circ$) in order to allow a large distance between the target and the chamber walls (see Fig. 6). In this geometry, most of the forward-scattered radioactive ions will be deposited on the distant chamber walls, where they are out of the direct line of sight of the remaining Ge detectors. In experiments involving neutron-deficient nuclei, the most forward angles may be devoted to the neutron detectors, which benefit from the kinematic focusing of the evaporation neutrons at these angles. Also, the increased time of flight of the neutrons (due to the larger flight distance) would make it easier to distinguish the neutron from the gamma signals.

With the exception of the deep-inelastic collision reactions, which benefit from a 4π charged-particle detector (such as the Dwarf Ball of Washington University[4]), the experiments on the neutron-rich side are generally less demanding on the detection sensitivity and selectivity. This is due to the fact that the neutron-rich channels of interest, usually produced in (xn) fusion-evaporation or transfer reactions, are not masked by other competing channels. In contrast, the most neutron-deficient channels are usually produced with very small partial cross sections. Thus, deployment of highly selective ancillary detectors, such as RMS, is almost mandatory for these studies.

The advantage of the RMS lies in the fact that its selectivity, (σ_{Tot}/σ_x), is inversely proportional to the partial cross section, σ_x. Thus, for weak channels with σ_x=10-100 μb, the RMS would reduce the background by as much as 10^5-10^4, respectively. In contrast,

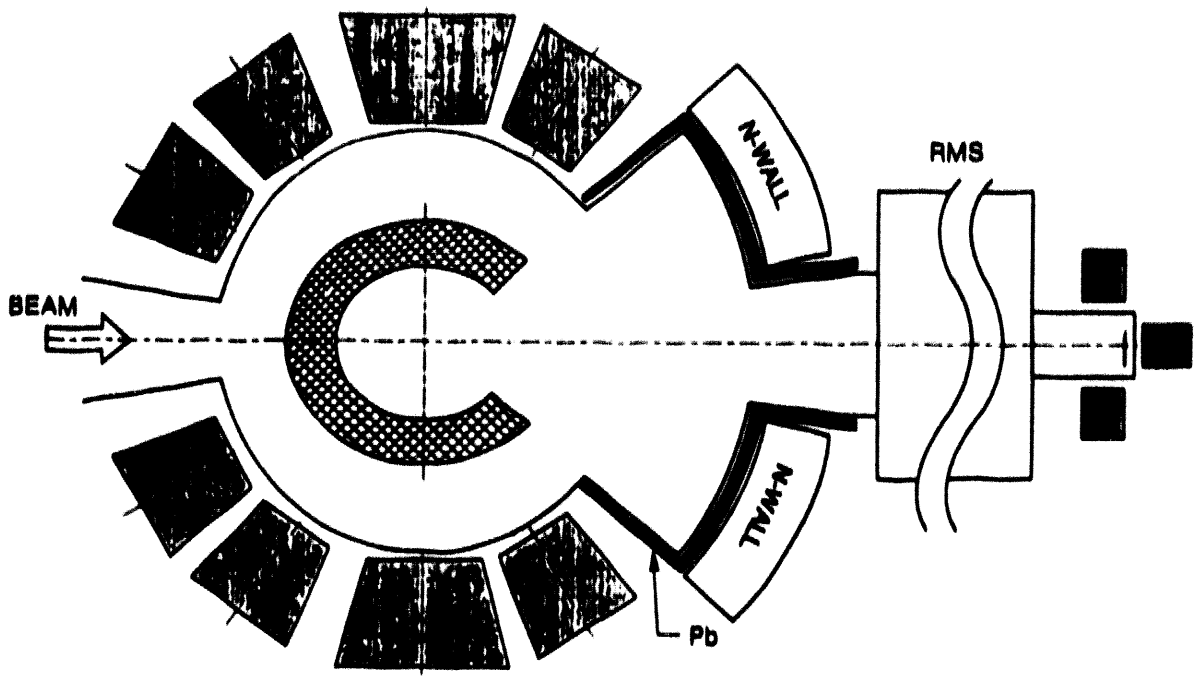

Fig. 6. A schematic drawing of a prototypical experimental set up that combines a large array of segmented Ge detectors (heavy shade), a nearly 4π charged-particle detection system (cross hatched), a neutron wall at forward angles, an RMS, and an array of particle, X-ray and gamma-ray detectors deployed at the focal-plane of the RMS. (The recess in the target chamber at forward angles is to reduce the background activity in the Ge detectors that originate from the scattered beam particles.) Nearly all these detectors are required for a detailed high-spin studies of the proton-rich nuclei.

gating on a known gamma ray in the band of interest, reduces the background in the gamma spectra by the Resolving Power of the system, which is about 10 for most Ge-arrays that are equipped with Compton-suppression shields. (Resolving power is defined as the product (Photo peak/Total)*(S E_γ/FWHM), where (S E_γ) is the difference between the energies of two consecutive gamma rays in a rotational band, and FWHM is the gamma energy resolution.[30,31]) Thus, the RMS offers a clear advantage over gamma gating for the *weak* exit channels. On the other hand, γ–γ coincidence information is crucial for the construction of partial level schemes. Thus, the general practice has been to, first, use the γ-RMS coincidence information to identify a few transitions in the nucleus of interest. These transitions are then used for gating in the γ–γ coincidence mode to construct a partial level scheme. Two- and higher-fold gamma gating is also the preferred tool to isolate the weak cascades, such as members of a superdeformed band, in exit channels with a *large* partial cross section.

To take the full advantage of the selectivity of the RMS, both mass and Z identification are required. Unfortunately, Z identification, using the conventional gas counters at the focal plane, becomes increasingly difficult for the fusion-evaporation products with $Z \geq 50$, because of their relatively low recoil velocity. This problem may be partially remedied by the use of inverse kinematics. However, the resulting large Doppler broadening of the γ rays would severely limit the Ge resolution for angles between +45° and -45°, unless highly segmented Ge detectors are used. The clover detectors[32] of the EUROGAM, and the split detectors[31] of the GAMMASPHERE are examples of such large volume, segmented detectors. Furthermore, when deployed near the 90°, these segmented detectors provide polarization information, which is crucial for many gamma-ray spectroscopic studies.

An alternative solution would be to use the RMS in conjunction with a 4π charged-particle detector system, or an array of X-ray detectors with a large solid angle coverage. The 4π charged-particle array would not only provide information about the Z of the residues, but would also give the energies and the emission angles of the evaporation charged particles. Using this information, one may infer the velocity vectors of the residues and apply the necessary corrections to the Doppler-broadened gamma energies. Regarding the use of large arrays of X-ray detectors, thin room-temperature HgI_2 detectors may offer an elegant solution in the next few years.[33]

Having a wide variety of ancillary detectors at hand would allow the construction of properly tagged reference gamma ray spectra (e.g., 1p 1n, 2p 1n, 1p 2n, etc.) that may be used to identify unknown gamma rays. For example, the peaks belonging to the (2p 1n) channel would be, respectively, enhanced and reduced in the (2p 1n)/(1p 1n) and (2p 1n)/(2p 2n) ratio spectra. (A related technique, namely the ratios of the gamma intensities in spectra gated by neutron, protons and alphas, were used to infer the multiplicity of the evaporation particles in Ref. 34.) Alternatively, "pure" (xp yn) spectra may be constructed from a linear combination of the various spectra formed from the above reference spectra.

6. Summary

Radioactive ion beams will usher a new era for nuclear physics in general, and high-spin structure physics in particular. Some of the exciting new physics opportunities that will become accessible with RIB were outlined in this paper. Undoubtedly, as with other facilities in the past, we shall encounter unexpected new phenomena that will lead to new applications for these beams that are unforeseen at present.

The most critical parameter for these high-spin studies is the intensity of the very proton- and neutron-rich beams produced at the future RIB facilities. This implies that actinide targets are needed to produce neutron-rich radioactive beams of acceptable intensity. To maximize the scope of this program, a wide range of odd- and even-Z beam species are desirable. The most useful energy range is around 5MeV/nucleon, although lower energy beams may be useful for Coulomb excitation, and beams of up to 10MeV/nucleon would be needed for quasi-elastic reaction studies.

Last, but not least, to fully realize the potentials for these exciting explorations, the future laboratories should pay particular attention to the detection systems. Large arrays of Ge detectors with high efficiency and granularity, nearly 4π charged-particle arrays, neutron walls, recoil mass separator and a variety of detector systems around its focal plane are *necessary* equipment at any future RIB facility. It would be highly desirable to develop the tools and techniques required for these challenging experiments on the first generation of the radioactive beam facilities.

Acknowledgment

Discussions with J.D. Garrett, W. Nazarewicz and R. Wyss are gratefully acknowledged. I would like to thank W. Nazarewicz and R. Wyss for sharing several results of their calculations prior to publication. Oak Ridge National Laboratory is managed by Martin Marietta Energy Systems, Inc. under contract DE-AC05-84OR21400 with the U.S. Department of Energy.

References

[1] W. Nazarewicz *et al.*, Nucl. Phys. **A435** (1985) 397.
[2] W. Gelletly *et al.*, Phys. Lett. **B253** (1991) 287.
[3] A. Gavron, Phys. Rev. **C21** (1980) 230; modification PACE2S by J.R. Beene.
[4] D.G. Sarantites *et al.*, Nucl. Inst. and Meth. **A264** (1988) 319.
[5] P. Nolan and P. Twin, *Ann. Rev. Nucl. Part. Sci.* **38** (1988) 533; and references therein.
[6] R.V.F. Janssens and T.L. Khoo, *Ann. Rev. Part. Sci.* **41** (1991) 321; and references therein.
[7] C. Baktash *et al.*, Phys. Lett. **B255** (1991) 174; ORNL physics Division Progress Report, 1988, ORNL-6508, p. 75.
[8] I. Ragnarsson, in *Proc. Workshop on the Science of Intense Radioactive Ion Beams*, ed. B. McClelland and D.J. Vieria, Los Alamos National Laboratory Report LA-11964, Oct. 1990, p. 199.
[9] J. Dudek *et al.*, Phys. Lett. **B211** (1988) 252.
[10] R.R. Chasman, Phys. Lett. **B302** (1993) 134.
[11] W. Nazarewicz, Phys. Lett. **B305** (1993) 195.
[12] R. Wyss (private communication).

[13] I. Ahmad and P.A. Butler, *Ann. Rev. Part. Sci.* (1993) (in press).
[14] I. Ragnarsson, Phys. Rev. Lett. **62** (1989) 2084.
[15] W. Nazarewicz, Nucl. Phys. **A435** (1990) 333c.
[16] J. Skalski, Phys. Lett. **B238** (1990) 6.
[17] J. Dudek, in *High Spin Physics and Gamma-Soft Nuclei*, ed. J.X. Saladin *et al.* (World Scientific Press, Singapore, 1991), p. 146.
[18] S. Aberg, H. Flocard, and W. Nazarewicz, *Ann. Rev. Part. Sci* (1993) (in press).
[19] R. Wyss and A. Johnson, in *High Spin Physics and Gamma-Soft Nuclei*, ed. J.X. Saladin *et al.* (World Scientific Press, Singapore, 1991), p. 123; P.H. Regan *et al.*, Phys. Rev. **C42** (1990) R1805.
[20] S. Cwiok *et al.*, Comp. Phys. Comm. **46** (1987) 379.
[21] D. Cline, Ann. Rev. Nucl. Part. Sci. **36** (1986) 683.
[22] I.Y. Lee *et al.*, Phys. Rev. **C42** (1990) 1953.
[23] M. Oshima *et al.*, Nucl. Inst. and Meth. **A312** (1992) 425.
[24] C.Y. Wu *et al.*, *Ann. Rev. Nucl. Part. Sci.* **40** (1990) 285.
[25] P.D. Bond, Comm. Nucl. Part. Phys. **11** (1983) 231; and reference therein.
[26] W. Satula et al., Nucl. Phys. **A529** (1991) 289.
[27] K.G. Helmer et al., Phys. Rev. **C44** (1991) 2598.
[28] U. Schroder and J. Huizenga, *Treatise on Heavy -Ion Science*, Ed. D.A. Bromley (Plenum Press, New York, 1984) Vol. 2, p. 115.
[29] H. Takai *et al.*, Phys. Rev. **C38** (1988) 1247.
[30] GAMMASPHERE, A National Gamma-Ray Facility, The Proposal, ed. M.A. Deleplanque and R.M. Diamond, LBL Report No. 5202 (1988).
[31] F.S. Stephens, in *Proc. Int. Conf. on Nuclear Structure at High Angular Momentum*, Ottawa, May 1992, AECL 10613.
[32] F.A. Beck *et al.*, in *Proc. Int. Conf. on Nuclear Structure at High Angular Momentum*, Ottawa, May 1992, AECL 10613, p. 364.
[33] J.S. Iwanczyk *et al.*, IEEE Trans. Nucl. Sci. **39** (1992) 1275.
[34] R. Schubart *et al.*, Zeit. Phys. **A 343** (1992) 123.

November 19, 1992

STUDY OF NUCLEAR REACTIONS AT AN ISL FACILITY

F. D. Becchetti
University of Michigan

I. Introduction

We are entering an exciting period of nuclear science. As discussed in the previous ISL "white paper" [1] the severe constraints imposed by using stable beams, (i.e. those which typically have N ≈ Z, are in the g. s. , have zero or low spin, and are close to spherical) can be removed by the use of unstable nuclear beams (RIB/RNB). Thus in many ways, we are starting anew in nuclear physics. Obviously we do not want to just repeat 80 years of nuclear science but, instead, we should concentrate on the new information that can be realized using RIB/RNB.

Although study of reactions related to nuclear astrophysics will certainly play a significant role at ISL, nuclear astrophysics alone should not dictate the operating parameters. It now appears [2] that much of the needed astrophysics-related data can be obtained from high-energy RIB/RNB reactions. As an example breakup information can be used in lieu of low energy (p,γ) or (n,γ) data. Also some of the most significant results may well come in non-astrophysics related experiments. (Of course, almost all of nuclear science is related to astrophysics in some way).

II. ISL Nuclear Reaction Studies

We already have a small "learning" curve regarding the use of RIB/RNBs in nuclear reaction studies via the use of fragmentation beams and accelerated ^{13}N [2]. However, except for ^{13}N and perhaps ^{8}Li, this information is skewed towards experiments (Fig. 1) which can be done with rather low RIB/RNB intensities e.g. $< 10^6$/sec. This includes a large number of RIB/RNB breakup experiments where, however, the target is mostly a spectator. Thus, these experiments study primarily the **structure of the RIB/RNB** itself (^{11}Li, ^{8}He,...) rather than the projectile-target system or the reaction mechanism. At intensities $< 10^6$/sec, the experiments can be done with **in beam** detector systems [3]

and **active targets** (Figure 2). Also, the beam itself does not necessarily present a major background problem since, for example, many "beams" are only $10^2 - 10^4$/s.

Many of the present types of RIB/RNB experiments and setups, while certainly feasible at ISL, will **not** be typical since the intensities at ISL will hopefully be much higher ($10^6 - 10^{10}$/s) and one will likely do those experiments (and use setups) which can exploit the higher intensities (Figure 1). Thus, the ISL experiments will not generally employ in-beam detector arrays or active targets, and there will be experimental problems associated with dumping a high-intensity RIB/RNB near detector arrays, particularly for the proton-rich β^+-emitting beams. Also RIB/RNB tend to fragment easily (with large cross sections) so many break-up products (including neutrons) may be produced from the target.Thus γ-ray and neutron, proton, and other backgrounds of $> 10^4$/sec may be present. (In some instances, accurate **time-of-flight** using a pulsed beam will be necessary to suppress such background.)

i) Fusion, fission, elastic and inelastic scattering

At the low-end of ISL intensities ($10^6 - 10^8$/sec), RIB/RNB-induced studies of fusion-fission, fusion-evaporation, CN, total reaction cross sections [4], elastic scattering, Coulomb excitation, and inelastic (nuclear excitation) are feasible (Fig. 1). (The interesting physics aspects of these measurements are discussed in the original ISL white paper [1]). Coulomb-nuclear interference measurements, which require accurate measurements of $\sigma(\theta)$ near the grazing angle are obvious types of ISL experiments one can use to determine differences in neutron and proton deformations for nuclei with $N \gg Z$ or $Z \ll N$.

Experimentally, fusion-evaporation reactions using RIB/RNB will generally be **high-multiplicity** events, even at rather low energies, since excess protons or neutrons are involved when using RIB/RNB and the reactions are generally **highly exothermic**. High-multiplicity particle arrays will likely be employed, again requiring good intrinsic (beam) TOF and a "clean" dump for the RIB/RNB. Some crude **energy** variation will be desirable for excitation functions.

Elastic and inelastic scattering will require **good absolute energy resolution** ($\delta E <$ 1 MeV) to separate elastic scattering from inelastic scattering. RIB/RNB with stable, low-lying excited states may have very **large** BE $\uparrow$ or BM $\uparrow$ or the target (Fig. 3) may have such levels which must be resolved to permit a quantitative analysis. This is particularly

true at large angles where details of **both** the elastic and inelastic cross sections should be measured, yet the inelastic scattering [5] may be as large or larger (Fig. 3). This can become even more pronounced depending on the **spin** of the RIB/RNB and its **breakup** (i.e. absorption) properties. [Much of the presently-reported RIB/RNB "elastic " data ($^{11}\mathrm{Li} + X$) are really measurements of a combination of elastic and inelastic scattering i.e. "quasielastic" scattering.]

Methods to achieve good resolution in the residual **excitation** spectrum, (i.e. techniques which cancel some of the energy spread in the RIB/RNB itself) include multi-detector, kinematic coincidence "**Q-value**" measurements (projectile and target) and **dispersion** matching using magnetic elements (quads and magnetic spectrometers). **Both** techniques should be utilized at ISL, the latter if a **magnetic spectrometer** and suitable dispersive, beam preparation system are available.

ii) Utilization of Reverse Kinematics

A typical setup [6] for a kinematic-coincidence experiment using a heavy RIB/RNB on a light target (e.g. $^{1}\mathrm{H}$ or $^{2}\mathrm{H}$) is shown in Figure 4. Many of the ISL nuclear reaction experiments will likely utilize such **reverse kinematics**. At the high ISL intensities, one has the problem of the projectile often being close to (or in) the RIB/RNB itself. Large, special chambers with multi-hit detectors will be needed **or** a combination of a magnetic device (for small θ recoils) and an **associated particle** array. Again intrinsic TOF capability and a clean beam dump are both advantageous. In addition, exploiting reverse kinematics with heavier RIB/RNB will require **energetic** RIB/RNB (E/λ > 10 MeV) with a **good emittance** ($\leq$ a few mm-mr) to minimize the angular spread in the beam.

The reverse-kinematics mode will be particularly useful for studying **proton** and **α-particle** scattering (and reactions) from unstable nuclei—including excited, isomeric nuclei (if available). One- and two-nucleon transfers e.g. (d,p) and ($^{3}\mathrm{He}$,d) to study single-particle levels far from stability, should prove particularly interesting. Again RIB/RNB energies E/A > 10 MeV are typical with a magnetic device advantageous for small-θ recoils.

iii) Transfer reactions and near-barrier nucleon tunneling

In addition to light-ion reactions, heavy-ion reactions, such as Coulomb excitation for BEλs, and transfer reactions will likely be studied. These are often done at **low** c.m. ener-

gies in normal kinematics *viz.* the RIB/RNB on a heavy target. Here, the **intrinsic** beam energy resolution and purity become important along with the availability of magnetic devices for dispersion matching, and gamma detectors for particle-γ coincidences. Again background from the RIB/RNB could be a limit for particle-γ coincidence work.

Other special RIB/RNB reactions, which are not uncommon since $Z \gg N$ or $N \ll Z$ and $Q \gg 0$, involve the detection of one or more **particle-unstable** excited ejectiles. As an example $^{6}He + p \rightarrow t + \alpha^{*}$ where $\alpha^{*} \rightarrow d + d$ (Fig. 5) or $^{7}Be + d \rightarrow p + {}^{8}Be^{*}$ where $^{8}Be^{*}$ (and $^{8}Be_{g.s}$) $\rightarrow \alpha + \alpha$. Reverse kinematics is again particularly useful for this type of measurement and, of course, TOF.

Near-barrier one- and multi-nucleon transfer using selected RIB/RNB can exhibit special features (Fig. 6) since the transfers, unlike most stable-beam reactions, often will involve the highly exothermic transfer of a loosely-bound set of nucleons. The reaction Q-value can then be optimal w.r.t. the "Q-window" (Fig. 7) and, in addition, the "Q-window" will often be centered at **high excitation** in the residual nucleus [7], often resulting in intense quasi-elastic transfer groups close in energy to the original RIB/RNB, hence often difficult to separate from the elastic scattering. Good particle i. d. , usually using TOF, and energy resolution are needed. Again, a large solid-angle magnetic device for detection and i. d. of the reaction products will be advantageous. However unlike previous cases, measurements at **large** Θ (beyond 90° c. m.) will often be necessary and will involve sub-mb/sr cross sections (Fig. 6). This can obviously complicate the design of such a device. Also, only one angle/measurement can be done with a typical magnet which is a problem compared with using detector arrays since, even at 10^{9}/sec, the better part of a day may be required for a single data point. A **multi-gap** type magnet or similar device may be needed to permit **simultaneous** measurements at **several** angles.

iv) Isomeric and other short-lived "tagged" RIB/RNB

Very short-lived β^{+}/β^{-} beams ($\tau <$ few sec) and excited, **isomeric** beams (**INB**) offer the possibility of "tagging" the beam via a β^{+}/β^{-} particle decay (and annihilation γ's)-or via the INB γ-decays [8]. This is particularly useful if one can rapidly shut off the beam for a certain period after an interesting event is detected. This usually requires a **gated ion source** with macroscopic (msec) and, preferably, microscopic (MHz) gating e.g. $\frac{1}{n}$ pulse selection for an RF accelerator. The use of short-lived INB (100 to 500 nsec)

allows one to do elastic scattering (Fig. 4) on light targets using the INB γ-tag (Fig. 8) to ensure that the INB is not excited or that one (in first order at least) is not scattering a non-INB component in the beam.

The unusual properties of INB, including their **internal excitation**, often unusually **high spin** ($\rightarrow 20^+$) and **unusual shapes** ($\beta \gg 0.2$) obviously make these beams interesting for a wide variety of reaction studies [6]. It will be a challenge to produce such beams at ISL owing to the short lifetimes involved. One may need to produce them as **secondary** beams from another, primary stable beam or RIB/RNB. Likewise, production of very neutron-rich RIB/RNB may require a similar secondary beam capability, e. g. a **high-efficiency fragmentation** capability using an intense, stable beam or RIB/RNB from the main ISL accelerator. Obviously, such a capability places additional requirements on the accelerator design. Again one must decide if the potential, new science justifies this (I think it does).

III. Conclusion

Taking all of the above into consideration, we can conclude that the study of RIB/RNB induced nuclear reactions at ISL would be best served by a facility with:

1.) Low to at least **moderately high beam energies** [e.g. 1 to 30 MeV/u as this would overlap with the lowest energy (E/A $\geq$ 30 MeV/u) MSU-NSCL fragmentation RIB/RNB.]

2.) **Good** intrinsic RIB/RNB **energy resolution** and **TOF capability** (δE < 1 MeV absolute for light RIB/RNB; $\delta t \leq$ 1 nsec e.g. using a postbuncher).

3.) **Gated beam** and pulse selection capability (e.g. gated ion source)

4.) At least **moderate beam purity** (< few% impurity)

5.) At least **crude energy variation** (10% steps)

6.) **Capability** to produce high-intensity ($\geq 10^6$/s) short-lived RIB/RNB and isomeric beams, as well as neutron-rich RIB/RNB **via fragmentation** or other secondary reactions [e.g. with an intense H.I. primary stable beam (μA) or intense RIB/RNB ($> 10^9$/s)].

Since the ISL, if built, may be the **only** new nuclear science facility built in the foreseeable future,it is important that,where cost-effective, its capabilities be broad enough to include most of the potentially new physics that can be done with RIB/RNB.

References

[1] *The Isospin Laboratory - Research Opportunities with Radioactive Beams*, LALP 91-51, eds. R. F. Casten, et. al. (Los Alamos Laboratory, 1991).

[2] *Radioactive Nuclear Beams 1991 - Proceedings of the Second International Conference on Radioactive Nuclear Beams, Louvain-la-Neuve, Belgium, 19-21 August 1991*, edited by Th Delbar (Adam Hilger, Bristol, 1992).

[3] M. Lewitowicz, *et. al.* "Elastic Scattering of a secondary ^{11}Li beam on ^{28}Si at 29 MeV/n", GANIL preprint P 92, 20 (1992).

[4] R. E. Warner, *et. al.* "Total Nuclear Reaction Probabilities and Average Cross Sections for 16 to 23 MeV ^{6}Li in Silicon", Nucl. Phys. **A516**, 416–428 (1990).

[5] A. Nadasen, *et. al.* "Inelastic scattering of 210 MeV ^{6}Li ions from ^{12}C, ^{28}Si, and ^{58}Ni: Test of unique ^{6}Li potentials", Phys. Rev. **C 40**, 1237 (1989).

[6] J. .A. Brown, in *Radioactive Nuclear Beams 1991*, proceedings of the International Conference, Belgium, edited by Th Delbar (Adam Hilger, Bristol, 1992).

[7] F. D. Becchetti, *et. al.* (submitted to Phys. Rev. C).

[8] F. D. Becchetti, *et. al.* "Production of an isomeric, excited radioactive nuclear beam", Phys. Rev. **C 42**, R801 (1990).

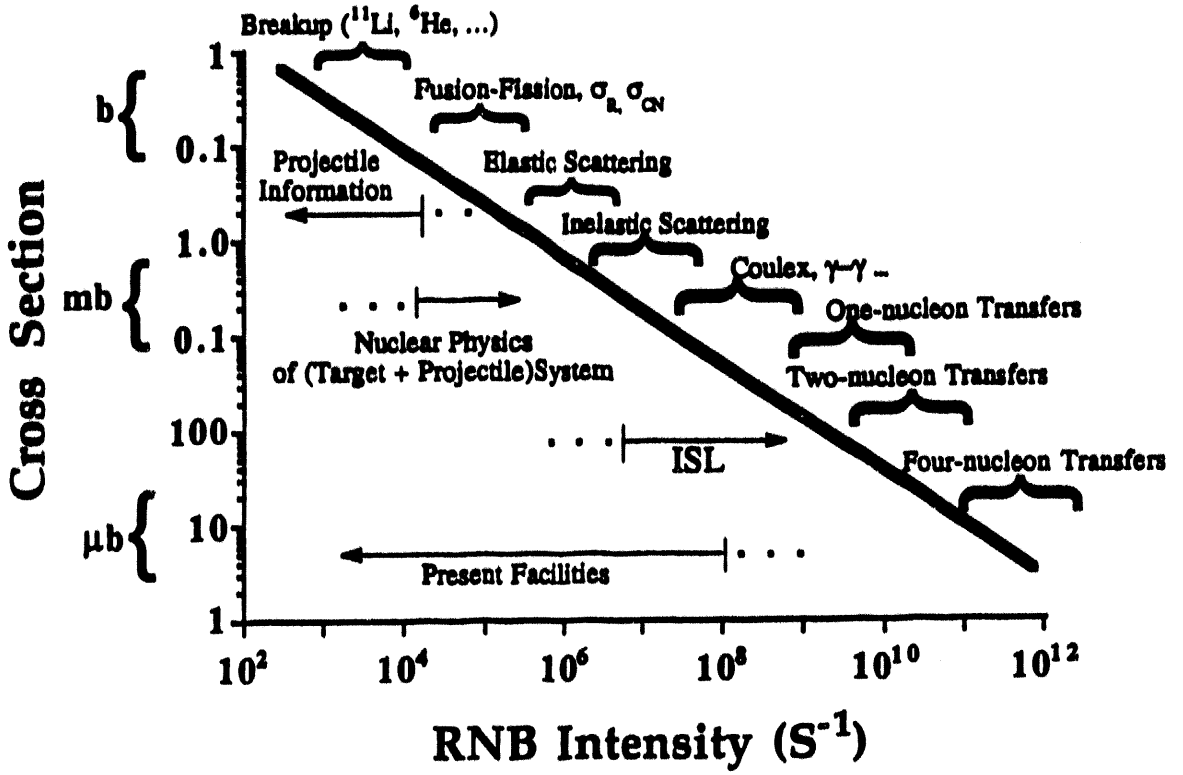

Fig. 1. Qualitative representation of RIB/RNB-induced reactions at various intensities.

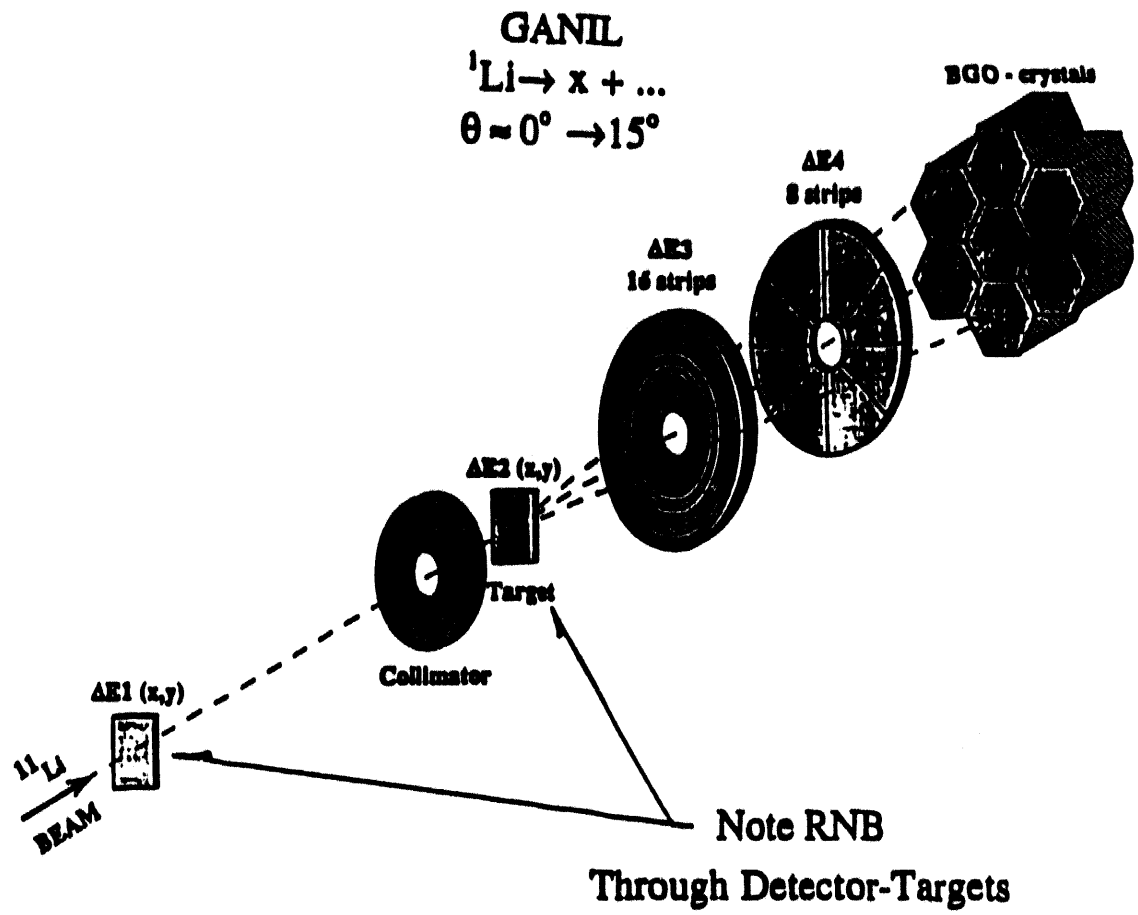

Fig. 2a. Schematic representation of the in-beam detector system used at low intensities ($< 10^{6}$/sec) by Lewitowicz et al. (see Ref. 3).

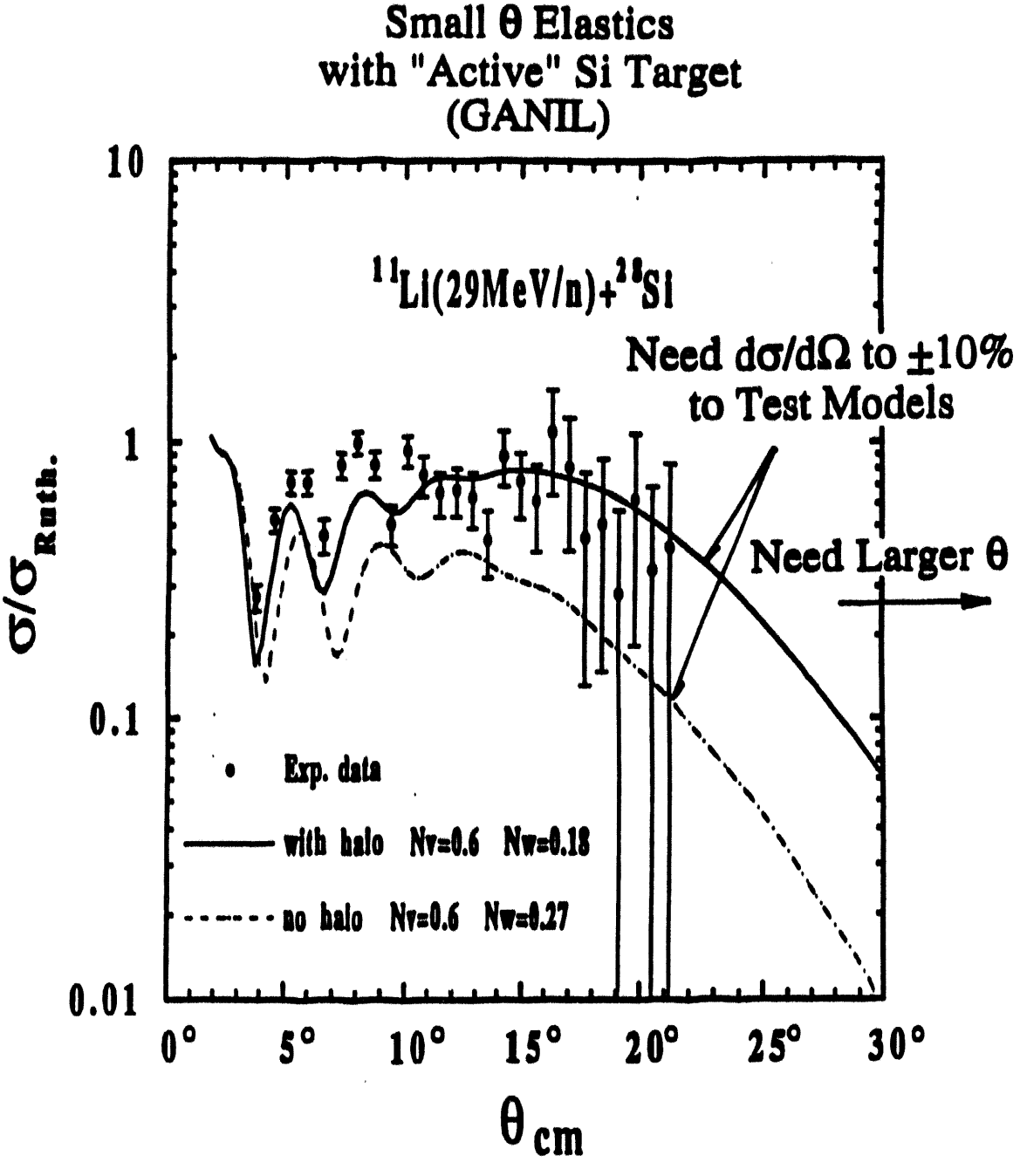

Fig. 2b. Small θ elastic angular distribution for ^{11}Li + ^{28}Si (see Ref. 3).

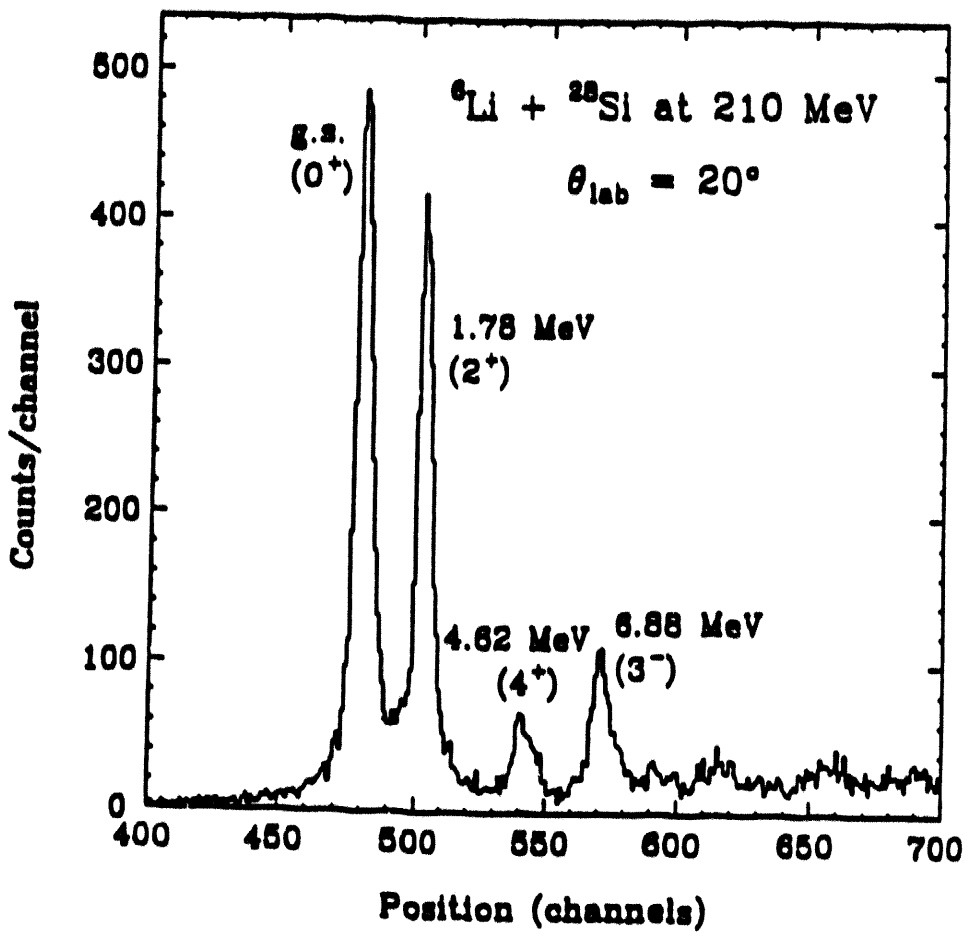

Fig. 3. Elastic and Inelastic Scattering of ^{6}Li + ^{28}Si at 210 MeV studied by Nadasen, et al. (see Ref. 5).

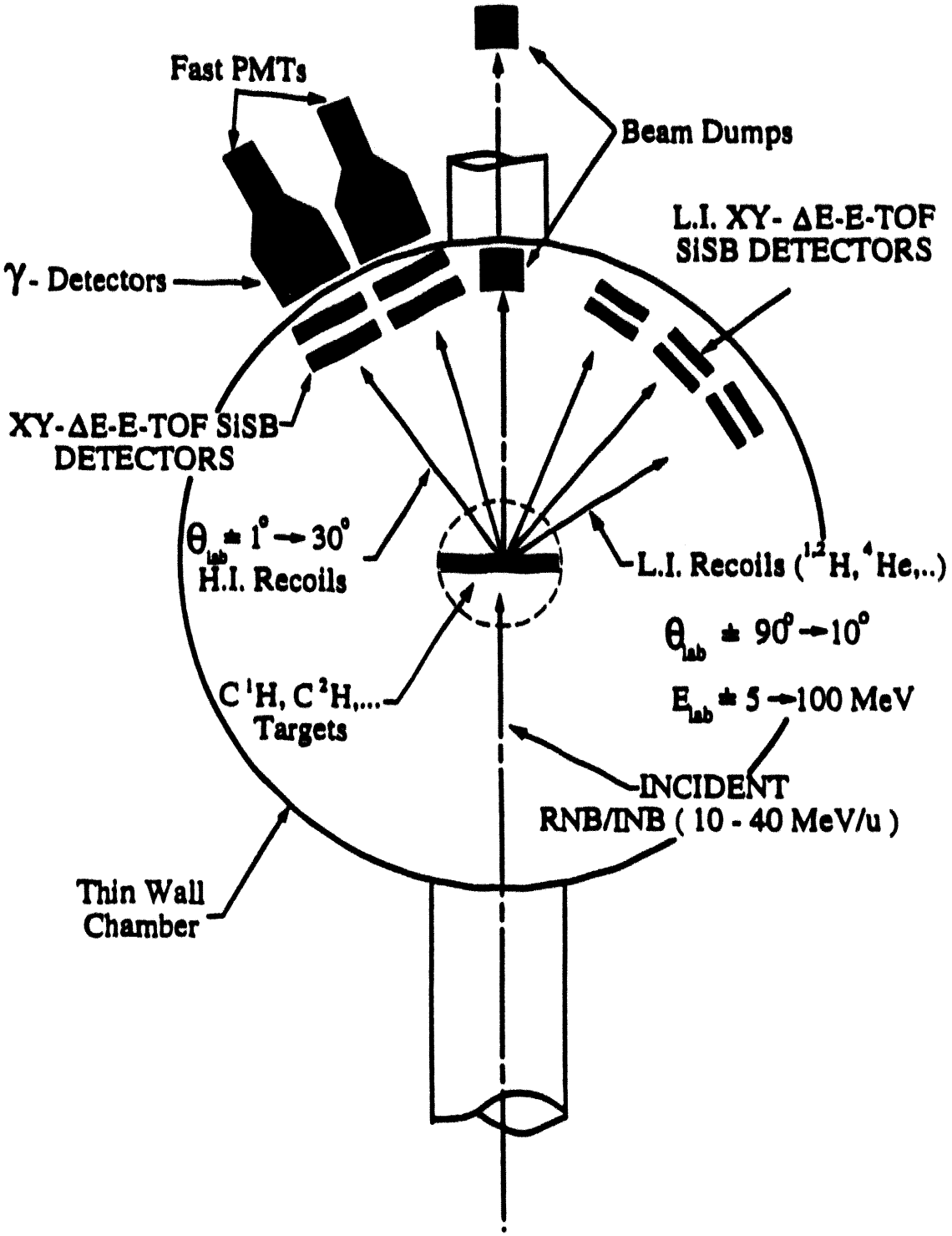

Fig. 4. Representation of an experimental setup for kinematic-coincidence and γ-tagged experiments.

Example: RNB-Induced Transfer Reactions to Ejectile Excited Levels (Since $Q_{RNB} >> 0$):

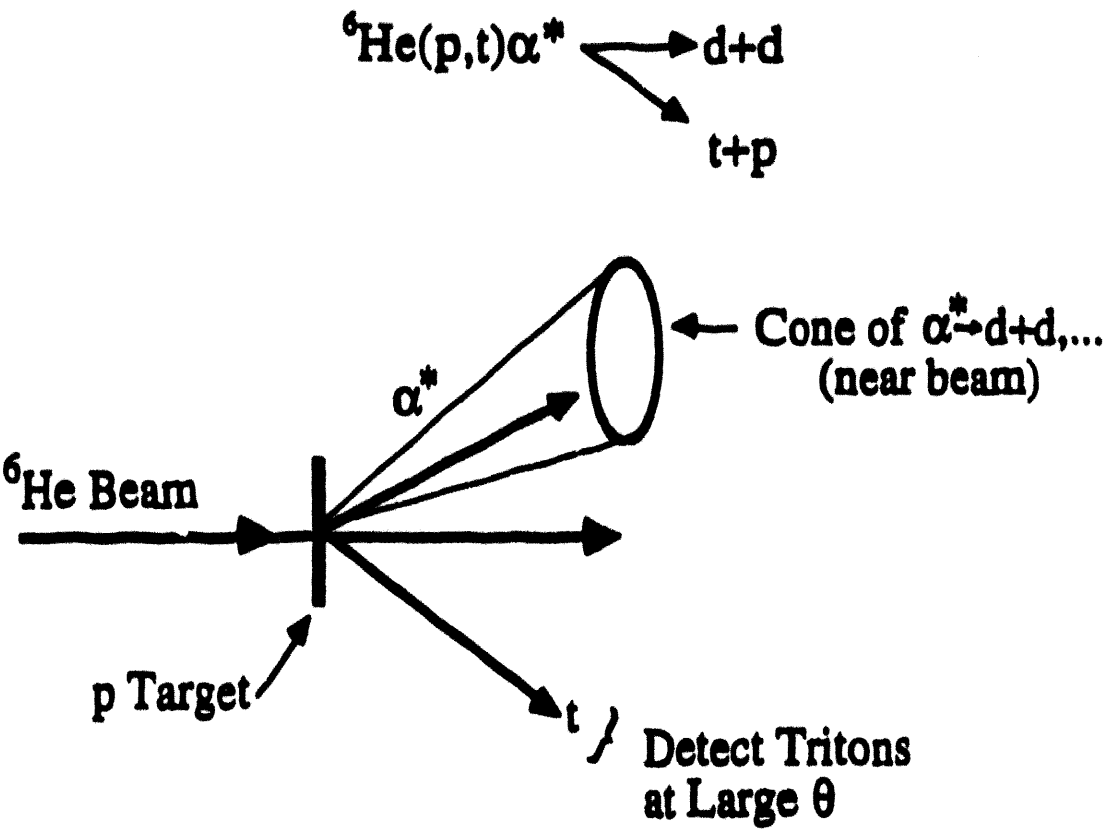

Thus: Need (For $\theta \simeq 0^\circ$) multi-hit detector arrays and/or spectrometer (?).

Good T.O.F. Important
Measure Q Value To Reduce δE in Beam

Fig. 5. An example of RNB-induced transfer reactions to excited ejectile levels—done in kinematic-coincidence mode.

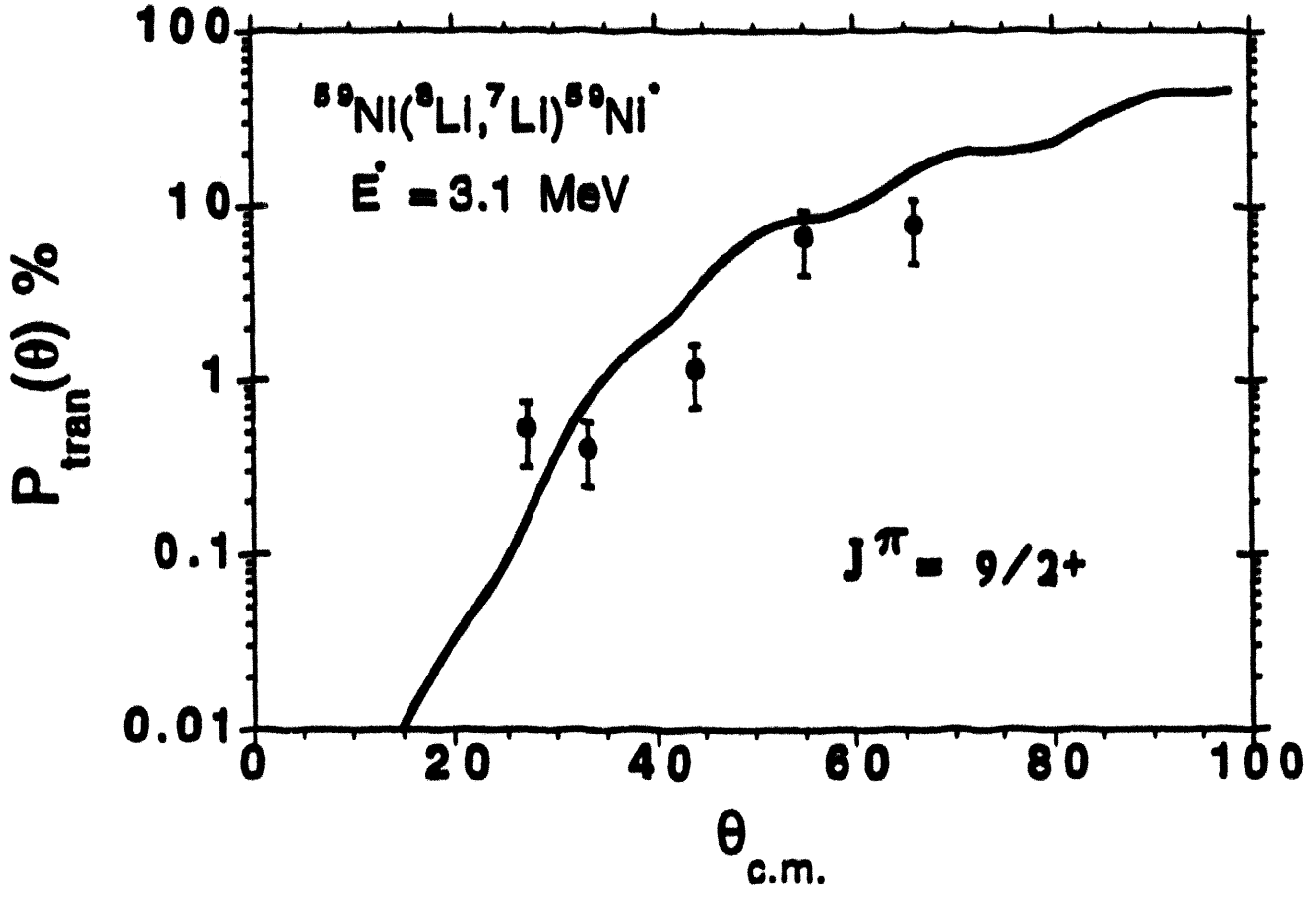

Fig. 6. Near-barrier RNB-induced single neutron "tunneling" reactions on ^{58}Ni at E ≐ 19 MeV.

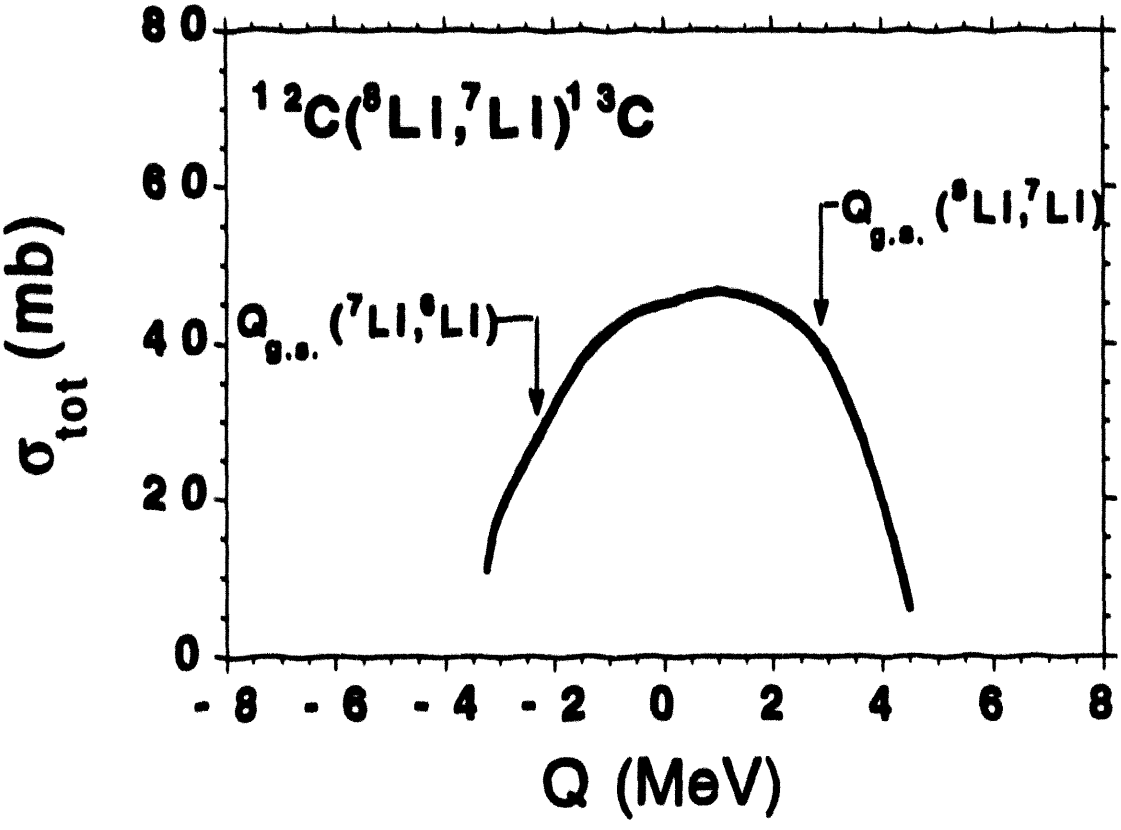

Fig. 7. Calculated "Q-window" of the $^{12}C(^{7}Li,^{8}Li)$ and $^{12}C(^{8}Li,^{7}Li)$ reactions with the appropriate $^{12}C \rightarrow {}^{13}C_{g.s.}$ Q-values indicated.

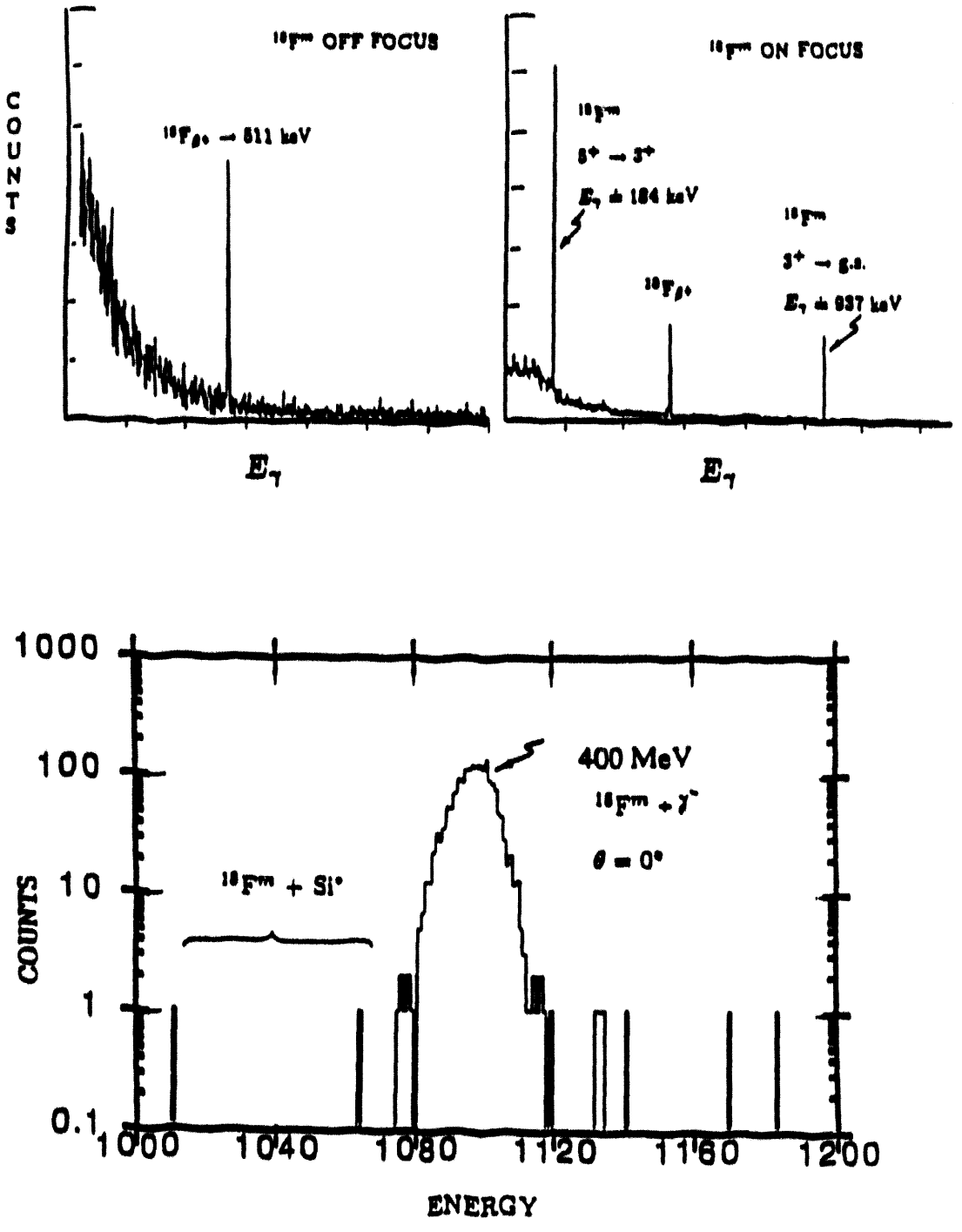

Fig. 8. Particle-γ coincidence spectra from an ≈450 MeV $^{18}F^{m}$ beam stopped near $\theta = 0°$.

Prototypical Experiments: Proton-Rich Nuclei

Reaction Studies with Inverse Kinematics

by

J.C. HARDY

AECL Research, Chalk River Laboratories
Chalk River, Ontario, Canada K0J 1J0

ABSTRACT

Several prototypical experiments are described which exploit single- and two-nucleon transfer as well as charge-exchange reactions — all in inverse kinematics — to study nuclear spectroscopy. The examples chosen relate to the N~Z nuclei with $56 \leq A \leq 100$ and to the study of superallowed β decay, but the potential usefulness of these reactions extends far beyond. It is concluded, however, that this rich potential can only be tapped at a future radioactive-beam facility if the beam energies reach at least 25 MeV/u and preferably 50 MeV/u.

1. INTRODUCTION

There is an enormous variety of radioactive-beam experiments possible among proton-rich nuclei. I cannot possibly outline them all, let alone describe fully representative ones, in a short presentation. I have decided instead to focus on one region of the nuclear chart — the N~Z nuclei between ^{56}Ni and ^{100}Sn — and on one class of experiments — transfer (and charge-exchange) reactions in inverse kinematics. These particular nuclei were chosen because my own interests in physics lead me to them; I should not want to leave the impression, however, that inverse-reaction studies are so limited. Their fascinating possibilities in fact extend far beyond one small group of nuclei. In my view, such studies should form a major component of the nuclear-physics research program at any future radioactive-beams facility.

Why select N≈Z nuclei above ^{56}Ni? Overall, these nuclei span an extraordinarily broad range of nuclear structure, starting with the doubly magic ^{56}Ni, passing through some large and possibly exotic deformations in the light-strontium neighbourhood, and terminating at another doubly magic (but still elusive) nucleus, ^{100}Sn. Not only is the structure rich and varied but the similarity of neutron and proton numbers highlights symmetry and correlation effects, and provides fertile grounds for the study of Gamow-Teller transitions.

It is the study of $0^+ \rightarrow 0^+$ beta transitions that has piqued my own interest in this region. To date, there are eight nuclei from ^{14}O to ^{54}Co with precisely measured superallowed $0^+ \rightarrow 0^+$ beta decays. Their experimental ft-values, all known to better than a part in 10^3, have been used to determine the vector coupling constant, G_V; probe the conserved vector current (CVC) hypotheses; and test the three-generation Standard Model via the unitarity of the Kobiyashi-Maskawa matrix[1]. By now, these tests are limited not by experimental precision but by uncertainties in the theoretical "radiative" corrections, particularly those charge-dependent effects that lead to differences between the parent and daughter analogue 0^+ states. There is no independent way to measure the total transition strength lost by charge mixing from the daughter state so it is necessary to

make nuclear-model calculations of the effect; the results show substantial scatter[1] from one model to another, which ultimately limits the precision of the tests.

So far, the only potential route around this obstacle has appeared to depend on measurements of neutron β decay, for which no charge correction is necessary. Unfortunately, neutron decay presents far more complex experimental problems than do the $0^+ \rightarrow 0^+$ nuclear decays, so the value of G_v as derived from the neutron has an uncertainty four times larger than the nuclear result including its calculated corrections[2]. There are no obvious ways to improve the former by a large factor.

Now, with radioactive beams, it is possible that the nuclear $0^+ \rightarrow 0^+$ results can actually be improved by our gaining a firmer handle on the charge corrections. The only viable method yet devised to check any aspect of the mixing calculations is to measure the intensity of "forbidden" $0^+ \rightarrow 0^+$ beta transitions between the same nuclei[3]. These transitions populate excited 0^+ states in the daughter via admixed components of the analogue state; their measurement can provide an important constraint on the model-dependent mixing calculations. The difficulty, displayed in figure 1, is that very few excited 0^+ states are energetically available to beta decay in the familiar $A \leq 54$ nuclei and, because of the E^5 dependence of β-decay intensity, fewer still are fed by measurable transitions. However, as radioactive beams make accessible the heavier N~Z nuclei, this situation should change dramatically; it should become possible to observe several $0^+ \rightarrow 0^+$ transitions from each emitter and to determine the charge correction with greater precision than has ever been possible before.

To complete these difficult measurements requires not only the production of the 0^+ parent so that its decay can be observed, but also requires that the decay energy be measured precisely and that excited 0^+ states in the daughter be identified. Reaction experiments with inverse kinematics will make this possible: for example, the decay energy of the 0^+ superallowed emitter ${}^{66}_{33}As$ can be determined from the measured threshold of the reaction $p({}^{66}Ge, {}^{66}As)n$; and the 0^+ states in its daughter, ${}^{66}Ge$, can be located via the reaction $p({}^{68}Ge, t){}^{66}Ge$.

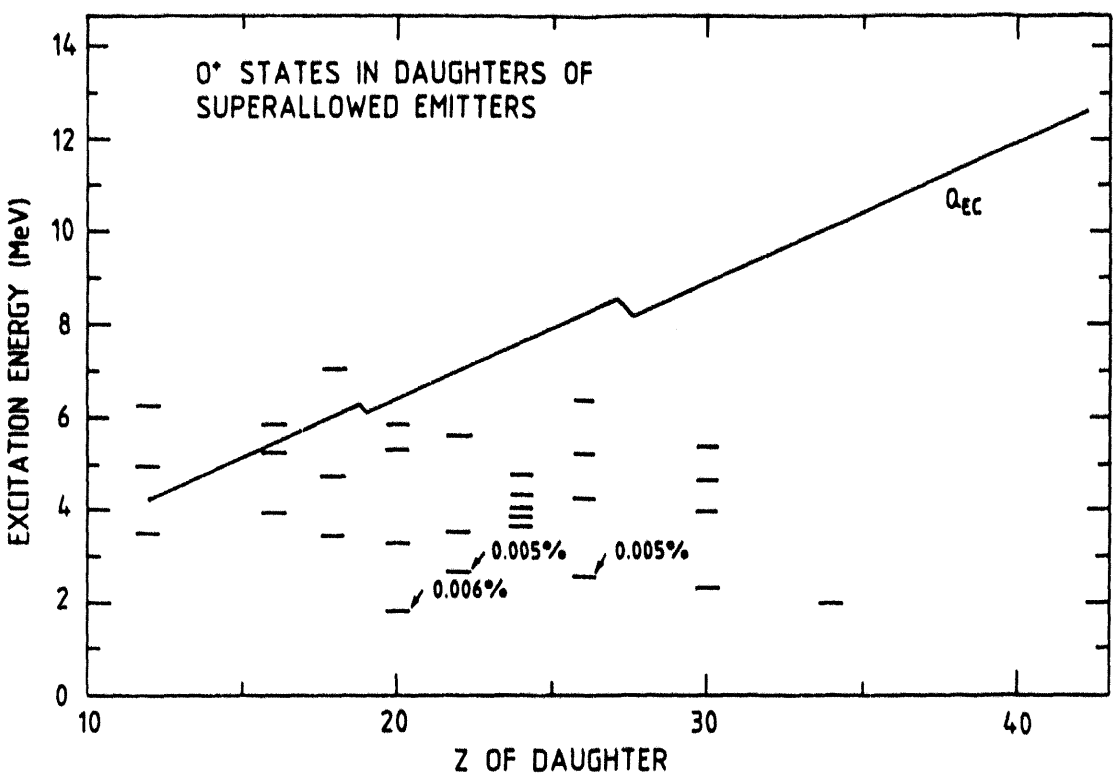

Figure 1: Level schemes of known 0^+ states in the T_z=1 daughters of superallowed emitters. The lightest seven shown (^{26}Mg, ^{34}S, ^{38}Ar, ^{42}Ca, ^{46}Ti, ^{50}Cr and ^{54}Fe) have been well studied, with the measured feeding of excited 0^+ states shown in three cases where they are known. Superimposed is a plot of Q_{EC} values (emitter to daughter) indicating which states are accessible to β decay; note the increasing "energy window" beyond Z=26 and the paucity of known 0^+ states.

2. TRANSFER REACTIONS

Rather than focusing on the specific examples just quoted, I shall illustrate the more general properties of a variety of inverse stripping and pick-up reactions by choosing projectiles in the neighborhood of the closed-shell nucleus, ^{56}Ni. Such experiments would themselves be intrinsically interesting from a nuclear-structure point of view, and their general characteristics can easily be generalized to other cases. Furthermore, transfer reactions with normal kinematics have been well studied in nearby nuclei, making count rates and angular distributions easy to predict. A typical example of a measured one-nucleon transfer reaction (in "normal" kinematics) is ^{58}Ni(p,d)^{57}Ni, which was reported in reference 4: at a proton

energy of 27.5 MeV, differential cross sections covering the range $10^{-2} \leq d\sigma/d\Omega \leq 10$ mb/sr were obtained between 8° and 120°, although it is evident from the published results that angular distributions up to, say, 60° would have been sufficient to provide the same spectroscopic information. A good example of two-nucleon transfer, $^{58}Ni(p,t)^{56}Ni$, appears in reference 5: in this case, the proton energy was 40 MeV, and differential cross sections in the range $10^{-3} \leq d\sigma/d\Omega r \leq 1$ mb/sr were measured between 5° and 60°. These two measurements will provide the standards of comparison for the following proposed inverse reactions.

Figure 2 illustrates the relationship between "normal"- and inverse-kinematic views of the same pick-up reaction. Part A of the figure shows the "normal" case in which a projectile, moving right to left, picks up a nucleon (or nucleons) from a heavy target and is ejected at a forward angle, θ. (In this simple illustration, the difference between the laboratory and centre-of-mass frames is small and can be neglected.) The equivalent inverse reaction (figure 2B) reverses the role of target and projectile: the heavy projectile, moving left to right, strikes the light target, resulting in the light ejectile emerging at a forward angle, ϕ. The figure shows the relationship between θ and ϕ. In the centre-of-mass system, note that the forward angle in "normal" kinematics becomes the same angle in the backwards direction for inverse kinematics.

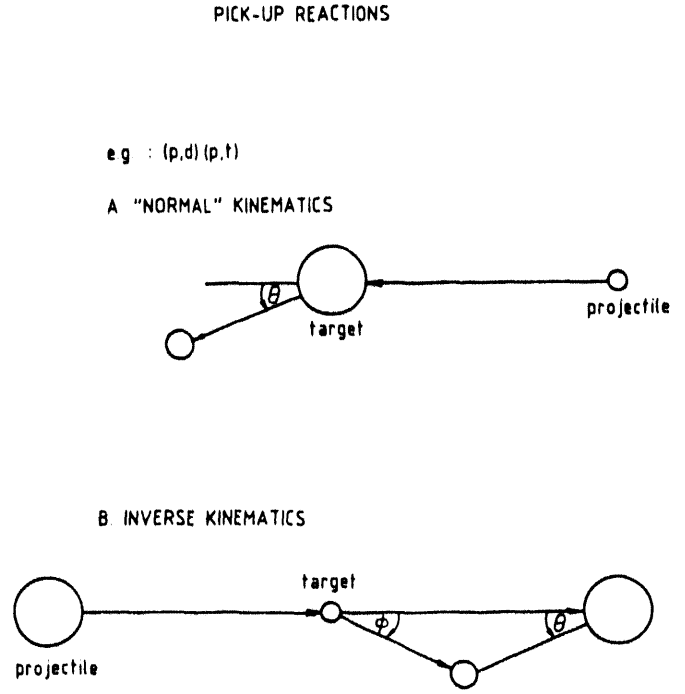

Figure 2: Illustration of the relationship between "normal" and inverse kinematics for pick-up reactions.

The details of a specific example, $p(^{57}Ni,d)^{56}Ni$ at 25 MeV/u, are shown in figure 3. In the top part of the figure is plotted the laboratory energy of the ejected deuterons as a function of their laboratory angle, θ_{lab} (equivalent to ϕ in figure 2), for three putative final states in ^{56}Ni (the ground state and two excited states at 5 and 10 MeV). Superimposed on the figure are lines indicating the equivalent centre-of-mass angles, θ_{cm}, of the deuteron in "normal" kinematics ($\approx \theta$ in figure 2). Note that at each laboratory angle there are two deuteron groups observed for each final state in ^{56}Ni, and that no deuterons emerge beyond 35° in the laboratory frame.

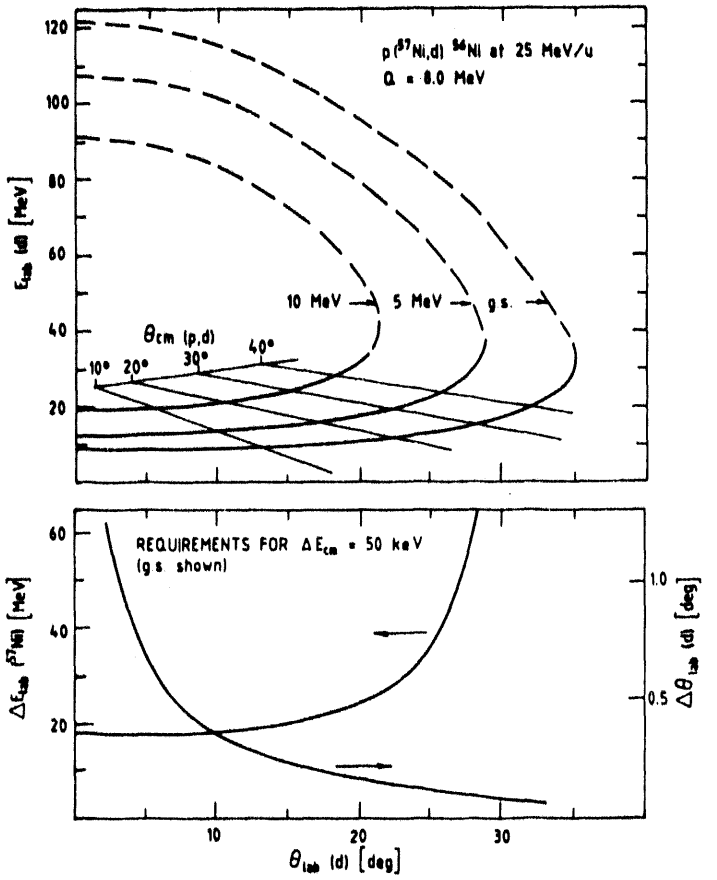

Figure 3: Kinematics calculated for the reaction $p(^{57}Ni,d)^{56}Ni$ at 25 MeV/u. The details are explained in the text.

Based on the results of ref[4] and many other similar measurements, one can set an approximate requirement for generating useful data from this experiment: the experimental energy resolution (FWHM) for detected deuterons should be less than 50 keV (centre-of-mass energy). This puts constraints on the energy spread in the primary ^{57}Ni beam and on the angular acceptance of the deuteron detector. The limiting values of these parameters are shown at the bottom of figure 3 as a function of laboratory angle. Evidently, the

constraints on beam-energy spread (~1%) and angular acceptance (~0.1°) are not particularly daunting.

The equivalent information for a two-nucleon pick-up reaction, $p(^{56}Ni,t)^{54}Ni$ at 50 MeV/u, is shown in figure 4. In all aspects the experimental demands are greater. The emerging tritons are compressed into forward angles below 25°; the beam spread must be ~0.3% and the angular acceptance ~0.03° to deliver 50 keV resolution for the detected tritons.

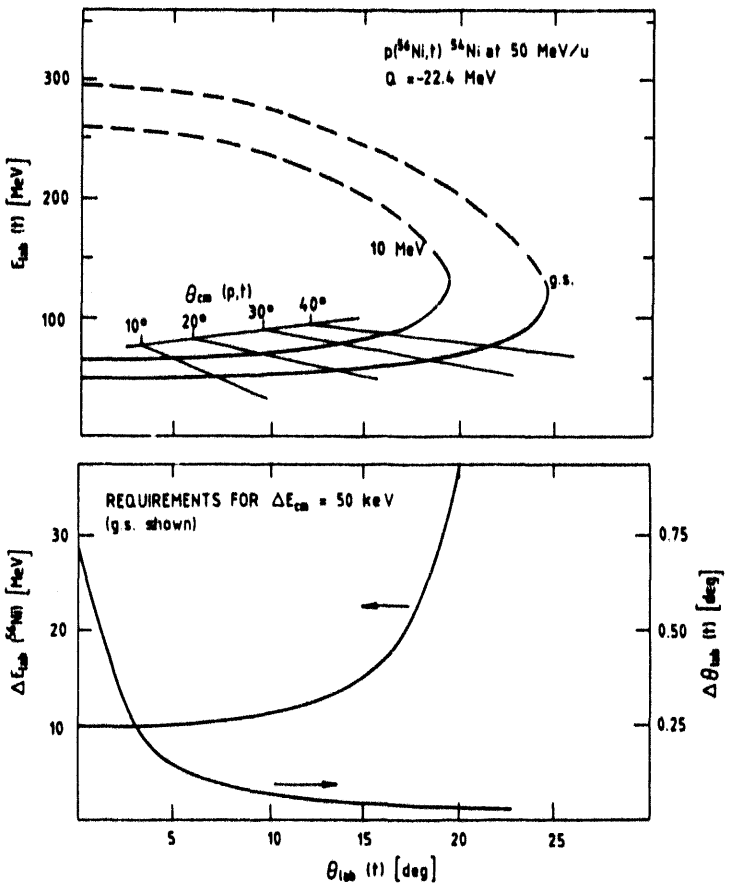

Figure 4: Kinematics calculated for the reaction $p(^{56}Ni,t)^{54}Ni$ at 50 MeV/u. See figure 3.

Stripping reactions present a quite different picture. As illustrated in figure 5, the important forward angles for the light ejectile in "normal" kinematics actually correspond to backward laboratory angles for the ejectile in inverse kinematics. In fact, this leads to a rather more favourable

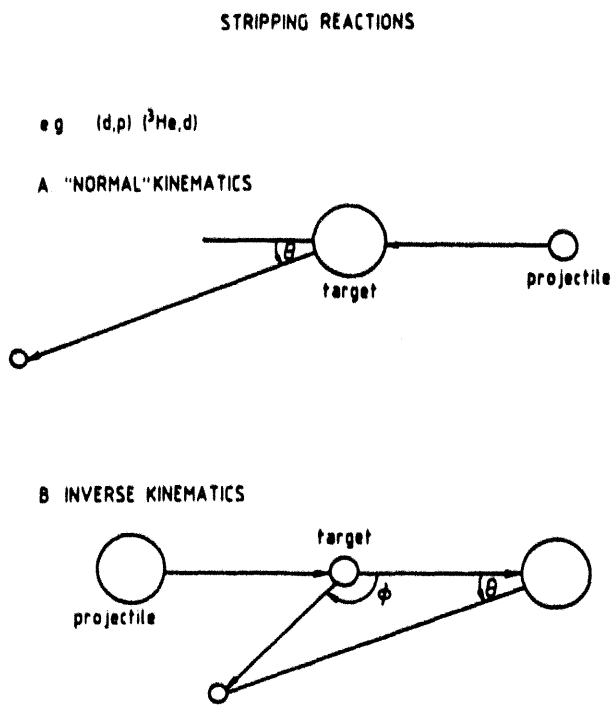

***Figure 5**: Illustration of the relationship between "normal" and inverse kinematics for stripping reactions.*

experimental situation. Figures 6 and 7 demonstrate this for two specific examples — $d(^{56}Ni,p)^{57}Ni$ at 15 MeV/u and $^{3}He(^{56}Ni,d)^{57}Cu$ at 20 MeV/u, respectively. For such reactions only one light-particle group appears at each laboratory angle, and angular distributions should be measurable from very close to 0° (in the centre-of-mass system viewed in "normal" kinematics — see abscissa labelling at the top of the figures) out to at least 60°. Furthermore, the constraints on beam-energy spread (~0.2%) and angular acceptance (~0.1°), though challenging, are not too severe.

3. PRODUCTION RATES

The projected count rate for an actual experiment naturally depends on a variety of factors, some of which cannot easily be generalized. Considered here is a specific example — $p(^{57}Ni,d)^{56}Ni$ at 25 MeV/u — which was also illustrated in figure 3. The assumptions are as follows:

a) **Beam current.** The Isospin Laboratory proposal[6] tabulates and illustrates projected currents for radioactive beams over the entire chart of nuclides. The value shown for ^{57}Ni is about 10^{8} atoms/s, a fairly representative result for N~Z nuclei in this region.

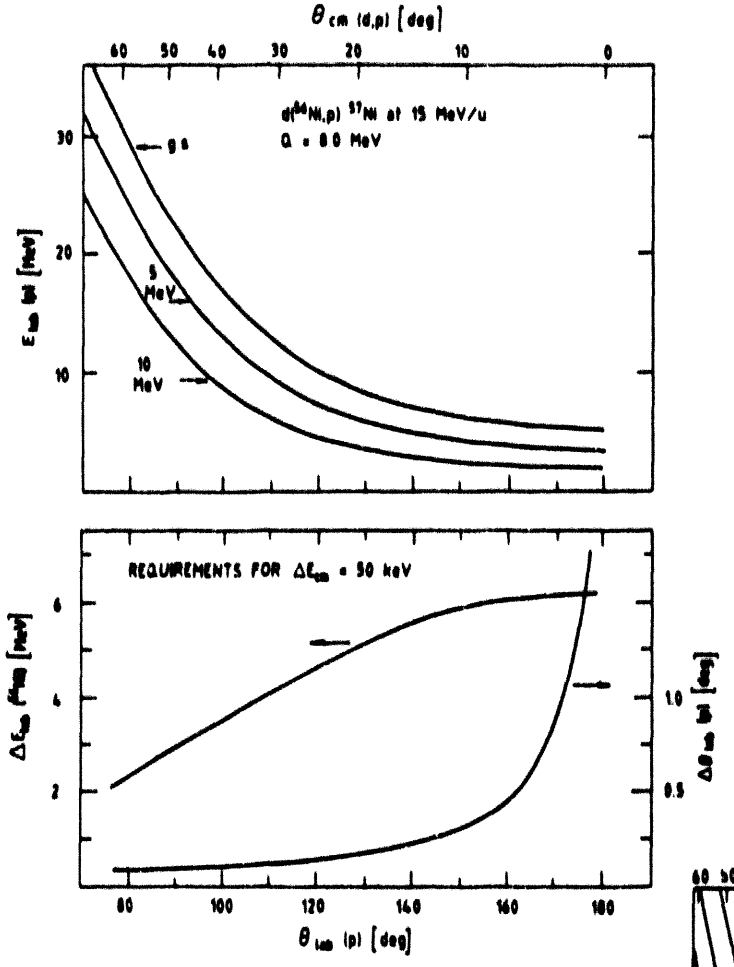

Figure 6: Kinematics calculated for the reaction $d(^{56}Ni,p)^{57}Ni$ at 15 MeV/u. The details are explained in the text.

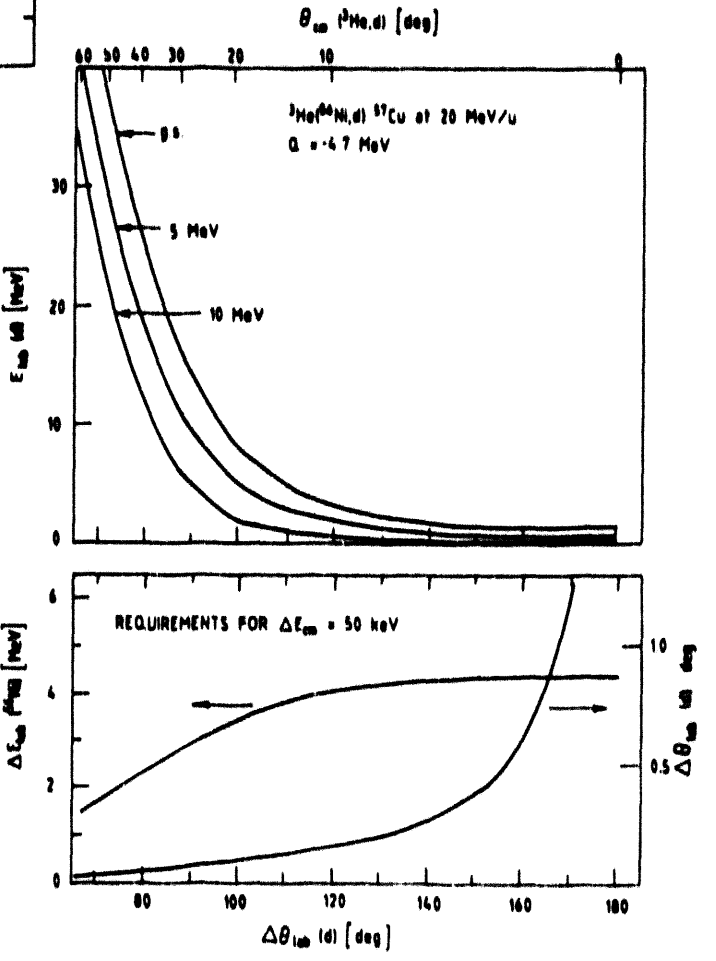

Figure 7: Kinematics calculated for the reaction $^{3}He(^{56}Ni,d)^{57}Cu$ at 20 MeV/u. See figure 6.

b) Target. Gas jets, gas cells and solid $(CH_2)_n$ targets were considered. A gas jet would certainly yield the cleanest spectrum from a localized source but the effective target thickness is likely limited[7] to ~15 $\mu g/cm^2$. A gas cell, however, ~2 cm in diameter and containing hydrogen gas at atmospheric pressure, would have an effective thickness ten times greater, yet would only degrade the ^{57}Ni beam[8] by about 6 MeV, an amount well below the limiting value required to achieve 50 keV deuteron resolution (see fig. 3). This same effective hydrogen thickness of ~150 $\mu g/cm^2$ also characterizes the thickest acceptable $(CH_2)_n$ target as determined by the maximum allowable ^{57}Ni energy loss (~18 MeV). It is this value that is used in subsequent calculations.

c) Detector. In the past (e.g., refs.[4,5]), transfer reactions were typically studied with a counter telescope having an angular acceptance of $\Delta\theta \approx 0.2^\circ$ and a total solid angle of $\sim 10^{-4}$ sr. Clearly, considerable improvement is possible today and indeed would be required by the beam currents likely to be available at a radioactive beam facility. With a suitably designed array of silicon strip detectors placed annularly about the beam path, it would be possible to maintain an angular acceptance for each strip of 0.1° but with a total solid angle subtended by each strip approaching 10^{-2} sr. At angles not requiring such high angular resolution, the solid angle could be increased still further by adding together the signals from neighbouring strips.

With these assumptions it is now possible to calculate the count rate expected for the $p(^{57}Ni,d)^{56}Ni$ reaction. If we consider the range of differential cross sections measured[4] for the $^{58}Ni(p,d)^{57}Ni$ reaction ($10^{-2} \leq d\sigma/d\Omega \leq 10$ mb) to be representative, then the counting rate, R, for each final state should be in the range

$$10 \leq R \leq 3 \times 10^3/\text{hr/strip}.$$

This is an entirely reasonable rate if one considers that with sufficient strip detectors all required angles could be measured simultaneously.

Admittedly, single-nucleon pick-up reactions are particularly favourable examples. The stripping reactions illustrated in figures 6 and 7 would be limited by beam-energy spread to targets a factor of three thinner, but even that does not preclude convenient measurements. Only the two-nucleon transfer reaction of figure 4 is a really doubtful case, with even more stringent detector requirements, and cross sections a factor of ten[5] smaller.

4. THRESHOLD MEASUREMENTS

An important requirement in the study of superalloved $0^+ \rightarrow 0^+$ β^+ decay is a very precise measure of the Q_{EC} value for each transition. Among the transitions studied to date, many of the Q_{EC} values have been determined from (p,n) threshold measurements on the β-decay daughter nucleus, which itself is stable and provides a suitable target. In the cases expected with A > 56, none of the T_z=1 daughters is stable, so it would be particularly useful if such threshold measurements could be made in inverse kinematics.

Superficially there is a real problem. Consider, for example, the well studied decay of $^{54}Co \xrightarrow{\beta} {}^{54}Fe$. Its Q_{EC} value has been determined in several ways, one being from the measured threshold[9] for the reaction $^{54}Fe(p,n)^{54}Co$. The beauty of this technique is that, with a pure enough target, no activity whatsoever is observed below threshold; the excitation function is thus established from a measurement of ^{54}Co activity ($t_{1/2}$=193 ms) as a function of proton beam energy (~9.2 MeV), the ^{54}Co recoils having stopped easily in the target. The situation would be much more complicated for the inverse reaction, i.e., a 500 MeV ^{54}Fe beam (~9.2 MeV/u) impinging on a hydrogen gas target. It is hard to conceive of a simple arrangement in which the ^{54}Fe beam or the high-energy ^{54}Co recoils would not interact with other materials — a gas cell window, or a stopper — thus producing a high rate of background activity.

With some added complexity, however, it appears that inverse threshold measurements could become viable. One possibility is to use a fully stripped $^{54}Fe^{26+}$ beam bombarding a hydrogen jet target, which is followed by a 0° magnetic spectrometer to separate the $^{54}Co^{27+}$ recoils from the $^{54}Fe^{26+}$ beam; the $^{54}Co^{27+}$ recoils could be counted directly on the focal plane of the spectrometer and their decays recorded in a β detector. Although cross-section figures are difficult to obtain, it appears[9,10] that in the $^{54}Fe(p,n)^{54}Co$ reaction the cross-section is about 1 mb at 8 keV above threshold (centre of mass). If we again assume a beam current of 10^8 atoms/s for the inverse reaction, this corresponds to a count rate of ~1/s.

Although these predictions relate to the A=54 system, which is, of course, well known, they strongly indicate that such measurements would be possible for the as-yet-unknown cases with A>56; in these cases, inverse reactions with radioactive beams provide the only means of access.

5. SUMMARY AND CONCLUSIONS

Based on several specific examples, it has been shown that inverse reaction studies are easily possible at a radioactive-beam facility with a modest investment in experimental equipment — a versatile array of strip detectors as a minimum, and possibly a gas-jet target and a magnetic spectrometer. The physics rewards of such studies could easily support several major experimental programs for many years.

It is important to realize, though, that these programs would require higher beam energies than the 10 MeV/u presently called for in the Isospin Laboratory proposal[6]. To provide useful spectroscopic information, the single-nucleon transfer reactions would require at least 25 MeV/u, and the two-nucleon transfer reactions up to 50 MeV/u. Even the inverse threshold measurements would require over 15 MeV/u near A=100 (see Q_{EC} plot in figure 1). It would seem shortsighted indeed to design a facility to preclude such an important source of information on nuclear spectroscopy.

6. ACKNOWLEDGEMENTS

I should like to acknowledge very helpful discussions with Gordon Ball, Alfredo Galindo-Uribarri and Erik Hagberg.

7. REFERENCES

1. J.C. Hardy, I.S. Towner, V.T. Koslowsky, E. Hagberg and H. Schmeing, Nucl. Phys. A509 (1990) 429.

2. I.S. Towner, J.C. Hardy, E. Hagberg and V.T. Koslowsky, Proceedings of the Int. Symp. on Weak and Electromagnetic Interactions in Nuclei (WEIN-92), Dubna, Russia, 1992 June 16-22 (to be published).

3. E. Hagberg, V.T. Koslowsky, T. Shinozuka, J.G. Hykawy, J.C. Hardy, G. Savard, P.P. Unger, H. Schmeing and I.S. Towner, Proceedings of 6th Int. Conf. on Nuclei far from Stability & 9th Int. Conf. on Atomic Masses and Fundamental Constants, 19-24 July 1992, Bernkastel-Kues, Germany (to be published).

4. F.M. Edwards, J.J. Kraushaar and B.W. Ridley, Nucl. Phys. A199 (1973) 463.

5. H. Nann and W. Benenson, Phys. Rev. C10 (1974) 1880.

6. "The Isospin Laboratory (ISL), Research Opportunities with Radioactive Nuclear Beams", report LALP 91-51 (1991).

7. G. Bittner, W. Kretschmer and W. Schuster, Nucl. Instr. and Meth. 167 (1979) 1.

8. L.C. Northcliffe and R.F. Schilling, Nucl. Data Tables 7 (1970) 233; F. Hubert, R. Bimbot and H. Gauven, At. Data and Nucl. Data Tables 46 (1990) 1.

9. S.D. Hoath, R.J. Petty, J.M. Freeman, G.T.A. Squier and W.E. Burcham, Phys. Lett. 51B (1974) 345.

10. S. Tanaka and M. Furukawa, J. Phys. Soc. Japan 14 (1959) 1269.

PROTOTYPICAL EXPERIMENTS: NEUTRON-RICH NUCLEI

K.-L. Kratz[1], P. Möller[1,2] and F.-K. Thielemann[3]

[1]Institut für Kernchemie, Universität Mainz, Germany
[2]Theoretical Division, Los Alamos National Laboratory, Los Alamos, NM 87545, USA
[3]Harvard-Smithsonian Center for Astrophysics, Cambridge, MA 02138, USA

1. Introduction

Over the last years, worldwide interest has developed in radioactive nuclear beam (RIB) science, which covers many significant areas ranging from nuclear structure and reactions, astrophysics, atomic physics, materials science to biology and nuclear medicine. Since it is impossible to do justice to all these interesting topics, and since some of them have been discussed in other contributions to this workshop, we focus in the present paper on the strong interplay between nuclear-structure properties of neutron-rich nuclei far from stability and stellar nucleosynthesis of elements beyond Fe by rapid neutron-capture processes.

In the past, at several stages in the development of an understanding of the r-process mechanisms, the major limitation to further progress has been - and still is - the degree to which the associated nuclear physics is known (for landmark papers or reviews, see e.g. [1-5]). Therefore, it is no surprise that even today the exact stellar site of the r-process ('where in a supernova?') is not known. With the close connection between not only *gross* but also detailed *microscopic* nuclear physics and whatever constraints can be imposed on models for the astrophysical environments, it is obvious that only additional and more accurate experimental data on exotic neutron-rich isotopes can lead to a better understanding of r-process nucleosynthesis. An interesting recent finding in this context is that with our present knowledge of nuclear physics, of isotopic r-process abundances in nature, and of supernova models, deficiencies in calculated abundance patterns seem to indicate nuclear-structure effects on the very-neutron-rich side of β-stability [7,8] for nuclei so far not observable in terrestrial laboratories. With the expected improvement in the production of far-unstable species at future ISOL and RIB facilities,

unique opportunities will be provided not only to answer questions on fundamental current nuclear-structure themes (as outlined, e.g. in [8]), but also to allow the study of new phenomena, obviously derivable from astrophysical 'observations' but not from present nuclear-model extrapolations.

2. Solar r-abundance fits and nuclear data

The observed isotopic r-abundances ($N_{r,\odot} \simeq N_\odot - N_s$ [9]) are the result of successive neutron captures along the r-process path and decay back to β-stability, thus depending – apart from stellar parameters – on nuclear properties of nuclei with extreme N/Z ratios. In the general case (see, e.g. Eq. 2 in [6]), among these properties ground-state masses (respectively Q_β-values), neutron-separation energies (B_n), β-decay half-lives ($T_{1/2}$), probabilities of β-delayed neutron emission (P_n), neutron-capture cross sections ($\sigma_{n,\gamma}$) and ground-state spins and parities (J^π) are the main ingredients in r-process calculations. For nuclei with $Z \geq 80$, fission barriers and rates of β-delayed as well as neutron-induced fission are also important.

Neutron-capture cross sections far from stability can so far only be obtained from the statistical Hauser-Feshbach (HF) model. This approach is justified as long as nuclear level densities in the compound nucleus are sufficiently high. The HF method requires a knowledge of the relevant physics quantities, such as optical potentials, giant dipole resonance parameters for γ-widths, level densities, ground-state J^π and reaction Q-values B_n, either from experiment or from theory (see [10] and Sect. 3 in [5]). Some experimental information on level densities of neutron-rich isotopes may be obtained from high-resolution spectroscopy of β-delayed neutrons; this decay mode can be considered as 'inverse process' to neutron capture (see, e.g. [11,12]). For nuclei near closed neutron shells, where the level density is small, the HF approach is no longer applicable and should be replaced by the Breit-Wigner resonance-capture formalism plus direct-capture (DC) contributions [13,14]. The latter DC rate may even be the dominant part of the total neutron-capture cross section for neutron-magic nuclei. Here, (d,p)-reactions in inverse kinematics, e.g. on $^{78}Ni_{50}$ and $^{132}Sn_{82}$, are a promising tool to determine the spectroscopic factors and J^π which are necessary for improved DC calculations [14].

If one considers a steady-flow r-process ('waiting-point' concept [1]), its path is not determined by the $\sigma_{n,\gamma}$, and the important nuclear properties are only B_n, (Q_β), $T_{1/2}$ and P_n. Recently, first experimental information in the $A \simeq 80$ and 130 regions (see, e.g. [15–18]) made it possible to analyze isotopic abundance patterns in the first two $N_{r,\odot}$-peaks [19] within the 'waiting-point' concept. This concept implies approximate equality of progenitor abundance ($N_{r,prog}$) times β-decay rate ($\lambda_\beta = \ln 2 / T_{1/2}$) for each isotopic chain. For a number of Zs at N=50 and N=82, only *one* isotope (i.e. ^{76}Fe to ^{80}Zn and ^{127}Rh to ^{130}Cd) contains the dominant r-abundance in the respective Z-chain. From the *measured* $T_{1/2}$ and P_n of the 'waiting-point' isotopes ^{79}Cu [18], ^{80}Zn [16–18] and ^{130}Cd [15], together with the known P_n-values of their isobars on the way to β-stability and the known $N_{r,\odot}$ of ^{79}Br, ^{80}Se and ^{130}Te [9], one can calculate their initial $N_{r,prog}$, and with these – in turn

- one can *predict* the $T_{1/2}$ for the progenitor nuclei in the r-process path and also for their so far unknown neutron-magic neighbors. As was shown in [18,19], these 'β-flow requests' on $T_{1/2}$ agreed closely with experimental and/or QRPA shell-model predictions, suggesting that, indeed, the 'waiting-point' concept seems to be valid - at least locally in the $N_{r,\odot}$-peak areas (see also [6]).

Since the vast majority of nuclei in or close to the r-process path are not (yet) accessible in terrestrial laboratories, a general understanding of their nuclear-structure properties may be obtained only through theoretical means. However, since a number of different quantities are needed in r-process calculations, in the past it was not possible to obtain them all from the same source. This has not only raised the question of consistency but has also strongly limited the predictive power far off β-stability (see, e.g. [5]).

Therefore, in Ref. [6] and in the r-process calculations presented in this paper, the *unified* macroscopic-microscopic approach of Möller et al. [20-22] has been applied, within which all necessary nuclear properties can be studied in a largely consistent way. A Folded-Yukawa (FY) single-particle (SP) model is combined with a finite-range droplet model (FRDM) and a Lipkin-Nogami (LN) pairing model. As a first step, nuclear ground-state masses and shapes are calculated. Once these quantities are known, nuclear wave functions are derived for the appropriate shapes. Matrix elements giving β-decay rates and other quantities of interest may then be determined. $T_{1/2}$ and P_n-values are deduced from theoretical Gamow-Teller (GT) strength functions calculated within the QRPA [23], generally taking the same FYSP levels as used for the shell corrections of the nuclear masses. To account for the retardation of low-energy decay rates, a simple GT residual interaction is added to the Hamiltonian which is studied in the QRPA. For a detailed discussion, see [23].

In principle, with the above approach, for the first time an internally consistent data set for astrophysical calculations is available. In addition to these theoretical model extrapolations, all recent experimental data on Q_β, B_n, $T_{1/2}$ and P_n were included. Furthermore, for nearby extrapolations, known nuclear-structure properties either model-inherently not contained in or not properly described by the above - still too simplistic - approach were taken into account (for details, see [6]). This combined theoretical and experimental data set is expected to yield more reliable predictions of nuclear-physics parameters than earlier approaches.

As is discussed in [6], the global r-abundance curve shown in Fig. 1 is the result of a superposition of several n_n-T_9 components at 'freeze-out' conditions. Clearly, the main features of the $N_{r,\odot}$-distribution [9] - in particular position and height of the three main peaks - are well reproduced; however, there remain several deficiencies: the region below A=78, the mass range $105 \leq A \leq 125$ and the $A \simeq 170$ area. Both, general agreement and local deficiencies are believed to represent nuclear-structure signatures far off β-stability. For developing a better understanding of the detailed *isotopic* $N_{r,\odot}$-curve and the underlying physics, one may phrase a number of questions:

- What is the origin of the $A \simeq 80$, 130 and 195 $N_{r,\odot}$-peaks?

- Why is the A≃80 $N_{r,\odot}$-'peak' no peak?
- Why is the A≃130 $N_{r,\odot}$-peak so narrow?
- Why is the $N_{r,\odot}$-curve in between the peaks so smooth?
- What is the origin of the A≃120 trough in the $N_{r,calc}$?
- What is the origin of the deviations in the A≃110 and 170 pygmy-peak regions?

In order to answer the above questions, a number of prototypical experiments may be

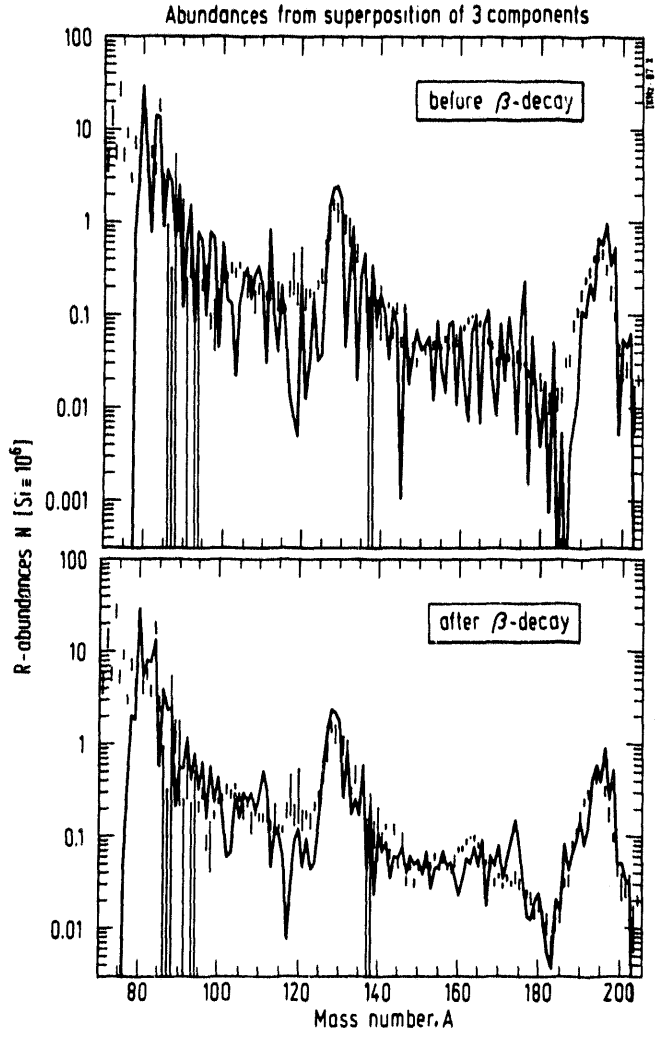

Fig. 1: R-abundance distribution obtained from a superposition of three time-dependent calculations with the 'best-fit' n_n-T_9 values for the A≃80 peak and the 90≤A≤130 and 135≤A≤195 mass ranges (from Ref. [6]). In the upper part, the calculated initial progenitor abundances are shown; in the lower part, the final abundances are given. The smoothing of the abundance curve is introduced by the P_n-branching during β-decay back to stability.

suggested which range from studies of simple-to-measure quantities (such as $T_{1/2}$ and P_n-values) to detailed spectroscopic investigations (e.g. to determine ground-state deformations, or to understand the proton-neutron (pn) residual interaction in exotic nuclei) and reaction studies (e.g. the measurement of single- and few-nucleon transfer reactions in the $^{78}_{28}Ni_{50}$ and $^{132}_{50}Sn_{82}$ regions).

3. Simple-to-measure quantities

As discussed in Sec. 2, among the most important nuclear properties for steady-flow r-process calculations are the $T_{1/2}$ and P_n-values of isotopes *in* the r-process path, in particular in the $N_{r,\odot}$-peak regions. The $T_{1/2}$ determine the relative isotopic r-abundances in each Z-chain - and, when normalized to a neutron-magic 'waiting-point' nucleus, the *absolute* r-abundances. The P_n-values are responsible for the considerable smoothing of the initial $N_{r,prog}$ during β-decay back to stability (compare the upper and lower part of Fig. 1). There is, however, one local exception. As a result of the specific structure of the N≃50 'waiting-point' isotopes, the odd-even (oe) variations of their P_n-values result in a pronounced oe-staggering of the $N_{r,\odot}$ in the A≃80 region.

Both quantities $T_{1/2}$ and P_n are usually determined via β- and β-delayed-neutron multiscaling experiments (see, e.g. [15,18,24]). However, as our recent measurements performed with a chemically non-selective plasma ion source have shown, contaminations by molecules (e.g. $[^{40}Ca^{90}Br]^+$ in the case of ^{130}Cd [15]), multi-charged species or strongly produced isobars (e.g. the 2.85 s βdn-precursor ^{79}Ga in the case of ^{79}Cu [18]; see Fig. 2) may severely disturb these experiments. Therefore, future measurements of $T_{1/2}$ and P_n-values of very-neutron-rich isotopes at ISOL-facilities require chemically selective ion sources (e.g. laser ion sources [25]), isobar separation [26] and/or the use of ion traps [27]. Of particular interest in the context of the 'classical' r-process are, of course, the unknown 'waiting-point' isotopes $^{76}Fe_{50}$ to $^{78}Ni_{50}$ and $^{127}Rh_{82}$ to $^{129}Ag_{82}$. Apart from these key nuclides, any 'new' $T_{1/2}$ and P_n-value on the way to the r-process path will be helpful in testing present model predictions far from stability.

With regard to nuclear structure, it is fortunate that already simple experiments, such as mapping the $E(2_1^+)$, $E(4^+)/E(2^+)$ or certain strong GT transitions (e.g. to the $\nu g_{7/2}$-orbital) over long chains of isotopes or isotones, may yield first information on the evolution of structure from β-stability to neutron drip-line, or along the r-process path from one shell closure to the next. To give an example for ISOL-experiments, $E(2_1^+)$ and $\nu g_{7/2}$ SP levels in the $_{48}$Cd isotopic chain, or $(\pi g_{9/2}\nu g_{7/2})1^+$ states in $_{47}$Ag nuclides are of interest not only from the point of view of the shell model in the region 'southwest' of ^{132}Sn (see, e.g. [28,29]), but also for an understanding of the A≃130 $N_{r,\odot}$-peak shape as well as the deficiency in the A≃120 mass region (see Fig. 1). The fact that one observes a rather narrow A≃130 r-peak over a wide range of n_n–T_9 conditions [6] can be related to the strong N=82 shell closure near ^{132}Sn, which seems to be well described by current mass models [21,32,33]. However, further below ^{132}Sn, for Z≤46 isotopes all nuclear mass

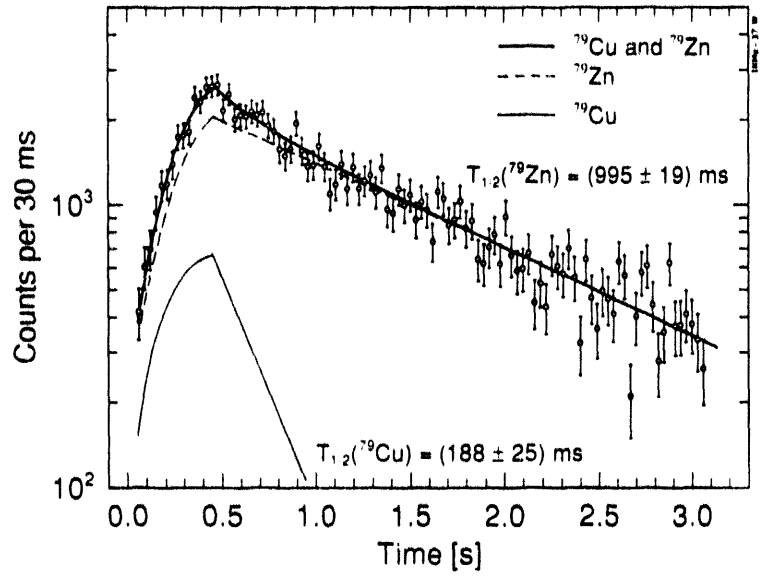

Fig. 2: Beta-delayed-neutron multiscaling curve for A=79, after subtraction of the 2.85 s activity of the isobar ^{79}Ga (from Ref. [18]). Besides the known $T_{1/2}$ of ^{79}Zn, another short-lived βdn-component was observed which could be attributed to the N=50 'waiting-point' isotope ^{79}Cu. In a case like this, the use of an element-selective ion source and/or isobar separation would be highly desirable.

extrapolations overestimate the N=82 shell strength, resulting in the A$\simeq$120 dip in the calculated r-abundances shown in Fig. 1. Because of the overly strong neutron shell in the models, the r-process path leaps over 13 mass units from $^{112}Zr_{72}$ to $^{125}Tc_{82}$ (see Fig. 3), producing *not a single* $B_n \simeq 2$ MeV 'waiting-point' isotope in this region. Therefore, gross β-decay properties, nuclear masses (respectively B_n-values) as well as detailed nuclear-structure studies (for the latter, see Sect. 4) are required in this mass region in order to understand the shape transition far off stability from N=66 neutron mid-shell around Z=38 to N=82 shell closure at Z$\geq$45.

Another attractive opportunity to investigate shape transitions across entire shells is the measurement of B(E2)-values in Coulomb excitation experiments [32]. In certain mass regions, e.g. around the nearly-superdeformed ($\beta \simeq 0.40$) isotope ^{100}Sr, low-energy $K^{\pi}=1^{+}$ intrinsic excitations and associated M1 strengths [31] may be studied, which are not accessible in present β-decay experiments.

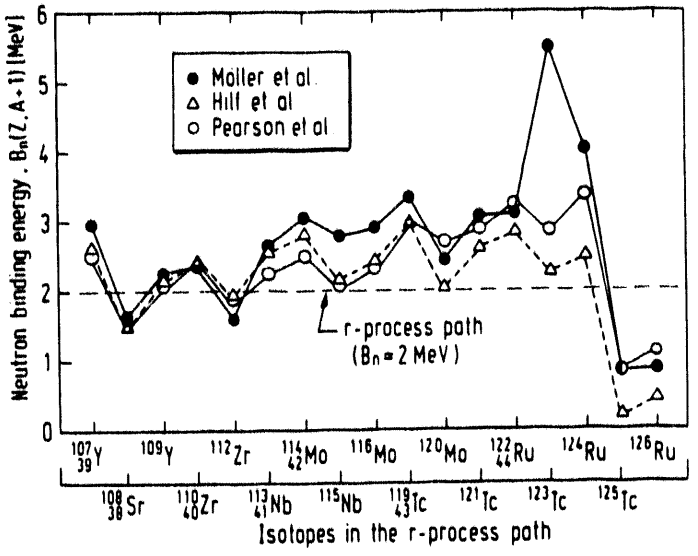

Fig. 3: Neutron binding energies B_n for r-process nuclei in the $105 \leq A \leq 125$ mass region (from Ref. [6]). Before the N=82 shell, the recent microscopic mass models of Möller et al. [20,21] and Pearson et al. [30] predict somewhat larger B_n-values than the old Hilf et al. [31] mass formula. With the general trend in all three models, too few $B_n \simeq 2$ MeV 'waiting-point' isotopes exist between A=112 and A=125, resulting in the pronounced abundance trough in the calculated N_r-distribution shown in Fig. 1.

4. Detailed spectroscopic investigations

With ISOL and RIB techniques a large variety of nuclear-structure phenomena can be addressed (for a broad coverage of this topic, see e.g. [8]). With regard to astrophysics applications, shell strengths around ^{78}Ni, and below ^{132}Sn and ^{208}Pb are of special interest for an understanding of the shapes and isotopic abundances of the $A \simeq 80$, 130 and 195 $N_{r,\odot}$-peaks [9]. Furthermore, evolution of nuclear structure in the $A \simeq 100$ and 150 phase-transitional regions is important for an understanding of the formation of the $A \simeq 110$ and 170 $N_{r,\odot}$-pygmy-peaks. Finally, any new information on neutron-rich trans-lead isotopes may help to resolve the still existing puzzles on the ^{208}Pb isotopic anomaly and the long-lived r-process chronometers [5,6,34].

As an example of detailed nuclear-structure studies near closed-shell nuclei, Fig. 4 shows a comparison of the experimental level scheme of ^{80}Ga (obtained from β-decay of the N=50 'waiting-point' nucleus ^{80}Zn [35]) with our QRPA predictions for spherical and deformed shapes [36]. The key result of this comparison is that the lowest $J^\pi = 1^+$ states in ^{80}Ga can only be reproduced when assuming the β-decay daughter to be deformed, at least above 600 keV. The observed splitting of the spherical 2QP 1^+ states, as well as the fair agreement of theoretical logft, $T_{1/2}$ and P_n values with experimental data [16-18,35] strongly suggest that also the ground state of the mother isotope ^{80}Zn is prolate and

not spherical as one might expect in the close vicinity to the doubly-magic nucleus ^{78}Ni [21]. The above observation implies a rather rapid weakening of the N=50 shell strength above ^{78}Ni, which may be one of the reasons why the A≃80 $N_{r_{\odot}}$-'peak' is not as well developed as the r-peaks at A≃130 and 195. Nevertheless it is evident, that further nuclear-structure information from β-decay and reaction studies is needed in the ^{78}Ni region.

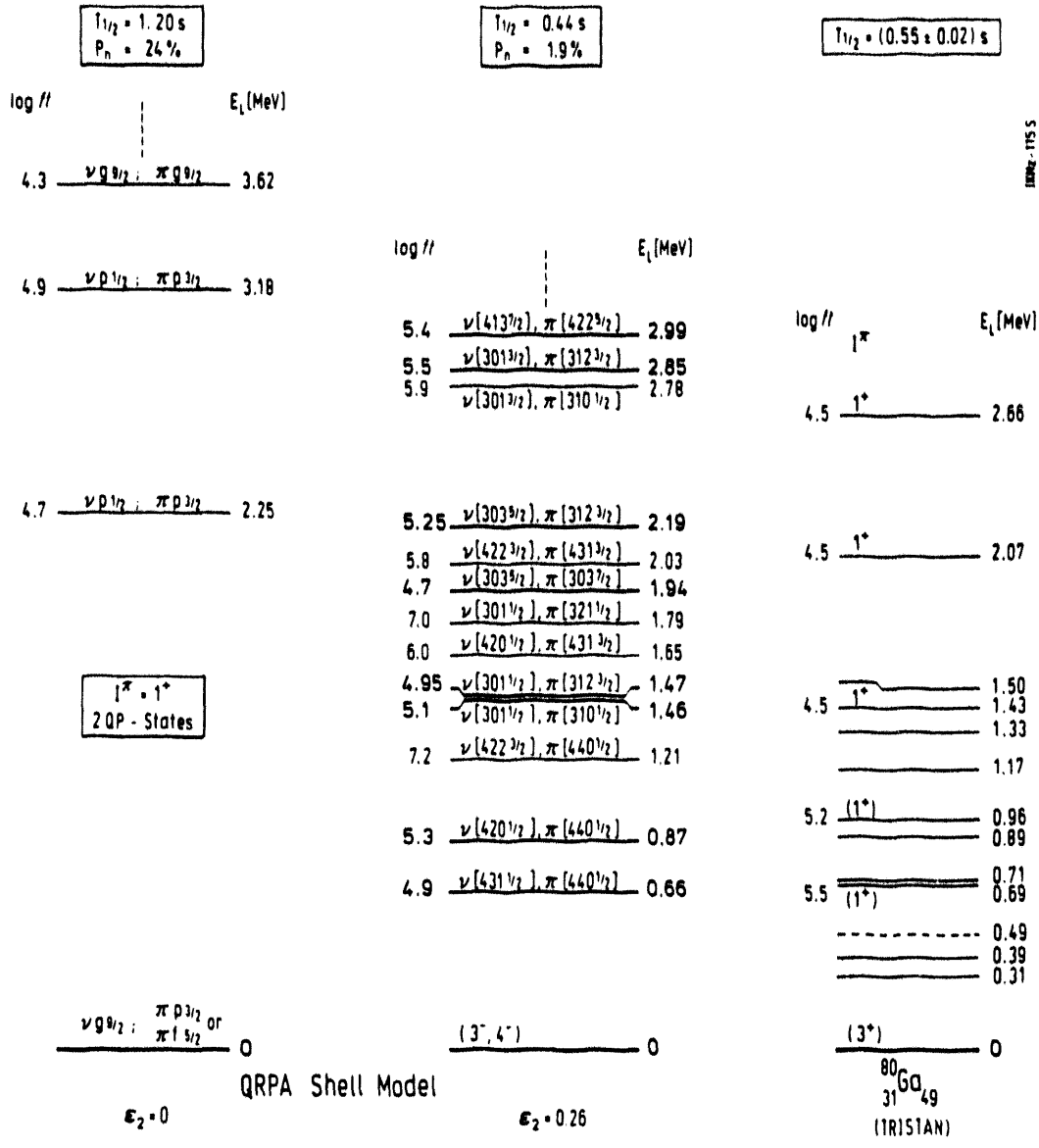

Fig. 4: Comparison of measured decay scheme and $T_{1/2}$ of ^{80}Zn from the TRISTAN group [35] with QRPA shell-model predictions for two different assumptions on quadrupole deformation (from [36]).

Similar arguments also hold for the doubly-magic nucleus ^{132}Sn and its neighbors. The β-decay properties and the low-energy level structure in this region are strongly dependent on the available shell-model orbitals and their modulation through the proton-neutron residual interaction (see, e.g. [28,29]. In particular, the very fast β-transition connecting the $\pi g_{9/2}$ and $\nu g_{7/2}$ orbitals dominates the GT strength in quite a number of neutron-rich In and Ag isotopes. The observed regularities, tested against improved model extrapolations, may be helpful in predicting the main decay properties of still unknown or only little known nuclei, such as the 'waiting-point' isotopes ^{129}Ag and ^{133}In. As an example of the important $\pi g_{9/2}$-$\nu g_{7/2}$ interaction – which is neglected in the recent QRPA models of [23,37] – the resulting modulation of the SP energies between $^{91}_{40}Zr_{51}$ and $^{131}_{50}Sn_{81}$ is shown in the left part of Fig. 5 (taken from Heyde [38]). With the filling of the $\pi g_{9/2}$ shell, the $\nu g_{7/2}$ orbit is lowered by as much as 3 MeV. As a consequence of the missing pn interaction, the QRPA models calculate the $\nu g_{7/2}$ state in the ^{132}Sn region roughly 3 MeV too low compared to the experiment. This results, for example, in a $T_{1/2}$(QRPA)for

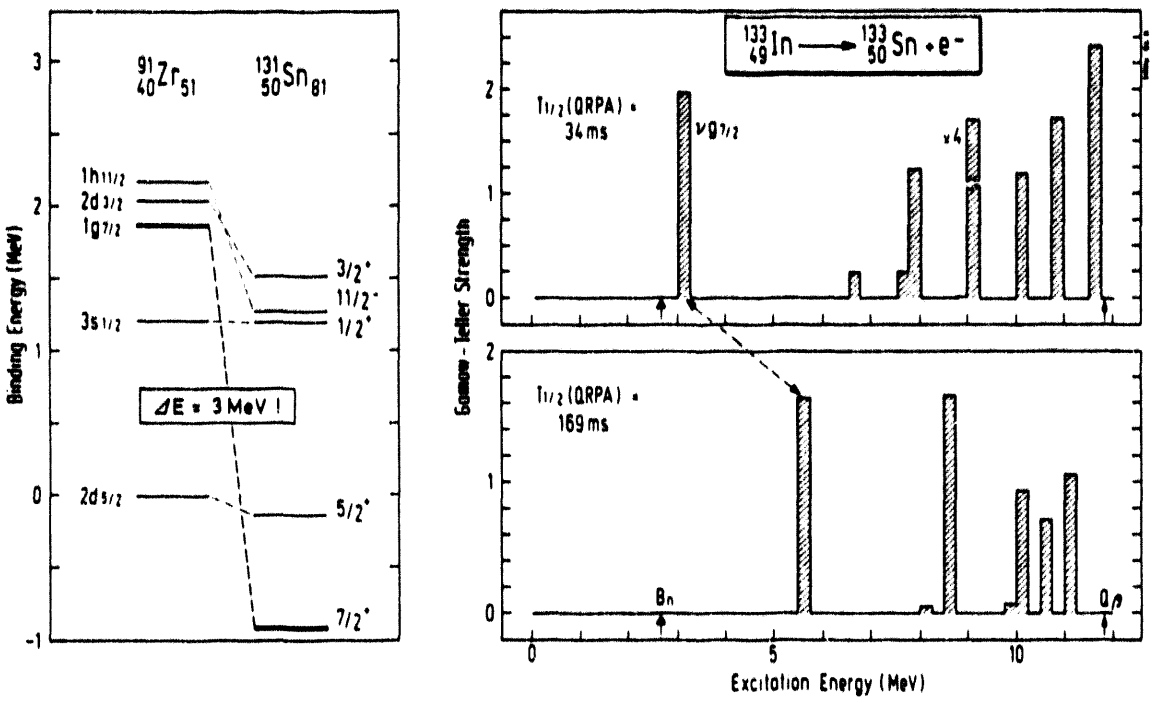

Fig. 5: Left part: SP energies in ^{91}Zr and ^{131}Sn (adopted from [38]). With the filling of the $\pi g_{9/2}$ shell, a dramatic lowering of the $\nu g_{7/2}$ orbit occurs as a consequence of the monopole pn-interaction. Note, that even the order of the $\nu d_{5/2}$ and $\nu g_{7/2}$ shell-model states is inverted. Right part: GT strength functions for ^{133}In decay. With the use of the standard Nilsson SP parameters, the QRPA [23] calculates the $\nu g_{7/2}$ level about 3 MeV too low, resulting in a too short $T_{1/2}$(QRPA). When choosing, instead, experimentally known SP energies, the $\nu g_{7/2}$ level is shifted up to E$\simeq$6 MeV, and the $T_{1/2}$(QRPA) comes close to the measured value of 195 ms [39].

^{133}In decay which is a factor six lower than the measured value (see right part of Fig. 5). Such model deficiencies can presently only be overcome by choosing *experimental* SP levels for local regions instead of the global Nilsson model parameters. In our opinion, this is a more reasonable solution than the procedure of the Klapdor group [37]. In order to obtain the 'correct' $T_{1/2}$ in this area, they reduce the low-lying GT strength - and, in this case, also that to the $\nu g_{7/2}$ SP level at the *wrong* excitation energy - by reducing the GT coupling constant for Z=49 by about the above factor of six. Analogously, depending on the prediction of the $\nu g_{7/2}$ level in $^{129}Cd_{81}$ (without or with taking into account the effect of the pn-interaction), the $T_{1/2}$(QRPA) for the N=82 nucleus ^{129}Ag varies between 17 ms and 140 ms, thus drastically affecting a test of the r-process 'waiting-point' concept of the A≃130 $N_{r,@}$-peak. If the $T_{1/2}$(QRPA) of 34 ms for ^{133}In and 17 ms for $_{129}$Ag - obtained when neglecting the $\pi g_{9/2}$-$\nu g_{7/2}$ attractive interaction - were 'true', no A≃130 r-peak would exist in nature. Turning around the arguments, one may conclude that the large abundances observed for ^{126}Te to ^{132}Xe [9] *require* long $T_{1/2}$ of their r-process progenitors.

In addition to decay spectroscopy, the measurement of single- and few-nucleon transfer reactions in the ^{132}Sn region will be of great importance for providing new information on simple collective modes and SP states. And indeed, experiments of this type have been proposed for the ESR at GSI [40]. A beam of ^{132}Sn and thin gas targets of p, d, ^{3}He and ^{4}He would enable the mapping of particle and hole states in this region. First (d,p)- measurements in inverse kinematics in this mass region using radioactive $^{134}Te_{82}$ beams will presumably be carried out at GSI at the end of next year. Once the SP states are identified, in a next step one may study two-particle and particle-hole energies (e.g. the $(\pi g_{9/2}\nu g_{7/2})1^+$ states) in neighboring nuclei. For technical details of such measurements, we refer to J.C. Hardy's contribution [41] in which reactions in inverse kinematics on the proton-rich doubly-magic isotope $^{56}_{28}Ni_{28}$ are discussed in detail.

Another example related to the pn-residual interaction is the development of nuclear structure in transitional regions. In this context, neutron-rich isotopes near A≃100 are especially interesting owing to the unusually large number of different shapes and excitation modes within a small range of proton and neutron numbers (for a recent review, see e.g. [42]). Z≃40 isotopes near stability experience the strong spherical subshell closure at N=56, whereas between N=58 and 60 a dramatic lowering of the 2_1^+ energies of the $_{38}$Sr and $_{40}$Zr isotopes indicates the well known *sudden onset of deformation*. Recent systematics of level energies and ρ^2(EO)-values in these isotopes [43] suggest that with increasing occupation of the $\nu g_{7/2}$ and $\nu h_{11/2}$ orbitals, their interaction with the $\pi g_{9/2}$ shell rapidly lowers a deformed minimum from about 1.5 MeV at N=58 over 0.6 MeV at N=59 down to the ground state at N=60 (see Fig. 6). However, contrary to former interpretations [44], it is the 0_3^+ state and not the 0_2^+ level in $^{96}Sr_{58}$ and $^{98}Zr_{58}$ which is associated with the second potential-energy minimum that at N≥60 becomes the strongly deformed ground state . Beyond N=60, recent band-structure and lifetime measurements have indicated a steady increase of deformation for $_{40}$Zr and $_{42}$Mo isotopes towards neutron midshell, whereas the $_{38}$Sr nuclides show the rather unique feature of a saturation of ground-state deformation immediately at its onset (see, e.g. [45]). In addition, identical rotational bands at low spin

and low excitation energy have been found in four contiguous N≥60 $_{38}$Sr isotopes [43]. Despite all this recent progress in the understanding of nuclear-structure phenomena in the A≃100 region, there remain features which are not yet understood, and hence should be subject to future γ-ray and laser-spectroscopic investigations.

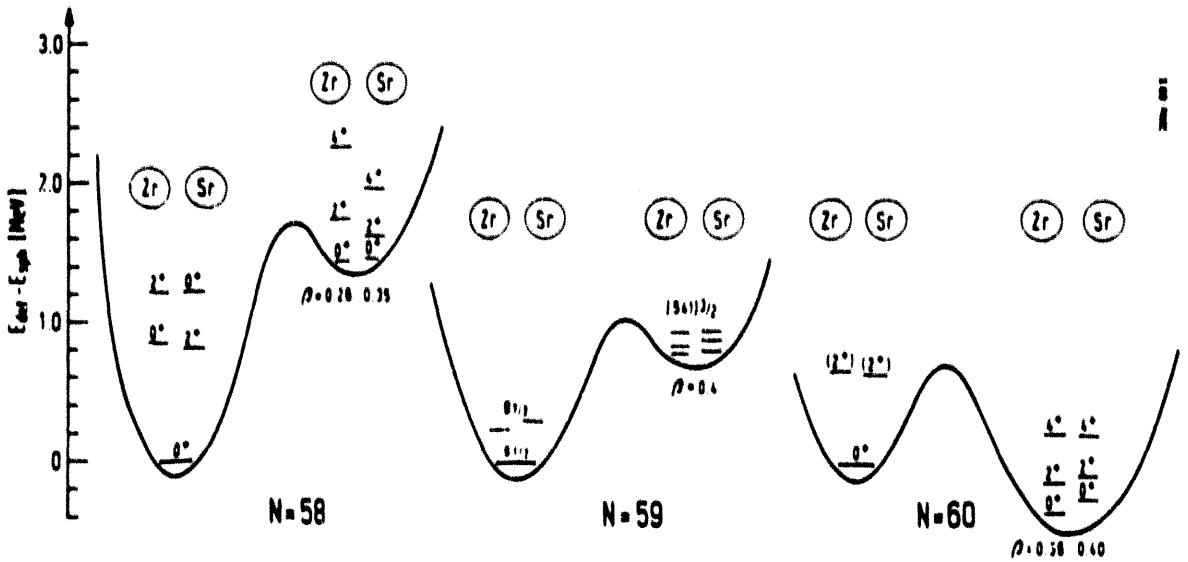

Fig. 6: Systematics of intruder states in N=58 to 60 Sr and Zr nuclei. The potential-energy curves are only a guide to the eye (from [43]).

With regard to r-process abundances just beyond the A≃80 'peak', more information is needed on neutron-rich $_{32}$Ge to $_{36}$Kr isotopes. An interesting question in this context is for example: Is the N=60 isotone ^{96}Kr deformed as predicted by current models [20,21,30], or is it still spherical as may be inferred from recent experiments [46,47]? This has – via the prediction of unknown β-decay properties, which are strongly dependent on the assumed N=56 subshell strength below Z=38 (see e.g. Fig. 7) – an important impact on the nucleosynthesis origin of the heaviest stable zirconium isotope ^{96}Zr. This nuclide is not only strongly abundant in the bulk solar system, but has recently also been observed as an isotopic anomaly (correlated with an overabundance of ^{50}Ti) in certain EK-5 inclusions of the Allende meteorite [48]. While so far ^{96}Zr was believed to be an *r-only* isotope [9], recently Gallino et al. [49] claimed that it must have received an important contribution from a high-neutron-density s-process component through the branching point at ^{95}Zr. However, based on experimental data and short-range predictions of nuclear-physics properties, our steady-flow calculations of r-abundances in the A≃95 [6] indicate fair agreement with the observed $N_{r,\odot}$. As can be seen from Fig. 8, this is most evident from the simultaneous reproduction of the abundance of the r-only isotope ^{100}Mo and the $N_{r,\odot}$ of ^{99}Ru which both originate from ^{100}Kr which is predicted to have a 'long' $T_{1/2}$(QRPA). The

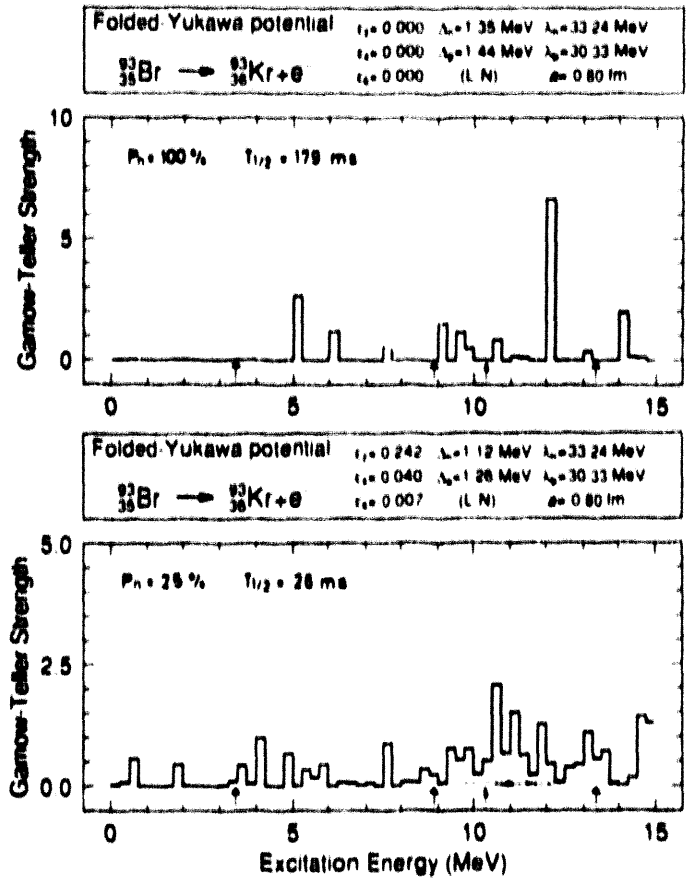

Fig. 7: Gamow-Teller (GT) strength functions of $^{93}_{35}Br_{58}$ decay obtained from QRPA calculations [23] using the FYSP potential, the LN pairing model and two different values for the quadrupole-deformation parameter ϵ_2. Upper part: assumption of spherical shape, which corresponds to recent findings from γ-ray and laser-spectroscopic studies [46,47]; lower part: assumption of prolate deformation, as predicted by the mass model of Möller et al. [21]. Substantial differences in the astrophysically important parameters $T_{1/2}$ and P_n are observed.

large ^{96}Zr abundance originates mainly from β-delayed neutron decay of the progenitor ^{97}Br. From this, we conclude in contrast to Gallino et al. [49], that most ^{96}Zr ($\geq$80%) observed in both the solar system as well as in the EK-5 meteoritic inclusions [48] has presumably been produced under r-process and not under s-process conditions. A final statement can, however, only be given when the relevant β-decay properties of the progenitor isotopes are measured and *understood* in terms of nuclear structure.

A last aspect discussed in the present paper with regard to an improved understanding of changes in collectivity in the neutron-rich A$\simeq$100 and 150 mass regions, is the question of how nuclear deformation develops from its onset at N=60, respectively N=90

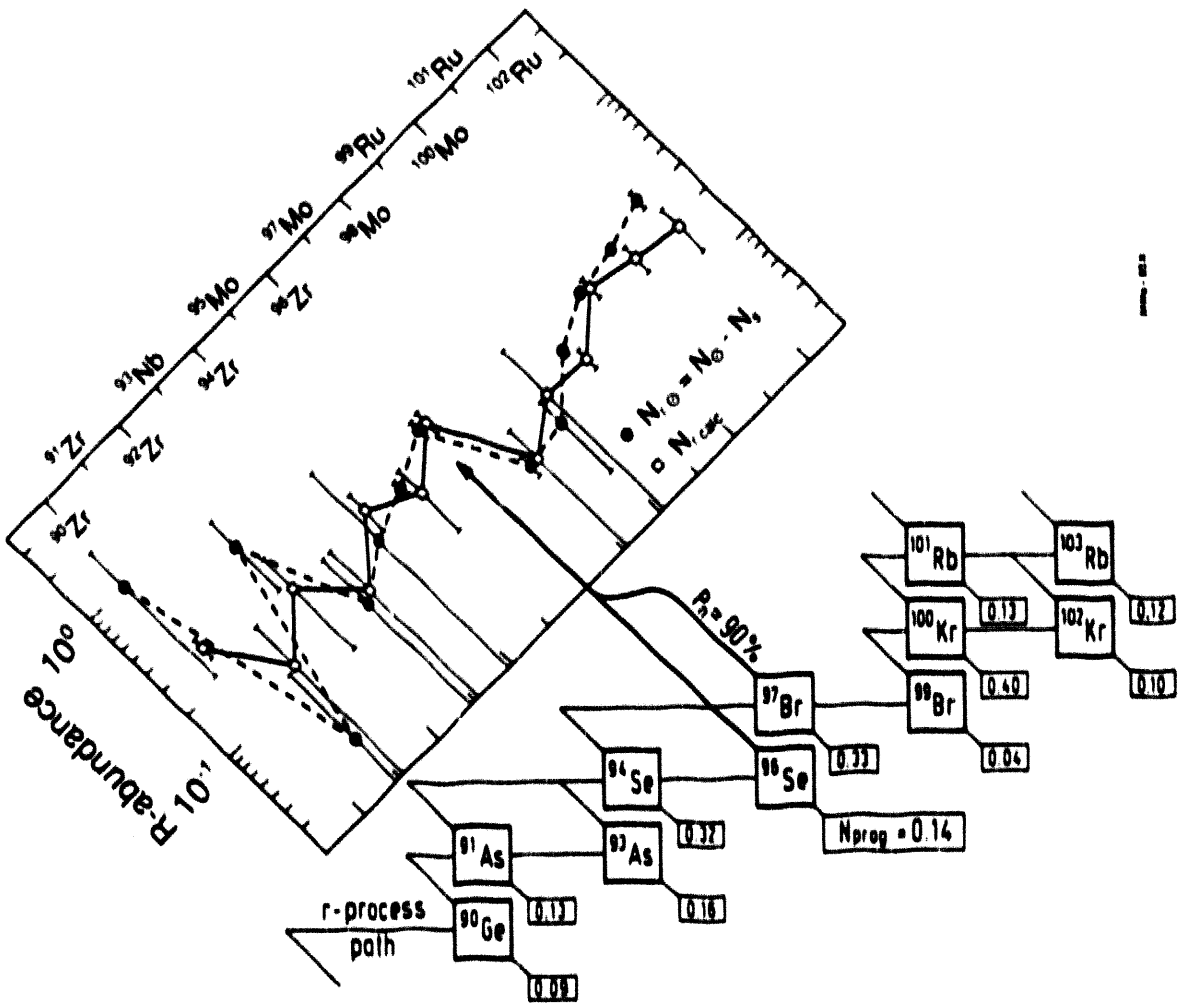

Fig. 8: Schematic view of the r-process path in the A≃95 region at freeze-out conditions [6]. The calculated r-abundances ($N_{r,calc}$) derived from the progenitor abundances ($N_{r,prog}$) by taking into account P_n-branching during β-decay back to stability, are compared to the solar r-process residuals ($N_{r,\odot} \simeq N_{\odot} - N_s$) from [9].

towards midshells at N=66, respectively N=104, and how and where the expected transition between deformation and sphericity occurs when approaching the N=82, respectively N=126 shell closures. This question is related to the sinusoidal deviations in the A≃110 and 170 pygmy-peak regions in our r-process calculations (see Fig. 1) when using the internally consistent nuclear-data set of Möller et al. [20,21,23]. As can be seen, for example, from Fig. 9 for the 107≤A≤126 mass region, presumably correlated with the too slow decrease of the B_ns far from stability (see Fig. 3), the model of Möller et al. predicts ground-state deformations up to N=80. An abrupt change from prolate to oblate shapes is observed at N=72 for 42≤Z≤46 isotopes N≃72 . Also the model of Pearson et al. [30] predicts very strong prolate deformations beyond N=66; however, the change to oblate

shapes occurs somewhat earlier, and spherical ground-state shapes are reached already around N=78. In contrast to the two recent microscopic models, the older mass formula of Hilf et al. [31] obtains a smoother decrease of (by construction only *prolate*) deformation as a consequence of the assumption of 'symmetry' relative to the N=66 neutron midshell. Having in mind, that both microscopic mass models predict the onset of deformation in the neutron-rich A≃100 region too early due to the missing N=56 spherical subshell (see, e.g. the discussions in [6,46]), one may suspect that deformed shapes will also be maintained too long beyond neutron midshell. Assuming somewhat lower quadrupole deformation would result in slightly lower B_n-values since these quantities are interrelated in microscopic models. For given n_n–T_9 conditions [6], this would shift the r-process path closer to β-stability and – in consequence – change the isotopic $N_r(Z)$-ratios in each Z-

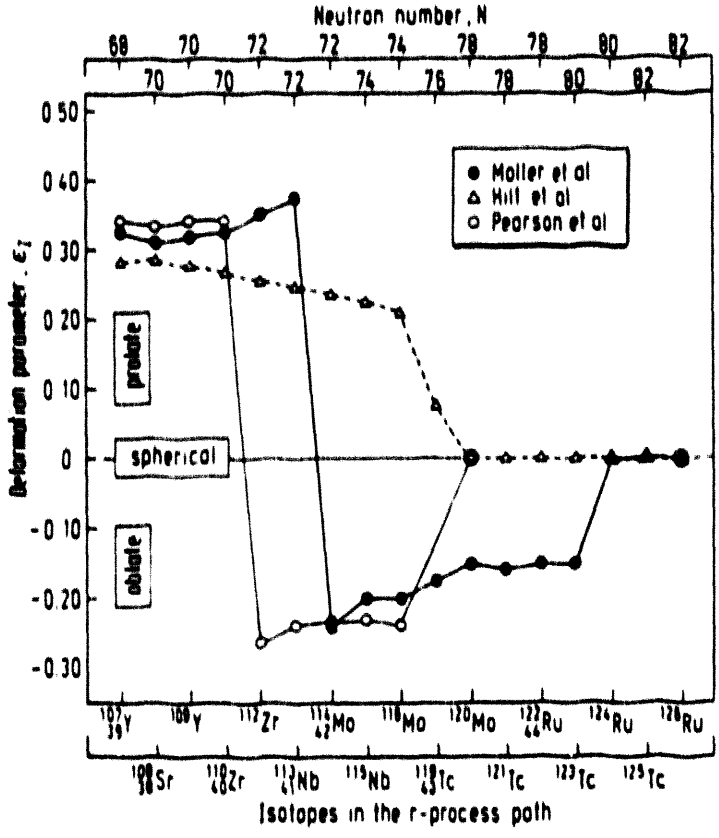

Fig. 9: Quadrupole-deformation parameter ϵ_2 for 'waiting-point' nuclei in the 107≤A≤126 mass region from three mass models [21,30,31]. Clear differences in the transition behaviour from strongly deformed near-midshell isotopes to spherical nuclei in the vicinity of the N=82 shell closure are observed, which are also reflected in the $T_{1/2}$ and P_n predictions. For example, when using the ϵ_2-value of Möller et al. [21], one obtains for $^{112}Zr_{72}$ (the last 'waiting-point' isotope before the A≃120 r-abundance trough) a $T_{1/2}$ of 45 ms; with the ϵ_2-value of Pearson et al. [30], the $T_{1/2}$ becomes 28 ms; and with the ϵ_2 of Hilf et al. [31], one obtains 21 ms. For a further discussion, see [6].

chain, giving the lighter isotopes a higher weight. In our specific case, this would cause a shift of the maximum abundances in the $37 \leq Z \leq 40$ chains from nuclei with (Z,N) to (Z,N-2) isotopes and an additional modulated by the corresponding changes in the $T_{1/2}$ and P_n-values (see, e.g. Fig. 22 in [6]). This results – at the same time – in a filling of the local $A \simeq 103$ deficiency and in a lowering of the $A \simeq 111$ 'spike'. A similar situation exists in the $160 \leq A \leq 175$ mass region involving 'waiting-point' isotopes beyond the N=104 midshell. Also here, lowering quadrupole deformation together with the interrelated changes in the B_n, $T_{1/2}$ and P_n would simultaneously result in a fill of the $A \simeq 160$ part of this deviation and lower of the $A \simeq 175$ 'spike'. In any case, one may speculate that both 'pygmy' $N_{r,\odot}$-peaks around $A \simeq 105$ and 165 have their origin in the β-decay properties of *deformed* progenitor isotopes with 'longer' $T_{1/2}$ than those predicted for spherical shapes. With this, the earlier interpretation of large fission contributions would no longer be necessary.

As was already discussed in Sect. 3 (see Figs. 1 and 3 in this paper, or Fig. 10 in [22]), the sinusoidal deviation in the $A \simeq 110$ region is followed by the r-abundance trough around $A \simeq 120$, which seems to originate from the assumption of a too strong N=82 shell 'southwest' of ^{132}Sn in the two microscopic models [21,30]. When using, instead, the much more simplistic mass formula of Hilf et al. [31], which by construction and maybe intuition gives a more smoothly decreasing B_n-trend towards N=82, the $A \simeq 120$ abundance trough will start to fill up. However, even then the $N_{r,calc}$ are too low in this mass region, on the average by a factor of five. Since possible astrophysical reasons for this deficiency – e.g. from a *fast s-process* [49] [50]– can probably be ruled out, the remaining abundance dip may be due to additional unexpected nuclear-structure effects. One possibility is 'longer' $T_{1/2}$ than predicted by the present QRPA model [23]. This seems not impossible around $A \simeq 120$, provided the respective 'waiting-point' isotopes exhibit some kind of shape coexistence as, for example, observed in the nearby, somewhat closer-to-stability $A \simeq 110$ $_{43}$Tc to Ru region. Partial hindrance of specific GT transitions connecting states with different shapes can so far not be treated properly by our QRPA shell-model approach, thus resulting, in almost all cases, in too short theoretical $T_{1/2}$. Therefore, it would be particularly important to continue *detailed* nuclear-structure studies mainly in the $100 \leq A \leq 125$ mass range, but also in the exotic $A \simeq 165$ rare-earth region, in order to learn about the shape changes beyond neutron midshells in very-neutron-rich isotopes.

5. Summary and outlook

In this paper, we have tried to demonstrate that there exists a close connection between macroscopic and microscopic nuclear physics on the one hand, and whatever constraints can be imposed on astrophysical r-process models on the other hand. The existence of so far only a few experimental data on 'waiting-point' isotopes at the N=50 and 82 magic neutron shells, together with recent mass- and shell-model predictions of unknown properties very far from β-stability, have considerably improved the nuclear-physics basis for r-process calculations. Summarizing the present situation, one may conclude that both the overall success in reproducing the r-abundance peaks and parts of the regions

in between as well as the local failures discussed above, seem to indicate new and partly unexpected nuclear-structure signatures of extremely neutron-rich isotopes, the vast majority of them not yet accessible in terrestrial but only in stellar laboratories. Therefore, many more experiments on gross properties, such as $T_{1/2}$, P_n and Q_β, respectively B_n, as well as a more profound understanding of the development of nuclear structures between stability and neutron drip line are required in order to further pin down the constraints on astrophysical parameters and stellar sites of rapid-neutron-capture nucleosynthesis. With future powerful ISOL and RIB facilities, fascinating perspectives will open up in the entwined fields of nuclear and astrophysics for experimentalists and theoreticians.

6. Acknowledgements

We want to acknowledge many stimulating discussions on nuclear structure with K. Heyde, G. Lhersonneau, F. Münnich, W. Nazarewicz, J.R. Nix, J.M. Pearson, I. Ragnarsson, W.B. Walters and N. Zeldes, and on astrophysical aspects with H. Beer, A.G.W. Cameron, M.F. El Eid, R. Gallino, W. Hillebrandt, W.M. Howard, F. Käppeler, B.S. Meyer, K. Takahashi and S.E. Woosley. We also thank W. Böhmer for his help in preparing this manuscript. This work was supported by grants from DFG (Kr 806/1), BMFT (06 MZ 106), GSI (MZ Kra K), and NSF (AST 89-13799).

References

[1] E.M. Burbidge, G.R. Burbidge, W.A. Fowler, F. Hoyle, Rev. Mod. Phys. **29** (1957) 547.

[2] P.A. Seeger, W.A. Fowler, D.D. Clayton, Ap. J. Suppl. **97** (1965) 121.

[3] W. Hillebrandt, Space. Sci. Rev. **21** (1978) 639.

[4] G.J. Mathews, R.A. Ward, Rep. Prog. Phys. **48** (1985) 1371.

[5] J.J. Cowan, F.-K. Thielemann, J.W. Truran, Phys. Rep. **208** (1991) 267.

[6] K.-L. Kratz, J.-P. Bitouzet, F.-K. Thielemann, P. Möller, B. Pfeiffer, Ap. J. (1992) in press.

[7] B.S. Meyer, W.M. Howard, G.J. Mathews, S.E. Woosley, R.D. Hoffman, Ap. J. (1992) in press.

[8] Proc. Workshop on the Science of Intense Radioactive Ion Beams (compiled by J.B. McClelland, D.J. Vieira), Los Alamos, LA-11964-C (1990).

[9] F. Käppeler, H. Beer, K. Wisshak, Rep. Prog. Phys. **52** (1989) 945.

[10] F.-K. Thielemann, M. Arnould, J.W. Truran, Advances in Nucl. Astrophys., Editions frontières, Gif sur Yvette (1987) 525.

[11] K.-L. Kratz, W. Ziegert, W. Hillebrandt, F.-K. Thielemann, Astron. Astrophys. **125** (1983) 381.

[12] K.-L. Kratz, F.-K. Thielemann, J. Phys. **G14** (1988) 742.

[13] G.J. Mathews, A. Mengoni, F.-K. Thielemann, W.A. Fowler, Ap. J. **270** (1983) 740.

[14] K.-L. Kratz, E. Krausmann, H. Krauss, T. Rauscher, H. Oberhummer, submitted to J. Radioanal. Nucl. Chem. (1992).

[15] K.-L. Kratz, H. Gabelmann, W. Hillebrandt, B. Pfeiffer, K. Schlösser, F.-K. Thielemann, Z. Physik **A325** (1986) 483.

[16] B. Ekström, B. Fogelberg, P. Hoff, E. Lund, A. Sangariyavanish, Physica Scripta **34** (1986) 614.

[17] R.L. Gill. R.F. Casten, D.D. Warner, A. Piotrowski, H. Mach, J.C. Hill, F.K. Wohn, J.A. Winger, R. Moreh, Phys. Rev. Lett. **56** (1986) 1974.

[18] K.-L. Kratz, H. Gabelmann, P. Möller, B. Pfeiffer, H.L. Ravn, A. Wöhr and the ISOLDE Collaboration, Z. Physik **A340** (1991) 419.

[19] K.-L. Kratz, F.-K. Thielemann, W. Hillebrandt, P. Möller, V. Harms, A. Wöhr, J.W. Truran, J. Phys. **G14** (1988) 331.

[20] P. Möller, J.R. Nix, W.D. Myers, W.J. Swiatecki, Nucl. Phys. **A536** (1992) 61.

[21] P. Möller, J.R. Nix, W.D. Myers, W.J. Swiatecki, At. Data Nucl. Data Tables, to be published.

[22] P. Möller, J.R. Nix, K.-L. Kratz, A. Wöhr, F.-K. Thielemann, Proc. Int. Symp. on Nuclear Physics in the Universe, Oak Ridge, Sept. 1992, IOP Publ., in press.

[23] P. Möller, J. Randrup, Nucl. Phys. **A514** (1990) 1.

[24] Proc. Specialists' Meeting on Delayed Neutron Properties, Birmingham, England, ISBN 07044 0926 7 (1987).

[25] V.I. Mishin, V.N. Fedoseyev, H.-J. Kluge, V.S. Letokhov, H.L. Ravn, F. Scheerer, Y. Shirakabe, S. Sundell, O. Tengblad and the ISOLDE Collaboration, Nucl. Instr. Meth. **B**, in press.

[26] H. Wollnik, Contribution to this Workshop.

[27] R.B. Moore, Contribution to this Workshop.

[28] J. Blomqvist, Proc. 4th Int. Conf. on Nuclei far from Stability, Helsingør, Denmark, CERN 81-09 (1981) 536.

[29] B. Fogelberg, Proc. Int. Conf. on Nuclear Data for Science and Technology, MITO, Japan, JAERI (1988) 837.

[30] J.M. Pearson, Y. Aboussir, A.K. Dutta, R.C. Naya, M. Ferris, F. Tondeur, Nucl. Phys. **A528** (1991) 1.

[31] E.R. Hilf, H. von Groote, K. Takahashi, Proc. 3rd Int. Conf. on Nuclei far from Stability, Cargese, France, CERN 76-13 (1976) 142.

[32] R.F. Casten, Contribution to this Workshop.

[33] W. Nazarewicz, Priv. Communication during this Workshop.

[34] F.-K. Thielemann, J.-P. Bitouzet, K.-L. Kratz, P. Möller, J.J. Cameron, J.W. Truran, Phys. Rep. (1992), in press.

[35] J.A. Winger, J.C. Hill, F.K. Wohn, R. Moreh, R.L. Gill, R.F. Casten, D.D. Warner, A. Piotrowski, H. Mach, Phys. Rev. **C36** (1987) 758.

[36] K.-L. Kratz, V. Harms, A. Wöhr, P. Möller, Phys. Rev. **C38** (1988) 278.

[37] A. Staudt, E. Bender, K. Muto, H.V. Klapdor-Kleingrothaus, At. Data Nucl. Data Tables **44** (1990) 79.

[38] K. Heyde, Proc. Int. Workshop on Nuclear Structure in the Zirconium Region, Bad Honnef, Germany, Res. Rep. in Physics (1989) 1.

[39] G. Nyman, B. Jonson, Priv. Communication (1990).

[40] SIS/ESR Proposal No. 56, GSI (1987).

[41] J.C. Hardy, Contribution to this Workshop.

[42] Proc. Int. Workshop on Nuclear Structure in the Zirconium Region, Bad Honnef, Germany, Res. Rep. in Physics (1989).

[43] G. Lhersonneau, K.-L. Kratz, J. Äystö, H. Gabelmann, J. Kantele, B. Pfeiffer, the OSTIS and ISOLDE Collaborations, Proc. 6th Int. Conf. on Nuclei far from Stability, Bernkastel-Kues, Germany, IOP Publ. (1992) in press.

[44] A. Etchegoyen, P. Federman, E.G. Vergini, Phys. Rev. **C39** (1989) 1130.

[45] G. Lhersonneau, H. Gabelmann, N. Kaffrell, K.-L. Kratz, B. Pfeiffer, K. Heyde, Z. Physik **A337** (1990) 143.

[46] A. Wöhr, H. Gabelmann, G. Lhersonneau, B. Pfeiffer, K.-L. Kratz and the ISOLDE Collaboration, Proc. 6th Int. Conf. on Nuclei far from Stability, Bernkastel-Kues, Germany, IOP Publ. (1992) in press.

[47] E. Arnold, W. Borchers, U. Georg, M. Keim, A. Klein, P. Lievens, R. Neugart, R.E. Silverans, L. Vermeeren, Proc. 6th Int. Conf. on Nuclei far from Stability, Bernkastel-Kues, Germany, IOP Publ. (1992) in press.

[48] C.L. Harper, L.E. Nyquist, C.-Y. Shih, H. Wiesmann, Proc. Int. Symp. on Nuclear Astrophysics, Baden/Wien, Austria, MPA/P4 (1990) 138.

[49] R. Gallino, H. Beer, M. Busso, L. Corcione, C.M. Raiteri, Proc. 6th Workshop on Nuclear Astrophysik, Ringberg Castle, Germany, MPA/P5 (1991) 48.

[50] A.G.W. Cameron, F.-K. Thielemann, J.J. Cowan, Phys. Rep. (1992) in press.

Future Uses of Radioactive Ion Beams in Materials Science

HEINZ HAAS
PPE Division, CERN, CH-1211 Geneve 23
and the ISOLDE Collaboration, CERN

Abstract

A short summary of the present use of radioactive beams for condensed matter research in the ISOLDE program is presented. Future uses of high intensity and high energy radioactive ion beams beyond the scope of the present projects are discussed. As examples the study of diffusion in immiscible systems by deep implantation of radiotracers, the deposition of decelerated ion beams on surfaces, the technique of beta-NMR following tilted-foil nuclear polarization and the transmutation doping of wide-bandgap semiconductors are presented. The major requirements for use of a future radioactive ion beam factory in the field of materials research are derived. Particularly important is a wide energy range from 20keV to 500keV/A, a frequent recurrence of a given beam and a suitable infrastructure.

1. Introduction

Radioactive nuclei from various sources have been used in condensed matter investigations for a long time. The earliest application of radiotracers was the investigation of diffusion processes /1/. Radioactive ^{31}Si nuclei for transmutation doping of silicon are of great technological importance. Nuclei are now being routinely used as probes of their environment in metals and semiconductors via various methods. More recently these techniques have also been applied to the study of complex biomolecules, surfaces and interfaces. This off-spring of nuclear physics research has been steadily expanding. With the routine availability of high purity radioactive ion beams from isotope separators the possibilities for such investigations have been greatly expanded, allowing technologically ever more demanding experiments.

In particular the use of on-line isotope separation at the CERN / ISOLDE facility has demonstrated the great potential for applications. Since the first solid state physics experiments at this facility some 15 years ago the number of users out of the materials research field has grown steadily to some 100 at the time of the shutdown of the SC / ISOLDE separators in December 1990. Up to one third of the beamtime at this installation was finally dedicated to such work. The applications to condensed matter studies will also be an important part in the research program of the new Booster / ISOLDE facility at CERN /2/, that has started operation recently.

If one then plans a high intensity radioactive ion beam (RIB) facility for the next decade, it appears clear that the applications in materials science are going to be an important research field there too. The future user of a RIB factory would be able to utilize the higher beam intensities and energies available there. The present paper will therefore, after a short summary of the ongoing ISOLDE program in condensed matter physics, concentrate on novel uses of radioactive ion beams. In order to demonstrate the conditions posed on a RIB facility for condensed matter studies four examples are selected from the fields of tracer diffusion, surface physics, nuclear probe studies and device research.

2. The ISOLDE solid state physics program

Nuclear methods allow the investigation of impurities in condensed matter at a very low concentration. The intense pure beams of radioactive ions from ISOLDE are ideal for such research as evidenced by the increasing number of users in this field. The solid state experiments take advantage of the practically unlimited choice of isotopes at ISOLDE which can be implanted into the matrix under investigations. During the last three years of running of the ISOLDE-2 and ISOLDE-3 separators at the CERN-SC condensed matter experiments used yearly about 800 hours of beamtime, more than one third of the total running time.

As may be seen from the summary presented in Table 1, the major effort of the solid state program is in the study of impurity implantation into semiconductors, a process of high technological importance. A whole spectrum of modern techniques is being used by the ISOLDE experiments, including tracer diffusion (TD), Mössbauer spectroscopy (MS), emission

channeling/blocking, perturbed angular correlation (PAC), deep-level transient spectroscopy (DLTS) and conversion electron spectroscopy (CESVEC).

Most of these techniques, together with low temperature nuclear orientation (NO), are also being employed to investigate final lattice sites of implanted atoms as well as magnetism and diffusion in metals. A relatively new field of study is surfaces and interfaces.

3. Diffusion in highly immiscible systems

Diffusion studies with the radioactive tracer technique, whether they are followed by sectioning of the sample or by some sort of depth sensitive radiation counting, require a certain solubility of the diffusing element for the development of the characteristic diffusion profile. In cases where strong forces keep the impurity atoms at the sample surface these methods are not applicable. It is here where deep implantation could find a very interesting application. Typical implantation profiles for a wide range of implantation energies are shown schematically in Fig.1. It may be noted that the degree of localization in a predetermined depth improves with energy on a relative scale, even though the absolute width of the range distribution due to straggling naturally grows with energy.

The system of isolated impurity atoms at a specific depth lends itself perfectly to the investigation of diffusion even for immiscible systems. Such systems produced by forced alloying are of increasing technological importance. Their systematic study at high implantation depth and very low concentration could lead to a better understanding of the processes occurring in the materials with practical applications.

In order to illustrate the great potential of the proposed diffusion technique, the study of astatine diffusion in alkali metals shall be discussed. This is obviously a system far from any technological interest, but in earlier experiments we have found indications for such an unusual behaviour, that a careful study appears to be highly rewarding. Part of the existing evidence can be seen in the alpha spectra of Fig.2, measured after implantation of ^{205}Fr into K. The broad energy distribution of the alphas from ^{205}Fr decay is characteristic for the diffusion profile of these atoms in the matrix. The difference of the two spectra as function of time after activation can be completely understood in this way. A careful

measurement of such spectra as function of time and temperature has allowed us to extract reliable diffusion coefficients for Fr in several alkali metals. As the longest living Fr isotope has a halflife of only 22 minutes, this element can only be studied on-line to a production facility. The results are well in accord with present ideas about diffusion in simple metals. The sharp alpha line in the spectra of Fig.2 is actually the unusual feature. It stems from the decay of the radioactive daughter of ^{205}Fr, ^{201}At. Since these daughter nuclei are produced virtually at the site of the parent Fr nucleus, one would expect a broadened energy distribution as well. The sharp line spectrum actually shows unambiguously that the At nuclei have reached the surface of the sample before they decay and are trapped there. From similar data on ^{221}Fr, where the halflife of the daughter ^{217}At isotope is only 30ms, we could estimate that the diffusion constant for At in K is at least three orders of magnitude larger than that for Fr, itself enhanced by a factor of 10 over self diffusion. Naturally this unexpected phenomenon of a new type of fast diffusion calls for a systematic measurement of the diffusion constant in a wide temperature range.

Since At has a strong tendency for binding to the sample surface, the measurement of diffusion profiles following deep implantation using alpha spectroscopy as a depth profiling technique is virtually the only possibility. One would have to implant the At isotopes with energies up to 500keV/A. A typical evolution of the alpha spectra expected from such a measurement is shown in Fig.3. Measuring with different halflife isotopes implanted at different depths the diffusion constants could be determined over at least 8 orders of magnitude. If not the alpha particles but the heavy recoil nuclei could be employed for depth profiling, another 4 orders of magnitude could become accessible, coming close to the best diffusion data available to date for any system.

The typical requirements for the proposed experiment are beams in the energy range of 20keV to 100MeV for the isotopes ^{199}At (7s) and ^{209}At (5h) and of 1MeV to 100MeV for ^{217}At (30ms). The needed intensities for the shortlived isotopes are typically 10^5 ions per second, while measurements with the longlived ^{209}At could be performed off-line, so that collections for a short time would be sufficient, making use of high intensity beams.

4. Deposition of ion beams on surfaces

Surfaces and interfaces are a field of great interest in several areas of physics and chemistry. For the study of pure surfaces or for monolayer coverages a wide variety of experimental methods has been developed. Very sparse data, however, exist for isolated impurities or defects on surfaces. It therefore would be quite important to get microscopic information on electronic and lattice structure for such systems.

In recent years the corresponding problem for impurities and defects in bulk metals has been very successfully attacked with the use of nuclei as probes. Particularly experiments with perturbed angular correlation (PAC) and Mössbauer spectroscopy (MS) have in this case given detailed insight. Both techniques require as little as 10^{11} atoms in favorable cases. Virtually isolated probe atoms can thus be investigated on a surface of typically 1 cm^2, certainly much less than monolayer coverages ($10^{15}/cm^2$). The application of these methods to study surfaces therefore can give unique microscopic information.

The nuclear techniques PAC and MS should also be particularly well suited for the investigation of interfaces, where the standard surface techniques are not applicable at all. Both the lattice structure and the magnetism at interfaces are a topic of great present interest. Well defined interfaces may e. g. be produced by controlled coverage of previously characterized surfaces.

The central problem in the use of radioactive atoms for the study of surfaces is the sample preparation and the clean deposition of the probe nuclei on the surface. The use of an isotope separator, particularly in on-line mode with a production accelerator, allows to obtain clean beams of radioactive isotopes, in most cases even without contamination from stable isotopes. A procedure for depositing these on surfaces by evaporation after implantation into an oven has been tested at the ISOLDE-2 facility for Cd, In and Rb.

As a pilot project PAC experiments could be performed at ISOLDE with ^{79}Rb, ^{111m}Cd and ^{111}In /2,3,4/, complementary to laboratory experiments at Konstanz with ^{111}In using chemical techniques /6,7,8/. A series of experiments has allowed us to follow the history of the Cd and In adatoms on Pd(111) from the first landing site on the terraces to their

final incorporation into the lattice /5/. In Fig.4 the identified sites are shown schematically. At quite low temperatures, 100 K already, surface diffusion on the terraces sets in and the atoms move to the ledges. At higher temperatures diffusion along the ledges occurs, leading to binding at kink sites. The next stage observed is the incorporation of the adatoms into the ledges and finally into the terraces. Thus, all the surface diffusion steps could be followed in a microscopic way via the measurement of the electric field gradient by PAC. It has thus been established that the PAC technique is able to characterize isolated impurity sites on metal surfaces. The number of systems investigated up to now is very small, however, calling for further systematic measurements. For the new ISOLDE facility at the CERN PS-Booster a beamline in UHV standard and a dedicated surface physics chamber has been constructed and successfully tested.

The scope of possible uses of nuclei for surface studies would be greatly enhanced if a direct deposition of the radioactive ion beam from the isotope separator on surfaces could be accomplished. This would furthermore open up many new possibilities for creating thick layers of radioactive nuclei e.g. as targets for nuclear reactions, since the sputtering does not limit the accumulation as it does at energies above several 100eV.

With the high beam quality from an isotope separator it should in principle be possible to slow down the radioactive ion beam to a few eV and deposit it on a surface. This possibility has therefore been investigated theoretically. The blow-up of the beam spot size generally accompanying deceleration can be largely avoided if the retardation is performed in a very strong magnetic field that can coil up the ion path. The beam-optical calculations performed in collaboration with B. Moore, Montreal, have confirmed this idea. The designed deceleration system is shown in Fig.5. The present concept is for the use of an available 10T magnet and the surface physics chamber installed at the ISOLDE facility.

To demonstrate that "soft landing" has occurred one would deposit ^{111}In ions on Pd(111), where the PAC signature of all surface sites is known from the previous experiments. The beam intensity needed for such a test would be quite small. It must be possible, however, to work with sufficiently small acceleration voltage to reduce the effects of ion

optical aberrations and to limit the voltages within the deceleration device to reasonable values. We have chosen 20keV as the incoming beam energy in our test calculations.

5. Beta-NMR with tilted-foil polarization

Beams of polarized radioactive nuclei open the possibility for interesting investigations in several fields. In addition to possible uses in nuclear beta decay studies, such beams would be well suited for beta-NMR studies with shortlived isotopes. The combination of a RIB facility with the tilted-multifoil method allows the production of such nuclei, their subsequent polarization and then measurement of the hyperfine interaction of the nuclear moments with the fields of their surroundings using the beta-NMR technique. The tilted foil polarization technique has been used successfully to induce in-beam polarization of nuclei at the several percent level /9/.

If an ion beam is passed through a very thin foil, tilted with respect to the beam direction at an oblique angle, the electronic states of the outgoing ions are polarized. Polarization is initially induced in the orbital motion of the ionic electrons by a surface interaction on exit of the ion from the foil. During flight in vacuum some of this electron polarization (which is in the direction n # v= x, where n is the unit vector perpendicular to the outgoing surface of the foil and v is the ion velocity vector) is transferred via hyperfine interaction to the nucleus. By a successive passage of several such foils, interspaced with regions of free flight to allow a significant nuclear precession around the total angular momentum F=I+J in flight between successive foils, the effect can be enhanced. The expectation is that rather sizeable nuclear polarizations can be obtained for a wide variety of elements.

Tilted foil nuclear polarization has also been used in the past for the measurement of signs of quadrupole moments of high spin isomers /10/ and, recently, in a measurement of parity violation in the 17/2$^-$ isomer of ^{93}Tc, again a high spin state /11/. In those experiments the ion velocity was generally in the range 0.01c-0.03c. Conditions relevant to experiments at a radioactive beams facility would differ substantially from these earlier experiments. Nuclei of generally lower nuclear spin I would be used, requiring only a small number of foils. The lower ion

velocity in the range of 50 to 100keV/A should lead to a larger polarization, though this expectation has not been verified by experiments up to now. The smaller size, angular divergence and energy spread of the radioactive beam and the typically higher count rates should also render the experiments easier.

The very simple experimental setup is sketched in Fig.6. The polarized ions are stopped in a crystal generally cooled to low temperature in order to increase the spin-lattice relaxation time. A holding magnetic field, best produced by a superconducting magnet, is also applied parallel to the polarization direction. For radioactive nuclei, the polarization is most conveniently determined by measuring the angular distribution of the emitted beta particles. It has the form $W(\Theta) = 1 + B_1 A_1 \cos(\Theta)$, where Θ is the angle with respect to the polarization direction. An rf field is applied to the stopped, polarized nuclei and tuned until the polarization (and hence the asymmetry) is destroyed. The frequency of this NMR resonance can be measured to high precision.

Beta-NMR has the potential to become a very powerful tool for the investigation of condensed matter. It would complement well the other nuclear probe techniques available at a radioactive beams facility for studies of the environment of implanted nuclei in solids. Until now only a few probe nuclei have been useful for this method, due to the difficulty in producing polarized nuclei. The only somewhat universal technique is capture of polarized neutrons. Experiments on ^{8}Li, ^{12}B, ^{20}F, ^{110}Ag and ^{116}In have been successful /12/. The usefulness of this technique for solid state applications is, however, seriously limited by the fact that the samples have to contain a large amount of the element to be studied, thus forbidding the investigation of dilute impurities, otherwise characteristic for the nuclear methods. The exceptions are ^{12}N and ^{12}B, the only nuclei suitably polarized following nuclear reactions /13/. Nevertheless the few applications of the beta-NMR method have demonstrated the power of NMR coupled to nuclear detection. Pioneering studies of nuclear relaxation, diffusion, radiation defects and glass structure have been performed.

With the development of the tilted foil technique the possibility of obtaining polarized ion beams will open up the wide spectrum of isotopes available at a RIB facility for applications of the beta-NMR technique. Clearly the strength of the method lies with the lighter elements, where

spin-lattice relaxation times are sufficiently long for investigations over a wide temperature range. For these technologically important implants generally no probe atoms suitable for the other nuclear methods like MS, PAC or PAD are available. It is difficult, however, to predict which isotopes will be most suitable for condensed matter studies. Exploratory measurements of the beta asymmetries for several of the most interesting cases are necessary before one can discuss a solid state research program with the new technique in detail.

Measurements of the spin-lattice relaxation or Knight shift for light elements in metals are still very scarce. Together with the hyperfine fields in the few ferromagnets they would give direct information on the conduction electron density at the impurity site, one of the few ways to test band structure calculations on a microscopic scale.

The elements of the first two periods are especially important as dopants and impurities in presently used semiconductors and even more so in diamond, one of the semiconductors of the future. Beta-NMR could give direct information about electronic and lattice structure, in particular since also the nuclear quadrupole interaction can be measured with NMR accuracy. The further development of radioactive beams of the reactive light elements (B,C,N,O, and Al,Si,P,S) would be of great significance in this respect. Especially the mirror decays of ^{11}C, ^{13}N, ^{15}O, ^{17}F, ^{19}Ne, ^{21}Na, ^{23}Mg, ^{25}Al and ^{27}Si are well suited for this new technique.

As a representative example of an actual experiment one could consider the investigation of implantation of C and Si into SiC by way of the electric field gradients acting on the probe nuclei ^{11}C and ^{27}Si. For both elements there are actually no stable isotopes at all that would allow the measurement of nuclear quadrupole coupling constants. One therefore would have to test the technique first by implantations into non-cubic solids like graphite. Then a series of measurements of the beta-NMR pattern at different temperatures could be performed and interpreted to determine the defect configurations present. Later a series of double resonance experiments with the stable nuclei of the matrix could give further details on the lattice sites taken up after implantation. The silicon atoms occupying carbon sites (antisite defect) e.g. would show a stronger coupling to the matrix Si spin system than the substitutional atoms. One would probably also investigate a few samples with different

doping levels to detect the influence of charged lattice defects. Such a program would typically run for 2-3 years, depending on the suitability of the probe nuclei chosen and the significance of the initial results.

The required beam energies are about 100keV/A, with a large uncertainty in the present expectations, however. Various test runs to find the optimal conditions for the experiment would certainly have to be made. Intensities of 10^7 ions per second should be largely sufficient.

6. Transmutation doping of wide-bandgap semiconductors

Much of the interest in the studies of implantation into semiconductors comes from the central role this technique presently plays in device manufacture. To date radioactive beams have only been applied to study implantation in order to obtain a microscopic insight into the atomic processes. Radioactive transmutation doping of silicon following neutron capture, on the other hand, is a standard procedure in semiconductor technology. It has thus been realized quite early, that radioactive implants for doping semiconductors would offer special features like site specificity /14/.

There has been a long standing scientific and technological interest in the use of wide-bandgap semiconductors like diamond and SiC for device manufacture. In principle these would offer sizeable advantages for high power, frequency and temperature applications. With the recent progress in thin film growth of these materials /15/ the interest has grown very large. Actually the first devices from these materials have been produced.

One of the major problems in the use of wide-bandgap semiconductors is the reliable doping of these materials. At least for diamond the application of implantation is the only possible route. Even high energy implantation has been suggested /16/. An abundant research material has been collected /17,18/, and it is now clear that the residual radiation damage after dopant implantation and annealing does strongly affect the electrical properties /19/.

The technique to dope diamonds via nuclear transmutation following radioactive beam implantation is at present obviously highly speculative. Since self-implantation even to a very high dose is possible into diamond at elevated temperature, one would implant C and Si isotopes into the

crystal at the right depth and structure required for the wanted electronic device. These would then decay to the dopant atoms in situ, eliminating the strong lattice damage generally accompanying the impurity implantation process. The most suitable isotopes for this purpose would be ^{11}C, decaying to B with a halflife of 11min, and ^{31}Si, decaying to P in 2.6hrs. Due to the short halflives only small areas could be doped at a time. Clearly the physics underlying the proposed procedure would have to be studied first. At least at this stage areas of $1mm^2$ should be highly sufficient.

The beams required for doping purposes would by necessity have to be quite intense. As the expected intensity of ^{11}C at a facility using 100μA protons should exceed 10^{12} ions per second, however, doping levels of $10^{18}cm^{-3}$ in a 1μm thick layer, much larger than required for most purposes, could be achieved within a time much shorter than the halflife of ^{11}C. Beams of ^{31}Si are much harder to produce, but 10^{10} per second should be within reach. Since the energies of the implanted beams would have to be only very modest, a simple high voltage platform would suffice for post-acceleration in most cases. Such a device has been installed at ISOLDE for a variety of purposes. For future device production it could be very important to have extremely small spot sizes for an economical use of the precious radioactive ions. A specially designed (magnetic) fine focussing system should be considered. Also it is not quite clear whether on-line production is the most efficient path to a ^{31}Si beam. Off-line production in a batch mode should at least be considered, because it would allow a greater flexibility in choice of the optimal target material. One severe problem in the use of radioactive beams for doping could be the requirement of beam purity. Stable contaminants and the use of molecular beams are not allowed.

7. Conclusions

Materials research will certainly be an important topic at any RIB facility. For a wide program it is obviously essential to have as many isotopes as possible available for the different experimental requirements. The purity of the beams from stable contaminants is of great importance even for the methods that use nuclear counting.

Undoubtedly most of the applications will call for the standard beam energies from an isotope separator between 20 and 200keV. There are, however, a number of interesting applications for accelerated beams up to 500keV/A. At present it is hard to imagine uses of beam energies in the nuclear regime, 5MeV/A, for condensed matter studies.

Important for any research in materials science is also the infrastructure existing on site. Radioactive laboratories, clean rooms, etc. should be available. A good vacuum at the beam port can be essential for some cases. Very often experiments in materials science require the use of the same type of beam quite regularly. A repetition period of more than 4 months makes most work in this field intolerably ineffective.

8. References

/ 1 / J. Groh und G. Hevesy, Ann. der Physik 63 (1920) 85

/ 2 / E. Kugler, D. Fiander, B. Jonson, H. Haas, A. Przewloka, H.L. Ravn, D.J. Simon, K. Zimmer and the ISOLDE Collaboration, Nucl. Instr. and Meth. B70 (1992) 41

/ 3 / E. Hunger, H. Haas, V. Marx and M. Menningen, in: Nuclear Physics Applications on Material Science, Eds. E. Recknagel, J. C. Soares (Kluwer Academic, 1988) p. 429

/ 4 / E. Hunger, H. Haas and H. Grawe, Hyperfine Interactions 60 (1990) 999

/ 5 / E. Hunger and H. Haas, Surf. Sci. 234 (1990) 273

/ 6 / T. Klas, J. Voigt, W. Keppner, R. Platzer, R. Wesche and G. Schatz, Hyperfine Interactions 34 (1987) 577

/ 7 / R. Fink, R. Wesche, T. Klas, G. Krausch, R. Platzer, J. Voigt, U. Wöhrmann and G. Schatz, Surf. Sci 225 (1990) 331

/ 8 / J. Voigt, X.L. Ding, R. Fink, G. Krausch, B. Luckscheiter, R. Platzer, U. Wöhrmann and G. Schatz, Phys. Rev. Lett. 66 (1991) 3199

/ 9 / W.F. Rogers, D.L. Clark, S.B. Dutta and A.G. Martin, Phys. Lett. B177 (1986) 293

/ 1 0 / E. Dafni, J. Bendahan, C. Broude, G. Goldring, M. Hass, E. Naim, M.H. Rafailovich, C. Chasman, O.C. Kistner and S. Vajda, Nucl. Phys. A443 (1985) 135

/ 1 1 / C. Broude, G. Goldring, M. Hass, N. Takahashi, S. Hoffmann, F.P. Hessberger and V. Ninov, Z. Physik A336 (1990) 134

/12/ H.Ackermann, P.Heitjans and H.-J.Stoeckmann, Hyperfine Interactions 24/26 (1985) 395
/13/ T.Minamisono et al., Hyperfine Interactions 15/16 (1983) 547
/14/ G. Weyer et al., Phys. Rev. Lett. 44 (1980) 155
/15/ R.F. Davis and J.T. Glass, Advances in Solid State Chemistry 2 (1991) 1
/16/ A.M. Zaitsev, Nucl. Instr. and Meth. B62 (1991) 81
/17/ R.E. Clausing, L.L. Horton, J.C. Angus and P. Koidl, Eds., Diamond and Diamond-like Films and Coatings, NATO ASI Series B, Vol. 266, Plenum Press (New York) 1991
/18/ J.T. Glass, R. Messier and N. Fujimori, Eds., Diamond, Silicon Carbide and Related Wide Bandgap Semiconductors, MRS Symposium Proceedings, Vol. 162, Materials Research Society (Pittsburgh) 1990
/19/ J.F. Prins, Materials Science Reports 7 (1992) 271

Table 1: The ISOLDE Solid State Program -techniques, isotopes, groups and topics

1. Moessbauer Spectroscopy ^{57}Mn ^{119}In ^{119}Sb
(Aarhus-CERN-Groningen-Leuven)
Defects in metals,
Impurities and defects in semiconductors

2. Perturbed Angular Correlation ^{73}As ^{77}Kr ^{79}Rb ^{111m}Cd ^{199m}Hg
(Berlin-Bonn-CERN-Erlangen-Konstanz-Lisbon-Munich)
Impurities in metals
Defects and impurities in semiconductors
Adatoms and diffusion on surfaces
Motion of biomolecules

3. Channeling ^{8}Li ^{112}In ^{205}Fr
(CERN-Goteborg-Konstanz-Leuven)
Implantation into semiconductors and metals

4. Tracer Diffusion ^{121}Te ^{195}Au ^{221}Fr
(Argonne-Berlin-CERN-Kuwait-Muenster)
Bulk diffusion in semiconductors and metals
Grain boundary diffusion

5. Beta - NMR ^{8}Li ^{23}Mg
(CERN-Goteborg-Mainz-Marburg-Oxford-Rehovot)
Nuclear relaxation in semiconductors

6. Conversion Electron Spectroscopy ^{73}Ga ^{119}Sb
(Aarhus-CERN-Zuerich)
Electronic structure at impurities

7. Deep Level Transient Spectroscopy ^{195}Au
(Aarhus-Erlangen)
Impurities in semiconductors

8. Surface Desorption ^{47}Ca ^{105}Cd
(Saclay-Berlin-CERN-Tel Aviv)
Nuclear recoil from surfaces

9. Low Temperature Nuclear Orientation many
(Berlin-Bonn-CERN-Daresbury-Delft-Gent-Leuven-Lyon-Manchester-Munich-Orsay-Oxford-Paris-Strasbourg)
Nuclear relaxation in metals

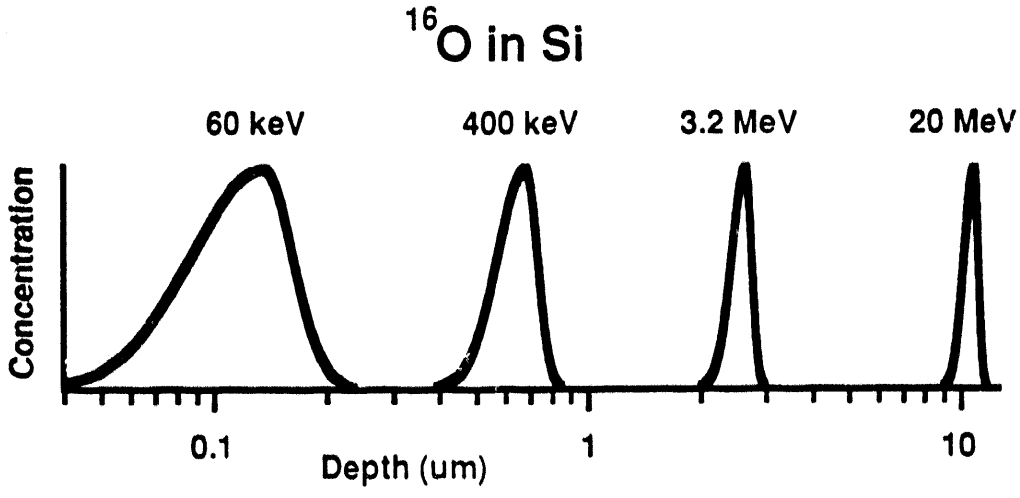

Fig.1: Typical range profiles for implantation into solids at various energies. It is apparent that a well defined depth of order μm can be obtained at typically 50keV/A

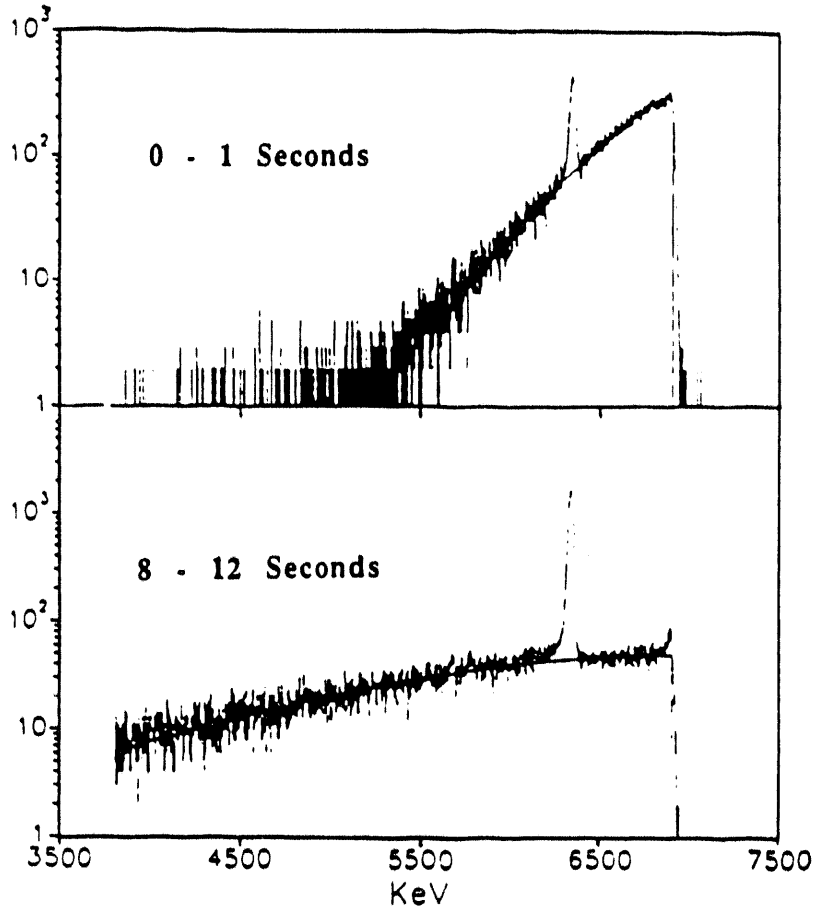

Fig.2: Alpha spectrum of ^{205}Fr at different times after implantation into potassium at 320K

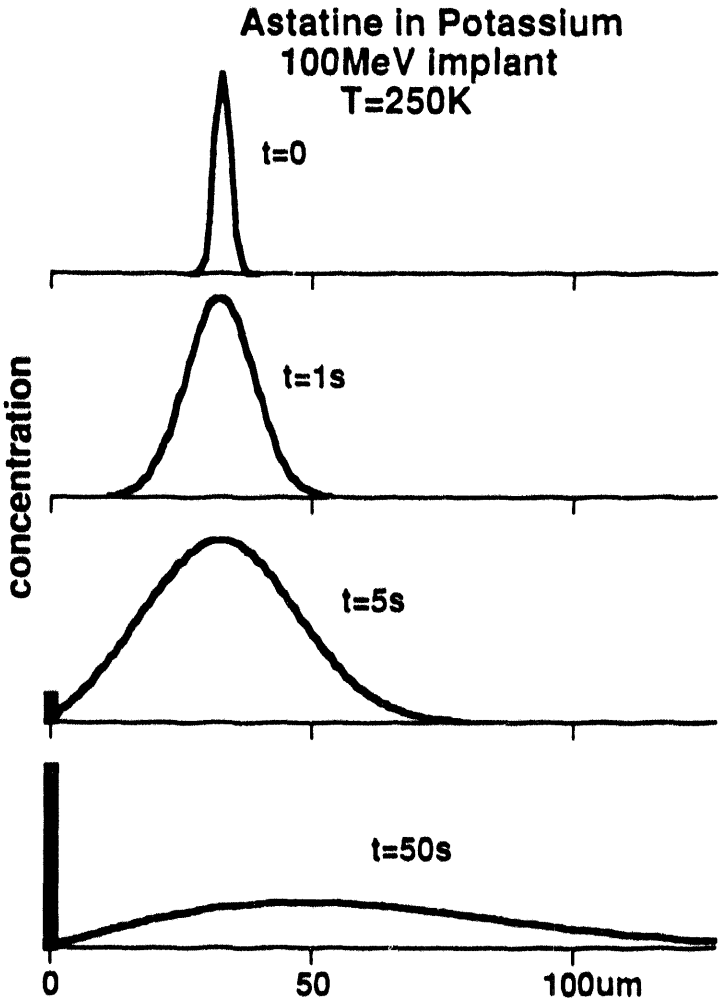

Fig.3: Expected diffusion profile for At in K following implantation at 100MeV

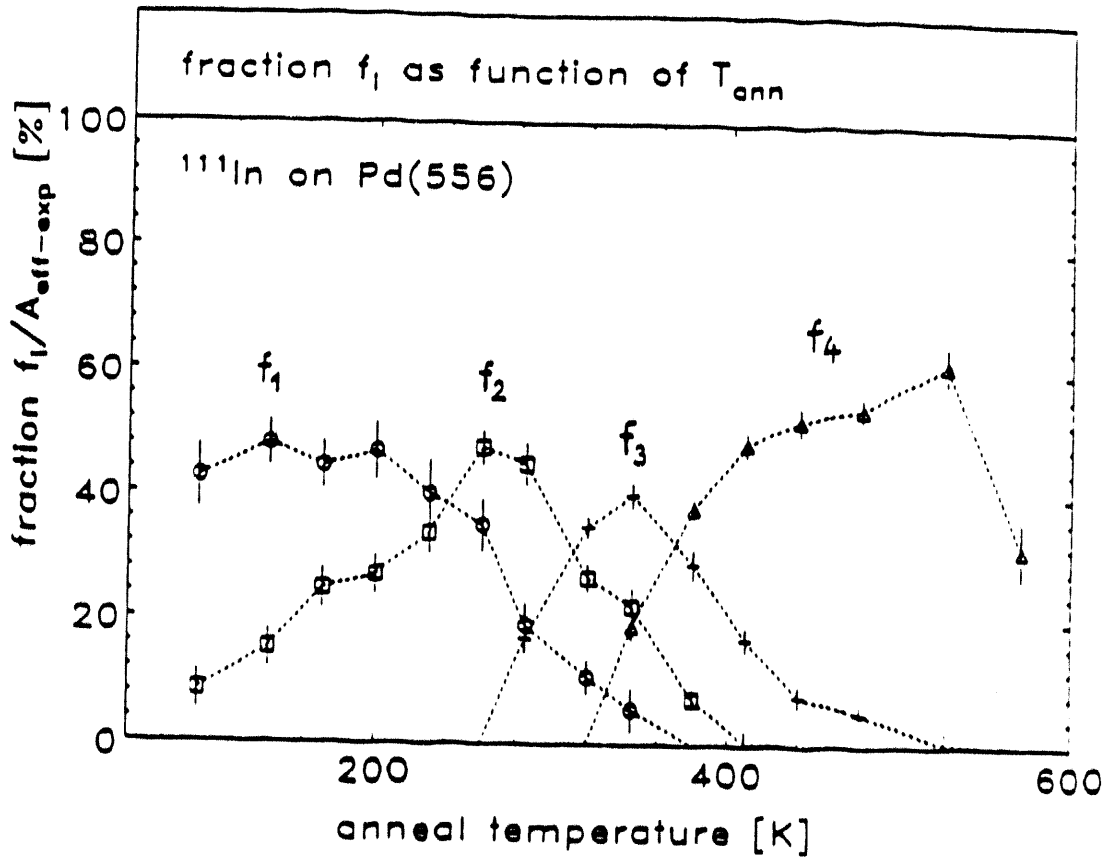

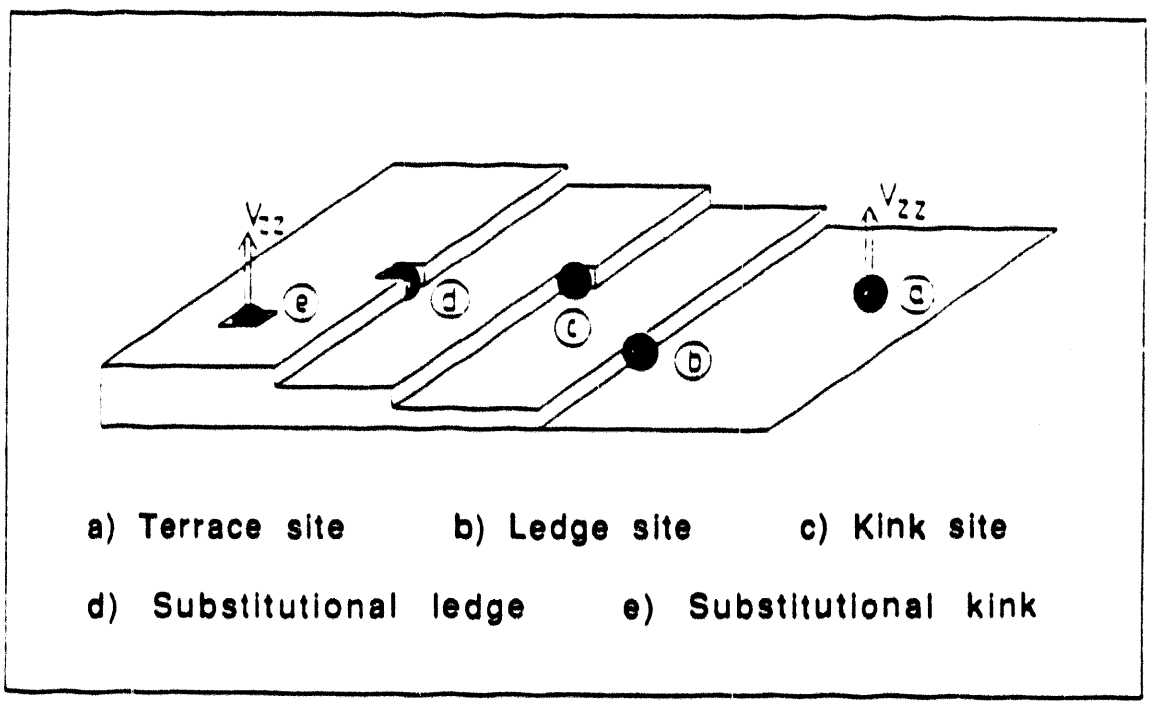

Fig.4: Identified surface sites occupied by In and Cd adatoms on Pd(111) (Bottom) and fractional occupation on a vicinal surface as function of annealing (Top). The fractions f_1 to f_4 correspond to sites b to e

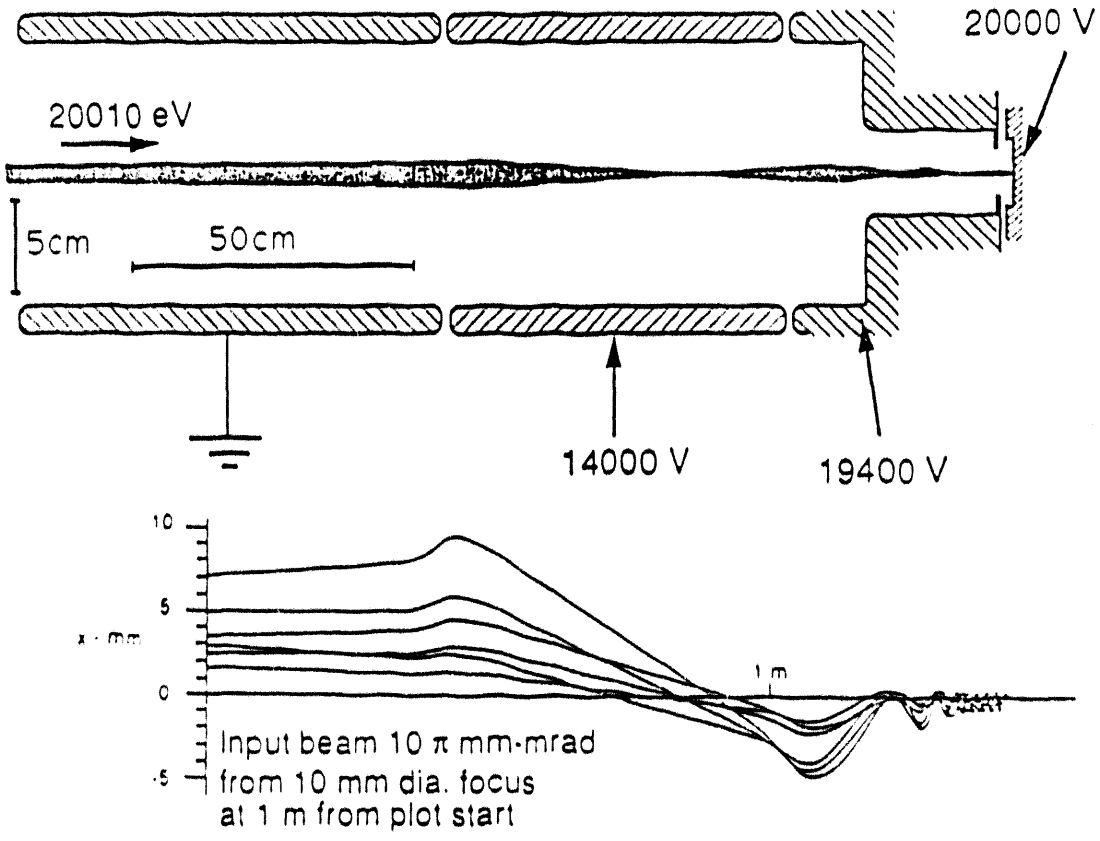

Fig.5: Ion optical system for "soft landing" experiment. Top: Electrode configuration; Bottom: Ion trajectories into 10T magnet

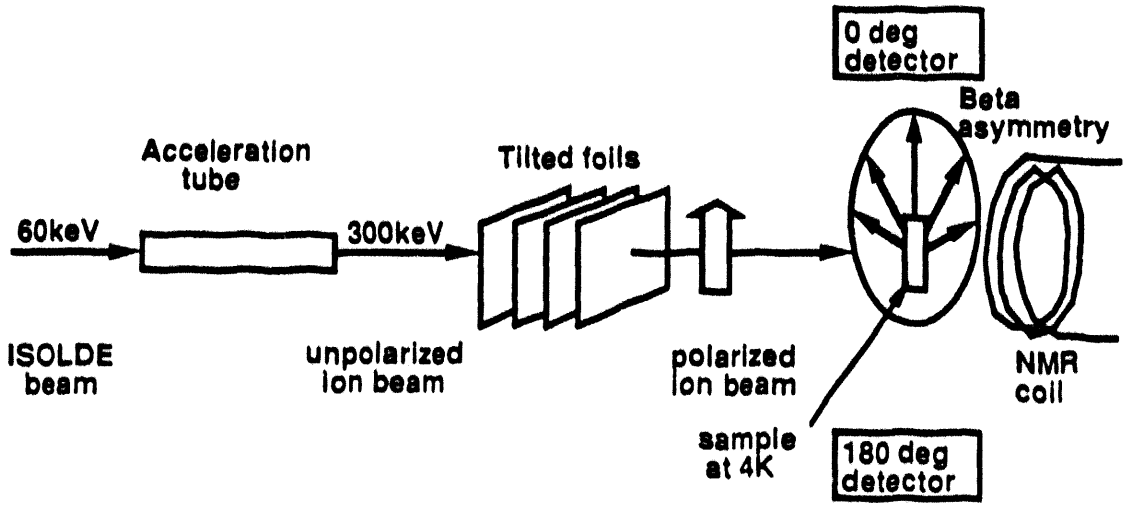

Fig.6: Schematic representation of the multifoil polarization technique

Section I
Report from Discussion Group

Section I

Report from Discussion Group on Experiments with Radioactive Beams

D. J. Vieira and M. Wiescher

Abstract

During the course of the workshop, a wide range of futuristic radioactive-beam experiments was discussed. These extended from the study of electroweak interactions in nuclei to materials science, nuclear astrophysics, and a host of nuclear physics investigations. Emphasis was placed on illustrating how these prototypical experiments could be accomplished, discussing what types of detection systems would be needed, exploring the new problems that would confront the radioactive-beam experimenter, and better defining the beam requirements.

Introduction

In general, the types of experiments that can be accomplished at a variable-isospin, heavy-ion facility, such as the IsoSpin Laboratory (ISL), are dictated by the range of beams that is available, the energy of those beams, and their intensities. The initiative outlined in the ISL White Paper seeks the most general type of radioactive-beam facility and covers nearly all of the nuclidic chart up to A = 240. The maximum energy of the ISL benchmark was set at 10 MeV/μ, and intensities as high as feasibly achievable were specified, with the nominal production choice being a high-intensity, ISOL-based system. At this workshop, considerable discussion was devoted to the maximum energy of the facility. Several participants argued that the maximum energy should be increased to 30 MeV/μ or more (especially for beams with A < 140) to take advantage of inverse-kinematic reactions with large negative Q-values; moreover, this increase in energy would provide complete energy coverage up to the lower energy region now covered by projectile-fragmentation-based, radioactive-beam facilities.

Figure 1 qualitatively illustrates the different types of experiments discussed at this workshop and their related technologies vs beam energy. At the low end of the energy range, ion- and atom-trap technologies were described. These methods hold promise for a variety of studies of nuclear mass and decay spectroscopy, atomic physics, and weak

interactions. A whole new class of important experiments will be possible by using trapped, cooled, and fully polarized radionuclides. Naturally, a variety of other experiments, especially some in the fields of biology and materials science, will take advantage of the high-intensity radioactive beams that can be collected for use in chemical radiotracer studies.

With post-accelerated beams of energies up to 500 keV/μ, a variety of surface-physics and materials-science investigations based on sensitive radiotracer implantation techniques become possible. A reliable source of such radioactive beams would be of considerable importance to materials studies. With radioactive beams in the 0.2- to 2-MeV/μ energy region, a series of key nuclear astrophysical reactions await measurement. Many of these reactions cannot be measured with stable beams and targets. At slightly higher energies of 2 to 5 MeV/μ, several subbarrier and coulomb-excitation experiments were discussed.

At or just above the coulomb barrier, in the 5- to 10-MeV/μ energy range, a variety of fusion-fission and high-spin investigations are of interest. A wealth of experiments will be done at these energies with 4π gamma-ray, charged-particle, and/or neutron detector arrays. Naturally, special precautions must be taken to protect these large detector arrays from becoming contaminated or overwhelmed by radioactive emissions from the scattered radioactive beam itself or from decay daughters. Well-collimated beams and the use of disposable liners are likely to be required in many cases.

In the 10- to 30-MeV/μ energy range, various one- or two-nucleon-transfer or charge-exchange reactions were discussed. As mentioned above, many of these reactions will be done in inverse kinematics to take advantage of the kinematic concentration of reaction products at forward angles, where magnetic spectrometers can be efficiently employed. Above the Fermi energy (about 35 MeV/μ), projectile-fragmentation reactions become increasingly more dominant. Albeit at much lower beam intensities, beams at this energy and even higher energies are presently available from several existing projectile-fragmentation-based, radioactive-beam facilities. The ISL initiative does not intend to compete with these facilities, but rather to concentrate on nuclear structure, nuclear astrophysics, and other more applied areas where a wide range of high-intensity, high-quality radioactive beams is required but where they are not as yet available.

Figure 2 reviews the basic intensity requirements of a variety of nuclear reactions and is taken from a figure presented by Fred Becchetti (University of Michigan). Although each experiment's intensity requirements will depend on the process being investigated and the experimental setup used, Figure 2 shows that the intensities range from less than 10^5 to 10^{12} particles per second, where most reactions require beams of 10^6 to 10^9 particles per second. Such intensities (at the energies and beam quality desired) are available (at Louvain-la-Neuve or projected for the Radioactive Ion Beam Facility now under

construction at Oak Ridge) for a limited number of light- to medium-mass radioactive beams that lie only a few nucleons away from stability.

For long-lived species (those with a half-life of 1 h or more), the preferred experiment may be to accumulate the mass-separated ISOL beam as an on-line radioactive target and to use a stable beam from the heavy-ion post-accelerator. In addition, a low-energy neutron generator of the 3-MeV-proton, 150+—μA type that uses the ^{7}Li(p,n) reaction to produce a stellar-like, neutron energy spectrum, was suggested for use with on-line accumulated radioactive targets for the measurement of (n,γ) cross sections for s-process studies. Thus, an on-line radioactive-target station, a stable-beam injector (that also could be used in tuning and operating the post-accelerator), and possibly a low-energy neutron generator should seriously be considered for ISL.

Within these basic parameters, the workshop participants discussed prototypic experiments, detector and experimental systems, and desired beam requirements for the ISL. Clearly, not all topics were represented at this workshop. These discussions represent only a sampling of the experiments that could be done at such a facility, but a great amount of credit is due the workshop participants and to the members of the wider radioactive-beam community who contributed these forward-looking ideas.

Prototypical Radioactive Beam Experiments

In this section, we proceed from low- to high-energy beams, regrouping the discussion according to topic. A complete listing of invited speakers and "discussion leaders" appears in the workshop agenda, and more details are contained in the invited or contributed papers published elsewhere in these proceedings.

Weak-Interaction Experiments

Weak-interaction studies in nuclei are expected to become more and more feasible as higher beam intensities and more sensitive experimental techniques become available. Towards this end, Gene Sprouse (Stony Brook) presented an outlook on parity-nonconservation experiments of francium atoms that could provide a high-precision test of the Standard Model of electroweak quark-electron interactions at low momentum. This experiment involves the measurement of the 7S-to-8S atomic transition rate with circularly polarized laser light at the transition energy in crossed electric and magnetic fields. To increase the sensitivity of the experiment so radioactive species can be used, a Zeeman optic trap (ZOT) is proposed to trap, concentrate, and cool atomic francium isotopes that have been mass separated, stopped, and neutralized. The combination of high-intensity ISOL

beams and a ZOT laser could also enable a variety of other nuclear studies, such as the decay of polarized nuclei and electron-neutrino angular correlations.

Another weak-interaction investigation was highlighted by Moshe Gai (Yale). It involves the first forbidden beta-delayed alpha decays in mirror nuclei, such as ^{20}F and ^{20}Na. The branching ratios are expected to be very small (on the order of 10^{-6}), but if such determinations can be made, new insight into parity-violating contributions that arise from the subnucleonic (meson) degrees of freedom may be revealed. Gai went on to discuss a more-precise measurement of parity-violating beta-delayed alpha emission in ^{18}F. Previous work on ^{18}F indicates a suppression of isovector ($\Delta I = 1$), neutral-current weak interactions in the nucleus. This experiment also involves the measurement of very small branching ratios ($\sim 10^{-10}$); thus, both of these weak-interaction experiments will require the highest ISOL intensities available and a specially designed high-geometry detection system.

Also related to this subject is the study of $0^{\pm}0^{+}$ superallowed beta decay for $N \cong Z$ nuclei. This topic was discussed by John Hardy (AECL, Chalk River). Radioactive beams are needed to produce and characterize the beta decays of heavier nuclei between A = 56 and A = 100. Such measurements, especially for "forbidden" $0^{\pm}0^{+}$ transitions, will provide an experimental check of the charge-dependent radiative corrections whose uncertainty now limits such work. With improved charge corrections, the high-precision measurements of superallowed transitions will further probe the conserved-vector-current hypothesis and test the Standard Model via the unitarity of the Kobiyashi-Maskawa Matrix.

Materials-Science (Condensed-Matter) Experiments

Heinz Haas (ISOLDE, CERN) presented an overview of materials-science applications by using radioactive beams. Nuclear methods, such as radiotracer diffusion, Mössbauer spectroscopy, emission channeling/blocking, perturbed angular correlations, deep-level transient spectroscopy, conversion electron spectroscopy, and low-temperature nuclear orientation, provide excellent diagnostic tools for investigating impurity effects in condensed matter at very low concentrations. Experiments that address diffusion in immiscible systems by deep radiotracer implantations, surface migration, and interface studies were described. The techniques that would be employed in these studies include the use of decelerated, "soft-landed" radioactive beams; local-magnetic-field measurements with beta-NMR with tilted-foil-polarized radioactive beams; and transmutation doping of wide-bandgap semiconductors. In general, these studies require a variety of radioactive beams with doses of 10^{9} to 10^{11} atoms in small areas (<1 mm^2) at implantation depths of <10 μm. Meeting these specifications requires tightly focused, fairly intense (>10^{8} particles per second) beams with energies up to 500 keV/μ. For the semiconductor-doping

experiments, intense (10^{10} to 10^{12} particles per second) beams of ^{11}C and ^{31}Si were suggested. To make progress in this field, frequent short experimental runs must be made with ready access to radiochemical laboratories, clean rooms, and other related experimental equipment.

Concentrating on Mössbauer experiments and their application to materials studies, Jerzy Sawicki (AECL, Chalk River) outlined an experiment that involves the implantation of ^{197}Hg, which, once implanted, would decay to ^{197}Au. Through on-line Mössbauer spectroscopy, the diffusion of gold in silicon could then be investigated. Such work has direct applications to the development of fast, very-large-scale integrated circuits. Another area of high interest in materials science is the study of doped diamonds and their potential use as wide-bandgap semiconductors. The use of radioactive beams to implant ions, such as ^{57}Mn, ^{73}As, ^{119}In, and ^{197}Hg, which are not readily available to the materials science community, would greatly advance the use of such nuclear techniques in addressing condensed-matter issues.

Nuclear-Astrophysics Experiments

In the field of nuclear astrophysics, ISL offers a unique opportunity to extend the experimental study of stellar nucleosynthesis processes towards unstable short-lived nuclei, which are of extreme importance for the understanding of explosive stellar scenarios. The discussion focused on three nucleosynthesis processes:

1. the r-process, which is thought to occur in supernova explosions
2. the s-process, which determines the production of heavy elements in red-giant stars
3. the rp-process, which determines the nucleosynthesis in nova events

The understanding of these three processes requires a detailed knowledge of the nuclear-structure parameters of isotopes that lie away from the line of stability; however, because of the substantially different nature of these processes, different experimental approaches are needed to study the various nuclear "input" parameters. This viewpoint was developed from extended discussions of the nuclear astrophysics working group, which was stimulated by the invited talk of Art Champagne (University of North Carolina) and contributions by Dick Boyd (Ohio State), Joachim Görres (Notre Dame), and Franz Käppeler (Karlsruhe).

The r-process is a rapid-neutron-capture process, and its reaction path runs along the neutron-rich side of stability near the neutron drip line, as determined by (n,γ)-(γ,n) equilibrium. Its understanding mainly requires the measurement of nuclear masses, beta-decay lifetimes, and decay properties near or even on the r-process path. These studies

largely use the front-end, isotope-separator part of ISL with its improved mass-resolution capabilities without beam post-acceleration.

The s-process, a slow-neutron-capture process, runs close to the line of stability and mainly involves neutron-capture reactions on stable nuclei but may also involve neutron capture on unstable isotopes. The study of these reactions allows the determination of the macroscopic stellar parameters, such as temperature, neutron density, and mass density. For the measurement of these reactions, the ISL will be used as an implantation facility to produce relatively thick samples of long-lived isotopes for off-line or even on-line neutron irradiation. A similar approach is possible for the study of the p-process, which is characterized by (γ,n) reactions on long-lived isotopes on the neutron-deficient side of stability. In this case, the measurement of (n,γ) reactions on long-lived samples can be used to study the inverse photodisintegration process.

The rp-process is characterized by a sequence of proton-capture reactions and beta decays on the proton-rich side of stability. Understanding this process requires a detailed knowledge of the reaction rates of the various (p,γ) processes along the reaction path, which is sensitive to both the temperature and density of the site of this process. The cross sections of these reactions can be measured at the ISL in inverse kinematics after accelerating the isotopically and isobarically separated radioactive nuclei to energies of 1 to 2 MeV/μ on a hydrogen target. An alternative is to study transfer reactions to determine the nuclear structure of proton-rich isotopes above the proton threshold. This approach allows one to calculate the resonant reaction rates for the (p,γ) processes that produce these nuclei.

r-Process Experimental Requirements. The main goal of these measurements is the determination of masses, lifetimes, and decay modes of nuclei far from stability. For this purpose, the isotopically separated nuclei are implanted with a typical energy of about 100 keV into a transport system (a tape or gas jet) and positioned before an appropriate detector system to measure their decay properties. The experimental limitations of such measurements at current ISOL systems like ISOLDE are the beam intensities and beam purities. Beam intensities can be improved by increasing the primary-beam intensity and/or decreasing the transport and release times for the produced radioactive isotopes. The beam purity can be improved with the introduction of an isobar separator; limitation of impurity concentrations to 10^{-5} or less may be required. Another suggestion was to selectively ionize particular isobaric members with a laser ion source. These measurements require that the beam be deflected before the post-accelerator system, which is not needed for such studies.

s- and p-Process Experimental Requirements. The measurement of neutron-capture reactions on radioactive isotopes requires the production of two unstable nuclei. In addition to the ISL, an efficient neutron source is necessary. The isotopically and isobarically purified beam will be fanned out before the post-accelerator so it is implanted at an energy of about 100 to 200 keV into an appropriate backing material (e.g., carbon). For neutron-capture measurements, a target thickness $\geq 10^{14}$ atoms seems necessary. After the sample is produced, it will be irradiated in a neutron beam to measure the cross section by using activation techniques (i.e., measuring the characteristic decay signal of the reaction product). In most cases, the important reactions for the s-process only involve very long-lived radioactive isotopes ($t_{1/2} \leq 10$ years); therefore, it is not necessary for the neutron source to be on site. The measurement of neutron-capture reactions on short-lived nuclei ($t_{1/2} \leq 1$ day), however, requires an on-line neutron source. A 3-MeV high-intensity proton machine was suggested as a favored source for producing neutrons in a stellar velocity distribution via the ^{7}Li(p,n) reaction with about 2-MeV protons. An on-line neutron-production facility would have large advantages for the study of p-process reactions. Such studies would require (n,γ) measurements on fairly short-lived, neutron-deficient targets. Those measurements can be determined from the (γ,n) cross section by detailed balance. This technique, however, may require larger neutron energies than would be available from the ^{7}Li(p,n) neutron source.

rp-Process Experimental Requirements. The study of proton-capture reactions with the ISL requires a more complex experimental setup and puts more stringent requirements on the beam quality. The isotopically and isobarically separated ions need to be accelerated to between 0.2 and 2.0 MeV/μ, the range of astrophysically relevant energies. A solid-hydrogen target (C_nH_x) or a hydrogen-jet target was suggested. While the gas target system is technically more demanding, the solid target has an unfavorable stoichiometry that may reduce the reaction yield by a factor of 3. Both targets will cause substantial beam losses (10^{-5}) by scattering either on the target material itself or on the beam-defining collimators. These scattering losses will lead to a substantial buildup of background activity in the target area and lead mainly to 511-keV annihilation radiation. This buildup will lead to a large background count rate in the gamma-detector system causing pileup problems. This type of experiment will require a beam intensity of at least 10^{9} particles per second, a beam energy resolution of <15 keV/μ, and a beam-energy calibration of better than 2 keV/μ. In addition, a gas target system will require a beam focused to a diameter of ~1 mm so it can pass the entrance collimators without substantial losses. An isobaric purity of better than 10^{-5} seems necessary to avoid potentially intense background reactions. To

reduce the background in the detection system, a pulsed beam with adjustable pulse duration for activity measurements of reaction products may be favored.

The following requirements were formulated for the detector system. For the gamma detector, a highly segmented NaI array was suggested to reduce the total count rate, resulting mainly from the background activity. The poorer resolution in comparison to that of a germanium detector system is not serious because the gamma lines are expected to be Doppler broadened, anyway. The time structure of the beam will be used to improve the peak-to-background ratio. An additional combined recoil separator/velocity filter will help to separate the recoiled reaction products from the initial beam, allowing coincidence measurements between the prompt-gamma radiation and the separated recoil products. In some cases, the expected resonance strengths of (p,γ) reactions would be too weak to measure directly. In these cases, measuring single-particle transfer reactions in inverse kinematics with ISL beams was suggested as a way to determine the single-particle spectroscopic factors of the proton unbound states in the reaction product. Such measurements require a beam energy of up to about 20 MeV/μ. This energy is significantly higher than that originally anticipated in the ISL White Paper; however, the multitude of possible applications for the study of resonant-proton-capture rates [e.g., by measuring (3He,d) reactions] and of resonant- and nonresonant-neutron-capture rates [e.g., by measuring (d,p) transfer] may justify a modification to higher energies in the long term.

Coulomb Excitation and Other Subbarrier Experiments

In the subbarrier energy region, Rick Casten (Brookhaven National Laboratory) described a coulomb excitation (Coulex) experiment to measure B(E2) values for the decays of the first 2^+ and 4^+ states in even-even radioactive beams. This low-spin information, if done for a broad set of species, would provide invaluable insight into the nuclear structure (e.g., collectivity, nuclear shapes, and the role of p-n interactions) of these nuclei and into how this structure changes as functions of N and Z. Given the large excitation probabilities and the relatively low gamma-ray multiplicities expected, the experiment could be accomplished with fairly modest beam intensities (on the order of 10^6 particles per second) at energies of 1.5 to 3 MeV/μ with only a small number of germanium detectors placed in close geometry around the target. If the experiment were done in inverse kinematics with medium- to heavy-mass beams on a hydrocarbon- or possibly a hydrogen-gas target (about 1 mg/cm^2), count rates on the order of about 1 Hz could be estimated. Thus, a whole series of measurements could be made relatively quickly.

In other discussions, the idea of investigating subbarrier neutron-transfer, fusion, and fission reactions was explored. The use of radioactive beams with large neutron halos or

skins could make such experiments particularly interesting; however, most of these species lie along the dripline and possess very short half-lives, so hold-up times and decay losses in the target/ion source would combine to limit these exotic beams to low intensities ($<10^5$ particles per second), which would, naturally, limit such investigations.

Fusion-Fission and High-Spin Experiments

Near and above the coulomb barrier, in the energy region from 5 to 10 MeV/μ, radioactive beams make possible a wide variety of reactions for the production of nuclei with interesting configurations that cannot be produced with stable-heavy-ion beams. They would also make possible a variety of reaction-mechanism studies. Unfortunately, at this workshop we were not able to explore all of these topics, so only a few areas have been highlighted, among them, high-spin physics.

The invited talk of Cyrus Baktash (Oak Ridge National Laboratory) and contributions from Irshad Ahmad (Argonne National Laboratory) and I-Yang Lee (Lawrence Berkeley Laboratory) painted a broad picture of the different types of high-spin studies that may be undertaken. Baktash concentrated on studies in proton-rich nuclei. In particular, he mentioned:

1. The search for predicted, new, exotic shapes, such as hyperdeformation (a 3:1 ratio of major to minor axes), for example, in the neutron-deficient barium region with a ^{64}Ge beam and Y_{31} (banana-shaped) octupole deformations
2. The study of N $\equiv$ Z nuclei between ^{60}Zn and ^{92}Pd
3. The investigation of p-n interactions that involve identical high-j neutron and proton orbitals (e.g., the $g_{9/2}$, $h^{11/2}$, and $i_{13/2}$ orbitals in the A $\approx$ 80, 120, and 170 mass regions, respectively)
4. The study of octupole and superdeformed shapes "southwest" of ^{208}Pb (e.g, in the neutron-deficient mercury isotopes)

All of these could be produced via compound nuclear reactions with radioactive beams that have intensities of 10^8 to 10^{10} particles per second and energies around 5 MeV/μ. The general theme here was that the extreme isospin beams will lead to the most dramatic results. With large germanium arrays, such as GammaSphere and Euroball, and their accompanying arrays of charged-particle or neutron detectors, the detection system can be easily overloaded. Thus it may be better to exploit reactions with large cross sections with small beam intensities than ones with small cross sections at high beam intensities; however, when small cross sections (<0.5 mb) must be investigated, the use of a recoil separator to tag outgoing reaction products can be very powerful.

Ahmad, filling in for Mike Carpenter (also of Argonne National Laboratory), outlined a high-spin experiment that would use neutron-rich radioactive beams. The idea was to study "complete" J and E^* spectroscopy in stable rare earth nuclei, such as for a series of erbium nuclei (e.g., ^{162}Er to ^{168}Er). (^{166}Er is also a candidate for hyperdeformation.) Extensive information on low-spin states is known for erbium nuclei, but because of the lack of suitable target-projectile combinations with stable beams, high-spin studies of these nuclei have not been possible; however, with neutron-rich radioactive beams, such studies could be done. Conditions that favor these studies are:

1. The large fusion cross sections
2. The smaller fission losses compared to the currently accessible neutron-deficient nuclei
3. The smaller charged-particle-evaporation losses

Thus, an acceptable gamma-gamma double-coincidence experiment could be mounted with a detector array like GammaSphere and with beam intensities of 10^7 to 10^8 particles per second for neutron-rich radioactive beams, such as $^{46\text{-}52}$Ar on a ^{124}Sn target with a thickness of about 1 mg/cm^2. Complete spectroscopy investigations are expected to be possible for other stable nuclei throughout the Sn to Pb mass region.

Lee explored what high-spin studies could be attempted with the coulomb-excitation approach. The specific case examined was a 4.5-MeV/μ ^{168}Dy neutron-rich radioactive beam on a ^{208}Pb target (of about 1 mg/cm^2), where spins up to 22 $\hbar$ are expected to be populated. The problem, however, is the large scattering of the radioactive beam into the forward hemisphere ($\pm 60^{o}$). This part of the gamma array would have to be removed, thus reducing the multiple-gamma detection efficiency. Nonetheless, low but acceptable counting rates were estimated for a gamma-gamma-particle coincidence experiment with ^{168}Dy-beam intensities of 10^6 to 10^7 particles per second.

Turning to the heavy mass region, Jerry Wilhelmy (Los Alamos National Laboratory) reminded us that the ISL will provide copious amounts of isotopes in the region between lead and thorium that were previously inaccessible because of the lack of stable or long-lived targets. Such radioactive beams provide a unique opportunity to extend our knowledge of the fission process, most notably how changes in fission barriers and shell structure influence the fission observables (mass distributions, kinetic-energy release, etc.). A particularly interesting region of study lies "northwest" of ^{208}Pb (i.e., the neutron-deficient pre-actinides). For the most neutron-deficient isotopes in this region, fission will be the dominant decay process. In a specific example, Wilhelmy described a fission experiment that uses the (d,pf) reaction in inverse kinematics with a radioactive beam of ^{209}Th at 8 MeV/μ. Because of the inverse kinematics, the fission products are concentrated

at forward angles, and their energies are "boosted" to higher energies. Both of these characteristics help in making the detection more efficient and the dE/dx particle identification more precise. Acceptable data rates could be obtained with beam intensities of 10^6 particles per second. Finally, Wilhelmy said that this same region holds promise as being a rich source of new fission-shape isomers. With the inner barrier dropping below the outer barrier by 1 to 3 MeV in the neutron-deficient radium isotopes, relatively high isomer populations (10^{-2} to 10^{-3} in contrast to typical actinide fission isomer populations of 10^{-4} to 10^{-6}) are expected. These projected populations of isomers imply that a whole set of shape-isomer experiments would be possible with a GammaSphere-type array at the ISL.

For the chemical and nuclear investigation of the heaviest long-lived transactinides, Ken Gregorich (Lawrence Berkeley Laboratory) explored the production of rutherfordium (Z = 104) isotopes with $^{248}Cm(^{20}O,xn)$ compound nuclear reactions. With ^{20}O at the beam intensities cited in the ISL White Paper, some 100 atoms per day of ^{264}Rf could be produced via the 4n reaction. Another investigation mapped out the production rates of neutron-rich nuclei with Z from 94 to 100 via a ^{93}Rb beam on a ^{248}Cm target. For several species, the production appears sufficiently high to consider a variety of β-decay ($t_{1/2}$, β-n, and β-fission) studies. In closing, Gregorich made a pitch for the accumulation of online radioactive targets (RT). He showed that for species with half-lives longer than 1000 seconds, higher luminosities can be achieved with radioactive targets and stable beams than with radioactive beams and stable targets.

Transfer Reactions and Reactions with Isomeric Beams

The use of radioactive beams will allow a wide array of nuclear-reaction investigations. Many of these reaction studies, some of their general characteristics, and the technical needs and/or equipment were discussed in the talk of Becchetti. It was noted that reactions with radioactive beams often have more positive Q-values than do their stable-beam counterparts. Thus, Q-window matching guarantees that more excited states, exhibiting a larger variety of nuclear properties, are accessible to study. The resulting particle-transfer spectra are thus likely to be more complicated and rich. In the case of the most extreme T_z beams, which are weakly bound, cross sections may be significantly reduced because of entrance-channel breakup losses. Becchetti pointed out that many experimental tricks could be employed to help facilitate such studies. These tricks include the use of multiple detectors, kinematic coincidences, dispersion matching with spectrometers, reverse kinematics, ejectile breakup detection, large solid angle devices, and time-of-flight measurements. In closing, Bechetti highlighted reactions that could be studied with

isomeric beams. Given that isomers are internally excited and that they often correspond to a nucleus that has an unusual shape, a variety of experiments can be imagined that exploit these features. For example, a better understanding of the spin-dependent ($\ell \cdot \ell$ and $\ell \cdot s$) parts of the nuclear potential may be obtained. In the case of short-lived isomers that are produced as a secondary beam from a stable or radioactive beam, gamma (or beta) tagging techniques can be used to identify the reaction products. Thus, reactions that involve either entrance-channel or exit-channel isomeric-state populations may be investigated.

Hardy outlined a set of prototypical radioactive-beam experiments that involve transfer reactions near doubly magic ^{56}Ni, which could be studied in inverse kinematics. Pickup and stripping reactions [such as d(^{56}Ni,p)^{57}Ni, ^{3}He(^{56}Ni,d)^{57}Cu, p(^{57}Ni,d)^{56}Ni, and p(^{56}Ni,t)^{54}Ni], leading to single- and two-particle excitations with respect to the ^{56}Ni doubly closed shell, are interesting nuclear-structure studies. They not only provide the single-particle states relative to the N = Z = 28 shell but also establish the two-particle correlations. Hardy reported that reasonable energy spreads (about 0.2%) and angular resolutions (about 0.1°) were required to achieve a 50-keV resolution for the light ejecule in the center of mass. With either a gas-jet or a gas-cell (at about 150 μg/cm^2) target with a microstrip detector telescope array to measure the outgoing light particles, acceptable counting rates (between 10^{-3} and 1 Hz per strip for $d\sigma/d\Omega$ = 10 μb/sr to 10 mb/sr) are achievable with radioactive-beam intensities of 10^8 particles per second. Desired beam energies for the single-nucleon transfer reactions on hydrogen varied from 15 to 25 MeV/μ depending on the Q-value. And in the worst case, that of the p(^{56}Ni,t)^{54}Ni reaction, where the Q-value was very negative (Q = -22.4 MeV), a beam energy of 50 MeV/μ was sought. Higher energies could be achieved at the expense of beam intensity by selecting a less-favored, higher charge state after stripping. Additional measurements, such as p(^{66}Ge,^{66}As)n and p(^{68}Ge,t)^{66}Ge and the Q(EC)-value determination via the reaction-threshold measurement of p(^{54}Fe,^{54}Co)n, were also discussed as being of interest to the 0^+-0^+ superallowed beta-emitter work mentioned previously. Along similar lines, Brad Sherrill (Michigan State University) mentioned the calculations of Walter Henning (Argonne National Laboratory) on the inverse-kinematic stripping reaction d(^{132}Sn,p)^{133}Sn at about 15 MeV/μ. A very promising program of transfer and charge-exchange reactions would clearly be possible at ISL; however, some reactions would require beam energies greater than 10 MeV/μ, at least for certain mass ranges.

Sherrill reviewed current activities on the nuclear structure of and reactions with dripline nuclei, especially neutron-halo nuclei. Of interest in the case of ^{11}Li are the $(s_{1/2})^2$ and $(p_{1/2})^2$ contributions to the ground state, which could be mapped out via one- and two-neutron stripping reactions. For the p(^{11}Li,^{10}Li)d reaction (where the ^{10}Li rapidly breaks up into ^{9}Li + n), Sherrill estimated that a feasible experiment could be done at an

intensity of 10^5 particles per second; however, a beam energy of 30 MeV/μ would be desirable. To exploit and further investigate the nature of the neutron-halo extension, subbarrier energies should be explored. Such speculative effects as halo-assisted, cold fusion, and enhanced neutron-transfer cross sections could prove interesting.

Experimental Equipment and an Outline of the Experimental Areas

One session was devoted to experimental equipment needs and the discussion of what new problems the radioactive-beam experimenter is likely to face. Marc Huyse (Catholic University, Leuven) started by recounting some of the experiences confronted in Louvain-la-Neuve radioactive-beam experiments. The major experimental problems were:

1. Low beam intensities (compared to stable-heavy-ion beams)
2. Small, astrophysically interesting cross sections
3. High backgrounds

The solutions generally involved a combination of:

1. The use of a large-solid-angle detection system, often with a high degree of granularity
2. Tailoring the experiment to be highly selective to the process of interest and as insensitive as possible to other processes (i.e., by employing specialized equipment)
3. Effective disposal of and shielding from the radioactive beam and its decay daughters

In the latter case, the incident beams were well collimated to remove beam halos, and the beam dumps were as well shielded and as far removed from the detection equipment as possible. During group discussions it was mentioned that a moving tape or screen arrangement could be used to remove the accumulation of scattered-beam activity. Long-lived radioactive beams or beams with long-lived decay daughters are a serious problem, not only for the post-accelerator but for the experimental beam lines and the experiments as well. Special precautions, such as the use of activation monitors and removable liners, must be taken to prevent long-term contamination of equipment should these beams be absolutely necessary.

Demetrios Sarantites (Washington University, St. Louis) talked about highly segmented 4π detector arrays. Clearly, such large-solid-angle detector systems are what will make radioactive-beam experiments feasible in most cases. Highly segmented devices, such as the GammaSphere, are ideal for multifold, gamma-gamma de-excitation studies.

Although multiplicity selection is a powerful tool and it will help to reduce the annihilation-radiation problem associated with scattered positron decaying beams, in many cases it cannot do it all. The addition of a charged-particle-detector array, such as the Microball (an array of CsI and plastic detectors), and/or recoil tagging with a recoil mass separator will have high utility in picking out the desired neutron-deficient or neutron-rich species of interest. Other large-solid-angle devices (such as neutron arrays, silicon microstrip arrays, gas detectors arrays [i.e., PPACs or Bragg counters], or a time projection chamber) also have merit; however, in all of these expensive and manpower-intensive detection systems, special precautions must be taken to prevent contamination by scattered radioactive beams. To this end, inverse-kinematic reactions (i.e., heavy beams on light targets) may become the rule rather than the exception as it exists today with stable beams. Many of these radiation-background issues could and should be addressed today with stable beams so that we are better prepared to deal with the problem when a broad set of radioactive beams become available in the future.

Turning to recoil separators, Cary Davids (Argonne National Laboratory) described the operation and performance of the Fragment Mass Analyzer (FMA), a separated-function E x B recoil separator now in operation at Argonne. Because of scattered-beam problems, this device is not well suited to inverse-kinematic reactions, but for fusion reactions for which it was designed it works quite well. Future developments of such recoil separators are likely to have one or more intermediate foci to:

1. Improve the rejection of the primary beam
2. Help decouple and reduce (via strategically placed multipoles) the effects of leading second-order aberrations, which now limit the resolution
3. Facilitate better recoil particle identification or provide some Z separation

(Some of these improvements have been incorporated in new recoil separators, such as MARS at Texas A&M University or the recoil-mass separators now being constructed for the Oak Ridge RIB Facility.) Acceptances as large as $\Omega = 20$ msr, $\delta(m/q)/(m/q) = \pm 10\%$, and $\delta E/E = \pm 20\%$ may be possible, and ray-tracing techniques may further enhance the performance where ion counting is possible.

Sherrill reviewed large-acceptance magnetic spectrometers. As mentioned earlier, such spectrometers will be useful for a variety of inverse-kinematic reactions where a large part of the angular distribution is concentrated at forward angles. Existing modern spectrometers have large acceptances ($\Omega = 20$ msr [$\pm 5^{o}$], $\delta p/p = \pm 5\%$), and momentum resolutions of 1 part in 10^4, and they employ ray-tracing techniques. Angular resolutions of a few mrad (about 0.1^{o}) can be measured. The S800 spectrometer currently being constructed at Michigan State was cited as an example. A general-purpose magnetic

spectrometer for ISL was seen as being more of a technological challenge in that it should be able to work with heavy nuclei as well as with light nuclei and the high radioactive-beam intensities would lead to background problems. A guestimated price tag for such a spectrometer is about $2 million.

Very large solid angle devices, such as superconducting solenoids, were discussed by Becchetti. The advantages of such a device are large solid angles (up to 2000 msr at $\varphi \approx 0^{o}$) and energy (±5%) acceptances, short flight lengths (giving reasonably isochronous performance), and a favorable beam-dump arrangement (on the centerline axis). The new 5-T supersolenoid device now on-line at Michigan State University was given as an example. Having very simple double-focusing optics, the strong solenoid device lends itself well to small circular, ring, or rod counters. The short flight path makes it ideal for the investigation of short-lived fragment or isomer reaction products. For secondary beams, a pair of supersolenoids has been used to produce a high-intensity secondary beam at GANIL (the so-called SISSI project). The idea of a dual solenoid that could operate as an achromat or with an intermediate crossover was also discussed. Finally, the use of a radial electric field and an axial magnetic field to produce a large-acceptance mass-to-charge separator was mentioned. Such devices (which should also include superconducting quadrupole devices and orange spectrometers) are good beam concentrators for the study of weak processes with moderately good primary-beam elimination; however, these devices are not, in general, for high-resolution work.

Other experimental equipment that was discussed ranged from storage rings to large-volume Penning traps. Dennis Moltz (Lawrence Berkeley Laboratory) presented a briefing on storage rings, which could have a variety of applications, extending from mass measurement of exotic nuclei to atomic physics. Although storage rings around the world have made impressive technological advances in electron cooling, laser cooling, and beam stacking, the large probability charge-state changing probability at low energies makes an ultrahigh vacuum essential. Moreover, the use of a gas-jet target does not look promising at these energies even with the possibility that a low-dispersion tune of the ring can be arranged. Although such devices, if designed to be flexible, could be operated in a synchrotron mode to further accelerate or decelerate radioactive beams, its undertaking would appear to be rather expensive. A storage ring/synchrotron device was therefore considered more as a possible upgrade to ISL rather than something to begin with.

Bob Moore (McGill University) briefly mentioned large-volume Penning (and Paul) traps that are on the technological horizon. Such ion traps could store a reasonably large number of ions (overcoming space-charge problems through increased size). Likewise, the development of dynamic Paul traps is expected to increase injection efficiencies. Thus, ion

traps hold promise for a variety of ISOL and high-charge-state, atomic-physics experiments.

There was not a dedicated discussion devoted to nuclear astrophysics or condensed-matter equipment per se; however, many of the experimental needs of those communities were presented in other talks or discussed in smaller groups. Like the experimental needs of the rest of the radioactive-beam community, their experimental needs are widely varied. Individually tailored experiments are likely to be the rule rather than the exception.

In an effort to spark researchers' interest and imagination, we have put together a rough outline of the experimental areas as composed of the major pieces of experimental equipment mentioned for ISL at this workshop. Out of necessity, this picture is incomplete, and it should only be considered as a starting point. Other equipment would, of course, be needed for the more specialized setups that we could not enumerate here.

The reader is encouraged to forward his or her experimental ideas to (and become involved with) the Experimental Instrumentation and Detection Equipment working group that is being formed as an outgrowth of this workshop. More information on this group is included in the summary by Casten.

In general, we feel that two experimental areas will be required for ISL:

- One for ISOL beams and perhaps modestly post-accelerated radioactive beams for implanted radiotracer studies
- The other for radioactive beams with energies between roughly 0.5 and 30 MeV/μ

A sketch of the low-energy ISOL area is presented in Figure 3. Lines are included for

1. Atomic physics, weak-interaction studies, and other nuclear-decay studies
2. Radioactive target accumulation for use with a neutron generator [e.g., for (n,γ) measurements]
3. Materials science (e.g., for radiotracer ion implantation)
4. Biology studies that use radioactive species and medical-isotope collection

A set of clean rooms and chemical laboratories will be needed to facilitate the work in the latter two areas. A serious materials science effort may also need one or more stable-ion implantors located nearby. Finally, a secondary beam of mass-separated species could be of high utility for many of these investigations that require frequent but routine access to radioisotopes.

Figure 4 is a rough sketch of the main radioactive-beam area. Major experimental equipment like a magnetic spectrometer, a recoil separator, and large detector arrays are highlighted. Many of these systems should be designed from the outset to mix and match because different experiments will require different combinations of these systems.

Experimental needs will naturally evolve as more radioactive-beam experiments are designed and as technology advances. That being the case, specialized setups (most of which have not been thought of as yet) will be very important for ISL.

In summary, at least two experimental areas are envisioned for ISL: one primarily for mass-separated ISOL beams and the other for post-accelerated radioactive beams. The capability of accumulating medium- to long-lived radioactive targets on-line should not be forgotten. To fully exploit the many potential uses of a wide-mass-range, high-intensity radioactive-beam facility like ISL, considerable equipment costs ranging from 20% to 50% of the overall costs of the facility are anticipated. These costs should not be hidden or overlooked but rather included up front in the costs of the facility.

Beam Requirements

A short time was spent reflecting on the basic ISL beam requirements needed by the prototypical experiments outlined at this workshop. These beam requirements are summarized in Table 1 in terms of (1) base requirements and (2) capabilities desired by many researchers. Naturally, large variations occur in the beam requirements from experiment to experiment, and we found those variations bewildering to quantify; however, an evolving consensus did develop, and we represented this position here.

The first point is a given. The ISL should be a broad-mass-range radioactive-beam facility that covers as wide a range of nuclides as possible with the highest possible intensities. The desired maximum energy of ISL was a matter of considerable debate. As the discussion developed, it became evident that most post-accelerating schemes that would provide 10 MeV/μ at A = 240 could deliver higher energies for lower-mass species. Impromptu estimates indicated that, with the same accelerating structure, which would deliver 10 MeV/μ at A = 240, about 20 MeV/μ could be achievable at $A \leq 140$ and about 30 MeV/μ could be reached for $A \leq 60$. Moreover, for those experiments that require even higher energies, some compromise may be struck between stripping losses (i.e., intensity) and beam energy. These issues of maximum beam energy vs mass and intensity must be carefully examined.

Most of the other beam qualities were fairly standard for heavy-ion accelerators. Beam energy resolutions of about 10^{-2} will be routinely required. In some cases, such as astrophysical-reactions resonance work, energy resolution on the order of 10^{-3} or better will be needed. Small beam emittances are required for many of these nuclear-structure experiments, and, for obvious reasons, a premium is likely to be placed on radioactive beams with only the smallest of beam halos. Many of these beam-halo problems can be reduced with collimators, but a high-quality beam is still required. Desired beam purities

varied widely from experiment to experiment. Some experiments were relatively insensitive to isobaric and/or isotopic beam impurities and required beam purities of only about 99%. Other experiments were very sensitive to such impurities and required 99.999% or better purity. Again, these impurity issues are ion-source- and production-rate-dependent, which translates into a strong Z and A dependence. For coincidence experiments, large duty factors are, in general, required. Finally, to facilitate beam timing techniques as a means of discriminating against random background problems, beam pulses with a width of about 1 ns and spaced every 100 to 300 ns were foreseen. The participants agreed that a compromise between good energy resolution and good beam timing can be arranged with either a beam buncher or the last cavity in a LINAC.

Outlook

The discussions of this working group on prototypical radioactive-beam experiments for ISL and their related experimental equipment were surprisingly productive. As such, this workshop represents a good beginning, and we would like to thank all of those who contributed to its success.

As one of the outcomes of this workshop, a specific working group on Experimental Instrumentation and Detection Equipment will be set up by Davids. We encourage all who are reading this summary to become actively involved in this working group. We know that many people could not attend this workshop, but we need your input in further developing and refining the research that should be undertaken at ISL and in defining the very nature of the facility itself. Your combined individual efforts are needed to advance the very strongest scientific case possible.

Acknowledgments

Special thanks are extended to Cary Davids (Argonne National Laboratory), Michael Smith (Oak Ridge National Laboratory), and Dave Cullen (Oak Ridge National Laboratory) for taking notes on the working-group discussions and to Dirk Rosenauer (Los Alamos National Laboratory/Giessen University) for helping to prepare these figures. We also appreciate the assistance of Fred O'Hara (Oak Ridge), Rick Casten (Brookhaven National Laboratory), and Jerry Garrett (Oak Ridge National Laboratory) in preparing this summary.

Table 1. Beam requirements as suggested by the experimental discussions.

Beam Qualities	Base Requirements	Desired Capabilities
Maximum energy	10 MeV/μ @ A = 240	10 MeV/μ ≤ A = 240 20 MeV/μ ≤ A = 140 30 MeV/μ ≤ A = 60
Energy resolution	$<10^{-2}$	$<10^{-3}$
Emittance	<2π mm-mrad	<1π mm-mrad (normalized)
Beam impurities	$<10^{-2}$	$<10^{-5}$
Beam structure		
Macro duty factor	>30%	100%
Microstructure	<2-ns beam pulses every 100 to 300 ns	<300-ps beam pulses every 100 to 300 ns

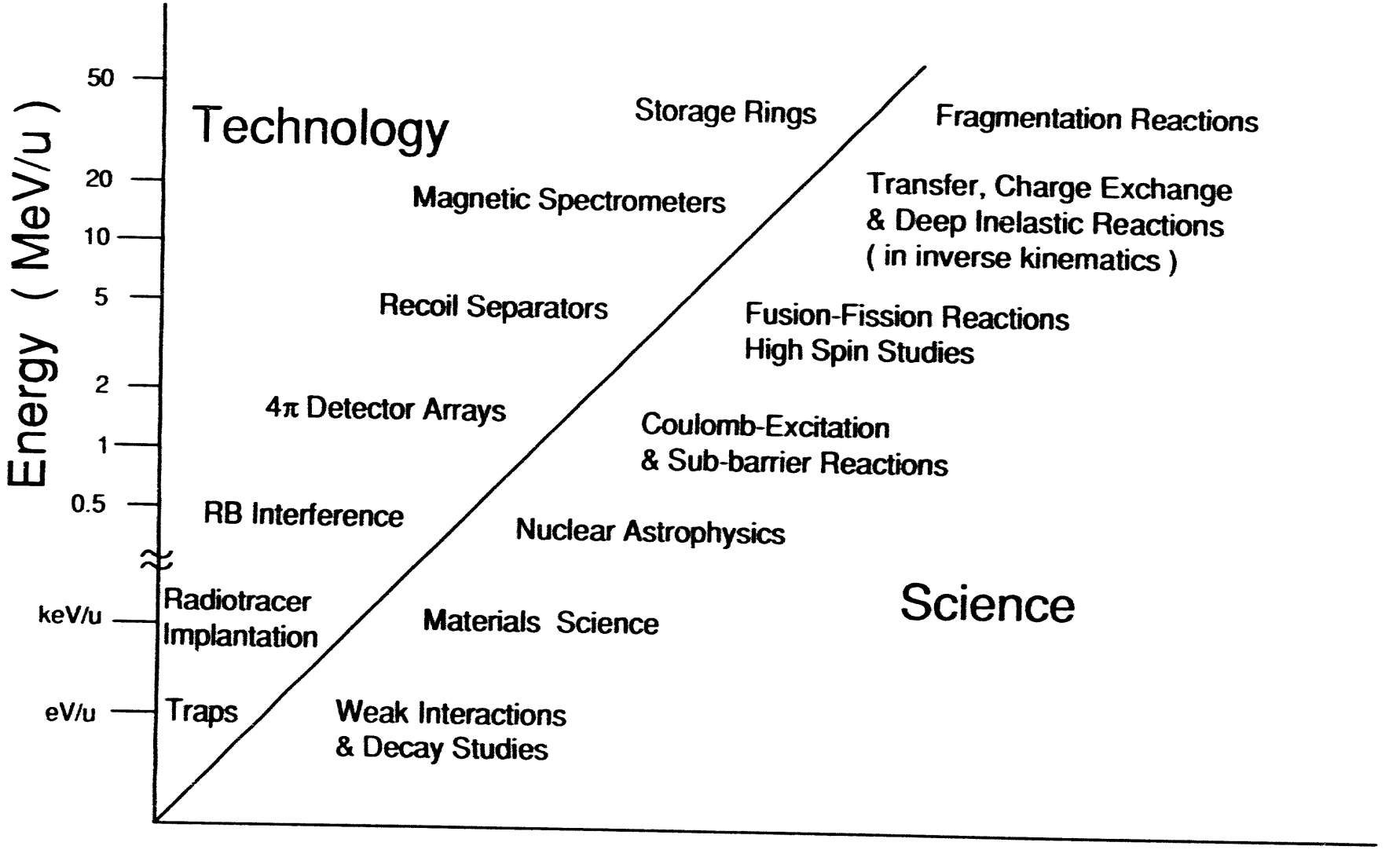

Figure 1. Science and technology made possible by or needed for radioactive beams with increasing beam energy.

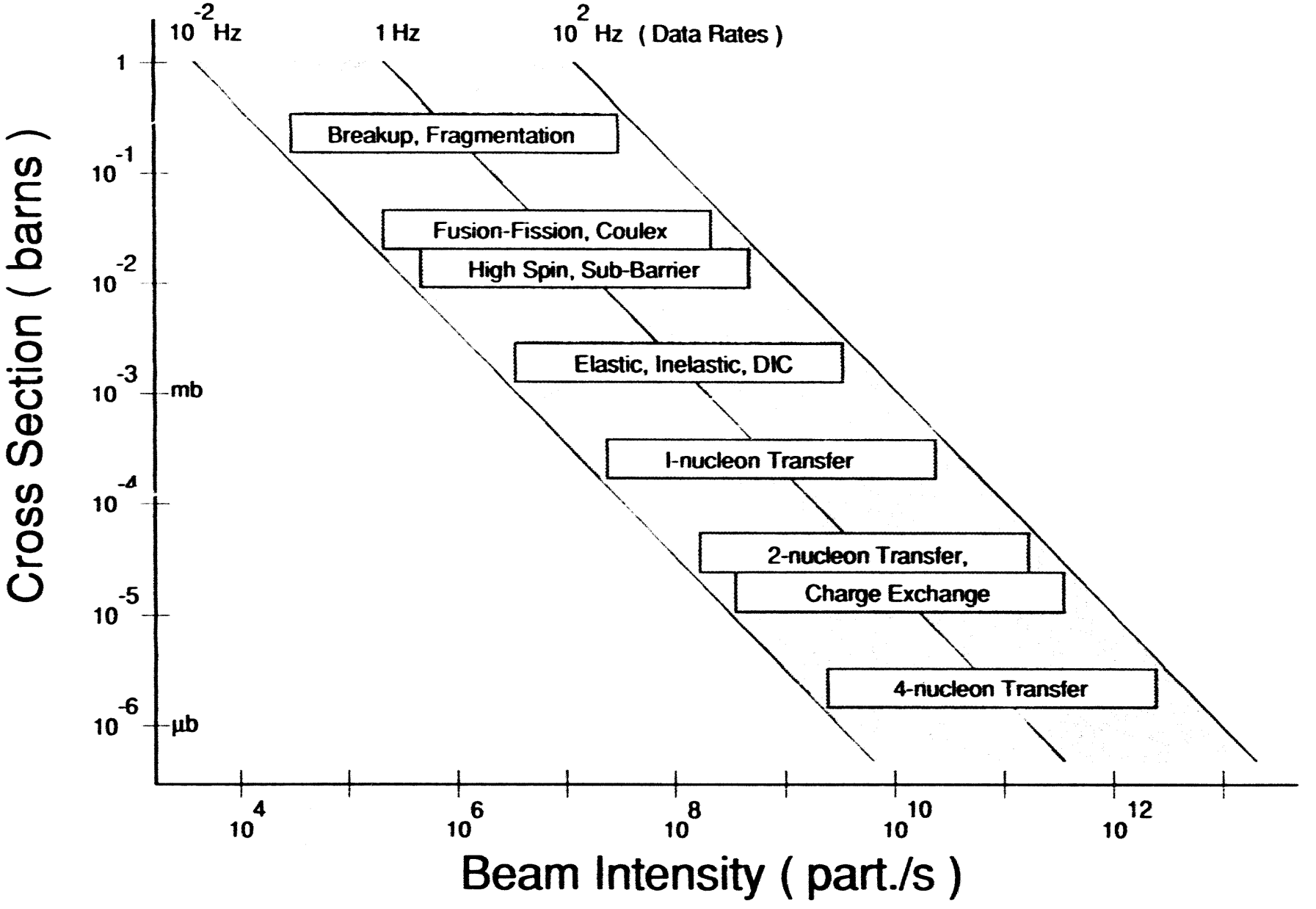

Figure 2. Beam-intensity requirements as a function of cross section, assuming a target thickness of 10^{18} atoms/cm^2 and an overall detection efficiency of 50% of 4π for several classes of reactions.

Low-Energy ISOL Experimental Area

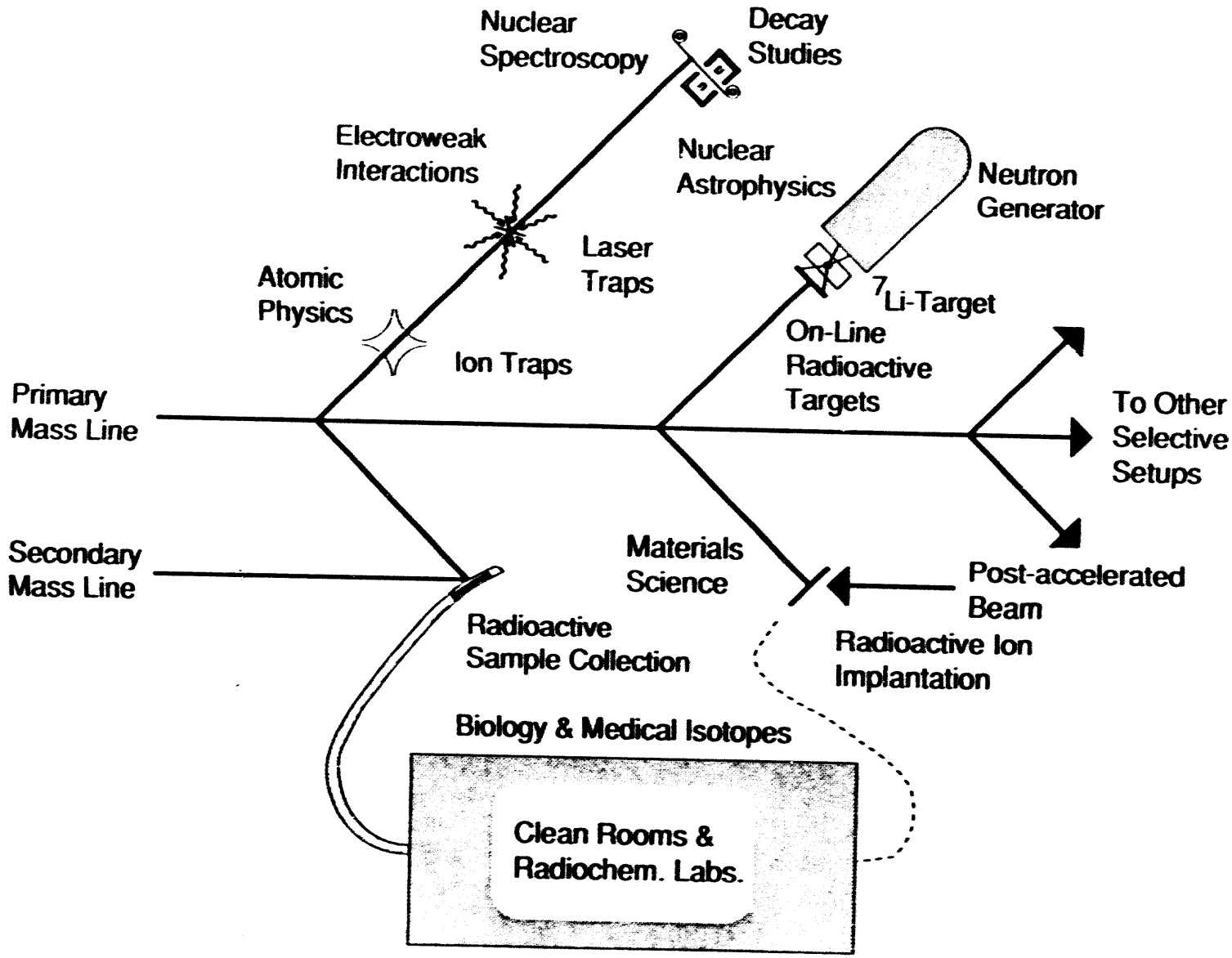

Figure 3. Rough layout of the low-energy (ISOL) experimental area of ISL as suggested by these discussions.

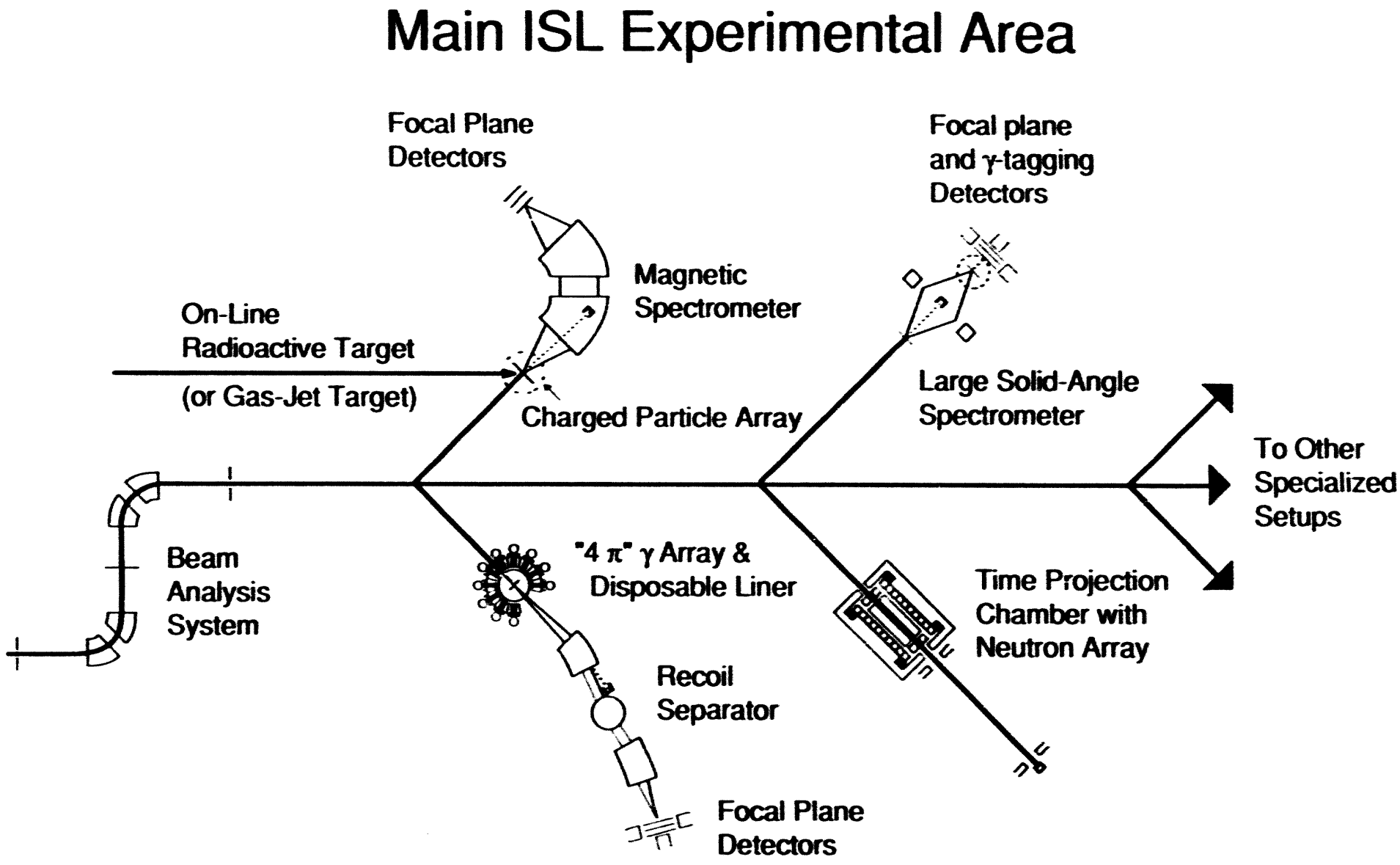

Figure 4. Rough sketch of the main ISL experimental area as suggested by these discussions.

Section I
Contributed Papers

Resonant Laser Ion Sources for High Elemental Selectivity

W. M. Fairbank, Jr. and A. Barrera
Physics Dept., Colorado State Univ., Fort Collins CO 80523

H. K. Carter
UNISOR, Oak Ridge Institute for Science and Education, Oak Ridge TN 37831

K. R. Newton and A. C. Trivedi
Dept. of Physics, Mississippi State Univ., Mississippi State MS 39762

Abstract

Laser ion sources based on resonance ionization of neutral atoms are reviewed. Progress on the development of a laser ion source based on helium jet transport, laser ablation and resonance ionization is reported.

Introduction

Production rates in fusion and fission reactions characteristically fall off rapidly in the regions farthest from stability. Consequently, when pure beams of such isotopes are needed for nuclear spectroscopy experiments or for the production of radioactive ion beams, a high level of isotopic and isobaric discrimination in the system is required. In this paper we review progress in the development of laser ion sources with high elemental selectivity based on Resonance Ionization Spectroscopy (RIS). After a short discussion of the work of others, our limited progress toward demonstrating a laser ion source based on helium jet transport, laser ablation and resonance ionization is reported.

Resonance Ionization Spectroscopy

The fields of Resonance Ionization Spectroscopy (RIS) and Resonance Ionization Mass Spectrometry (RIMS) have been very active in the last decade and a half, with major efforts taking place in laser isotope separation and low level elemental and isotopic analysis [1-3]. The different methods for RIS can be classified according to the types of laser systems used: a) high resolution, low power continuous lasers pumped by argon or krypton lasers, b) high repetition rate, moderate peak power pulsed lasers pumped by copper vapor lasers, and c) low repetition rate, higher power pulsed lasers pumped by excimer or Nd:YAG lasers.

The high laser power available in the latter case allows greater flexibility in choosing the ionization scheme, and a single dye laser is usually all that is needed; but the low duty cycle of the process can lead to low overall efficiency when the influx of atoms is continuous. In such cases the higher repetition rate systems (a and b) may be preferred, but the tradeoffs are generally of insufficient intensity to saturate the final ionization step and reduced wavelength range. To combat these problems multi-step resonance ionization is often used, with the final step occurring through field, collisional or autoionization of high-lying states.

Laser ion sources based on RIS

Three types of resonant laser ion sources are currently under development for nuclear physics, to our knowledge. In the hot cavity approach [4,5], radioactive atoms diffusing out of a thick target are stored between copper laser pulses in a heated cavity. Ionization efficiencies of 35%

for Yb [6], 17% for Sr [5], 13% for Tc [7], and 0.2% for Sn [8] have been demonstrated. A major limitation of this method is isobaric backgrounds due to surface ionization in the hot cavity. For example, at the highest Yb efficiencies (35%), the surface ionization efficiency was 0.2%, while the ratio of resonance to surface ionization was only about 2 for Ho [6]. At ISOLDE a measured selectivity between 10 and 10^4 for Tm has recently been reported [9].

An alternative method for storing atoms between laser pulses is the buffer gas method [10-13], which is related to the ion guide technique. In this type of laser ion source, recoil products of fusion or fission reactions are stopped in helium gas and stored long enough (~5 msec) to become neutralized. They are then transported to a separate region where lasers resonantly ionize the element of interest. The ions pass through a nozzle and skimmer at the entrance to a mass separator. Feasibility studies for this method are underway, but no experimental efficiencies have been reported [11,12]. A similar system has also been developed for laser spectroscopy studies [14,15].

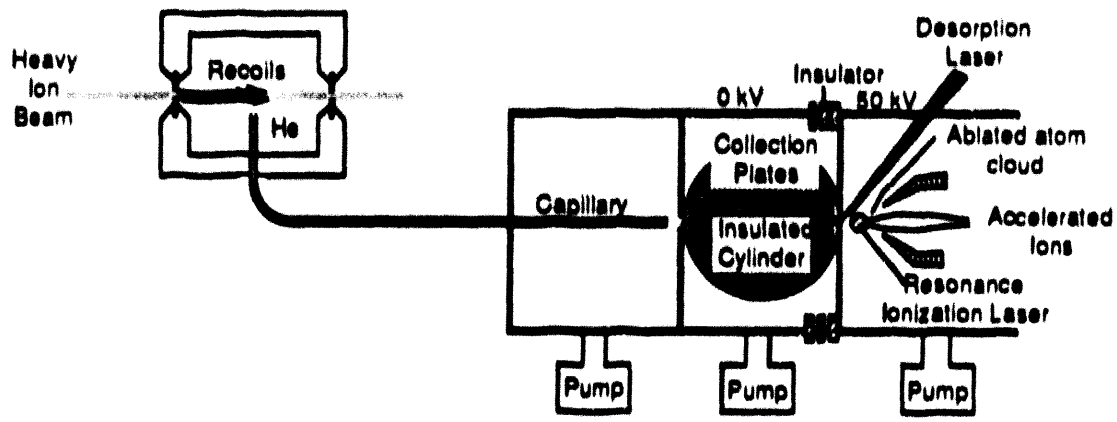

Fig. 1. Laser ion source based on helium jet transport, laser ablation and RIS.

We are exploring a third type of laser ion source based on storage of atoms on a metal surface. In this source (Fig. 1) recoil products are stopped in helium gas and transported through a capillary to the surface [16]. After a short collection period, perhaps equal to the time between laser pulses, the surface is rotated into a differentially-pumped region of high vacuum. There the deposited activity is ablated by a laser pulse and the desired species in the vaporized cloud above the surface is resonantly ionized by a tunable laser beam. The ions are then extracted into the mass separator. Based on limited experience, efficiencies on the order of 1-10% for this method are predicted. Our progress since the original publication in demonstrating the fundamental processes involved in this technique is reviewed in the following paragraphs.

Helium jet transport

It is desirable for the laser ablation step to minimize excess material transported with the reaction products to the collection surface. Thus a carrier-free helium jet is preferred, although the use of small refractory aerosols (e.g., metal spheres) is also worth exploring.

Previous studies (Table 1) with pure helium jets have shown that radioactive atoms can be transported with high efficiency over lengths up to 10-15 cm in room temperature helium gas [17] and up to 1 meter at 77K [18,19]. We have done additional experiments with unseeded helium gas at room

Parameter	Ref. 18	Ref. 19	This work
Capillary diameter	0.8 mm	0.4 mm	1 mm
Capillary length	100 cm	45 cm	45 cm
Chamber pressure	1.5 atm	1 atm	1 atm
Temperature	77 K	77 K	300 K
Max. efficiency	78%	90%	55%

Table 1. Results of helium jet experiments with pure helium for 0.5-1.0 m lengths.

temperature. The apparatus is shown in Fig. 2. A known amount (~1 μCi) of ^{67}Ga, ^{99m}Tc or ^{111}In is released into ~1 atm of helium gas by heating a filament upon which a dried salt solution is deposited. The helium gas and the activity pass through a 1 mm diameter stainless steel capillary, formed into a 5 cm diameter coil, to a collection chamber evacuated by a Roots pump. There the transported activity is collected on a silicon sample.

The results of our experiments were somewhat erratic, but quite promising. The measured transport efficiency ranged from 0% to 97% for capillary lengths of 1-45 cm [20]. For example, the measured efficiencies for ^{111}In are shown in Fig. 3. Most of the deposit on the sample was found to be within a 1-2 mm diameter spot. Since the vacuum system was not of high vacuum quality and unknown amounts of salt may have been attached to the radioactive atoms during transport, it cannot be asserted with surety that the transport was aerosol-free. However, in many cases the amount of extra material deposited was quite small, i.e., it was not visible. A RBS depth profile of one ^{67}Ga deposit indicated a deposit thickness of less than a monolayer.

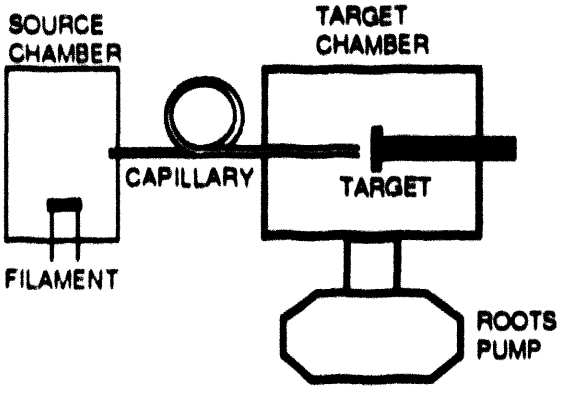

Fig. 2. Helium jet test apparatus.

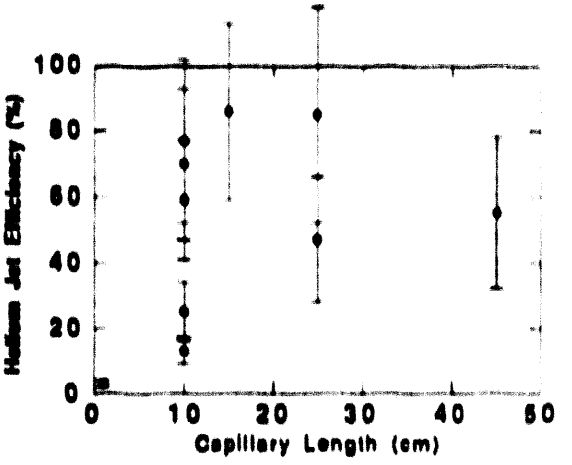

Fig. 3. Measured efficiency for pure He.

Laser ablation

For moderate laser intensities (<10^8 W/cm^2) and short pulse lengths (10-40 nsec), the local effect of an absorbed laser pulse on a surface can be described primarily by a thermal model [21]. In this regime, atoms on the surface evaporate with a thermal velocity distribution, with the temperature reaching 2000°C at the high end of the range [22]. For somewhat higher intensities, a shock wave forms and a velocity offset in the forward direction is

Isotope	Helium Jet Efficiency	Ablation Laser(s)	RIS Laser	Ablation Efficiency	Ionization and Transport Eff.
^{111}In	evaporated	Excimer	Nd:YAG dye	75%	0.06%
^{67}Ga	50%	Nd:YAG	none	89%	0.4%
^{67}Ga	50%	Nd:YAG dye/ Doubled dye	none	37%	0.65%
^{67}Ga	60%	Copper vapor	none	>50%	

Table 2. Results of laser ablation experiments. Each experiment represents thousands of laser shots.

observed [23].

We have investigated, in a limited way, laser ablation of radioactive samples of ^{111}In and ^{67}Ga using various lasers. Some of the results are presented in Table 2. In all cases it was possible to remove the activity on the sample with reasonably high efficiency in a few thousand laser shots. The evaporated salt solution samples, which had visibly thick deposits, were significantly more difficult to ablate than the invisible helium jet deposits. Unfortunately we have not yet done the tests which will answer the most important question: if a significant fraction of the activity in a helium jet deposit can be ablated without plasma formation in a single laser shot.

Resonance Ionization

It is known from previous Sputter-Initiated RIS (SIRIS) work in several laboratories that the efficiency for resonance ionization of atoms sputtered from a surface can be quite high (>10%). For example, in previous work at Atom Sciences, Inc. by one of us (WMF), the stable isotopes of Ga were used as a standard for tuning up the system. Typical RIS efficiencies measured were 2% for Ar^+ pulses 1μsec in duration and 10-15% for 0.2μsec pulses. One might expect even better efficiency for RIS of laser-ablated atoms since the energy distribution of thermally ablated atoms is narrower and the ablated atoms are generated at the same time.

The best test of this prediction is the experiment of Krönert et al. with ^{195}Au implanted into graphite [24]. The estimated efficiency factors for this experiment are summarized in Table 3. Overall an efficiency of 0.01% was expected, while the observed value was an order of magnitude smaller. The source of the discrepancy could have been errors in any of the factors plus losses due to molecule formation. In analyzing this result it is important to note that most of the efficiency losses in this experiment could be reduced dramatically. For example, most of the loss in the RIS process could be avoided by using a RIS scheme which could be saturated. This has been achieved for many elements. The mass spectrometer loss should be small for a laser ion source coupled to a mass separator (e.g., transmission was ~100% in the SIRIS instrument at Atom Sciences). Finally, one expects higher ablation efficiency for atoms bound weakly to a surface in a helium jet deposit than for implanted atoms. Thus we view the results of this experiment as very promising in spite of the low measured efficiency.

We have done one test of laser ablation and RIS with an ^{111}In sample evaporated from an acid solution. The deposit was visibly thick and took ~50,000 laser shots to ablate. The observed LARIS and transport efficiency was lower than desired, 0.06% (Table 2). There are many potential causes of this

Parameter	Efficiency	Comments
Ablation	50%	Higher for surface atoms
Temporal overlap	80%	
Spatial overlap	60%	
RIS	0.5%	Ionization step not saturated
Mass spectrometer	10%	
Theoretical total	0.01%	Could be 10-20% in a laser ion source
Experimental total	0.001%	

Table 3. Summary of efficiency factors in the Krönert et al. LARIS experiment.

low value which we did not investigate in detail, including lack of saturation of the ionization step.

It has been suggested that the ablation and RIS steps could be simplified by using a single resonant laser for ablation [25]. Consistent with the results of others, we have seen enhancements of up to ten times in the percentage of ablated ions for Ga, In, and Fe when the laser is tuned to resonance. With this method we obtained a total efficiency for ^{67}Ga LARIS and transport of 0.65% (Table 2). McLean et al. have reported enhancements of up to two orders of magnitude when grazing incidence angles are used [26]. Thus further investigation of this simplified approach is warranted.

The number of background ions generated in the ablation process is strongly dependent on the laser intensity used, i.e., the peak temperature of the surface. It has been shown in SIRIS work that pulsed electrodes, energy filters and pulsed detection are effective in reducing background ions to the 10^{-9} level and below [1, 27-30]. A similar high selectivity may be possible in the proposed laser ion source (except in the case of the single laser approach discussed in the previous paragraph), although there may be some tradeoffs in efficiency vs. selectivity.

Summary

Laser ion sources with hot thick targets have already been shown to have efficiencies up to 35% for elements which are volatile at intermediate temperatures. Progress on demonstrating a new laser ion source which would operate with cold thin targets and could be used for refractory elements has been reported here. Tests on different portions of the system have confirmed thus far the original expectations, which formed the basis for predicting an efficiency on the order of 1-10% for such a source.

Acknowledgements

The authors are grateful to Ray Garrett and Marvin Payne for their hospitality and the use of equipment at Oak Ridge National Laboratory in the LARIS measurements on evaporated ^{111}In samples. We also acknowledge the experimental assistance of Steve Allman and Susan Fischer in that work. UNISOR is a consortium of universities, State of Tennessee, Oak Ridge Associated Universities, and Oak Ridge National Laboratory and is partially supported by them and by the U. S. Department of Energy under Contract No. DE-AC05-76OR00033 with the Oak Ridge Associated Universities.

References

[1] G. S. Hurst and M. G. Payne, *Principles and Applications of Resonance Ionisation Spectroscopy* (I. O. P, Bristol, 1988).

[2] V. S. Letokhov, *Laser Photoionization Spectroscopy* (Academic Press, Orlando, 1987).

[3] See also the series *Resonance Ionization Spectroscopy* (I. O. P, Bristol, 1984, 1986, 1988, 1990, 1992).

[4] H.-J. Kluge, F. Ames, W. Ruster and K. Wallmeroth, Proceedings of the Accelerated Beams Workshop, Parksville, L. Buchmann and J. M. D'Auria, eds., TRIUMPF Report No. TRI-85-1, 1985, p.119.

[5] S. V. Andreev, V. I. Mishin and V. S. Letokhov, Opt. Commun. 57, 317 (1986).

[6] G. D. Alkhazov et al., Nucl. Instrum. and Methods A306, 400 (1991).

[7] F. Ames, T. Brumm, K. Jager, H.-J. Kluge, B. M. Suri, H. Rimke, N. Trautmann and R. Kirchner, Appl. Phys. B51, 200 (1990).

[8] F. Scheerer et al., Rev. Sci. Instrum. 63, 2831 (1992).

[9] V. I. Mishin, "Resonance Ionization Laser Ion Sources for Nuclear and Atomic Spectroscopy", abstract for the Fourth Workshop on Ion Guide Based Isotope Separation, Rydzyna, Poland (September, 1992).

[10] J. Ärje et al., Phys. Rev. Lett. 54, 99 (1985).

[11] Z. N. Qamhieh et al., Nucl. Instrum. and Methods B70, 131 (1992).

[12] P. van Duppen et al., "A laser Ion Source Based on Resonant Ionization in a Buffer Gas Cell", abstract for the Fourth Workshop on Ion Guide Based Isotope Separation, Rydzyna, Poland (September, 1992).

[13] M. Oshima et al., Nucl. Instrum. and Methods B70, 241 (1992).

[14] H. Backe et al., Nucl. Instrum. and Methods B70, 521 (1992).

[15] H. Backe, M. Hies, W. Lauth, H. Schöpe, P. Schwamb, N. Trautmann and S. Zauner, "An Ion Guide Quadrupole Mass Spectrometer for Resonance Ionization Spectroscopy", abstract for the Fourth Workshop on Ion Guide Based Isotope Separation, Rydzyna, Poland (September, 1992).

[16] W. M. Fairbank, Jr. and H. K. Carter, Nucl. Instrum. and Methods B26, 357 (1987).

[17] J. Äysto and K. Valli, Nucl. Instrum. and Methods 111, 531 (1973).

[18] J. Äysto, S. Hillebrand, K.-H. Hellmuth and K. Valli, Nucl. Instrum. and Methods 120, 163 (1974).

[19] A. G. Martin, S. B. Dutta, W. F. Rogers and D. L. Clark, Nucl. Instrum. and Methods A247, 520 (1986).

[20] A. C. Trivedi, M. S. Thesis, Mississippi State University (May, 1991).

[21] J. F. Ready, *Effects of High Power Laser Radiation* (Academic Press, New York, 1971).

[22] J. S. Bakos, I. B. Földes, P. N. Ignácz and M. A. Kedves, in *Resonance Ionization Spectroscopy 1990*, J. E. Parks and N. Omenetto eds. (IOP Conf. Ser. 114, 1991) p. 443.

[23] D. W. Beekman and T. A. Callcott, in *Resonance Ionization Spectroscopy 1984*, G. S. Hurst and M. G. Payne eds. (IOP Conf. Ser. 71, 1984) p. 143.

[24] U. Krönert, St. Becker, G. Bollen, M. Gerber, Th. Hilberath, H.-J. Kluge and G. Passler, Nucl. Instrum. and Methods A300, 522 (1991).

[25] F. R. Verdun, G. Krier and J. F. Muller, Anal. Chem. 59, 1393 (1987).

[26] C. J. McLean et al., Int. J. Mass Spectrom. Ion Proc. 96, R1 (1990).

[27] J. E. Parks, D. W. Beekman, L. J. Moore, H. W. Schmitt, M. T. Spaar, E. H. Taylor, J. M. R. Hutchinson and W. M. Fairbank, Jr., in *Resonance Ionization Spectroscopy 1986* , G. S. Hurst and C. G. Morgan eds. (IOP Conf. Ser. 84, 1987) p. 157.

[28] C. E. Young, M. J. Pellin, W. F. Calaway, B. Jorgensen, E. L. Schweitzer and D. M. Gruen in *Resonance Ionization Spectroscopy 1986* , G. S. Hurst and C. G. Morgan eds. (IOP Conf. Ser. 84, 1987) p. 163.

[29] W. M. Fairbank, Jr., R. D. LaBelle, J. E. Parks and M. T. Spaar, in New and Exotic Phenomena, O. Fackler and J. Tranh Van eds. (Lee, Singapore, 1987).

[30] W. M. Fairbank, Jr., G. S. Hurst, J. E. Parks and C. Paice, in *Resonance Ionization Spectroscopy 1984* , G. S. Hurst and M. G. Payne eds. (IOP Conf. Ser. 71, 1984) p. 287.

BETA-DELAYED (ALPHA) PARTICLE EMISSION; A PROBE OF WEAK INTERACTIONS IN NUCLEI

Moshe Gai
A.W. Wright Nuclear Structure Laboratory,
Yale University, New Haven, CT 06511

ABSTRACT

We propose proto-typical experiments for the Iso-Spin Laboratory: measurement of the beta-delayed alpha-particle emissions of ^{20}F and ^{20}Na with an estimated branching ratio of the order of 10^{-6}, to study rank one first forbidden beta decay of mirror nuclei, and the beta-delayed alpha-particle emission of ^{18}N with an estimated branching ratio of 10^{-10}, to study parity violation in ^{18}O. These experiments are natural extensions of the Yale experiment that measured the beta-delayed alpha-particle emission of ^{16}N, with a sensitivity for the branching ratio in the range of 10^{-9} to 10^{-10}. These experiments will utilize the high intensity secondary (radioactive) beams of the IsoSpin Laboratory, but will not require post acceleration.

Beta-delayed alpha-particle emission of light nuclei could be used to study beta-decays with small branching ratios due to their selection rules and selectivity. In particular an observation of alpha-particle decays of non-natural parity states is a direct evidence for parity violation. First forbidden beta-decays, on the other hand, are known to be governed by sub-nucleonic (meson) degrees of freedom, where significant mesonic contributions are found in the time-like axial current operator, [1] and are used to study mesonic effects in nuclei.

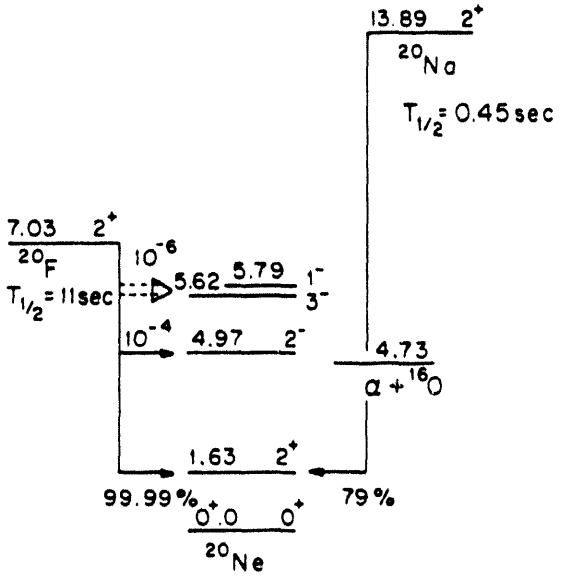

Fig. 1: First Forbidden beta-decays of the mirror nuclei ^{20}F and ^{20}Na.

The rank zero first forbidden beta decay of the 2^+ ground state of ^{20}F to the 2^- state in ^{20}Ne, was measured to have a branching ratio of 1.0×10^{-4}. Using this ft value we estimate for rank one first forbidden beta-decay to the 1^- and 3^- states, branching ratios of the order of 10^{-6}. In this estimate we assumed the matrix elements of the rank one operator are a factor of ten smaller then rank zero. In Fig. 1 we show these decays and the expected branching ratios for ^{20}F. In the case of the beta-decay of ^{20}Na, we expect a larger branching ratio due to the increase in phase space.

In order to measure these rank one first forbidden beta-decays one needs to measure the beta-delayed alpha-particle emission of ^{20}F and ^{20}Na with a sensitivity for the branching ratios of the order of 10^{-7}, at alpha-particle energies of the order of 1 MeV. As we shall describe below such experiments can be performed, and in fact even smaller branching ratios have been observed at such an energy range.

The Queens-Florence [2,3] experiments on parity violations in ^{18}F suggest that $\Delta I=1$ (iso-vector) neutral current weak interactions in nuclei are suppressed.[4] These experiments allow for a model independent extraction of neutral current interactions given by the pion weak interaction (F_π), with an upper limit which is a factor of 3-4 smaller then predictions of the quark model. While in the 70's Cabibo, Gari and others suggested that neutral current weak interactions are expected to be enhanced in nuclei, the Queens-Florence ^{18}F experiment suggest the contrary to be correct. The hindrance observed in ^{18}F of neutral current interactions ($\Delta S=0$) was proposed [4] to be reminiscent of the well known $\Delta I=1/2$ rule, for charge current interactions ($\Delta S=1$) and may suggest an ill understood iso-spin dependence of weak interaction in hadrons. These two hindrances if connected, may suggest a new puzzle in non-perturbative QCD.

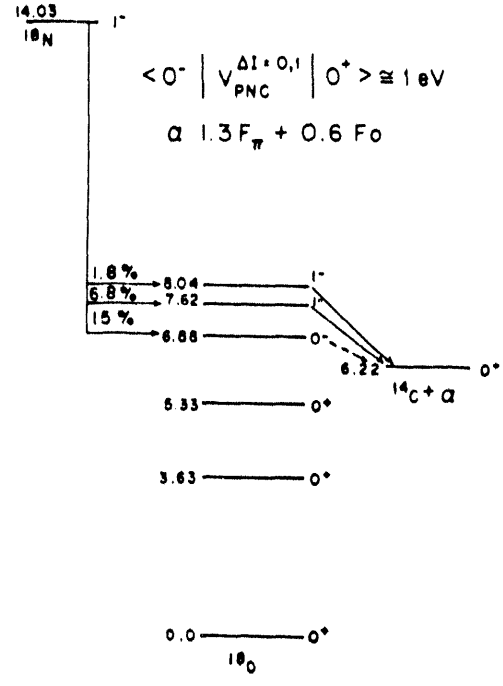

Fig. 2: The parity violating alpha-decay of the 0^- state at 6.88 MeV.

Attempts to perform an improved ^{18}F experiment, are currently in progress at Yale University. Here we propose to measure the parity forbidden alpha-particle decay of the 0^- state at 6.88 MeV in ^{18}O, following the beta decay of ^{18}N, as shown in Fig. 2. Extensive shell model calculations of the parity forbidden alpha-particle width suggest [5] it is proportional to: $1.3F_\pi + 0.6F_0$, and thus could be used as a testing ground for hindrance of F_π. In these calculations all three known and seven unbound predicted 0^+ states are included, but it is shown that the largest effect arises from the cluster 0_2^+ at 3.63 MeV. The complicated structure of the higher lying states leads to cancellations and small contributions to the parity forbidden alpha-particle width, reminiscent of the cancellations that are characteristic of E1 decays. These calculations predict the alpha-decay width of the 0^- state at 6.88 MeV to be of the order of 10^{-11} eV with a branching ratio of the order of 10^{-10}. This branching ratio is dependent on the (unknown) lifetime of the 0^- state, and a shorter lifetime yields a smaller branching ratio.

Attempts to calculate parity violations in nuclei were met with great difficulties in several nuclei. However it appears that the nuclear structure of ^{18}O may allow an improved situation and the possible extraction of the fundamental weak interaction coupling constant, due to the fact that such calculation could be tested against a large body of data of measured electric dipole decays (E1s).

The beta-delayed alpha-particle emission of ^{18}N has been measured by the Yale-MSU collaboration, [6] and the beta-delayed alpha-particle emission of ^{16}N was measured at Yale University.[7] The ^{16}N experiment used some 10^7 ^{16}N/sec produced in the $^{15}N(d,p)^{16}N$ reaction, and the time of flight for low energy alpha-particles was measured off line. This experiment exhibited low background at low energies (1 MeV alpha-particles) and a sensitivity for a beta-decay branching ratio of the order of 10^{-9} to 10^{-10}, as shown in Fig. 3.

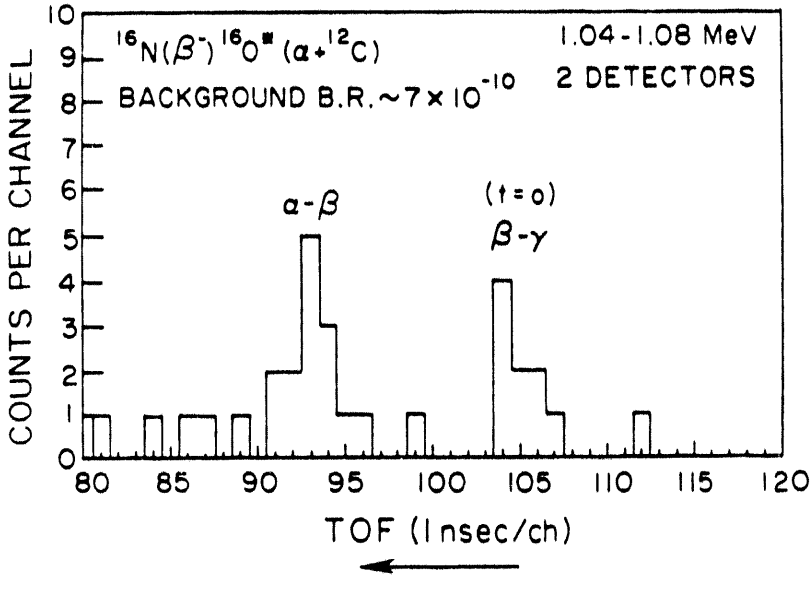

Fig. 3: The beta-delayed alpha-emission of ^{16}N measured at Yale [7] with a sensitivity for branching ratios of the order of 10^{-9} to 10^{-10}.

The ^{16}N Yale experiment can be used as a bench mark for the proposed parity experiment in ^{18}N, which requires an improved sensitivity (by approximately a factor of 10). We then propose to study the β–α time of flight of beta-delayed alpha-particle emission of ^{18}N, as performed in Ref. 7. The low energy ^{18}N ions produced by the IsoSpin Laboratory and mass analyzed, would be collected on a thin carbon catcher foil. We emphasize that in this case contaminant molecular ions such as $^{16}N_2$ should be removed so as not to interfere with collection of $^{18}N^{14}N$ molecules.

In the following we list the differences between the Yale ^{16}N experiment and the proposed parity experiment. These differences need to be studied in detail prior to embarking on this very difficult experiment. At first we note that the predicted intense production of some 10^8 ^{18}N/sec, estimated for the isoSpin laboratory, with a moderate β–α time of flight detection efficiency of 1%, will result for a beta-decay branching ratio of $1x10^{-10}$, a detection rate of 10 events per day, very similar to the event rate of the Yale ^{16}N experiment. The intense beta rate and alpha rate require a large segmentation of the beta and alpha counters, e.g. 100 plastic scintillator beta-counters (covering 40% of 4π) and 100 Si detectors (covering 10% of 4π), so as to yield a count rate of 200 kHz maintained in the Yale experiment. As observed in the Yale experiment at these rates the random coincidence rate at low energies, allows for the observed low background. One major difficulty in the ^{18}N experiment is the possible existence of a new broad state observed [6] in the beta-delayed alpha-particle emission of ^{18}N. One needs to measure the width of this state as well as its alpha-particle partial width in order to assess the "physics background" from this state at small energies (0.5 MeV). Current estimates suggest that the background is in fact below the predicted parity violating alpha-decay signal.

REFERENCES

1. See for example, E.K. Warburton; Phys. Rev. C44(1991)233.

2. H.C. Evans, G.T. Ewan, S.-P. Kwan, J.R. Leslie, J.D. MacArthur, H.-B. Mak, W. McLatchie, S.A. Page, P. Skensved, S.-S. Wang, A.B. McDonald, T.K. Alexander, C.A. Barnes, and E.T.H. Clifford; Phys. Rev. Lett. 55(1985)795, ibid Phys. Rev. C35(1987)1119.

3. M. Bini, T.F. Fazzini, G. Poggi, and N. Taccetí; Phys. Rev. Lett. 55(1985)791, ibid Phys. Rev. C38(1988)1195.

4. E.G. Adelberger, and W.C. Haxton; Ann. Rev. Nucl. Part. Sci. 35(1985)501.

5. B.A. Brown and M. Gai, Cyclotron Laboratory, MSU, annual report, 1987, p. 128.

6. Z. Zhao, M. Gai, B.J. Lund, S.L. Rugari, D. Mikolas, B.A. Brown, J.A. Nolen, Jr, and M. Samuel; Phys. Rev. C39(1989)1985.

7. Z. Zhao, R.H. France III, K.S. Lai, M. Gai, and E.L. Wilds; Bull. Amer. Phys. Soc. 37(1992)1256, and Z. Zhao, Ph.D. thesis, Yale University, 1992.

ELECTROMAGNETIC TRAPS AND RADIOACTIVE ION BEAMS

R.B. Moore

Introduction

Recently electromagnetic traps have been gaining a great deal of attention in physics. This has been demonstrated vividly by the sharing of a Nobel prize in Physics for 1989 by Dehmelt and Paul.

This may seem a little odd considering that electromagnetic traps were invented a long time ago. The Penning trap, used by Dehmelt in the measurement of the g-factor of the electron to an accuracy 400 times better than any previous, was developed by Penning in the mid 1930's for the investigation of electrical discharges. The Paul trap, until recently called the radio-frequency quadrupole (RFQ) trap, was developed by Paul in the mid 1950's. However, except for a select few such as Paul and Dehmelt, electromagnetic traps were not considered as practical devices for serious scientific work until recently.

In my opinion, practical considerations are what have suddenly made them gain respectability as scientific instruments. These are the recent developments in high quality, long-holding-time superconducting solenoids, high stability and low noise electronics, reliable commercial ultra-high vacuum equipment and, last but not least, the personal computer which is now used to control most of these devices. The chemists around the world now have several thousand in operation. The physicists have probably several hundred.

A general feature of the use by chemists is very sensitive detection of the products of various reactions. Typically they will have 1000 to 100 000 ions in a trap at any one time. The general use by physicists is for precision measurements. They will typically have from 1 000 ions down to only one ion in a trap at any one time.

There are excellent reviews of these uses in print. The bible for Paul trap theory and usage is still Peter Dawson's book[1]. A more recent update on the uses by chemists is the excellent review by March[2]. This is being further updated in a new two-volume issue by the Chemical Rubber Publishing company, also edited by March[3]. A recent review of the uses by physicists has comprised an issue of the Journal of Modern Optics[4].

This presentation will not be on the use of electromagnetic traps themselves for measurements in the experimental sciences. Rather it is about the possible uses of electromagnetic traps as ion manipulation devices for preparing an ion collection for an experiment or for other manipulation such as acceleration to high energies. One example of such a use is the system we have developed at ISOLDE at CERN for high-accuracy mass measurements on radionuclides. Here a Penning trap is used for the collection and cooling of radionuclide ions for delivery as a small cloud of precisely defined phase space to a precision Penning trap for mass-measuring. The separation of the function of the two traps allows the design of the first trap to be optimized for efficiency of collection and cooling and the second trap to be optimized for precision and accuracy. Another possible use of a trap in such a manner would be to prepare a collection of radionuclide ions into a precisely defined phase space for collinear laser spectroscopy.

The basic principles of electromagnetic trapping

Many electric and magnetic field configurations can lead to the confinement of charged particles. The simplest is probably the "magnetic bottle" formed by a cylindrically symmetric axial magnetic field with a local minimum at the center of confinement and which has been used in plasma physics. Another that is well known would be any circular particle accelerator.

However, these familiar devices are not generally regarded as electromagnetic traps. This is because they are either leaky for some low energy particles or do not allow particles to be localized around a particular point in space. The aim of electromagnetic trapping is to confine low energy charged particles in all three spatial coordinates about a fixed center.

Again, there are many electric and magnetic field configurations that can achieve this. However, there are only two that have been used to any great extent. These have come to be known by the names of their inventors as the Penning and Paul traps.

The Penning trap

The Penning trap is probably the simplest trap to understand at an elementary level. In this device a high magnetic field is used to confine a charged particle's motion to a spiral about a particular magnetic field line. The motion is completely confined by superimposing a restoring electric field along the axis of the magnetic field. The simplest such restoring field is shown in Fig 1 in which two end electrodes are at a potential which repels the charged particle and there is a ring electrode surrounding the confinement region at a potential which attracts the charged particle.

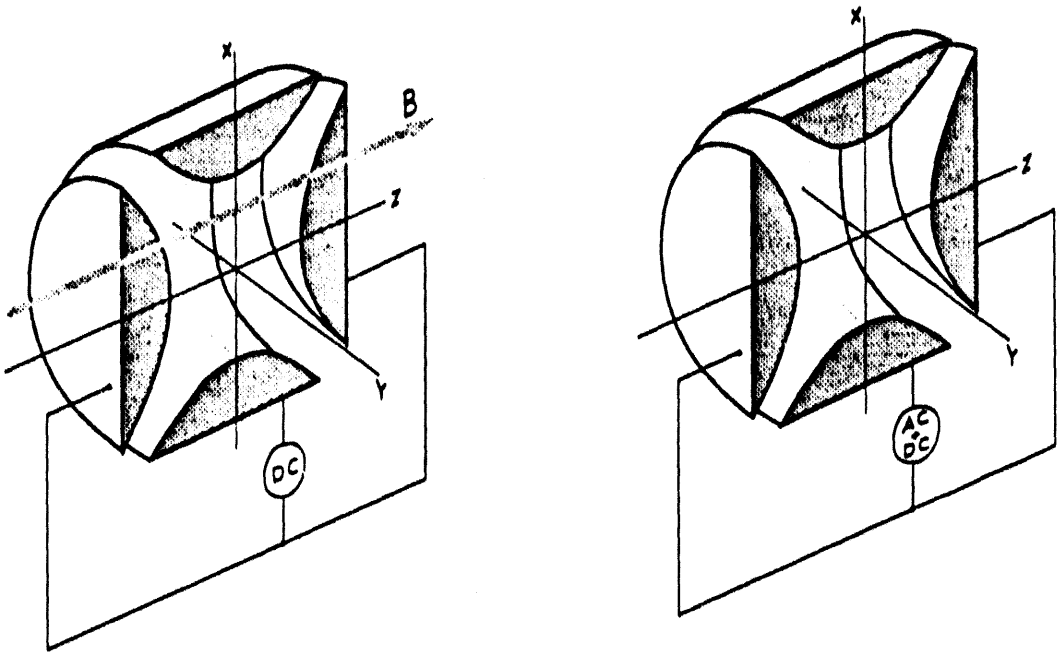

Fig. 1 Cross-sectional views of the two most common electromagnetic traps. On the left is the Penning trap which combines a DC electric field with a DC magnetic field. On the right is the Paul trap which has only an electric field with an oscillating component.

The Penning trap has several disadvantages. An obvious one is the requirement of the high magnetic field. The apparatus to provide this field is expensive and makes the apparatus massive, generally obscuring most of the trapping region.

A less obvious disadvantage is that the particle is not confined if there is general energy loss. This is because of the attraction of the particle to the ring electrode. Any random energy losses, such as from collisions with gas molecules, will cause the particle to migrate toward the ring electrode and eventually reach it and be lost. The radially repulsive electric field, because it counteracts the Lorentz force of the magnetic field, also reduces the cyclotron frequency and causes a slow magnetron precession of the cyclotron orbits.

Despite these disadvantages, the Penning trap has become a very important form of electromagnetic containment device. It was the form of trap used to observe the single electron and the trap used to contain antiprotons at CERN. However, it is obviously desirable to have an electromagnetic trap which provides a spring-like action returning a charged particle to a center for excursions in all three dimensions of space using only electric fields. Such a trap, of the Paul type, was used by Dehmelt for making a photograph of laser fluorescence of a single Barium ion.

The Paul trap

The electrode configuration of the Paul trap is the same as that of the Penning trap; i.e. two end electrodes and a ring electrode producing an axially symmetric electric quadrupole field. However, instead of a magnetic field along the axis of the cylinder, the electric potential between the cylinder and the end electrodes is oscillated, usually at a radiofrequency (figure 2). This has the effect of continually changing the action of the electric field on the particle. At the one instant the field will be repelling the particle from the end electrodes and attracting it to the ring and at the next it will be attracting the particle to the end electrodes and repelling it from the ring.

At first it would seem that these two actions would cancel each other, leading to no net push of the particle toward the trap center. However, with weak fields oscillating at high frequency there is a net attraction impulse toward the trap center over a full RF cycle.

A simple mechanical analogy is a ball resting on a horizontal membrane which has a circular rim, the rim being capable of being deformed so as to be high on two opposite sides and low in the regions between these two highs.

Fig. 2 The rubber membrane analogy to the Paul trap. In the diagram on the left, the ball will be forced toward the rim due to the downward slope. One half period later, represented by the diagram on the right, it will be forced back toward the center. However, because the ball is farther from the center, the slope at this point is greater resulting in a net impulse toward the center.

If the regions of highs and lows are oscillated up and down, then the action of gravity on the ball will be very similar to that of the electric field in a Paul trap on a charged particle. If the motion of a ball is observed in such an apparatus it will be seen that the ball can be made to roll about the center of the membrane just as if it were in a round-bottomed dish.

The theory of trap dynamics will not be presented here. That is available in the references given. As for typical operating parameters, Penning traps are typically one to two centimeters between end electrodes and operate in a magnetic field of about 6 Tesla with several tens of volts between the ring and the end electrodes. For such operation, a singly charged ion of mass number A = 100 will have cyclotron frequencies of about 1 MHz with axial oscillation frequencies of about 100 kHz and magnetron precession frequencies of about 10 kHz. Paul traps are about the same size as Penning traps and are typically operated at up to several kV_p RF between the ring end and the end electrodes and at frequencies of typically 1 MHz. For such an operation, a singly charged ion of mass number A=100 can experience a net restoring force sufficient to result in simple harmonic motion at about one-quarter of the RF in both the radial and axial directions.

Of course, other forms of electromagnetic traps are possible, using more complicated electrode configurations. However, none of these traps seem to offer significant advantages over the Penning and Paul traps and so none of them have received widespread attention.

The uses of electromagnetic trapping as ion cloud preparation devices

Electromagnetic traps have already been used in many ways to prepare ion clouds for a particular type of investigation. What follows is a brief description of the principal usages.

The elimination of unwanted ions

One of the uses of an electromagnetic trap for subsequent experiments on a selected ion is to eliminate species of other ions that may be present in an initial collection. This is being carried out in the collection/cooling trap at ISOLDE by using a ring electrode which is split into azimuthal quadrants. By loading the trap with helium at 10^{-3} Pa as a background buffer gas and using a voltage configuration on the electrodes which produces a radiofrequency azimuthal quadrupole field at the cyclotron frequency of a particular ion, only the motion of that ion is cooled so that the ion condenses into a small volume at the center of the trap[5].

The unwanted ions of species with cyclotron frequencies different from that of the selected ion will be heated by this applied electric field so as to be driven toward the ring electrode. If desired, this process can be accelerated for a particular species of contaminant by using the same quadrants of the ring to produce an oscillating azimuthal dipole field at the cyclotron frequency of that contaminant. In this way, contaminants in the ion clouds collected in the ISOLDE mass measurement system have been removed from the desired collection with a mass resolution of 1 part in 10^5.

Similarly, clouds of ions in Paul traps are routinely purged by chemists by resonantly exciting the axial simple harmonic motion of a particular unwanted species until it is driven from the trap.

Cooling to miniscule phase space volumes

The cooling mechanism referred to in the previous item has been used in the ISOLDE system to cool clouds of ions down to the temperature of the ambient background gas. This cooling is achieved in less than 0.1 s. The phase space volume of the resulting ion clouds is typically less than 1 eV-microsecond in each canonical displacement coordinate. When delivered to the measurement Penning trap, this results in a small oblong collection which is about 2 mm long and about 0.3 mm in diameter, making the extremely precise mass measurements possible.

At McGill, similar cooling has been achieved for collections of ions in a Paul trap. Again helium buffer gas cooling was used but in this case at a background pressure of about 10^{-2} Pa. For collections of less than 1000 ions, cooling has been achieved to phase space volumes of less than 0.5 eV-μs microseconds in each coordinate of the motion. The cooling times to reach these volumes appear to be about 10 ms.

The ionization of a small collection to high charge states

One of the advantages of the Penning trap is that an ion of a given mass will become more strongly confined as its ionization level is increased. This means that a given ion cloud can be bombarded by high energy electrons until as many of the electrons as desired are removed from the ion's nucleus.

This is the basis of the so-called EBIT (electron bombardment ion trap) high-charge state ion source. Such a source is being mounted for a high accuracy mass measurement system for stable nuclei at the Manne Siegbahn Institute in Stockholm.

For radioactive ions to be treated in this way, the rate at which high ionization states can be achieved must be taken into account. From present results it would appear feasible to bring a cloud of medium mass ions to charge states of over 4^+ in several tens of milliseconds.

The breakup of unwanted molecules

Chemists routinely use collision-induced dissociation of molecules in electromagnetic traps. The most common application is in Paul traps where axial oscillations are resonantly excited in the presence of a background gas. The products of the dissociation are then analyzed to give an unambiguous identification of the original molecule.

Electron bombardment can also be used to break up molecules in electromagnetic traps. This could be of particular use on some physics experiments where an ionized molecule could be an isobar of a particular rare radionuclide of interest.

Separation of different ions of interest

Once a collection of ions has been cooled to a small phase space volume in an electromagnetic trap, varying the trap operating parameters can result in ions of different species within that cloud being extracted from the trap at different times. Chemists do this routinely in Paul traps as a means of identifying the reaction products of a dissociation procedure.

The injection and extraction of ions from traps

The techniques outlined above should have a wide variety of applications in adapting or preparing a given collection of ions for different experimental observations. However, to make them generally useful there must be efficient injection and extraction schemes for the electromagnetic traps to be used. This has been primarily the drive of the research effort at McGill.

Essentially, the problem of injecting charged particles into and extracting them from electromagnetic traps is very similar to that of injection and extraction from circular accelerators. Injection of any one beam pulse into a trap merely involves time manipulation of the electric fields decelerating the ion pulse until the pulse has the phase space volume corresponding to that of a stable oscillating cloud in the trap. This phase space volume will be characterized by ellipses in each of the 3 momentum-displacement projections of the phase space volume (Fig. 3).

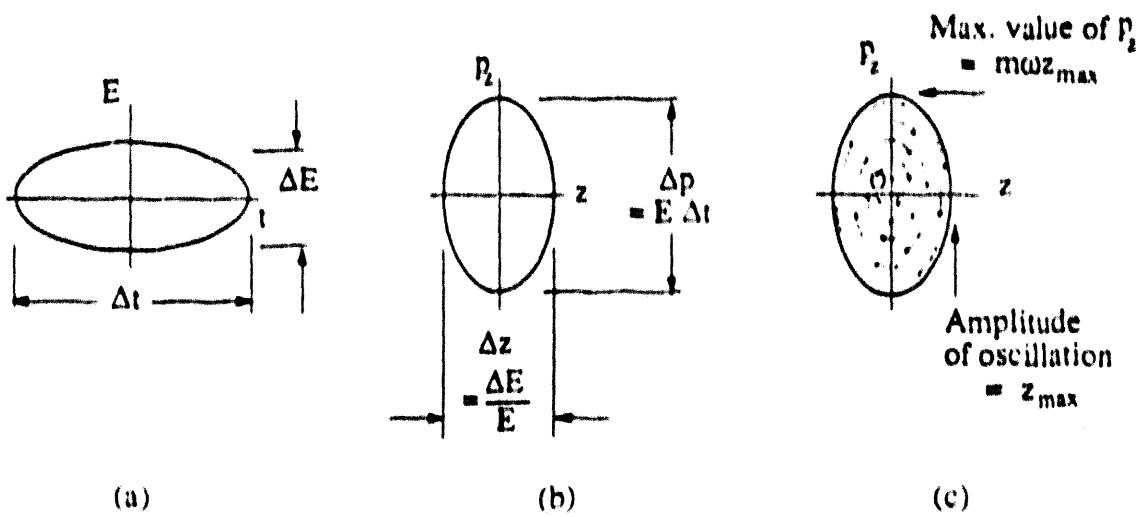

Fig. 3 Projections of the phase space volumes of a beam and a trap for the motion in the axial coordinate (z). (a) is the presumed ellipse for the beam pulse with the vertical axis representing the energy spread and the horizontal the pulse duration. (b) is the momentum-displacement plot for this pulse if its center of mass is quickly decelerated to rest in an electric field of E. (c) is the diagram for a trap with ion oscillations to amplitude z_{max} at angular frequency ω.

By Liouville's theorem, in a linear system, the areas of the diagrams in fig. 3 will be the same for the manipulation of an ion pulse into a trap. These areas are usually referred to as longitudinal emittance. All that is required for complete capture is therefore that the phase apace volume of the trap be greater than longitudinal emittance of the original beam pulse.

The phase space volume available in a typical trap can allow a very large longitudinal emittance (several keV-μs). It is therefore relatively easy to capture one beam pulse. However, the capture of a continuous beam requires the stacking of successive longitudinal bites of the beam in different radial sections of the phase space volume. This requires more careful manipulation of the beam into these different regions. Also, for continued filling of the trap indefinitely, the ion cloud already within the trap will have to have its phase space reduced by cooling.

Methods have been developed for accomplishing this leading to the expectation that close to 100% injection efficiency of a DC ion beam into a trap should be possible in the near future[6].

The space charge limitation of electromagnetic traps

There is, however, a severe limitation on the use of electromagnetic traps for charged particles. This is because of the space charge of the particles. In a typical trap that has been used up to now, the maximum number of particles that can be kept for even a limited time is about 10^6. For a Paul trap the limitation is even more severe if one wants a cold ion cloud. This is because the radiofrequency motion associated with the oscillating electric field can heat the cloud. In our work at McGill, room temperature could only be achieved for a cloud of no more than 1000 ions.

For holding larger numbers of cold ions, a long Penning trap would be recommended. For such a trap it is probable that up to 10^8 ions could be stored for long periods of time. By heroic measures it might be possible to store up to 10^9.

Conclusions

The conclusion of this presentation is that electromagnetic traps could be very useful devices for preparing and manipulating collections of small numbers of ions. This rules them out from having a significant part to play in manipulating beams of ions of more than about 10^9 per second. However, that still leaves a considerable number of possibilities i. dealing with the very rarely produced radionuclides far from beta stability.

References

[1] Dawson, Peter H., 1976, *Quadrupole Mass Spectrometry*, (Elsevier)

[2] March, Raymond E. and Hughes, Richard J., 1988, *Quadrupole Storage Mass Spectrometry*, (John Wiley & Sons)

[3] March, Raymond E. and Todd, John F.J., editors, to be published 1993, *Modern Mass Spectrometry - Practical Aspects of Ion Trap Mass Spectrometry*, (CRC Press Series)

[4] Blatt, R., Gill.P., and Thompson, R.C., editors, 1991, *Special Issue Physics of trapped Ions* , Jour. Mod. Optics **39**

[5] Savard, G., Becher, St., Bollen, G., Kluge, H.-J., Moore, R.B., Otto, Th., Schweikhard, L., Stolzenberg, H. and Weiss, U., "*A New Cooling Mechanism for Heavy Ions in a Penning Trap*", 1991, Phys. Lett. A **158**, 247.

[6] Moore, R.B., Lunney, M.D.N., Rouleau, G. and Savard, G., "*Collection, Cooling and Delivery of ISOL Beams*", 1992, Proceedings of the 12th International Conference on Electromagnetic Separators and Techniques Related to Their Applications, Sendai, Japan, Sept 1991. Nucl. Instr. & Meths. **B70**, 482.

Materials Science Experiments in the ISOSPIN Laboratory

J.A. Sawicki

AECL Research, Chalk River Laboratories, Chalk River, Ontario KOJ 1JO, Canada

Construction of a high-intensity, broad-mass-range, second-generation radioactive beam facility in North America would offer fantastic research opportunities in many areas of materials science and engineering, atomic physics, chemistry and medicine, as well as nuclear physics and astrophysics, the primary interest of this workshop. The range of possible applications of exotic radioactive beams in areas outside of nuclear physics and astrophysics, and various specific examples, has been discussed earlier during Workshops in Parksville (1) and Argonne (2,3), and a recent extensive survey of applications in materials science has been presented by the author in the ISOSPIN Laboratory proposal (4). As we have learned from the very interesting and comprehensive review of various programs in CERN (5), the portion of research projects related to atomic and materials sciences at ISOLDE is increasing continuously; recently it approached about 40% of the total number of projects there. The list of experiments given in ISOSPIN proposal is quickly growing, and detailed discussions of specific ideas and projects will be held during the special Workshop in Chicago next year. The immense research opportunities offered by the ISOSPIN laboratory should be quickly and energetically brought to the attention of condensed-matter physicists and materials scientists in America, as well as to their funding agencies and professional societies.

The interface between nuclear and materials physics has always been a fertile ground for discovering new phenomena and attractive applications. One of the most prominent regions is Mössbauer spectroscopy, which combines nuclear, atomic, solid-state and chemical phenomena in a beautiful quantum effect, widely employed in materials science, chemistry, metallurgy, geology, biology, environmental research and other sciences. Mössbauer spectroscopists used to be the leaders in applications of radioactive ion beams from isotope separators and accelerators, in their studies of ion implantation and ion beam modification of materials. As a result, Mössbauer spectroscopy papers usually constitute a major part of the program in the conferences on the applications of unstable nuclei and particles in studies of condensed matter. This was clearly seen at the conference held in RIKEN a month ago (6).

As the Mössbauer spectroscopist at AECL Research, I am especially interested in applications of radioactive ion beams in the studies of materials and processes related to CANDU-type nuclear power reactors, and to the nuclear industry in general. We use Mössbauer spectroscopy extensively in studying the properties of advanced (Zr-based) alloys, corrosion phenomena in primary (cooling) systems and secondary (steam generating) systems, behavior of fission products and nuclear by-product (waste) management, as well as catalysts for environmentally safe chemical processing. Since we are constantly looking for new or improved methods of analysis of very low-concentration impurities in

radioactive/irradiated materials, the application of radioactive beams to produce the sources or to probe the absorbers offers many advantages. Because each Mössbauer isotope has its own specific features and methodology of measurements, it is impossible to generalize at this point. For instance, in the most often used case of 14.4 keV Mössbauer resonance in ^{57}Fe, one usually works with a long-lived ^{57}Co ($T_{1/2}$=270 d) source, and less often with a Coulomb-excited ^{57}Fe source. The use of a short-lived ^{57}Mn ($T_{1/2}$=1.7 min) source recently obtained at ISOLDE would allow us to probe, for instance, the behavior of Mn in materials, and particularly in irradiated Zr alloys.

Research projects in materials science and especially in applied analytical work are generally much shorter in time and smaller in scale than basic nuclear or astrophysics projects. This implies that the ISOSPIN facility should be very flexible and responsive to many future impatient and unwealthy users regarding type of experiment, beam, energy, current, length of shifts, etc. Although it is impossible to predict precisely the scope of projects that will be undertaken about ten years from now, one can be sure that materials for energy generation, semiconductors and biomaterials will continue to be of major interest. The newly emerging physics of doped-diamonds, nanostructures and soft condensed-matter studies may especially profit from the availability of exotic beams. In particular, in addition to studies with ^{57}Co, ^{119}Sn and ^{197}Pt sources, I would like to explore ion implantation in diamond, VLSI silicon devices and nuclear materials by on-beam Mössbauer spectroscopy with, for instance, ^{57}Mn, ^{73}As, ^{119}In and ^{197}Hg, which are not readily available using conventional irradiation techniques.

1. J.A. Sawicki, "Applications of Radioactive Beams in Nuclear Solid State Physics and Materials Analysis", Proc. of the Accelerated Radioactive Beams Workshop, Parksville, Canada, 1985, TRIUMF, 1985-1, eds. L. Buchanan and J.M. D'Auria, p. 307-314.

2. J.A. Sawicki, "Applications of Radioactive Ion Beams in Materials Science", Proc. of Workshop on the Science of Intense Radioactive Ion Beams, Los Alamos, 1990, LA-11964-C, pp. 231-248.

3. E.D. Arthur, J.E. Crawford, P.L. Dyer, W.D. Hamilton, S.S. Hanna, C.J. Maggiore, H.A. O'Brien, D.R. Phillips, J. Sample, J.A. Sawicki, G.D. Sprouse, R.D. Taylor, J.R. Tesmer and B.H. Wildenthal, "The Border Regions of Medicine, Condensed Matter, Atomic and Nuclear Physics", *ibid.*, pp. 82-83.

4. North American Steering Committee for the ISOSPIN Laboratory with J.A. Sawicki, K.E. Gregorich, L.Buchmann, G.J. Mathews, L. Orozco, G.D. Sprouse, M. Hass and J.M. Wouters, "The ISOSPIN Laboratory (ISL): Research Opportunities with Radioactive Nuclear Beams", Los Alamos, 1991, LALP 91-51.

5. H. Haas, "Prototypical Experiments in Materials Science", this Workshop.

6. International Conference on Applications of Unstable Nuclei and Particles in Condensed Matter Studies, RIKEN, Japan, Sept. 1992, Proc. to be published in Hyperfine Interactions.

A New Region for Fission and Fission Isomer Studies.

J. B. Wilhelmy and P. Möller

Los Alamos National Laboratory
Los Alamos, N.M. 87545

An IsoSpin Laboratory would offer a unique opportunity to greatly extend our knowledge of the fission process. Near barrier studies of fission have been largely limited to a relatively narrow region of actinides (Th-Cf). Over the past decade the most exciting areas of fission studies have been associated with the very heaviest elements where rapidly changing barrier and shell properties have resulted in strong variations in mass distributions and kinetic energy release. These areas are, however, extremely difficult to access and only limited quantities of data have been obtained. With an ISL facility it will be possible to produce copious quantities of previously inaccessible isotopes (due to a lack of any stable or long lived targets) in the region between Pb and Th. Using the ISL prototypical design it is estimated that over 300 isotopes will be produced in the Pb-Th region having beam intensities > 10^6 part/sec.

Since the fissility of an isotope is $\propto Z^2/A$, a large number of the neutron deficient isotopes in this new region will be more fissile than many well studied actinides (^{235}U, ^{239}Pu, ...). These isotopes will have their fission probability controlled by the outer barrier which, unlike that of the more familiar actinide isotopes, is always substantially larger than the inner barrier. Calculations imply that these outer barriers will be complex in nature with discrete minima associated with both symmetric and asymmetric shapes. This is just the desirable condition to learn the most about the influence of the barrier potential energy properties on the fission observables. To maximize the information about the barrier it is necessary that fission be the predominant decay channel, i.e. the neutron binding energy should be greater than the fission barrier ($B_n \geq B_f$). This is just the condition that occurs in the neutron deficient preactinide region. As the neutron number decreases the fissility increases, the fission barrier decreases, and the neutron binding energy increases. Fig. 1 presents the calculated fission barrier and neutron binding energy for a series of Rn (Z=86) isotopes. For isotopes below A=204 fission will become the dominant decay channel. The peak in the

fission barrier at A=212 is caused by the N=126 shell closure which greatly increases the ground state binding energy.

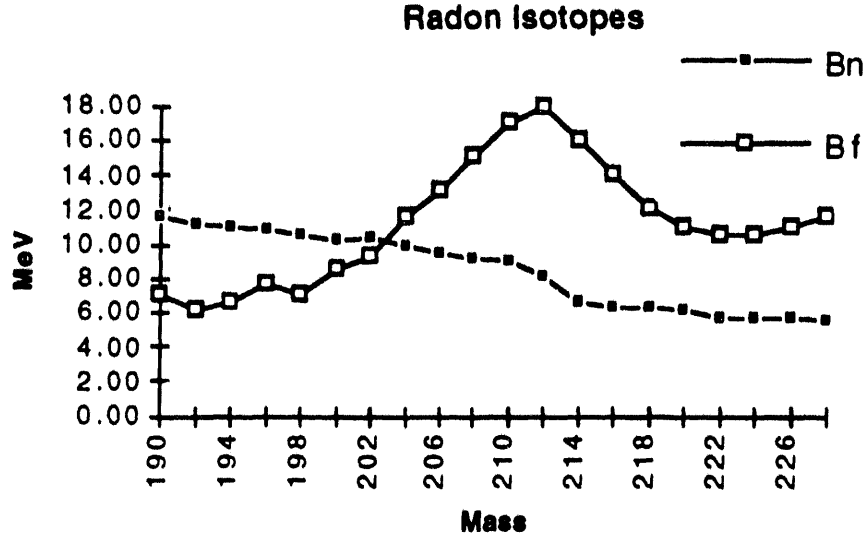

Figure 1. Calculated neutron binding energies and fission barriers for Radon isotopes.

With the ISL, fission barrier studies would use simple direct reaction mechanisms, such as (d,pf), but perform them in an inverse kinematic manner by accelerating the radioactive heavy element species. Typical beam energies would be in the 7-10 MeV/A region. These high energy heavy ion projectiles would have an appreciable usable range in realistic targets ($\approx$ mg/cm^2). Due to the inverse kinematics the emerging fission fragments would be focused in a small forward cone (permitting high solid angle detection) and have high laboratory velocities (moving them well above the Bragg peak and thus permitting accurate dE/dx particle identification). Beam currents of 10^6 ions/sec would, for a typical heavy element in this region, result in the measurement of over 10^6 particle/ fission coincidence events per day.

In addition to extensive new fission barrier studies, experiments with these preactinides would open up an entirely new region for shape isomerism studies. As stated above, the fission process will be dominated by the outer barrier. However, there is still an inner barrier for all of these isotopes which will provide an isolation region for shape isomeric trapping. Figure 2 shows the calculated values for the neutron binding energies, inner and outer fission barriers and the isomeric levels for a series of Radium (Z=88) isotopes.

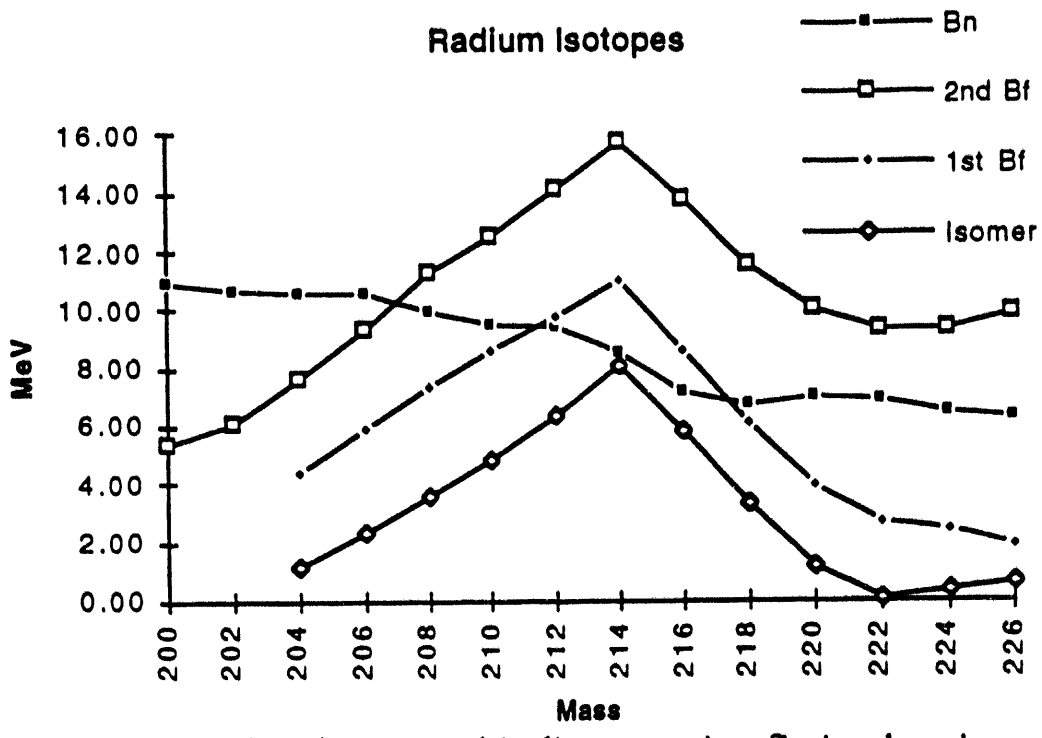

Figure 2. Calculated neutron binding energies, fission barriers and isomeric levels for Radium isotopes.

The inner barrier is substantially below the outer barrier while the isomer level is 1-3 MeV below it. This means that any trapping in the isomeric level will be strongly inhibited against fission and will predominantly decay by tunneling and gamma emission in the first well. The "specialization energy" will inhibit the decay back to the first well and thus make the isomers long enough lived for experimental detection and spectroscopic study. The relatively high neutron binding energy will result in an increased $\Gamma_{isomer}/\Gamma_{g.s.}$ population. Simple scaling estimates imply that isomer population will be in the 10^{-2} - 10^{-3} range (whereas typical actinide fission isomer population is in the 10^{-4} - 10^{-6} range). This implies that ISL experiments using a GammaSphere type photon detector array could result in detecting some 10^5 isomeric decays/day.

PRODUCTION OF BEAMS OF NUCLEI FAR FROM STABILITY

R.N. Boyd

Department of Physics, Department of Astronomy

The Ohio State University, Columbus, OH 43210 USA

and

M.C. Wiescher

Department of Physics

University of Notre Dame, Notre Dame, IN 46616

A scheme is considered for producing extremely neutron rich nuclides in which a secondary radioactive nuclear beam is accelerated and fragmented to produce the (tertiary) beams of interest. Although little is known about some of the cross sections involved, the scheme appears sufficiently promising to warrant further investigation.

Although numerous schemes [1] have been suggested, and utilized, for producing radioactive nuclear beams, none yet devised would produce copious amounts of heavy nuclides, i.e., nuclei 200 amu or more, near the neutron drip line. The present study is directed toward a scheme intended to produce usable intensities of such nuclides. Why study such nuclei? The nuclides near the proton or neutron drip lines produce the most stringent tests possible of nuclear mass formulae. The possibility of new collective nuclear phenomena, such as the neutron halo

discovered for light nuclides, also becomes greater as one moves further from stability. Finally, understanding the astrophysical r-process, the succession of neutron radiative captures which has synthesized many heavy nuclides and all of those heavier than 209 amu, requires study of the nuclei at the neutron drip line, perhaps as many as 20 neutrons beyond stability. Since the r-process requires study of the most extreme neutron rich nuclides, I will focus on it as motivation for their study.

A recent study of the r-process by Kratz et al. [2] allows definition of the processes necessary to fully understand the r-process. One of their equations gives the rate of change of the abundance Y(Z,A) of nuclides characterized by proton number Z and mass number A as

$$dY(Z,A)/dt = n_n Y(Z,A-1)\sigma_{A-1} + Y(Z,A+1)\lambda_{A+1} - Y(Z,A)(n_n\sigma_A + \lambda_A + \lambda_{\beta n}{}^A + \lambda_{\beta 2n}{}^A + \ldots) + Y(Z-1,A)\lambda_\beta{}^{Z-1,A} + Y(Z-1,A+1)\lambda_{\beta n}{}^{Z-1,A+1} + \ldots ,$$

where n_n is the neutron density in the r-process environment, σ_A is the (n,γ) cross section on nucleus (Z,A), λ_A is the rate of destruction of nucleus A by (γ,n), the terms multiplying Y(Z,A) represent processes which destroy nucleus (Z,A) via (n,γ) or (γ,n) (the first two terms) or by decays of that nucleus via emission of a β and some number of neutrons, and the last two terms represent creation of nucleus (Z,A) from decays of more massive nuclei via emission of a β and some number of neutrons. While some approximations can be made, this equation shows that in general one needs to know the β-decay rates of each nucleus involved, the relative strengths of each mode of decay (whether β, βn, $\beta 2n$, etc.), and the cross sections for (n,γ) or (γ,n). This is, even with unrestrained enthusiasm, impossible at present, due to the unavailability of radioactive beams of extremely neutron rich nuclides together with a neutron target of sufficient

density for reactions to ever be observed. However, if even low intensity beams of some of the relevant nuclides could be produced, enough masses could be measured to define nuclear mass formula parameters to the point where they could be trusted to predict masses and, if some lifetimes and β-decay modes could be measured, β-decay systematics as well. Such measurements would represent an extremely important advance for understanding the astrophysical r-process. In addition, in many instances, (d,p) reactions could be used to obtain similar information to that required for the (n,γ) reactions.

To study possible schemes of producing extremely neutron rich heavy nuclides, we have selected W isotopes as a test case. The relative yields of W isotopes from high energy proton bombardment of a U target were first predicted. The code used utilized the Silberberg-Tsao formalism [3]. The relative production intensities for W isotopes (via fission) were found to fall off exponentially with N, with that for ^{206}W, 20 neutrons beyond stability, being a factor of 10^4 lower than that for ^{188}W, the lightest even-mass unstable W isotope.

However, if one accelerated the W isotopes produced from the p+U interactions (which is required anyway to produce an analyzable output), up to roughly 100 A MeV, one then could bombard another target, possibly a neutron rich one such as ^{48}Ca, to shift the isotopic distribution peak (of the tertiary beam!) further to the neutron rich side of stability. If enough of a shift occurred, it might compensate for the loss in intensity due to the second scattering for the most neutron rich isotopes. In this context we have performed two sets of yield predictions, one with a ^{190}W beam on ^{48}Ca and the other with a ^{196}Os beam on a ^{48}Ca target, using code INTENSITY [4]. The former case, assuming an acceptance solid angle into a subsequent analyzer of 6.4 msr, predicts an attenuation factor of about 3000 for ^{194}W and ^{196}W compared to ^{190}W, with decreasing yields as one goes to more neutron rich nuclides. However, the peak of the distribution does

indeed occur further to the neutron rich side of stability than with the p+U production scheme, giving yields which begin to compete with those from the p+U scheme. Furthermore, there are several obvious ways to increase the tertiary beams, probably by at least an order of magnitude. The ^{196}Os on ^{48}Ca scheme predicts that the fragmentation yields actually increase out to ^{200}W! While this seems unrealistic, there are, of course, no data to contradict this result. The beam intensities from this second scheme would thus certainly exceed those from the p+U production for W isotopes beyond about ^{204}W, but the veracity of the predictions must certainly be tested.

While the trustworthiness of the predictions on which the present study is necessarily based is questionable, those predictions do suggest that it might be possible to enhance the yields of very neutron rich heavy nuclides with the tertiary beam approach suggested here. However, data to test the predictions of the codes would certainly be helpful, especially data for isotopic fragmentation yields for high energy heavy ions on isotopes of, e.g., Ca. Then combination of those measurements with the codes should allow us to predict whether or not the scheme suggested in this paper can succeed.

This work was supported in part by NSF grants PHY89-20606 and PHY89-11831. The assistance of W. Talbert and B. Sherrill in performing calculations is gratefully acknowledged.

[1] R.N. Boyd and I. Tanihata, Physics Today **45**, 44 (1992).

[2] K.L. Kratz, J.-P. Bitouzet, F.-K. Thielemann, P. Moller, and B. Pfeiffer, Astrophys. J. to be published, 1992.

[3] R. Silberberg and C.H. Tsao, Astrophys. J. Suppl. **25**, 315 (1973); ibid, **25**, 335 (1973).

[4] J.A. Winger, B.M. Sherrill, and D.J. Morrissey, Nucl. Instr. Method. B**70**, 380 (1992).

rp–Process Measurements with High–Intensity RNBs

Joachim Görres

University of Notre Dame

The reaction yields Y for the direct measurement of resonances of importance to the rp–process can be calculated from the estimated resonance strengths $\omega\gamma$ from the relation:

$$Y = \frac{m_t + m_p}{m_t} \frac{\lambda^2}{2\,\varepsilon}\,\omega\gamma,$$

with $m_t(m_p)$ the mass of the target (projectile), λ the proton wavelength and ε the stopping power in the lab–system. Table 1 shows the resonance parameters for several reactions of interest. The reaction yield has been calculated for a RNB intensity of 10^{10}/s. A comparison with the $^{13}N(p,\gamma)$ reaction, which has been recently measured at Louvain–la–Neuve [1], reveals that an improvement of at least two orders of magnitude is needed for the direct measurement of these resonances. The limiting factor in these experiments will be the background induced by the RNBs. In the following, several experimental aspects of such a measurement will be discussed.

Table 1: expected yield for several reactions of importance to the rp–process calculated for a RNB intensity of 10^{10}/s. As a comparison, the parameters for the $^{13}N(p,\gamma)$ reaction are also listed.

Reaction	E_R [MeV/u]	E_γ [MeV]	$\omega\gamma$ [meV]	Y [1/h]
$^{19}Ne(p,\gamma)$	0.45	1.6	6.2	440
$^{31}S(p,\gamma)$	0.59	2.2	32	1720
$^{39}Ca(p,\gamma)$	0.36	0.9	0.003	0.3
$^{56}Ni(p,\gamma)$	1.70	2.4	63	1520
$^{13}N(p,\gamma)$	0.545	5.17	2400	$1.5 \cdot 10^5$

Hydrogen Target

The major advantage of a jet gas target over a solid target (CH_2) is the stoichiometry (pure H_2). The presence of Carbon in a solid target increases the stopping power, and thus the yield for a solid target is decreased by nearly a factor of three compared to a pure H_2 target. A common problem of both targets is the deposition of activity from the RNB near the target area. For a solid target this is caused by large angle scattering on Carbon and for the jet gas target by scattering on collimators, which are necessary because of the small diameter of a jet (typically 3 mm). However, it appears possible to reduce this activity by a careful design of the jet gas target area.

γ–Detection

The main problem for the detection of prompt γ–rays from the reaction is the beam induced background. A γ–flux of ~10^5/s (mainly 511 keV γ–rays from the β^+–decay) is expected for a RNB intensity of 10^{10}/s if one assumes that 10^{-5} of the beam is deposited close to the target area. This can lead to pile–up extending into the energy range of interest ($E_\gamma \leq$ 2.5 MeV, s. table 1). A high segmentation of the detector system is therefore important to limit the count rate in the individual detectors to reduce the pile–up probability.

The choice of the γ–detector is determined by the need for high efficiency. This requirement favors the use of NaI detectors. The advantage of Ge detectors is the good energy resolution, which improves the peak to background ratio compared to a NaI. However, the limiting factor for the energy resolution is the Doppler broadening of the peaks ($\Delta E/E \leq$ 1 %) caused by the inverse kinematics. An additional disadvantage of Ge–detectors is the large response time compared to a NaI detector. This leads to increased pile–up and limits the total count rate of the detector to ≤ 25 kHz.

Example: A array of 30 NaIs (7.5 cm × 7.5 cm) has a total peak efficiency of up to 30% at E_γ= 2 MeV. This would lead to a reaction count rate of 0.15/s for the $^{31}S(p,\gamma)$ reaction (E_γ= 2.2 MeV). However, a pile–up rate of ~ 100/s is expected from an extrapolation of the test

results of Bonnet et al. [2]. The problem is even more severe in the case of the $^{39}Ca(p,\gamma)$ reaction, where the γ–energy is only 0.9 MeV. These examples show that γ–spectroscopy alone is in general not sensitive enough for the direct measurements of resonances in the range of $\omega\gamma$= 1 – 100 meV.

Recoil detection

A second approach is the detection of the recoil particles. The required recoil spectrometer must be able to separate the recoils from a primary beam with ΔM = 1 and similar momentum ($\Delta p/p$ = 2 – 5 %). Best suited for this task appears to be a combination of energy filters (Wien filter) and magnetic dipoles. Such a device has been recently tested at Caltech [3] using the reaction $^{12}C(p,\gamma)$, and a beam rejection ratio of 10^{-10} has been achieved. Assuming a beam intensity of 10^{10}/s and a total detection efficiency of 50%, a count rate of 0.25/s is expected for the $^{31}S(p,\gamma)$ reaction with a background rate of 1/s. The reaction to background ratio can be further reduced by a combination of γ– and recoil detection, and a ratio of 10000 : 1 appears realistic. An alternative in many cases is the observation of the characteristic decay products from the decay of the recoil either at the focal plane of the spectrometer or at a low background area using a tape transport system.

Beam requirements

A RNB of the order of 10^{10}/s is essential to measure resonances in the range of $\omega\gamma$ = 1 – 100 meV within a realistic time frame.

For the direct measurements an energy range of 0.2 – 2 MeV/u is necessary. Desirable is an energy of up to 20 MeV/u to allow the search for resonances by indirect measurements, e.g. transfer reactions. This would allow the determination of the exact locations of the resonances of interest, thus avoiding the time consuming search for the resonances in the direct measurement, while also allowing the study of reactions where either the beam intensity or the strength of the resonances is too low for a direct study.

Because of the low level densities at the excitation energies of interest, a beam energy resolution of ≤15 keV/u would be sufficient to resolve resonances in the direct measurements. However, to insure maximum reaction yield (the thick target yield) a better resolution is needed. Depending on the specific reaction, a resolution of better than 30–50 keV is needed assuming a target thickness of $10^{18}/cm^2$.

The RNB energy has to be known within 1–2 keV/u to avoid the time consuming search for the resonances, and the beam spot should be well defined (~1 mm) to reduce the scattering of the beam in order to keep the accumulation of activity in the target area at a minimum.

The demand on the beam purity will strongly depend on the reaction to be measured. The main problem is the contamination of the beam with isobars of the reaction product of interest and with isotopes which lead to strong background reactions, e.g. ^{19}F. For these cases a beam impurity of 10^{-5} or better is required.

[1] P. Decrock et al., Phys.Rev.Lett. 67 (1991) 808

[2] L. Bonnet et al., NIM A292 (1990) 343

[3] M.S. Smith, C. Rolfs, and C.A. Barnes, NIM A306 (1991) 233

SAMPLES FOR *s*- AND p-PROCESS STUDIES

F. Käppeler[1], M. Wiescher[2], and P. E. Koehler[3]
[1]Kernforschungszentrum Karlsruhe, Institut für Kernphysik, [2]University of Notre Dame
[3]Los Alamos National Laboratory

MOTIVATION

The abundance patterns of *s*-process branchings carry important information on the physical conditions of the stellar site, e.g. they allow for the determination of the neutron density, temperature, and mass density. Hence, their study yields information on the reliability of stellar *s*-process models.

In the first place, the analysis of these branchings requires the stellar neutron capture cross sections of the involved isotopes. Since the *s*-process abundances are uniquely determined by the respective stellar (n,γ)-cross sections, these data need to be known with an accuracy of better than 5% for performing reliable branching analyses. While the stable *s*-only isotopes, that define the branchings, can meanwhile be measured by optimized techniques with typical uncertainties of 1% [1], experimental information for the unstable isotopes is still missing for practically all branch point isotopes. For these nuclei, statistical model calculations have to be used so far, but even with the most sophisticated methods, the calculated cross sections exhibit uncertainties of typically 20 to 30%, often not sufficient for a detailed interpretation of the observed abundance pattern.

Recently, there was renewed interest in the *p*-process, that is responsible for the production of the rare, neutron-deficient isotopes, which cannot be ascribed to the *s* - or *r*-process. To date, these studies are almost completely based on data derived via statistical model calculations [2]. This situation needs to be improved by a subset of experimental cross sections to be used for testing and/or adjusting the cross section calculations. In this context, (n,γ)-cross sections on radioactive isotopes are needed as well.

EXPERIMENTAL TECHNIQUE

Given the specific problems of neutron capture cross section measurements, a direct on-line measurement at the ISL-facility does not appear very promising. Therefore, we propose to use ISL for the preparation of samples that can be investigated off-line. For the cases listed below, capture cross sections can be measured with existing techniques provided that the samples satisfy the following conditions:

(i) Isotopic enrichment sufficient to reduce unwanted background from impurities.

(ii) Safe handling with respect to radiation hazard and possible contaminations.

(iii) Prompt availability to minimize ingrowth of daughter nuclei.

These requirements could be met by using a radioactive ion beam for implanting the unstable isotopes in an appropriate backing. The optimal implantation energy is approximately 200 keV. This requires a fan-out of the beam after the isotopic/isobaric separation at ISL. This technique has been demonstrated recently at ISOLDE [3] for the cesium isotopes 131, 134, and 135.

In the following, we propose a number of cases, where such samples could successfully be used in cross section measurements. We anticipate that limitations on the available beam current and beam time at a forthcoming RIB facility will limit sample sizes to about 10^{14} atoms. As a result, the activation technique seems to be the only method sensitive enough for the proposed (n,γ) measurements. This restricts the number of branch points that can be investigated in a straightforward way to ~16 cases of importance or the *s*-process and to ~6 cases for the *p*-process. If, however, the RIB yields would be high enough to produce samples of 0.1 to 1 mg total mass, many more cases would become accessible by using the Moxon-Rae setup at Karlsruhe [4] or the 4π detector at Los Alamos [5].

This contribution summarizes those cases that are relevant for the most important *s*-process branchings and that can be investigated with the activation technique.

COMPILATION OF POSSIBLE SAMPLES

Our estimates for sample production are based on the yields reported by the ISOLDE group [6]. In particular, we assume a RIB current of 10^9 particles/s and an implantation time of ~2 days. The examples are restricted to cases with

$t_{1/2}(\text{target}) \gg t_{1/2}(\text{product})$ and $E_\gamma(\text{target}) < E_\gamma(\text{product})$,

so that the induced activity can be unambiguously separated from the activity of the

sample. The electron background due to the beta decay of the target appears to be manageable in practically all cases.

We illustrate our proposal at the example of the target/product pair $^{155}Eu/^{156}Eu$. Implantation of 10^9 atoms/s of ^{155}Eu for 2 d with an efficiency of 50% results in a sample of $N = 8 \cdot 10^{13}$ atoms. Irradiation in a neutron flux Φ for a period t produces

$$Z = \Phi \cdot N \cdot \bar{\sigma} \cdot t$$

^{156}Eu nuclei. For simplicity, the decay during activation was neglected. This is a reasonable approximation, if the activation time is restricted to one half-life of the product nucleus. The $^7Li(p,n)^7Be$ reaction has been used routinely at energies just above threshold to approximate the stellar spectrum for a typical *s*-process environment with a total neutron flux of $\Phi = 10^9\ s^{-1}$ [7]. With $t = t_{1/2}(^{156}Eu) = 1.3 \cdot 10^6$ s, one obtains $Z =$

TABLE 1 Branch point nuclei on the *s*-process path. The relevant sample data are given for those cases, which can be studied with the activation technique.

Isotope	Relevant sample data				*s*-Process parameter
	$t_{1/2}$	E_γ [keV]	$\langle\sigma\rangle$ [mb]	A_β / A_γ [Bq]	
^{134}Cs	2.06 yr				temperature
^{135}Cs	$2 \cdot 10^6$ yr	no γ	200	0.18/ -	
^{137}Cs	30 yr	662	50	$2 \cdot 10^4 / 1.5 \cdot 10^4$	
^{147}Nd	11 d				neutron density
^{147}Pm	2.6 yr	121	1000	$8 \cdot 10^5/24$	
^{148}Pm	5.4 d				
^{154}Eu	8.5 yr				temperature
^{155}Eu	5.0 yr	~100	1900	$1.2 \cdot 10^5 / 7 \cdot 10^4$	
^{163}Ho	4570 yr	no γ	2600	only K X-rays	mass density
^{169}Er	9.4 d				temperature
^{170}Tm	128 d				
^{171}Tm	1.9 yr	67	1000	$2.5 \cdot 10^5 / 400$	
^{179}Ta	1.7 yr	no γ	1250	only K X-rays	mass density and temperature

The quoted activities A_β / A_γ refer to a sample of 10^{14} atoms.

10^5 atoms of ^{156}Eu per activation, if the calculated stellar cross section, σ = 2000 mbarn, is correct.

After irradiation, the decay of ^{156}Eu can be followed via the associated gamma-ray activity. In total, 65% of all decays yield gamma-rays between 646 and 2098 keV; using a large Ge detector in close geometry, these can be measured with an efficiency of about 10%. If the activity is counted for one half-life, one obtains

$$C = Z \cdot \ln 2 \cdot \varepsilon_\gamma \cdot I_\gamma \cdot t = 5 \cdot 10^3$$

counts. In this expression, ε_γ is the efficiency for gamma-ray detection and I_γ denotes the gamma-ray intensity per decay. Even if the signal-to-background ratio is 0.5 as a result of the long counting time, the statistical uncertainty would be already as small as 4% in a single activation, illustrating the feasibility of such measurements on short-lived targets.

The most important *s*-process branchings covered by this proposal are listed in Table 1. The respective branch point isotopes are given in the first column, followed by the relevant sample data for those cases that are accessible to the activation technique discussed here. The last column indicates the respective physical parameter of the stellar plasma, to which the various branchings are particularly sensitive.

It is to be noted that samples of the longer-lived species could also be made by off-line techniques. However, radiochemical methods are often very time-consuming and may also depend on the isotopic purity of the batch material.

The samples of interest for the *p*-process, which can be studied with the same technique, include ^{68}Ge, ^{148}Gd, ^{150}Gd, ^{154}Dy, ^{194}Hg, and ^{202}Pb.

REFERENCES

[1] K. Wisshak, F. Voss, F. Käppeler, G. Reffo 1992, Phys. Rev. *C45*, 2470.

[2] M. Rayet, N. Prantzos, M. Arnould 1990, Astron. Astrophys. *227*, 271.

[3] R. A. Naumann, D. Burke, H. L. Ravn, G. Hlawatsch, T. von Egidy, J. de Boer 1987, Nucl. Instr. Meth. *B26*, 59.

[4] Th. W. Gerstenhöfer, S. Jaag, K. Wisshak, F. Käppeler (In preparation).

[5] P. E. Koehler, In "Capture Gamma-Ray Spectroscopy and Related Topics", ed. W. Hoff, AIP Conference Proceedings 238 (American Institute of Physics, New York 1991), p. 892.

[6] ISOLDE User Handbook IV (1987).

[7] H. Beer, F. Käppeler 1980, Phys. Rev. *C21*, 534.

Section II
Target Ion Sources and Mass Separation

J. M. D'Auria, Coordinator

Section II
Invited Papers

PRODUCTION OF HIGH INTENSITY RADIOACTIVE ION-BEAMS BY MEANS OF THICK TARGET TECHNIQUE

H. L. Ravn
CERN ISOLDE
CH-1211 Geneva 23, Switzerland

ABSTRACT

Target and ion-source techniques which allow rapid separation of thermalized radioactive nuclei from 1-500 g/cm^2 thick irradiated target material and continuously convert them into a mono-isotopic ion-beam present themselves as a new method of radiochemical separation. These techniques combine nuclear reactions with high temperature chemistry, metallurgy, solid state diffusion and ionization phenomena. Developed at the many mass separators on-line at various accelerators or reactors they are today widely used to produce radioactive ion-beams for physics experiments. For some years they have reached a stage of development that allows the production of low-energy high-intensity beams of radioactive isotopes of most elements in the periodical system. In this paper the parameters that determine the intensities of these most often singly charged ion-beams are discussed in view of injection into a post accelerator. First a short introduction is given to the technique of on-line mass separation. This is followed by a detailed discussion of the three factors which determine the production rates in the target: i.e. reaction cross sections, beam properties and target thicknesses and by a discussion of the more decisive factors which control the efficiency with which the radioactive nuclei produced in the target can be transformed into a final ion-beam of typically 10-60 keV energy.

Throughout the discussion the influence and direction of new developments are assessed. Finally, selected examples of realistic

beam intensities are given, which may be used for comparison of the different production methods.

1. INTRODUCTION

The interest in the study of nuclei lying far from ß-stability has led to the development of a powerful technique for production of ion beams of radioactive nuclei. The production is achieved by the bombardment of a target material of sufficient thickness to stop the nuclear reaction products. In this case the products have to be separated from the bombarding beam and the target in order to continuously convert them into an ion beam. The advanced technological processes which are needed to produce pure beams of radioactive nuclei are strongly dependent on the physical and chemical properties of the individual elements. They take place in the target and ion-source unit, which forms the heart of these facilities and has to be developed specifically for each element or group thereof. Once this is achieved, the method has a number of advantages for production of high intensity radioactive ion-beams. Today the development of such systems has reached a stage which allows the production of low-energy beams of the radioactive isotopes of most elements in the periodical system.

Particularly high beam intensities have been obtained when the on-line mass separator is combined with an intense proton beam of about 1 GeV energy. Due to the thick targets (~500 g/cm^2) that may be used, primary beam conversion rates into secondary radioactive beams of up to $R = 5 \cdot 10^{-2}$ are achieved. However, R&D projects proposed at HI accelerators and reactors suggest that similar intensities may now be obtained there. After a short introduction in section 2 to the concept of on-line mass separation a discussion follows of each of the parameters given in equation (1) which determine the radioactive beam intensity.

$$I = \sigma * \Phi * N * \varepsilon_1 * \varepsilon_2 * \varepsilon_3 \qquad (1)$$

In section 3 the formation cross sections s for the nuclear reactions of interest are discussed followed in section 4 by a discussion of the

primary beam intensities F, target thicknesses N and the resulting power densities. The product release and transfer efficiency ε_1, the ion source efficiency ε_2 and the delay transfer efficiency ε_3 are described in sections 5-7 respectively. A more extensive overview of recent developments in the field may be found in the proceedings of the last EMIS conference[1,2]. Finally, in section 7 selected examples of experimentally determined cross sections and beam intensities are given, which allows a comparison of the different production methods.

2. THE ON-LINE MASS SEPARATOR CONCEPT

The concept of on-line mass separation[3], where thermalized nuclear reaction products are continuously transferred from the target to the ion source of a small heavy-ion accelerator equipped with a mass analyzing magnet, is shown in Fig. 1. The essential point here is that the nuclei of interest are formed in very complex nuclear reactions with many exit channels. Only a mass separation combined with a chemical separation in the target and ion source unit can produce isotopic beams of sufficient purity. In Fig. 2 an example of the heart of such a facility, the target and ion-source unit of ISOLDE[4] is shown. The radioactive nuclei formed in the target according to the equation $Y_0 = s \cdot F \cdot N$ are thermalized in the thick target and have now to be transformed into an ion beam. This operation can be broken down into three distinct processes which each have an efficiency as defined in section 2: (ε_1) diffusion to and release from the target surface and transfer by diffusion through the transfer line from the target to the ion source, (ε_2) ionization and (ε_3) decay during the entire process. The many different on-line mass separators in operation which are finding ever-widening applications in the areas of nuclear and other sciences are reviewed in ref.3. The growing interest[5,6] in the application of short-lived radioactive ions as projectiles, has revived the ideas of post acceleration of the beams available from on-line mass-separators. This was in fact already discussed at the 1965 Lysekil conference on nuclei far from stability[7] which marked the start of the field. Since then the on-line mass-separator technology has progressed considerably and reached the stage where it now is a technical feasibility. At the CERN ISOLDE

separators 600 different radioactive ion-beams[8] of the elements shown in Fig. 3 with intensities of up to 10^{12} atoms per second have been obtained with an incident 600 MeV proton beam of $2 \cdot 10^{13}$ protons/s (3μA). This facility is by far the most ambitious project in the field[9]. It was recently reconstructed in a new experimental hall on-line the 1GeV, 2 μA proton beam of the CERN PS Booster and enjoys the collaboration of more than 200 physicists from 50 laboratories. With a physics programme[10] which ranges from the study of nuclei far from stability over atomic, solid state, surface and elementary particle physics, to medical applications. From the layout shown in Fig. 4 it is seen that two mass separators will be used. A low current general purpose separator (GPS) and a medium current high resolution mass separator (HRS) both serve a common experimental area. The design parameters of these machines are to be found in ref. 2. By alternating the operation of the two separators, 3200 hours/year of radioactive beam time may be given to the users. For the planned ISOLDE post-accelerator the HRS seems most advantageous since it may resolve isobaric molecular-ions or possibly isobaric masses if the subsequent accelerating stages are unable to do this.

3. NUCLEAR REACTIONS AND CROSS SECTIONS

The particular radioactive nuclei which it is desired to post accelerate may be produced by a variety of bombarding particles and nuclear reactions. The three reactions which most often are used to produce the nuclei of interest are spallation, fission and fragmentation for which the mass yield curves at different energies are shown in Fig. 5 for the reaction of protons on a heavy target[11]. Somewhat similar reactions may be induced with relativistic light to heavy ions which in addition allows the use of projectile fragmentation. The independent formation cross-sections can be calculated by the formulas of Rudstam[12], Silberberg and Tsao[13] and others. Since these calculations have relatively large uncertainties the following discussion is based only on published experimentally determined cross sections. Such values for all three reactions are found in the compilation of Silberberg and Tsao[14].

Whereas reactions with protons and heavy ions allow us to produce all nuclei of interest, the thermal neutron induced fission of ^{235}U can only be used to produce the neutron-rich isotopes of the elements shown in Fig. 6.

For protons, the total reaction cross-section not only increases considerably between 500 MeV and 1GeV, in the region of target fragmentation and fission as seen in Fig.5[15] but the cross section also rises for deep spallation reactions. A typical example of this is shown in Fig. 7 where the excitation curve for the production of krypton isotopes by spallation of silver[15] shows a weak optimum close to 1 GeV. The gains are from a factor of two near stability at mass 84 rising to a factor of 5 at mass 78 and estimated to end up being a factor of 10 far from stability. For spallation leading to products close to the target and the line of stability the maximum cross-sections are already reached at ~200 MeV proton energy as seen on the excitation curve for the production of argon isotopes by spallation of scandium[15] shown in Fig. 8. By rising the proton energy, gains are expected in the cross sections for target fragmentation reactions leading to neutron-rich light nuclei. This is indicated by the excitation function[14] for production of ^{24}Na and ^{18}F from lead and uranium targets respectively shown in Fig. 9.

Thanks to the recent development of ECR ion sources the intensity of heavy-ion beams (HI) with energies of 30-100 MeV/u has been greatly increased so that they may become of interest for the production of radioactive ion-beams. The higher excitation energy which the slow heavy particle can deposit in the target nuclei gives a cross-section increase for the reactions shown in Fig. 5 of 1-10 times over the 3 GeV proton curve with the highest values for the short ranging heaviest ions. The somewhat longer ranging light ions ^{3}He and ^{12}C show a cross section advantage for deep spallation and target fragmentation reactions as shown in Fig. 10. Here it is seen that the ISOLDE beam intensity ratio[16] of sodium beams formed in 600 MeV proton and 86 MeV/u ^{3}He and ^{12}C fragmentation of uranium increases a factor of 10 near stability increasing to a factor of 50 on the far neutron-rich side. Fig. 11 shows a comparison[17] of isotopic distributions of rubidium produced by fission of ^{238}U with protons of

various energies, 77 MeV/u ^{12}C ions and thermal neutron fission of ^{235}U. It is seen that the cross sections for the HI reaction are 2-5 times higher for ^{12}C than for 1GeV protons whereas the thermal neutron fission yields are up to three orders of magnitude higher. Only small gains were observed for close spallation reactions (DZ = 3) with the HI[16]. A further interesting possibility might be to use the projectile fragmentation in thick targets as a production technique.

It can be concluded that the highest cross-sections are found in the thermal fission of uranium followed by the HI reactions which generally are somewhat higher than for the corresponding proton reactions. It should, however, be noted that the cross sections alone do not allow us to conclude on the best suited bombarding particle. The other factors in equation 1 change the picture given in this section dramatically.

4. PRIMARY BEAM INTENSITIES AND TARGET THICKNESSES

The production rates in the target are generally determined by the product F * N rather than by the cross-section discussed in the previous section. In Table 1 a collection is given of important beam and target parameters i. e: the primary-particle energy loss, maximum available driver beam intensity, maximum target thicknesses and the resulting power deposited in the target.

For thermal neutrons the level of technical development allows presently in Studsvik[18] to use target amounts of the order of 1 gram in a flux density of $3 * 10^{11}$ neutrons/cm^2 * s. An increase of F * N by one order of magnitude seems to be feasible with a moderate R&D effort and will not exceed the total power deposit already handled with other particles. To use the maximum available flux density of 10^{14} neutrons/cm^2 * s seems to require a major R&D effort which may be started at the ILL Laboratory in Grenoble[19].

Protons of 30 MeV are currently used in the pioneering two accelerator RIB project[20] at Louvain-la-Neuve. The short range of these protons is offset by the available beam intensity of 500 mA. The present technological limit is presently around 200 mA which gives a total power of 6 kW. In contrast the long range of the ~1 GeV

protons allows the use of targets of the order of moles/cm^2; a target thickness of 400 g/cm^2 of ^{238}U has been chosen for the calculations as the worst case due to the additional fission power. Targets of this thickness have only been tested with prototypes of lead at ISOLDE whereas targets of 150 g/cm^2 are routinely used. Total power of 5kW (electrical and beam heating from 3 mA of protons) is handled without problems due to the low power density in such big targets. As a logical consequence of the change at ISOLDE from a 600 MeV driver beam to one of 1 GeV it is now suggested to double the target length to 40 cm. Calculations show[21] that for solid refractory targets it is technically possible to use proton-beam intensities of the order of 100 μA and tests of ISOLDE-like targets at the spallation neutron source of the Rutherford Appleton laboratory[22] are in preparation.

For HI the high specific energy loss limits the target thickness to the level of what can be used by low energy protons but due to their energy the total power and power density are the highest in the field. It should be noted that high power density has both beneficial and deleterious effects on the target. On one side it has shown a reduction in the release from the target material as will be discussed in sections 5 and 7. On the other side it tends locally to overheat windows and the target material and to dissociate chemical compounds which may give rise to an unwanted gas load of the ion source. The target and ion-source development programme started at GANIL.[23] will most certainly address these effects.

5. RELEASE AND TRANSFER OF PRODUCTS FROM THE TARGET

The general problem is one of mass transfer, i.e. per second to separate typically between 10^{12} and 10^{-1} wanted nuclei from the 10^{23} target atoms and to transfer them to the ion source. The different steps of this process and the losses from various effects are illustrated in Fig. 12 . They determine the most important parameters of the system: the release yield and the target to source transport efficiency which are combined in the factor ε_1. In the following each of these steps is discussed separately and references to further information are given.

5.1 Target material and product release

The separation of the products from the bulk of the target can be done merely by heating a target material with a low vapor pressure to a sufficiently high temperature so that the more volatile nuclei of interest which are stopped in the target, are released by diffusion and desorption processes. Only in this way can the flow of material be kept sufficiently low to allow the ion-source to perform optimally. A number of such materials have been found and their release properties studied[2] and in the good cases the release from the target occurs with 90-100% efficiency with only small losses in strongly bound sites in the solid targets. Often an element is retained in the target due to too low vapor pressure or chemical bonds to the target surface. By in-situ synthesis of a more volatile compound, a technique often referred to as chemical evaporation, [24,25] a number of less volatile elements have recently successfully been brought on-line. This is illustrated in Fig. 13 which shows the selenium beams obtained from a ZrO_2 target[26] where the volatile CO_2 homologous COSe compound was synthesized on the surface of the target by O_2 addition. Similar reactions may be used to release the two other members of the group VIA elements which also are difficult to separate from a target due to their tendency to form refractory compounds.

A particularly elegant and precise method to study the release from the target or catcher materials has recently been demonstrated by the GSI group[27] as indicated in Fig. 12. They implant a high energy HI beam of the element of interest directly into the real target and ion-source system and record the intensity of the fraction of the originally implanted HI which are released and reionized. In this way they obtain not only the release efficiency of the system but also the time distribution function and the ion-source efficiency.

5.2 Target-to-source transfer

The chemical affinity of the desired species to the walls of the target container, the transfer tube and the ion source determine the losses by adsorption and diffusion. Since these surfaces often are kept at high temperatures the main effect is a delay of nature analogous to the release of the product from the target materials

which is discussed in section 6. For extreme cases where the hold-up time on the surfaces is long or the diffusion speed in the tube construction material is very high, losses through the container and tube walls have been shown to be of importance like the losses through unavoidable mechanical leaks. The use of the chemical evaporation technique may also here speed up the transfer and help to keep the products in the gas phase. A careful choice of construction materials with minimum affinity to the wanted species should be made as discussed in ref. 2 and in many cases a transfer efficiency of 80-90 % is obtained.

6. IONIZATION EFFICIENCIES

The widespread use both in basic research and industry of stable heavy-ion beams has led to a large variety of sources. Since the amount of input material for these purposes usually is unlimited only little emphasis has been put on their efficiency. Despite this, most of our inspiration for development of sources comes from work in this field which is reviewed in ref. 2. There is no universal source that will be best suited for all the elements. Most often the source has to be optimized for each element or group of elements. The alkali, the alkaline earth and the rare earth elements are efficiently ionized (>50%) by means of surface ionization sources[28] or thermal ionization sources[29] which have the particular advantage of working at temperatures around 2000 °C. Also the halogens may efficiently be ionized as negative ions by means of surface ionization[30]. The group of noble gases is conveniently ionized in hot cathode plasma discharge sources in yields of 1 to 60%. Most of the remaining elements seem only to be ionizable in useful yields (>1%) by means of plasma discharge sources kept at high temperature so that atoms which impinge on the walls may be desorbed again. In fact, the efficiency of the ionization process itself is usually very high; it is the often irreversible losses of atoms and ions by condensation on the walls of the sources that determine their efficiency. The major difficulties in maintaining the temperature needed (often above 1800 °C) is the unavoidable chemical reaction between the anode insulators and the

conductive part of the source which eventually will give rise to leaks and an uncontrollable gas pressure in the source.

The hot cathode plasma-discharge ion-sources probably have reached their limits of development. Only a careful choice of construction materials with minimum affinity to the products or the chemical reactions discussed in section 5 may reduce the losses to the walls and keep the products in the gas phase. An example of this is seen in the production of oxygen beams from a platinum target combined with a graphite ion-source[31]. New techniques like laser and ECR ion-sources seem at present to be the most promising way to make further progress. At Gatchina and ISOLDE a concept for an on-line laser ion-source has been developed[32),33,34]. It makes use of stepwise resonant laser ionization in a cavity as shown in Fig. 14. Up to three laser beams of different frequency are directed through the analyzing magnet to overlap with the flow of reaction products in a hot tubular cavity connected to the target as shown in detail in Fig. 15. The advantage of this source is high element selectivity. Suppression of neighboring rare earth elements by a factor of 10^4 has been achieved with ion-source efficiencies of 10-20 %. Since the lasers are pulsed with 10 kHz the ion beam has the same pulse frequency and a pulse width of 25 μs as shown in Fig. 16. This width can be understood in terms of the electrical heating potential applied to the cavity which accelerates the ions out of the tube. In fact the beam is bunched since it can be shown that the tubular cavity has an ion storing effect. Other advantages of this concept are that it is insulator free and employs only an exceedingly simple mechanical construction in the vicinity of the target. On the other hand the source delivers only singly charged ions. This is contrary to the ECR ion source which promises high charge states, pulsed beams and high efficiency. Due to its rigorous plasma confinement ionization efficiencies of 10-40 % have been demonstrated for singly charged ions of light gaseous elements as seen in Fig. 17 where the layout of the TISOL[35] ion-source is shown together with the ionization efficiencies measured at the Louvain-la-Neuve on-line ECR source[36,37]. Similar efficiencies for the light noble gases, but in high charge states, are now reported from GANIL. Judged from the stable

metal consumption of accelerator ECR sources ionization efficiencies of moderately volatile elements like Ca in a given high charge state seems to be of the order of 1 %. It remains however to be shown that this high efficiency is not obtained at the expense of a very high delay time in the ion source since the wall temperature of these sources is so low that atoms which reach the walls remain there for a very long time. This is obviously not a problem in operation with stable material which in equilibrium has saturated the inner surfaces of the source.

7. DELAY TRANSFER EFFICIENCY

The time taken by the processes discussed in the previous sections causes a decay loss of the radioactive products. This loss can theoretically be described in terms of diffusion and desorption processes. A detailed discussion is found in a previous paper[38]. So far the fastest systems developed are based on solids in the form of foils, wires and powders kept at high temperature. The crucial parameter is a function p(t) which can be measured for the entire system but is often determined by the slowest step in the process. A primitive description of this function is the delay half-time i.e., the time it takes for one half of the produced atoms to leave the target. For a powder target characterized by an average grain radius R and a product diffusion constant D, in the case where the delay is governed by the diffusion in the target grains, the probability p(t) per unit time that an atom produced at time zero crosses the grain boundary at time t is:

$$p(t) = \frac{6D}{R^2}\sum_{n=1}^{\infty}\exp\left[\frac{-n^2\pi^2 D t}{R^2}\right] \qquad (2)$$

Expressions of similar types describe p(t), if the delay is governed by diffusion in other shaped solids, diffusion in the pores of the target material or diffusion to and in the source. With reasonable assumptions for D and R, good fits to the experimentally observed release data can be obtained. For a product with mean life-time T_m

much shorter than the average delay time the delay transfer efficiency is given by:

$$\varepsilon_3 = \frac{3\sqrt{DT_m}}{R} \qquad (3)$$

as shown for Rb isotopes as a function of half-life in Fig. 18. The most powerful method to determine p(t) and hence ε_3 is the HI implantation method described in section 5. Recently a number of systems dominated by the surface desorption process have been investigated by the GSI group [27] and successfully related to the enthalpies of desorption as shown in Fig. 19 for the overall efficiencies of some non volatile elements.

The rate of chemical reactions giving rise to release from the surfaces was studied for nitrogen by the Louvain-la-Neuve group[39] who found that a partial pressure of stable nitrogen had to be present in order to release the strongly surface bound ^{13}N atom as the stable ^{16}N -^{14}N molecule. This is illustrated in Fig. 20 which shows the intensity of the ISOLDE ^{14}N -^{13}N beam as function of $^{14}N_2$ partial pressure. The corresponding p(t) for ^{15}N -^{15}N, ^{14}N -^{15}N and $^{15}N_2$ molecules released from a typical ISOLDE target and ion system[40] is shown in Fig. 21. It is seen that the delay increases in the order listed above indicating that they are formed by dissociation including a surface adsorption step of the ^{15}N.

The power deposition and the cascade of nuclear reactions and secondary particles are found strongly to enhance the release times i.e. p(t). This makes the targets faster as indicated by the delays measured by the Orsay group in their PS experiment where the protons are delivered in 2 μs long bursts every few seconds. They observe[41] delay half times of 50 ms. In the first test of the PS-booster ISOLDE[42] the delay half time for Ne produced in a MgO target was reduced from 1 s to 400 ms as seen in Fig. 22. With such targets the beam is now bunched and a number of experiments can improve their signal-to-noise ratio by only activating the data-taking during the pulse.

8. CONCLUSIONS AND COMPARISONS

With the existing on-line mass separator technique we have today a very powerful injector for radioactive beam accelerators and many beams have already been developed that will produce accelerated beams of nA intensities. It is clearly seen that the techniques developed for high energy protons presently lead the field of intensity and variety of ions although it has been demonstrated that low energy protons play a role for a limited number of beams. Cross-section considerations indicate that also thermal neutrons and energetic heavy ions deserve consideration as production particles. In the two latter cases the degree of success will depend on substantial R&D work which only recently has been started. A comparison of the three methods suffers from the fact that only for the protons has the essential development reached the critical stage where experimental values of sufficient intensity emerge. For the other particles we will have to rely on the projected outcome of the R&D work. The authors view of the present status is seen in Fig. 23 which shows the routinely obtained rubidium beam intensities at ISOLDE and OSIRIS. Added to these are the intensities that may be obtained with 77 MeV/u ^{12}C which are calculated from the experimentally known cross-sections the maximum usable target thickness and $\epsilon_1 = 0.8$, $\epsilon_2 = 0.95$ and $\epsilon_3 = 0.9$ as measured at ISOLDE. This picture may change by as much as a factor of 0-5 in other regions of the nuclidic chart. For all three particles major R&D work is planned especially in the direction of making use of the maximum available driver beam intensities mentioned in Table 1. If it is assumed that the future R&D work is accomplished with equal success the picture may change into the one displayed in Fig 24.

Although it is said above and shown in Fig. 23 that many beams exist that would give sufficient intensity if post accelerated, they are not necessarily the ones needed for a physics programme. In order to make a better comparison and to inspire those who plan the physics programme, the list of radioactive ion-beams for which the European projects have specific experiments is shown in Table 2. It should be noted that the beams are chosen among the groups of elements for which it is most easy to develop on-line technique. They would

therefore in an early stage of development give the highest beam intensities. In order to illustrate the present state of beam intensities the ones measured at the old ISOLDE, not always with the ideal target thickness and ion source, are listed in Table 2. Presently a study group under NuPECC[43] is working out the intensities of these beams as they would be under optimal conditions with the different production particles discussed above.

REFERENCES

[1] Proc. 12th Int. Conf. on Electromagnetic Separators and Techniques Related to their Applications, Sendai, Japan, Sept. 1991, eds M. Fujioka, T Shinozuka and Y. Kawase Nucl. Instr. and Methods B70(1992)1

[2] H. L. Ravn, Nucl. Instr. and Methods B70(1992)107

[3] H.L.Ravn and B. Allardyce, Treatise on Heavy-Ion Science Ed. D. Allan Bromley Vol. 8 (Plenum Press New York 1989) p 363.

[4] S. Sundell and H. L. Ravn, Nucl. Instr. and Methods B70(1992)160

[5] Proc. First Int. Conf. On Radioactive Nuclear Beams, 16 Oct. Berkeley California, Eds. W. D. Meyers, J. M. Nitchke and E. B. Norman, World Scientific Singapore 1990

[6] Proc. Second Int. Conf. On Radioactive Nuclear Beams, Louvain-la-Neuve, Belgium Aug. 19, 1991, Ed. Th. Delbar Adam Hilger Bristol 1991

[7] J. Bondorf, Proc. Internat. Symposium on Why and How should we Investigate Nuclides Far Off the Stability Line, Lysekil, 1966, eds. W. Forsling, C. J. Herrlander and H. Ryde, Ark. Fys. 36(1967)681

[8] H. L. Ravn in ISOLDE User's Guide, Ed. H. -J. Kluge, CERN 86-05 (1986).

[9] E. Kugler et.al., Nucl. Instr. and Methods B70(1992)41

[10] H. -J Kluge in User's Guide, Ed. H.-J. Kluge, ISOLDE CERN 86-05 (1986)

[11] J. M. Miller and J. Hudis, Ann. Rev. Nucl. Sci. 9(1959)159

[12] G. Rudstam, Z. Naturforsch. 21A(1966)1027

[13] R. Silberberg, C. H.Tsao, The Astrophys. J. Suppl. 25(1973)315

[14] R. Silberberg, R. Tsao, C. H., NRL Report(1973)7593

[15] S. Regnier, Thesis CEN Bordeaux CENBG(1977)7726

[16] T. Bjørnstad et. al. Z. Phys. A. Atoms and Nuclei 303(1981)227

[17] M. de Saint Simon et. al. Phys. Rev. C. 26(1982)2447

[18] S. Borg, I. Bergström, G. B. Holm, B. Rydberg, L. E. de Geer, G. Rudstam, B. Grapengiesser, E. Lund, and L. Westgaard, Nucl. Instr. and Methods 91(1971)109

[19] J. L. Belmont et. al. Proc. Int. Workshop on the Physics and the techniques of secondary nuclear beams. Dourdan March 23-25 1992

[20] P. Van Duppen et. al, Nucl. Instr. and Methods B70(1992)393

[21] T. Eaton and H.L. Ravn, Nucl. Instr. and Methods B26(1987)190

[22] Proposal for a Radioactive Beam Test Bed Facility at the Rutherford Appleton Laboratory, Unpublished

[23] GANIL Report, 92 04

[24] J.C. Puteaux et al., Nucl. Instr. and Methods 186(1981)321

[25] P.Hoff et al., Nucl. Instr. and Methods 186(1981)186

[26] E. Hagebø, P. Hoff, O. C. Jonsson, E. Kugler, J. P. Omtvedt, H. L. Ravn and K. Steffensen, Nucl. Instr. and Methods B70(1992)165

[27] R. Kirchner, Nucl.Instr. and Meth A 292 (1990) 203.

[28] H.L. Ravn, Phys. Rep.54(1979)201

[29] R. Kirchner, et. al. Nucl. Instr. and Methods B26(1987)235

[30] B. Vosicki, T. Bjørnstad, L.C. Carraz, J. Heinemeyer and H.L. Ravn, Nucl. Instr. and Methods 186(1981)307

[31] H. R. Andreasen, Eder, H. Haas, E. Hagebø, P. Hoff, H. L. Ravn, K. Steffensen, and S. Sundell, Nucl. Instr. and Meth. B58(1991)247

[32] G. D. E. Alkhazov, Ye Berlovich, and V. N. Panteleyev, Nucl.Instr. and Meth. A 280 (1989) 141.
[33] F. Sherer et. al. To be published in the proceedings of the 4th Int. Conf. on Ion Sources Bensheim-Germany Sept 1991. Rev. Sci. Instr.
[34] V. I. Mishin et. al. Chemically Selective Laser Ion-Source For The CERN ISOLDE On-line Mass-Separator Facility, Submitted to Nucl.Instr. and Methods. B
[35] Buchmann, L. J. Vincent, H. Sprenger, M. Dombsky J. M. D'Auria, P. McNeely and G. Roy, Nucl.Instr. and Methods. A295(1990)291
[36] P.Van Duppen, An ECR ion-source for the LISOL facility, Nucl.Instr. and Methods. A295(1990)
[37] P. Decrock et. al. Nucl.Instr. and Methods. B58(1991)252
[38] H. L. Ravn, Phys. Rept. 54(1979)201
[39] P. Decrock et. al. Nucl.Instr. and Methods. A295(1990)182
[40] The ISOLDE Collaboration to be published
[41] F. Touchard et al., Nucl. Instr. and Methods 186(1981)329
[42] E. Kugler The ISOLDE FAcility at the CERN PSS BOOSTER, To be published in Nucl. Instr. and Methods B
[43] Report On The European Radioactive Beam Facilities,Nupecc Study Group Ed. R. Siemssen Unpublished

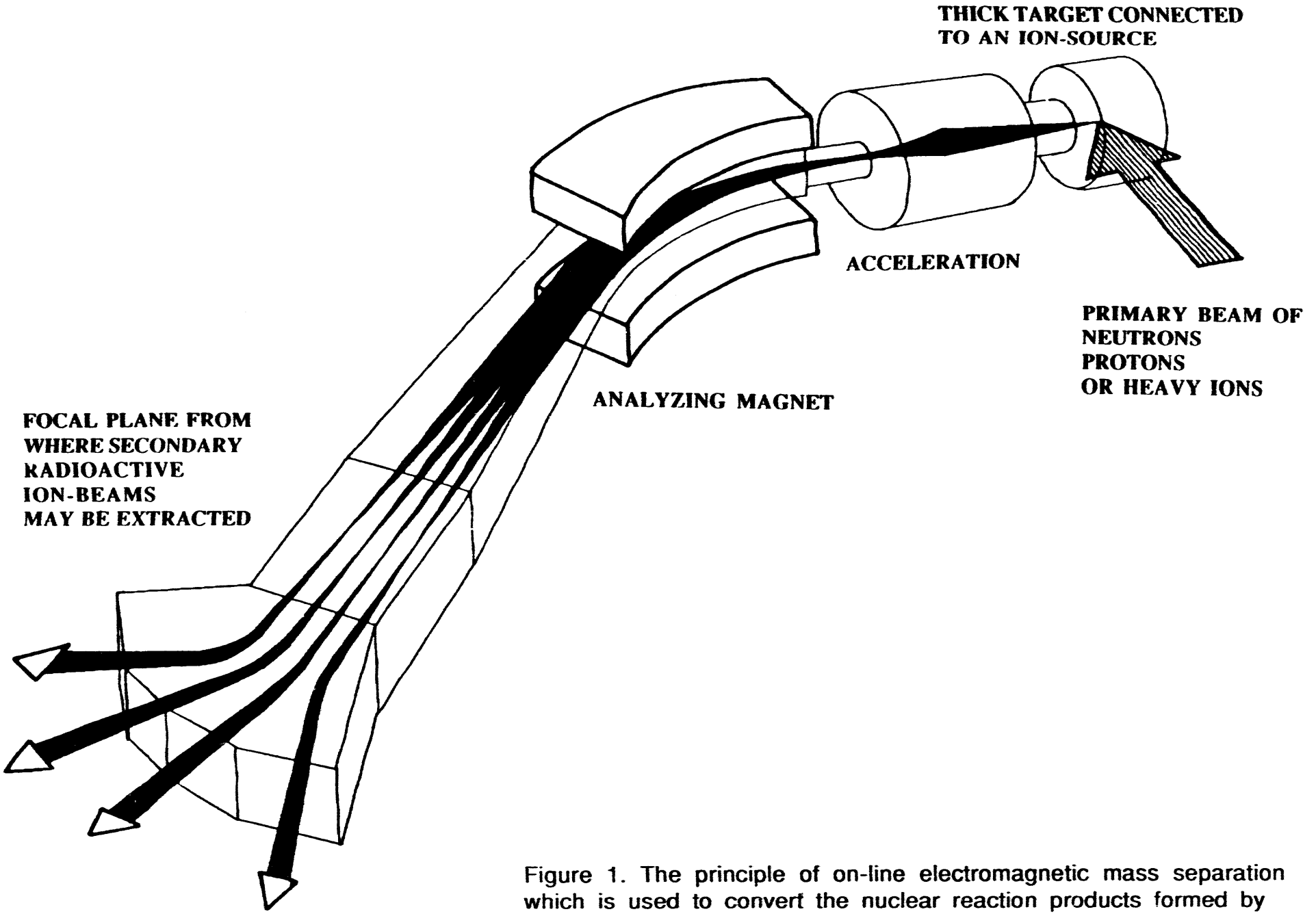

Figure 1. The principle of on-line electromagnetic mass separation which is used to convert the nuclear reaction products formed by bombarding a thick target into an array of mono isotopic ion-beams.

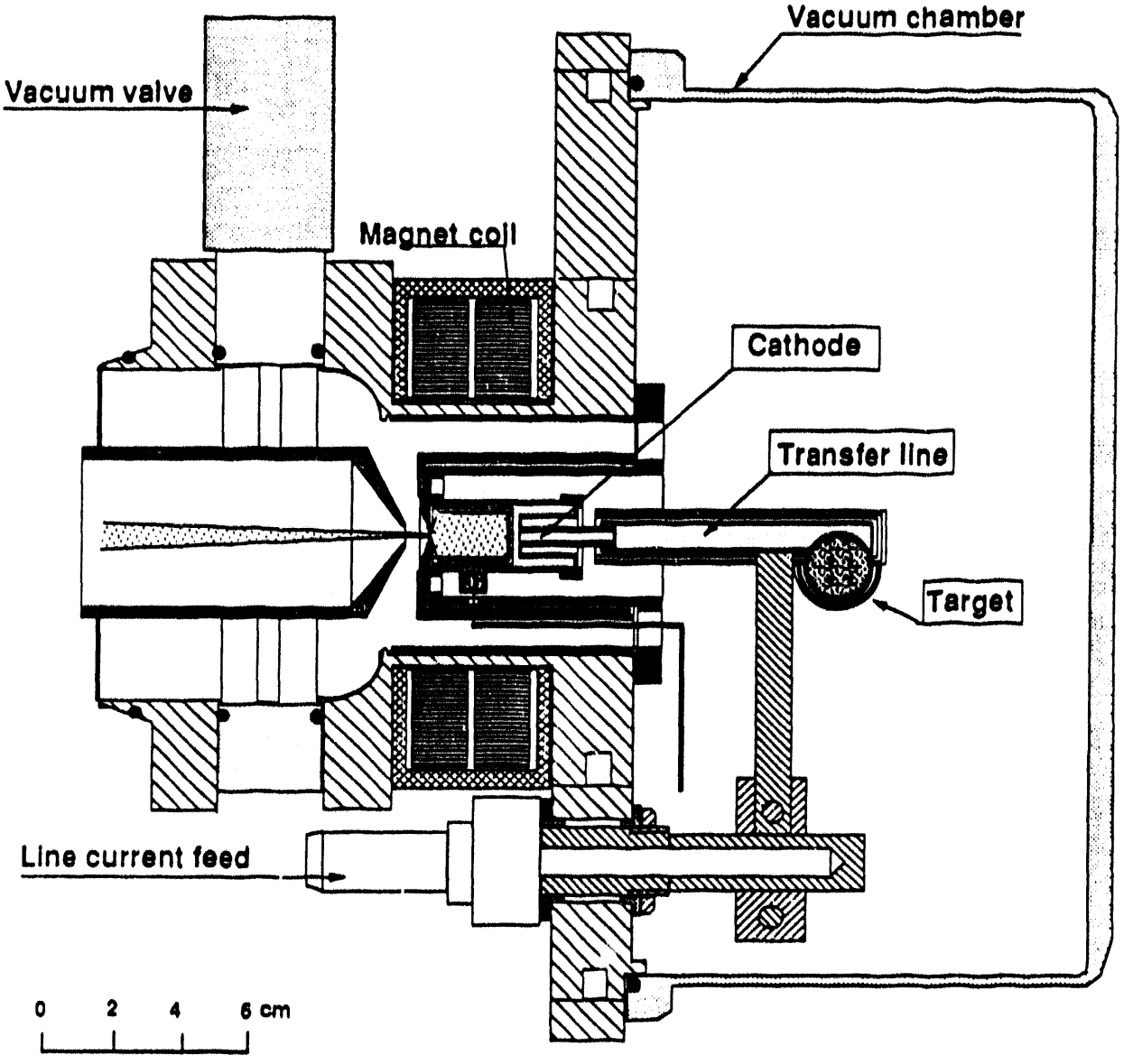

TARGET ION SOURCE ASSEMBLY

Figure 2. A typical target and ion-source unit where the target container is connected to an ion-source via a transfer tube.

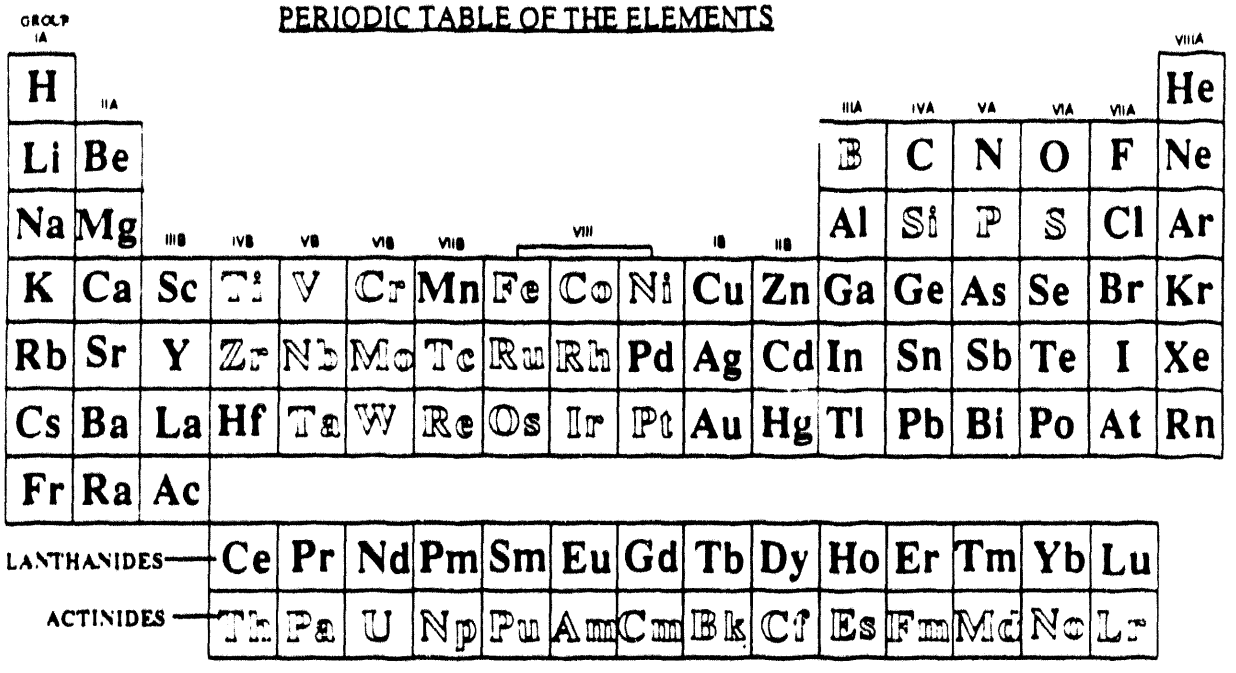

Elements in bold characters are available as beams at ISOLDE

Figure 3. Periodical table of the chemical elements which shows those for which target and ion-source techniques at present have been developed. Note that all the elements with outlined symbols which are unavailable as on-line beams from thick targets belong to the elements which are refractory or form refractory compounds.

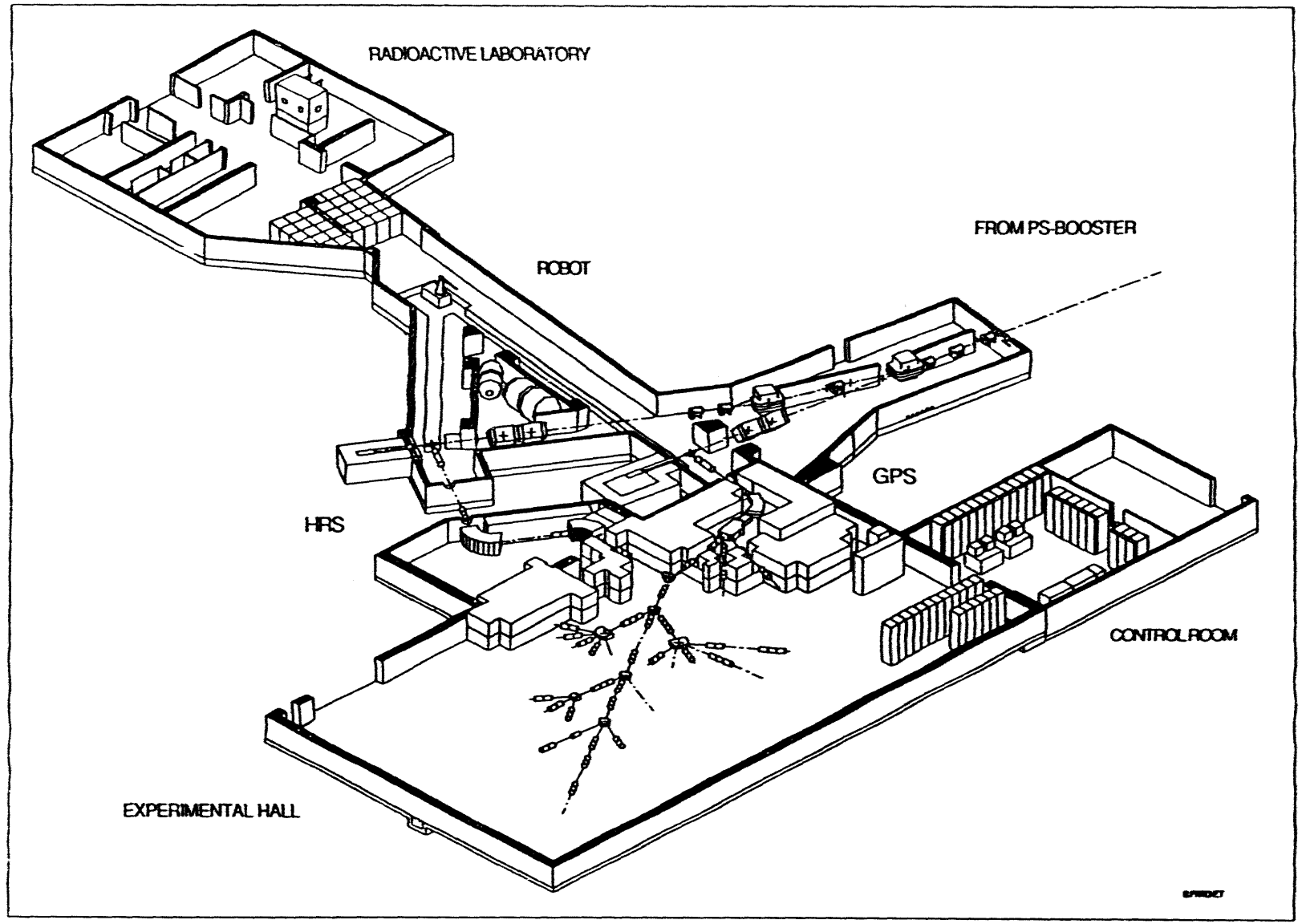

Figure 4. Layout of the new CERN ISOLDE facility with its two on-line mass separators which feed a common experimental hall separated from the proton beam and target handling area.

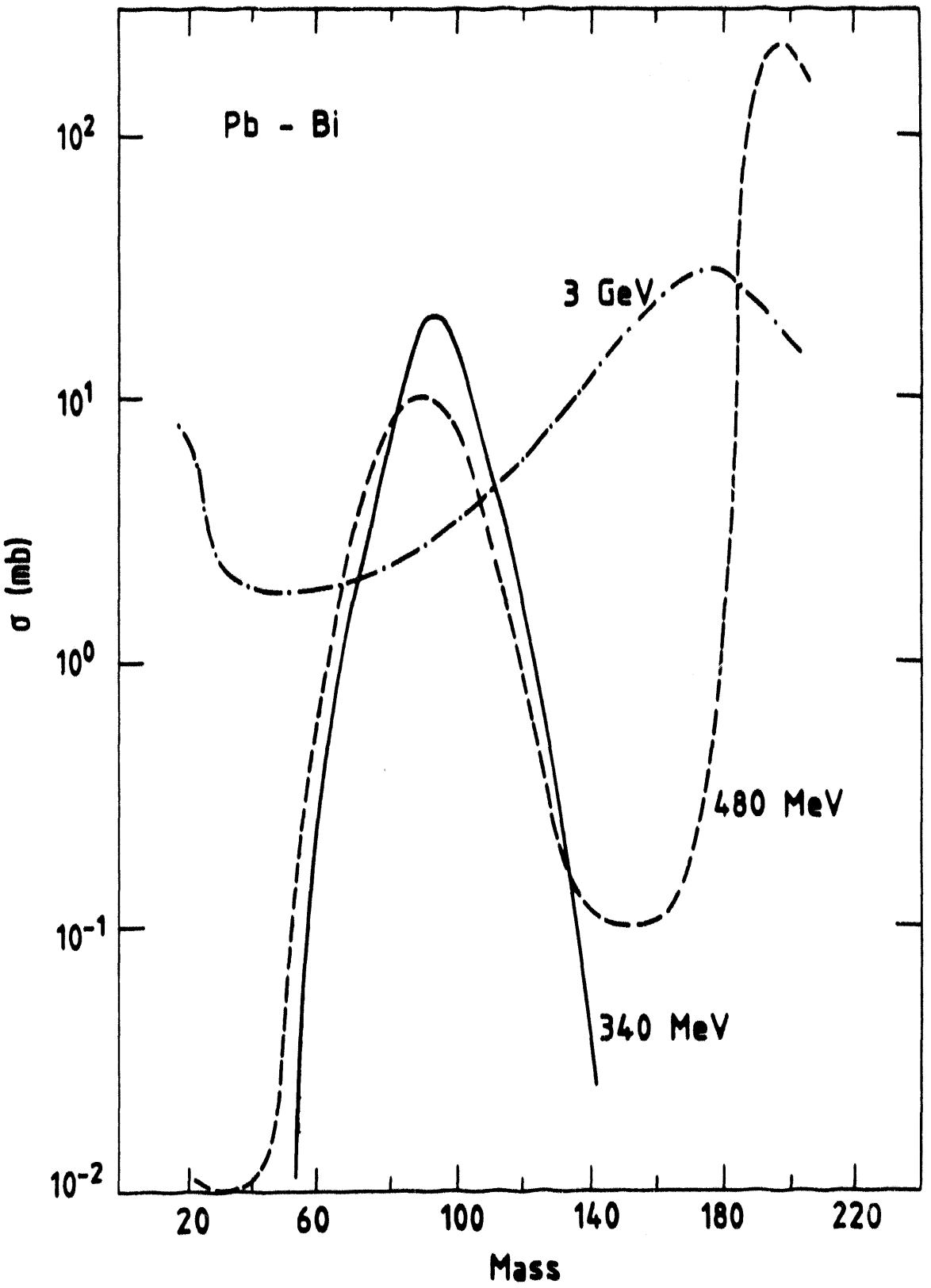

Figure 5. Mass yield curve for bombardment of Pb and Bi with protons of various energies.

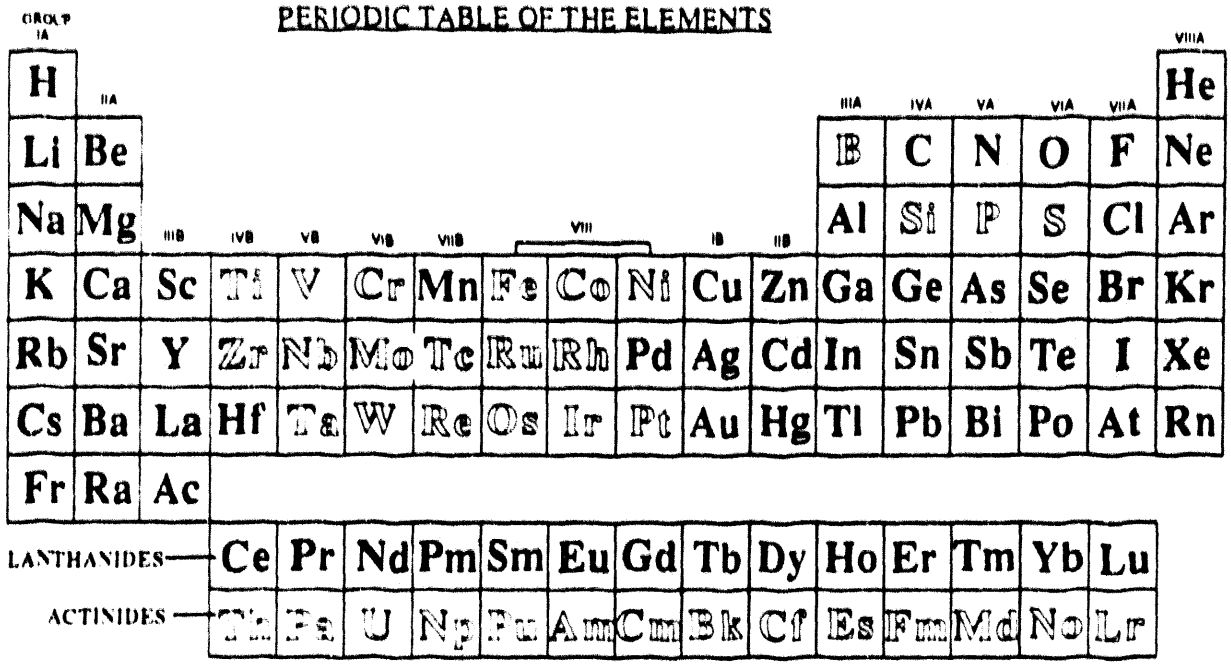

Elements in bold characters are available as beams at ISOLDE

Figure 6. Periodical table of the chemical elements which shows by shading those for which the neutron rich isotopes can be produced by thermal neutron fission of ^{235}U.

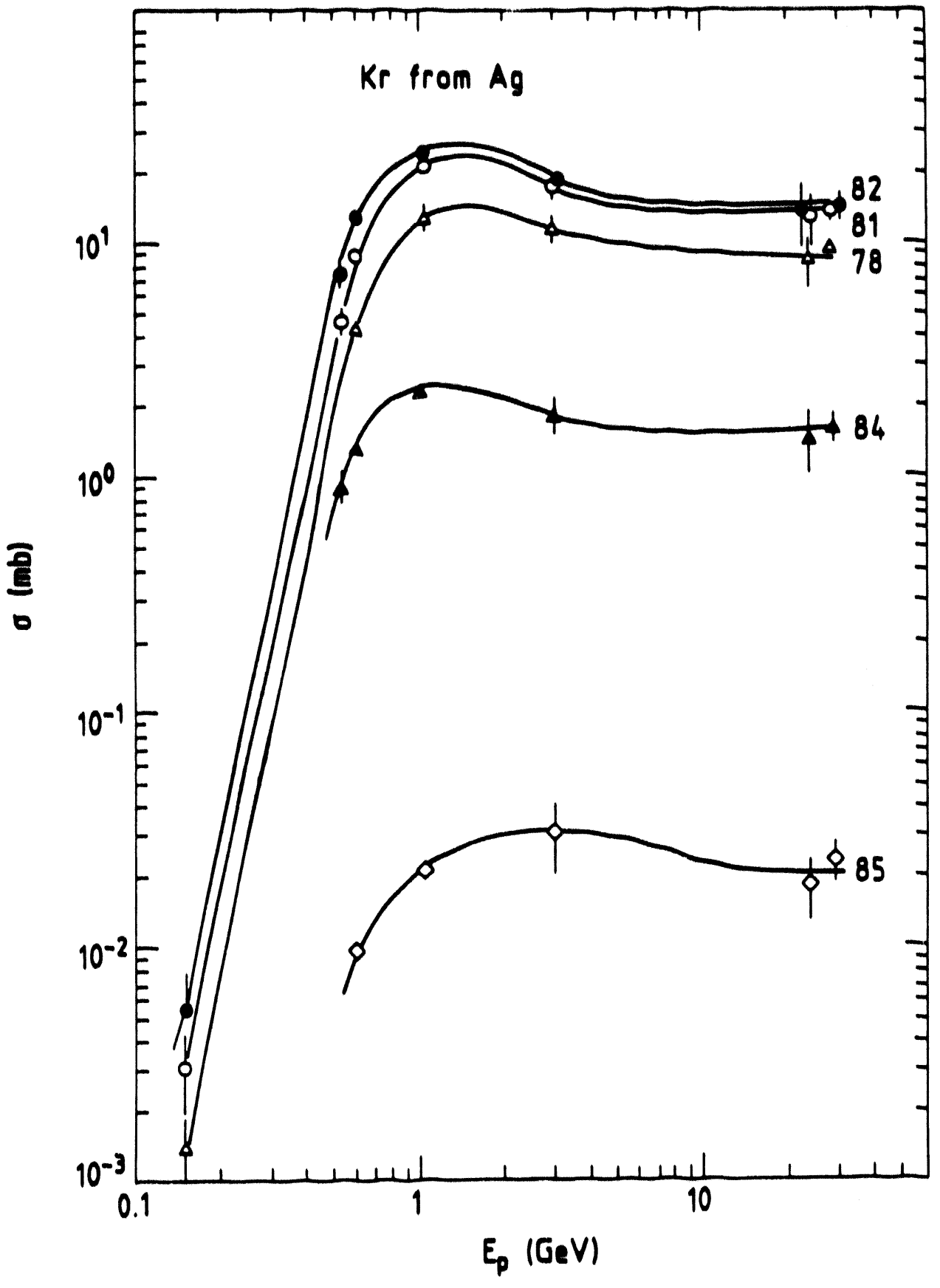

Figure 7. Experimentally measured excitation function for the spallation of silver (DZ = 11) leading to krypton isotopes.

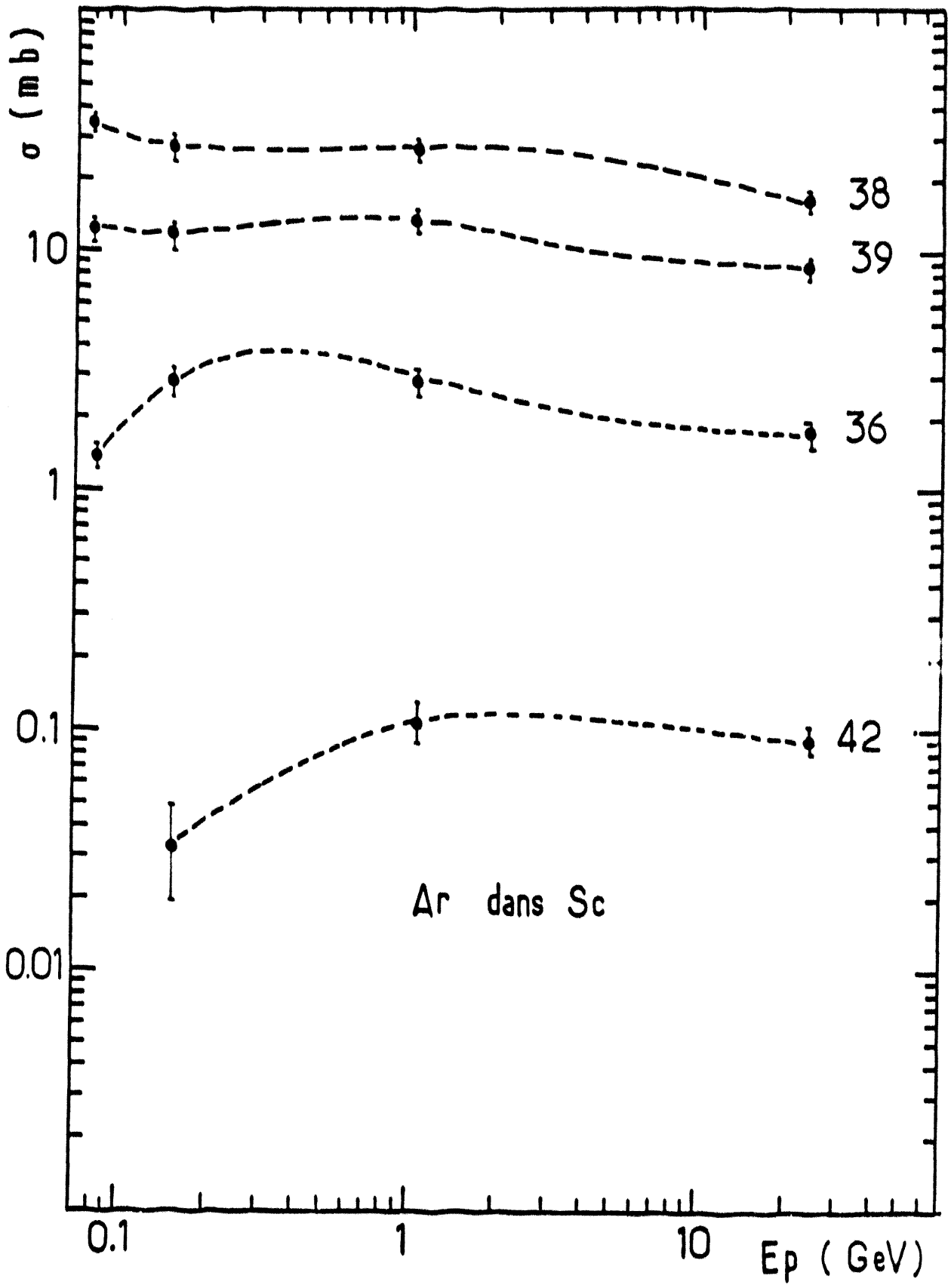

Figure 8. Experimentally measured excitation function for the spallation of scandium (DZ = 3) leading to argon isotopes.

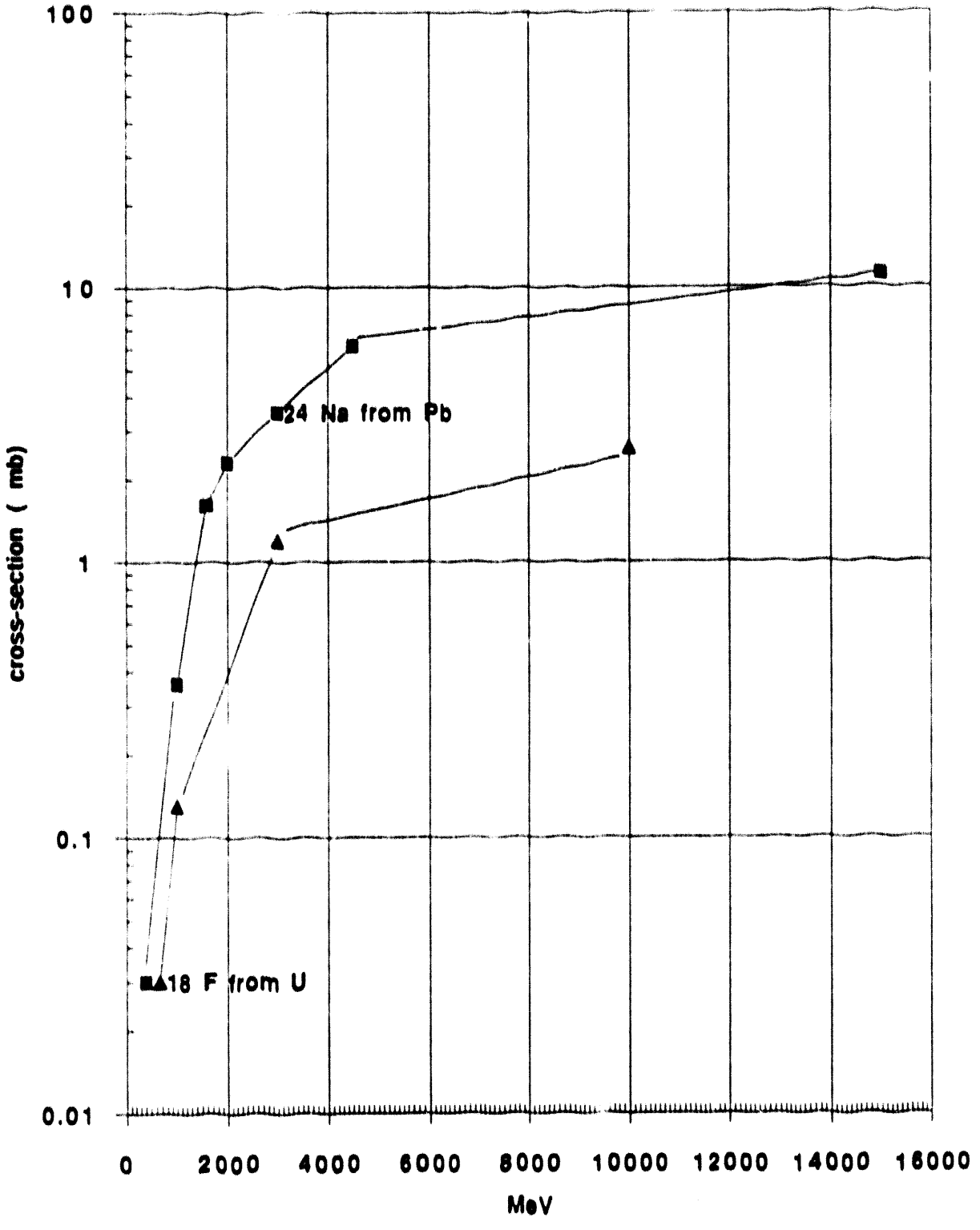

Figure 9. Experimentally measured excitation function for the fragmentation of lead and uranium leading to ^{24}Na and ^{18}F respectively.

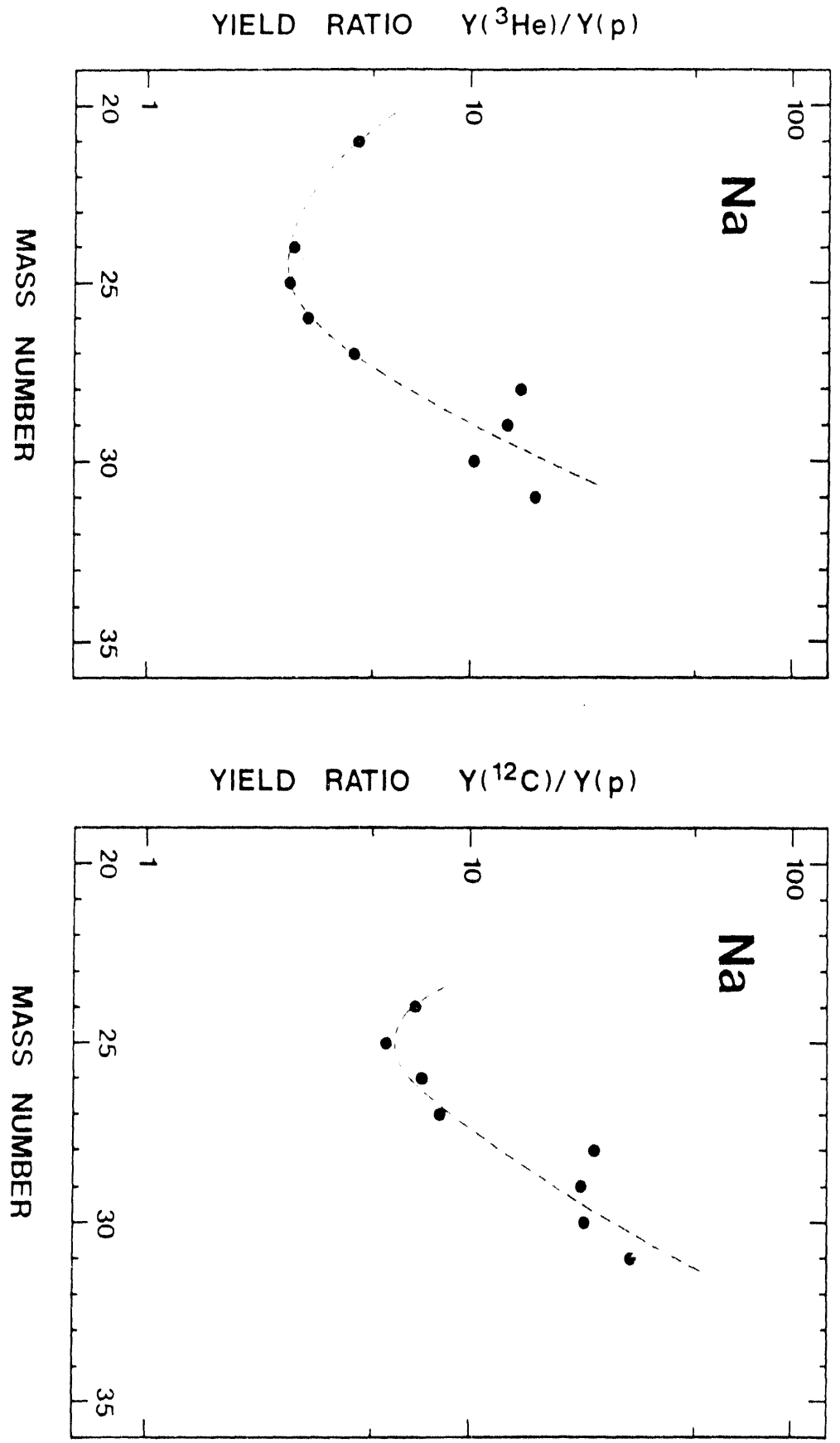

Figure 10. Ratios of sodium beam yields obtained by fragmentation of uranium by means of 86 MeV ^{3}He and ^{12}C over fragmentation of uranium by means of 600 MeV protons.

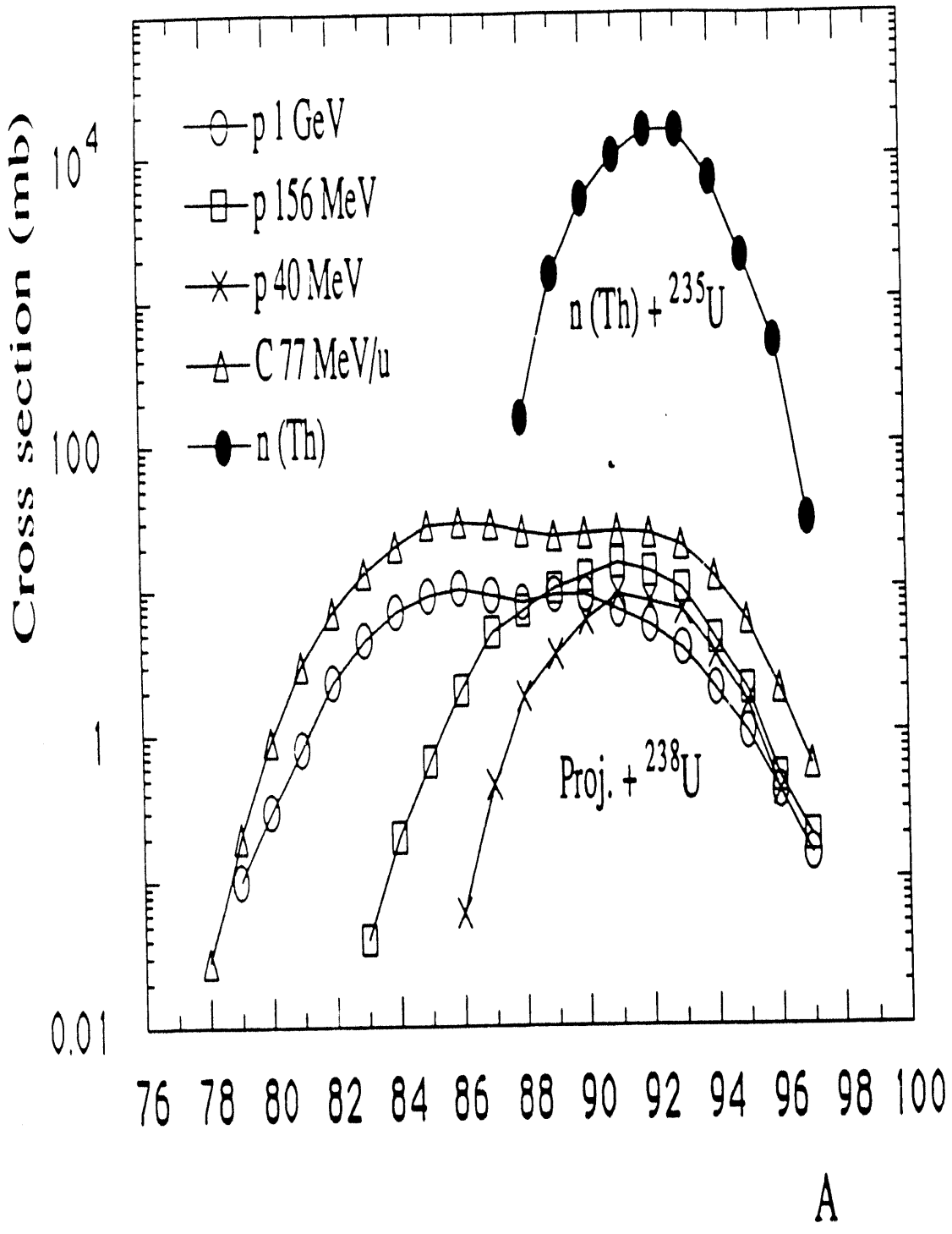

Figure 11. Cross sections for production of rubidium isotopes by various nuclear reactions.

IMPLANTATION OF ENERGETIC HEAVY IONS

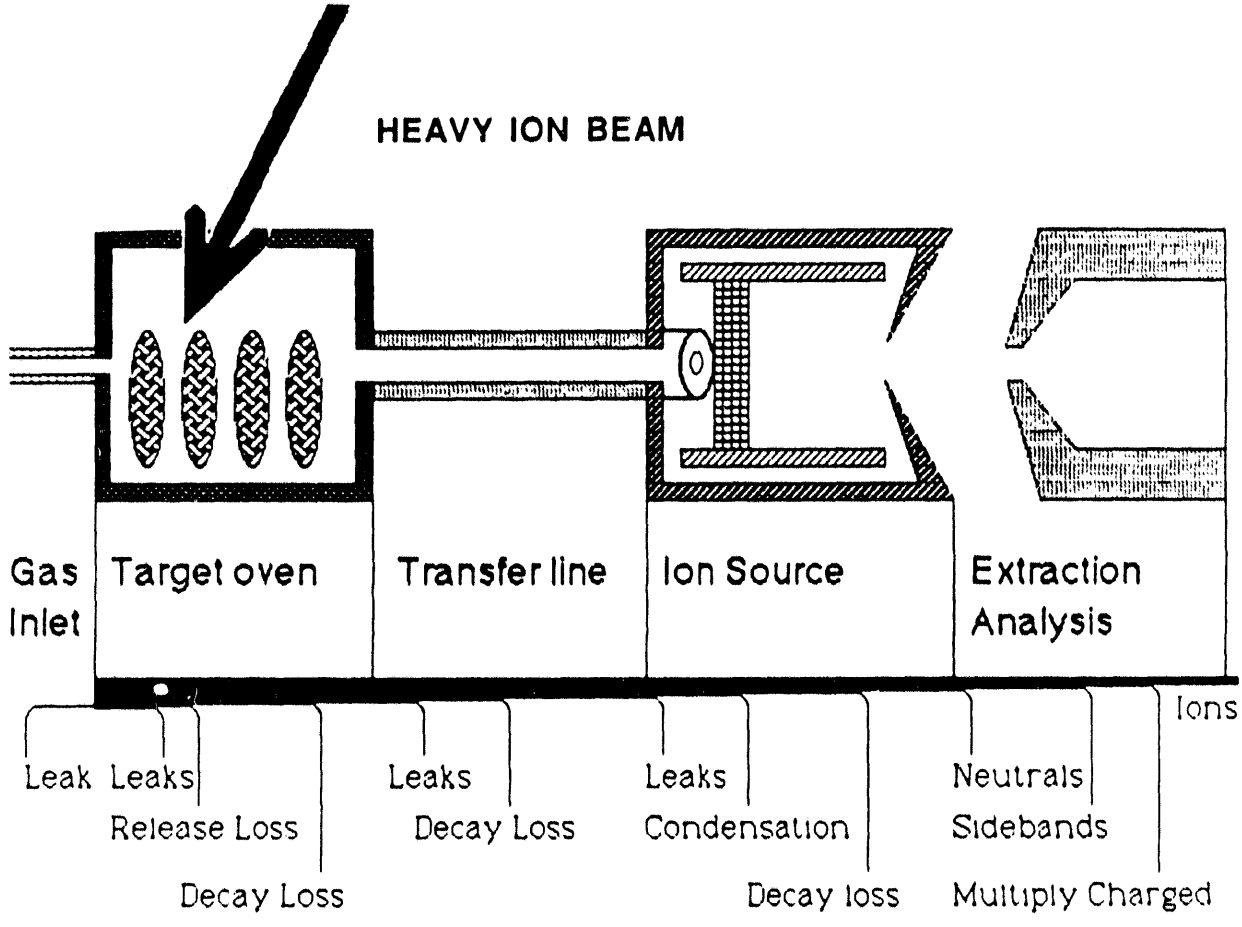

Figure 12. Schematic representation of the transfer of the reaction products from the target to the ion source and the possible loss mechanisms. The heavy-ion beam indicates that these effects can be studied in a particularly precise way by means of energetic HI.

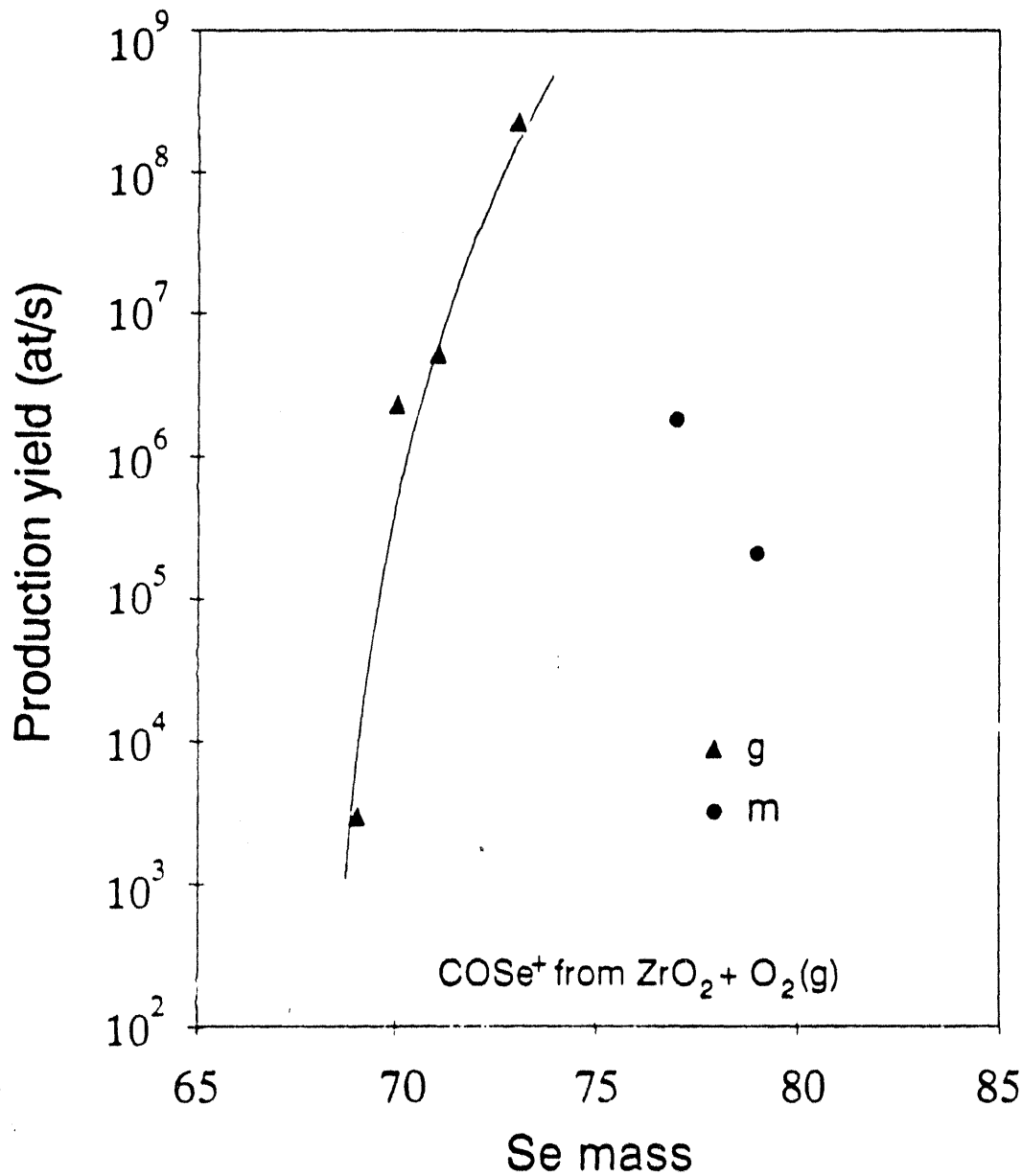

Figure 13. Beam intensities of only the most neutron deficient Se isotopes obtained by irradiating a 6.2 g/cm$_2$ ZrO_2 target combined with a high temperature plasma-discharge ion-source to which O_2 gas was added.

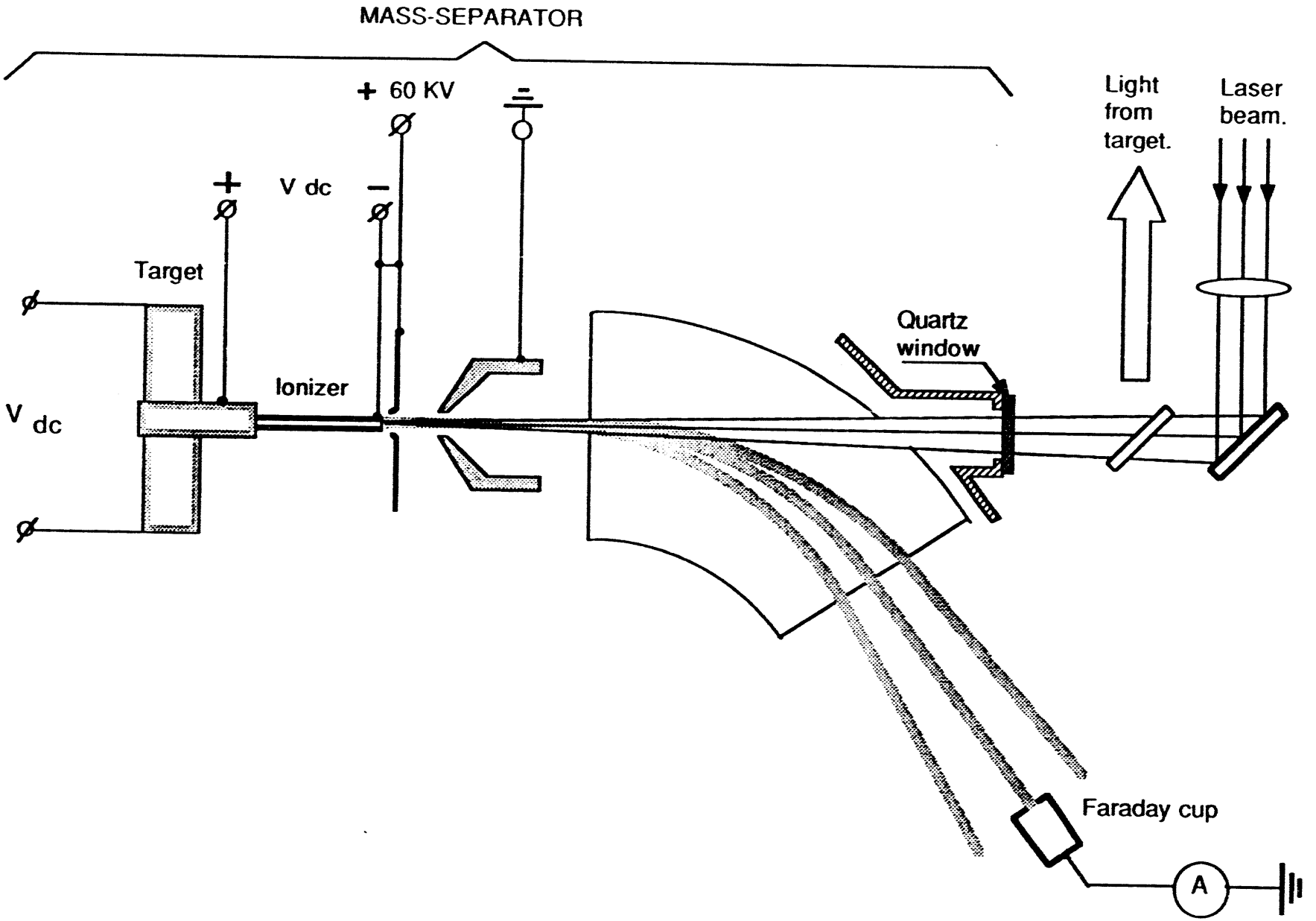

Figure 14. The principle of the ISOLDE laser ion-source.

Layout of the ISOLDE laser ion source.

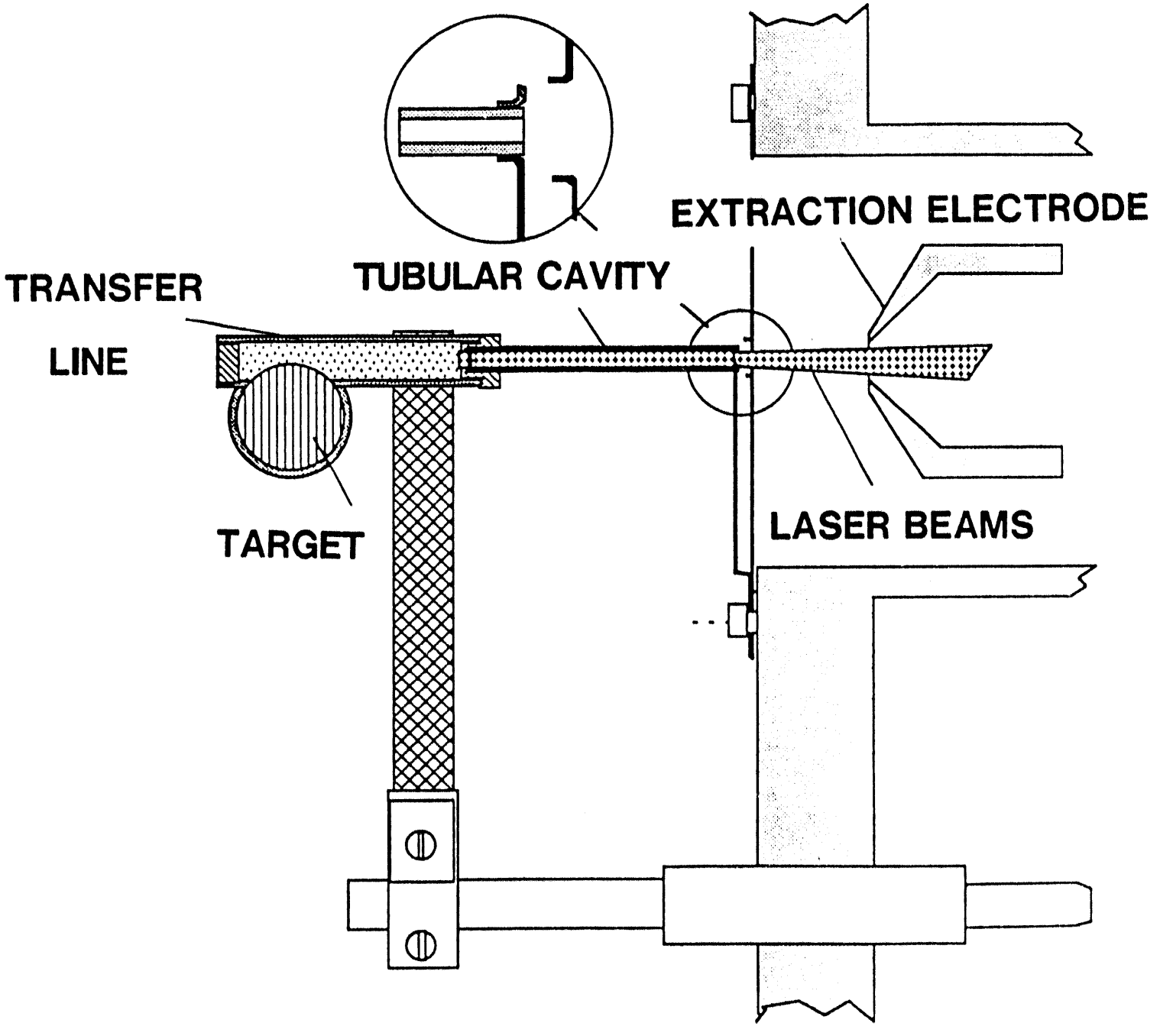

Figure 15. Layout of the ISOLDE target and laser ion-source unit.

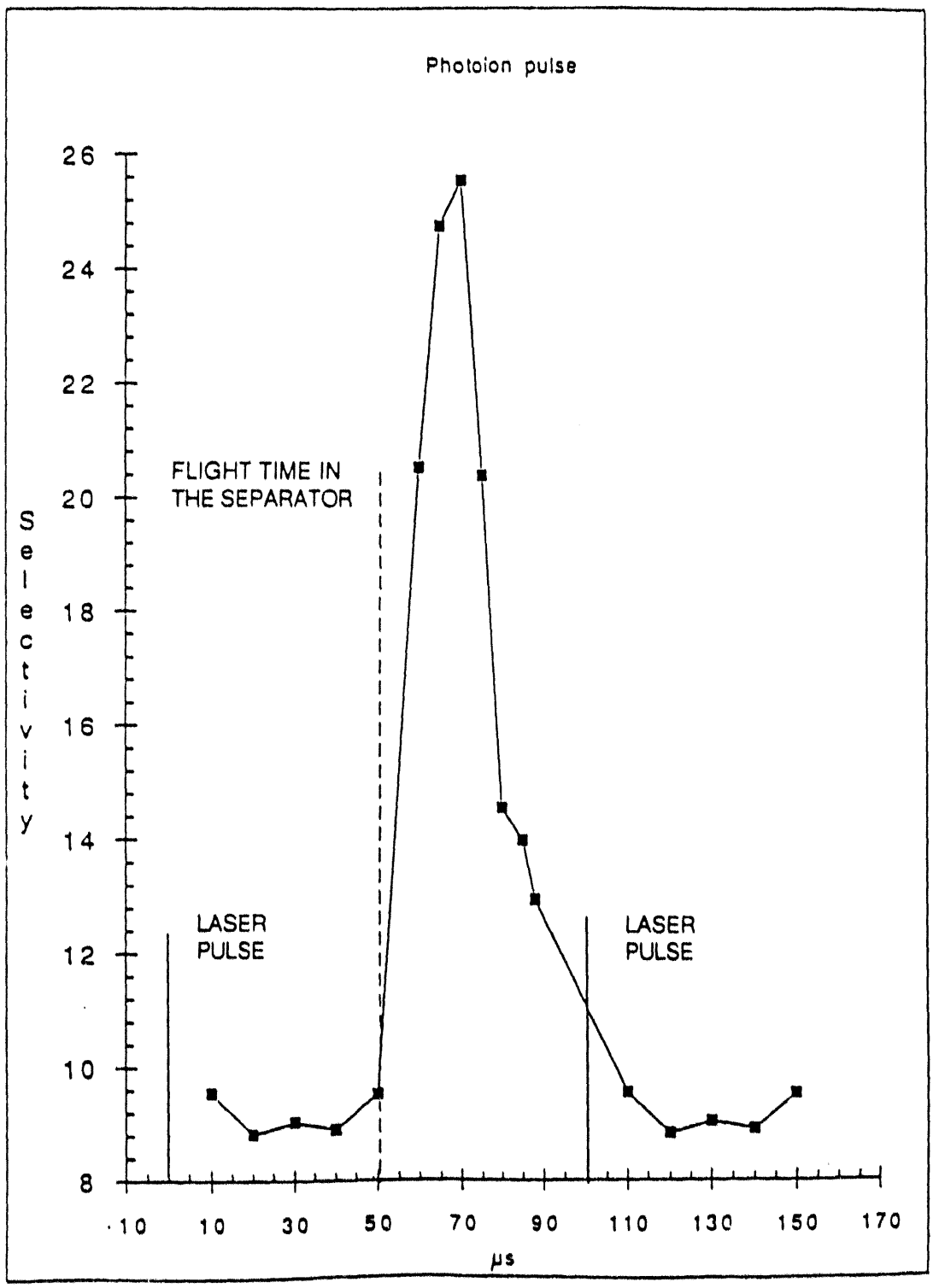

Figure 16. Pulse structure of the laser produced ions.

ELECTRON CYCLOTRON RESONANCE (ECR) ION SOURCES

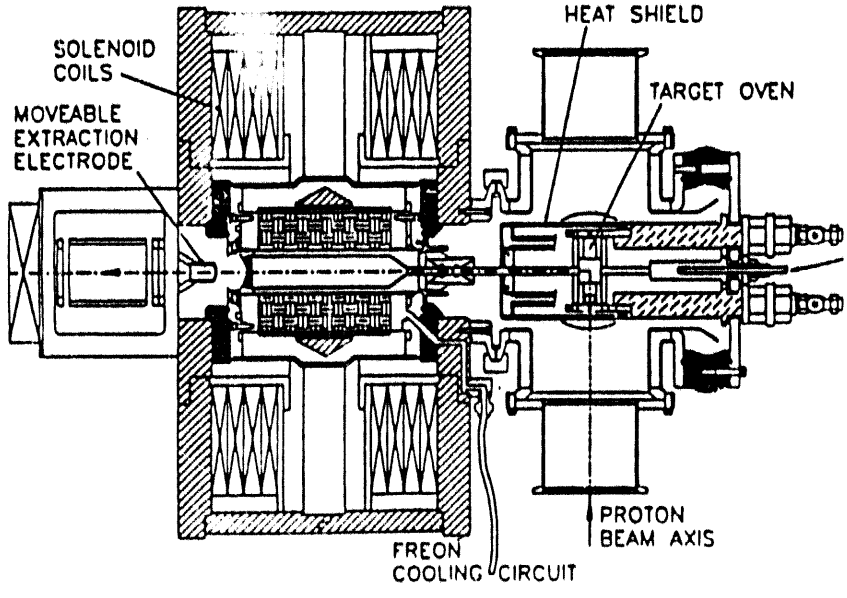

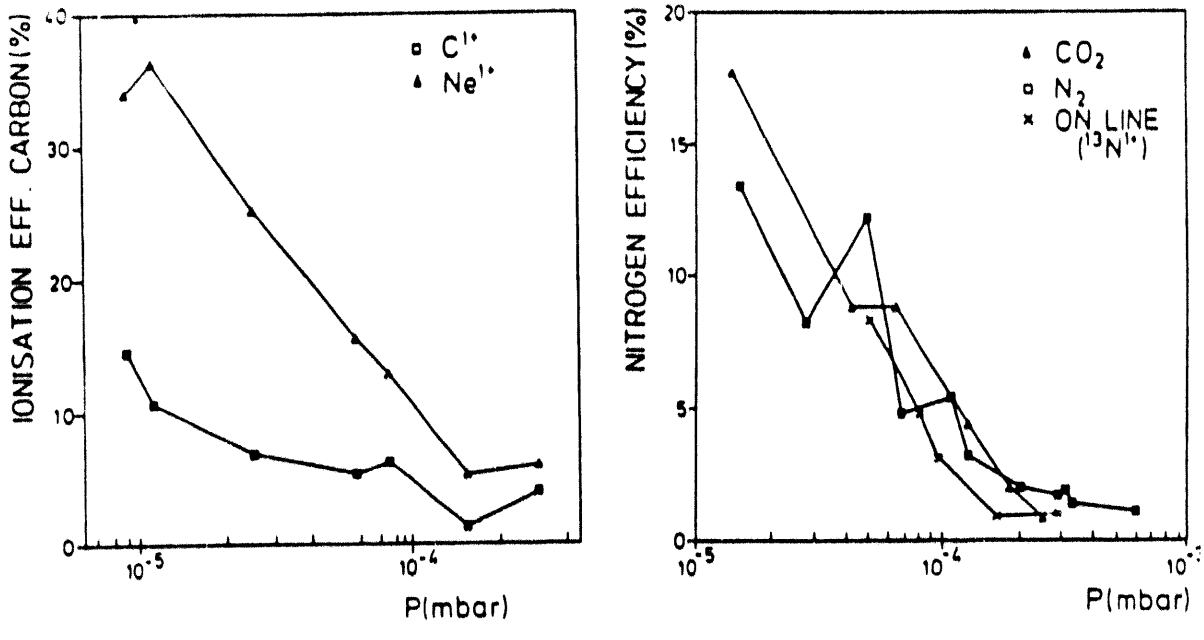

Figure 17. Layout of the TISOL on-line ECR source and gas yields measured with the Louvain-la-Neuve ECR source.

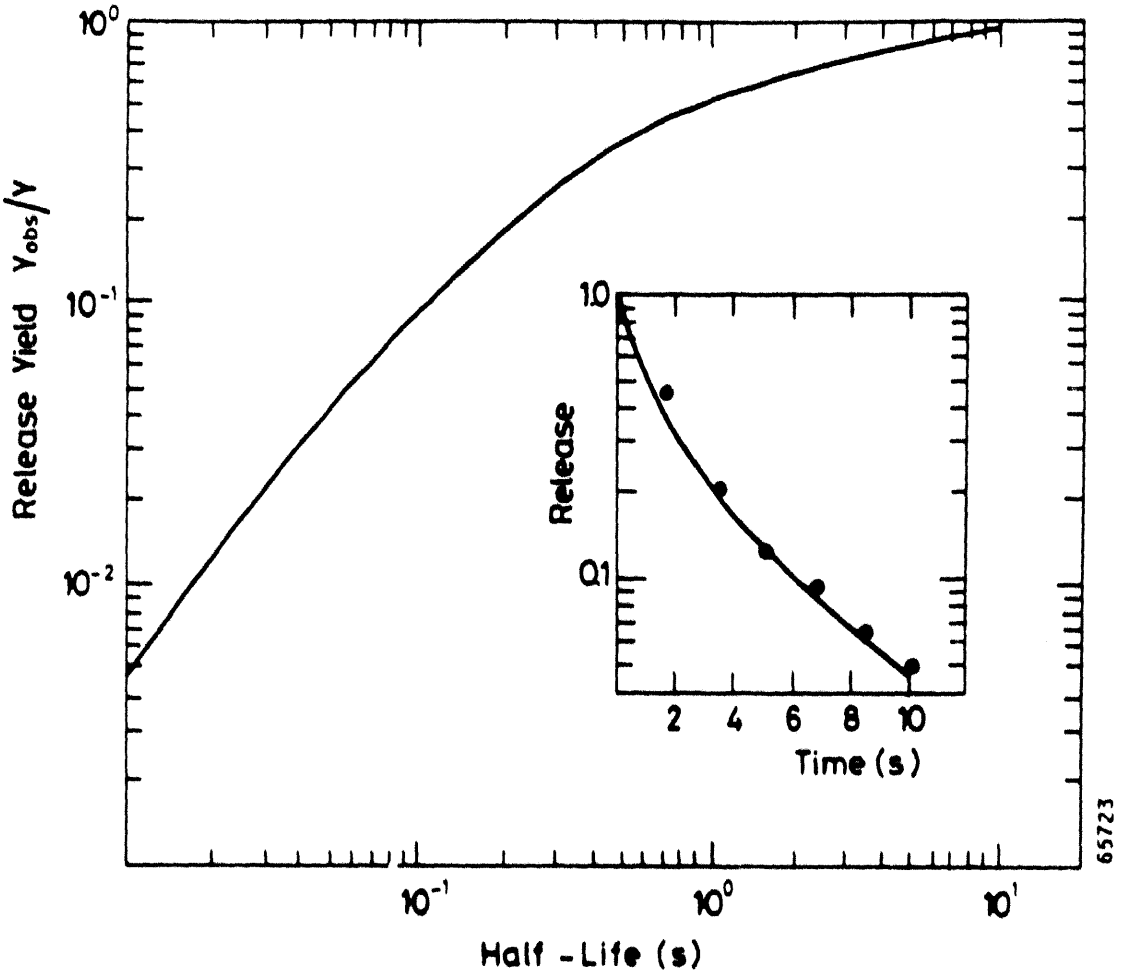

Figure 18. Decay loss of Rb isotopes as a function of half-life. The insert shows the delay curve from which the p(t) is derived. It is in this case obtained by sampling the radioactive ion beam intensity as a function of time after switching off the proton beam.

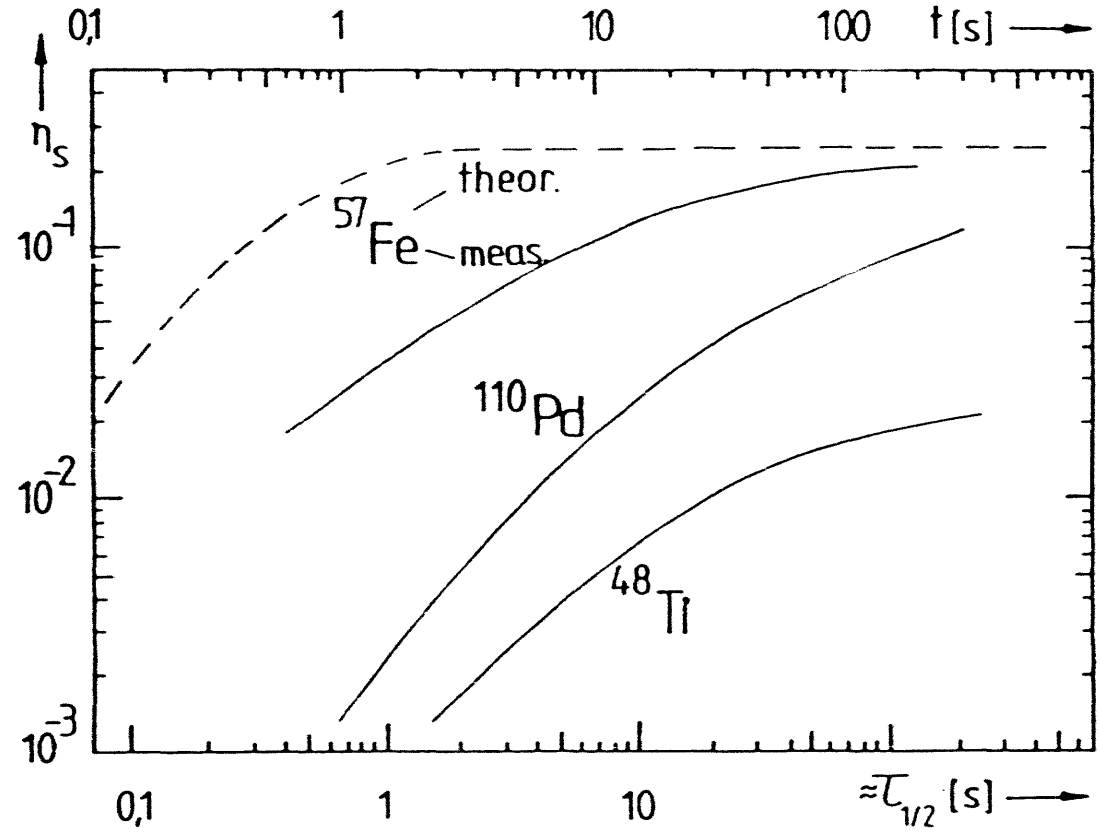

Figure 19. Overall efficiencies of Ti, Fe and Pd as a function of half-life measured by means of the previously implanted stable high energy heavy-ions.

Release of $^{16}N^{14}N^+$ from a mixed Platinum-graphite target as function of $^{14}N_2$ partial pressure.

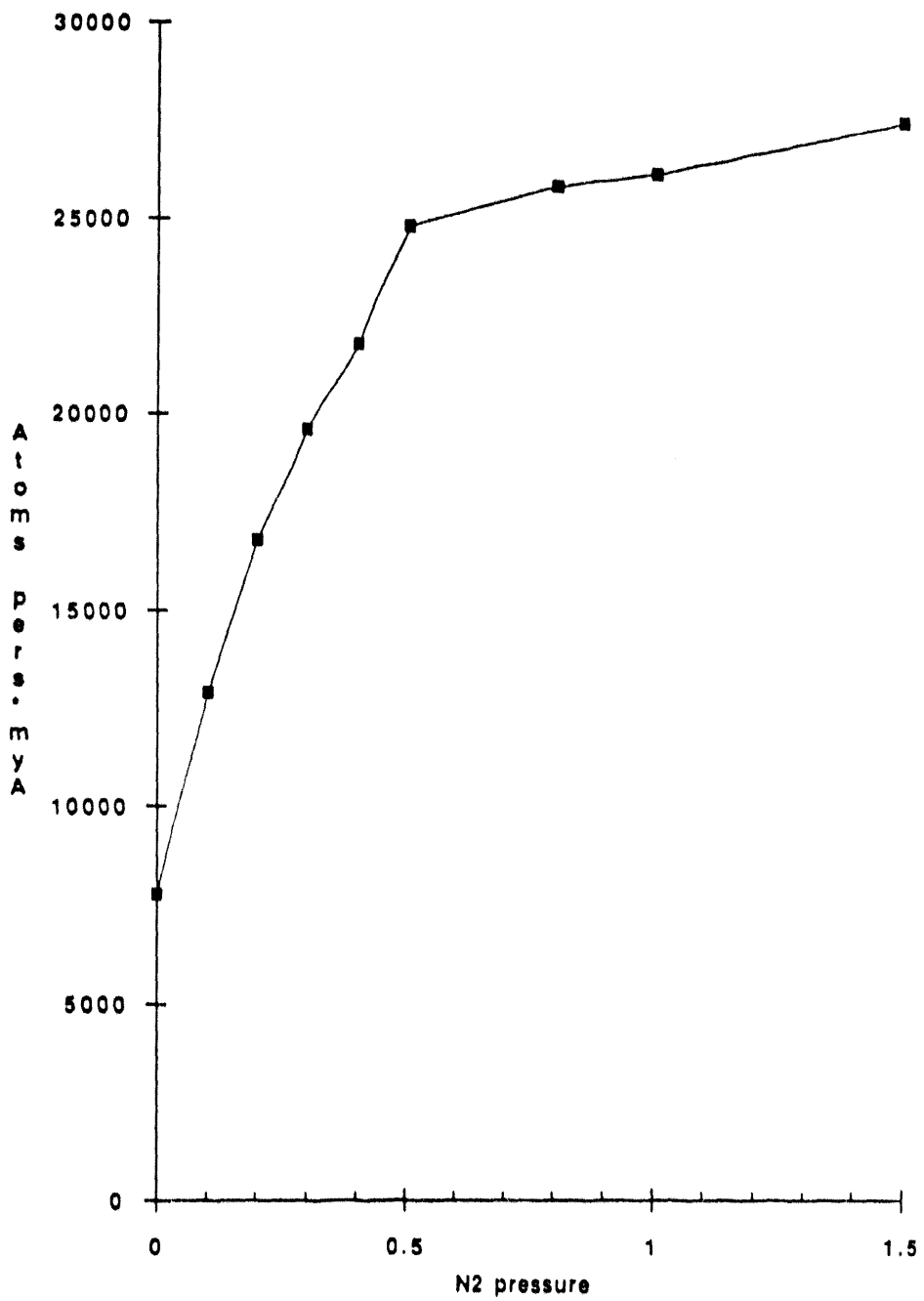

Figure 20 Release of ^{16}N -^{14}N ions from a graphite platinum target as a function of $^{14}N_2$ partial pressure.

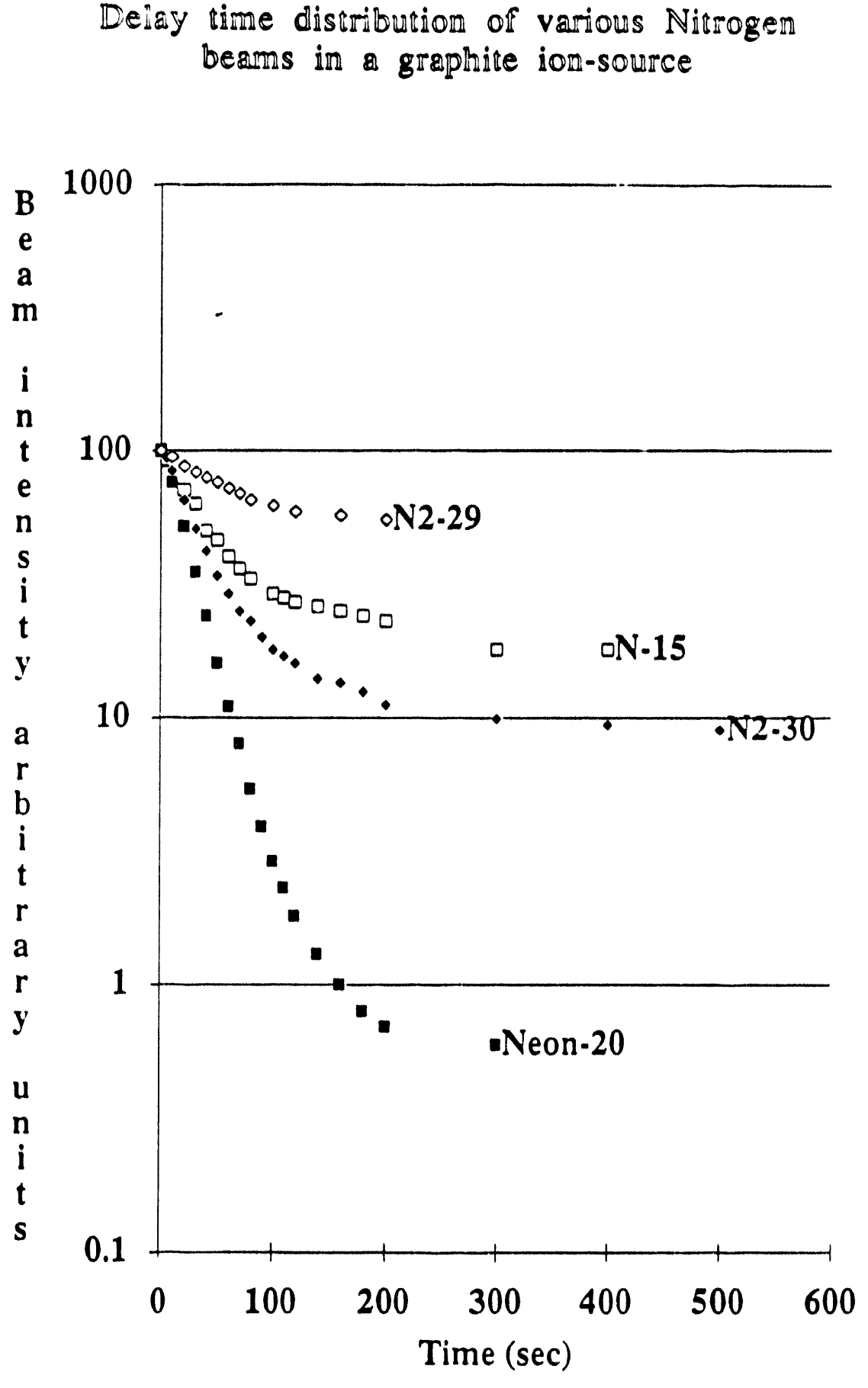

Figure 21. Delay time distribution of various nitrogen beams from a graphite ion-source.

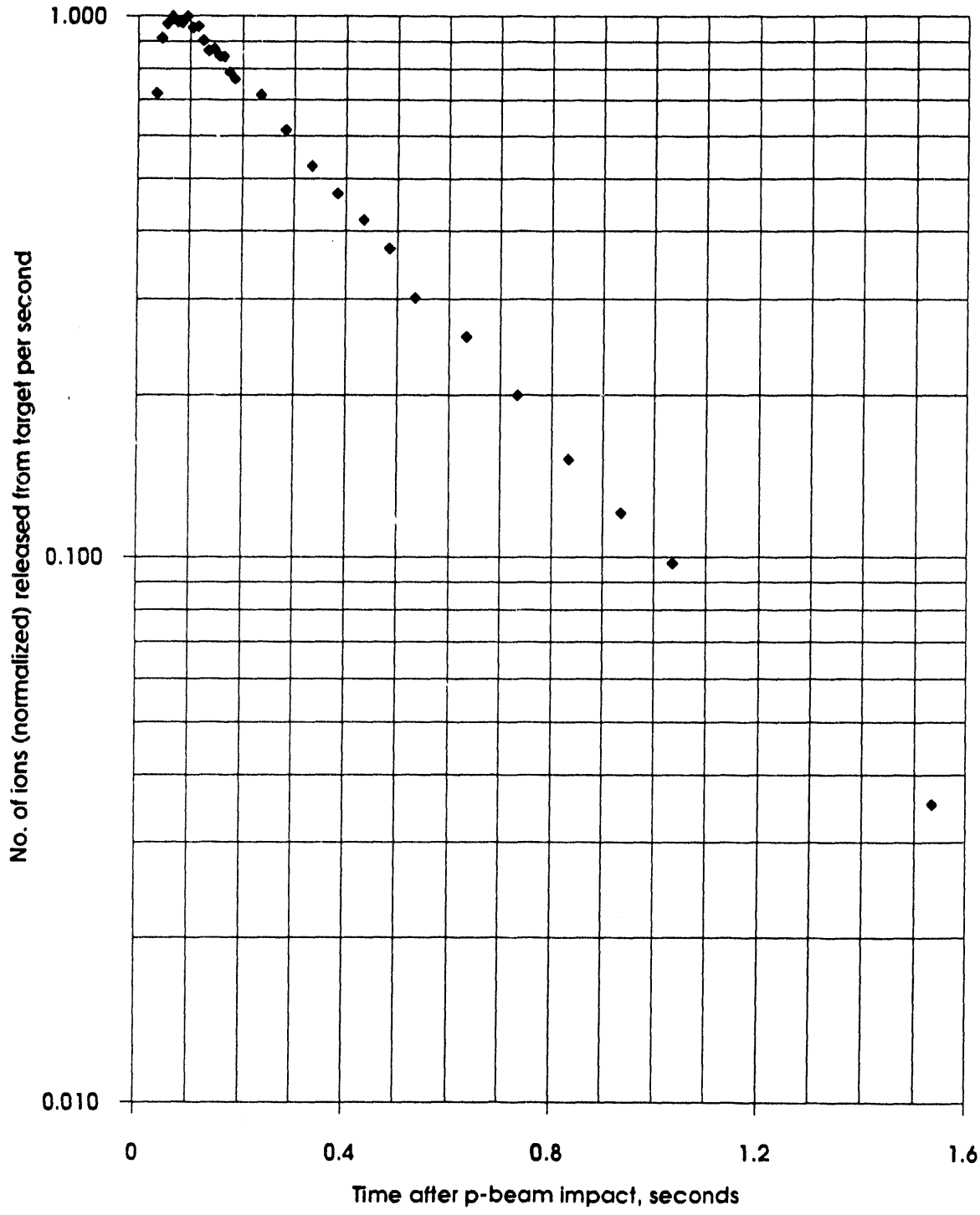

Figure 22. Delay time distribution p(t) of Ne from the ISOLDE MgO target irradiated with $3 \cdot 10^{13}$, 1GeV protons in 2.4 μs wide bursts.

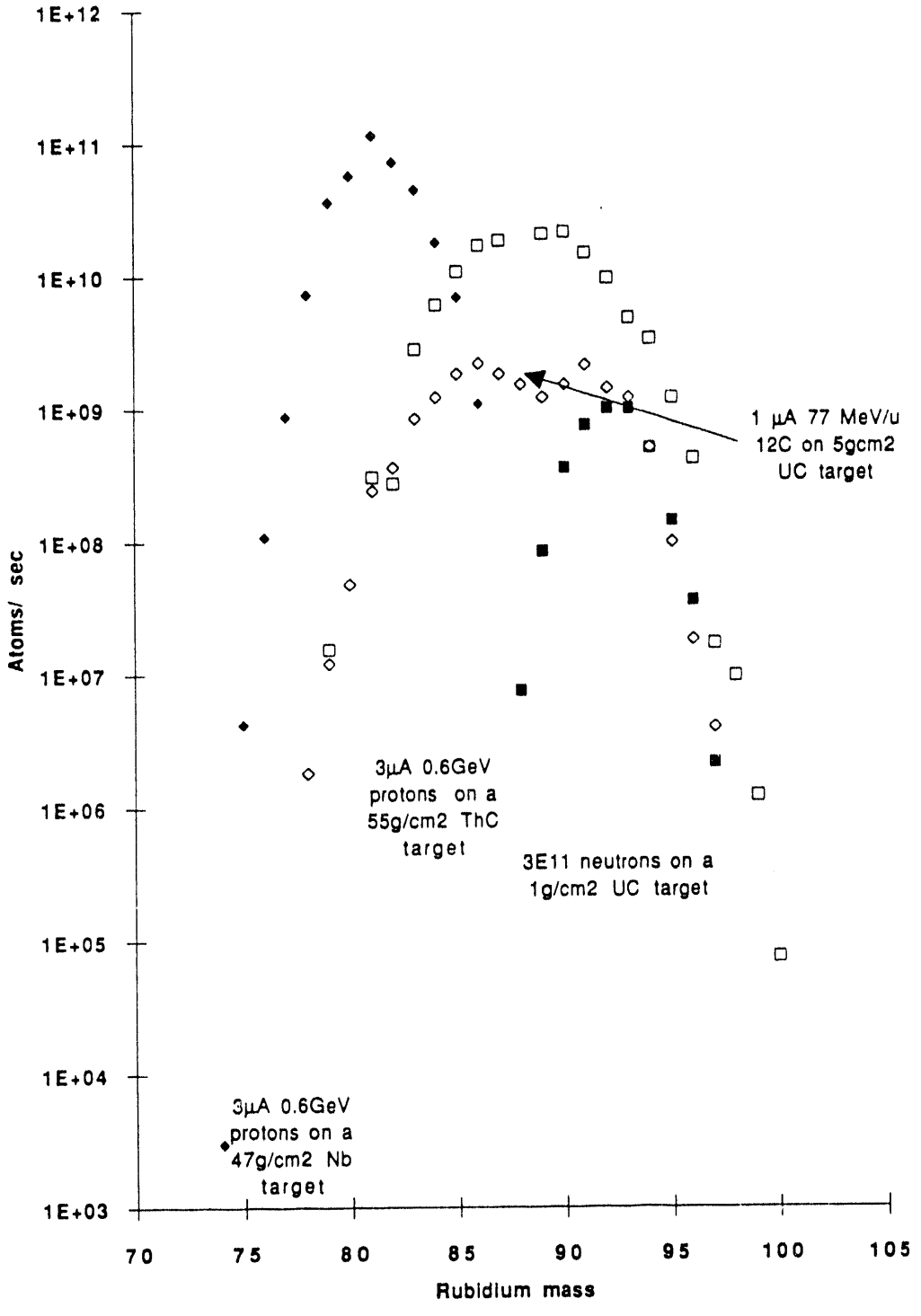

Figure 23. Measured production rates of Rb isotopes produced by means of 1GeV protons and thermal neutrons compared to calculated production rates with 77 MeV/u ^{12}C-ions.

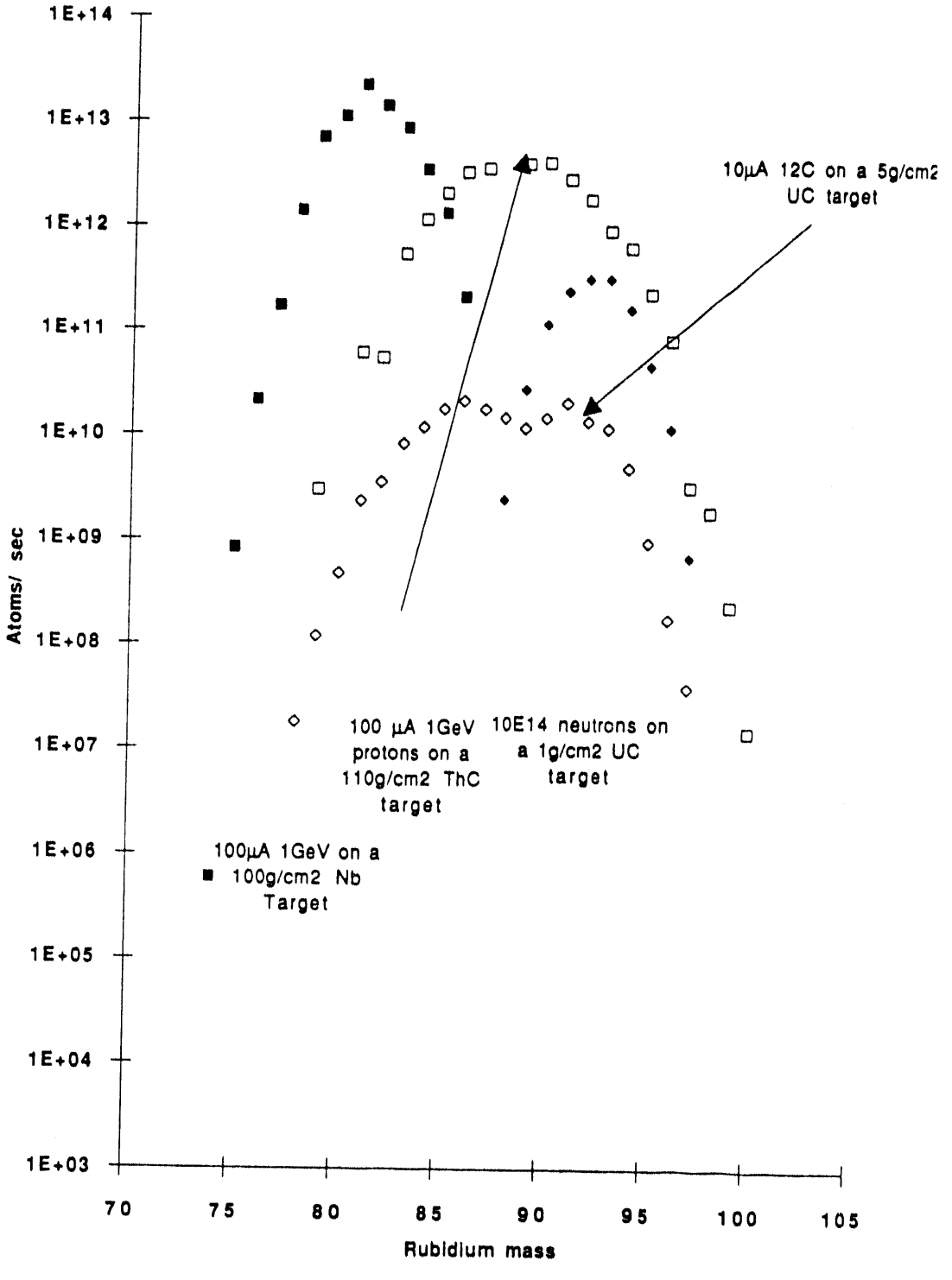

Figure 24. Measured production rates of Rb isotopes produced by means of 1GeV protons and thermal neutrons compared to calculated production rates with 77 MeV/u ^{12}C-ions. The intensities have here risen to the levels expected from the outcome of the respective R&D work which aimed at using the maximum beam intensities listed in table 1.

Power densities

Particle	Energy MeV	Energy loss dE/dx MeV/g*cm2	Target thickness, element g/cm2	Total power for a beam of: 6.25E12 particles/s (1μA) W	Power density W/cm3	Maximum available beam particles/s
Neutrons	thermal	160/fission	1, U-235	300	375	1E+14
Protons	1000	1.2	406, U-238	1600	31	6E+14
Protons	30	16.7	0.9, carbon	30	75	3E+15
12C	1152	200	4, Tin	800	1200	6E+13
36Ar	3456	2351	0.9, Carbon	2100	5250	6E+13

Table 1. Important beam and target parameters.

Beam	Half life	Target Material	Target Mass	Experimentally obtained beam intensities Atoms/s*μA
8He	122ms	UC	238	6.6E+05
8Li	842ms	Ta	181	3.9E+08
11Li	9ms	Ta	181	3.0E+03
11C	20m	MgO	24	6.8E+05
13N	10m	MgO	24	9.2E+03
14O	71s	Pt	195	2.0E+04
15O	2m	Pt	195	3.0E+04
19O	27s	Pt	195	1.0E+04
22O	2,3s	Pt	195	4.0E+02
17F	65s	Al	27	1.0E+07
19Ne	17s	MgO	24	3.0E+07
26Ne	162ms	U	238	7.0E+03
20Na	446ms	Al	27	2.4E+01
30Na	53ms	UC	238	6.0E+02
34Ar	844ms	CaO	40	3.8E+06
35Ar	1.8s	CaO	40	4.1E+07
72Zn	46h	U	238	2.7E+06
73Se	7h	ZrO2	90	3.0E+08
74Kr	12m	SrO	93	7.6E+01
91Kr	8.6s	U	238	1.5E+08
94Kr	0.2s	U	238	1.4E+06
97Rb	170ms	U	238	5.6E+06
111In	2.8d	Sn	118.7	1.0E+09
105Cd	56m	Sn	118.7	3.5E+08
108Sn	10m	TeCl4	127.6	5.0E+06
132Sn	40s	U	238	1.0E+05
121Cs	2.3m	La	139	7.3E+09
144Cs	1s	U	238	1.0E+09
142Xe	1.2s	U	238	4.2E+06
144Xe	1.2s	U	238	8.6E+04

Table 2. Radioactive ion-beams for which the European projects have specific experiments.

Isobar Separators for Radioactive Beam Facilities

Hermann Wollnik

2. Physikalisches Institut, University of Giessen, Germany

Abstract

Efficient high performance on-line isotope separator designs are discussed as needed in radioactive ion beam (RIB) facilities. It is described that good results can be expected only from multistage systems which should advantageously act on the ions at different acceleration levels.

Introduction

Energetic neutron rich or neutron deficient nuclei allow the study of astrophysical processes [1] but at higher energies they are also most interesting for the formation of neutron rich or neutron deficient heavy elements [2]. However, also for the study of materials [3] energetic short lived nuclei are of interest.

1. The production of radioactive ion beams

There are two ways to produce isotopically pure radioactive ion beams (RIB) of high energy:

1. One can bombard a thin target by energetic heavy ions and form beams of energetic reaction products from which one can select a beam of ions of a desired species by a high energy separator and either use them as they are as radioactive ion beams [4,5] or accelerate them in additional structures.

2. One can bombard a thick heavy element target by energetic light mass ions, so far preferably protons, thermalize the reaction products in the target, extract them by thermal diffusion and feed them into an ion source [6,7]. Alternatively one can bombard thin targets from which

the ions recoil into a high pressure gas where they are thermalized and swept into an ion source together with the gas [8]. In both cases the formed ions then can be mass separated in an isotope separator [6,7,9] and accelerated in a heavy ion accelerator.

The present paper focuses on the second method and proposes isotope separators that are capable of rendering isotopically pure radioactive ion beams. The production of such beams is difficult since their mass cross contamination must be extremely low because of the drastically different production rates of nuclei of neighbouring masses [10]. Since the ions of interest are often produced in minute quantities only, the isotope separators in question must feature high separation efficiencies and high transmissions simultaneously [11,12,13].

2. Properties of efficient isotope separators

For an efficient separation of isotopically pure beams of ions of mass m_0 and energy K_0 from all others it is necessary [7,11] to build a separator that consists of at least two stages that together:

1. efficiently eliminate fully accelerated (energy K_0) ions of wrong mass m_1 that are scattered - by collisions with residual gas atoms - into the exit slit optimized to collect ions of mass m_0 and energy K_0. This mass cross contamination is usually about 10^{-4} for a one-stage[1] and about 10^{-8} for a two-stage momentum analyzer.

2. efficiently eliminate ions of wrong mass $m_1 > m_0$ formed by charge-exchange processes or molecule-breakup reactions at places in the acceleration region from where the newly formed ions are accelerated only to energies $K_1 < K_0$. Of these ions only those can pass a first magnetic

[1]The number of 10^{-4} can be appreciated if one considers a magnetic sector field of one meter radius and an overall path length of about 3 meters. By using an exit slit of about $1mm$ such a system usually achieves a mass resolving power of $M/\Delta M \approx 1000$. If in this system a pressure of $\approx 10^{-6}$mbar exists, one finds there about $3 * 10^{10}$atoms/cm^3 so that after the said 300 cm flight path about 1% of all ions have interacted with one of the residual gas atoms assumed to have a cross section of about 10^{-15}cm^2. If those ions are distributed in the image plane over a length of perhaps 100 mm one finds that about 1% of all scattered ions pass through the exit slit of 1mm width.

separator stage[2] whose energies are $K_1 = K_0\, m_0/m_1$.

Since those ions have the same momentum as the ions of mass m_0 and energy K_0, they can only be eliminated by electrostatic sector fields [11]. However, a second momentum analyzer is also applicable if it operates at a different electrostatic potential [6,13]. This method is especially advantageous if a postacceleration of the mass separated ions is anticipated anyhow.

3. feature a combined mass resolving power that is high enough to separate neighbouring elements of the same isobar simply by their different nuclear binding energies which result in slightly different masses. In case of short-lived nuclei these mass differences are reasonably large (for instance several MeV for ions of perhaps 100 daltons) so that mass resolving powers in excess of $M/\Delta M = 30000$ usually suffice.

Additionally to the postulate that the separator must consist of two stages one should

1. postulate that the geometrical and chromatic image aberrations of both separator stages are reduced reasonably.

2. postulate that small variations in the ion-source behaviour do not jeopardize the good mass-separation properties of the ion-optical system.

3. find ways that increased ion currents do not deteriorate the mass resolving properties of the separator in a big way (due to space-charge problems).

4. design the isotope separator such that it can provide different mass resolving powers for different applications, thus allowing in special cases better mass separating properties even if that requires special efforts and possibly a loss in transmission.

[2] As an example one may assume ions of masses $m_0 = 100$dalton and $m_1 = 101$dalton as well as of energies of $K_0 = 60$keV and $K_1 = 60 * m_0/m_1 \approx 59.4$keV, respectively. Downstream from a first stage separator of resolving power $M/\Delta M = 1000$ the energy range of the transmitted ions of mass m_1 is $K_1 \approx 59.4(1 \pm 0.0005)$. Postaccelerating all ions after this first separator stage by another 60keV one must thus separate ions of momentum $\sqrt{2 * 100 * (60 + 60)}$ and $\sqrt{2 * 101 * [60 + 59.4(1 \pm 0.0005)]}$ differing by $(0.245 \pm 0.013)\%$. This can be achieved by a second-stage mass analyzer that has a mass resolving power $M/\Delta M \geq 1000$ or a momentum resolving power of $p/\Delta p \geq 500$.

3. The proposed separator geometry

To achieve all these features it is advantageous to design the isotope separator with at least two stages. Each of these stages can be constructed as proposed in ref. [13] and outlined in Fig.1 in which the ion beam is matched to the magnetic sector magnet by an astigmatic focusing quadrupole multiplet, preferably a quadrupole quadruplet. In this two-stage system the first-stage separator must mainly eliminate the bulk of the undesirable ions of neighbouring elements and neighbouring mass numbers, but its mass resolving power $M/\Delta M$ does not need to exceed 1000 or 2000. The resultant ion beam then must be purified by the second-stage separator which should feature a rather high mass resolving power ($\geq$ 30000) if neighbouring elements of the same isobaric chain must be separated from each other.

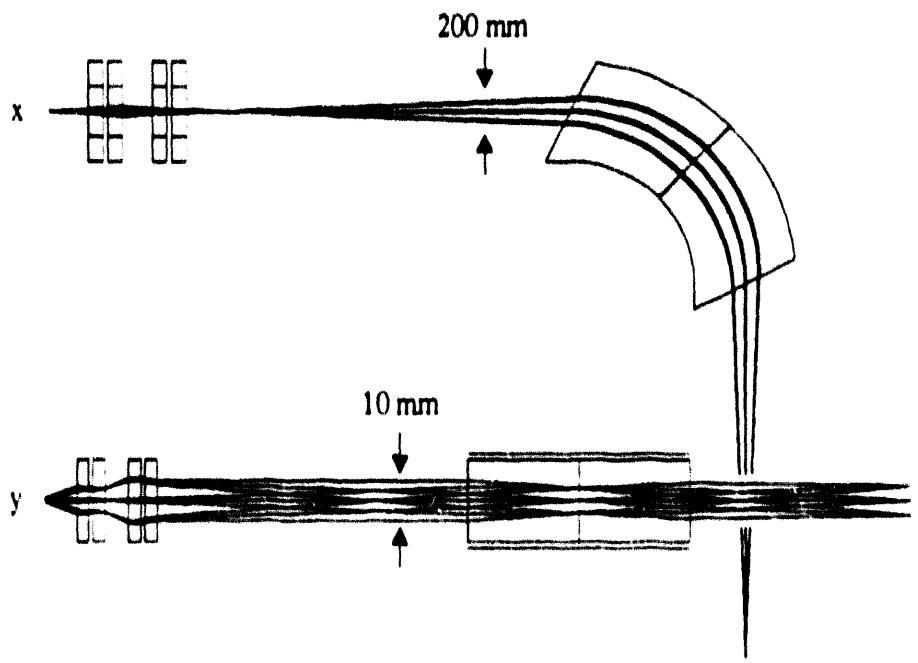

Figure 1: A mass separator is shown equipped with a preceding four quadrupole matching unit. Note that the x- and y-scales are very different and that the x-width of the ion beam is considerably larger (for instance $\approx \pm 100mm$) than the y-width (for instance $\approx \pm 5mm$).

3.1. The first-stage separator

For the first-stage separator the matching system is especially important since it follows the ion source immediately. In this case it serves the following purposes.

1. It separates the separator system from the high radiation levels at the production target which except for the He-jet approach is inevitably close to the ion source.

2. As far as the xz-plane of deflection is concerned the initial ion source exit is imaged to the entrance slit of the actual separator, i.e. at the position of the separator entrance slit an image is formed of the small area ($\approx \pm 0.1 * 0.1\ mm^2$) from which the ions seem to originate in the ion source, though the source aperture is much larger ($\approx \pm 1.0 * 1.0\ mm^2$). Usually this area is the virtual pupil of the ion source aperture formed by the lens action of the acceleration field.

   Varying the strengths of the quadrupole lenses one can

   (a) ensure that this image is formed at the separator entrance slit also if the ion-source parameters have varied slightly and so has the x- or the z-position of the virtual ion-source area.

   (b) vary the x-magnification at the position of the entrance slit which in combination with the unchanged dispersion of the sector magnet allows to vary the mass resolving power of the separator [12,13]. Note, however, that an N-times smaller image at the entrance slit inevitably causes an N-times larger angle of divergence of the ion beam and thus a wider beam in the sector magnet as far as the xz-plane of deflection is concerned [14].

3. in the yz-surface perpendicular to the xz-plane of deflection the quadrupole lenses in all cases can form a relatively wide beam at the position of the entrance slit, perhaps $\approx \pm 3mm$ or $\approx \pm 6mm$. In detail it is advantageous to postulate that the ion beam in all cases keeps more or less the same y-height throughout its travel through the sector magnet. This has the following advantages

   (a) all space-charge problems are grossly relieved since the beam cross section area stays reasonably large even at the position of the

entrance slit (perhaps $\approx \pm 0.1 * 5\ mm^2$) . Note here that in case of a stigmatic image of the small virtual ion-source area (perhaps $\approx \pm 0.1 * 0.1\ mm^2$) the ion-current density would considerably exceed that at the ion-source orifice (perhaps $\approx \pm 1.0 * 1.0\ mm^2$).

(b) the ion beam in the magnet can be much smaller in y-direction (perhaps $\approx \pm 5mm$) than in x-direction (perhaps $\approx \pm 100mm$) which reduces considerably all final image aberrations in x-direction that are due to the y-extension of the ion beam in the sector magnet, i.e. to second order the aberration coefficients (x,yy), (x,yb), (x,bb) as outlined for instance in ref. [14]. Thus no measures need to be taken to correct these aberrations. Consequently quite weak multipole fields or only slightly contoured field boundaries suffice to correct the usually still large image aberrations in x-direction that are due to the x-extension of the ion beam in the sector magnet, i.e. to second order the aberration coefficients (x,xx), (x,xa), (x,aa). This in turn does not - as is usually the case - inflate the third-, fourth- and fifth-order aberrations.

Furthermore, the magnet air gap stays small which allows a cheaper and lighter magnet since the magnet costs are usually proportional to the overall stored magnetic energy, i.e. approximately the magnetic flux multiplied by the magnet air gap.

So far it has only been stated that the matching system should consist of astigmatically focusing quadrupole lenses, but no decision has been made whether these lenses should be magnetic or electrostatic elements. In case of high radiation levels at the ion source position, however, one could state that it would be quite desirable to use magnetic quadrupoles since in this case a feasible radioactive contamination in the vacuum system could simply be eliminated by replacing the vacuum tube. Furthermore an existing space-charge compensation of the ion beam by low energy electrons or ions would stay undisturbed while electrostatic fields would extract such low energy particles [11]. On the other hand one should note that all magnetic quadrupole strengths must newly be adjusted for every change of the ion mass while electrostatic quadrupoles can be left alone as long as the ion energy stays constant. However, one should mention here also that electrostatic elements are subject to possible surface charge ups that modify the field distribution.

3.2 The second-stage separator

The second-stage separator should achieve a high mass resolving power. If the energy spread of the ions is about ±0.5eV or ±1.0eV the ion energy must be a few 100keV if this energy spread shall not significantly deteriorate a mass resolving power of $< M/\Delta M = 30000$. Furthermore the mass dispersion of the second-stage separator must be larger than 30000 times the width of its entrance slit. This usually requires the radius of the optic axis to be several meters. Furthermore it is most advisable to precede also the second-stage separator by an astigmatically focusing matching unit. This matching unit should

1. provide a y-waist more or less in the middle of the sector magnet so that its image aberrations can be corrected efficiently as described in point 221 of section 3.1.

2. provide an x-focus at the entrance slit with variable magnification so that a magnification $|M_x| < 1$ can be chosen for cases in which a high mass resolving power is required and in all other cases a magnification $|M_x| > 1$. Note here, however, that the angular magnification is always $1/|M_x|$.

4. Connection of an isotope separator to a post-accelerator

In section 3 it was outlined how ions should be accelerated by precision DC voltages from the ion source to the first-stage and then to the second-stage mass separator (see Fig.2). However, nothing was said about where this chain of potentials should be grounded.

In case of a DC postaccelerator it certainly is most convenient to position the second-stage separator at ground potential while the first-stage separator is fixed at some chosen potential[3] for instance $100kV$ relative to the ion source potential. In case of an AC accelerator one must not only control the potential differences from the ion source through the first- to the second-stage separator but also ensure that the velocities of ions of all masses are the

[3]Note that we speak only of the potential of the vacuum chamber and not of the total separator. Thus one can still choose whether one wants to float the whole first-stage separator or whether one wants to insulate the vacuum chamber from the entrance to the exit slit and float it relative to the magnet which can stay at ground potential.

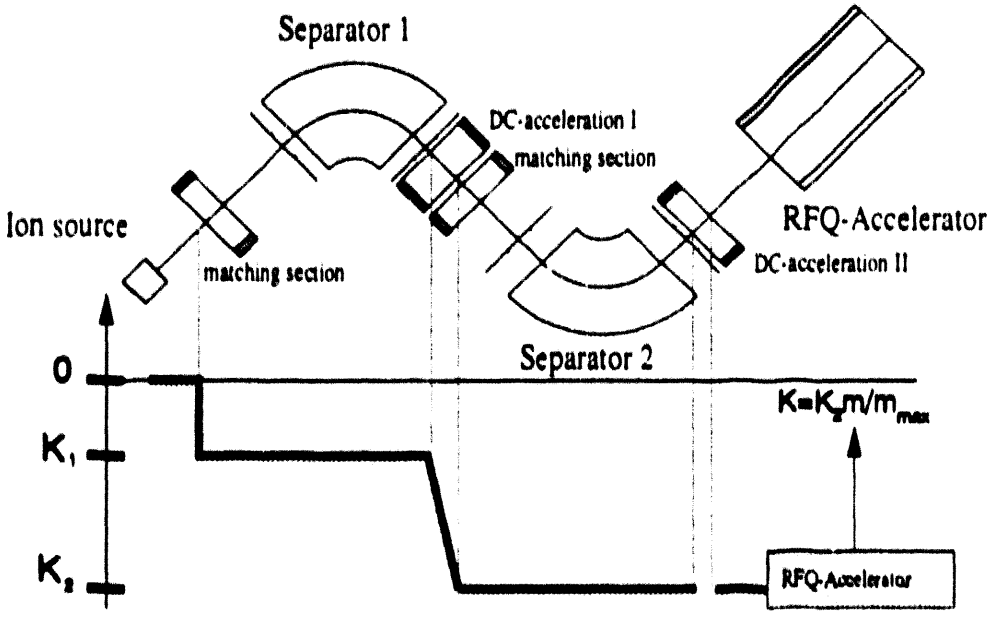

Figure 2: A feasible two stage mass separator is characterized by the ion energy K_i at the electrostatic potentials of its different parts. Note that here an RFQ AC-accelerator is indicated the potential of which is varied such that $K_i = K_0 m_i/m_0$ assuming that ions of mass m_i are to be accelerated. Note also that all indicated potentials are the potentials on the optic axis. In the sector magnets the indicated potentials are those of the vacuum chamber where the magnet itself can be at an arbitrary potential. In the RFQ accelerator the indicated potential here is that of the accelerating structure while the vacuum envelope can also be at an arbitrary potential. Note furthermore that one still can decide where to ground the potential chain. There may be reasons to postulate the AC accelerator to be at ground, however, there may also be reasons to postulate one of the separator stages to be grounded and in cases of very complex ion sources there may be reasons to float both the separators as well as the AC accelerator while the ion source stays at ground potential.

same when they enter the AC-accelerator. Thus the ions may all have to be accelerated or decelerated after the exit of the second-stage separator. If the accelerator is at the same potential as the second-stage separator, only ions of a specific mass m_0 and energy K_0 have the correct velocity for the AC accelerator. For ions of other masses m_i the potential of the AC-accelerator must be changed relative to the second-stage separator such that the ion energy is $K_i = K_0 m_i/m_0$ and both ion velocities are equal.

If ions of masses $m_i = 8u$ to $m_i = 250u$ should be accelerated, it may be advantageous to choose the proper velocity for the AC-accelerator to be that of ions of mass $m_0 = 250u$ and energy K_0. In order to accelerate ions of other masses m_i then the accelerator potential must be varied such that the ion energy varies between K_0 and $0.032K_0$, i.e. that the low mass ions are decelerated to almost the potential of the ion source. Note, however, that this deceleration can be smaller if for different mass ranges the ion charges are varied, for instance such that ions up to mass ≈ 50 are singly, from mass ≈ 50 to ≈ 150 are doubly and above mass ≈ 150 are triply charged.

Acknowledgements

For fruitful discussions I am thankful to A.Przewloka, M.Winkler and C. Weil and for financial support to the Bundesminister für Forschung und Technologie.

References

1. C.A.Barnes, Rad. Nucl. Beams, ed. T.Delbar; Adam Hilger New York (1991) p.250

2. D.D.Warner, Rad. Nucl. Beams, ed. T.Delbar; Adam Hilger New York (1991) p.139

3. E.Arthur et al. and I.Sawicki, Rad. Ion. Beams, eds. J.Mclelland and D. Viera, LANL report LA-11964-C (1990)p.82, p.231

4. H.Wollnik, Nucl. Instr. and Meth. **B26**(1987)267

5. G.Muenzenberg et al., Rad. Nucl. Beams, eds W.Myers et al. World Scientific, Singapore (1989)91

6. C.Geisse et al., Nucl. Instr. and Meth. **B26**(1987)120

7. H.Wollnik, Nucl. Instr. and Meth. **A258**(1987)289

8. H.Wollnik, Nucl. Instr. and Meth. **139**(1976)311

9. H.Wollnik et al., Rad. Nucl. Beams, eds W.Myers et al. World Scientific, Singapore (1989)603

10. H.Ravn, Nucl. Instr. and Meth. **70**(1992)107

11. H.Wollnik, Int. J. Mass Spectr. and Ion Proc. **30**(1979)137

12. K.Becker and H.Wollnik, Nucl. Instr. and Meth. **187**(1981)167

13. H.Wollnik, Nucl. Instr. and Meth. **B56/57**(1991)1096

14. H.Wollnik, "Optics of Charged Particles", Acad Press 1987, Orlando

RADIATION PROBLEMS AT AN ISL FACILITY

I.M. THORSON
TRIUMF
4004 Wesbrook Mall
Vancouver, B.C. Canada V6T 2A3

ABSTRACT

The problems associated with the high radiation field and large quantities of residual radioactivity induced in beam-line components and shields and released from production targets in a high beam power (~50 kW) ISL facility are estimated. A conceptual design that accommodates these constraints is described.

1. INTRODUCTION

The radiation fields produced in the vicinity of the high beam power, 50 kW (500 MeV, 100 μA), radioisotope production target of an ISL facility are estimated and described in section 2 of this report. The shield requirements to achieve tolerable levels of personnel exposure during operation as well as the residual fields from induced radioactivity in areas of closest personnel approach during maintenance operations are estimated. The dose-rates expected near the production targets, required for materiel damage estimates, are also defined. A very brief description of the phenomenology of surface contamination and adsorption is also included in section 2.

Section 3 describes a conceptual design for a high beam power ISL facility based on our experience and the same generic approach that has been employed successfully at the TRIUMF meson factory, and will be employed in the design of the KAON facility when it proceeds to detailed design and construction. The principal specific requirement for ISL is the need for a two-stage vacuum system capable of tolerating 200° C temperature rises in the radioactivity containing primary vacuum system for distillation of loosely adsorbed radioactive species from the walls and internal components to a cryogenically pumped trap and auxiliary vacuum pumping system.

Section 4 enumerates a few of the more important components and systems called for by the design in section 3 that should proceed to prototype development and firm conceptual design in the early stage of an ISL construction program.

2. RADIATION ESTIMATES

2.1 Operating Radiation Fields: Shield Requirements

The radiation field produced by the bombardment of thick targets by an intense beam of 500 MeV protons has been estimated from Bertini's[1] intra-nuclear cascade calculations parameterized by Alsmiller et al[2]. The cumulative reactions of the incident protons colliding in stopping thickness targets of carbon, aluminum, copper and lead were derived from the compilation of proton range and reaction probabilities tabulated by Measday and Richard-Serre[3] and are shown in Fig. 1. Using the 7 energy groups implied in Fig. 1, the cascade proton and neutron yields into the 4 angular segments tabulated in reference [2] were estimated per incident primary proton and shown in Fig. 2. Fig. 3

shows the secondary nucleon kinetic energies in the 4 angular segments as fractions of the original 500 MeV proton kinetic energy. The evaporation neutron and proton yields and kinetic energy fractions are also shown in Figs. 2 and 3, assumed to be isotropic and normalized per steradian, as for the cascade nucleon results. The results are summarized in Tables Ia and Ib. Figs. 4a and 4b summarize the forward direction yields extrapolated linearly back to the origin from Figs. 2 and 3 as a function of target mass number, A. Fig. 5 shows the exponential relaxation widths of the cascade nucleon angular distribution expressed as 1/10 relaxation widths. The results are also tabulated in Table II.

The results, particularly for the cascade neutrons, the dominant deep-penetration radiation component, are not strongly target dependent. Table III shows the dose-rate from the unattenuated cascade and evaporation neutron field in the forward and lateral directions from a proton stopping thickness target of the various representative materials. Although tertiary, and higher order, protons and γ-radiation from the proton and neutron collisions and neutron capture will make some contribution, the dominant field will come from the neutrons, even close to the target. The evaporation neutron component dominates for high mass targets at shallow shield depths because of their high multiplicity. After one or two decades of attenuation, however, the cascade component will become dominant, particularly in the forward direction where neutrons up to the incident proton energy contribute significantly. At angles above 90° the cascade neutron spectrum effectively cuts off at approximately 100 MeV (for 500 MeV protons incident) for all targets extending the onset of exponential relaxation and the depth where secondary evaporation neutrons contribute significantly to the dose.

The dose distribution in shields surrounding targets bombarded by protons above a few hundred MeV can be approximated by an extended Moyer Model using the relationship:

$$D(\theta,r) = \beta_D e^{-(\theta/\theta' + d/\lambda)}/r^2$$

where: θ' is the angular relaxation width for e^{-1} reduction (0.43x relaxation widths quoted in Table II),
d is the thickness of the shield, of equilibrium relaxation length λ,
r is the distance from the source to the field point,
and β_D is the dose build-up and normalization factor that is expected to saturate to a constant value at large depths.

The experience at higher energies (E > 1 GeV) indicates values of $\theta' = 1$ radian (57°)[4]. The results shown in Fig. 5 are consistent with this value on the plausible assumption that the radiation transport to large depths is proportional to the secondary neutron kinetic energy distribution. Experience at TRIUMF (E = 0.5 GeV) indicates[5] that the β_D value from higher energies, namely,

$$\beta_D = 2.8 \times 10^{-13} E^{0.8} f \qquad \text{Sv p}^{-1} \text{ GeV}^{-0.8} \text{ m}^2,$$

can be extended to the lower energy by inclusion of a discount factor f, for the fraction of the primary energy suffering nuclear collisions (Table Ib).

At the lower energy and large depths, the normalization factor β_D given above, extrapolated from higher energies gives similar estimates to one based on plausible assumptions about the equilibrium spectrum (E^{-1}), fluence-to-dose-equivalent conversion factors (NCRP-38)[6] and fraction of secondary and higher order spectrum above the effective reaction cross-section cut-off (~75 MeV) of concrete shields. At shallow depths in shields β_D is expected to depend on incident energy and angle,

particularly at higher energies, but the empirical formulation quoted above should give useful approximations to the cascade neutron component.

To obtain estimates of the physical dose in other materials the QF factors quoted in NCRP-38 have been removed from the fluence-to-dose-equivalent relationship giving 2.6 x 10^{10} cm^{-2} evaporation neutron fluence for 1 Gy dose and 8.5 x 10^{9} cm^{-2} cascade neutron fluence to deliver 1 Gy dose. The change in absorbed dose-to-fluence ratio for other materials can be ignored given the qualitative understanding of radiation effects on materials and the approximations in estimating the neutron fluences.

To obtain the 10 $\mu Sv\ h^{-1}$ dose-equivalent rates required for uninhibited occupation by experimenters and operators of ISL facilities, the total shield attenuation must be 10^{-9} in the forward direction from 50 kW targets and 10^{-4} in the lateral direction. Approximate shield thicknesses to provide such protection are quoted below. Two intermediate stages of shielding are of interest: the point, or points, where various materials, such as organics, may suffer significant radiation damage and the point at which residual radioactivation begins to inhibit maintenance and disassembly/reinstallation operations. The latter is the more constraining. The annual dose to components in the lateral direction from a 50 kW beam at 50% overall duty factor at a distance of 1.6 m behind 1.0 m of iron and 0.3 m of water, or equivalent hydrogen content, is estimated by the model described above to be 10^{5} Gy. Most materials will survive such abuse without significant problems. The semi-saturated residual γ-dose rate at the surface of an iron component at that point would however, be of the order of 1 $mSv\ h^{-1}$. To obtain the desirable situation of 50 $\mu Sv\ h^{-1}$ dose rates for extended work following substantial operations without inhibiting personnel exposures, the shield thickness needs to be increased to 1.5 m of iron and 0.4 m of water equivalent outside the assumed "stay clear" void of 0.3 m radius for target components and services. To obtain the 10 $\mu Sv\ h^{-1}$ operating fields at inhabited space an additional 4.5 m of concrete are required in the lateral direction and about 5.5 m in the forward direction. Such an array would require about 400 tonnes of iron and 350 - 500 m^{3} of concrete if it was arranged in a compact configuration.

2.2 Radioactivation

Fig. 6 shows the mass chain yield parameter for spallation reactions in ^{56}Fe for various proton energies, based on Silberberg and Tsao's [7] elaboration of Rudstam's [8] original formulation. The Z dependence width, ΔZ ($\sim$0.59 to 0.67 amu), which is not reaction energy dependent, but is slightly dependent on the product mass, produces slight variations and small (< factor 1.3) renormalization factors for the precise integral mass yields from those shown in Fig. 6. There are also some ad hoc corrections that are applied for particular even/odd combinations of protons and neutrons and for certain elemental species but these are also less than a factor 1.5, maintaining the gross variations in A shown in Fig. 6. For 500 MeV reactions, the total estimated yield is 0.64 neutron deficient species, 0.034 neutron rich species, 0.11 isolated, central valley species, as well as 0.53 stable species, all per 500 MeV proton reaction. The peak in the Z-distribution is never further than 1 amu from a stable element and the fractions of multiple decays are of the order 3% for the total saturated radioactivity production. The residual γ-radiation field decay curve for iron is shown in Table IV from Barbier and Coopers [9] compilation based on Rudstam's formula. The reaction spectrum is approximated by equal weighting for the 50, 100 and 600 MeV danger parameters from reference [9]. The slow decay of the long lived species (first factor 2 in 10 days, second factor 2 in 6 months) indicates the need for considerable caution with regard to long term radioactivation.

Thermal neutron capture can also lead to difficult radioactivation problems. Capture in cobalt (leading to 5 year half-life ^{60}Co) at the 100 ppm level in stainless-steel or iron in a water-moderator environment can be the dominant long lived species. Capture in the ~2% sodium in some concrete is also a problem, especially for bare high mass targets in accelerator/beam line enclosures. Low sodium concrete and/or concrete with natural or additive boron concentrations of ~0.1% by weight can each reduce the ^{24}Na production by an order of magnitude.

Radioactivity in cooling water is not a serious problem in an isolated closed-loop system; the dominant β sources that accumulate are ^{3}H and ^{7}Be, the latter of which is removed in the ion-exchange system required for corrosion control. The short lived β^{+} emitters, quickly dominated by ^{11}C, decay at the rate of approximately 1 decade per hour.

The γ-radiation field from the ion-exchange resin beds may be dominated by corrosion products or even recoil species from the high field container wall surface, but it represents a very small fraction of the induced radioactivity.

Radioactivation of air, mostly from spallation reactions in the nitrogen and oxygen giving the short live β^{+} emitters can be a problem, especially where interstitial space in close proximity to high power production targets contains heat sources that can drive thermal convection currents. Chimneys are very efficient and effective devices for mass transport and can require substantial and expensive ventilation facilities to prevent uncontrolled radioactivity releases. Radioactivated air can pose two problems of a lower threshold than the obvious one of personnel exposures. The first is the background problem to experimental equipment in the experimental areas. The second is the background interference with environmental and contamination egress monitoring at control boundaries. The most satisfactory solution to these problems is to suppress radioactivation of the air at its source by eliminating the air from the vicinity of targets.

2.3 Radioactivity Contamination

The major difference between an ISL facility and existing high power facilities, such as the meson factories, is the loose radioactivity contamination problem. In the meson factories loose contamination represents a very small fraction, of the order of 10^{-6} or 10^{-5} of the total radioactivity production; most of it is deeply buried in targets, structural components and shields. Even in accidents the scenarios get to be only marginally credible for releases greater than 10^{-4} or 10^{-3} of the total inventory. Thus the closest relevant experience with the handling of loose radioactivity remains with the existing on-line ion source system such as ISOLDE[10]. The step that is envisaged in going to an ISL facility, however, is a factor 10^{2} which probably requires a revolutionary, as distinct from evolutionary, approach to the anticipated problems.

Because the objective will be to release as much of the radioactivity induced in production targets as possible the design will need to accommodate the anticipated disposition of all species evolved, i.e. we must understand at least the basis of surface physics[11]. Fig. 7 shows the expected dwell times for species adhering to surfaces with an adsorption energy Q_A at the various temperatures shown parametrically. It is simply the general relation for the mean dwell time, t, of an atom on the surface,

$$t = \tau e^{Q_A/kT},$$

where τ is of order 10^{-13}s, the time for a thermal atom to traverse the distance of one atomic surface layer without sticking. If it is bound by energy Q_A its dwell time is enhanced by the exponential factor shown. The bonding mechanism can be anything from van der Waal's force at the low Q_A end to molecular or chemical bonding at the high Q_A end. The annotation on Fig. 7 gives a few surface-gas combinations in the range of their determined or expected Q_A values. The Q_A values will in general depend on the existing contamination layers already on the surface and may well change as the surface contaminants are deposited or removed. The only general tool one has available to adjust the surface concentrations is the surface temperature. If a particular elemental species encounters different surfaces with different adsorption energies in a vacuum system it will migrate toward the one with the highest bonding energy, the relative distribution being inversely proportional to the dwell times and directly proportional to the size of the surface areas. There is a second constraint, however, namely the time for equilibration. If, for example, a species were bound to a surface at 500° K with a binding energy of 30 kcal mole^{-1} the mean dwell time at any one point would be 1 second and if we were attempting to move it to a surface or a port that represented 0.1% of the contaminated surface area, the mean relaxation time for the transfer would be 1000 seconds, ~15 minutes. Presuming that the receiving surface or port had a much higher bond energy or lower temperature so that there was no return, the transfer would go at a rate of one decade reduction from the warmer surface every 35 minutes, a conveniently short transfer time. If the bonding energy was 40 kcal mole^{-1}, the individual dwell periods would increase to about 3×10^4 seconds and the mean transfer time, again for 0.1% receiving surface fraction, would be 3×10^7 seconds i.e. 1 year! However, when the temperature of the (de-) contaminated surface is brought back to room temperature (300° K) the dwell time of the species bound at 30 kcal mole is now $\sim 7 \times 10^6$ seconds and for 40 cal mole species, 10^{16} seconds. Given the 4×10^{14} Bq total saturated radioactivity inventory from a typical target under 100 μA bombardment the contamination loss rate would appear to be manageable under such a decontamination regime.

The point is that raising the temperature ~200° C and extracting the evaporated species into traps that can be isolated would allow at least gross decontamination of the components of an ISL facility, at least of those species that are the most susceptible to migration during transport to maintenance facilities.

3. DESIGN REQUIREMENTS - POSSIBLE SOLUTION

Although other conceptual designs are probably feasible, the most flexible approach where substantial shields are required is from the top, especially where highly radioactivated components may require some shielding for transport to hot-cell maintenance facilities. Such an approach implies the availability of a substantial (25 - 30 tonne) crane for rapid access to the buried components and the ability to transport heavy shield flasks. Personnel access is then limited to elevations above a distance set by the residual radioactivation consideration. All components at beam line elevations are mounted under top-shielded columns which are removed and transported with their components. All insertion and installation operations must be accomplished remotely, or at least at a distance, putting a considerable burden on good mechanical design. While pre-alignment should be used whenever possible, the ability to at least monitor the position of critical components is probably a practical necessity. For close tolerance alignment, it is also probably necessary to keep the alignment devices near the critical components; this will probably require "soft coupling" of the critical components to their services and top shield plugs. The services connections are all made at the top of the removable columns, of course.

3.1 Monolithic Shield/Secondary Vacuum System

The approximately 4.4 m x 4.4 m x 3.6 m monolithic shield in which the proposed facility is imbedded is mostly made of iron - approximately 400 tonnes - as shown in plan view in Fig. 8. Figs. 9a and 9b show the lateral and longitudinal vertical sections, a heavy secondary vacuum tank grouted into place using, preferably, a water-saturated grout made from a limestone based aggregate and loaded with about 0.1% boron to suppress long term thermal neutron radioactivation, primarily for ultimate disposal. This design essentially eliminates the air radioactivation problem. The size of this secondary vacuum tank will need to be balanced between cost, not just capital but also operational costs arising from more massive components, and future flexibility and contingency. The 0.6 m width of the slots and 0.4 m bottom clearance for the primary and secondary beam lines shown in Fig. 8 and 9, appear to be reasonable but by no means firm. Because the difference in shield cost for substantial targets, say 25% removal, and complete stopping is not large, the beam stop should be mounted close to the target in the monolithic shield. The secondary channel slot is extended back beyond the target primarily to allow the installation of cryo-vacuum pumping system as near the target-ion source assemblies as thermal heat loads will allow and large ducts to the auxiliary systems for volatile species mounted in the service space above.

The shielding required outside the target block can be designed for minimum cost, with the possible exception of minimizing the length of the secondary channel. That usually means standard concrete; the 4.5 m thickness will translate to 350 - 500 m^3 total, much of which could probably be used as a permanent installation without sacrificing future flexibility significantly.

3.2 Two-Stage Vacuum System

Fig. 10 shows an expanded view of the secondary beam channel conceptual design. The most critical aspect of the proposed conceptual design is a two stage vacuum system. The secondary vacuum system contained by the imbedded vacuum tank shown in Figs. 8,9 and 10 is all-welded construction in the vicinity of the beam plane. The demountable seals at the top of the assembly are all removed far enough from the target that good organic material can be used. The pumping system for the secondary enclosure must be capable of only modest vacuum, say 10^{-2} torr. This essentially eliminates the radioactivation of air and the atmospheric mechanical load on the primary vacuum system. It should also eliminate most of the convective heat transfer from the primary vacuum system, allowing baking of the whole primary system at, say, 200° C, for decontamination purposes. During operation the target-ion-source-secondary beam channel would operate at unconstrained temperatures; some of the secondary channel more remote from the hot target should operate at low temperatures for cryogenic pumping/trapping of radioactive contamination. The secondary channel could even employ a modest dog-leg for more complete trapping of such activity, especially if it could be combined with gross isotopic beam separation, at the obvious cost of extending the length of the secondary beam channel beyond that shown in Figs. 8,9 and 10.

One of the more important components for the primary containment system are the primary vacuum seals. The "pillow" seals employed in the redesign of the Paul Scherrer Institute primary beam-line[12] are proposed because of their simplicity and their remote installation/extraction features. PSI uses double seals with intermediate vacuum pumping to obtain 10^{-8} pressure differentials. In this application which should require only 4 or 5 decades reduction in residual gas pressure from the secondary vacuum and no atmospheric mechanical load, single stage seals should, hopefully, be adequate. These all-metal seals must however, retain their integrity through the 200° C temperature

cycling described above. Clearance for insertion/removal of the components and their shield columns may require the auxiliary bellows, as shown in Fig. 10, to achieve enough travel of the seals.

To decontaminate any or all of the primary vacuum system, the primary vacuum system valves at the exit from secondary vacuum enclosure would be closed before the nearby in-line cold traps were warmed-up. The temperature of the whole primary system, including the open vacuum valve between the target ion-source facility and the cryo/auxiliary pumping system port would then be raised to 200° C and held for several hours to distill over all species below a cutoff surface bonding energy to the cryo-pumping-and-trapping system. At the end of the decontamination period the vacuum valve would be closed and the system returned to room temperature in preparation for letting both the primary and secondary vacuum systems up to atmospheric pressure, probably simultaneously. The secondary beam-line component to be serviced should now not contain contaminations that would be vulnerable to release, at least during transport.

4. DEVELOPMENT REQUIREMENTS

Several critical components and system designs must be perfected and demonstrated with prototypes before building even a full-scale prototype of such an ISL target. Two obvious components are the "pillow" vacuum seals and the radiation-hard vacuum valve, which must tolerate a temperature swing of at least 200° C and still maintain their seal integrity. Proof tests of the conceptual regime should be done by exposing test plates in an operating ISOL target environment of various materials and removing them to a temperature controlled distillation facility similar to that proposed.

Considerable conceptual design work on the mechanical installation, extraction and, particularly, alignment and alignment monitoring of the components and systems is required. Production and testing of prototypes of the more critical components and systems would also be prudent.

5. ACKNOWLEDGEMENTS

I would like to thank the organizing committee of this meeting for the opportunity to discuss the problems and possible solutions for an ISL facility from my perspective and experience at a meson and aspiring kaon facility, and in particular, John D'Auria whose patience and perseverance have been sorely tested.

6. REFERENCES

[1] H.W. Bertini, Phys. Rev. 131, (1963)1801 and Phys. Rev. 138 (1965)AB2.

[2] R.G. Alsmiller Jr., M. Leimdorfer and J. Barish, ORNL - 4046 1967, *Analytical Representation of Non-Elastic Cross-Sections and Particle Emission Spectra from Nucleon-Nucleus Collisions in the Energy Range 25 - 400 MeV.*

[3] D.F. Measday and C. Richard-Serre, CERN 69-17, 1969, *Loss of Protons by Nuclear Reactions in Various Materials.*

[4] R.H. Thomas and G.R. Stevenson, *Radiological Safety Aspects of the Operation of Proton Accelerators*, IAEA Technical Report Series No. 283, Vienna 1988.

[5] *KAON Factory Study - Accelerator Design Report*, TRIUMF, 4004 Wesbrook Mall, Vancouver, B.C., CANADA, V6T 2A3, 1990.

[6] *Protection Against Neutron Radiation*, National Council on Radiation Protection and Measurements, NCRP Report No.38, January 4, 1971, 4201 Connecticut Ave., N.W. Washington, D.C. 20008

[7] R. Silberberg and C.H. Tsao, The Astrophysical Journal Supplement Series, No. 220(I) 25, 1973, pp 315-333 and No. 220(II) 25, 1973, pp335-368.

[8] G. Rudstam, Phil. Mag. 46, 1955, p. 344, and Nuclear Physics, A126, 1969, p401.

[9] M. Barbier and A. Cooper, CERN Report, 1965, 65-34, *Estimates of Residual Radioactivity in Accelerators.*

[10] H.L. Ravn and B.W. Allardyce, *On-Line Mass Separators*, p. 363. Treatise on Heavy-Ion Science, Vol.8. Nuclei Far from Stability, Edited by D. Allan Bromley, Plenum Press, New York and London, 1989.

[11] J.H. de Boer, *The Dynamical Character of Adsorption*, 2nd Edition, Oxford University Press, Oxford UK, 1968.

[12] SIN Jahresbericht 1984, Schweizerisches Institut für Nuklearforschung, CH-5234 Villigen, pJB17.

TABLE Ia: NUCLEON PRODUCTION FROM 500 MeV PROTONS ON THICK TARGETS

	C	Al	Cu	Pb
Collision Fraction	0.768	0.751	0.704	0.691
Cascade Protons	1.20	1.18	1.04	0.75
Cascade Neutrons	0.70	0.81	0.92	0.97
Evap. Protons	0.40	0.76	0.58	0.26
Evap. Neutrons	0.26	0.42	1.82	5.85
Totals	2.56	3.17	4.36	7.83

TABLE Ib: ENERGY FRACTIONS FROM 500 MeV PROTONS ON THICK TARGETS

	C	Al	Cu	Pb
Collision Energy	0.545	0.527	0.485	0.475
Casc Proton K. Energy	0.336	0.290	0.228	0.156
Casc. Neutron K. Energy	0.158	0.159	0.143	0.157
Evap. Proton K. Energy	0.005	0.009	0.009	0.007
Evap. Neutron K. Energy	0.003	0.004	0.013	0.033
Total Sec. K. Energy	0.502	0.462	0.393	0.353
Residual	0.043	0.065	0.092	0.122

TABLE II: ANGULAR DISTRIBUTION PARAMETERS
500 MeV PROTONS ON THICK TARGETS

		C	Al	Cu	Pb
$_pY(0)$	steradian^{-1} proton^{-1}	0.64	0.55	0.45	0.30
$_p\theta_Y{}^{0}$		86°	97°	102°	109°
$_pKE\ (0)$	steradian^{-1} proton^{-1}	0.49	0.35	0.22	0.14
$_p\theta_{KE}{}^{0}$		46°	51°	58°	61°
$_nY\ (0)$	steradian^{-1} proton^{-1}	0.31	0.32	0.32	0.30
$_n\theta_Y{}^{0}$		102°	110°	120°	135°
$_nKE\ (0)$	steradian^{-1} proton^{-1}	0.17	0.15	0.11	0.12
$_n\theta_{KE}{}^{0}$		54°	58°	66°	71°

TABLE III: DOSE RATES FROM THICK TARGETS
100 μA, 500 MeV PROTONS BOMBARDMENT

		C	Al	Cu	Pb
$_nY\ (0°)$	steradian^{-1} proton^{-1}	0.31	0.32	0.32	0.30
$_nY\ (90°)$	steradian^{-1} proton^{-1}	0.040	0.049	0.057	0.065
$_n\Phi_i\ (0°)$	cm^{-1}s^{-1} @ 32 cm	1.9×10^{11}	2.0×10^{11}	2.0×10^{11}	1.9×10^{11}
$_n\Phi_i\ (90°)$	cm^{-1}s^{-1} @ 32 cm	2.5×10^{10}	3.1×10^{10}	3.6×10^{10}	4.0×10^{10}
$_n\Phi_t$	cm^{-1}s^{-1} @ 32 cm	1.3×10^{10}	2.1×10^{10}	9.0×10^{10}	2.9×10^{11}
$D_i\ (0°)$	Gy s^{-1} @ 32 cm	22	24	24	22
$D_i\ (90°)$	Gy s^{-1} @ 32 cm	2.9	3.6	4.2	4.7
D_t	Gy s^{-1} @ 32 cm	0.5	0.8	3.5	11.2
$D_{\text{total forward}}$	Gy s^{-1} @ 32 cm	23	25	28	33
$D_{\text{total backward}}$	Gy s^{-1} @ 32 cm	3	4	8	16

TABLE IV: RESIDUAL SURFACE DOSE RATE FROM IRON
(for 4 x 10^9 cm^{-2} s^{-1} Cascade Neutron Flux Saturated Bombardment)

Decay Period	Surface Dose Rate ($\mu Sv\ h^{-1}$)
0	146
1 hour	118
1 day	106
7 days	88
30 days	67
180 days	44
360 days	29

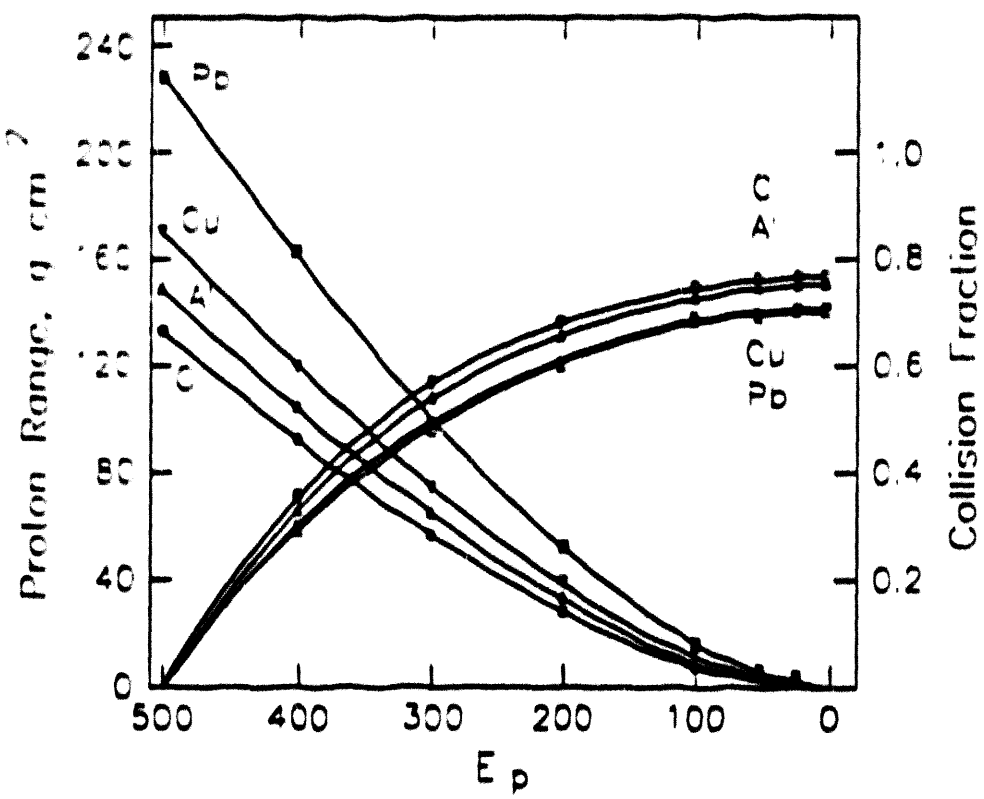

Fig. 1 The residual range and cumulative proton reaction probabilities are shown as a function of the remaining proton kinetic energy in stopping thickness targets of carbon, aluminum, copper and lead bombardment by 500 MeV incident energy protons.

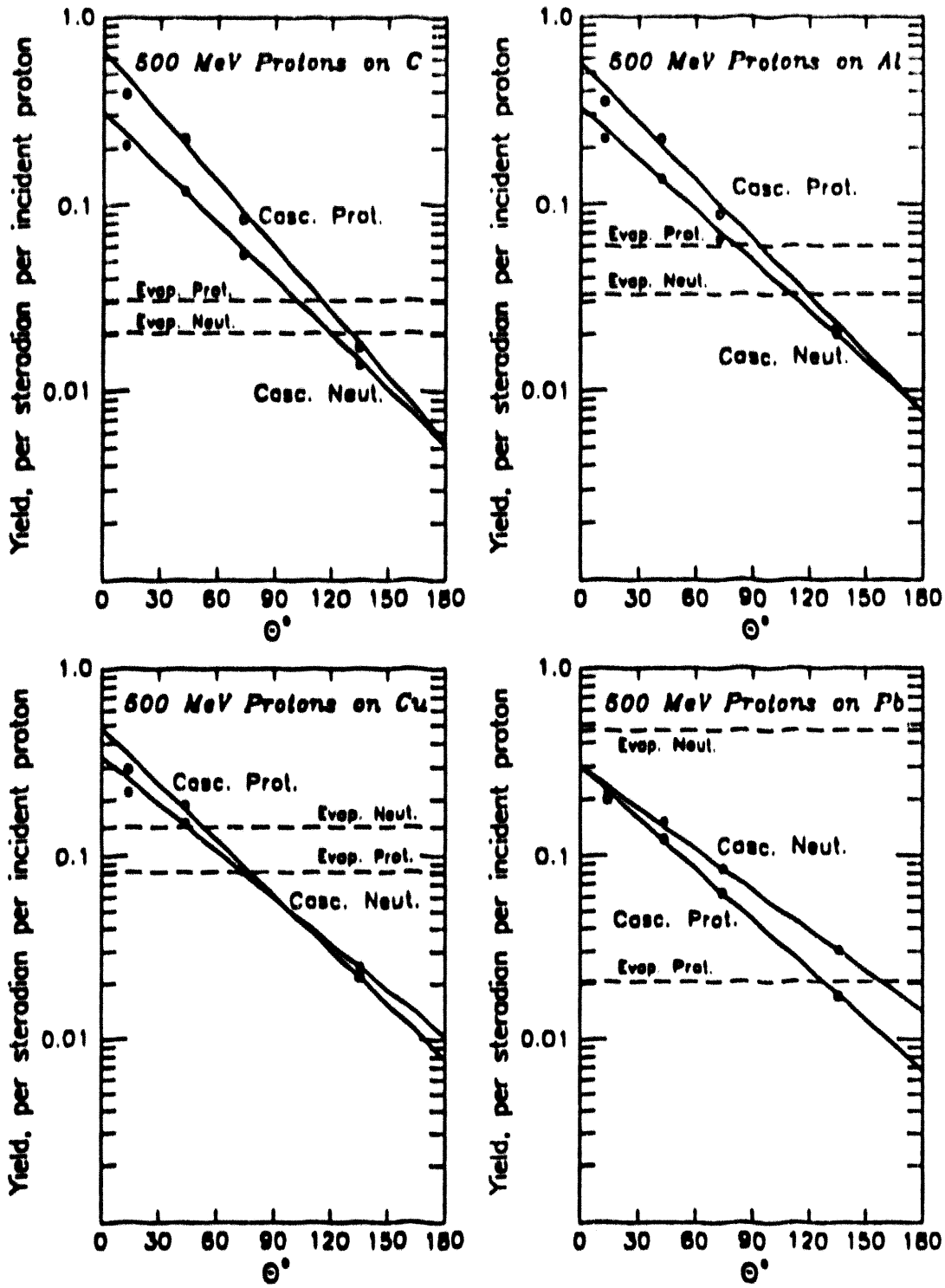

Fig. 2 The yield of secondary cadscade and evaporation neutrons and protons from 500 MeV protons stopping in thick targets of carbon, aluminum, copper and lead are shown as angular distributions from the primary proton beam direction. The yields are integrals over both primary (stopping) and secondary (spectral) energies.

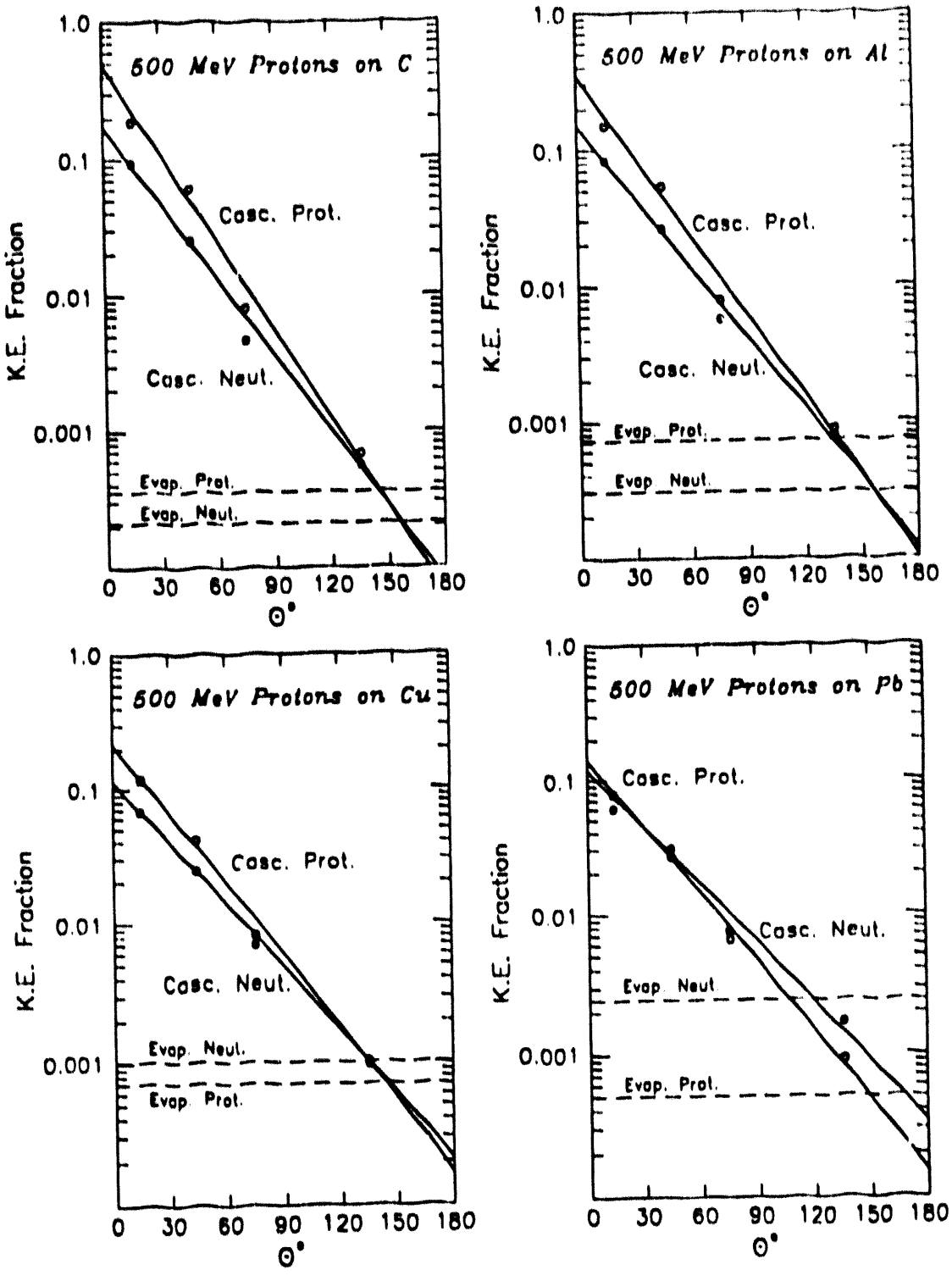

Fig. 3 The secondary nucleon kinetic energies are shown as angular distributions fractions of the original 500 MeV primary proton kinetic energy incident on stopping thickness targets of carbon, aluminum, copper and lead.

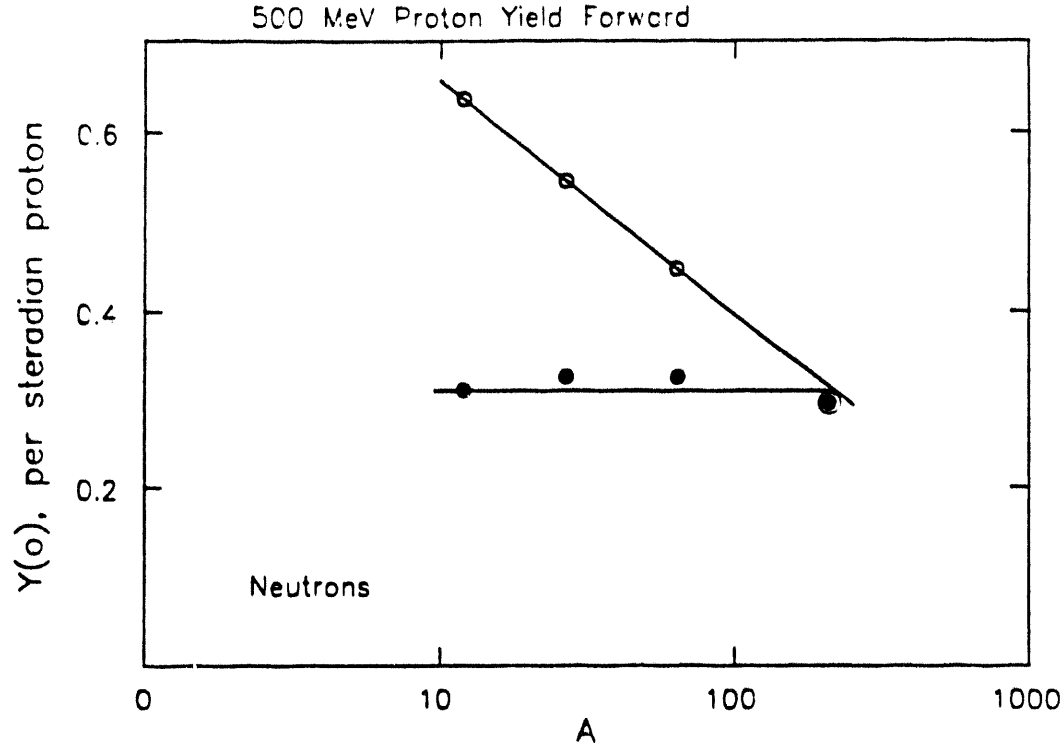

Fig. 4a Shows the cascade nucleon particle yields in the forward direction from the log-linear extrapolation of Fig. 2, as functions of the target mass number.

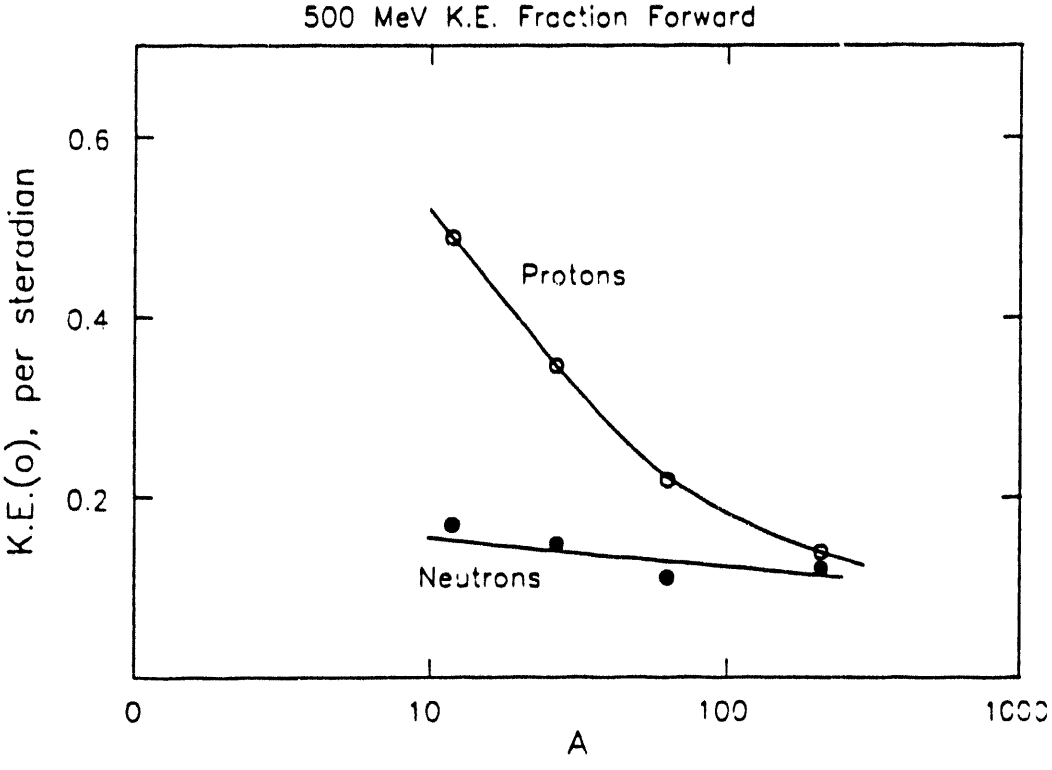

Fig. 4b Shows the cascade nucleon kinetic energy fraction in the forward direction from the log-linear extrapolation of Fig. 3, as functions of the target mass number.

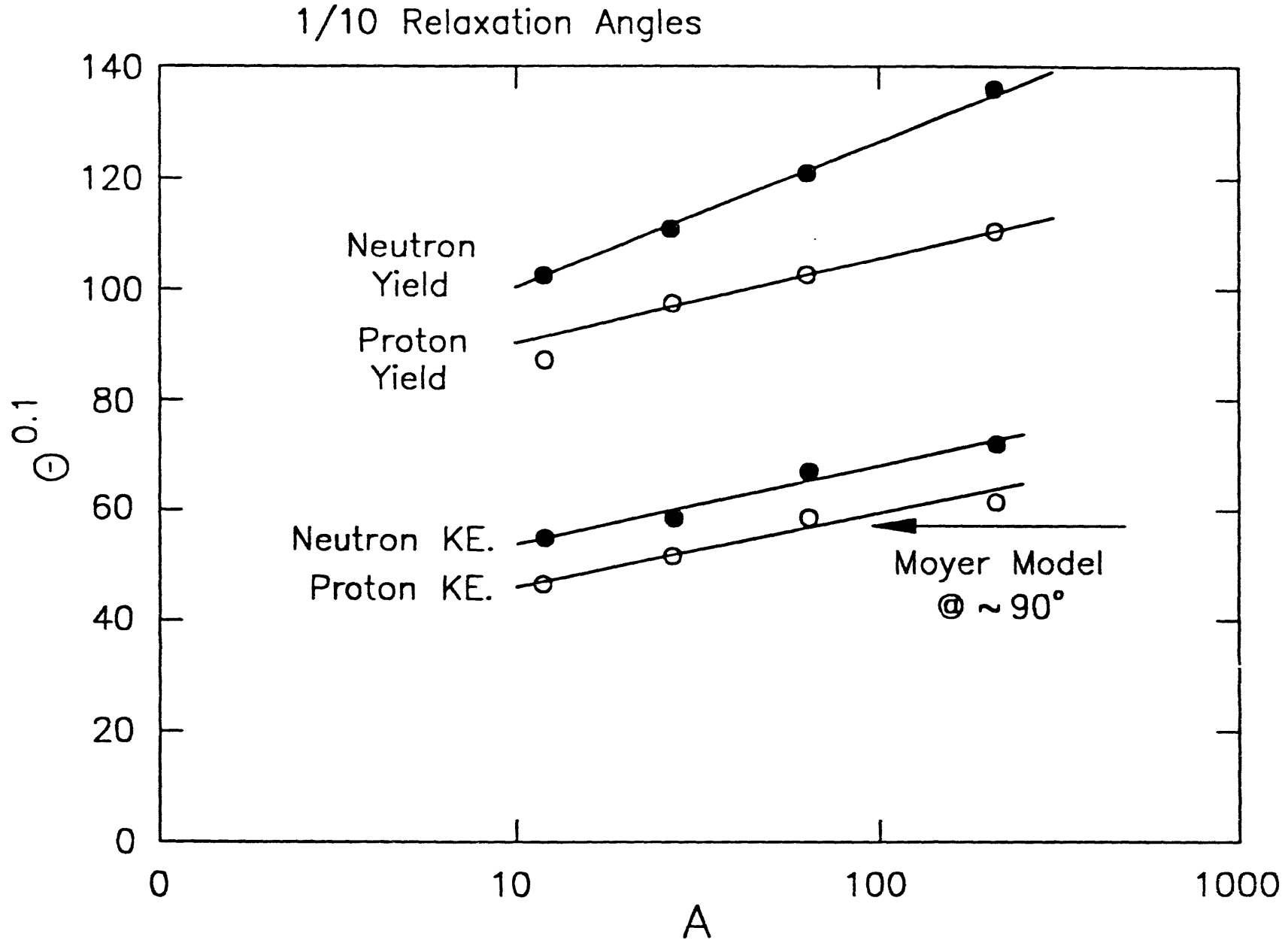

Fig. 5 Shows the 1/10 angular relaxation widths from the slope of the angular distributions shown in Figs. 2 and 3, also as functions of target mass number A.

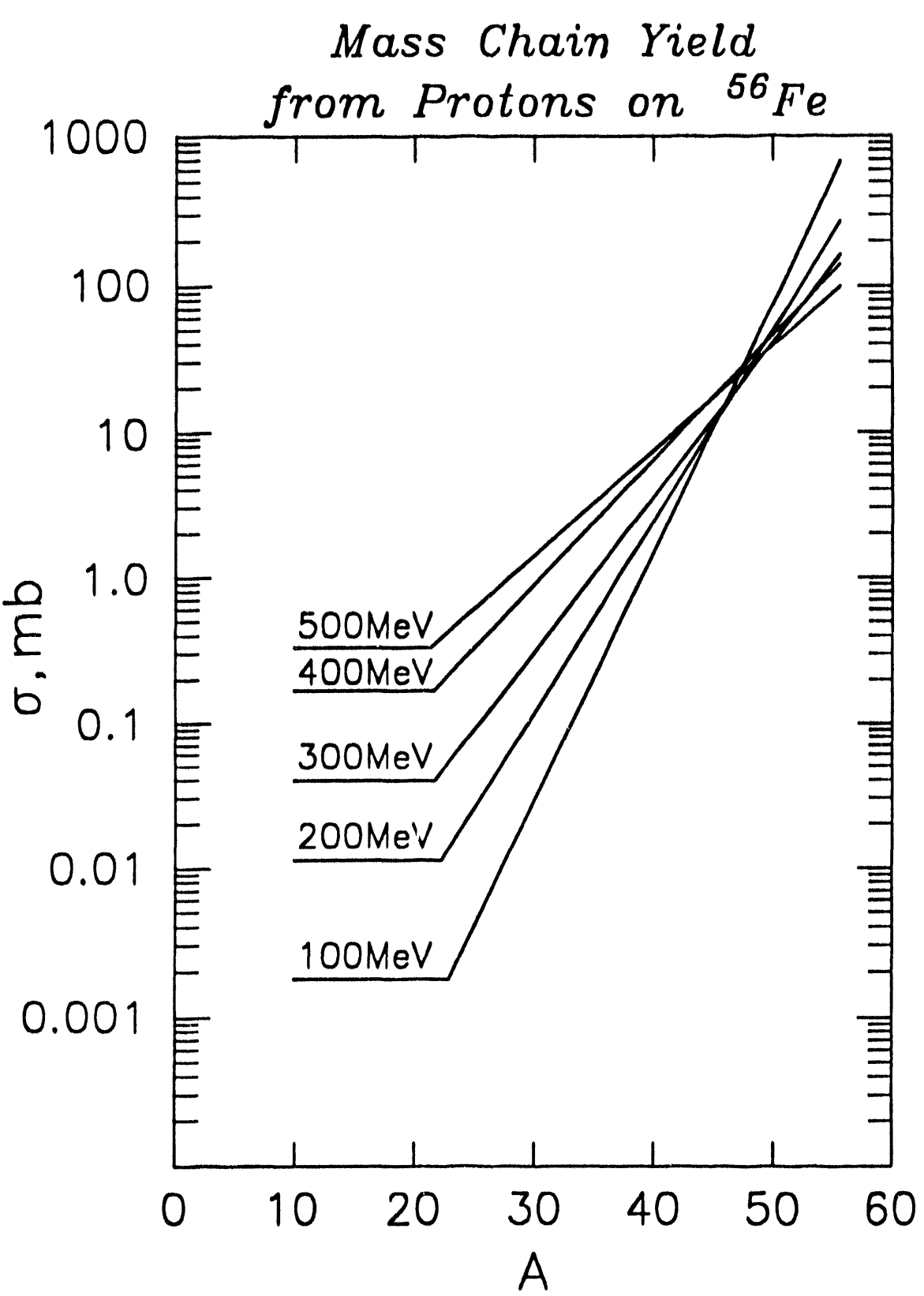

Fig. 6 Shows the mass chain yield distribution from proton reactions of various energies with ^{56}Fe. The estimates are based on the empirical fits of reference [7] without renormalization for the Z-distribution and various small detailed corrections in the range 0.7 - 1.5.

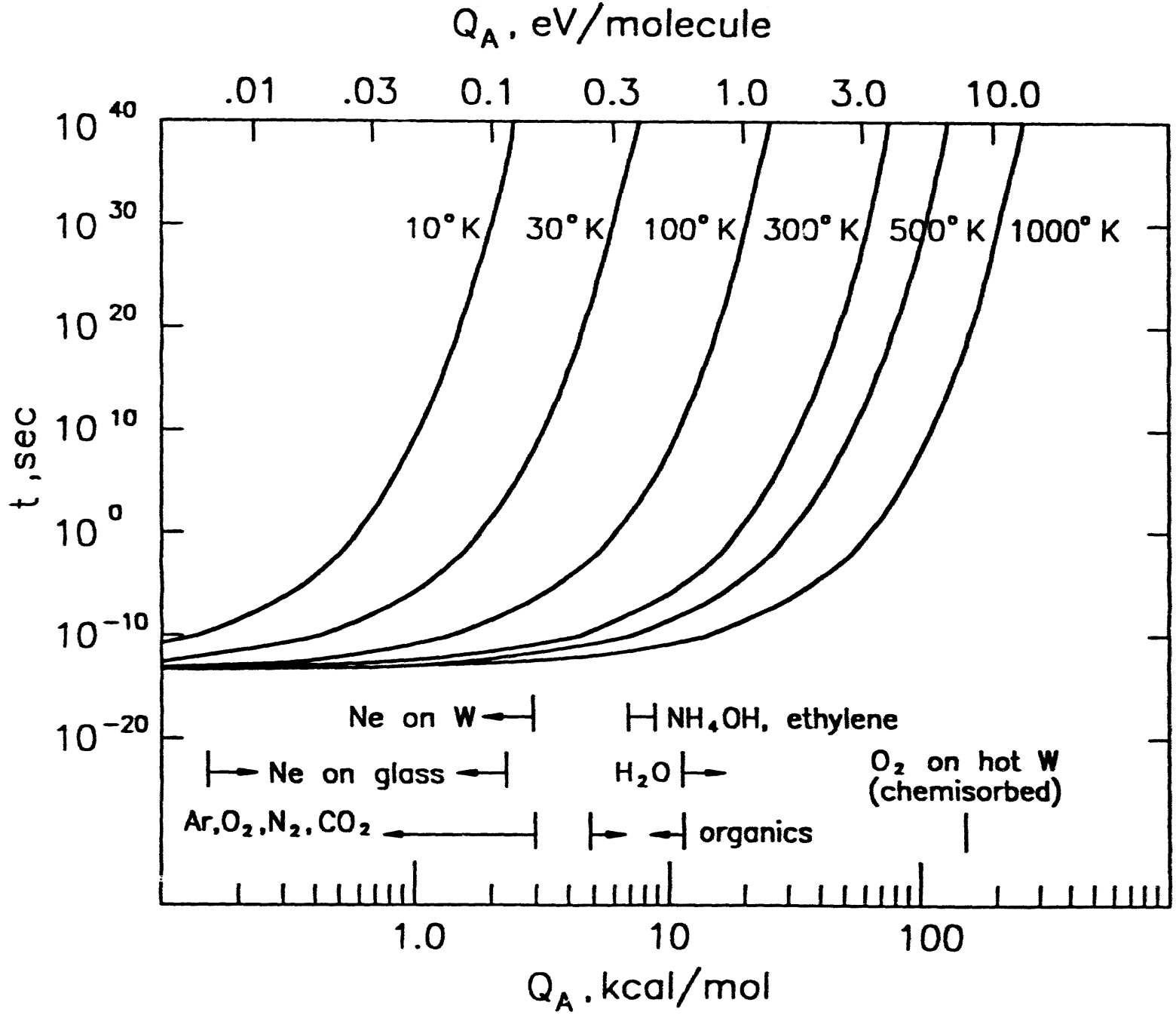

Fig. 7 The sticking times of atoms bound to a surface at various temperatures by a bond energy Q_A.

Plan View

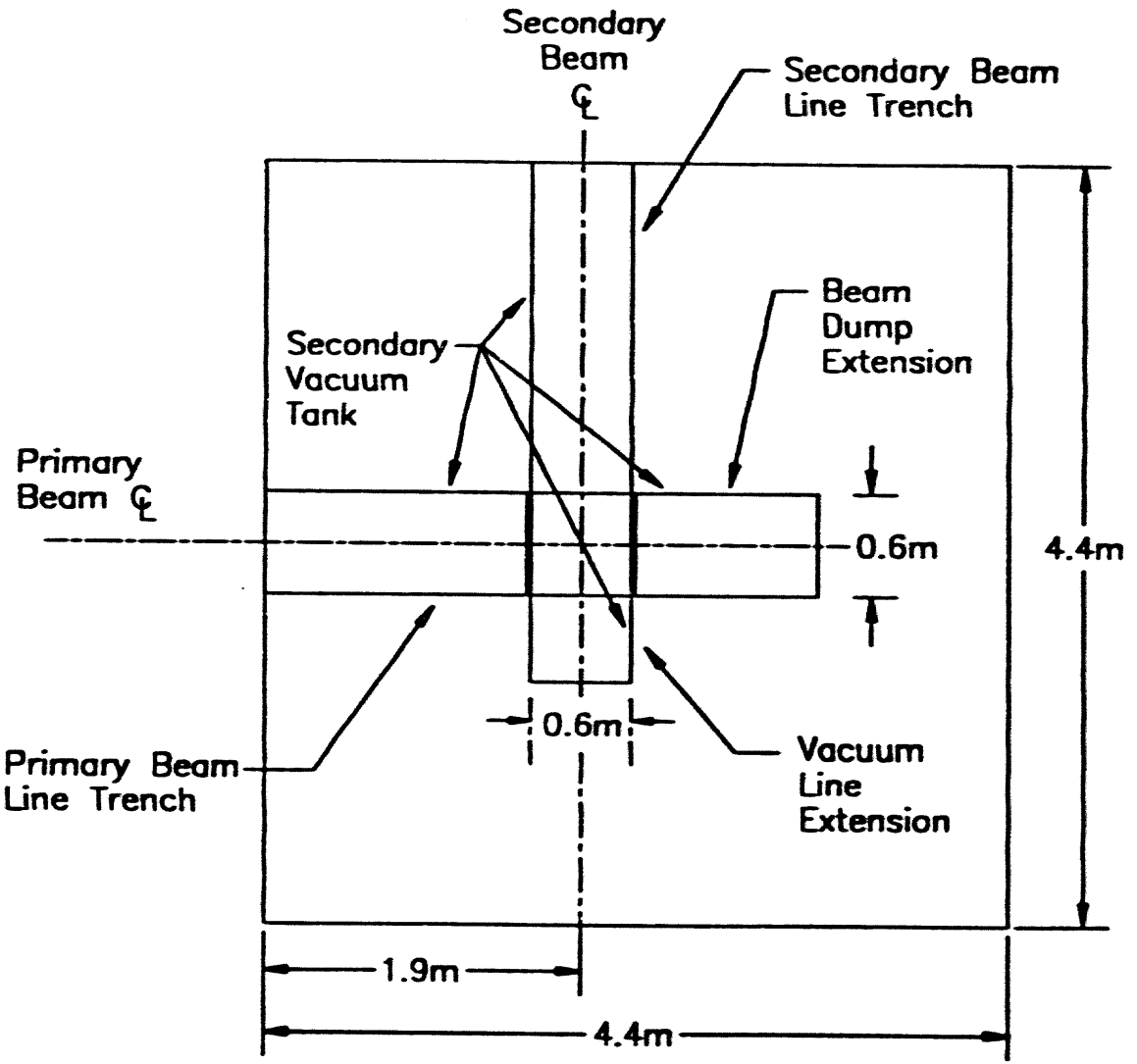

Fig. 8 The plan view is shown of the proposed secondary vacuum tank embedded in a monolithic iron shield. The intersecting trenches shown for the primary and secondary beam lines are both 0.6m wide and 2.6m deep with all component access and servicing from above.

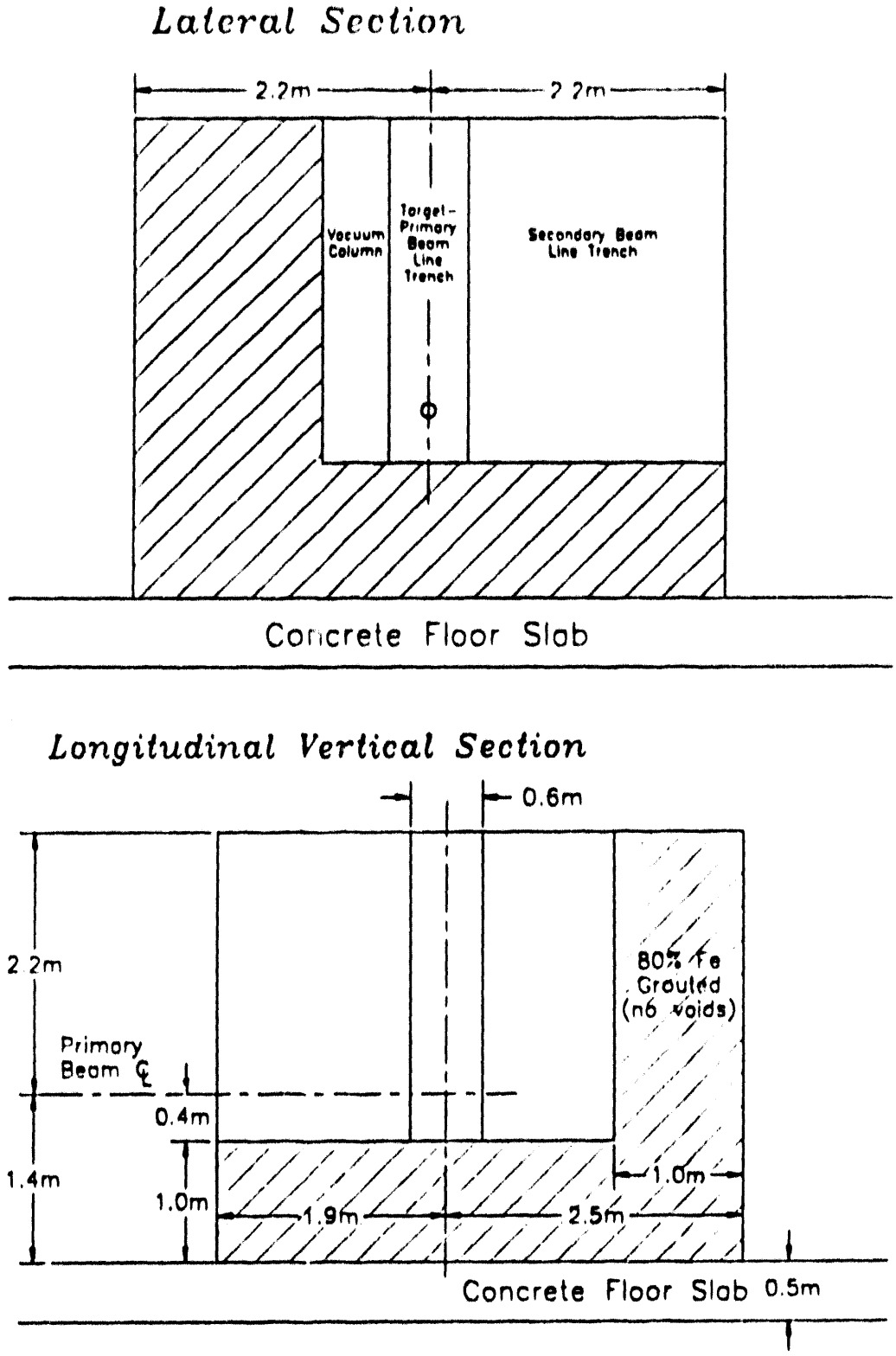

Fig. 9 Shows the orthogonal vertical sections along the primary and secondary beam center lines of the proposed secondary vacuum tank embedded in a monolithic iron shield.

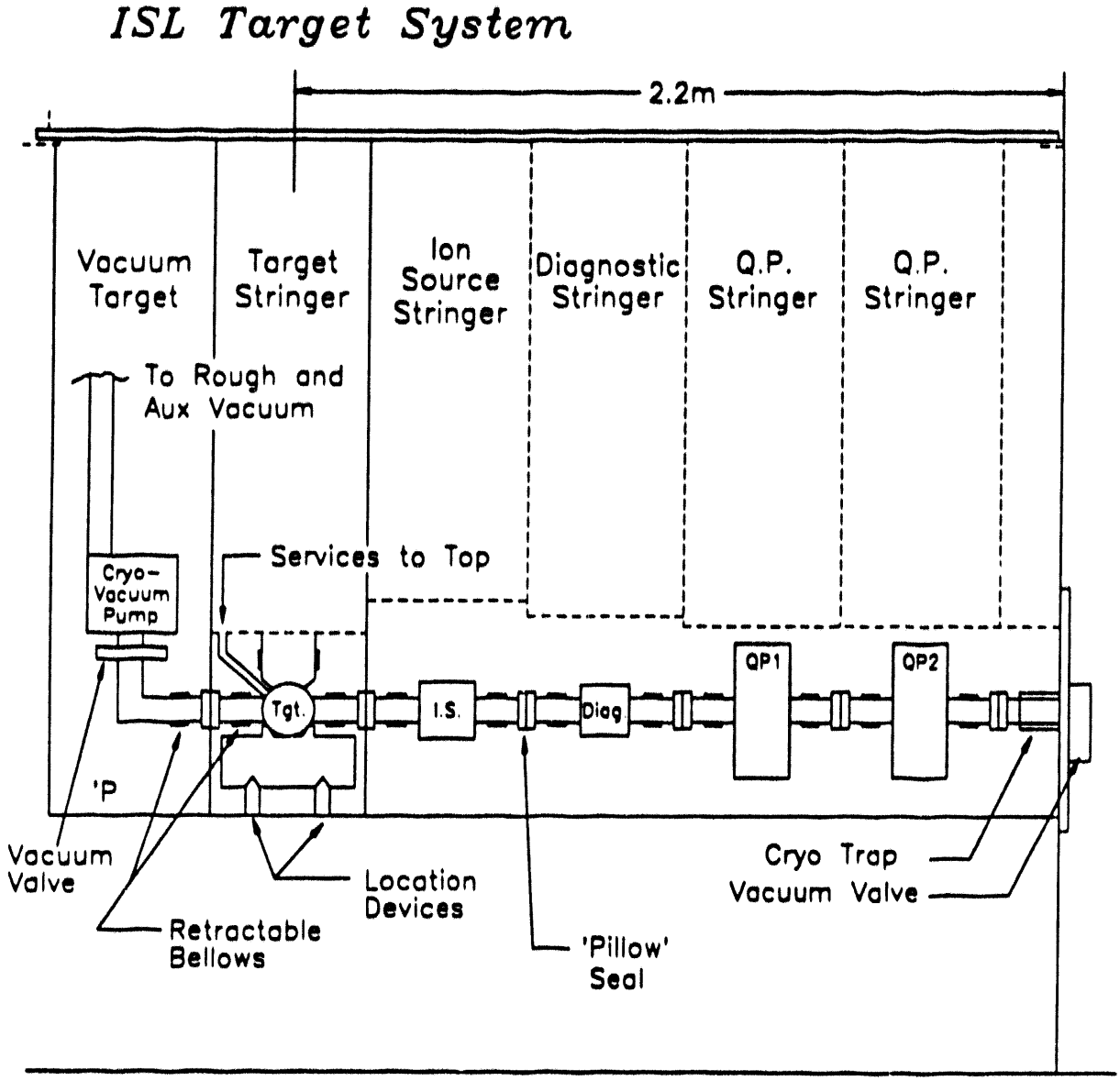

Fig. 10 An expanded longitudinal section along the secondary beam channel shows the primary and secondary vacuum systems and generic components with the services and access from above. All components near the beamline would be mounted below shield columns that would be extracted with their captive components.

Section II
Report from Discussion Group

Section II
Report from Discussion Group on Targets, Ion Sources, and Mass Separators for ISL

J. M. D'Auria

General Objective/Purpose of the Session

The present conceptual plan for an ISL facility is the so-called benchmark facility (BMF) described in the ISL white paper. This conceptual plan is a first version of a high-intensity, accelerated-radioactive-beam facility that meets the desired specifications of an ISL. This approach is based upon a thick-target ISOL system combined with a post-accelerator. The purpose of this section of the workshop was to provide a thorough review of the technical aspects of the front end of this proposed facility by experts and interested observers. The specific goals of this session were:

- To receive advice from experts and interested observers on technical aspects of the front end of the ISL (BMF).
- To discuss identified and unidentified problem areas and questions, indicating their importance and priority, and proposing paths to their solution.
- To indicate areas requiring further research and development studies.
- To develop lines of communication for providing assistance for the ORNL RIB project.

The discussion included, but was not limited to, problems related to target systems (including realistic production yields with protons and heavy ions); ion sources; extraction systems; ion-beam elements (including the mass-separator systems); isobaric separators; radiation effects on materials; robotic and remote-handling systems; shielding requirements; vacuum and pumping requirements; space, manpower, and cost requirements; and related items. High-priority research and development projects were identified for further study.

An extensive list of key questions related to specific technical problems was circulated prior to the workshop and served as an initial focus of discussion.

Invited Papers

Participants in the workshop included scientists and engineers who have expertise in a variety of specific areas of importance to the final ISL project. But these scientists and

engineers also need to be aware of concepts and to deal with problems outside the areas in which they are expert. For this reason, a series of invited talks was scheduled to bring all participants up to about the same level of expertise in key areas of the front end.

In the question-and-answer period following Ravn's talk and in subsequent discussions, Ravn made the following points:

- ISOLDE's success is due to collaboration among laboratories, and the ISL would benefit from similar collaborations.
- Regular meetings and open discussions among experts should be held.
- ISL scientists do not need to "reinvent the wheel" but rather should use available technology.
- ISL's expected performance specifications should be realistic.

Introduction

The series of questions related to the design and operation of an ISL facility that was circulated prior to the workshop was used as the starting point for discussion. Some of these questions were dealt with in the invited talks; for others, individuals were asked to provide short discussion papers. The work sessions consisted of short presentations on pertinent topics, followed by discussion. Some of the presenters followed up by submitting written reports, which are the contributed papers that follow this working group report. Some of the presentations, however, are not available in written form. Key illustrations from those presentations and summaries of all the discussions are presented below. A summary of the activities of this working group is presented at the end along with recommendations.

Production of Radioisotopes

Comments

Nuclear-physics research is currently experiencing a rapidly growing, worldwide interest in the use of radioactive-ion beams (RIBs). The challenges and technical complexities inherent in this research make close cooperation necessary among the various groups interested in producing and accelerating radioactive-ion beams.

The success of ISOLDE is based in large measure on the collaborations among participating groups; experimenters get deeply involved in design and operation issues. Groups at CERN, ORNL, GANIL, Louvain-la-Neuve, GSI, and RAL keep in close

contact and meet regularly to discuss problems. At these meetings, the researchers often propose solutions to problems associated with the production and acceleration of high-intensity, highly radioactive ion beams.

In North America, TRIUMF, LAMPF, ORNL, and other labs should meet often to solidify ideas about the ISL. Such meetings would provide a basis for further cooperation.

CERN has accumulated more than 20 years of experience in target/ion-source technology. This resource should be exploited fully. Repetition is not needed if similar developments or studies have already been brought to fruition at another institution.

The background material in the literature should also be read thoroughly. What has been done previously should be exploited, as should all available talent. Cooperation in North American projects is essential because of the small number of researchers involved in the two ongoing projects.

NUPECC is a European organization with members from several centers. The committee meets periodically to discuss progress on projects and proposals. The strategy being followed by NUPECC is to join European nuclear physicists around central facilities (RIBs, electron accelerators, etc.). It compares, evaluates, and makes recommendations based on proposals submitted by the European scientific community.

The NUPECC meetings and deliberations during the past year have been very productive. Newcomers are being involved, and the NUPECC structures offers an excellent model for the ISL community. That community must wrestle with the fact that one accelerator cannot provide particles to investigate the whole periodic table. The development of facilities to investigate potential isotopes must be evolutionary. Techniques that are already available must be built upon. As a result, we may want to redefine what beams are desired first and how to make use of existing experimental facilities. Techniques that work nicely now for specific elements should be pursued first, leaving other beams for future development.

Once the beam capability is set, the target and ion source must be selected. Here, NUPECC has developed a list of priorities to guide the researcher. NUPECC recommends choosing combinations that have been demonstrated experimentally. Its list of priorities uses intensities from the ISOLDE handbook, but it only goes up through ^{144}Xe. This list was derived from the desires and interests of the ISOLDE customers; the ISL community would very likely produce a different list of priorities for experimental investigation.

To date, more than 600 beams of ions of the elements shown in boldface type on the periodic table (see Figure 3 in Ravn's invited paper) have been created at ISOLDE. The elements that can be released are Group IA, Group IIA, noble gases, halogens, Mn, Hf, Pd, Cu, Ag, Au, Zn, Cd, Hg, Ga, Sn, Pb, As, Sb, Bi, Se, Ta, Po, and certain members of the lanthanide series.

In thick targets, the production ratio from the target may reach 10^{-2} of the primary beam. Special techniques can be used to increase the release from targets, such as the use of CO or CO_2 to enhance the release of Se by forming COSe compounds.

The half-lives of quickly decaying isotopes like ^{11}Li (8 ms) dictate the type and geometry of the target. ISOLDE's yield of this isotope is 3000 [atoms per second per μA of incident proton beam], and it is believed that, at best, only 1/1000 of the atom yield is obtained.

No target or ion-source system is universal; the system must be optimized for each element under consideration. The physical lifetime of an ion source and target assembly at ISOLDE is about one week.

A picture of an ISOLDE-type target/ion source was shown by Ravn. He then showed a list of elements provided by ISOLDE (see Table 2 in his paper). The list is very limited and includes beams observed experimentally at CERN. These beams range from a yield of 24/s (^{20}Na) to one of about 10^{10}/s (^{121}Cs). The list included only about 30 beams. In addition, ^{7}Be and certain lanthanides can be produced. Also, very high beam intensities of ^{122}Cs (10^{12}/s) have been produced, but no experimenters have requested this beam.

The question of whether mass-production distribution is nearly independent of production means was discussed. If based on cross-sections alone, that assertion would be right; but other factors come into play, such as target thickness and release. The production of Rb by various projectiles was discussed (see Figure 24 of Ravn paper). While there are advantages and disadvantages associated with both protons and heavy ions as projectiles, there is not a clear case for any projectile being better than protons, except for the use of heavy ions to produce very proton-rich species.

The possibilities of using neutron guides to deliver 10^{11} neutrons per second to the target or of using spallation reactions as sources of fast neutrons were mentioned. Problems arise from immersing a target/ion source in a large (more than 10^{12} n/cm^2-s) neutron flux, however; for example, insulators fry.

Radioisotope Production in Thick Targets with Heavy Ions

P. Bricault spoke about the use of heavy ions for the production of RNB. He stressed that no target or primary ion beam can be used universally. Two approaches can be used to produce radioactive-ion beams with primary heavy-ion beams: projectile fragmentation and the ISOL technique. Both can be used with high-energy, heavy-ion beams.

Projectile fragmentation is a good production mechanism. It involves the use of high-energy, heavy-ion projectiles incident on a thin target. The fragment of interest has a momentum close to that of the projectile and, therefore, has a low angular spread. The

beams of interest can then be selected for RIB usage. A figure showed the projectile-fragmentation scheme with a heavy-ion primary beam going through a thin target. The projectile is fragmented and used as the RIB. The technique can produce a wide variety of nuclei. The angular distributions of the fragments are sharply peaked for mass fragments.

The beam can also be stopped in a thick target in an ISOL for thermal release and subsequent use, similar to ISOLDE. A test of this ISOL method at GANIL involves the use of light heavy ions (^{12}C) incident on thick, high-atomic-number targets. The reaction products are thermally released from the high-Z target material (usually at high temperatures), ionized in an ion source (e.g., an ECR, as used in GANIL), and extracted for acceleration to final energies.

With the heavy-ion technique, range is a problem, but the scale factor in the cross-section is related to the total cross-section. Very far from stability, heavy ions make produce larger yields of radioactive isotopes for reacceleration; ^{12}C at 84 MeV/amu on uranium targets produces yields of sodium that are higher than those from 600-MeV protons by factors of 5 to more than 50. Similarly, ^{12}C at 84 MeV/amu on uranium targets produces yields of potassium that can be higher than those from 600-MeV protons by a factor of 2 or 3. Other advantages of high-energy heavy ions include:

- The distribution of fragments becomes energy independent above a certain threshold of the projectile's total kinetic energy.
- The scale factor in the cross-section is close to the total reaction cross-section.
- The production of species very far from stability is enhanced through the use of heavy ions.
- The best projectile-target-fragment combination can be chosen to optimize the production rate of the desired species. This technique can be used to get around basic problems. (For example, a ^{48}Ca beam is easier to make than a ^{48}Ca target.)

The useful target thickness depends on the half-life of the release of the product.

One problem of heavy ions is the power density in the target. The deposited power is about 1 kW/cm^3. The target could be damaged if the beam is made too small (less than a few millimeters). The GANIL targets are heated with a deposited power of only 0.6 kW/cm^3. At Louvain-la-Neuve, targets are routinely run with a beam power of 6 kW, although these targets are water cooled directly. This design is feasible given that the beam energy is only 30 MeV.

To overcome this problem, thin-foil targets can be used, or the target can be cooled. At GANIL, 1-mm-thick MgO target disks are mounted in a cylindrical holder in which they are separated by about 1 mm and edge-cooled.

Ravn made the comment that for light-projectile-fragment products, heavy ions may be 2 or 3 times better than protons as a primary beam.

The reaction between an MgO target and a ^{28}Ne beam produces both projectile fragments (largely Ne isotopes of mass 18, 19, 21, and 22) and target fragments. For projectile fragments, target thickness leads to a 10% energy loss. With the ^{20}Ne energy as 20 MeV/u, the yield ranges from 2.8×10^7 to 8×10^9 with an efficiency of about 0.6%.

T. Antaya asked if radiation problems for heavy ions are less than those from protons. The group felt that heavy ions produced less beam radiation but that target-handling difficulties are the same.

Producing exotic beams with the projectile-fragmentation-recoil method has a number of advantages:

- Access to nuclei with very short half-lives
- High collection level
- Relatively good selectivity
- Easy target fabrication

and a number of disadvantages:

- Very thin target because of $\Delta p/p$
- Very poor emittance
- Very high momentum spread
- Small energy range
- Deceleration and cooling is difficult without intensity loss
- Moderate beam purity
- Very high energy needed (500 MeV per nucleon for uranium)

Producing exotic beams with the online-isotopic-separation method also has advantages:

- Thick targets
- High beam purity
- Low energy spread
- Excellent beam quality
- Accumulated experience in target design

and disadvantages:

- Delay from diffusion and desorption
- A post-accelerator is necessary
- Elaborate target handling needed

Target Heating from Beam Power

Will Talbert presented results of using the LAHET computer code to study the energy deposited in different thick targets by protons of different energies. See Figure 1. Complete details have been published in NIM (B70 (1992) 175).

A view graph of deposition features indicated:

1. The LAHET code developed at ORNL is used to calculate total energy deposition. These results agree well with an earlier CERN theoretical study, with the exception of cases with tantalum or binary targets.
2. Bulk-density dependence is most important for predicting power deposition. Predictions can be extended to targets larger than 20 cm and proton energies exceeding 100 MeV.
3. Power deposition increases monotonically with proton energy.
4. The energy-deposition profile differs from the profiles found by Eaton et al. LAHET distributions show that the beam becomes depleted in the central region and blooms because of multiple scattering as it progresses down the length of the target. At the emergent end of the target, the energy-deposition density profile becomes relatively uniform, as expected.

See Figure 2 and Table 1.

Talbert described simulating cylindrical-geometry solid targets in a solid conductor. Annular regions between an outer solid conductor and a water-cooled jacket are used to exhaust He through. This technique allows control of the target's temperature. Two configurations were shown, one in axial view (the water-cooled jacket) and the other in lateral view (the sodium heat pipe). See Figures 3 and 4.

These studies led to the following conclusions. Some targets can be cooled by radiation losses at beam intensities of 10 μA (e.g., Ir, Nb, Ta, Ti, and Zr) to 100 μA (e.g., Ir). Enhanced radiation cooling can be used to operate targets above these beam intensities. Conductively cooled targets can be designed that permit 40 kW of energy deposition. The following designs are under study:

1. A simple conductor with a helium-filled annulus
2. A sodium heat pipe with an outer, helium-gas-filled chamber to remove the heat

A number of specific details must be worked out for each target that would be used at a high-intensity facility like ISL.

High-Intensity Targets

Calculations similar to those by Talbert at LANL are being performed by M. Nitschke at LBL on a system consisting of radiatively cooled cylindrical targets with fins.

Early deposition was modeled with LAHET, the 3D code developed at ORNL, with a beam that was assumed to be Gaussian. Most of the energy was distributed at the beam entrance of the target. The beam was "wobbled" to give more-uniform distribution. The longitudinal distribution profile is controlled by running fins along the length of the cylinder so that the target temperature is more uniformly distributed. Experiments are being planned to simulate heat transfer with electrons from a resistance-heated wire along the axis. See Figures 5-10.

The possibility was raised that perhaps more time and money should be spent at various labs to develop ion sources and targets that can survive the severe environments to which they will be subjected. Certainly, attention should be given to increasing the ionization efficiencies of ISOL sources so that the power deposited in the target can be reduced.

Ian Thorson indicated that at TRIUMF a lead target has been in use for a long time, and experimental information is available for a 50-kW beam on a lead beamstop. LAHET could be used to calculate its "temperature profile," and the results could be compared with the experimental particulars.

Radiation Effects

Given the high-production beam intensities being considered for an ISL facility, radiation effects will obviously be important, both for the materials at the front end of the ISL and in terms of the required shielding around the target. The expected radiation levels are considered both in the invited talk of I. Thorson and also in the brief report submitted by R. Donohue (LBL) below. In addition, this topic was considered by others, and their comments are summarized below.

Radiation Damage to Materials

M. Borden (LANL) provided information based upon experiences at the LAMPF meson facility, which uses a proton beam with intensities of the order of 2 mA (LA-UR-92-1211). He recommends that all units in severe radiation fields be of welded construction. Reliable materials include stainless steel, copper, aluminum (which gives less residual activity), and Inconel.

At LAMPF, beam stops and beam windows are subjected to up to 10^{22} protons/cm^2 with minimal problems. The performance of the LAMPF beam-entry window under irradiation was reviewed. The double-walled flat plate on the beam stop is made of Inconel 718 and has a lifetime of 17,500 h at an average beam intensity of 20 to 30 μA/cm^2 measured at the beam's center. It has been exposed to 1.3×10^{22} protons/cm^2 with minimal problems.

A polycrystalline-graphite rotating target is used at the A-1 and A-2 target stations at LAMPF. The operating parameters for LAMPF targets are summarized in Table 2. The targets at the LANSCE facility at Los Alamos is made of a tungsten alloy. Table 3 shows the performance of LAMPF beam windows under irradiation.

The penetration of the beam into a copper beam stop at LAMPF was detailed along with the beam-intensity distribution. Material damage was also characterized with an illustration from an Argonne report. See Figures 11 and 12.

Other aspects about materials that have to be considered include:

1. Transmutation effects:
   - Swelling by helium bubbles and voids formed in metals by stopped alpha particles
   - Displacement-per-atom effects caused by helium; this effect can cause nickel in iron to be displaced significantly
   - Chemically active elements raising or lowering the surface energies and forming stress fields around voids
2. Changes in alloying-element content (impurities) induced by the radiation, altering phases and properties (e.g., vanadium is changed to chromium, nickel to iron, and aluminum to silicon)
3. Mechanical-property alterations influenced by the collection of trans-mutants at grain boundaries, flaws, crack tips, and precipitates

Classes of materials that should be examined for susceptibility to radiation damage are given as follows:

1. Structural materials
   - Aluminum and alloys
   - Ferritic and martensitic steels (Fe and Fe-Cr-based)
   - Stainless steels and high-alloy Fe-Ni-Cr materials
   - Zirconium and alloys
   - Vanadium and alloys
2. Target materials
   - Lead-bismuth or liquid or solid lead

- High-Z refractories and alloys
- Uranium and alloys
- Thorium and others

3. Barrier and cooling materials
   - Ceramics
   - Coatings and claddings
4. Advanced applications
   - Composites for enhanced radiation performance and NDE [nondestructive examination] (e.g., aluminum-silicon carbide, silicon carbide-silicon carbide, and carbon-carbon composites)

Targets and containers that have survived about 10^{21} protons include beam stops, LANSCE targets, and ion-production targets. Stainless steel, Cu, and Inconel materials have been reliable. Aluminum gives less residual activity. A beam stop has survived 1×10^{23} protons/cm^2 with no observable problems.

Material performances under different temperature regimes were characterized as follows:

Temperature Regimes (Tm is the melting temperature)	*Effects*
T < 0.3Tm	No swelling or very low swelling Embrittlement (loss of ductility) Hardening (affecting strength) Thermal creep not important Transient irradiation creep possible Hydrogen embrittlement possible Helium effects possibly important Irradiation-induced precipitation Segregation minimal Corrosion a minor concern Fatigue and crack growth possible
0.3Tm < T < 0.55Tm	Swelling Thermal creep and irradiation creep Hardening and embrittlement (loss of ductility) Fewer and less severe hydrogen effects than at low temperatures Hydrogen attack of material possible

	Helium effects important Irradiation-induced effects and segregation Corrosion Fatigue and crack growth
O.55Tm < T	Less swelling, but rate effects and helium effects may occur Hardening less of a concern Embrittlement by radiation-induced segregation and helium Low mechanical strength Thermal creep High corrosion rates

H. Ravn stated that the typical ISOLDE target withstands 500 mA-h before the elastomeric O-rings break down, but some hardier components do not break down until 1000 mA-h. Sintering, which starts at about the same exposure as elastomer breakdown, also causes target loss. The targets lose their high release at about 500 mA-h for some unknown reason. Evaporation of minor constituents or powder sintering may be the cause. The target must then be discarded. Aluminum oxide may be a better insulator than MACOR.

The general conclusion arrived at by the participants is that a great deal of information is available on this topic, and it is not an insurmountable problem.

Shielding Requirements

Radiation problems may be experienced at the ISL. Under the assumed operating conditions of the ISL, two types of neutron will be emitted: isotropic-evaporation neutrons and intranuclear-cascade neutrons.

Type of Neutron	*Mean Free Path* (g/cm^2)	*Tenth Value Layer* (Thickness of Concrete)
Evaporation	30	30 cm
Cascade	110	1 m

Evaporation neutrons can be ignored in designing bulk shielding; but because they are much more numerous than cascade neutrons, they may contribute significantly to radiation

damage close to the target cell. To achieve occupational radiation levels, about 10 m of concrete shielding will have to be provided in the forward direction of the beam, and 8 to 9 m laterally [around the target cell].

Examples of the residual activity produced are

- Target - kCi activity tens of rads per hour at 1 m
- Target cell after operation, without equipment - a few to tens of rads per hour.

Integrated doses:

Location	*Dose (rads/y)*	*Operation (h/y)*
Target Cell	~109	8760
Instrument Cell	106	see J. Domingo et al., ISOLDE/SIN Proposal

Remote Handling

A key area of concern is how the fragile target and ion-source systems can be handled given the high levels of radioactivity involved. The possibility of contamination and the question of personnel safety are of utmost importance. These topics have been touched on to some extent in the invited talk by I. Thorson. In the work sessions, short reports were given by H. L. Ravn on the ISOLDE robot system, E. Steiner on vertical-access techniques used at the meson facility in Switzerland (PSI), J. N. Herndon (ORNL) on the latest robotics systems used in high radiation fields, and J. Vincent (TRIUMF) on a planned upgrade to the TISOL facility that will incorporate new handling systems. As pointed out by several speakers, the major choice is between (1) a direct hardware, crane-based, vertical- or horizontal-access system or (2) a remote, robotic-manipulation system. The virtues and vices of these approaches were part of the subsequent discussion.

The TISOL Upgrade

TRIUMF is considering upgrading its TISOL facility to accommodate beam intensities >10 μA. Vertical access to components is the preferred approach for target handling. As part of the TISOL upgrade, a hexagonal, iron, 1.5-m shielding block was incorporated in the design. The shielding calculations were done with a code from Moscow.

Hands-on maintenance for the present TISOL produces an exposure of 10 mSv/hr; as a result, the dose-out time is quite short.

TRIUMF uses thick targets (10 g/cm^2) for meson production at 150 μA and 500 MeV. The techniques used there should and will be evaluated for use at TISOL (and ISL). At

TISOL, present operations call for manhandling, and personnel doses must be kept to <50 mR per day. For the planned upgrade to TISOL, the design specifications call for a target change in a period of a few hours, regardless of how high the radiation fields are, and an ion-source change in about one day. These tasks will be accomplished with remote-handling systems and within acceptable doses to personnel. Some strategies that should be considered are:

- Incorporating decontamination and disposal in situ
- Operating on an ion source on-deck

At TRIUMF, target handling is accomplished by vertical access, and all work on the targets and ion sources is performed in a working area that is separate from the target cell. The 1985 proposal for TISOL also sought to use this technique. The design philosophy is to replace the target/ion source as a unit except for the ECR. This strategy requires a redesign of all of the components.

A question arose about the use of robotics. Vincent has one, but does not like it very much; they would like to have force feedback so that they would have the capability to respond to some variant movements.

In high fields (on the order of kilocuries), failure modes must be taken into consideration.

Ravn voiced an opinion that shielding should not 'hug' the target.

In an ECR source, the SmCo magnets should last for years, but weak points do exist, such as insulators and quartz tubing.

When modules are removed, all systems should be valved off to avoid gases' escaping.

With vertical access, a hot cell can be installed above the shielding, and all operations can be done as part of a confinement enclosure by going through the hot cell.

System Handling at the PSI Facility

At PSI, horizontal access was used to replace targets. These targets are not as complicated as ISOL ion sources, but the latter could be treated as just another insert in the beam area. Radiological protection is provided with a 4-m-thick iron shield. Covering the iron with marble (inside) was suggested to protect people from the radiation resulting from iron activation.

With the upgrading of PSI to 1 mA (from 200 to 300 μA), the beam line must be redesigned. The spallation target was changed to lead instead of lead/bismuth because the latter produced a lot of alpha activities. Self-aligning vertical inserts are used; when they are removed, they are transferred to a remote handling cell with an overhead crane. No

manipulators are used; all servicing is done in a hot cell. Air control is used to control the dispersal of loose activities; to do this, shielding-block joints must be made nearly airtight.

The system has several crucial elements, including vacuum seals (sliding pillow seals; these were not used for SINQ out of concern for target leakage). A vacuum of 10^{-5} μtorr has been achieved with this system. Inserts are of a common design; all kinds of complicated targets, collimators, etc. can be hung within inserts. Such inserts can be lifted into a cask with a crane and moved to a hot cell. Old components have been disposed of by incorporating all but the aluminum components into a concrete (shielding) block.

To avoid alpha emitters in ISL, materials of $Z > 83$ should be avoided. Uranium targets launch the operation into another level of handling.

Another concern is beam scattering at windows, particularly with a tightly focused beam (e.g., 3 mm), where scattering may be significant. Perhaps a foil would be a good solution. (Further discussion and details of the PSI system can be found in the Steiner paper.)

Robotics and Intelligent Systems

J. Herndon (ORNL) described the RISP (Robotics and Intelligent Systems Program) used at Oak Ridge and elsewhere to handle components in the high radiation fields at nuclear reactors, at deposits of waste products from reactors, and in reprocessing plants. The goal is to reduce human risk, and the systems emphasize mobility, manipulation capability, and good communication with the control system. Two approaches are used: transfer the hot object to a hot cell, where the work is performed, and/or bring the dexterous equipment to the job site.

The philosophy of the second approach is to open up the system and to work on it with remote manipulators. All such procedures should first be tried out on a mock-up of the remotely maintained system because you do not want any surprises when the operation counts.

A very different approach is used at the Hanford Purex Canyon, where processing equipment with levels 104 R/h is serviced. Here, a crane is used to remove equipment to another location. Equipment with remote connectors creates an absolute maze, but it is serviceable from the crane access.

Experience shows that:

1. System flexibility is essential.
2. Maintenance tends not to be repetitive, structured, or planned.
3. Complex tasks can be performed.
4. Work-task efficiency depends on:

- Manipulation dexterity.
- Remote-sensing fidelity.
- Human-machine interface.
- Operator skill levels.

A fully remote design is essential to work-task efficiency. "Task provisions" need to be defined, and mobile remote operations require more robotics.

Such units can also be quite expensive, depending upon the tasks required. Clearly defining the task or tasks that will be performed and maximizing efficiency are very important. Thinking about remote-handling concepts and incorporating them at the beginning of the design of the facility are also important. A further discussion on guidelines for remotely maintained equipment can be found in ORNL/TM-10864. Additional comments are indicated in Figures 13, 14, and 15.

Participants commented that it is important to be able to recover from failures. The planning of robotic or remote systems needs to take into consideration what types of problems might arise and what capabilities need to be built into the system to allow the problems to be rectified without incurring human radiological exposure. Also, there is a trade-off between removing equipment to a hot cell for handling versus bringing manipulators to the job site, and that is the enormous quantities of concrete that must be handled.

The cost involved in a large overhead system is $2 to 3 million. Large hot cells may be cheaper. Designing the beam-line equipment for remote handling also involves added costs that must not be forgotten. The susceptibility to radiation damage of the materials and electronics used in the manipulators has to be considered. Color TV cameras can withstand 10^5 to 10^6 R/h, but black and white TV that will survive a lifetime of 10^9 Rads can often suffice for this type of operation.

ISL should probably use a combination of approaches (i.e., vertical access and robotics), but in any event, it should use a modular approach to allow for the easy replacement of components. Whatever approach is used, the demands of that approach must be taken into account in the planning, design, and layout of the facility and its equipment from the beginning.

Robotics Systems at ISOLDE

H. L. Ravn (CERN) briefly described the ISOLDE industrial-robot system used to perform simple tasks and, in particular, for disposal, changing, storing, and simple repair of the target system. The ISOLDE approach uses disposable targets and is only good up to

about 10 μA. An industrial robot of the type used for auto spray-painting removes the targets for disposal, storage, or (occasionally) repair in a hot cell. The robot has six degrees of freedom and operates on 25 m of track. Next year, it will be replaced at a cost of 200,000 SFr with one of a simpler design (like an automatic drill press) that will be controlled with a simpler set of instructions.

Manhandling is also used for simple, short jobs. This approach is probably good only for systems that use beams of less than 10 μA. The separator front end, for example, requires hands-on maintenance; it can be disconnected in 10 min. The entire front end is enclosed in an aluminum cage that can be easily decontaminated by hosing it down. Loose activity is avoided by valving off the target/ion-source-assembly separator. In addition, the front end (with the vacuum system) can be replaced as a module (for about 200,000 SFr).

For higher currents, a hot cell would be desirable for the target cell (like ISIS), but the target/ion-source assembly must be able to be removed. ISOLDE makes 45 assemblies each year. The elastomer seals on the valves are a weak point, but the ultimate lifetime of the target/ion source is not much longer because of the problems in materials used for the target or ion source.

When a target run stops, the residual activity is about 2 R/h and remains about 1.5 R/h when the target/ion source is removed. The activity could come from a combination of deposited radioactive material and activation.

Beyond 10 μA, the main insulator and vacuum seals are causes of worry.

The design of the facility should accommodate completely remote removal of the targets. Strategies and factors to take into consideration in planning the facility and its design include:

- Avoiding large amounts of metal.
- Making a shell (reduce the air volume).
- Planning carefully for waste disposal (treacherous waters, especially mixed waste).

In regard to the planning that must be done for the disposal of radiological waste and mixed waste, it was noted that the ISIS facility at the Rutherford Appleton Laboratory produces 1 g of ^{239}Pu in the beam stop each year at an operating level of 800 MeV and 100 mA.

Discussion

Participants commented that:

- Vertical access to and handling of highly active targets is feasible, including the precise alignment of the target and associated equipment.

- It is important that the handling approach be considered in designs and plans from the beginning.

Other Topics

Ion Sources for ISOL Devices

Four types of ion sources can be considered for the ISOL and post-acceleration: low-pressure, gaseous-discharge ion sources [NIM, B70 (1992) 186; NIM, A236 (1985)]; surface-thermoionization sources [NIM, A232 (1990) 203]; ECR ion sources [NIM, B58 (1991) 252]; and laser ion sources.

For this workshop, P. Van Duppen concentrated on the ECR ion source. A complete discussion can be found among the contributed papers. A plot of efficiency against pressure in the extraction region is presented here.

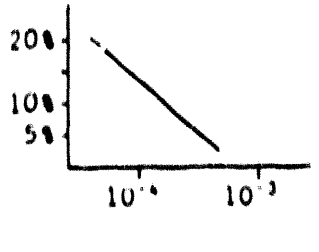

An ECR source is quite efficient for noble gases: up to 50%. But gas-pressure dependence is worse for light gases.

Questions remain about such sources:

1. What is the efficiency for higher charge states (>1) and for different elements?
2. Can the gas load from the heated targets be handled, given the demonstrated pressure-dependence?
3. Can metals be efficiently ionized, and what is the sticking time associated with the transfer from the target to the ionizer?

Delay times, sticking times, and other effects on efficiency need to be measured.

Comments

GANIL has a small ECR for high charge states; it has a 70-mm cross-section and a 400-mm length. The yield of neon beams from the GANIL ECR system is affected by trace oxygen contamination. Nevertheless, a 7-mA beam of Ne^{4+} has been extracted from the ECR IV. If one puts in an argon leak, Ar^{7+} and Ar^{8+} are seen with the beam on; but the

argon disappears, and the gas load from the target changes when there is no beam. This result is seen on both small-ECR and large-ECR IV types of sources.

The efficiency of a small ECR source is a factor of 10 lower than that of the larger ECR IV system. The field configuration is not optimum in the smaller source. This system uses a 10-GHz radiofrequency and has a 5-mm extraction opening. The release time of Kr^{+6} is about 1 s. At present, this configuration is only good for noble gases, but we are studying what happens when other species hit the walls. Also, studies are in progress on both target-desorption effects and transfer-line-desorption effects to find out what happens when reactive species hit the walls of the transfer lines and the ion source.

T. Antaya commented that an ECR ion source can be used to extract ion beams of metals with the use of a support gas of O_2 at about 10^{-7} torr to extract metallic oxides into the source.

Laser Ion Sources

Background-free collinear laser spectroscopy is being developed to study refractory elements, to study short-lived isotopes near the drip lines, to produce cleaner beams, and to offer a wider choice of targets. At this point, Fairbanks concentrated on laser-resonant ion sources. The lasers used are:

	Frequency (Hz)	*Power (mJ)*
Nd: YAG (IR, green)	10 - 30	300 - 1000
Excimer (UV)	10 - 100	~100
Copper-vapor (green and yellow)	6000	5

Three conceptual designs of ion sources were reviewed: the ISOLDE laser ion source, the Leuven laser ion source, and the laser ablation and resonance ionization laser ion source (LARIS), which involves a gas jet. The requirements for a LARIS are:

	Expected	*Demonstrated*
Helium-jet transport efficiency	>50%	60-90%
Time required	<10 s	<1 s
Laser ablation efficiency	>50%	90%
Time required	<10 s	
Resonance ionization efficiency	1-10%	15%

Time required	10 ns	10 ns
Ion-source-system efficiency	1-10%	-
Time required	<20 s	-

A more complete report can be found in the contributed papers.

Thin Target Production System

Considerations about integrated target-ion sources are that:

1. Reliable operation of target-ion sources has never been demonstrated at 100 μA.
2. Certain elements are not available from an integrated target-ion source.
3. The release times of certain elements from the target are known to be long.
4. Optimization of the ion source is complicated by the high-radiation environment.

A helium-jet-fed ion source has a short, predictable delay time of the reaction products that is largely independent of the element; is remotely located from the high-radiation environment and can be more easily maintained, reused, and optimized. And, it is decoupled from the target, placing a simpler system in the beam. On the other hand, a helium-jet-fed ion source has a thin target limited to tens of milligrams in thickness. With a 1-mA proton beam for helium-jet-system production, yields are about a thousand times larger for an integrated target-ion source operating at 100 μA. A comparison of transport efficiencies favors the helium jet for short half-lives.

A two-year study of the helium-jet concept is currently under way at LAMPF and is concentrating on direct detection during the first year and on the ion source and mass separator during the second.

Pioneering experiments at LAMPF have demonstrated that the helium jet works at lower beam currents and achieves a 60% efficiency for fission and spallation products. Questions still remain, however, about whether the system can work at a full 1-mA current and about the long-term reliability of the system.

The goals for the next two years are to show that a helium jet can operate efficiently and reliably in a 1-mA proton beam, to measure yields of specific nuclei, to demonstrate offline that a helium jet can be coupled to an ion source and achieve good efficiency, to emphasize ionization of nonvolatile elements, to couple an online helium jet to an ion source and mass separator, and to demonstrate coupled performance with short-lived radioisotopes.

A number of observations were offered by the participants:

- Measured flow rates are short.

- Ion-source coupling is limited by inner surfaces.
- Ion-source coupling was characterized as being 1 to 10% routine; mocked-up flow studies have been performed.
- Helium-jet efficiencies were reputed to be 1/10 those of other sources for elements of medium volatility, although this assertion was debated.
- Coupling is a real issue because backstreaming of the plasma must be avoided.
- A medium-current separator and a slit ion source are needed.
- Getting the best pressure possible in the optics system is crucial.
- Clusters are needed for efficient operation of the transport system.

Complete details of the project are given in the contributed paper by J. Wouters.

Mass Separators

A brief report on a new separator system was given by H. Wollnik. The essential elements are:

1. Ion-source matching system
2. "Modest" mass separator
3. High-resolution "isobar" separator with a section at high potential
4. System velocity matched to post-accelerator

Either a linear accelerator or a small cyclotron could be considered for acceleration after separation.

During the following discussions, the proposal was made that the front end of the ISOL device should be operated at ground and the back end at high potential (e.g., 300 kV).

Future Developments

Single-Ion Production

The future developments in ion production were reviewed by Ravn, and he started with the laser ion source. It directs a laser into a small tube, heating the contents to 2000°C. The ions produced are stored along the tube axis, and they drift because of a 0.6-V gradient.

Pulsed ion beams 20 μs wide are produced, the length of the pulse reflecting the drift time through the tube. These devices produce a limited field because of the small voltage. The use of a heated ceramic tube would make a larger drift field possible but would add to

the energy spread. A pulsed electrode in front of the extractor, though, may be able to compensate for that energy spread.

Another problem with this technique is that there is not a suitable laser light for all elements. At this point, only about a 20% efficiency can be attained for all rare and alkaline earths, alkalis, silver, tin, and cadmium.

Continuous-wave lasers have not yet been developed, and an R&D program to make them reach an 80% efficiency may not be worthwhile. The best strategy might be to stick with pulsed lasers.

The Kirchner approach uses a cooled-spot ion source. A variant is to use laser desorption (ablation) instead of controlled heating, as is done at GSI.

The general subject of pulsed ion sources was discussed, and the possibility of new parameters was raised. It is not inconceivable that lasers could be used to bunch beams, and these beams could be matched to the accelerator input frequency or sent to storage rings. Other possibilities might also exist.

Multiple-Ion Production

ECRs offer an excellent possibility for producing ions, including multiply charged ions. More studies are needed to measure their performances in terms of η_{ion} as a function of gas load and of sticking time (τ). Online systems exist at GANIL, TRIUMF, and Louvain, and these should be used to make such measurements.

Direct injection into the high-plasma region is being studied at Grenoble. This direct injection is accompanied by pumping at the sides of the plasma zone.

Bricault reported using pulsed rf power on an ECR source to increase the current by a factor of 3 with a rather faithful following of the pulse in the output power. A width of about 1 ms resulted. Between pulses, ions may reside in the source. Nitschke asked if it might be possible to store ions in the ion source and then pulse them, and Alton suggested using a cold spot and sputtering them off or ablating them with a laser.

Electromagnetic Traps for an ISL

Electromagnetic traps were suggested not for experiments but to manipulate ions prior to experiments. The Penning trap was first devised in 1935; it uses an electromagnetic DC magnetic field. The Paul trap, which was invented in 1956, uses an AC electric field. Thousands of chemists now use the Paul trap for studies of ionized species. Normally, they use it as an analytical tool, trapping and looking at 10^3 to 10^6 ions. Physicists, on the other hand, have fewer than a hundred of these devices for research purposes, and they

typically use them for precise measurements of 1 to 10^3 ions. As an example, a Penning trap can be used to separate ^{84}Rb from ^{84m}Rb.

At CERN/ISOLDE, a cooling Penning trap is followed by a cyclotron-resonance Penning trap (the measurement trap). The cooling is done with helium gas at about 10^{-5} torr. But a Paul trap can be used as a first-catcher and buncher. Traps can eliminate unwanted ions (to 1 in 10^5), eliminate unwanted molecules (as is done by chemists), and ionize high charges (which is done at EBIT in MSI in Stockholm).

Cooling to a minuscule phase space is done at McGill and CERN in a time range of 10 ms to 10 s. A pulsed dump is not required; the captured ions can be leaked. Different ions can be ejected at different times. But to do this, you first need ions in the trap!

The injection and extraction of ions into and out of traps follow the basic cyclotron principles. Tests at CERN show that 0.2% of a DC beam can be collected in a 2.5-cm chemist's trap, and 2% can be bunched. The phase space is proportional to the dimensions of the trap. An 8-cm trap is being constructed to increase the phase space by a factor of 7000 with the aim of capturing all of the ISOLDE beam.

One proviso is that the beam must not exceed the space-charge limit:

Trap size:	2.5 cm	8 cm	25 cm (feasible)
Choke level:	10^6	3×10^7	10^9
Swallow level:	10^4-10^5	3×10^5 to 3×10^6	10^7 to 10^8

Moore felt that traps should be considered useful for production rates greater than 10^6/s and for times of 10 ms to 10 s. Furthermore, they could be used for precise beam manipulation; indeed, they may be very versatile for dealing with high charge states.

Conclusions, Summary, and Recommendations

Key invited international experts presented an in-depth overview of the production of high-intensity radioactive beams with various projectiles; a technical review of magnetic mass separators, particularly for isobaric separation; and detailed estimates of expected radiation fields, residual fields, and required shielding for the highest-intensity proton beams being considered. Intense beams of high-energy protons are still considered the projectile of choice for production purposes, and 100 μA beams are now considered attainable.

A realistic conceptual design of a system was advanced to provide for the handling of production targets and beam-line elements subjected to high radiation and beam power while minimizing the release of contamination. The concept of using mass-separation devices at high tensions (e.g., 300 keV) to compensate for ion-source drifts as well as to

provide high-velocity ions for injection into post-accelerators was proposed for further study.

The general conclusion was that the benchmark facility (BMF) does not have fatal flaws in these areas. That laboratories openly cooperate and discuss issues was seen as imperative, and realistic performance characteristics based upon known technology must continue to be pursued.

The in-depth technical discussions cannot be adequately summarized here, but these conclusions and recommendations on technical issues were reached:

- The concept of ISL as put forward in the BMF can be considered technically feasible although optimization of certain aspects of the conceptual design do require additional study.
- Experimental production yields are needed for both thick-target, heavy-ion production and thin-target, high-energy-proton production to allow for proper comparison with thick-target proton production.
- The operation of a thick-target-ISOL approach should be studied at high proton-beam intensities (e.g., greater than 10 μA).
- Beam-heating and power-dissipation studies for proton-beam intensities approaching 100 μA should be studied, particularly in off-line simulation studies.
- More systematic data are needed for both single- and multiple-ion ionization with an ECR ion source because this capability could reduce the cost of the post-accelerator system.
- Laser ion sources and pulsed sources are potentially very powerful for providing radioisotopic-beam purity; more studies are needed.
- An ISL facility must incorporate a philosophy of remote handling in the early design stages, probably incorporating a combination of robotics and vertical-access, remote-handling.
- Higher extraction energies from the front end might be realized if units of the mass separator operated at high potential, but this novel idea requires demonstration of principle.
- The establishment of interlaboratory working groups on such project areas is strongly recommended; external funding is needed to make these operate.

Acknowledgments

The laborious and vital task performed by the rapporteurs, namely W. Talbert, G. Alton, and, to a limited extent, J. Wouters, is gratefully acknowledged. The assistance of B. Ward in the typing of the summary is noted.

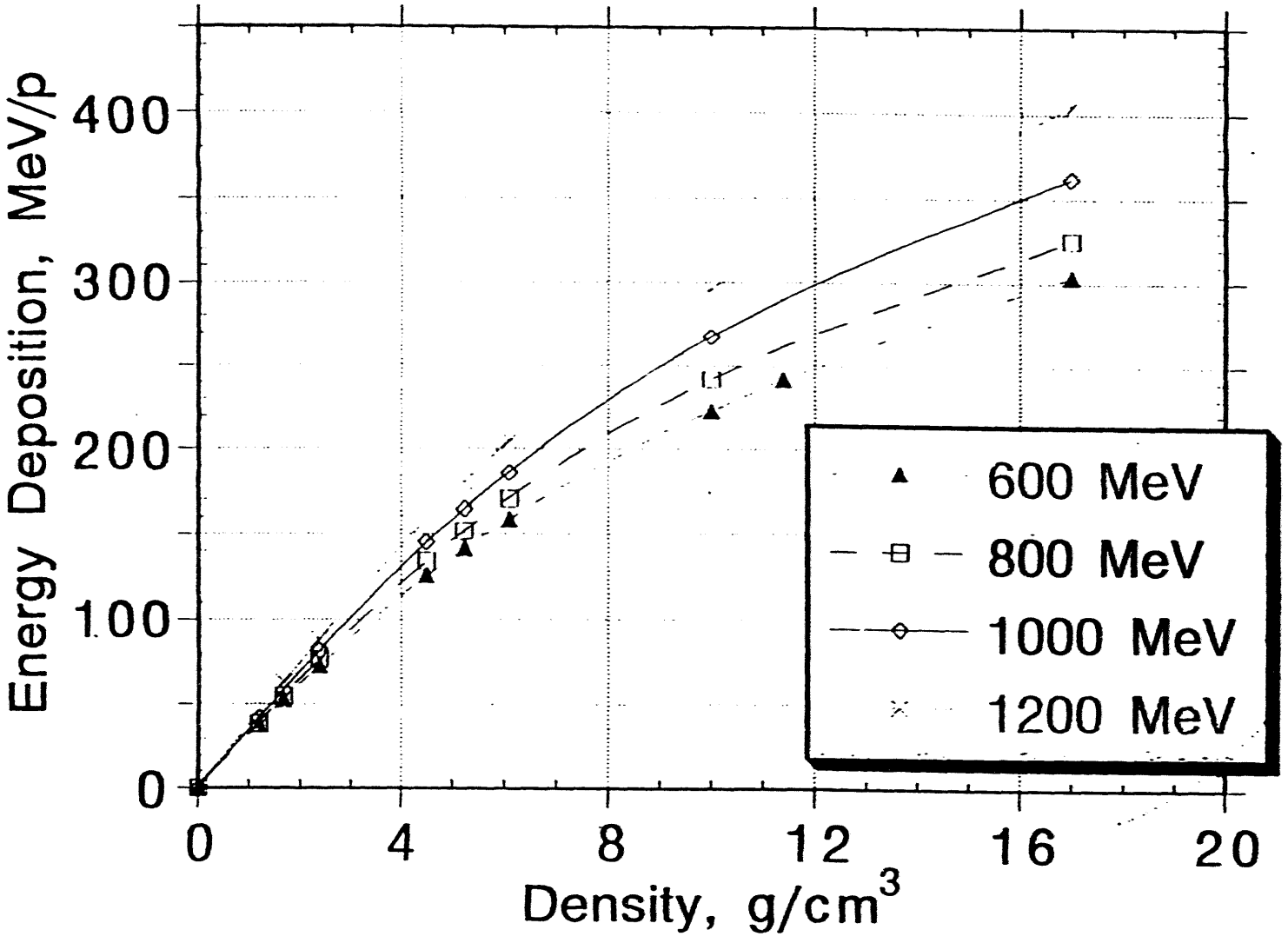

Figure 1. Energy deposition versus bulk density.

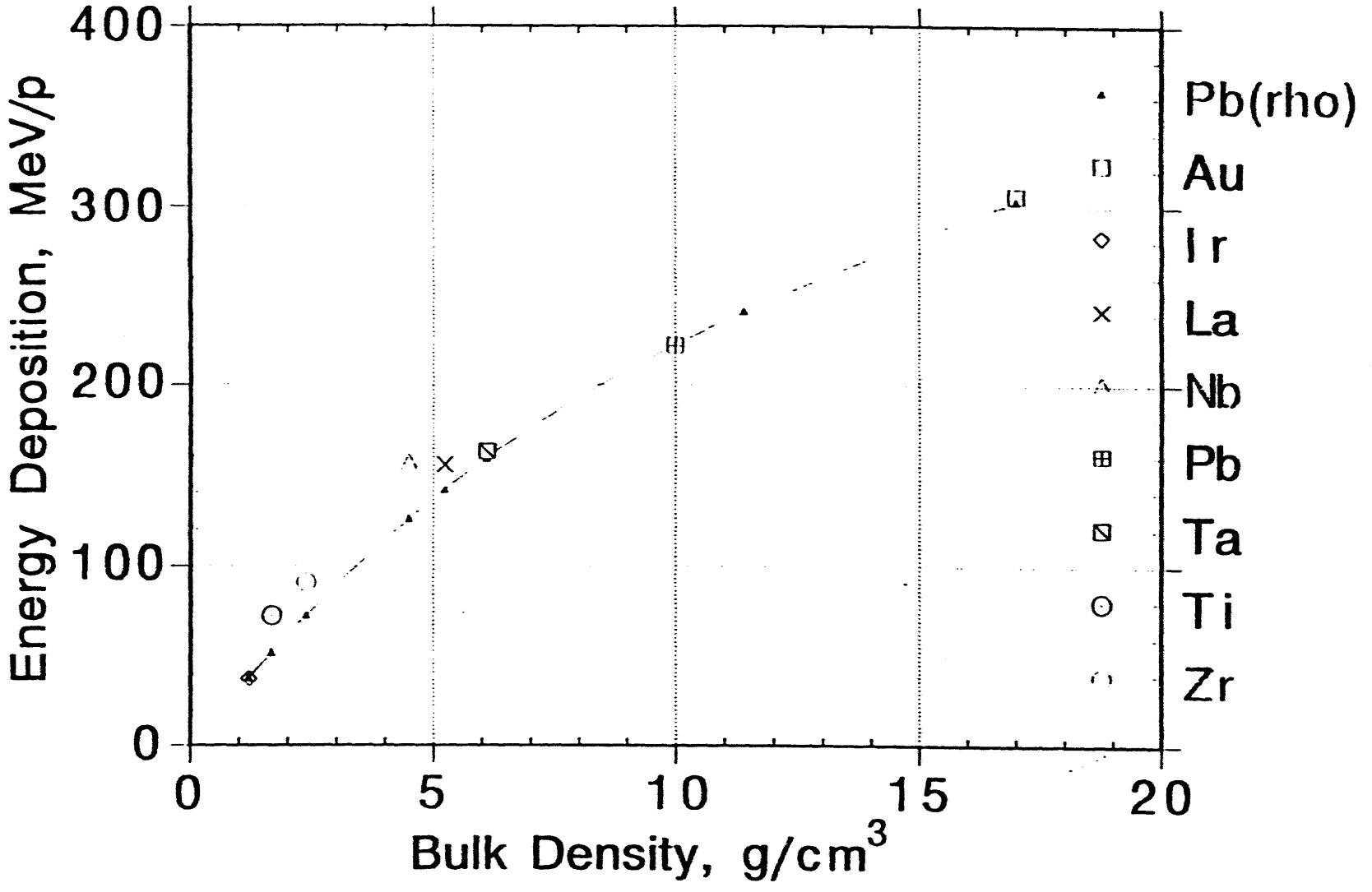

Figure 2. Energy-deposition rate at proton energies of 600 to 1200 MeV for various targets (Zr, Ti, Ta, Pb, Nb, La, Ir, and Au); higher beam intensity results in higher energy deposition; energy deposition increases with bulk density.

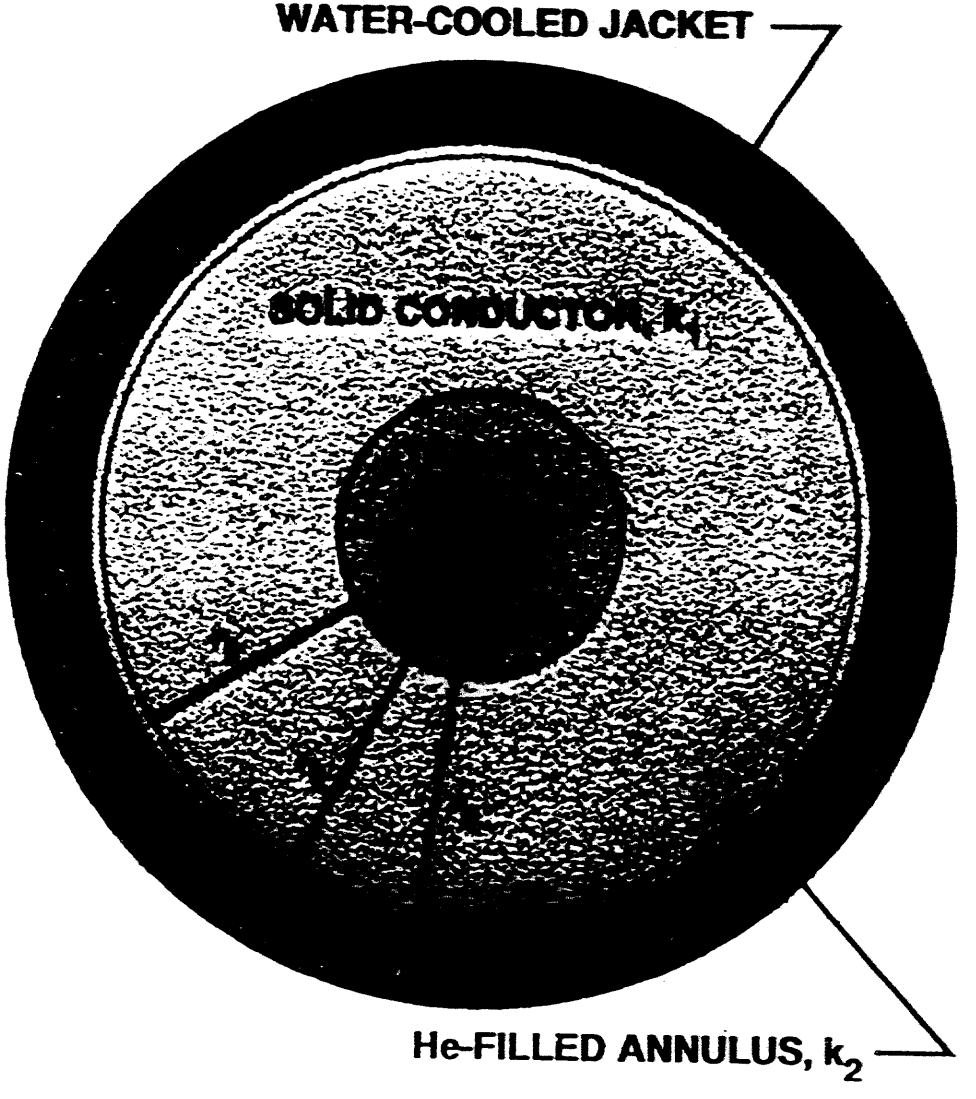

Figure 3. Conductively cooled target (in an axial view).

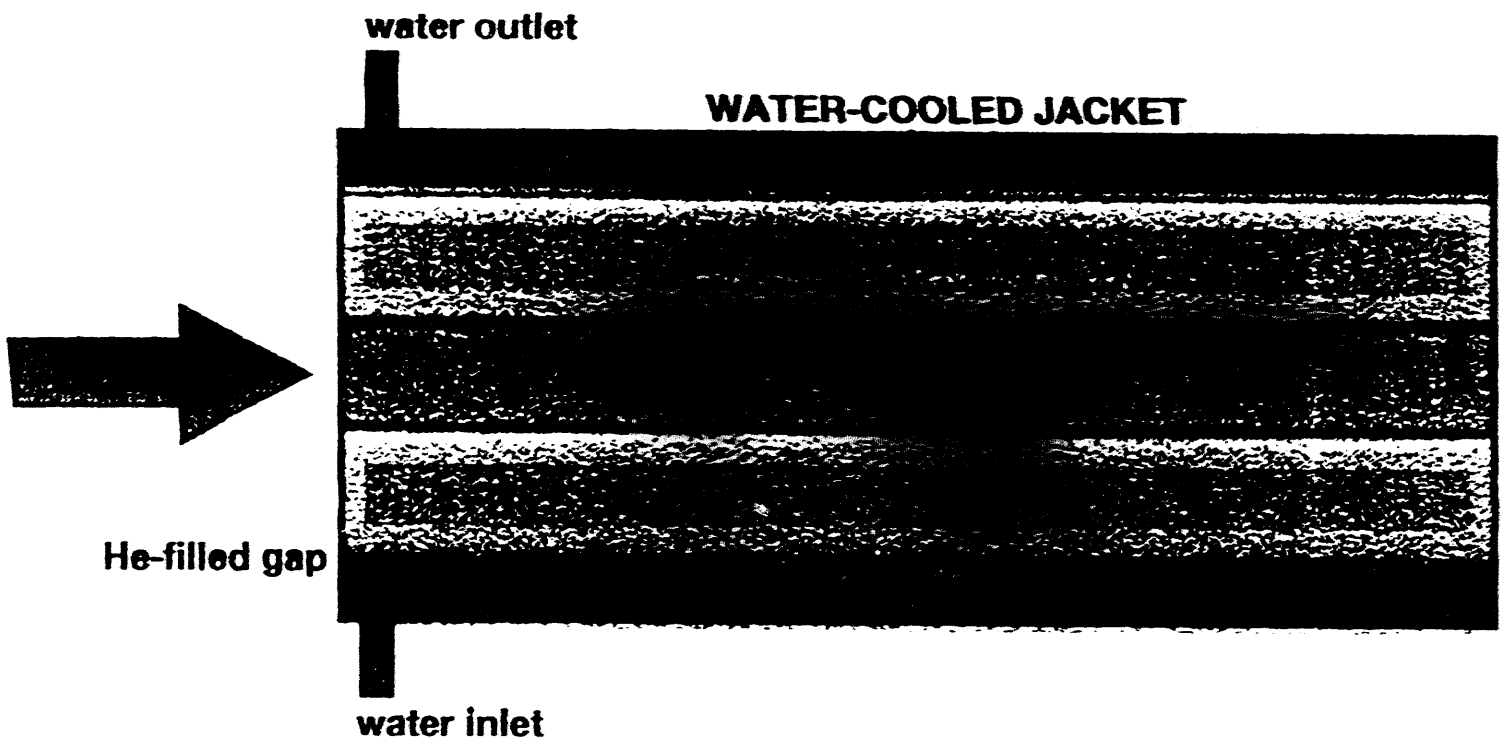

Figure 4. Heat-pipe cooled target (in a lateral view).

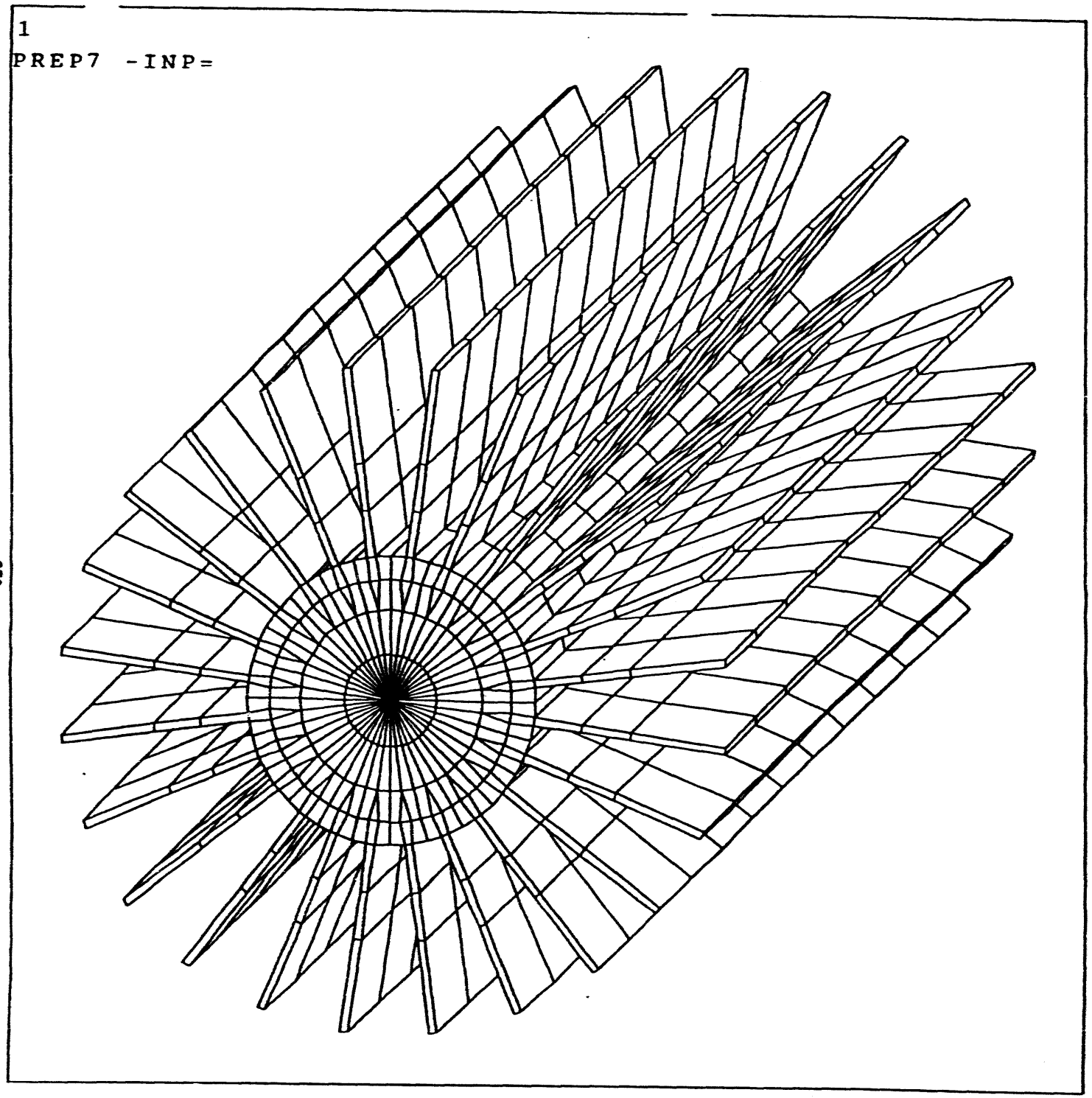
1
PREP7 -INP=
ANSYS 4.4A
MAR 19 1992
11:51:32
PREP7 ELEMENTS
TYPE NUM
XV =1
YV =1
ZV =10
DIST=0.035366
ZF =-0.1015
PRECISE HIDDEN

Figure 5.

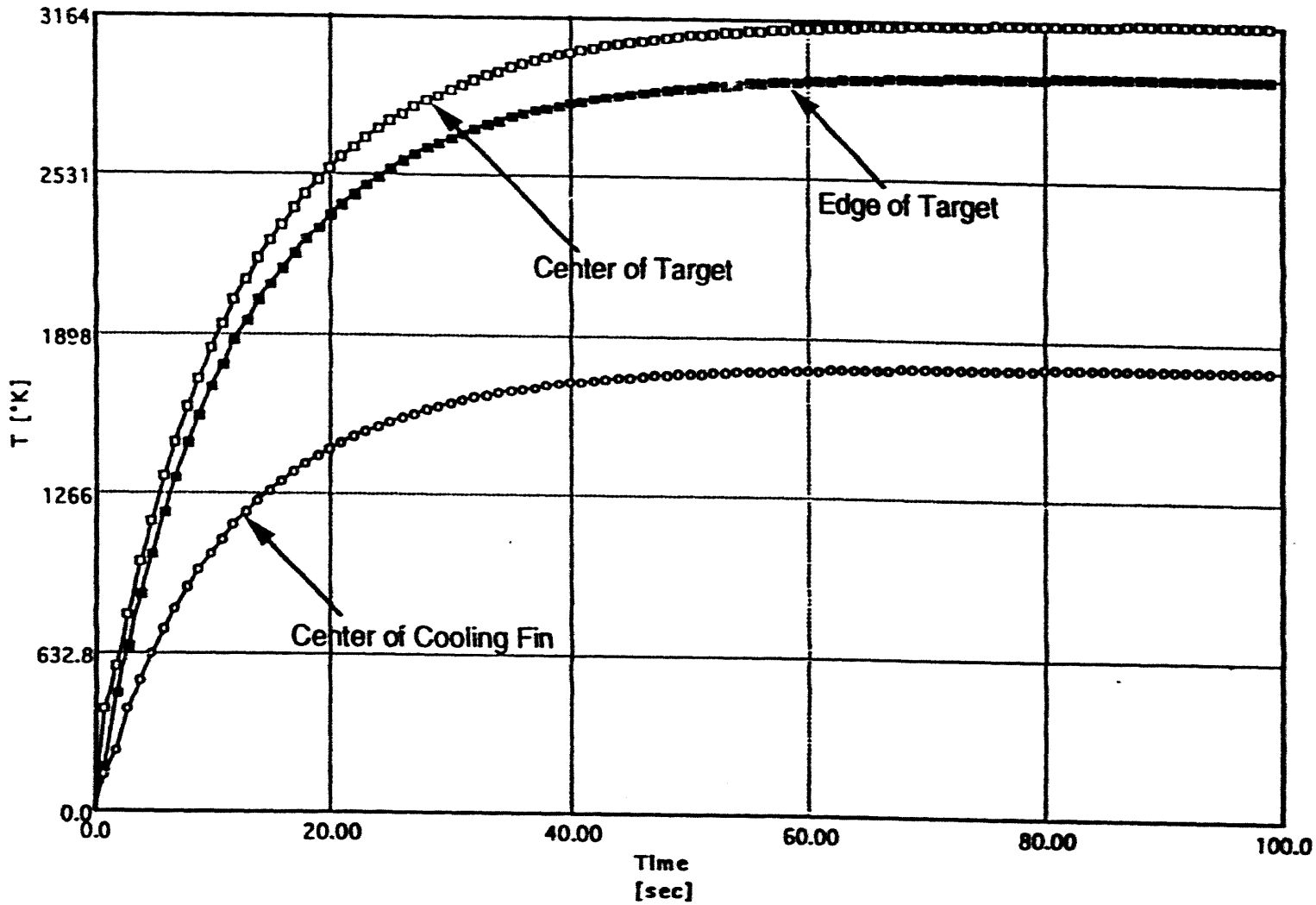

Figure 6. Temperature versus time: sigma = 3 mm; wobble radius = 5 mm.

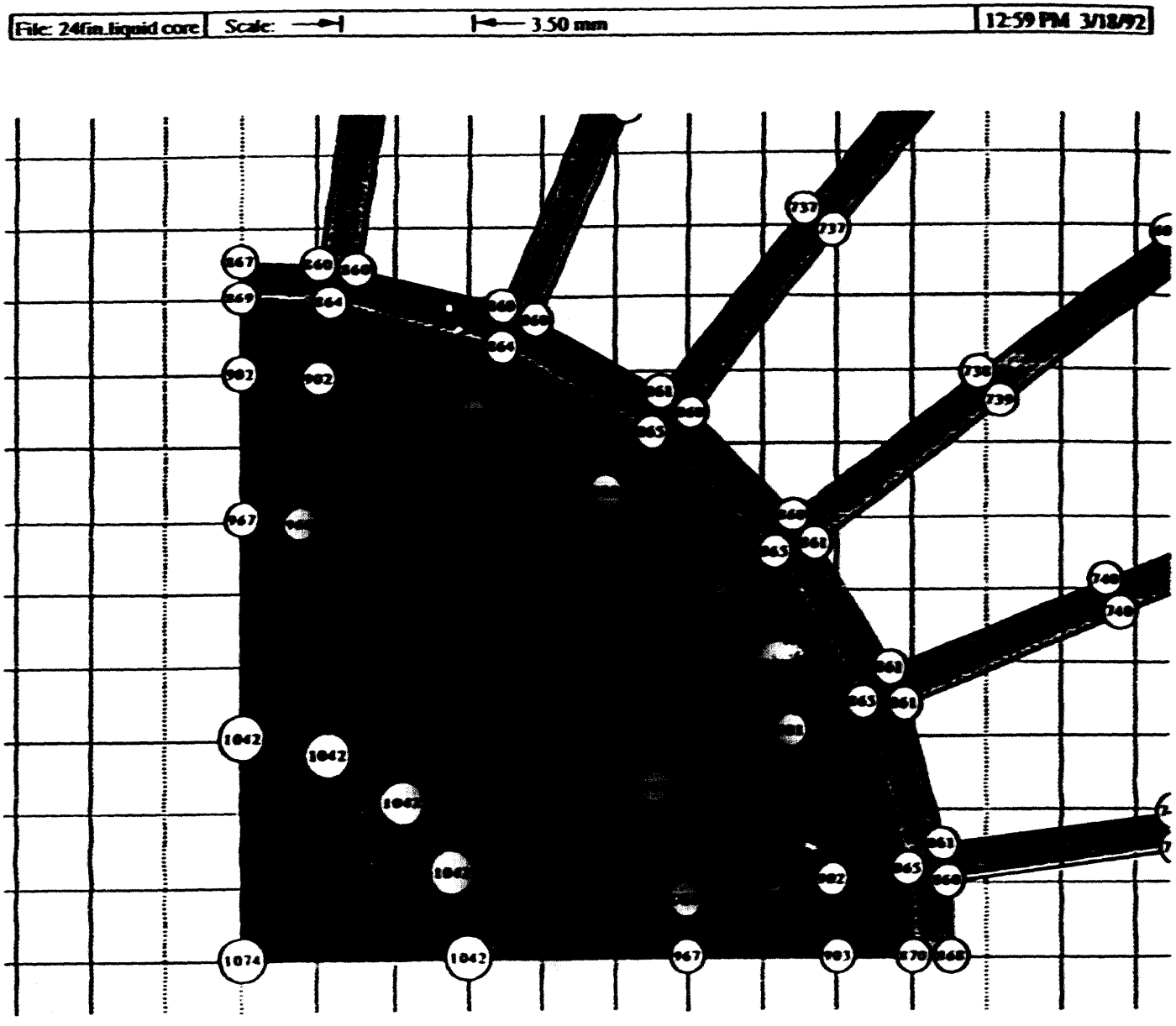

Figure 7. Wobble Gaussian beam heating molten lead target. 6.8 kW are deposited into the target. (Temperatures are given in °K.) The standard 24-fin Ta cooling setup is used with a .5 mm-thick Ta shell used to hold the Pb.

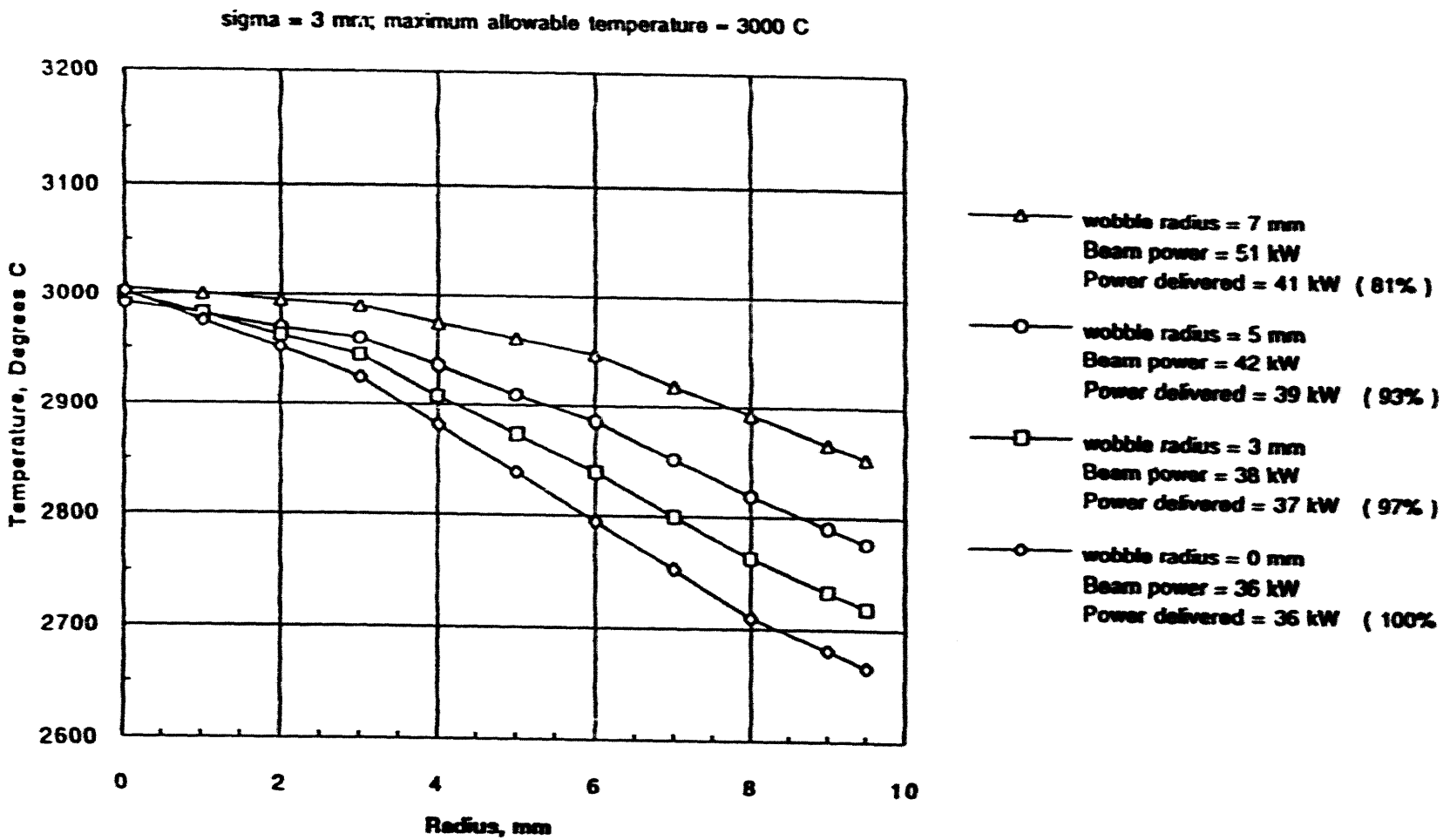

Figure 8. Temperature distributions for wobbled Gaussian beams.

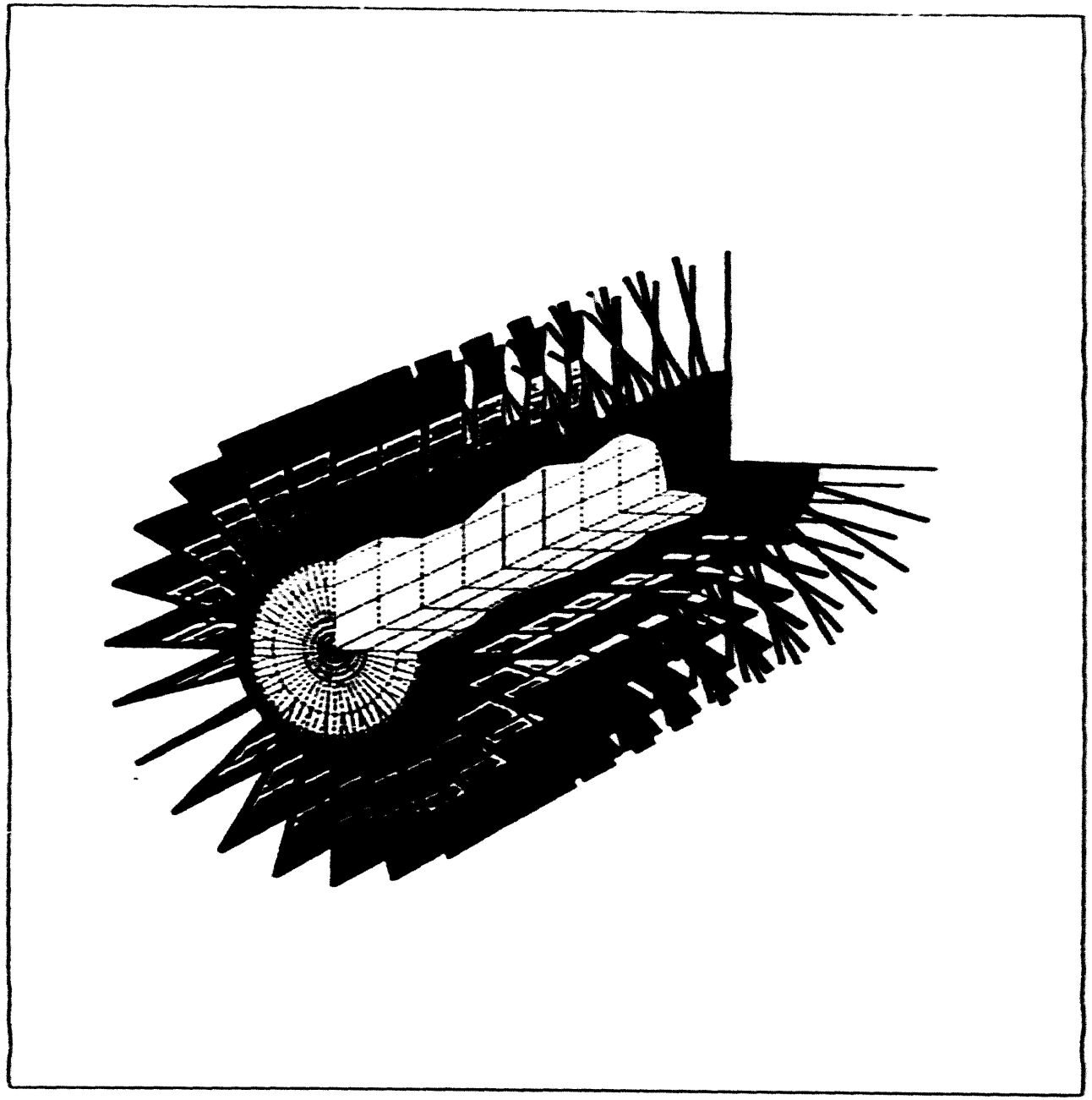

ANSYS 4.4A
MAY 19 1992
15:01:24

ISL TARGET- Version 3A
L= 20 cm; D= 2 cm; heat sink= 100 C

PROTON BEAM:
800 MeV; 61 microA; 28 kW
sigma(Gaussian)= 3 mm
wobble radius= 0

TARGET MATERIAL:
solid Ta; density= 16.6 g/cc

CODE: FLUKA89

TEMPERATURES:
373 K
1200 K
2000 K
2600 K
3027 K

Figure 9.

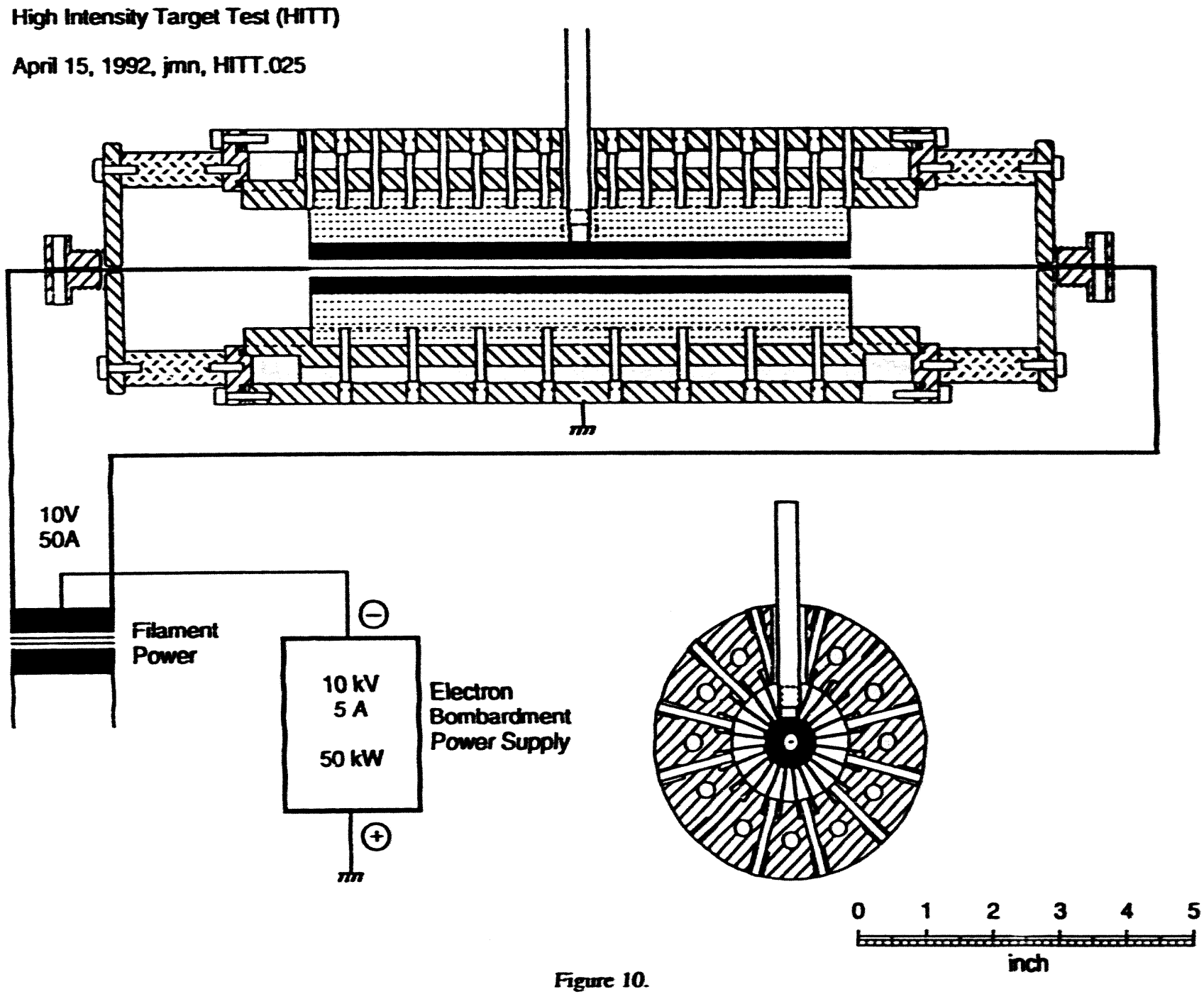
High Intensity Target Test (HITT)
April 15, 1992, jmn, HITT.025
10V
50A
Filament
Power
10 kV
5 A
50 kW
Electron
Bombardment
Power Supply
0 1 2 3 4 5
inch

Figure 10.

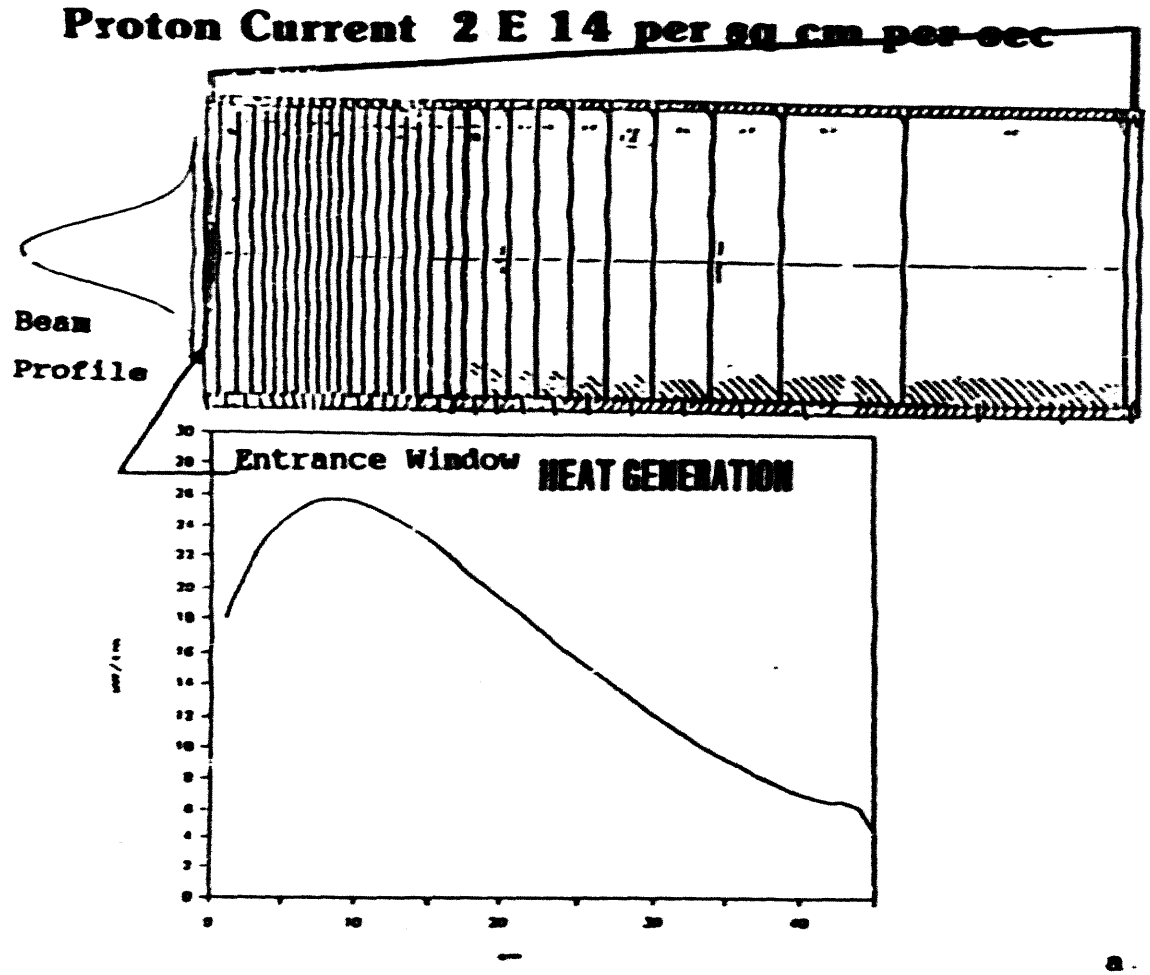

Figure 11. Diagram (a) of the copper beam stop used at LAMPF target station A-6. Photograph (b) of a beam stop, with part of the housing removed, after irradiation.

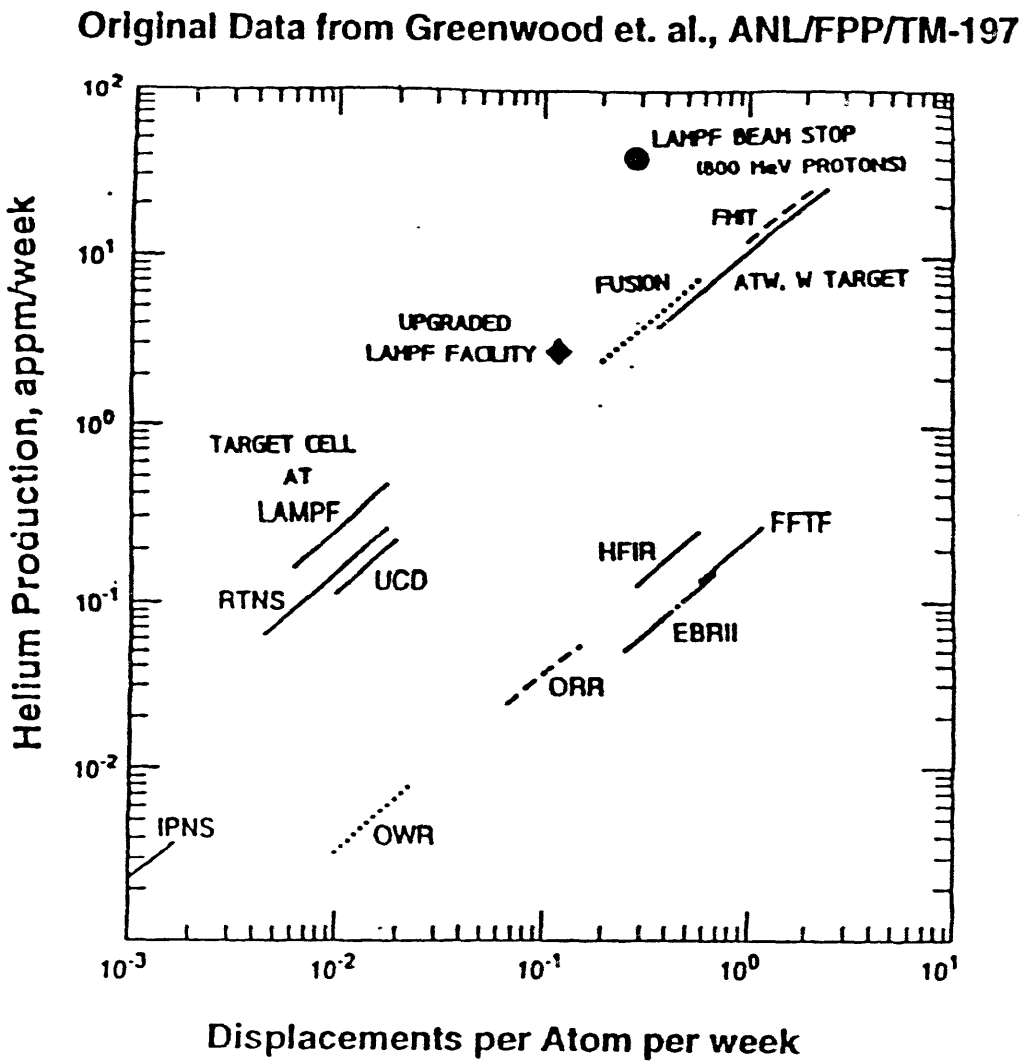

Figure 12. Material damage comparison.

THE RISP PROGRAM...

- Serves as the ORNL Focal Point for Research and Development in Robotics, Teleoperation, and Intelligent Machines
- Addresses Research and Development Goals for Extending Human Senses and Dexterity into Unstructured or Semi-Structured Hostile Environments
- Develops Systems Which Minimize Human Risk by Allowing Effective Remote Operation while Preserving Work Task Efficiency Through Automation and Attention to Human Factors
- Integrates R&D Efforts in Three ORNL Divisions
  - Engineering Physics and Mathematics
  - Robotics and Process Systems
  - ORNL Engineering
- Performs Robotics R&D for the Department of Energy and Other Federal Agencies

Figure 13. Robotics and Intelligent Systems Program (RISP) at ORNL.

- Remote Systems/Equipment Design & Demonstrations
- Manipulation Research and Development
- Precision Servomechanisms
- Advanced Control Techniques; Low-Level and High-Level
- Mobility and Navigation
- Sensor Systems
- Intelligent Systems
- High-Performance Embedded Computing
- Human-Machine Interfaces
- Rapid and Complete Prototyping Capabilities

Figure 14. RISP technologies are uniquely diverse.

Remote Technology Has Been Used Widely In The Nuclear Industry for Over 45 Years ... The Experience Shows That ...

- Maintenance system flexibility is essential to typical repair tasks because they are typically NOT repetitive, structured, or planned
- Very complex tasks can be successfully performed (even with remote crane-based maintenance)
- Work task efficiency is a strong function of the maintenance system elements
  - manipulation dexterity and transporter flexibility
  - remote sensing fidelity
  - human-machine interface efficiency
  - operator skill levels
- Fully remote design (manipulation, task provisions, remote tooling, and facility synergy) is essential to work task efficiency

Figure 15. Remote operations and robotics in nuclear facilities.

Target (ρ)	600 MeV	800 MeV	1000 MeV	1200 MeV
Au (17.00)	306.36 (6.98)	330.65 (6.72)	366.59 (6.86)	408.77 (7.33)
Ir (1.20)	37.50 (4.69)	39.70 (4.46)	41.60 (4.65)	44.25 (5.02)
La (5.24)	155.12 (7.78)	164.53 (6.96)	177.82 (6.85)	191.85 (7.31)
Nb (4.50)	156.72 (6.86)	166.02 (6.55)	177.51 (6.62)	191.17 (7.13)
Pb (10.00)	222.52 (8.32)	241.51 (7.98)	267.02 (7.99)	294.73 (8.27)
Ta (6.10)	162.57 (8.42)	175.55 (7.66)	190.84 (7.47)	208.72 (7.62)
Tl (1.67)	72.53 (4.64)	75.30 (5.11)	79.29 (5.56)	84.26 (6.04)
Zr (2.38)	90.84 (5.51)	94.08 (5.49)	99.37 (5.73)	105.54 (6.32)

Table 1. Energy deposition rates for incident proton beam energies from 600 MeV to 1200 MeV (in MeV/proton; Ta case deposition in parentheses).

Target Station	Target Type	Target Material	Beam Size, mm FWHM	Heat Generated, kW Current in (mA)
A-1	Rotating Wheel	Polycrystalline Graphite	3.2 Vertical 3.9 Horizontal	13 (1.0)
A-2	Rotating Wheel	Polycrystalline Graphite	5.3 Vertical 6.5 Horizontal	14 (0.92)
A-5	Stationary Water Cooled	Pyrographite	5.3 Vertical 8.9 Horizontal	40 (0.75)
A-6	Various	1) Various for Isotope Production 2) Copper Beam Stop	35 Vertical 35 Horizontal	600 (0.75)

Table 2. Operating parameters for LAMPF targets.

Double Walled Flat Plate on Beam Stop	
Material	Inconel 718
Service	17500 hours, 20-30 uA/cm^2 average in beam center - instantaneous ~ 17 X greater
Fluence	1.3 X 10^{22} protons/cm^2 plus high energy neutrons
Double-Walled Spherical Vacuum-to-Air Interface	
Material	Inconel 718
Service	4000 hours, 20-30 uA/cm^2 average in beam center - instantaneous ~ 17 X greater
Fluence	2.9 X 10^{21} protons/cm^2

Table 3. Performance of LAMPF beam entry windows under irradiation.

Section II
Contributed Papers

A TEST FACILITY FOR RADIOACTIVE IONS GENERATED BY INTENSE BEAMS OF HIGH ENERGY PROTONS

J R J Bennett[1] T A Broome[1], C J Densham [1],
W Gelletly[2], H G Price[2], and D D Warner[2]

[1] SERC, Rutherford Appleton Laboratory, Chilton, Didcot, Oxon, OX11 OXQ. UK
[2] SERC, Daresbury Laboratory, Daresbury, Warrington, Cheshire WA4 4AD, UK.

ABSTRACT

A proposal for a radioactive beam test-bed facility at the Rutherford Appleton Laboratory is described. The facility is aimed at testing and developing target/ion source technology with proton beam intensities of up to 100μA.

In essence we have two main ways of producing beams of radioactive nuclei. One technique makes use of the forward focussing of reaction products in peripheral nuclear reactions at high energies. The second method involves a two step process in which radioactive nuclei are produced when a target is bombarded with an energetic primary particle beam and subsequently thermalized, ionized and re-accelerated to ~5MeV/u to overcome the Coulomb barrier. The isotope separator ISOLDE on the PS-Booster at CERN[1] is the most notable example of the first stage of this process.

In principle the primary particle beam might be almost any projectile which will initiate nuclear reactions. In practice, if the aim is to produce intense beams of secondary particles the favoured beams are ions at >100 MeV/u or high energy protons (~1GeV). Before any choice of projectile is made for a major facility it is essential to show that one can realise the expected intensities from the target/ion source. In Europe a test bench to determine if heavy ions can be competitive with high energy protons for the production of exotic nuclei has been set up at GANIL[2]. The use of high energy protons is already well-proven at ISOLDE where the intensities of the proton beams are of the order of 1 to 3 μA. To reach the intensities required of a future, major accelerated radioactive beam facility would necessitate an increase in proton beam currents to some 100μA. In order to achieve this increase, existing target technology has to be tested and developed to accommodate the much increased power input.

Here we report briefly a description of a radioactive beam test bed facility to be sited at ISIS, the spallation neutron source situated at the Rutherford-Appleton Laboratory. ISIS is an intense, pulsed neutron source, which creates neutrons by the proton-induced spallation of a depleted uranium or tantalum target. The primary proton beam has an intensity of ~200μA and an energy of 800 MeV. This ideally matches the requirements of an intense, accelerated radioactive beam facility.

THE TEST BED FACILITY

The test facility will consist of a suitable target capable of withstanding the 80 kW of power imparted by the ISIS beam with a system for transporting the radioac-

tive ions from the target to an ion source. This is followed by an extraction system and ion optics together with a suitable magnetic system for analysing the mass of the particles. Finally a variety of instrumentation for collection and diagnostic purposes will be set up for the radioactive species produced. The layout is shown schematically in figure 1.

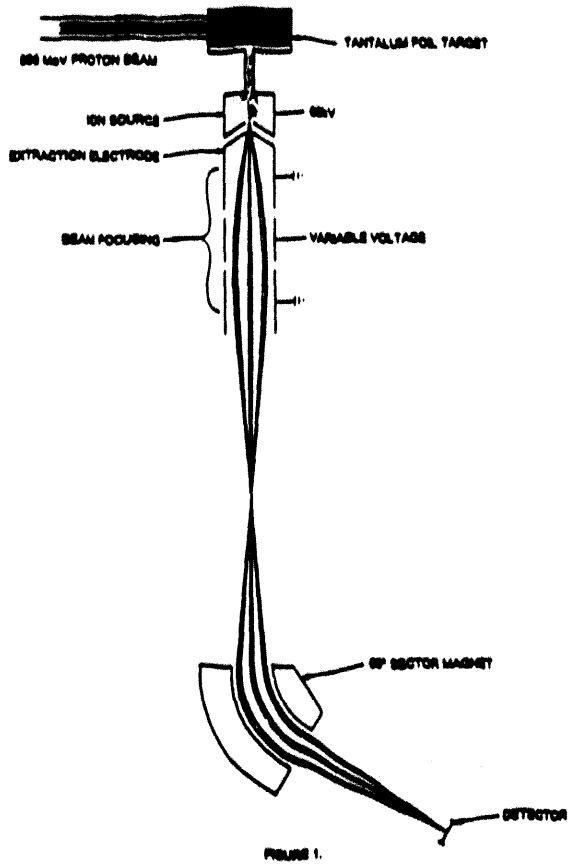

FIGURE 1.
SCHEMATIC LAYOUT OF THE RADIOACTIVE ION SOURCE TEST FACILITY

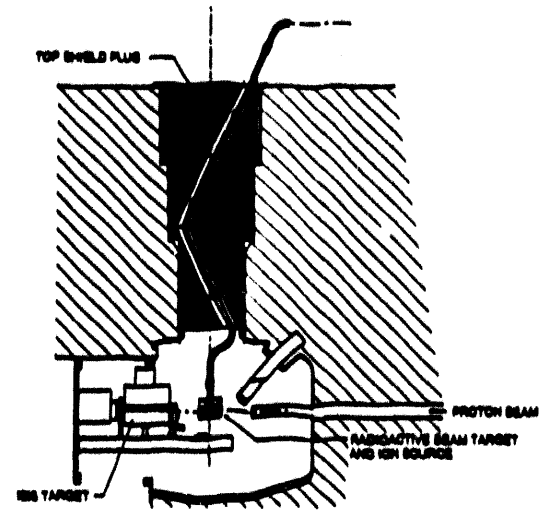

FIGURE 2.
THE ION SOURCE TEST FACILITY IN THE ISIS TARGET STATION

The most cost-effective location at ISIS for the test facility is the existing target station of the spallation neutron source. This allows the beam line shielding, active air ventilation system etc to be used. Crucially the test rig can be installed and used with no interruption of operation for neutron production. This choice of location limits flexibility but the crucial, high power target tests can be carried out.

Fig 2 shows the test facility in the target station. The ISIS target is rolled back on its trolley to allow the ion source target to move into position from above through a plug in the shielding. The source is directly above the target, followed by an extraction electrode and electrostatic bending and focusing to bring the beam through the shield plug to the top of the target station. The path through the plug has bends for shielding purposes to prevent direct line of sight from the target. The beam then passes through a 60° bending magnet to separate the ions of different mass. The whole system bears many similarities to ISOLDE at CERN. Indeed, the source and target geometry will be closely copied to ensure good performance with minimum development.

A new shield plug will be made for the target station. This plug and the whole test facility will be moved in and out of the target station during the two weeks short shut downs on ISIS. The equipment will be designed for easy, simple and

speedy exchange. Experimental runs with proton beam on target will generally be of only one day duration each shut down. The impact on the neutron beam operation will be minimal.

A "cold" tantalum target and ion source combination has been chosen for the initial tests because it will minimise the levels of activity and contamination. Tantalum targets produce mainly light nuclides, such as He, Li, Be and Na as well as the rare earths. Except for He these elements will condense as the cool surfaces surrounding the target and ion source and will not contaminate the rest of this facility. Small, but measurable quantities of the noble gases will be produced. These are the beams which will be measured first. The tantalum target is also one of the easiest to use at the high input power involved, since it is a refractory material.

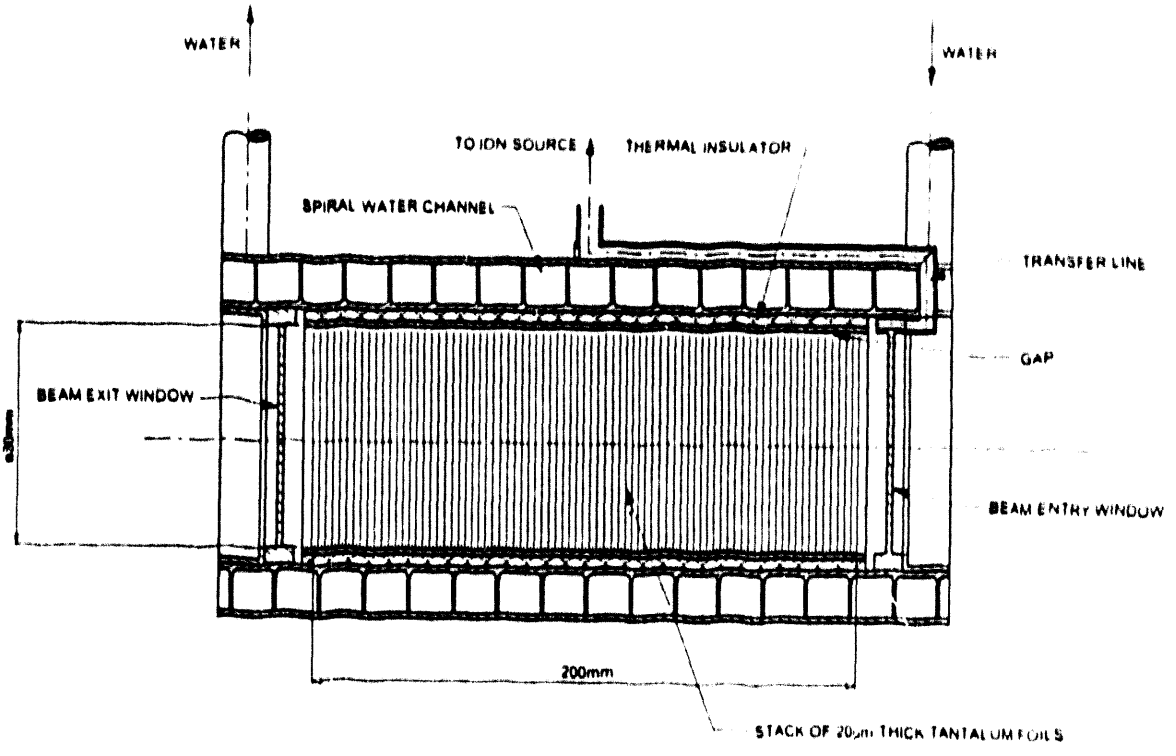

FIGURE 3.
TANTALUM FOIL TARGET WITH COOLED TRANSFER LINE

The cold target shown in fig 3 will consist of Ta foils, 20μm thick, forming a stack 20 cm long with a packing fraction of ~50%. At 100μA beam current the power dissipated will be no more than 3.5 kw per cm length of Ta. The simplest target will have loose discs of Ta foil in a water cooled Ta tube, and the heat from the foils will radiate to the walls of the tube. The radioactive products will infuse from the foils via a transfer line to the ion source. A second target for higher power dissipation will consist of Ta foils cooled at their edges by welding them to the enclosing tube. These targets will be heated by the proton beam and, where necessary, by passing a heavy current through the tantalum tube.

These initial tests will be followed by the construction of "hot" target/ion sources. Here all the surfaces in contact with radioactive products must be kept

hot to prevent condensation. The Ta foils will be welded into a gas tight Ta tube which will couple to the ion source through a heated tube. The Ta tube will be enclosed in an outer jacket designed to remove the heat but maintain the tube at ~2700k. The temperatures of the foils, tube and water will be monitored. Since the water cooling the target will become active when the target is bombarded with protons, the water current will be a doubly contained, closed loop system with deioniser and heat exchanger.

The initial ion source will be a close copy of the well tried plasma ion source on ISOLDE. Once a target with a "hot" body has been developed for non-gaseous ions, then a simpler surface ionization source can be used.

The target and ion source assembly will become highly active under bombardment. They are attached to the bottom of the shield plug and the system is designed to allow their removal from the target station on the main crane. The target assembly will then be placed in a steel pot and remotely disconnected from the rest of the test equipment. It will be allowed to cool in the pot before disposal by the same route as the ISIS targets and using the same flasks.

The target and ion source will be maintained at high voltage from a high voltage platform. Power will be fed to the platform through an isolating transformer. Monitoring and control will be via suitable light links. Following extraction from the ion source at +60kV the beam of radioactive ions will be focussed by Einzel lenses and electrostatic quadrupoles. Above the target shielding it will be rendered horizontal and passed into the magnet which currently constitutes the on-line isotope separator at the Daresbury Tandem Van de Graaff. This is based on a 60° sector magnet with 1m bend radius, and will provide a mass resolution of 1 in 500, assuming a 1mm beam diameter at the object position and negligible energy dispersion. A linear Einzel lens in front of the magnet will give some focussing in the direction of the magnetic field.

SUMMARY

The aim of the test facility is to establish first that the radioactive ion currents are comparable to those of similar sources, such as at ISOLDE, at the same proton current on target and then to show that the radioactive beam intensities increase in proportion to the proton beam current on target, up to 100 μA (mean). The facility will also allow an examination of the problems and possible solutions associated with the pulsed, high current drain from the high voltage supply on the ion source assembly, which is caused by ionization of the surrounding air and secondary emission of particles from surfaces by the proton beam, resulting in severe voltage fluctuations.

The test facility will be in operation in 1994. Since the Benchmark facility [3] proposed in North America has the same parameters as that proposed in Europe [1,4] it is hoped that there will be a common programme of research and development.

REFERENCES

1. B Jonson and D D Warner, Proc. of Int. Workshop on the Physics and Techniques of Secondary Nuclear Beams, Dourdan, France, March 1992; to be published.

2. J C Stechmeyer, Nuclear Physics News 2 No 3 (1992) p30.

3. The Isospin Laboratory, Report LALP 91-51

4. G Walker, Proc. of the Workshop on the Science of Intense Radioactive Beams, Los Alamos Laboratory, April 1990, Report LA-11964-C, p183.

Design principles for target stations and methods of remote handling at PSI

Erich Steiner *

Los Alamos National Laboratory, Los Alamos,NM 87545,USA

Abstract: Two design concepts for target stations used at PSI are shown. The method of the remote handling of activated elements is described and some conclusions with respect to a radioactive beam facility are given.

*permanent address: Paul Scherrer Institute, 5232 Villigen-PSI, Switzerland

Target Stations

At PSI all elements in high-radiation areas can be removed and transported into a specially designed hot cell for repair or disposal by means of an overhead crane. For the removal of elements which are known to need more-or-less frequent maintenance we have designed heavily shielded casks, which allow easy and safe removal of the elements. The systems are designed so that any repair or removal can be done with a minimum of exposure to personnel. For unforeseen problems there exists a simple, transportable power manipulator, which can be positioned in the proton channel. Proof that this is a good working concept which could be used for ISL is the fact that we have after nearly 20 years of operation at 100 - 300 μA dismantled two complete target stations and a beam dump with a total dose applied to all the workers of only 470 mSv (47 Rem), the average dose being 2.3 mSv and the maximum single dose 30 mSv. The maximum radiation field of an activated element that was handled was 400 Sv/h.

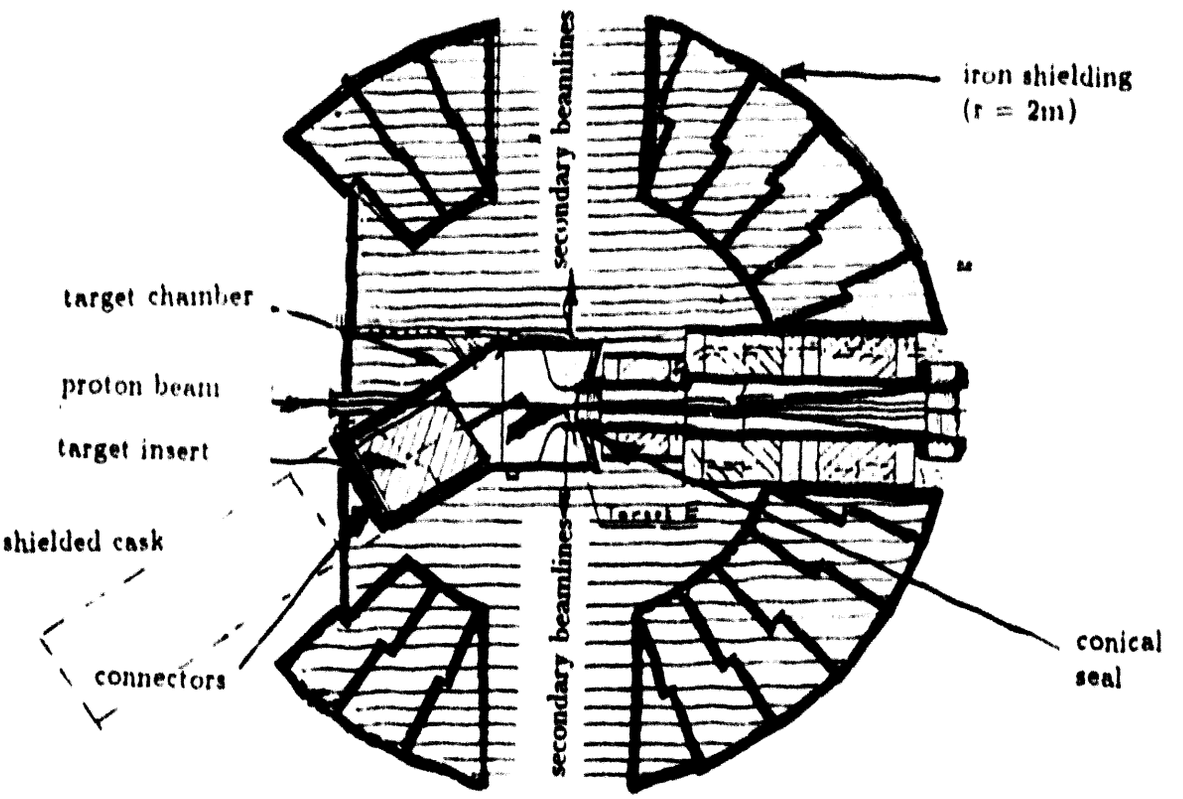

Figure 1: The first version of the thick-target station at PSI. The target insert is removed horizontally.

Our first concept of the target station (1972-1990) consisted of a target vacuum chamber that required the target structure to be inserted horizontally (see Fig 1). A cask, placed in front of this target insert, is opened remotely and then it grabs the insert and retracts it. After closing the shielding door, the whole cask with the target insert, is moved to the service area by crane. Only for a short time ($\leq$10 min) does a person need to work directly at the target station to unhook the power and cooling connections as well as to unscrew four bolts used to make the vaccuum seal (a rubber gasket is used between insert flange and target chamber).

The target vacuum chamber is connected to the vacuum system of the proton channel by a conventional metal seal at the entrance side and by a conical seal at the exit (the latter introduces a small controlled leak). This design worked well for currents up to 300 μA and 10-cm thick carbon targets.

It should be no serious problem to handle connections on the outside of the local shielding. For frequent routine operations (like weekly target-ion source changes, as expected for ISL) some improvements would have to be made. One such improvement would be to install a "marble" cladding ($\approx$20 cm of concrete enriched with calcium carbonate) at the entrance side of the target station to considerably reduce the radiation dose to personnel unhooking the target insert. The loss of protons at the entrance should also be kept as small as possible. This implies no entrance collimator to the target station and also no (or a well shielded) window at this place.

Going to higher intensities, we had to redesign our target system. We followed the same principles outlined above, but introduced the following improvements, which should also be considered for ISL. I would like to mention that these improvements have been in use at the thin target station (with a 5-mm C target) since 1985 with operating currents of 100-500 μA.

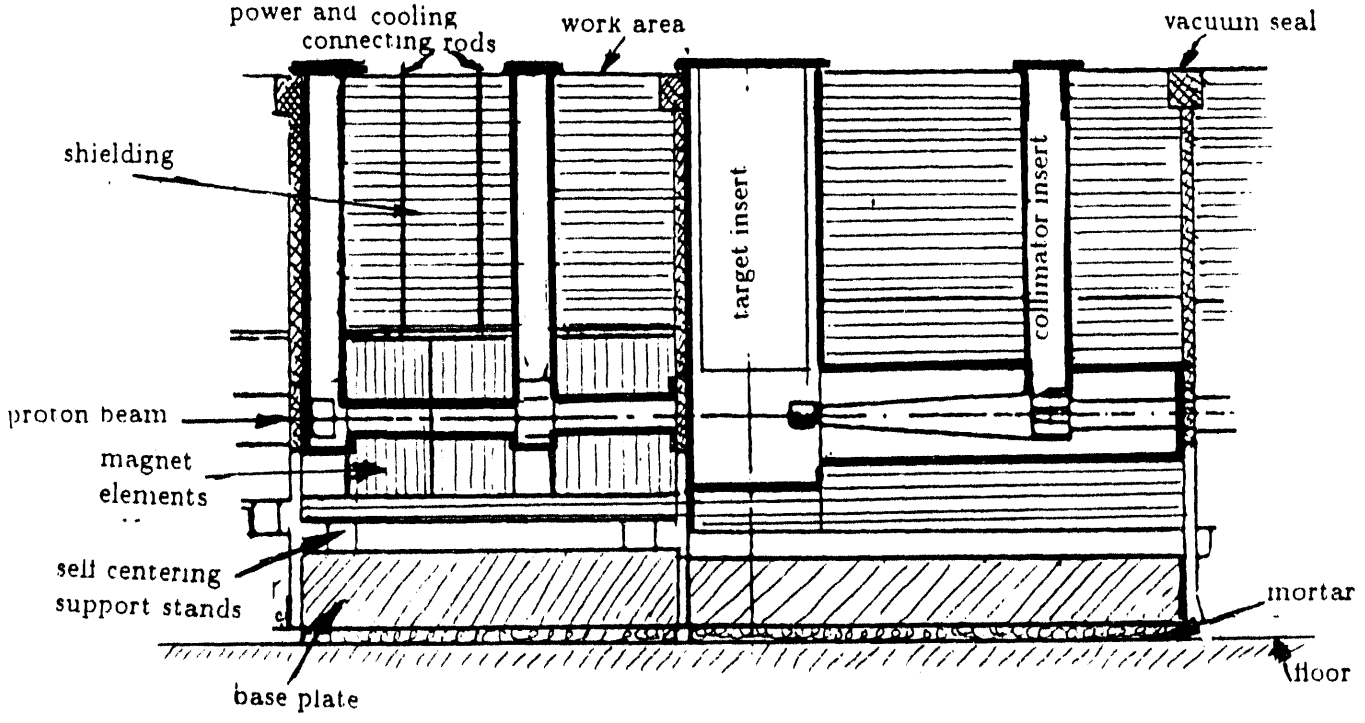

Figure 2: New design of the thick-target station at PSI. All the inserts are removed vertically.

The key ideas of the new concept are

- self-centering mounts;
- making vacuum connections with "pillow seals";

- increased shielding between places of beam loss and the working area (important for disconnecting the elements);
- quick disconnects for power, water, and signal connections (connections between work area and elements going through the local shielding);
- easy retractability of all the elements that are directly exposed to primary protons and that are designed to be maintainable in a hot cell.

The basic design is shown in figure 2: A base plate of steel (25-30 cm) is equipped with the lower part of self-centering support stands (the counterparts of the support stands are attached to the elements). The base plate is held in place on the floor by centering pins which are precisely located in the floor. The whole plate is adjusted to the correct height by means of three machined iron plates leaving a gap of about 2 cm between the baseplate and the floor. This space is filled with mortar, to give an even floor loading. Iron shielding blocks of about 2-m height are positioned on top of the elements (magnets, vacuum chambers).

In order to get electric power and cooling water from the topside of the shielding blocks to the elements below, holes are drilled through these iron blocks. Copper rods and stainless steel tubes carrying electric power and water, respectively, can be inserted and engaged into receptacles attached on the top of the elements. These rods and tubes can be inserted or removed from the top of the shielding block without exposing workers to intense radiation.

The whole target setup is surrounded by a wall of concrete blocks (sides and top). In order to prevent activated air from leaking out, the joints between the blocks are sealed using a radiation- resistant mortar. In addition, the roof is sealed off by means of a plastic foil, inserted between two layers of concrete roof beams. This sealing of the walls also permits a slight underpressure in the proton channel to be maintained with only a minimum amount of air expelled through the exhaust stack.

An important part of the concept is the pillow seals; two versions are shown in Figure 3:

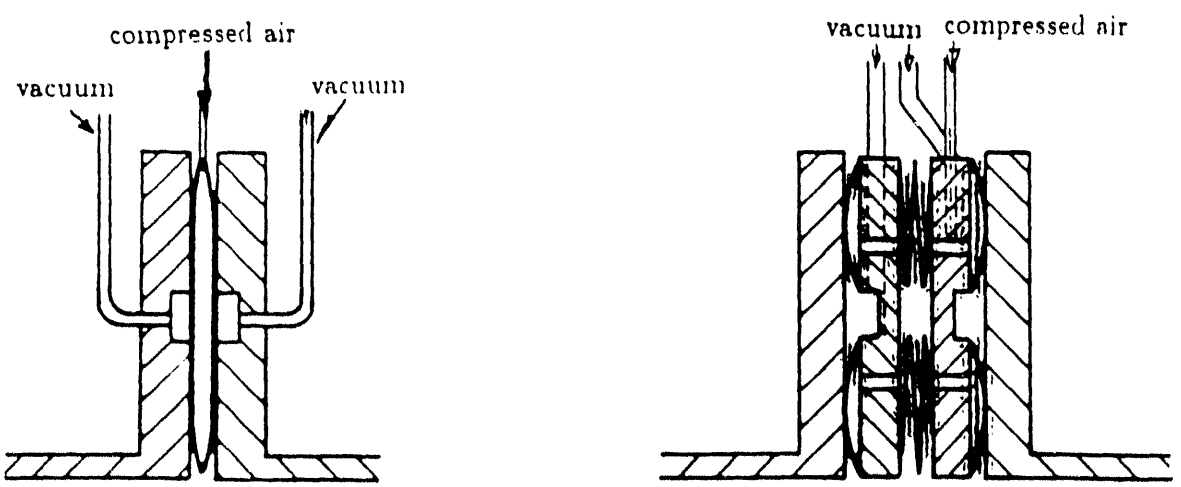

Figure 3: The two versions of pillow seals used at PSI.

These seals consist essentially of an inflatable ring made out of stainless steel foils. This ring can by inserted between two flanges. After applying pressure, the seal inflates and upon touching the flanges (which clearly have to be tied down to withstand the mechanical force), seals the connection. To remove the seal, the pressure is relieved (even vacuum may be applied) and the seal retracted. No clamping or unclamping is required. However, this type of seal leaks slightly and an auxiliary vacuum has to be applied. Our present type of pillow seal has been designed for a pressure of about 10 $\mu Torr$, but improvements could still be made. The achievable pressure depends also on the size and number of seals used as well as on the pumping speed. It must also be mentioned that radioactive gases created inside the vacuum system (such as the breakage of a target) might leak out into the surrounding region. In this respect, the safety aspects of these seals have to be investigated.

Remote Handling

To remove a highly activated insert, we use a shielding cask that can be precisely positioned

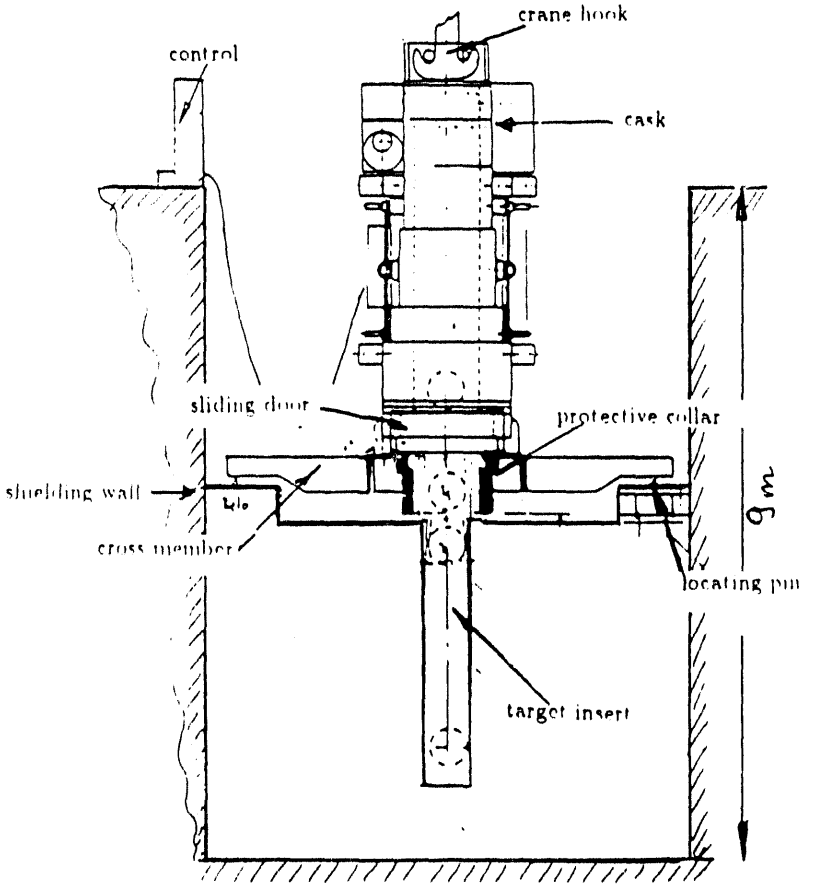

Figure 4: Removal of an insert from the proton channel.

over the insert (see Fig. 4). The door of the cask can be opened remotely and the insert retracted into the cask. After closing the door, the cask is lifted up by the overhead crane and brought to the service area. This allows the rapid removal of the insert and replacement by a spare unit. Ample cool-down time and the option to repair the insert is also made possible.

In case of potential contamination hazard in the air gap located between the bottom of the cask and the top part of the insert, a protective collar is used. The inserts are also put back in place with an overhead crane and cask system. The PSI inserts are positioned to within 0.5 mm, given that a higher precision is not needed. However, we can measure the position of the elements or support structures to within 0.01 mm so that, if required, the precision of repositioning can be improved to 0.1 mm.

Vacuum Windows

Of special interest in the context of a radioactive beam facility is the use of a window. A window that can withstand current densities of about 100 $\mu A/cm^2$ requires cooling. It usually is constructed as a double window with forced water cooling in between the two layers.

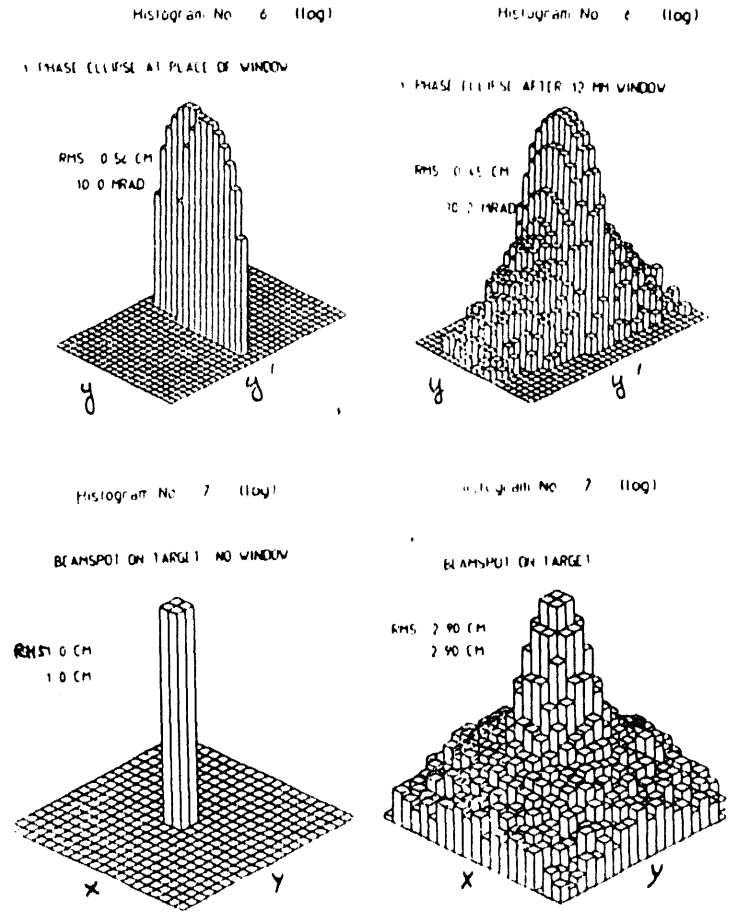

Figure 5: Effect of a 12-mm thick stainless steel window on the beam phase ellipse (top) and on the beam spot size (bottom) of an 800-MeV proton beam at the place of the target. The unaffected beam is shown in the left-hand part, the effect of the window in the right-hand part of the picture.

Stainless steel is the preferred material for such windows. Since each layer of the window is about 2 mm thick, the total thickness amounts to at least 4 mm. Such a window causes

significant scattering of the primary beam and the window has to be placed where the effect on the beam is kept minimal. This usually is at a focus position. However, at a focus the current density is rather high and easily exceeds 100 $\mu A/cm^2$. As an example I show in figure 5 the detrimental effect on the beam quality of two stainless steel double windows (one double window at the exit of the proton channel, one at the entrance of the target chamber, located one meter upstream from the target). The total thickness of the window assembly in this example is 12 mm. I have assumed that the beam diameter at the window is 1 cm, and the distance from the window to the target is 1 m.

Other solutions for the decoupling of the vacuum chamber and the proton channel could be considered such as a thin foil in the vacuum system for protection against a small leakage of radioactivity and a fast valve located several meters upstream in case of a sudden pressure surge. One could also think of a thick window immediately in front of the target and, in order to reduce the power density, one would have to wobble the beam ("hollow beam"). Since such windows require regular replacement, an efficient exchange procedure would have to be worked out.

Conclusion:

There exists a lot of knowledge and experience in designing, operating, and handling of target stations for proton beams of 600 to 800 MeV at intensity levels of 100 to 1000 μA. Several design concepts of target stations and beam stops have been used. I think, therefore, that the design of a target station for a radioactive beam facility that can be operated and maintained at the intensity level of 100 μA is feasible. Much thought and innovation, however, has to be put into the design of the target insert. One has to keep in mind, that no organic material, probably not even glass, can be used within a radius of 1.5 to 2 m from the target. It is of utmost importance that the methods of the remote handling of the activated parts are integrated into the design of the target station and of the target insert from the beginning. Later adaptions are extremely difficult and costly - if possible at all.

Considerations of the Low-Velocity Stage of a Radioactive Beams Accelerator

W. L. Talbert
Los Alamos National Laboratory
Los Alamos, NM 87545

Abstract: Studies of the low-velocity stages of a radioactive beams accelerator are summarized, highlighting the limitations of existing RFQ technology when applied to the specifications of the IsoSpin Laboratory.

1. Introduction

During June and September, 1992, visits by Peter Ostroumov of the Institute of Nuclear Research in Moscow, and A. Lombardi and A. Pisent of the Laboratori Nazionall de Legnaro, respectively, to Los Alamos resulted in studies to evaluate the possibilities of accelerating radioactive beams provided by an on-line mass separator according to the IsoSpin Laboratory (ISL) Benchmark Facility specifications.[1] This report summarizes the findings of these studies, including not only the systems resulting from the studies but also the constraints imposed by the ISL specifications for accelerator input, which are:

Mass range:	1 to 240
Charge/mass ratio (q/A) (singly-charged ions)	1/1 to 1/240
Transmission	≥ 90%
Input energy	1 keV/A
Input emittance (A_{in})	1 π mm-mrad.

2. Initial Considerations

The first stage of the radioactive beams accelerator is generally presumed to be of the radiofrequency quadrupole (RFQ) type.[2,3] The ISL transverse emittance specification provides a major constraint to intervane voltage and frequency, given the ion input energy, according to the scaling equation for the transverse focusing strength,

$$B\Psi = (q/A)(\sigma_t \lambda/A_{in})(eV/m_o c^2)(2/(m+1))^2, \qquad (1)$$

where $\Psi = (4\pi^2 + B)/(4\pi^2 - B)$, B is the transverse focusing strength, A_{in} is the input admittance (= emittance), σ_t is the transverse oscillation phase advance, V is the intervane voltage, λ is the rf wavelength for the chosen frequency, and m is the vane radial modulation factor.

Additional constraints are imposed by the attainable strength of the surface electric field for focusing (q/A small is harder to focus than q/A large), and the low input energy (1 keV/A - which makes rf defocusing strong). Most RFQ designs operate with a transverse focusing strength value of 5 or more - a value of 3 is pushing the margins of the design, but is adapted in these studies.

Two essential designs were considered by each visitor, one with prior external bunching, and one with adiabatic bunching in the RFQ. Because of the very low intensity of the ion beams (compared to high-current proton accelerators, for example) there is less benefit to adiabatic bunching, with the consequence that omitting the long bunching section of the RFQ can be considered.

3. Ostroumov Designs

The designs developed by Ostroumov encompass the concept of the radioactive beams accelerator to an energy of 1.5 MeV/A. For the purposes of this report, however, only the front-end design (with pre-bunching) is covered.

With conventional 2-cavity (room temperature) beam bunching, followed by RFQ acceleration in a superconducting structure having intervane voltage of 300 kV and operated at a frequency of 25 MHz, Ostroumov obtains acceleration to 10 keV/A for $A \leq 120$. The parameters of the RFQ are listed in Table 1, which also presents parameters for the other designs developed during these studies.

Ostroumov also considered the coupling between RFQs, and determined that a matching cavity is needed with sufficiently large longitudinal acceptance to provide for average energy matching (mass-dependent) and bunch phase space rotation.

In designing a single RFQ to provide adiabatic bunching and acceleration to 100 keV/A, Ostroumov required a 280-cell RFQ of length 12 m, with the first 150 cells being used for bunching and transverse matching (parameters not shown in Table 1).

4. Lombardi and Pisent Designs

Lombardi and Pisent considered both a pre-bunched design and one with adiabatic bunching. Their surface electric field assumption was more

conservative than that of Ostroumov (140 keV vane voltage), and their designs supported only ions with A ≤60, and acceleration to 4.2 keV/A (i.e., only the first of the RFQ structures).

The pre-bunched design included only one prebuncher, having more transmission loss to match longitudinal acceptance than the Ostroumov 2-cavity prebuncher. The parameters of the accelerator sections from both designs are summarized in Table 1.

Table 1: Summary of RFQ design parameters

Parameter	Ostroumov (Pre-buncher)	Lombardi (Pre-buncher)	Lombardi (Adiabatic)
Input energy, (keV/A)	1	1	1
Output energy, (keV/A)	10	4.2	4.2
Bunching	Pre-buncher, 2 cavities	Pre-buncher, 1 cavity	Adiabatic
Mean bore radius, (cm)	1.0	1.37	1.37
Modulation, m	2.1	1.1	1.15
Frequency, (MHz)	25	10	10
Intervane voltage, (kV)	300	140	140
Input phase	-40°	-30°	-40°
Surface field, (MV/m)	~40	14.8	13.3
Transmission, (%)	93	60	92.5
Length, (m)	0.67	4.21	9.35

5. Conclusions

Both design approaches resulted in low-β structures that could not meet the original ISL specifications and, indeed, were pushing the margins of current design (such as peak surface field) even for reduced input specifications (such as mass range). As a result of these studies, it is recommended that (a) the ISL heavy-ion acceleration input specifications be critically examined, and (b) further studies be commissioned to identify possible approaches that could result in a broader mass coverage while

optimizing the transmission and practicality (e.g., overall length) of the low-β stages.

In examining the input specifications, both studies recommended that the input energy be increased as high as feasible, possibly to 2.5 keV/A, and that the input admittance requirement be reduced through improvements in mass separator ion source performance. Every factor of two or so is needed. In addition, it may be required that the full ISL mass range be accommodated by independent low-β sections, each tailored to a portion of the mass range, but later feeding the following stages of the accelerator.

While the issue of superconducting versus room temperature structures was not explicitly addressed in these studies, it is clear that, with the intense electric fields required for even the smaller mass ranges in the designs, the superconducting option must be examined closely, not only for the RFQs, but for succeeding higher-energy structures.

Acknowledgments

This work was performed under the auspices of the U.S. Department of Energy. I am indebted to T. Wangler for a critical review of this report, and, of course, to Peter Ostroumov and to A. Lombardi and A. Pisent for their summaries of analyses and designs produced during their visits.

References

1. "The IsoSpin Laboratory (ISL) - Research Opportunities with Radioactive Nuclear Beams," North American Steering Committee for the IsoSpin Laboratory, Los Alamos report LALP 91-51.
2. I. M. Kapchinskij and V. A. Teplyakov, "Linear Ion Accelerator with Spatially Homogeneous Strong Focusing," Prib. Tekh. Eksp., No. 2, 19 (1970).
3. I. M. Kapchinskij and N. V. Lazerev, "The linear accelerator structures with space-uniform quadrupole focusing," IEEE Trans. Nucl. Sci. NS-24, 3463 (1979).

ION SOURCES FOR THE ISL–PROJECT

P. Van Duppen and M. Huyse
Instituut voor Kern– en Stralingsfysika, K.U.Leuven
Celestijnenlaan 200D, B–3001 Leuven, Belgium

"Over several decades now, ion sources have been used at on–line isotope separator facilities producing radioactive beams of virtually speaking every element from hydrogen to uranium, often with half lives down to a fraction of a second." One might draw the conclusion from such a statement that the problem of ion sources for the Isospin laboratory project is solved. THIS CONCLUSION IS WRONG. It is true that in some cases ion sources having an efficiency as low as 10^{-4}–10^{-5} for a particular short lived isotope, can give the opportunity to perform very interesting studies (e.g. decay studies far off stability). However these catcher-ion-source-systems (CISS) are of limited use for ISL.

In order to obtain reliable yields and to evaluate in what direction R&D is necessary we must consider every element/isotope in detail. We have nowadays a fairly good understanding of low– and medium pressure gaseous discharge ion sources [1], surface-ionization sources [2] and thermoionizing cavities [3] in such a way that we can define what the performances and limitations of these ion sources are. Detailed information on these sources can be found in the literature ([1-2-3], proceedings of the EMIS conferences [4] and review articles [5-6]). For information on laser ion sources, we refer to the contribution of W.B. Fairbank to this workshop. In this contribution we will concentrate on a few topics concerning Electron Cyclotron Resonance (ECR) ion sources.

The first ECR ion source for efficient ionization of trace elements (off–line) in a low–charge state, was developed by Bechthold et al. [7]. A copy of this source is installed at the TISOL facility, where the source is coupled to a thick–target system and various low–energy radioactive beams are produced [8]. A study to couple an ECR source with a He–jet system was initiated in Grenoble [9]. For the Belgian Radioactive Ion Beam facility, we developed a single stage ECR ion source for the

production of energetic radioactive beams of elements like nitrogen, neon, carbon, oxygen,... [10]). Based on the experiments performed with these single–stage, low–charge state ECR ion sources we can draw the following conclusions:

1. High ionization efficiencies (>20%) can be obtained for carbon, nitrogen, oxygen, neon, argon, krypton and xenon in a 1^+ charge state.
2. The ionization efficiency drops when going to higher charge states. Unfortunately only data on some specific charge states are available (e.g. Ne^{+4}: 4%; Ar^{+7}: ~1%; Xe^{+4}: 7%) [11])
3. For the light elements, the 1^+ ionization efficiency depends strongly on the pressure inside the ion source (gas load from the target). This pressure dependence disappears when going to heavier masses. For the higher charge states the pressure dependence becomes more pronounced and persists even for the heavier elements [10-11])
4. An atom that enters the ion source makes a large number of wall collisions before being extracted as an ion. This was shown by delay–time measurements using a calibrated leak filled with nitrogen gas enriched in ^{15}N. When closing the leak, the current at mass 15 dropped to half its original value after more than one hundred seconds. Furthermore the delay time was depending on the partial natural-nitrogen gas pressure in the source, evidencing the existence of an exchange reaction mechanism that released the trapped ^{15}N atoms [10]).

Recently tests were initiated at GANIL to get information on ionization efficiencies of the high–charge state ECR ion sources [12]). These ion sources are used for the production of intense multiply charged stable beams for injection in the GANIL cyclotrons. Ionization efficiencies up to 20% for Ar^{+9} were obtained but again depended strongly on the pressure inside the ion source. Many accelerator–based facilities have similar ECR ion sources for the production of multiply charged ions. Unfortunately, there is only very little information available on i) the ionization efficiencies of trace elements of gaseous as well as metallic species and on ii) the delay times of these sources (number of wall collisions, sticking times).

It is of utmost importance to measure these quantities in detail (preferentially for many different elements) using the existing ECR ion sources before starting a development program for the design and construction of a dedicated ECR source for

ISL. We need to get an understanding of the life of a single atom when it is converted to a highly charged ion in an ECR source. This information will determine to a large extent the choice that has to be made whether one starts from singly or multiply charged ions for the post–accelerator system. A great deal of the necessary information can be obtained from relatively simple measurements using calibrated leaks filled with: i) noble gases to measure the ionization efficiency and the intrinsic delay time of the source and ii) molecular gases from which the atomic components tend to stick to surfaces (like N_2, CO_2, CF_4,..) to measure the ionization efficiency and the delay times for these elements.

References:

1) R. Kirchner, Nucl. Instr. and Meth. B70 (1992) 186

2) B. Vosicki et al., Nucl. Instr. and Meth. 186 (1981) 307

3) R. Kirchner, Nucl. Instr. and Meth. A292 (1990) 203

4) Proceedings of the EMIS conferences: Nucl. Instr. and Meth. 186 (1981), B26 (1987), B70 (1992)

5) H.L. Ravn and B.W. Allardyce, in Treatise on Heavy Ion Science, ed. D.A. Bromley (Plenum Press, New York, 1989) vol. 8 p.363

6) P. Van Duppen et al., Rev. Sc. Instr. 63 (1992) 2381

7) V. Bechthold et al., Proc. of the 7th workshop on ECR ion sources, Jülich (1986) 248

8) L. Buchmann et al., Nucl. Instr. and Meth. B62 (1992) 521

9) G. Gimond et al., Nucl. Instr. and Meth. B70 (1992) 118

10) P. Decrock et al., Nucl. Instr. and Meth. B58 (1992) 252

11) P. Van Duppen et al., Proc. of the "International Workshop on the Physics and Techniques of Secondary Nuclear Beams", Dourdan, France, March 23–25 1992

12) P. Bricault et al., Rev. Sc. Instr. 63 (1992) 2494

A Radioactive Ion Production R & D Program Using a Helium-Jet Coupled Target Ion Source.

J. M. Wouters[1], W. L. Talbert[2], D. J. Vieira[1], and The LAMPF He-Jet Collaboration

[1]Isotope and Nuclear Chemistry Division, Los Alamos National Laboratory, Los Alamos, NM 87545, USA.
[2]Medium Energy Physics Division, Los Alamos National Laboratory, Los Alamos, NM 87545, USA.

Abstract. A brief outline of plans to test a He-jet fed mass separator at the Los Alamos Meson Physics Facility (LAMPF) is described.

1. Introduction

With the encouragement of the ISL users' community, we are planning an R & D program to develop a radioactive beam production technique complementary to the integrated target ion source approach. The primary consideration leading to the decision to undertake such a program is the potential resolution, using a He-jet coupled target ion source, of several known problems with the integrated target ion source system. Among these problems are: (1) the anticipated difficulties in operating an integrated target ion source at 100 μA, (2) the unavailability or slow release properties of nonvolatile elements, and (3) the complication of optimizing ion source operation in a high radiation environment. This article briefly describes several potential advantages of the He-jet coupled target ion source system and presents R & D plans to test such a system at LAMPF.

2. He-Jet Coupled Target Ion Source

Potential benefits of the He-jet coupled target ion source system over an integrated target ion source approach include: (1) short, predictable delay times for most reaction products that are largely element independent, (2) an ion source that is removed from a hostile environment facilitating maintenance and operational optimization, and (3) placement of a simple target system in the primary beam.

In order to highlight one of these areas, Figure 1 shows the fraction of recoils transported versus the half-life of the reaction products for both the He-jet and integrated target ion source systems. The He-jet calculation assumes a transport time, t_c, for the capillary and a sweep out time, t_s, of the target chamber for a reaction product half-life of $t_{1/2}$. Transport of activity from the integrated target ion source system is calculated using a

release time, t_r, where this release time is described by either a straight exponential dependence (Carraz *et al.* 1978) or a release derived from Fick's second diffusion equation (Carraz *et al.* 1979) for a molten or solid target, respectively. The figure shows clearly that for reaction products with slow release times, a He-jet coupled ion source system can be several orders of magnitude more efficient for short-lived reaction products.

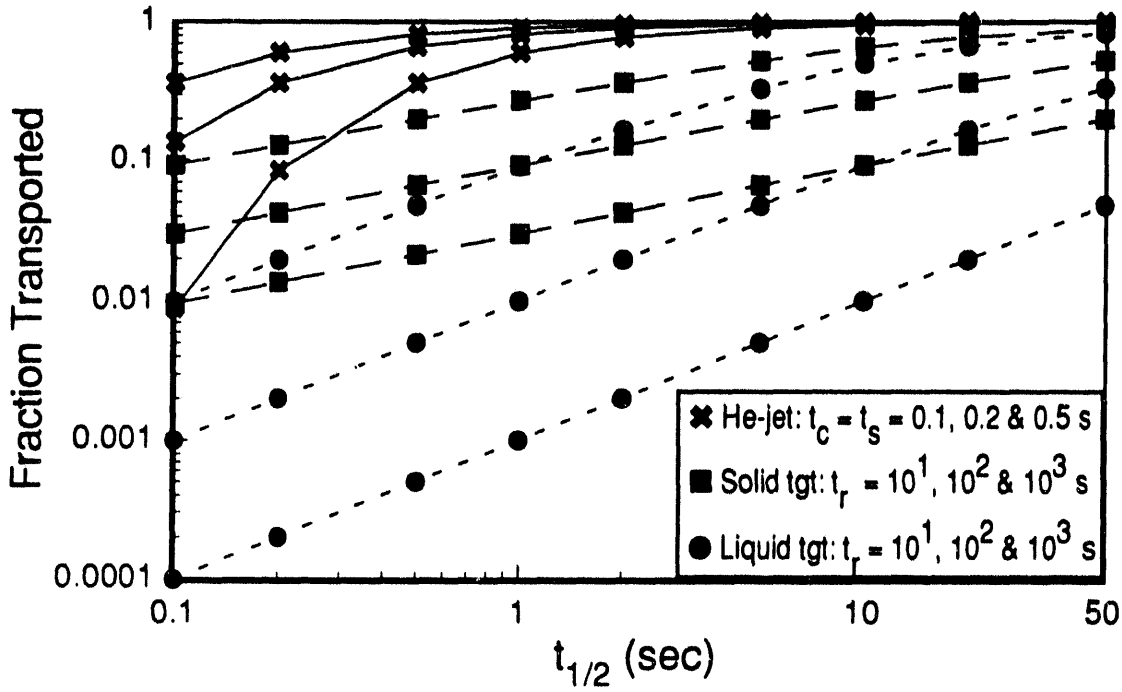

Fig. 1. Fraction of activity transported versus half-life for a He-jet system compared to two types (solid or liquid) of integrated target ion source systems.

3. An R & D Plan for the He-Jet at LAMPF

At LAMPF we are planning an R & D program in which a thin thorium metal or evaporated uranium target (~10 mg/cm^2) will be placed in the primary 1-mA 800-MeV proton beam. The high energy proton-induced fission products recoiling from the target will be collected and transported by a ~20-m long He-jet system to a low radiation area. Plans now are being made to follow a He skimmer chamber with a tape transport system that will be used to move the activity to a β-γ-n coincidence detection station. The yields of selected β-delayed neutron emitters will be determined using their unique decay signature to separate them from the plethora of other activity that is anticipated. Gross γ-ray spectroscopy will also be used to determine the yields of selected less exotic products.

In a subsequent experiment, an ion source and mass separator will follow the He skimmer box to establish yields through the entire target, He-jet, skimmer, ion source, mass separator system. In preparation for this second experiment we are planning an

extensive off-line program to study the coupling properties of a He-jet to an ion source. Our plan is to first efficiently transport and ionize several Cs isotopes as a starting point and then to develop a system for a refractory element that is not presently available with an integrated target ion source system.

Acknowledgments

This work was performed under the auspices of the U.S. Department of Energy. The LAMPF He-Jet Collaboration consists of members from Brookhaven National Laboratory, Los Alamos National Laboratory, Simon Fraser University, Utah State University, University of Giessen, University of Mainz, University of Oslo, Chalmers University of Technology and Oxford University. We are indebted to P. Chamberlin and H. Oona of the Isotope & Nuclear Chemistry Division for several fruitful discussions in preparing this article.

References

Carraz L. C., *et al.* 1978 *Nucl. Instrum. Meth.* **148** 217.
Carraz L. C., *et al.* 1979 *Nucl. Instrum. Meth.* **158** 69.

Section III
Accelerators—Primary and Secondary

J. M. Nitschke, Coordinator

Section III
Invited Papers

THE ROLE OF CYCLOTRONS

AS PRIMARY AND SECONDARY

BEAM ACCELERATORS

Yves Jongen

Ion Beam Applications s.a.
Chemin du Cyclotron, 2
B - 1348 Louvain-la-Neuve
Belgium

1. ABSTRACT

Different kinds of accelerators can meet the specifications of the primary accelerator of the ISL. Among those, positive and negative ion isochronous cyclotrons are more specifically discussed. A fixed field, alternating gradient ring accelerator could represent a new, but still unproven, alternative.

For the secondary accelerator, a high field, superconducting cyclotron could cover the required energy range, provided that a charge to mass ratio of 1/10 is available for the highest energies. The main quality of such a cyclotron would be its flexibility, and the main disadvantage would be a transmission probably smaller than required.

2. INTRODUCTION

Different kinds of accelerators can be considered for the primary and secondary beam acceleration at the ISOSPIN laboratory. Linear accelerators are the subject of another presentation of this session, and will therefore be excluded from this presentation.

Synchrotrons display certainly also some very desirable features in the frame of this subject, and should certainly also be considered as candidates.

However synchrotrons were also excluded from this presentation, mainly because the experience of the author does not extend to those accelerators.

3. THE PRIMARY ACCELERATOR FOR THE ISL : design specifications and technical options.

The design specifications of the ISL are illustrated in Table 1.

Table 1.

		Acceptable	Desirable
primary production source	projectile	P	p,d,^{3}He
	energy	≥500 MeV	~1 GeV
	intensity	~100 μA	≥ 100μA
	beam structure	CW or pulsed	CW

Table 1 : Design specifications for the ISL

while the basic data for protons from 400 MeV to 1 GeV are illustrated in Table 2.

Table 2.

GENERAL DATA								
Kinetic energy	MeV	400	500	600	700	800	900	1000
Total energy	MeV	1338,2	1438,2	1538,2	1638,2	1738,2	1838,2	1938,2
Beta		0,71	0,76	0,79	0,82	0,84	0,86	0,88
Gamma		1,43	1,53	1,64	1,75	1,85	1,96	2,07
Magnetic rigidity	T*m	3,18	3,63	4,06	4,48	4,88	5,27	5,65

Table 2 : Basic physical data for protons from 400 MeV to 1 GeV

The possible options for an accelerator meeting such specifications are :

a. Isochronous cyclotrons using either positive or negative ion acceleration

Similar cyclotrons have been built as meson factories (PSI, Triumf) and have been operating for many years well above 100 μA. The technical risk of such projects is therefore negligible. It should be noted that the present isochronous technology allows the acceleration of beam currents in excess of 1 mA. This current capability is not presently considered as usable in the frame of the ISL concept, and one could therefore object that the cyclotron carries a cost penalty in exchange for a beam current capability which is not really needed by the project.

Very large isochronous cyclotrons are normally built with a fixed field, excluding the possibility of accelerating other particles, or of changing the energy if protons are accelerated (H^- acceleration allows variable extracted energy with a fixed field). Doing such a very large cyclotron with a variable field is theoretically possible, but would probably be very difficult, expensive and would use a significant amount of electrical power in the correction coils.

b. The fixed field, alternating gradient ring accelerator.

This frequency modulated, fixed field ring accelerator with alternating gradient focusing has frequently been described, but has never been built in full-scale version. It represents an interesting, but yet unproven alternative.

c. A fast cycling, high current synchrotron

Such cyclotrons have been built at the Rutherford Appleton Laboratory or at the CERN, and have demonstrated the possibility to meet essentially the ISL specification, except for what concerns the beam structure.

Even so, the CERN ISOLDE experience shows that a very low duty cycle can sometime be advantageous.

d. A high current proton linac

This alternative is probably best represented by LAMF, for which specifications exceed those of the ISL project.

e. Positive ion isochronous cyclotrons

Accelerators of this family in this energy range are probably best exemplified by the ring cyclotron at Paul Scherrer Institute (PSI) in Switzerland. This 590 MeV cyclotron was completed in 1974 and has, since then, reliably supplied intense proton beams for meson production. Beam intensity grew with time, and is currently 300 μA on a daily basis.

The cyclotron R.F. system is currently being upgraded to allow the acceleration of beam currents up to 1 mA. The magnet system consists of eight separated sector magnets. The main coils use 650 kW, stabilized to 5x10-6. The fine tuning of the field is achieved by 18 pairs of trim coils, using 20 kW. The total weight of the steel is 1960 tons, and of the coils 28 tons. The R.F. system includes 4 single gap cavities, each fed by a 200 kW amplifier, ensuring an energy gain of 2.2 MeV/turn. An additional fifth cavity, operating at three times the main R.F. frequency, is used for flat-topping. The beam is injected from a 70 MeV, separated sector injector cyclotron able to provide more than 1 mA of beam with excellent optical properties. The beam is injected in the ring by a combination of electromagnetic and electrostatic channels. Beam extraction is carried by an electrostatic deflector. An excellent turn separation is obtained at extraction thanks to excellent beam optics, a large (2.2 MeV) energy gain per turn, and careful tuning of the cyclotron, resulting in an impressive (99.98%) extraction efficiency. At the end of the construction, in 1974, the cost of the ring cyclotron was estimated at 35 million Swiss Francs.

Based on the experience of the PSI ring cyclotron, some remarks can be made about the use of a similar cyclotron as primary accelerator for the ISL.

- Variable magnetic field and accelerating frequencies would be exceedingly difficult to achieve for such a cyclotron. As a result, both the particle and extraction energy should be fixed.

- Only one beam extraction is provided

- The PSI experience shows that with careful tuning, essentially 100% efficiency can be achieved both for acceleration and extraction, yielding the lowest possible accelerator activation for a given beam current. However, the tuning needed to reach such extraction efficiencies is critical and the machine is not forgiving in terms of tuning and injected beam quality.

- Although in theory, direct acceleration from an ion source is not excluded, actual design considerations (for instance mechanical design of the magnets) favors the use of a separate injector cyclotron.

- The positive ion cyclotron is smaller, lighter and probably altogether cheaper than its negative ion counterpart, especially for higher energies.

- Due to the need for thé highest flutter (to limit the amount of spiralization needed) a zero field in the valleys is desirable. Also, a larger turn separation at extraction is achieved if the average field is lower. Finally, with an optimized coil design, the magnet power in such a cyclotron can be reduced to a fraction of the total beam power. For those three considerations, it is the author's opinion that the use of superconducting coils is rather unattractive for such cyclotrons.

We have evaluated some key parameters of positive ion cyclotrons used as primary accelerators for the ISL as a function of the extracted beam energy.

Table 3.

POSITIVE ION CYCLOTRON								
Kinetic energy	MeV	400	500	600	700	800	900	1000
H+ Spiral angle for Qz=0.3	deg.	44	48	52	54	57	59	61
H+ average field (extr.)	T	1	1	1	1	1	1	1
H+ average field (centr.)	T	0,7	0,65	0,61	0,57	0,54	0,51	0,48
H+ extr. av. radius	m	3,18	3,63	4,06	4,48	4,88	5,27	5,65
H+ pole radius	m	3,38	3,83	4,26	4,68	5,08	5,47	5,85
H+ frequency	Mhz	10,61	9,87	9,23	8,66	8,17	7,72	7,32
H+ weight	Tons	1005	1465	2015	2659	3404	4253	5214
R.F. power	kW	636	721	801	879	955	1028	1100
Cost estimate	M$	24,66	29,41	35	41,45	48,84	57,22	66,63

Table 3. : Some key parameters of positive ion cyclotrons used as primary beam accelerators for the ISL as a function of beam energy.

The cost estimates in Table 3. are expressed in 1992 $US, and are based on an empirical formula developed by the author fitting various elements of the production costs of cyclotrons ranging from 10 to 30 MeV. The formula is therefore used very far from its established validity range and should be used with extreme caution. Those costs include direct costs related to the accelerator and related subsystems, including the manpower, but exclude overheads or contingencies.

f. Negative ion isochronous cyclotrons

Accelerators of this family are best illustrated by the large cyclotron at TRIUMF (Vancouver, Canada). This 520 MeV cyclotron was also completed in 1974 and has also, since then, supplied reliably intense proton beams for meson production. After several years of improvement, the beam intensity reaches now currently 150 μA, and plans are underway to boost the intensity to 350 μA and to achieve negative ion extraction without stripping to inject the beam in a system of synchrotrons to be used as a kaon factory.

The magnet is probably the world's largest cyclotron magnet, and is made of 4 large (radius = 7.8 m), low field, separated magnets with a common pair of circular coils. The gap is very large (52cm) resulting in a relatively large coil power : 1270 kW, with a stability of 2x10-7. 55 pairs of circular coils are used to fine-turn the field isochronism and use 68 kW.

The accelerating system uses a single accelerating gap, operated at the fifth harmonic of the orbital frequency.

Two sets of dee plates on the lower side, and two on the upper side are made of separated panels and are fed by a total RF power of 1100 kW to achieve a maximum dee to ground voltage of 85 kV.

The beam is injected axially at the center of the cyclotron by an electrostatic inflector. The external ion source is biased at 300 kV D.C. and the injected beam is transported to the cyclotron center by a 40 m beam line.

The beam is extracted by stripping the H^- ions into protons. Multiple extracted beams at different energies and with variable intensity ratios can be obtained and are actually routinely used.

The beauty of the extraction by stripping is that the efficiency is inherently 100%, even if the beam quality or the turn separation is less than perfect.

The H^- cyclotron is therefore a more forgiving machine in terms of beam optical quality. However, there is a price to pay for this easier extraction. In a negative ion cyclotron, some beam losses by stripping are always encountered during the acceleration process. This stripping is caused by interactions with the residual gas in the cyclotron vacuum tank. Another form of stripping is also present at higher energies : a negative ion is loosely bound and can be dissociated by an extremely strong electric field. The equivalent of such a field results from the combination of the velocity of the ion and the magnetic field (Lorentz force). As a result, only a very low magnetic field can be used to bend high energy negative ions, resulting in cyclotrons of extremely large size.

Even so, in a practical high energy negative ion cyclotron, the amount of beam lost by stripping can hardly be reduced to less than 1–5% of the beam intensity, resulting in a significant machine activation.

The construction cost of the Triumf cyclotron was estimated at 12 M Can $ in 1974. It is not clear, however, that any clear conclusion can be drawn from the comparison of this figure with the budget estimated for the P.S.I. ring cyclotron completed approximately at the same time, because the accounting methods are probably not similar on both projects.

The experience of the Triumf machine can be used to make some general remarks about a negative ion isochronous cyclotron used as primary accelerator for the ISL.

- In such a large cyclotron, practical reasons dictate a fixed magnetic field and a fixed frequency. Acceleration is therefore restricted to a single particle (normally H^-).However, thanks to the stripping extraction, variable energy extraction is possible, as well as multiple extractions at different energies and currents.

- The cyclotron is easier to tune than a positive ion machine, less critical and less demanding in terms of injected beam optical quality.

- However, a significant amount of beam losses is unavoidable during acceleration, leading on the long term to a significant activation of the machine.

- Low energy injection is possible, suppressing the need of an injector cyclotron.

- Electromagnetic stripping requires the use of lower and lower magnetic fields with increasing energy. As a result, such a cyclotron tends to become very large, heavy and expensive, especially at higher energies.

- Due to the low field requirements, superconductivity seems unattractive for a high energy, negative ion isochronous cyclotron.

We have evaluated in Table 4 some of the key parameters of negative ion cyclotrons used as primary accelerators for the ISL, as a function of the maximum beam energy. The remarks and restrictions about the validity of the cost estimations of Table 3 apply obviously here.

Table 4.

NEGATIVE ION CYCLOTRON								
Kinetic energy	MeV	400	500	600	700	800	900	1000
H- Spiral angle for Qz=0.3	deg.	56	60	63	65	67	69	70
H- hill field	T	0,66	0,58	0,52	0,47	0,43	0,4	0,37
H- average field (extr.)	T	0,53	0,46	0,42	0,38	0,35	0,32	0,3
H- average field (centr.)	T	0,37	0,3	0,25	0,22	0,19	0,16	0,14
H- extr. av. radius	m	6	7,83	9,79	11,88	14,11	16,46	18,95
H- pole radius	m	6,2	7,83	9,79	11,88	14,11	16,46	18,95
H- frequency	Mhz	5,62	4,58	3,83	3,26	2,82	2,47	2,18
H- flux / sector	Weber	9,08	12,32	16,78	21,92	27,76	34,33	41,66
Sector return srf. @ 1.8T	sq. m	5,05	6,84	9,32	12,18	15,42	19,07	23,15
Sector ax. width at R max	m	5,2	6,56	8,2	9,96	11,82	13,8	15,88
Return rad. width	m	0,97	1,04	1,14	1,22	1,3	1,38	1,46
H- weight	Tons	2363	3724	5889	8801	12605	17465	23562
R.F. power	kW	977	1233	1542	1872	2223	2594	2986
Cost estimate	M$	25,32	32,21	42,78	56,65	74,47	96,97	124,92

Table 4.: Key parameters of negative ion isochronous cyclotrons used as primary accelerators for the ISL as a function of maximum beam energy.

To illustrate the very large size of negative ion cyclotrons, Fig. 1 shows the conceptual view of the magnet of a 600 MeV, negative ion cyclotron.

Figure 1.

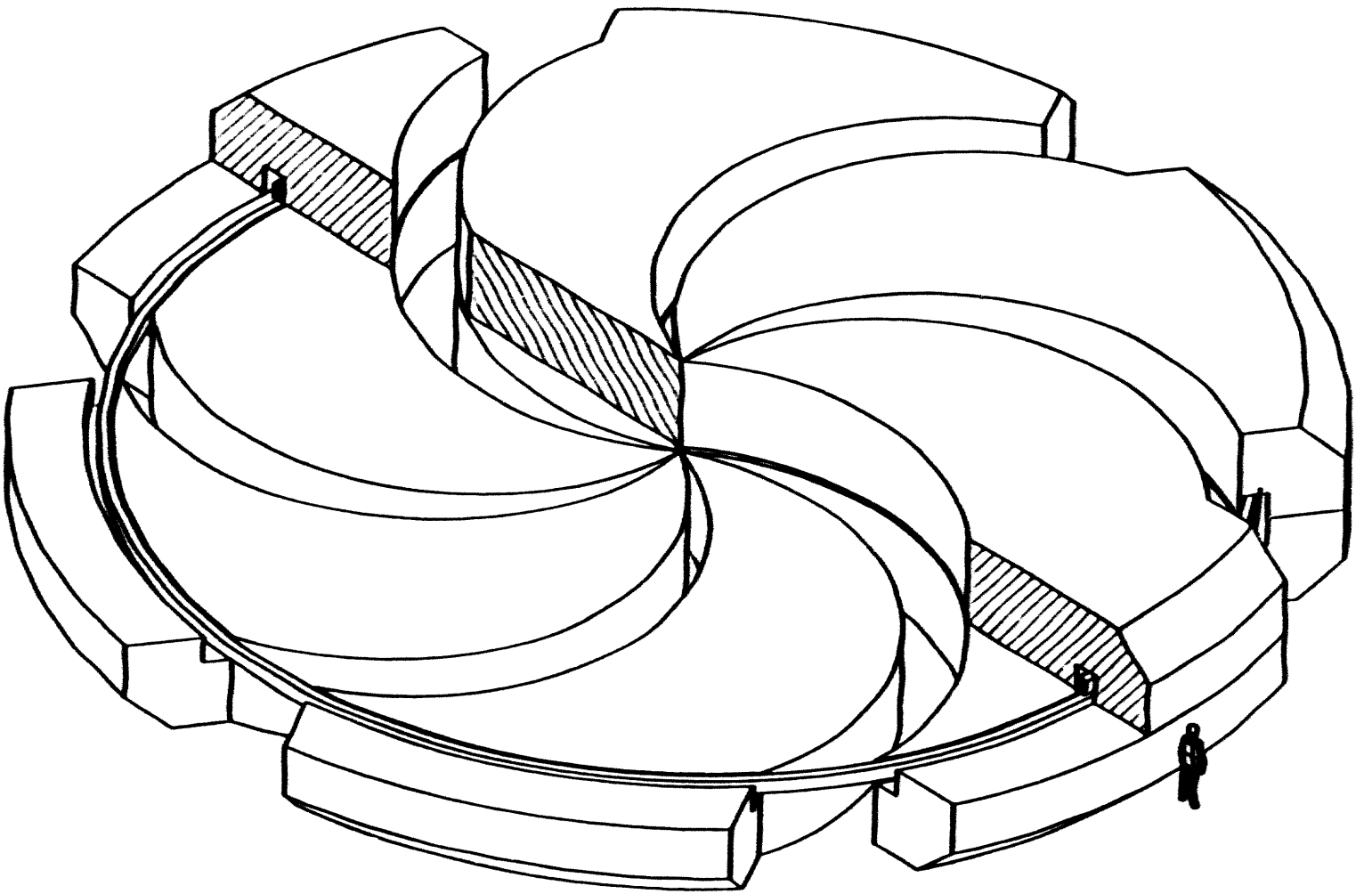

Figure 1 : **Conceptual view of the magnet of a 600 MeV, negative ion isochronous cyclotron. The human figure is indicating the scale.**

g. The FFAG.

The fixed field, alternating gradient ring accelerator could represent a new, alternative technical option for the primary accelerator of the ISL. The FFAG can be described as a ring accelerator where the field is fixed and the frequency is modulated to track the increase in orbital frequency of the ions from injection to extraction. The axial focusing is obtained, like in an isochronous cyclotron, by azimuthally alternating high and low field regions, and by spiralling the field boundaries. In order to reduce the radial extent of the ring, the injection and extraction trajectories are much closer than what they would be in an isochronous ring cyclotron. As a result, the field rises strongly with radius, and the revolution frequency of the ions increases with increasing energy. The acceleration system is therefore frequency modulated, and uses the phase focusing principle, as used in the synchrocyclotron. However, unlike the classical synchrocyclotron, the phase stable region is the rising part of the sinewave.

In order to stay away from dangerous resonances the betatron frequencies, Q_R and Q_Z remain quite fixed into a safe region during acceleration, either by keeping the flutter and the spiral angle constant (this requires, then, variable gap magnets) or, if fixed gap magnets are preferred, by matching the flutter and the spiral angle to obtain quite constant axial focusing.

The table 5 illustrates possible parameters for a conceptual FFAG that would accelerate protons from 100 MeV up to an energy of 1 GeV.

TABLE 5.

F.F.A.G.			
		INJECT.	*EXTRAC.*
Kinetic energy	MeV	100	1000
Total energy	MeV	1038,2	1938,2
Beta		0,43	0,88
Gamma		1,11	2,07
Magnetic rigidity	T*m	1,48	5,65
Radius	m	4,65	5,65
Average field	T	0,32	1
Field index		5,85	5,85
Hill to valley azim. ratio		0,32	1
Flutter		2,63	0,25
Spiral angle for Qz = 4.15	deg.	65	82
Approx. Qr		2,63	2,63
Orbital freq.	Mhz	4,4	7,4
Total weight	Tons	570	
R.F. power	kW	400	
Cost estimate	M$	15,28	

Table 5 : Proposed parameters for a conceptual 1 GeV FFAG.

The magnet described in Table 5 is illustrated in Figure 2.

Figure 2.
FFAG with separated magnets.

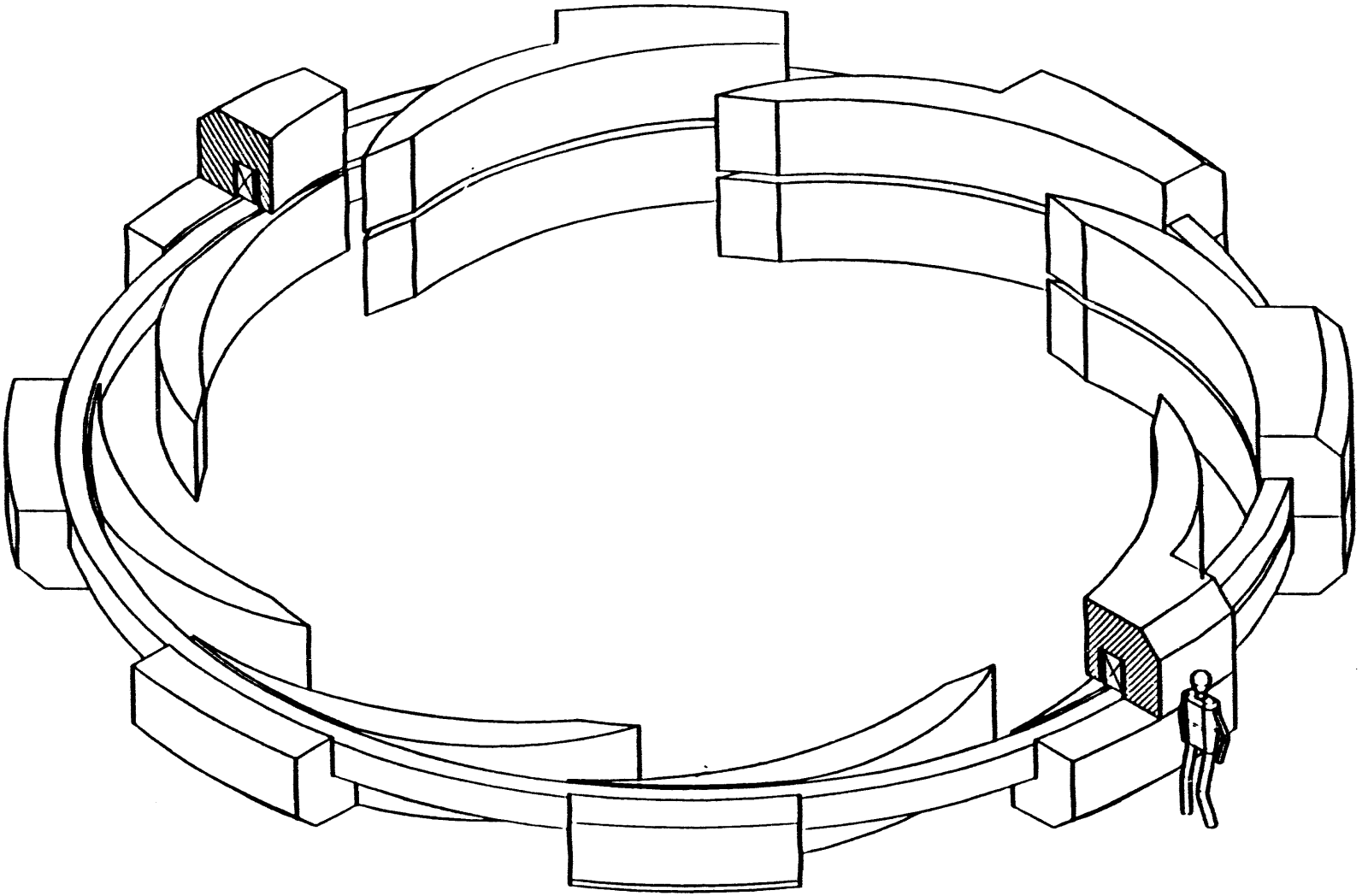

Figure 2 : **Conceptual view of the FFAG magnet described in Table 5. The scale is indicated by the human figure.**

The repetition rate of such an accelerator is dictated by the available accelerating voltage. A repetition frequency of 1000 hz would require a total acceleration voltage of 300 kV. Such a total accelerating voltage per turn represents an interesting challenge for a frequency modulated system, but could be achieved by the use of multiple cavities.

In that case, an average current of 100 μA corresponds to 6×10^{11} protons per pulse.

The circulating current at 1 GeV would be 730 mA and, if we assume a phase bucket of 60°, the peak beam current in the bucket would be 4.4 A. While this may sound like an extremely high current, specially for a low emittance beam, one can remark that the space charge forces associated with such a beam at 1 GeV are actually smaller than in a 5mA beam at 30 KeV (this last value is routinely used in the injection system of H^- cyclotrons) and the expected space charge induced tune shift would be negligible. One could however suspect that other kinds of collective effects similar to beam break up instabilities could appear.

In such an accelerator, a 10% time window in the cycle could be obtained for injection by providing a small isochronous region at the inner radius of the ring. By this way, the injected beam could clear the injection septum and be stored and accumulated on an orbit located a few centimeters outside the injection radius.

The injected beam could be provided by a separate isochronous cyclotron, providing pulses of 1 mA at 100 MeV. Approximately 500 turns storage would be necessary in the FFAG before starting the FM acceleration.

The extraction at 1 GeV could be achieved in a single turn mode using kicker magnets. Alternatively, one could think of a slow extraction using a still undefined resonance scheme.

Compared to an isochronous cyclotron, the advantage of such a FFAG would be the following :

- Due to the smaller radial extent of the magnet, the weight and the cost of the FFAG can be much lower than for an isochronous cyclotron of similar energy.

- The magnet tuning is less critical.

- The field being non isochronous, the acceleration of other light ions like deuterons, alpha particles, $^3H_e^{2+}$ could be possible with an appropriate modification of the frequency program.

The disadvantages of the FFAG, compared to an isochronous cyclotron are :

- The acceleration is cyclic, and not C.W.. The intensity is therefore lower than in an isochronous cyclotron, but larger than in a conventional synchrocyclotron., thanks to the larger injection energy. An average intensity of 100 μA seems feasible from space charge considerations.

- Unless a slow extraction method is devised, the extracted beam duty cycle would be very low, with a repetition rate of 100–1000 hz.

- The R.F. system, having to achieve a wide frequency sweep with a high energy gain per turn represents a significant technical challenge.

- The injection and extraction systems have never been studied in detail and are probably more complex than in an isochronous cyclotron. However, the provision of an isochronous region at injection seems possible and the extraction methods developed for synchrotrons (either fast or slow) should apply also here.

- Last but not least, no "full scale" FFAG was ever built, but only electron models (Midwestern Universities Research Association - MURA. at the University of Wisconsin at Madison).

h. The cyclotron as secondary accelerator for the ISL.

The specifications of the post-accelerator for the ISL are summarized in Table 6.

TABLE 6.

Design specifications for the ISL

	Acceptable	Desirable
Energy range	0.2 to 10 MeV/amu	
Energy resolution	<1%	<0.1%
Mass Range	1 to 240	
Z Range	1 to 96	
Transmission (not including stripping)	≥ 80%	≥ 90%
Intensity (at peak of observed mass distribution)	≤ 10^{11} part./s	≤ 10^{12}/part./s
RNB Production Luminosity	≃ 4 x 10^{38}(s^{-1} cm^{-2})	>4 x 10^{38}($s^{-1}cm^{-2}$)
Emittance (normalized)	~1 π.mm.mrad	< 1 π.mm.mrad

Table 6 : Design specifications for the ISL post accelerator.

Here again, different acceleration options can be considered :

- A C.W. linac (probably superconducting), or a combination of linacs separated by strippers, would probably offer the best possible transmission, and a very high beam quality. However, the flexibility required by the project may be more difficult to achieve.

- A small synchrotron is probably a very flexible and very light accelerator. However, due to the very long path stripping losses would probably be unacceptable. Also the short duty cycle of a synchrotron at injection does not match the essentially continuous nature of the radioactive ion beam source, and some kind of storage device would be needed to make the synchrotron usable in this case.

- The isochronous cyclotron is probably the most attractive accelerator in terms of flexibility : the magnetic field, the accelerating frequency and the harmonic number can be varied in order to match a wide range of experimental needs. The very large magnetic rigidities required by the heaviest beams indicate that a superconducting cyclotron would probably be desirable. However, the global beam transmissions achieved in today's superconducting cyclotron do not meet the ISL specifications. Lower field, separated sector cyclotrons as used at GANIL (France) have achieved higher transmission. There is however no physical basis preventing high field superconducting cyclotrons to achieve very high beam transmissions.

The maximum energy achievable for a given cyclotron magnet size is given by the following formula :

$$(E/m) = 47.94\ (B\rho)^2\ (Q/m)^2$$

E/m in MeV/amu

Bρ in Tesla-meter

the term $47.94\ (B\rho)^2$ is called the K-factor of the cyclotron magnet and is expressed in MeV.

The largest superconducting cyclotrons built today have a K-factor of 1200 MeV, corresponding to a magnetic rigidity of 5 T-m.

If such a cyclotron was built as a post accelerator, a Q/m of 1/10 would be needed to reach 10 MeV/amu.

Another important formula in a cyclotron relates the orbital frequency of the ions to the magnetic field :

$$f_{Mhz} = 15.26\ Q/m\ B_{Tesla}$$

Using those formulas, we can build the operating diagram of the proposed cyclotron.

Figure 3.

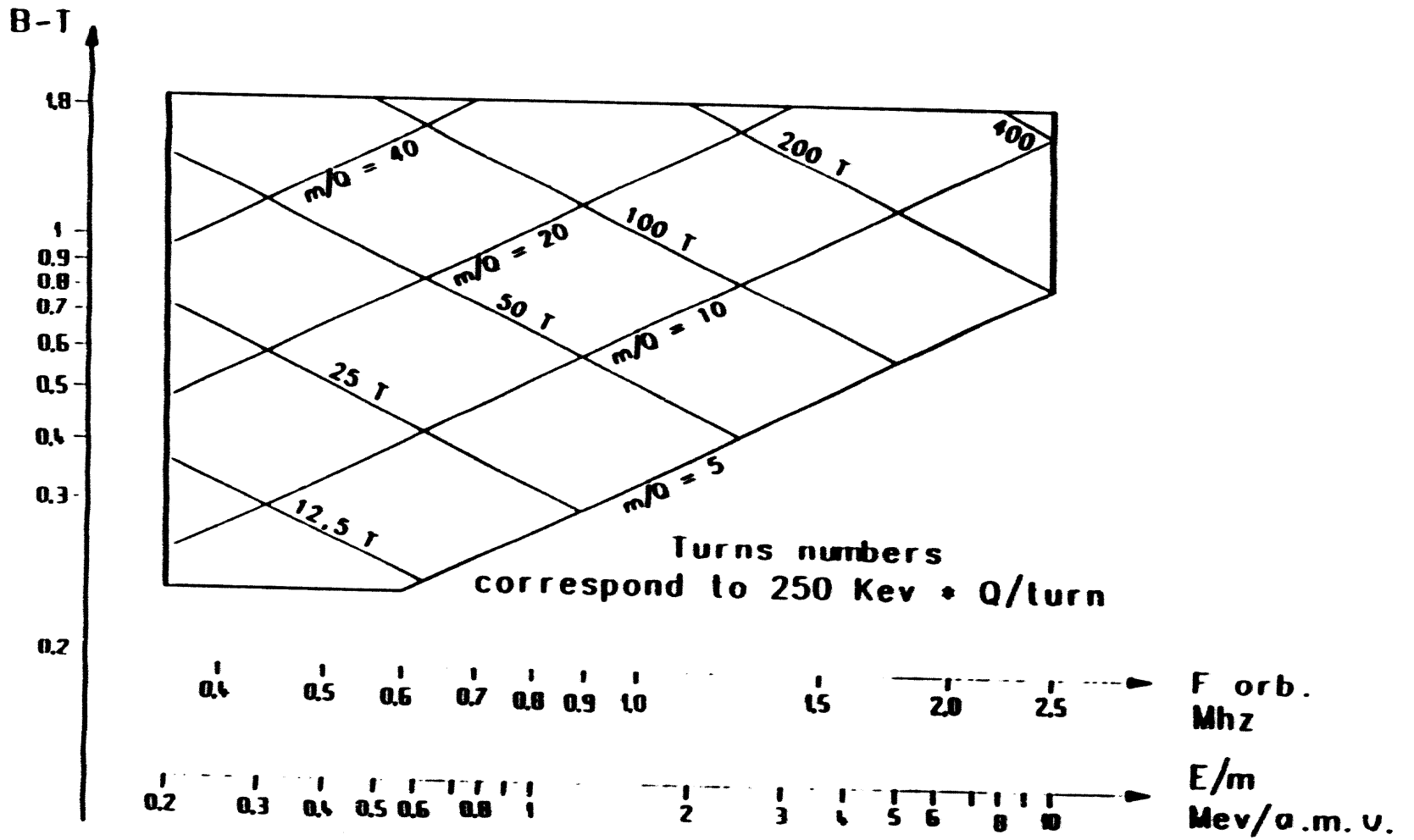

Figure 3 : **Operating diagram of a potential isochronous cyclotron with extraction radius = 3 m used as post-accelerator.**

SOME ASPECTS OF LINACS AS APPLIED TO THE ISL BENCHMARK FACILITY

K. W. SHEPARD
Argonne National Laboratory, Argonne, Illinois 60439

Introduction

This paper considers several aspects of using linacs in a radioactive beam facility in terms of the Isospin Laboratory (ISL) Benchmark Facility (BMF) plan, described in the 1991 white paper for a possible radioactive-beam laboratory [1]. The BMF is outlined schematically in Fig. 1. The intention is not to review comprehensively the application of linacs to an ISL facility, but to compare in outline form several linac options for such a facility. Particular emphasis is given to the use of superconducting rf technology for the secondary beam accelerator.

In what follows, first a possible normally-conducting light-ion linac for a primary beam accelerator is briefly outlined. Then the performance and cost of two options for a secondary beam accelerator are compared: a recent design for a normal-conducting cw linac, and an ATLAS-type superconducting linac. Finally, some of the problems which may be encountered at the entrance of a secondary beam linac are discussed.

I have included cost estimates with some reluctance and only because it is impossible to compare technical options without some discussion of costs. Although an effort has been made to indicate the sources and assumptions underlying cost estimates, please note that any costs mentioned must be considered as 'ball-park' numbers useful for only the most rudimentary planning. Even for elements of the BMF which can be modeled on existing linacs, cost comparisons between different institutions can be difficult to make. Cost estimates for elements based on untested designs or future technical development are necessarily highly speculative.

Primary Beam Linac

As has been pointed out elsewhere at this workshop [2], one option for a primary beam for ISL would be to use a 200 MV linac designed for a charge to mass ratio of 1/2. Such a linac would permit the use of a variety of fully stripped light ions (H_2^{1+}, $^2H^+$,..., N) for a spallation source. The particular linac discussed would deliver 100 MeV per nucleon ions at a 2% duty factor and a pulse rate of 100 Hz, and provide 100 KW of beam power. An ion linac of this size, or larger machines providing substantially more voltage, is commercially available at a cost of roughly 10¢ per volt for the linac itself, including rf and vacuum systems, but not including the ion source or building and utility costs [3]. Such a linac could also be used as the injector for a 500 - 1000 MeV proton synchrotron for a higher energy spallation source as discussed in the BMF plan.

Another possible option for the primary beam option could be a superconducting linac. The most nearly comparable existing machine may be the CEBAF electron linac, for

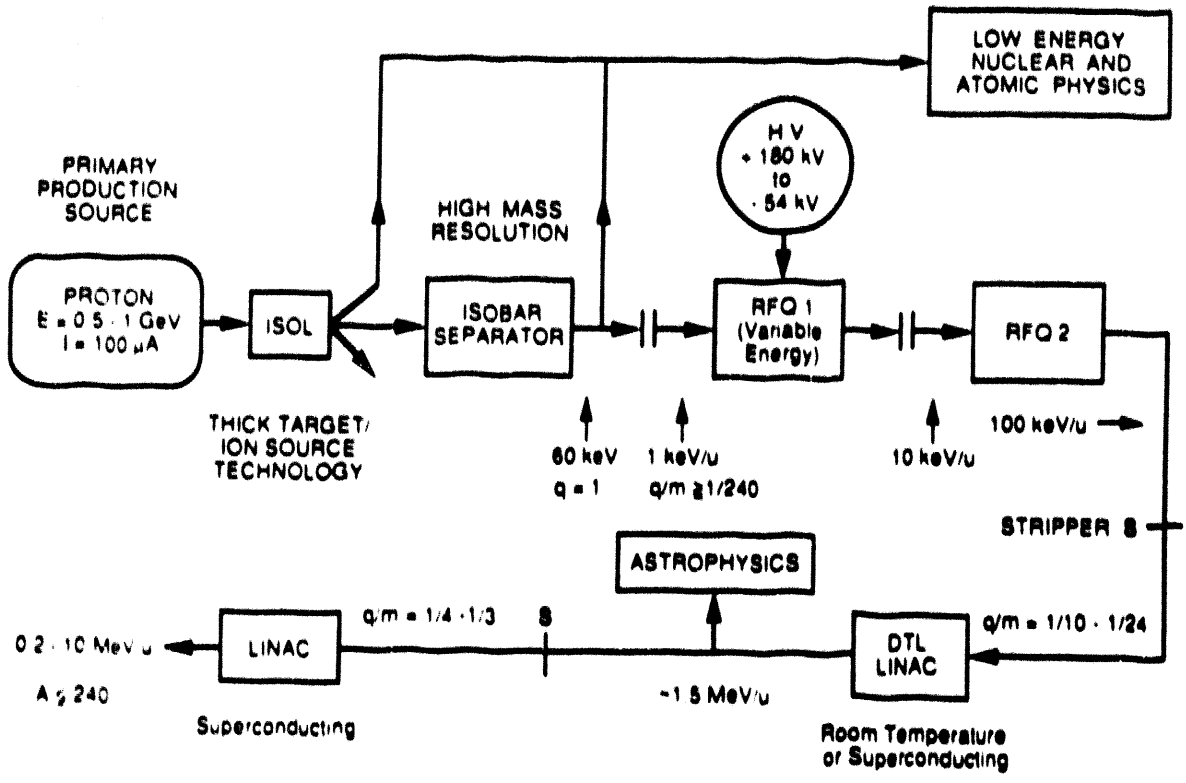

Fig. 1. Schematic diagram of the Benchmark Facility (BMF) discussed in reference [1] as a possible realization of the ISL.

which current construction costs are also roughly 10¢ per volt [4], assuming an operating gradient of 5 MV/m. Although no large superconducting proton linac has yet been built, accelerating structures for the necessary velocity range have been developed and show excellent performance in single-resonator tests [5]. If CEBAF or similar facilities prove able to operate at accelerating gradients substantially in excess of 5 MV/m, then the superconducting option for a primary beam accelerator could become advantageous.

Secondary Beam Accelerator

The secondary beam accelerator defined for the benchmark facility is straightforward after the first stripping. We will refer to this portion of the machine, with energy greater than 100 keV/u, as the secondary beam linac. For the linac, several options currently exist which can more or less satisfy the specifications [1]. More difficult problems are presented by the initial section of the secondary accelerator. We will refer to this portion, where energy less than 100 keV/u, as the secondary beam injector. The difficulties with designing the injector result primarily from requiring at the same time a normalized transverse acceptance of up to 1 $\pi \cdot$ mm $\cdot$ mrad, charge state as low as 1/238, and a final beam energy spread $\delta E/E \leq 10^{-3}$ or better [1].

We proceed by starting with the less speculative portion of the machine and compare two options for the secondary linac: an ATLAS-type superconducting linac [6] and a recent

design for a room-temperature, normally-conducting linac based on interdigital H-type accelerating structures [7].

Superconducting Linac

The high effective shunt impedance of superconducting low-velocity accelerating structures not only provides for cost-effective cw linac operation, but also enables design options which can provide exceptional beam quality and operational flexibility. Since the cavity geometry is not so strongly constrained by the need to minimize rf losses, for heavy-ion linacs the following design choices are typical:

1. Drift-tubes of large aperture provide exceptional transverse acceptance and excellent transmission.

2. Very short resonant cavities can be used, which intrinsically provide broad velocity acceptance (typically a factor of two range in velocity). By operating such short cavities in

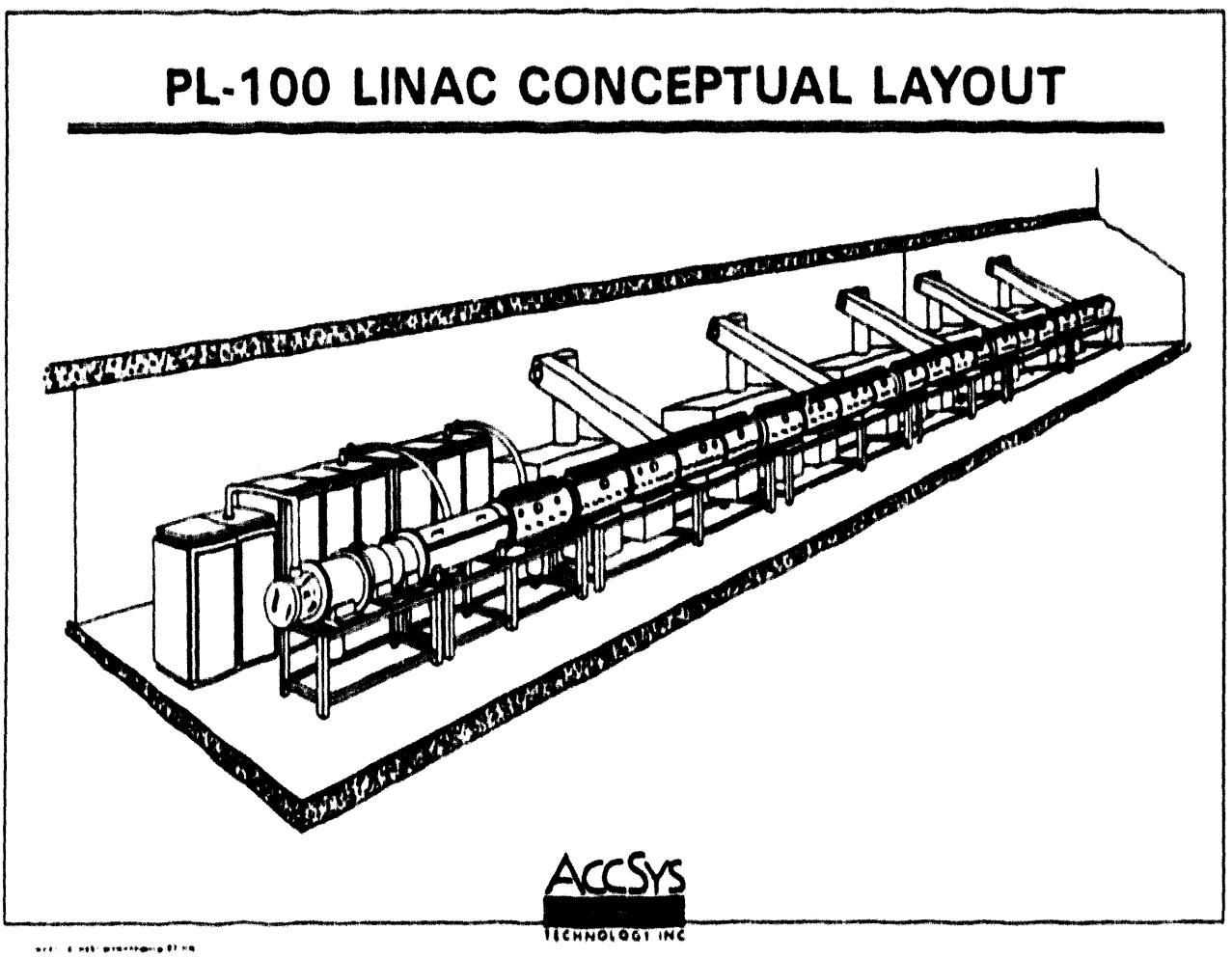

Fig. 2. Linacs suitable for a light-ion primary beam are commercially available. Shown is the layout of a 100 MV proton linac (courtesy of AccSys Inc.).

an independently phased array, one gains operational flexibility not only in being able to vary the linac velocity profile, but, more generally, in achieving a high degree of control over longitudinal phase space which, as is discussed below, has enabled heavy-ion beams of unprecedented quality.

In what follows, we take as representative of SC linacs the ATLAS accelerator which is typical of the technology and is the largest of the several superconducting heavy-ion linacs currently in operation [8]. ATLAS is presently configured to accelerate ions as heavy as uranium ($Q/A \approx 1/10$) from energies of 35 keV/u to 6 MeV/u and above: ATLAS could be used without modification as the BMF secondary beam linac from 35 keV/u on.

Normally-conducting IH-structure Linac

For a normally-conducting linac for radioactive beams, the most attractive option at this time seems to be a linac based on IH-structures [9]. The design discussed here is based on very high shunt-impedance structures recently developed specifically for radioactive beam application [7]. In particular, effort was devoted to obtaining a capability for cw operation and good transverse acceptance. The velocity ranges used in Table I below in fact correspond to the 5 different IH-structures developed by the Moscow group [7].

Comparison of Linac Parameters and Performance

Table I shows some basic parameters of the two linac designs, each evaluated at several different particle velocities. Linear accelerators being modular and extendable in fairly small increments, we normalize all parameters to the amount of linac required to produce a given amount, 1 MV, of effective accelerating potential. This enables, for example, scaling the linac design to accommodate different charge states.

Table 1A - Some parameters for the ATLAS superconducting ion linac [6, 10]. See text for details.

Velocity / c	.016	.024	.050	.086	.110
rf frequency	48.5 MHz	48.5	97	97	97
Length / MV	64 cm/MV	62	69	62	62
Power / MV *	13.5 KW/MV	9.5	11.5	7.6	7.6
Cost / MV	390 K$/MV	290	240	180	180

*Based on the ATLAS refrigeration efficiency of roughly 1 KW per watt: an up-to-date system could nearly double the efficiency, reducing the power requirement shown by nearly a factor of two.

The parameters shown are as follows:

rf frequency - operating frequency of the accelerating structure, not the bunch frequency which is usually a sub-harmonic

Length / MV - 'real estate' length of linac required to produce 1 MV of effective accelerating potential: a particle of charge Q gains energy $\delta E = Q \cdot 1$ MeV in traversing this length.

Power / MV - total 'wall-plug' electrical power required to operate the above 1 MV length of linac.

Cost / MV - equipment cost for the linac equipment only, including cryogenic refrigeration, rf, and vacuum systems, but not including any building or utility costs, or any elements preceding or following the linac proper. See further discussion below.

For the superconducting linac, the cost figures are based on construction experience with ATLAS, normalized to 1985 dollars. Costs for the IH linac designed by the Moscow group are more difficult to estimate. The cost figures shown are those given by H. Klein and R. Muller in 1985 for a similar IH linac design [11], and presumably reflects the construction experience at Munich and GSI.

Table 1B - Some parameters for normally-conducting ion linac based on IH structures [7, 11]. See text for an explanation of the cost estimates.

Velocity / c	.016	.024	.050	.086	.110
rf frequency	27 MHz	27	54	108	108
Length / MV	74 cm/MV	100	59	58	63
Power / MV	5.7 KW/MV	13.9	15.2	16.7	17.7
Cost / MV	-	210 K$/MV	210	-	-

A striking feature of the above tables is how similar in cost, length, and operating power the two very different technical options are. Performance characteristics, however, as discussed below, favor the superconducting option.

Output Beam Characteristics

Although the published requirements for the BMF specify only the energy resolution of the secondary beam, for many experiments the longitudinal emittance, or time-energy spread is a more important parameter. At ATLAS, where time-of-flight techniques have proven to be an important tool, the longitudinal emittance has been measured to be in the range 10 to 20 $\pi \cdot$ keV $\cdot$ nsec for a number of different beams [6]. Such beam quality will be hard to produce in a normally-conducting linac. For the IH linac designed by the Moscow

group, data given in reference [7] imply substantially larger values of longitudinal emittance, perhaps as great as 400 $\pi \cdot keV \cdot nsec$.

For the superconducting linacs, output energy can be varied easily and continuously with no degradation of beam. In an IH-structure linac, output energy can be varied by reducing the rf level in the final structure, in general the beam emittance would in general be substantially degraded in this technique.

Secondary Beam Injector

The desired specifications for an ISL secondary beam include:

Energy resolution	0.1%
Charge / Mass down to	1/240
Emittance (normalized)	$1\ \pi \cdot mm \cdot mrad$

Several designs have been presented for an RFQ injection section [7, 12] designed for Q/A of 1/60. A recent design also appears to provide the desired (very large) transverse acceptance [7]. CW operation, however, remains to be demonstrated for these designs, which are pushing state-of-the-art for cw field level.

Although very high rf electric field gradients have been obtained in tests of short superconducting RFQ structures [13], application of this technology to a BMF injector would not be straightforward. This is because the requirement of large transverse acceptance dictates a large beam aperture for the injector. This in turn forces the use of a low rf frequency to obtain an efficient accelerating structure. A fundamental problem with superconducting accelerating structures, particularly for heavy-ion applications, is maintaining sufficient structural rigidity to enable rf phase control in the presence of microphonic-induced phase noise [14]. At the present time, 50 MHz seems to be the lower limit of frequency for phase-controllable superconducting structures [14, 15], probably too high a frequency for a superconducting RFQ injector structure which can satisfy all the previously mentioned requirements.

Given the difficulty of producing sufficient electric field in an RFQ structure, it is surprising that all the designs presented to date include an adiabatic bunching section (producing no acceleration) that occupies as much as half the RFQ structure. Use of a separate bunching system to directly inject a more efficient RFQ might prove an attractive design choice for the following reasons:

1. Several existing systems use gridded-gap or double-drift bunching systems that can bunch more than 80% of the entrance dc beam and which have proven to be straightforward to use and cost-effective.

2. A properly designed gridded gap or double drift bunching system will produce substantially better (smaller) longitudinal emittance than an RFQ adiabatic bunching section.

3. With a separate bunching system, the bunch frequency can be chosen independently of the accelerating structure frequency or can even be varied for different beams and applications.

Conclusions

A variety of proven linac options exist for a primary beam linac, and for more than 90% of any secondary beam linac for an ISL facility. For the secondary beam, a superconducting linac presently offers the best beam quality, energy variability, and flexibility in terms both of system operation and upgrade options. Normally-conducting IH-structures at the present time probably provide lower costs at very low velocities (say below 250 keV/u).

The most problematic area is the secondary beam injector. At present, a low-frequency RFQ section seems to be the best choice and several designs for such RFQ sections have been published. However no design has even come close to meeting all the desired goals for the ISL BMF, nor is likely to in the immediate future. To facilitate machine development in this area, it would be helpful to more clearly establish requirements and tradeoffs concerning the various beam parameters. The following are suggested:

1. The ISL Design Specification should include a goal for longitudinal emittance of the secondary beam, and not just energy resolution, as is now the case. If time-of-flight techniques are to be available at ISL, then a longitudinal emittance below, say, 40 $\pi \cdot$keV$\cdot\cdot$ nsec would be desirable.

2. For design of the secondary beam injector, it would be helpful if guidelines were developed for the tradeoff required between transverse acceptance and initial charge state. Possibly more than one injector section might be desirable for ISL, to handle the various and sometimes conflicting requirements.

References

1. "The IsoSpin Laboratory (ISL), Research Opportunities with Radioactive Nuclear Beams", prepared by the North American Steering Committee for the IsoSpin Laboratory, copies available from Richard Casten, Physics Department, Brookhaven National Laboratory, Upton, N.Y. (1991).

2. J. Nolen, in this workshop - a schematic layout of such a linac is included in the summary by M. Nitschke in these proceedings.

3. R. Hamm, AccSys Technology Inc., 1177-A Quarry Lane, Pleasanton CA 94566.

4. R. Sundelin, private communication.

5. J. R. Delayen, et al., Proc. 1992 Linear Accelerator Conference, August 24-28, 1992, Ottawa, Ontario, AECL-10728, p695 (1992).

6. R. Pardo, et al., Proc 1992 Linear Accelerator Conference, August 24-28, 1992, Ottawa, Ontario, AECL-10728, p70 (1992).

7. S. K. Esin, et al., Proc 1992 Linear Accelerator Conference, August 24-28, 1992, Ottawa, Ontario, AECL-10728, p808 (1992).

8. L. M. Bollinger, Proc. 1992 Linear Accelerator Conference, August 24-28, 1992, Ottawa, Ontario, AECL-10728, p13 (1992).

9. U. Ratzinger, Proc. 1990 Linear Accelerator Conference, September 10-14, 1990, Albuquerque, New Mexico, LA-12003-C, p525 (1991).

10. K. W. Shepard, IEEE Trans. Nucl. Sci. NS-28, p3248 (1981).

11. H. Klein, et al., Proc. of the Accelerated Radioactive Beams Workshop, September 5-7, 1985, Parksville, Canada, TRI-85-1, p174 (1985).

12. H. R. Schneider, et al., Proc. of the Accelerated Radioactive Beams Workshop, September 5-7, 1985, Parksville, Canada, TRI-85-1, p189 (1985).

13. J. R. Delayen and K. W. Shepard, Appl. Phys. Lett. 57, p514 (1990).

14. N. Added, et al., Proc. 1992 Linear Accelerator Conference, August 24-28, 1992, Ottawa, Ontario, AECL-10728, p181 (1992).

15. P. Paul, in this workshop.

Section III
Report from Discussion Group

Section III

Report from Discussion Group on Accelerators—Primary and Secondary

J. M. Nitschke

Introduction

The ISL White Paper (WP) offers many options in the choice of primary and secondary accelerators, and existing facilities (such as ISIS, PSI, LAMPF, TRIUMF, ATLAS, ISOLDE, and Louvain) can serve as models in selecting a configuration. With the Benchmark Facility of the WP as a starting point, the ISL concept has now been expanded in several ways, some of which are shown in Fig. 1.

Three target stations are desired to ensure uninterrupted RNB delivery and the use of a variety of targets and ion sources:

- The first target station could be dedicated to conventional targets and ion sources similar to those used at ISOLDE.
- The second station could house both laser- and surface ion sources because they are mechanically similar.
- The third station could be designed specifically for targets coupled to ECR sources.

In addition, two separators are foreseen: (1) a general-purpose separator (GPS) for the ECR source operating at a constant E/μ of 10 keV/μ and (2) a high-resolution separator (HRS) for the first two stations operating with a constant ion energy of ~100 keV. The first RFQ would only be needed for the HRS branch to boost the energy from 1 or 2 keV/μ to ~10 keV/μ.

Primary Accelerator

Insights were sought on the operating and capital costs associated with different approaches to producing the primary beam (i.e., different kinds of cyclotrons, synchrotrons, and LINACs).

A 600-MeV sector-focused cyclotron for protons (about 10 m in diameter with an internal ion source and a total RF power of about 300 kW) costs about $35 million

without the infrastructure. The operating cost was estimated to be $4 to 5 million. This cost is about an order of magnitude less than, for example, LAMPF; however, a newer LINAC design could reduce the operating cost significantly. There did not seem to be much difference in price between normal-conducting and superconducting LINACs. Based on CEBAF cavities, costs of ~0.1 $/V were quoted, which would bring the price of a 600-MeV LINAC to $60 million.

The costs for a fixed-field alternating-gradient (FFAG) machine and a rapid-cycling synchrotron need to be looked at. Blosser suggested considering a K = 1200 cyclotron to produce a primary beam of 600-MeV deuterons.

No conclusions were arrived at for a preferred approach, and no requirement was set for variable energy although the opinion was voiced that the primary-beam current must be variable between 1 and 100 μA. The primary accelerator should be located at a site that has experience with the selected type of device.

The optimal primary-beam energy was discussed. The ISOLDE group has claimed that, for certain nuclei far from stability, an order of magnitude increase in yield can be expected when going from 600 to 1000 MeV in the primary-proton-beam energy. If cost were not an issue, the optimal proton energy would probably be ~1.5 GeV.

Little attention has previously been paid to the required beam quality of the primary beam. However, calculations have shown that it will be difficult to cool the center region of the target, and it has been suggested that a *hollow* primary beam be used. It can be produced from a conventional beam with quasi-Gaussian intensity distribution through the use of a "wobbler." This scheme requires a good transverse primary beam emittance of only a few π mm-mradians. No particularly stringent requirements are needed for the longitudinal emittance. A hollow beam would also have other advantages, as discussed in Section II.

The macroscopic duty factor of the primary beam can have a strong effect on the design of the front end of the postaccelerator. Extreme duty factors (i.e., ~10^{-6} at the Booster-ISOLDE at CERN) require pulsed-extraction power supplies for the ion source(s). Intermediate duty factors typical for fast-cycling synchrotrons, FFAGs, or pulsed LINACs invite further studies. The least complications are anticipated with a continuous wave (CW) beam structure.

The role of light ions as primary beams was discussed. A 10-pμA ^{12}C beam of 100 MeV/μ was said to be equivalent to a 100-μA proton beam at 500 MeV. However, it should be borne in mind that any comparison of protons and light ions as primary beams must depend on the nuclide being produced. Light-ion intensities were pointed out to be, in general, one or two orders of magnitude lower than proton beams, and the power densities in many target and window materials may exceed present technological limits.

Secondary Accelerator

The characteristics of the ion sources, in particular the q/A ratio of the produced ions, have a profound effect on the design of the postaccelerator. ECR sources are presently the only contender for the efficient production of highly charged ions.

The consideration of ECRs started with a discussion about the emittances (ECR emittances between a few tens and 800 π mm-mradians have been quoted) and included statements that the performance of ECRs has not been well characterized. ECRs, therefore, have great potential for R&D. Using ECRs for volatile products was suggested because it would allow isolating the target from the intense radiation by a transfer line from the target through shielding.

Purportedly, ATLAS now injects at a q/A of 0.1, and GANIL is basing its RNB project on $q/A = 0.15$ for $A \equiv 100$; if such high q/A ratios can be achieved routinely and efficiently, the first RFQ can be bypassed. For the second RFQ, the problem of high emittance can be handled more easily (see below).

Beam Purity

The question of beam purity was addressed in some detail. The most extreme demand came from astrophysics with impurity levels of $<10^{-5}$, for example in the case of ^{19}F.

Beam purity is affected by several machine parameters: primary beam characteristics, target matrix and temperature, selective ionization (including photoionization by lasers), chemical processes in the target and ion source (i.e., the formation of chemical compounds), physical and chemical separation steps (i.e., condensation and fractionation), electromagnetic analysis, stripping, and more. To obtain the required beam purity, several of these processes will have to be employed concurrently.

Shortly after the workshop, a new idea for additional beam purification was proposed by M. Nitschke. In that concept, a gas-filled separator would be used to obtain Z selection within a chain of isobars that previously had been separated by a conventional isotope separator. The basic idea is that the mean magnetic rigidity of an ion moving in a magnetic field is given approximately by $B\rho = \text{const.}\ A\ Z^{-1/3}$. It follows that the relative change in bending radius is related to the relative difference in Z via $\delta\rho/\rho = -0.33\ \delta Z/Z$. A gas-filled separator could, for example, be installed in one the stripper regions where ion energies are 1 to 2 MeV/μ. Whether the unavoidable emittance deteriorations introduced by the gas and the windows can be tolerated must be investigated.

RFQs

Two types of accelerators were considered for postacceleration—RFQs and cyclotrons.

If ECR sources with high metal efficiency ($^{238}U^{30+}$) can be developed, a cyclotron with K = 600, with no stripping, producing 10 MeV/μ U^{30+} or 50 MeV/μ O^{5+}, and with single-turn extraction for good beam quality might be an attractive solution for post-acceleration.

Conversely, RFQs and LINACs have been used successfully for the efficient acceleration of heavy ions in the past. However, RFQ focusing requirements make it difficult to achieve large acceptances for low ion velocities and low q/A ratios. Specifically, with present technologies, $^{238}U^{1+}$ at 1 keV/μ probably could not be focused in the first RFQ.

H. Schneider pointed out that, with B as the focusing coefficient for an alternating gradient field, the Matthieu equation defines the stability regime:

$$B = \frac{q\lambda^2 XV}{Mc^2 a^2} = \frac{q}{Mc^2}\lambda^2 \frac{V}{r_0^2} \quad .$$

If $q/\mu c^2$ is too low, B will be lessened and will have to be compensated for with increased V and λ. A B of less than about 3 will be underfocusing; and a B in the region of 4 to 8 would be desirable. Thus, reasonable designs should aim at B = 4, but not below. A V must be chosen that is as high as possible (~2 x Kilpatrick); at 25 MHz, it can go to 13 MV/m. As a point of reference, RFQ1 at Chalk River National Laboratory is designed for 1.8 Kilpatrick. Frequencies as low as 10 MHz may have to be considered.

Using an RFQ with no modulation was suggested for focusing the beam.

It was also suggested that a 10-T superconducting solenoid could be used for focusing, but it would take a big developmental step to do that in practice. Clearly, the RFQ was identified as needing a major R&D effort.

To achieve a constant input velocity (e.g., 2 keV/μ) for the fist RFQ, it has to be put on a high-voltage platform (e.g., 380 kV). Also, a rod-structure RFQ with rods floating on HV potential was suggested. Superconducting structures could also be put on a HV platform. The liquid-helium transfer may present a problem; however, CRYEBIS, for example, has a liquid-helium system going up to more than 100 kV. H. Schneider from TRIUMF discussed how high voltage could be put on the vanes of an RFQ. H. Wollnik and R. Moore suggested floating all or parts of the mass separators and keeping the target at ground potential. This would simplify many design problems in the high-radiation

field near the target. The efficacy of putting the RFQ on a HV platform was debated because RFQ focusing is independent of injection velocity. Clearly, details of the potential distributions along the front end of the ISL complex have to be looked at further.

W. Talbert reported on a study at LAMPF of an initial LINAC stage for the ISL by P. Ostroumov, A. Lombardi, and A. Pisent. They concluded that a factor of 2 or 3 in input energy (2 to 3 keV/μ) and a reduction in the transverse acceptance specifications would help a lot. The LANL study also indicates that a mass range of 6 to 240 is extreme and that different front ends may be needed for different mass ranges. Their feeling is that the maximum q/A that can be accomplished at this time is probably 1/60. Going beyond this value would require R&D and new technology. Some would say that even 1/60 is pushing the technology too far and may not work. Japanese researchers have evidently achieved 1/30, yielding 1.5 MeV/μ for ^{238}U and 5.0 MeV/μ for a mass of 80.

Another point of concern was the duty factor (DF) that can be achieved with RFQs. Chalk River has an operating CW RFQ. The Japanese group has a split-coax RFQ that is expected to operate at 30% DF for q/A = 1/30 and an energy gain from 2 to 170 keV/μ. TRIUMF has an RFQ design for q/A = 1/60 and an energy gain of 0.8 to 60 keV/μ operating at 25 Mhz. There was general agreement that it will be difficult to find an RFQ design that simultaneously satisfies the demands for CW operation, low input velocity, low q/A, and reasonable acceptance. The latter point also has to be addressed from the ion-source side, where reduced emittances would benefit the entire postaccelerator design. P. Paul discussed the design of superconducting RFQs, which would inherently have a 100% duty factor.

After the Workshop, we learned from A. Schempp about the development of a room-temperature "spiral RFQ" at Gesellschaft für Schwerionen Forschung for Xe^{1+}. It has an energy gain of 2.4 to 20 keV/μ and is claimed to be able to operate in the CW mode. The prototype is 4 m long and operates at 27 Mhz.

Substituting a cyclotron for the RFQ and the high-resolution spectrometer would combine the function of the mass separator and the accelerator. H. Blosser estimated that a K = 600 cyclotron would be required.

LINACs

Superconducting LINACs would be possible above 100 keV/μ. Such devices have very good energy resolution, but need development efforts for lower energies. To make use of the excellent energy resolution, it might be worthwhile considering whether a

LINAC could be used for isobaric mass selection when combined with a high-resolution spectrometer.

A weak point in the previous ISL Benchmark Facility was intensity losses caused by stripping. For very heavy ions, these can amount to more than an order of magnitude. The concept of a "charge state enforcer" presented by F. Selph and G. Loebner could greatly reduce such losses.

The next point in the discussion dealt with longitudinal emittances of post-accelerating structures. For example, at ATLAS, because the longitudinal beam emittance is very good (3 to 10 π keV-ns), the experimenters should be polled to see what the requirements for the ISL are. It seems that tens of keV-ns at $\Delta E/E = 10^{-4}$ are achievable.

RFQs can provide 50 to 60 keV-ns, which was reported for a design by P. Ostroumov, Moscow. However, the adiabatic bunching in an RFQ does not conserve longitudinal phase space. Independent bunching might be a solution because it would allow selecting independent bunching properties (frequency, for example).

It was stressed at several occasions that the transmission through all ion-optical devices has to be as high as possible (typically >90%) to avoid beam losses and radioactive contamination.

I.-Y. Lee reported on the use of a storage ring for RNBs. For beam currents of $\leq 10^6$/s, internal target experiments will give higher luminosities than single-pass experiments because of multiple target traversals. Considering the many attractive features of storage rings, their potential for the ISL should be further explored. The Europeans apparently have built a 10-MeV/μ storage ring for as little as $750,000.

Beam Parameters

The energy desired for the postaccelerator encompasses energies appropriate for experiments in astrophysics through the coulomb barrier and beyond. Some participants argued for energies up to 100 MeV/μ. It was, however, pointed out that this overlaps the range in which projectile-fragmentation facilities operate successfully, and a more modest energy vs mass profile emerged in the discussions:

30 MeV/μ up to A = 60
20 MeV/μ up to A = 150
10 MeV/μ up to A = 240

LINACs can always be added to. If a lower-energy LINAC were installed at the beginning, it could be upgraded at a later date to accommodate a higher range of energy to meet experimental needs. However, some argued that one should aim for ~30 MeV/μ right from the beginning.

An energy resolution of less than 0.1% would be needed for reactions of 10 MeV/A or greater. For several other experiments, 1% would be sufficient. The astrophysicists would like an absolute energy resolution of ≤ 15 keV and an energy-calibration accuracy of 1 to 2 keV.

Several experiments were proposed for heavy RNBs, confirming that the mass range needs to go up to A ≈ 240.

Much attention was paid to the actual execution of experiments and the required beam-spot sizes, divergences, and beam halos. This translates into the need for transverse emittances less than (and perhaps very much less than) 1 π mm-mradian. To manipulate the longitudinal emittance, a buncher/debuncher at the exit of the postaccelerator may be obligatory. The elimination of beam halos demands further study. Two kinds of beam structures are desired, CW for coincidence experiments and 100-ns micropulse spacing for time-of-flight studies.

After discussing many technical details, the general observation was made that, compared to conventional heavy ion accelerators, the ISL will require greatly increased reliability of all of its components because of its complexity.

Figure 1. ISL front end (particle flow and acceleration diagram).

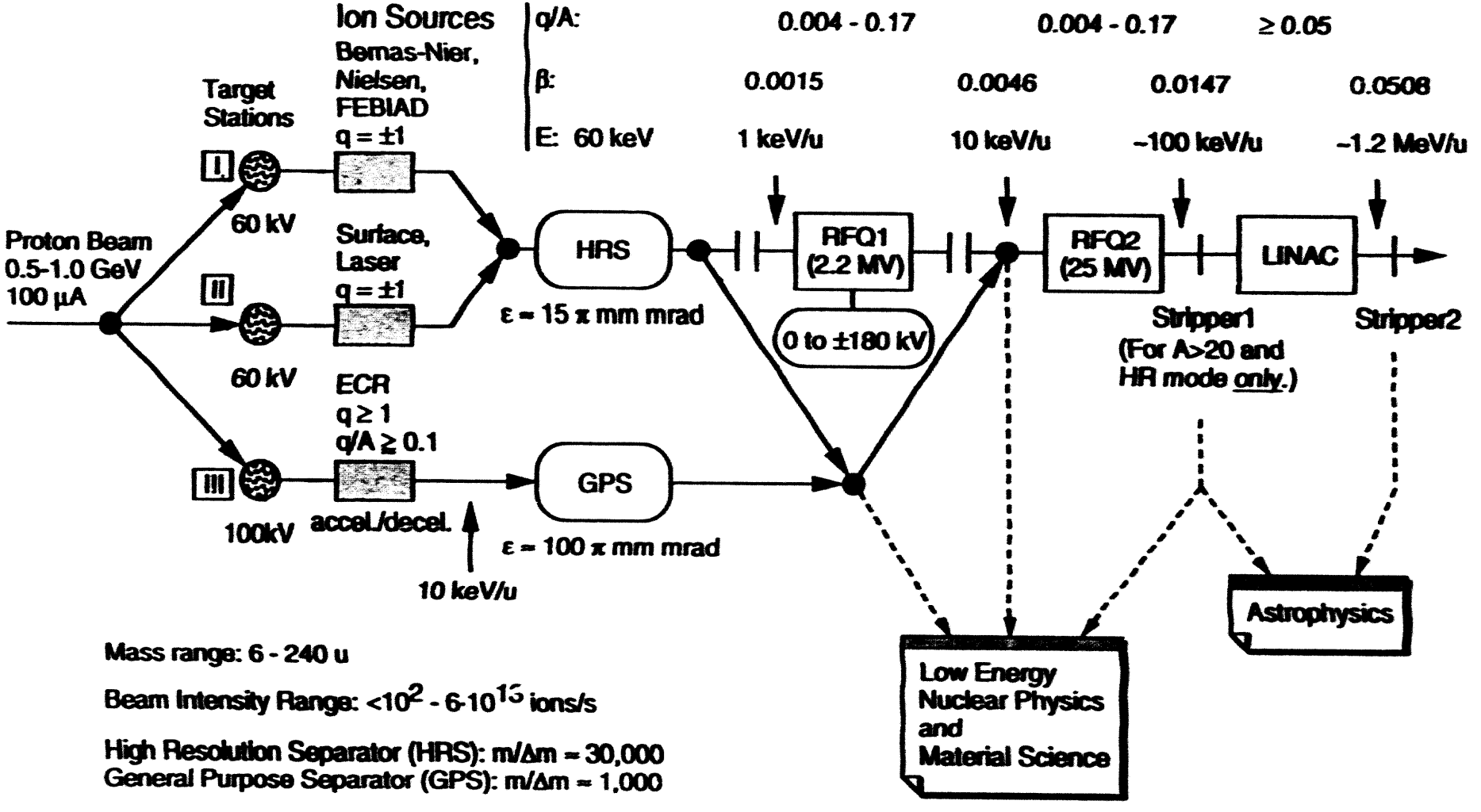

Section III
Contributed Papers

The "Charge State Enforcer" Revisited

K.E.G. Löbner
Sektion Physik, Universität München, 8046 Garching, Germany,
and Los Alamos National Laboratory, Los Alamos, NM 87547, USA

1. General concept of the charge state enforcer

For higher acceleration efficiency the acceleration of heavy ions to higher energies >1 MeV/u is usually done in 2 (or more) steps. In the second (and higher) acceleration step a high charge state is used. The problem is that the stripping process yields not just one charge state but a spectrum of charge states. However, since only ions of one charge state can usually be accelerated, this corresponds to a considerable loss of intensity which is especially bad for radioactive ion beams, where the intensities are very low to begin with.

The general idea of the "charge state enforcer" first proposed by John G. Cramer [1] is the following: Ions with low charge state ($Q_{start} = 1$) of intermediate energy (e.g. 0.1 or 1 MeV/u) strike a thin stripper foil (C-foil ≥ 3 $\mu g/cm^2$) yielding a spectrum of charge states (equilibrium charge state distribution). Particles of one charge state ($Q_{sel}>Q_{start}$) are selected and sent to the next acceleration step. Ions with other charge states ($Q=Q_{sel}$) are forced to recirculate back to the stripper foil and the stripping and subsequent selection process is repeated again and again until "nearly all" particles have the wanted charge state and are sent on to the next acceleration step.

This idea has been published by J.G. Cramer [1] and later by Franzke et al. [2] and V.P. Kukhtin et al. [3], but to my knowledge such a system has not been built.

Very recently the equilibrium charge state distributions of ions with Z=4 to Z=92 emerging from a carbon foil have been published by Shima et al. [4]. According to this compilation one has the following situation: For light ions e.g. ^{16}O approximately 50% of the ions are found in the most abundant charge state for E/u = 0.02 to 3 MeV/u. But for heavier ions the situation is much worse. Already for Br-isotopes only 22 % of the ions are in the most abundant charge state for E/u = 0.01 to 3 MeV/u. And for all heavier species (Zr to U) only approximately 20 % of the ions are to be found in the most abundant charge state for E/u = 0.01 to 3 MeV/u. This means one loses ≈ 80 % of the original heavy ion intensity with one stripping process and ≈ 96 % with two stripping processes. These high intensity losses lead one to think about ways of decreasing these losses. One possibility is the above mentioned charge state enforcer.

II. Distinguishing two problems

For the realization of a charge state enforcer one has to distinguish two problems:

1.) The physical difficulties causing the degradation of the beam quality due to
   a) energy straggling and energy losses in the stripper
   b) small angle scattering in the stripper
2.) Technical difficulties associated with selecting the ions of wanted charge state Q_{sel}.

In this contribution only the physical difficulties are discussed, whereas a possible technical realization addressing the second problem is discussed by Frank Selph in his contribution.

III. Physical difficulties with carbon-foil stripper

a) Energy losses in 3 $\mu g/cm^2$ C-foils

A medium mass nucleus $^{132}_{54}Xe$ with an energy of 1 MeV/u (dE/dx = Bragg maximum) loses in a 3 $\mu g/cm^2$ carbon foil (which is necessary to reach the maximum intensity of the most abundant charge state for heavy ions)

E_{loss} = 0.224 MeV according to Northcliffe-Schilling [5] and

E_{loss} = 0.212 MeV according to Ziegler [6]

(E_{loss} is of course less for lighter ions and higher for heavier ions).

Since the relative fraction of ions with Q_{sel} after N turns is $\eta(N,\varepsilon) = 1 - (1-\varepsilon)^N$

with ε=fraction of ions in most abundant charge state (with equilibrium charge state distribution) one obtains with ε=0.2 and N=7: η = 0.790 and energy differences of the ions (depending how often they have passed the stripper foil) of 1.26 MeV.

This energy loss is less at 0.1 MeV/u. For ^{132}Xe and carbon stripper foil 3 $\mu g/cm^2$

E_{loss} = 0.068 MeV according to Northcliffe-Schilling and

E_{loss} = 0.110 MeV according to Ziegler.

This is also very high. This yields for 7 turns an energy difference of 0.66 MeV (according to Ziegler).

A possible solution to this problem (already discussed by Franzke et al. [2]) may be the acceleration of the circulating ions in the ring [2] to compensate after each turn for the average energy loss in the stripper foil. To achieve this for all ions, the ions with different charge states must pass the high frequency acceleration gap at certain phase points of the high frequency, which should be possible in principle (see [2]). This should also reduce the energy spread of the ions due to energy straggling and foil thickness nonuniformities. How well this can be achieved should be calculated quantitatively.

b) **Small angle scattering in 3 $\mu g/cm^2$ C-foils**

For 1 MeV/u ^{132}Xe ions passing a 3 $\mu g/cm^2$ carbon foil, a half-width angle $\alpha_{1/2}$ due to multiple scattering is calculated to be: $\alpha_{1/2}$ = 0.12 mrad or $\alpha_{1/2}$ = 0.10 mrad according to Sigmund and Winterbon [7] using the Thomas-Fermi or Lenz-Jensen screening potential, respectively. For 0.1MeV/u ^{132}Xe ions $\alpha_{1/2}$ = 1.13 or 0.95 mrad are obtained for one pass of the C-foil, respectively.

It should be pointed out that the multiple scattering distributions have longer tails than Gaussian distributions (see fig. 5 of Sigmund and Winterbon), and depending on the actual situation such small angle multiple scattering may yield a considerable transmission loss (cf. e.g. Dollinger and Maier-Komor [8]).

IV. Physical difficulties with a gas stripper

A gas stripper has the following advantages in comparison to a foil stripper:

(1) Gas strippers can be very thin

(2) There are no problems with irradiation damage, lifetime, thickness changes of the stripper over time.

However, there is also one main disadvantage of gas strippers in comparison to foil strippers: The mean charge states are lower, for heavy ions ≈50 % lower than for solid material.

Until now mainly N_2-gas has been used as stripper gas. For N_2-gas and C-foils the stopping power (dE/dx) and the small angle scattering are very similar, only a reduced thickness of the gas stripper could help to decrease the energy loss and the small angle scattering.

How low one can go in thickness of the gas stripper is not well known, since the gas thicknesses to obtain equilibrium charge state distribution are not well determined. In principle one could use a very thin gas stripper which is below the equilibrium condition, but then the energy straggling can be expected to be relatively high, since the energy loss depends on the effective charge state of the ions.

V. Conclusions

In addition to the realization problems for the selection of ions with one charge state (which is certainly not simple and cheap) the introduction of the charge state enforcer yields a high degradation of the beam quality. For 1 MeV/u heavy ions the energy loss is the main problem which may be compensated by appropriate acceleration of the ions with charge states $Q \neq Q_{sel}$ for each turn.

For 0.1 MeV/u heavy ions, both the variation in energy loss and small angle scattering are expected to yield problems.

With a thin gas stripper the realization of a recirculating stripper system may be possible. However, it is certainly necessary to investigate the whole acceleration process and how the transmission is influenced by the degradation of the beam quality caused by the charge state enforcer and whether the pulsed beam structure behind the charge state enforcer can be properly accepted by the following acceleration steps.

It should also be investigated whether it would be possible (and simpler) to send the other charge states back to the ion source or the "target", in front of the ion source to increase the intensity of the radioactive ion beam, if the half-life of the specific isotope is long enough.

Acknowledgement

I would like to thank David J. Vieira for suggesting that I look into this problem and for valuable discussions. The author also expresses thanks to the TOFI group at LAMPF for their hospitality and to the Isotope and Nuclear Chemistry Division, Los Alamos National Laboratory for financial support.

References

[1] J.G. Cramer, NIM 130 (1975) 121
[2] B. Franzke, K. Blasche, B. Franczak, GSI-J-1-78, p. 157
[3] V.P. Kukhtin, Yu.P. Savergin, I.A. Shukeilo, Particle Accelerator Conference 1991, San Francisco, IEEE 91 CH 3038-7, p. 2035
[4] K. Shima, N. Kuno, M. Yamanouchi, H. Tawara, Atomic Data and Nuclear Data Tables 51 (1992) 173
[5] L.C. Northcliffe, R.F. Schilling, Nuclear Data Tables A7 (1970) 233
[6] J.F. Ziegler, Stopping Cross-Sections for Energetic Ions in All Elements, Pergamon Press, 1980
[7] P. Sigmund, K.B. Winterbon, NIM 119 (1974) 541
[8] G. Dollinger, P. Maier-Komor, NIM A282 (1989) 153

Storage Rings at ISL

D. M. Moltz
Lawrence Berkeley Laboratory

The idea of using a storage ring to perform many of the proposed physics experiments at Isospin Laboratory is extremely meritorious. The physics list is a subset of the ideas presented in many meetings and symposia. These ideas include reaction dynamics, high-spin gamma-ray studies, atomic physics, nuclear astrophysics, production of exotic nuclei, and atomic mass measurements. Except for this last experiment, operation of the ring would be in a traditional manner (a brief explanation of the alternative operation is given below). The technology necessary to construct such a ring exists and could easily be built and tested at a current low-energy physics installation. The primary drawback to such a system is the high cost of such an accelerator. The scientific payback, however, is large. The primary advantage is that large luminosities can be had for relatively low primary beam intensities. Of course this feature presupposes an internal cold-cluster gas target (these exist essentially as off-the-shelf commercial items) is installed in the ring. By utilizing particle or gamma-ray detector arrays around the target position, one can perform essentially all of the normal reaction and high-spin measurements. The ring also has an often overlooked advantage necessary for these measurements- it spreads the enormous background from the beam radioactive decay products over an enormous area, thereby significantly reducing the gamma background below what could ever be achieved for the same luminosity in a fixed target experiment.

Utilization of this storage ring as a mass measuring device would require its operation at the transition energy (the point where the flight path is the same for all mass particles within an isobar). This point is, however, an unstable operating condition. Thus the number of orbits which can be achieved is unknown. Since the mass determination is made via a simple time-of-flight measurement, increasing the number of orbits increases the mass precision which would be achievable. It is important to note that although the precision of this type of mass measurement cannot compete with that obtained via Penning traps, the long cooling and purification times limit this technique to activities with half-lives > 1 second. Thus the proposed method would be preferred near the drip lines.

Magnetic Ring for Stripping Enhancement

Frank Selph
Lawrence Berkeley Laboratory
University of California
Berkeley, CA 94720

Introduction.

A ring designed to recycle ions through a stripping medium offers the possibility for increasing output of the desired charge state by up to 4x. This could be a very important component of a Radioactive Nuclear Beam Facility. In order for such a ring to work effectively it must satisfy certain design conditions. These include achromaticity at the stripper, a dispersed region for an extraction magnet, and a number of first and higher order optics constraints which are necessary to insure that the beam emittance is not degraded unduly by the ring. An example is given of a candidate design of a stripping ring.

Statement of the Problem.

To take an example of stripping, U ions at 1 Mev in a carbon foil yield 20% in the most abundant charge state, q=39. The 2σ spread in charge states is about 5 (1). If the most abundant charge state is extracted, and the rest are recycled through the stripper, after 10 turns we can expect about 90% of the injected beam to be extracted in the desired charge state (2). Although storage of a beam for ten turns is a trivial accomplishment for a storage ring, we shall see that this imposes stringent conditions in a stripping ring, in order to preserve beam quality.

The use of a stripping ring as an "enforcer" of the most abundant charge is an attractive idea, which has been studied by several authors (2,3,4). The main difference between this type of ring and a conventional storage ring is the need to accommodate very large momentum spreads - on the order of +/-15% if the full capability is to be realized. Designing a ring to accommodate such large momentum spreads is not a simple task. First-order storage ring optics can be used to arrive at a basic design concept, but then a careful study of higher order aberrations must be made.

Design Goals.

1. At the stripper location the ring must be dispersion free, or doubly achromatic, ie η_x and η_x' must be zero [η_x is defined by the relation $\Delta x = \eta_x(\Delta p/p)$]. This insures that, to first order, ions with different momentum will return to the same position at the stripper.
2. The value of η_x in one of the ring straight sections should be on the order of 1 m, so that an extraction magnet which operates only on the most abundant charge state can be located there. If η_x is much smaller, the installation of the extraction magnet will be difficult. If η_x is much larger, the required apertures in adjacent magnets (which must accept all charge states) will become unacceptably large.

3. The tune of the ring, both horizontal (ν_x) and vertical (ν_y) should be integral or half-integral. This is so that when the incoming beam is focused on a foil stripper (for example), the recirculating beam will remain focused on the same spot. The tolerance in the tune must be held to a fraction of 1%. If the tune varies from integral or half integral by more than this there will be considerable spreading, which will translate into emittance growth in the extracted beam. In a storage ring, integral and half-integral tunes are avoided as any instability will be enhanced, leading to a beam blowup. In the stripping ring, as we expect ions will remain for only 10 revolutions at most, this will not be a problem.

4. A serious second-order effect which will degrade performance if it is not corrected, is due to the circumstance that quadrupoles focus particles with different momenta at different distances. In a ring this produces a tune shift as a function of momentum and is known as chromaticity, C_x or C_y, defined as:

$$C_{x,y} = \delta\nu_{x,y}/(\delta p/p).$$

For conservation of emittance both C_x and C_y should be zero. This will insure that the tune will be preserved for off-momentum particles.

Stripping Ring Design

As a minimum, the ring must have dipole magnets which bend through 360°. Four 90° magnets can make a compact ring, with edges providing vertical focusing, and quadrupoles to produce linear achromaticity, as shown in ref 4. To achieve the integral or half-integral tune, however, additional quadrupoles are required. This is necessary to allow some tuning range, as the focusing effect of fixed magnet edges cannot be predicted with sufficient precision. The quadrupoles used to produce dispersionless straight sections cannot be tuned.

Further, to correct the second order chromaticity requires two sets of sextupoles. They are only effective where there is dispersion in the ring. Dipole edges can be curved to provide a sextupole component, but to provide a tuning range some adjustable sextupole magnets will be necessary.

To illustrate these points, a candidate design for a stripping ring is shown in Fig. 1. Six 60° dipoles are used. The beam rigidity , after stripping, is taken as 1 T-m. Of the six straight sections, 3 are achromatic and 3 have dispersion. The dispersion is controlled in each straight section by two quadrupoles (QSF). An extraction magnet is placed in one of the straight sections, where ν_x = 0.84 m. This magnet bends the beam vertically, so that in a downstream straight section it enters a vertical septum magnet where the beam is deflected so as to clear the dipole yoke. This two-magnet extraction scheme greatly reduces the strength required for the first extraction magnet, so that it can be more compact.

The tune of this ring is ν_x=2, ν_y=1. This tune is achieved primarily by the focusing action of the dipoles and the QSF quadrupoles. The additional quadrupole sets Q1 and Q2 are used to provide a tuning range.

One set of sextupoles is achieved by making the QSF quadrupoles also sextupoles. In fact, they would have two sets of windings so that the quadrupole and sextupole fields can be treated independently. This is simply to save space; it would be equally valid to place independent sextupole magnets adjacent to these quadrupoles. The other necessary

set of sextupole corrections is made by curving the dipole edges adjacent to the dispersed regions, with some additional tuning range provided by poleface windings.

The stripper, which could be either foil or gas, is placed in one of the dispersionless straight sections. The injected incoming beam is taken into the ring through the yoke of a dipole, at an angle so that after stripping it has the proper ring orbit. The extracted beam is shown exiting the ring by being guided over the yoke of this magnet. There are other possibilities for the extraction arrangement, depending on the overall facility layout.

Acknowledgement

This work was supported by the Director, Office of Energy Research, Office of High Energy and Nuclear Physics, High Energy Physics Division, of the U. S. Department of Energy under Contract No. DE-AC03-76SF00098.

References

[1] K. Shima et. al., Atomic Data and Nucl. Data Tables 51, 173-241 (1992).
[2] J. G. Cramer, NIM 130, 121-123 (1975).
[3] B. Franzke, K. Blasche, B. Franczak, GSI-J-1-78, 157-158.
[4] V. P. Kukhtin, Yu. P. Savergin, I. A. Shukeilo, PAC 1991, IEEE 91CH3038-7, 2035-2036.

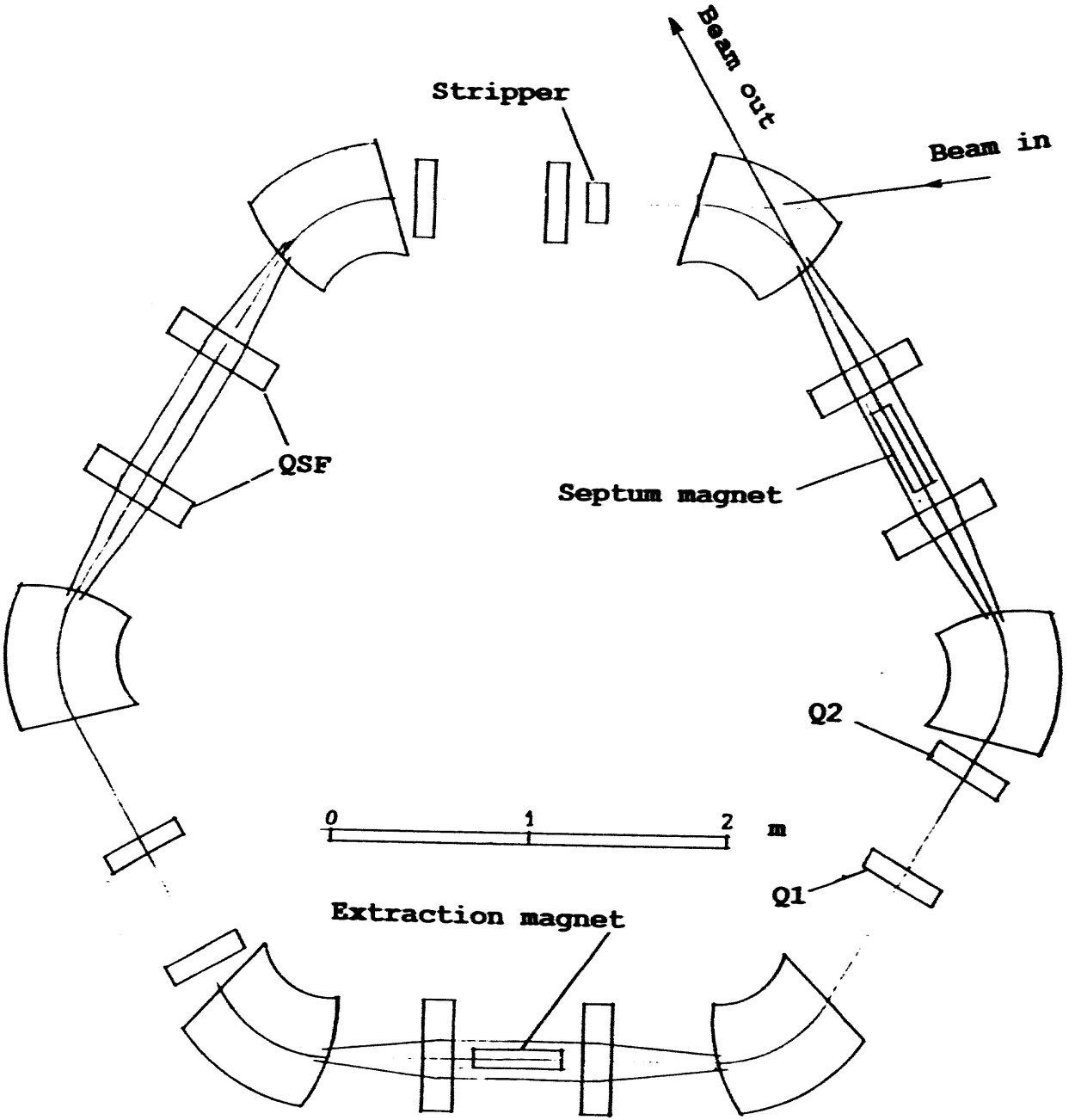

Fig.1 Ring for enhancing output of stripper

Air Core Superconducting Cyclotrons and Production of RNBs

K.Subotic, Institute of Nuclear Sciences Vinca, POB 522
11001 Beograd, Yugoslavia

Access to specific nuclide regions for the experimental study of exotic domains of nuclear matter depends strongly on the status of the beams available at a particular RNB facility. One of the most important requirements is sufficient intensity plus high quality and purity for a wide range of ion beams spanning the chart of nuclides. The two most effective methods for producing RNBs are PF and ISOL. These are actually the kinematic reverse of each other, and therefore in many cases the cross sections are similar. However, the ISOL luminosity, in the case of a proton beam, is higher than in the PF method, due to the higher respective target thickness and primary beam intensity. These two methods have complementary characteristics for producing RNBs from all regions of the chart of nuclides [1]. The advantages of the PF method are: short separation time, simple production targets, low radioactive load, high product collection efficiency, and reliable operation. The main disadvantages are: low intensity of primary heavy ion beam, high energies of secondary beams, poor emittance, moderate beam purity, large energy spread, and unavoidable intensity losses at deceleration or cooling. The main disadvantages of the ISOL method are: low yields for certain difficult elements, losses due to radioactive decay of secondary ions during time delays caused by diffusion and deadsorption, heavy radioactive load, and need for post acceleration. The advantages are: high yields of secondary beams of exotic nuclides, high purity and small emittance of secondary ion beams and convenient energies and intensities of the beam after acceleration. There has been more rapid development in the construction of facilities providing high energy secondary beams produced by projectile fragmentation than there has in the ISOL type facility [2]. The ISOL method is strongly recommended, however, because of better intensities and beam qualities with respect to experimental requirements for secondary reactions[1].

Yields from heavy ion reactions to produce isotopes near the beta stability line are six orders of magnitude lower than those observed from high energy proton reactions. This situation is dramatically changed for isotopes far from stability, where heavy-ion-induced compound nucleus reactions are the only means for producing such nuclei. In particular, it has been found that actinide and group VII elements, as well as the more exotic isotopes of groups 4A, 5A, and 6A are best produced in heavy-ion reactions. Refractory elements, elements that form refractory compounds, and noble metals are "difficult to produce" nuclei for the ISOL method, requiring the use of the inefficient He jet and IGISOL techniques. Fig. 1 illustrates the status of the beams available at existing production ISOL facilities, showing that almost 40% of the elements (enclosed by the thick line in Fig. 1) cannot be produced by the ISOL method in a satisfactory way due to their inconvenient thermochemical properties or low production cross-sections.

Design of a RNB facility which could integrate both production options seems to be extremely desirable. Air core superconducting cyclotrons that use a superconducting main coil and active multipole superconducting flutter configuration to ensure ion bending and focusing during acceleration may be basic components of this facility. The design of air core superconducting cyclotrons is discussed elsewhere [3,4], and only its main characteristics will be summarized here.

The prominent features of an air core design are mutually independent current settings in the superconducting main coil and multipole flutter configuration. The limiting phenomena that characterize iron core designs, such as the focusing limit, stop band limit and resonance limits are here controlled by independent coil settings [5]. The maximum

achievable energy depends only on the field symmetry, i.e., multipolarity of the active flutter configuration. The maximum energy for protons as a function of the field symmetry number N is given by T/A = 931.5 [(N-1.5)**1/2 -1] MeV. Fig. 2 shows a spherical main coil (b), which is characteristic of this design approach, providing the isochronous magnetic field (a) for a proton energy of 120 MeV at an extraction radius of 0.4 m. Fig. 2c shows the associated frequencies of radial and axial oscillations and related proton phase slip. An additional characteristic of an air core superconducting cyclotron design is the use of independently-powered main coil sections to produce the isochronous magnetic cyclotron field. The four independent main coil sections enable production of isochronous magnetic fields for the whole energy range up to 120 MeV for protons without use of correcting coils.

A similar design, with an increase in multipole order of the flutter configuration and in the number of independent main coil sections makes it possible to achieve higher energies. Four-fold field symmetry ensures bending and focusing of 400 MeV protons and of 400 MeV/nucleon Z/A = 0.5 heavy ions at an extraction radius of 2.5 m and current density of 30 kA/cmc in the straight edge flutter configuration. A 1 Gev proton and Z/A = 0.5 machine requires 8-fold field symmetry and an extraction radius of 5.5 m. Spiraling of the flutter configurations up to 40 degrees helps to avoid a negative curvature of particle orbits that may introduce an intolerable inclination of the particle orbits at intersections with multipole field edges. In this case, the average field may be raised to the level of 2.5 T, leading to a substantial reduction of extraction radii.

High flutter produces high axial frequencies, ensuring efficient transmission of required driver beam intensities. The respective second stage features, such as the accelerating/decelerating characteristics of cyclotrons and their accelerator mass spectrometric capabilities are discussed elsewhere [6,7]. Note that mass resolutions are of the order of R = 4nh, where n is the number of orbits executed and h is the operational harmonic number of the RF field employed, and a machine executing 1000 turns at h = 7 may resolve masses differing in one part in 30,000. Using air core superconducting cyclotrons as the basic elements, the construction of a high-performance multipurpose RNB facility that integrates the ISOL and PF method of production of exotic nuclides may be accomplished as shown schematically in Fig. 3.

References:

[1] The Isospin Laboratory,LALP 91-51
[2] G. Munzenberg: The separation techniques for secondary beams, Nucl. Instr. Meth. B 70(1992)265
[3] K.M.Subotic:Air Core Superconducting Cyclotron, Proc.X International Conference on Cyclotrons and their Applications,East Lansing 1984
[4] K.M. Subotic:Multipurpose Air Core Superconducting Cyclotrons,Proc. I European Particle Accelerator Conference, Rome 1988
[5] K.M. Subotic: Proton Window and Superconducting Cyclotrons,Proc. XII International Conference on Cyclotrons and their Applications,Berlin 1989
[6] K. M. Subotic et al: Superconducting mini cyclotron in AMS, Nucl. Instrum. Meth. B50(1990)267
[7] K.M.Subotic:Fragment Deceleration in Cyclotron,Proc. Workshop on Science of Intense Radioactive Beams,Los Alamos 1990

Fig. 1
Chart of nuclides with indicated Radioactive Nuclear Beams available at ISOL facilities (see legend for details]. Areas enclosed by thick solid line represent group of elements "difficult to produce" by ISOL method.

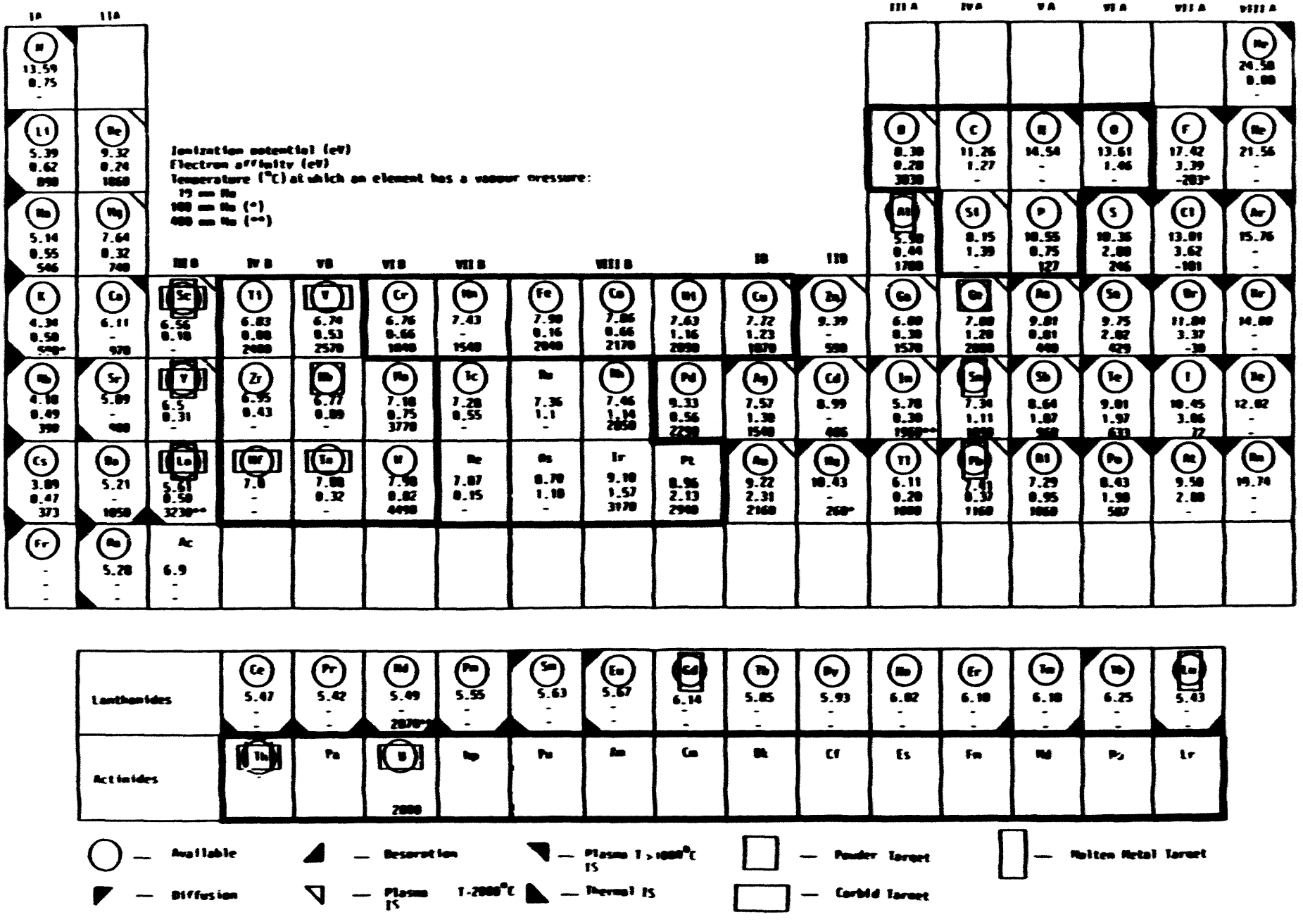

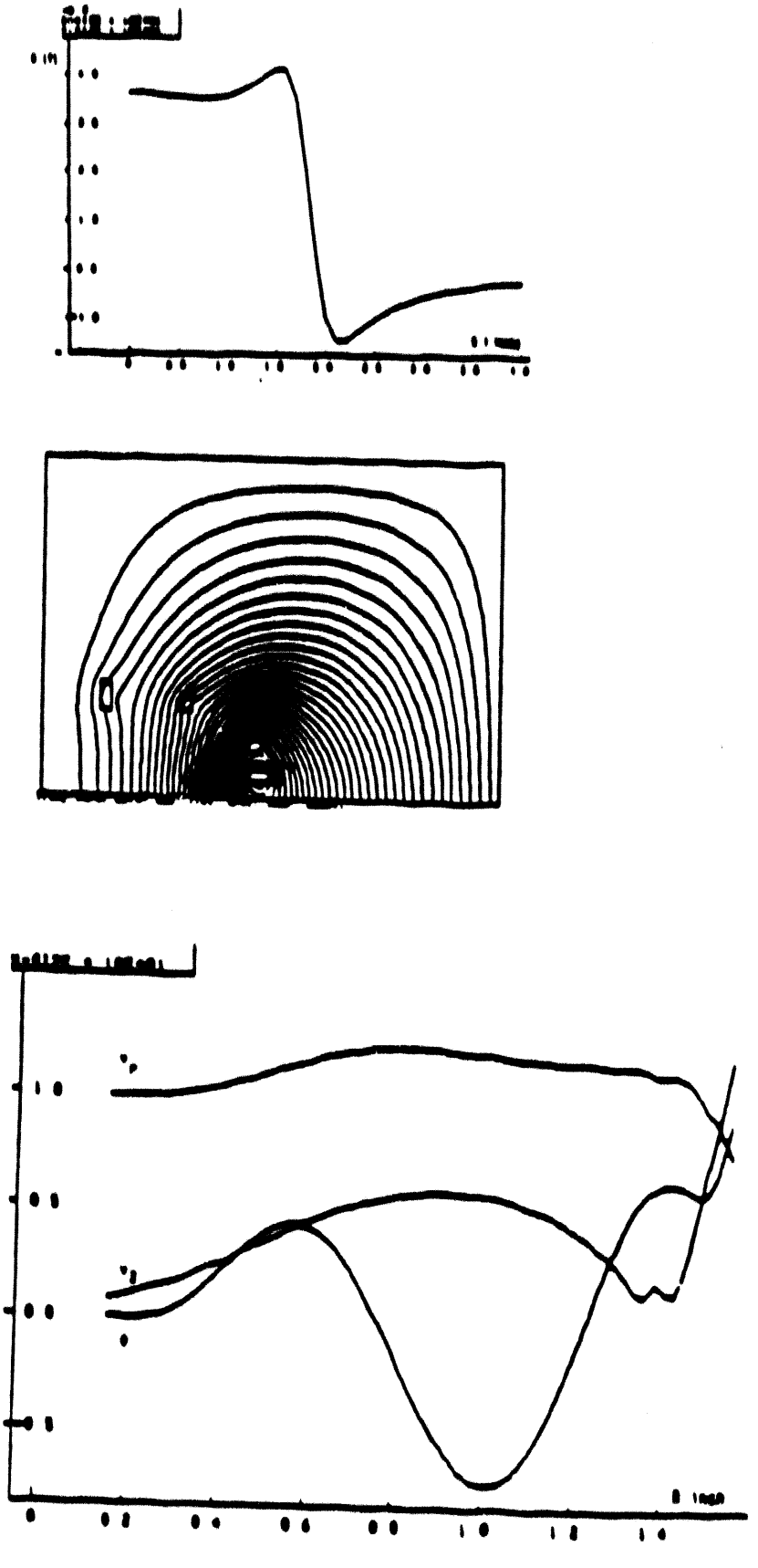

Fig. 2
Isochronous magnetic field(a) produced by spherical main coil of the superconducting air core cyclotron (b) and respective orbit characteristics for 120 MeV protons.

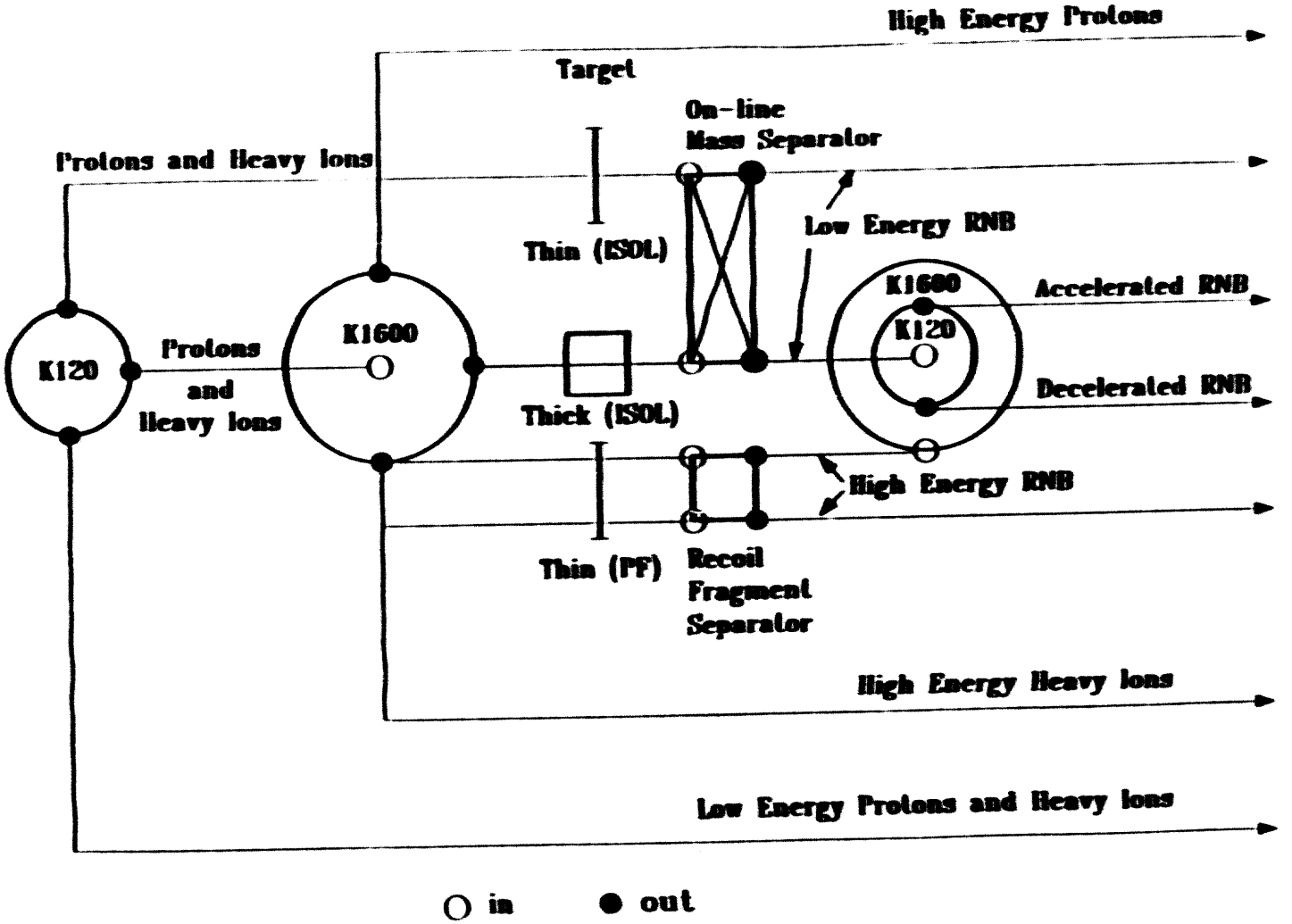

Fig.3
Multipurpose facility for production of Radioactive Nuclear Beams. Flexible operation range of the superconducting air core cyclotrons enables production of low energy protons and heavy ions (K120),which may be used in stand alone mode and/or to produce low energy RNBs using thin targets eventually combined with He jet and IGISOL techniques. Injected into K1600 cyclotron, protons and heavy ions may be accelerated in the domain of 1GeV A ,to be employed as primary beams for nuclear reaction studies or to produce RNBs by means of ISOL or PF method. Low energy(ISOL) and high energy(PF) RNBs may then be directly applied or accelerated/decelerated in K120/K1600 machine after accelerator mass spectrometric analysis (R=30000) during acceleration/decceleration.

Accelerator Complex for Unstable Beams at INS

M. Tomizawa, S. Arai, M. Doi, T. Katayama, K. Niki, N. Tokuda and M. Yoshizawa

Institute for Nuclear Study, University of Tokyo,
Midori-cho, Tanashi-shi, Tokyo 188 , Japan

1. Introduction

The construction of the prototype facility of the Exotic-arena in proposed Japan Hadron Project (JHP) [1,2] started in 1992 at INS[3]. The purpose of this facility is to study various technical problems of the Exotic-arena and to perform experiments with respect to nuclear and astrophysics with unstable nuclei beam. The prototype facility will be constructed in the existing building at the present INS campus. Its schematic diagram is shown in Fig 1. Unstable nuclei produced by bombarding a thick target with 40 MeV proton beam (~10 μA) from the existing SF cyclotron are ionized in the ion sources (positive surface ionization, ECR or FEBIAD type), mass-analyzed by an ISOL ($M/\Delta M$~5000), and transported to the following accelerator complex. The accelerator complex consists of an SCRFQ (split coaxial RFQ) and an IH (interdigital H type) linac. Unstable nuclei from the ISOL with an energy of 2 keV/u and a charge-to-mass ratio (q/M) greater than 1/30 are accelerated up to 170 keV/u by the SCRFQ. The beam is charge-exchanged by a stripper up to a q/M greater than 1/10, and is further accelerated up to 1 MeV/u by the IH linac. The output energy is variable over a range from 170 keV/u to 1 MeV/u by tuning the rf power and phase fed into the IH linac. The construction of the accelerators will be completed during the fiscal year 1994. In this paper, the present status of the accelerator complex is described with emphasis on a design of the IH linac.

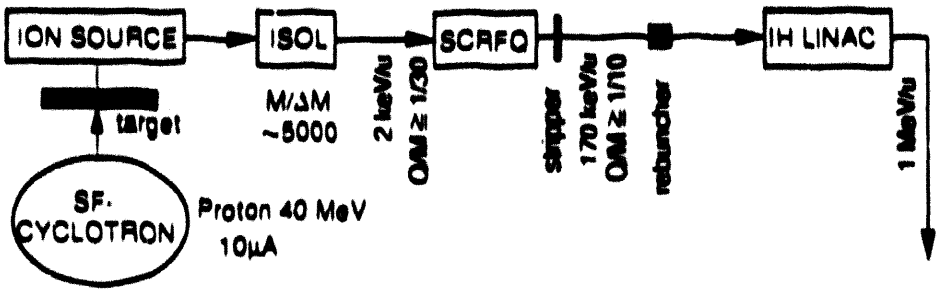

Fig. 1 Layout of the prototype facility at INS.

2. SCRFQ

An RFQ has a merit that it can accelerate a dc beam at very low energy with high transmission efficiency. In the case of accelerating the beam with a small q/M, the RFQ must be operated at a low rf frequency. The split coaxial structure keeps the size of the cavity small, compared with other structures such as a four-vane RFQ. In 1984, the development of a SCRFQ was started at INS. This SCRFQ has the following features[4,5]. (1) Modulated-vane electrodes are used to generate ideal accelerating and focusing fields. (2) By employing a multi-module cavity structure, vane electrodes are supported precisely and firmly at several points with stems.

In 1989, a 25.5 MHz-prototype model was constructed to obtain the know-how for practical use after studies with a cold model and a proton accelerating model working at 50 MHz [6 ,7]. The structure of the prototype model is illustrated in Fig.2. The prototype model consists of three-module cavities with 2.1 m in total length and 0.9 m in inner diameter, and accelerates ions with a q/M greater than 1/30 from 1 to 45.4 keV/u. Design parameters of the prototype model are the same as those of the JHP machine except the minimum q/M (=1/60). The modulated vanes were machined by two-dimensional cutting technique. The transverse radius ρ_T at the vane tip is constant at the mean aperture radius r_0=0.9458 cm. In high power tests, an intervane voltage of 114 kV, (which is higher than the design voltage of 109.3 kV for q/M=1/30 ions), was achieved by feeding an rf peak power of 75 kW under a pulse operation (repetition rate 150 Hz) with a duty factor of 9%. Acceleration tests were performed by using three ion species N_2^+,N^+ and Ne^+. The transmission efficiency obtained with a N^+ beam is better than 80% at intervane voltages (normalized by the design value) higher than 1.2. Details of these results are described in ref.[9].

The prototype model will be extended to an 8.5-m, 170-ke V/u machine for practical use. The following improvements or changes will be done[10]. (1) The coupling rings (see Fig. 2) will be removed to reduce the frequency-shift due to the local heating. It was confirmed that the mechanical stability of the electrodes can be kept without them. The flow rate of cooling water, about 300 l/min now, will be increased. By these improvements, the operation at higher duty factor (~30%) will be expected. (2) The injection energy is changed from 1 keV/u to 2 keV/u in order to make the beam transportation from the ISOL easier. (3) In order to achieve higher beam-transmission, the variable-ρ_T geometry of the vane tip will be employed for the low-energy part (the vanes are machined by three-dimensional-cutting technique), and the $\rho_T = r_0$ geometry for the high-energy part (by two-dimensional-cutting technique).

Parameters of the SCRFQ for practical use are listed in Table 1. Final design of the SCRFQ is now completed.

Table 1 Main parameters of the SCRFQ.

resonant frequency	25 5 MHz
energy	2 --> 170 keV/u
charge-to-mass ratio	≥ 1/30
duty factor	30%
repetion rate	20 ~ 1000 Hz
normalized emittance (out)	0 6 π mm · mrad
longitudinal emittance (out)	37 5 π keV/u · deg
tank diameter	0 9 m
vane length	8 6 m
mean aperture radius	0 9458 cm
intervane voltage	108 6 kV (q/M = 1/30 ions)
maximum surface field	178 2 kV/cm (2 5 Kilpatrick)
maximum rf power	280 kW
transmission	91%

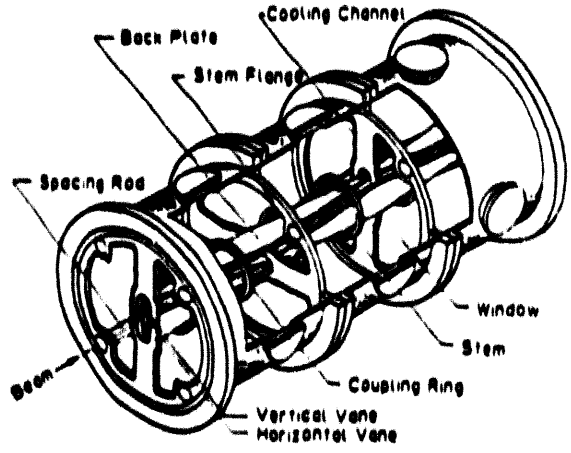

Fig. 2 Structure of the prototype SCRFQ.

3. IH Linac

With increasing beam energy, the acceleration by the RFQ becomes less efficient. The IH linac is suitable for the post-accelerator of the SCRFQ, since the shunt impedance of the IH linac in the energy range required in our facility is higher than those of other linacs such as an Alvarez type. The beam from the SCRFQ is charge-exchanged by a stripper, and injected into an IH linac. The IH linac has the following characteristics. (1) It accelerates the heavy ions from low energy (170 keV/u). (2) Synchronous phase is selected as -25 deg to assure the stable longitudinal motion in spite of the strong transverse rf defocusing force in the accelerating gaps. (3) To obtain high acceleration efficiency, a π-π mode is adopted as an acceleration structure, and no transverse focusing element is installed in the drift tubes. (4) The IH linac is divided into four tanks. Transverse focusing elements are placed between tanks. (5) Output energy is continuously varied in the IH linac. The parameters of the designed IH linac are listed in Table 2.

The resonant frequency of the IH linac is chosen to be twice as high as that of the SCRFQ. Its longitudinal acceptance is half of that with the same frequency as the SCRFQ. The length of drift spaces where magnetic quadrupole triplets are placed should be as short as possible to keep the phase spread in these spaces small. In the present design, the length of the drift spaces is

Table 2 Parameters of designed IH linac.

	tank-1	tank-2	tank-3	tank-4
resonant frequency (MHz)	51	51	51	51
charge-to-mass ratio	≥ 1/10	≥ 1/10	≥ 1/10	≥ 1/10
energy (keV/u)	170 ~ 292	292 ~ 471	471 ~ 721	721 ~ 1046
synchronous phase (deg)	-25	-25	-25	-25
tank diameter (m)	1 34	1 34	1.34	1.34
tank length (m)	0 59	0 84	1 15	1 53
cell number	9	10	11	12
effective shunt impedance (MΩ/m) *	751	510	345	244
maximum peak power (kW)	5 1	11	22	40

* Reducuon due to surface roughness and contact resistance is assumed to be 40%.

taken to be 48 cm. Figures 3 (A) and (B) show the calculated results of the energy and phase oscillations. In the calculation, the longitudinal emittance at the entrance of tank-1 is chosen to be 200 π keV/u·deg which is nearly three times larger than the predicted beam emittance from the SCRFQ.

Figures 3 (C) and (D) show the calculated transverse beam envelopes. The transverse and longitudinal emittances of the input beam are chosen to be 0.6 π mm·mrad (normalized) and 200 π keV/u·deg, respectively. The transverse emittance of the unstable nuclei is small, estimated to be less than 0.1π mm·mrad at the exit of the ISOL[11]. But an acceptance larger than this value is required, considering the emittance growth at the charge stripper, or the possibility for the acceleration of the stable-nuclei beams from other ion sources. The acceptance of 1.7 π mm·mrad is achieved by setting the bore radius of quadrupole magnets at 20 mm. Strong field gradients (about 5 kG/cm at maximum) and compact sizes are required for the quadrupole magnets to be placed in the 48 cm long drift spaces. Now these quadrupole magnets and their housing are being designed on the basis of calculation using the computer codes POISSON and TRIM.

The output energy of the IH linac can be continuously varied by tuning the rf power and phase in each tank. Its variation of output energies results from separating the IH linac into several tanks. Figure 4 shows the output energy and its spread as a function of the gap voltage. The output energy is continuously variable from 170 to 1046 keV/u. For example, if a certain energy in the range from 471 to 721 keV/u is needed, the gap voltage of tank-3 is varied without operating tank-4. The energy spread ($\Delta T/T$) is ±2~6% except at the exit of tank-1. Its spread, however, can be made smaller by adjusting the rf phase as well as the gap voltage.

The structure of four tanks is different from that of ordinary IH linacs, that is, axial length of the four tanks is shorter than or near the diameter needed for resonant frequency of 51 MHz. To estimate the resonant characteristics, equivalent circuit analysis was performed. In this analysis, the capacitance and inductance for accelerating cells and end cells were approximately obtained. The analysis predicts that diameters of four 51MHz-tanks are kept in the same size (134 cm) by adjusting the radius of the drift tubes of each tank in the range of 2~4 cm, and by adjusting the sizes of magnetic flux inducers. Predicted effective shunt-impedances are shown in Table 2 together with maximum peak powers. The view of the designed IH linac is shown in Fig. 5. Low power tests using a model will be performed during this fiscal year.

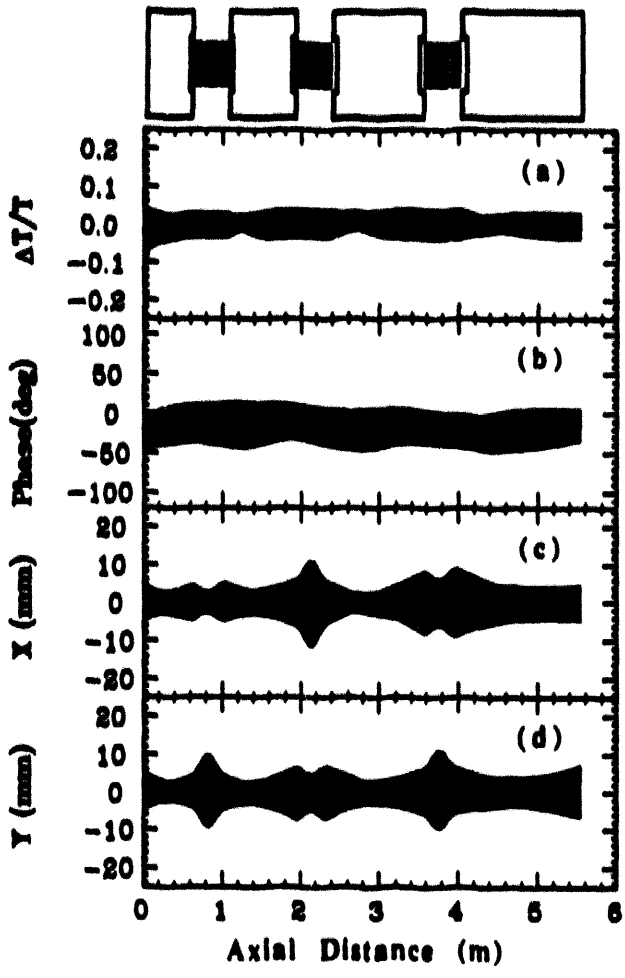

Fig. 3 Calculated beam profiles.

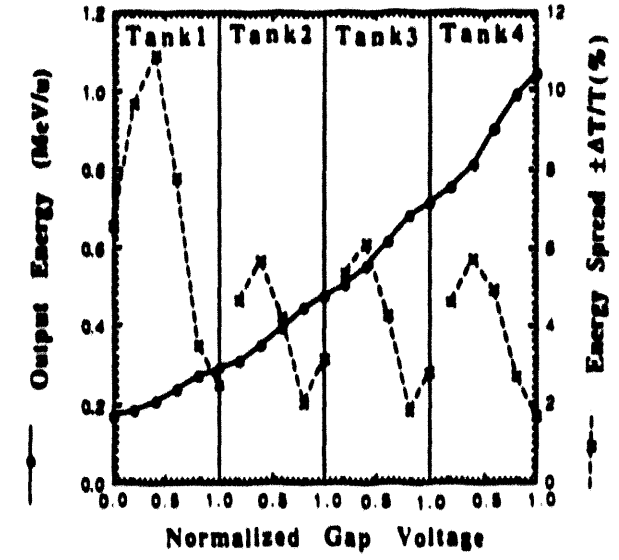

Fig. 4 Output energy and its spread as a function of normalized gap voltage.

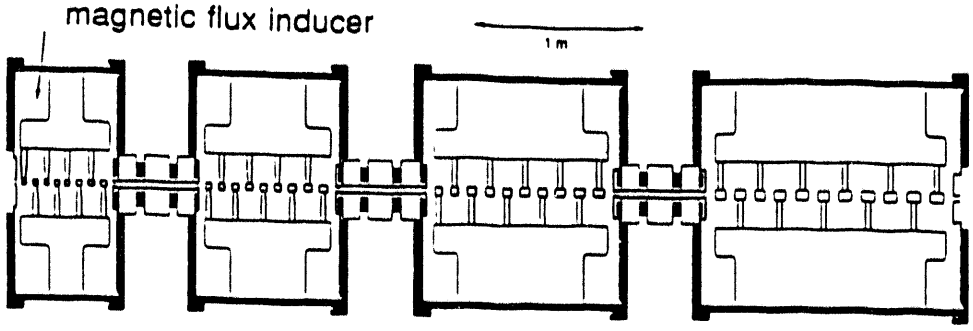

Fig. 5 View of the designed IH linac.

4. Charge Stripper and Beam Matching between SCRFQ and IH linac

Beam accelerated up to the energy of 170 keV/u by the SCRFQ is charge-exchanged by a stripper placed downstream of the SCRFQ, in order to increase the acceleration efficiency of the following IH linac. A carbon thin foil will be used as a stripper because of the easiness of the construction. For the beam of a low velocity, energy loss and its spread due to passing through the foil can not be neglected. Therefore very thin foil (5~10$\mu g/cm^2$) must be used as a stripper. The transverse emittance growth due to the multiple scattering depends on the beam size at the stripper position as well as the thickness of the foil. Therefore the stripper is placed just behind the exit of SCRFQ where beam sizes of both x- and y-directions are small. Considering the charge state distribution after passage through the carbon foil, a transmission efficiency is expected to be 30~50% for the ions with mass less than 30[12].

A buncher is necessary for the matching of longitudinal phase space between the SCRFQ and the IH linac. The correction of energy loss in the stripper as well as rebunching of the beam is performed in this buncher. The resonant frequency for the buncher, the same frequency (25.5MHz) as the SCRFQ, should be chosen to obtain better matching condition, since it reduces the effect of an aberration [13]. As a candidate for the buncher, a spiral cavity is proposed to keep the size of the resonator small. The mechanical stability and the resonant characteristics are now being investigated. Two sets of magnetic quadrupole doublets are placed for the transverse matching. A length of about 3 m is taken for matchings.

References

[1] T. Yamazaki, INS-Report-763 (1989).
[2] T. Nomura, INS-Report-780 (1989).
[3] T. Nomura et al., INS-Annual-Report-1990, pp.149.
[4] S. Arai et al., IEEE Trans. Nucl. Sci., Vol. NS-32 (1985) 3175.
[5] S. Arai, INS-T-464 (1986).
[6] S. Arai et al., INS-Report-764 (1989).
[7] N. Tokuda et al., INS-Report-794 (1989).
[8] S. Arai et al., INS-Report-875(1991).
[9] S. Arai, et al., Nucl. Instr. and Methods, B70(1992)414-420.
[10] N. Tokuda et al., INS-Report-920 (1992).
[11] T. Nomura, private communication.
[12] K. Shima et al., NIFS-DATA-10 (1991).
[13] K. Niki, private communication.

Section IV
The ORNL Radioactive Ion Beam Project

D. K. Olsen, G. D. Alton, R. L. Auble, C. Baktash, H. Blosser, H. K. Carter, J. Dellwo, D. T. Dowling, J. D. Garrett, D. L. Haynes, C. M. Jones, R. C. Juras, J. Kormicki, S. N. Lane, L. Lee, P. Mantica, F. Marti, M. J. Meigs, G. D. Mills, S. W. Mosko, L. Rayburn, C. A. Reed, R. L. Robinson, B. A. Tatum, and H. Wollnik

THE ORNL RADIOACTIVE ION BEAM PROJECT*

D. K. Olsen, G. D. Alton, R. L. Auble, C. Baktash, H. Blosser,[a] H. K. Carter,[b] J. Dellwo,[c] D. T. Dowling, J. D. Garrett, D. L. Haynes, C. M. Jones, R. C. Juras, J. Kormicki,[b] S. N. Lane, L. Lee,[a] P. Mantica,[b] F. Marti,[a] M. J. Meigs, G. D. Mills, S. W. Mosko, L. Rayburn,[b] C. A. Reed,[b] R. L. Robinson, B. A. Tatum, and H. Wollnik[d]

INTRODUCTION

On June 30, 1992, the Holifield Heavy Ion Research Facility (HHIRF) was shut down as an operating national users' facility for heavy ion physics research and became a construction project to reconfigure the existing accelerator system and develop a first-generation radioactive ion beam (RIB) facility.[1] During its 11 years of operation, the HHIRF had over 600 users, of which 200 were graduate students. During this time, nearly 39,000 hours of beam were delivered as beam-on-target for nuclear, atomic, and applied research. Table 1 lists the heavy ion beams that were provided for scheduled experiments. All together, 69 different isotopes from 36 different elements were accelerated for scheduled experiments. Most beams were produced with only the 25-MV tandem accelerator; however, for the most energetic beams and the heaviest ions, the Oak Ridge Isochronous Cyclotron (ORIC) was used as an energy booster. This paper will briefly review the concept of the ORNL RIB project and describe the progress being made on the various hardware components and physics factors required to produce RIBs with the HHIRF accelerator system.

*Research sponsored by the U.S. Department of Energy under contract No. DE-AC05-84OR21400 with Martin Marietta Energy Systems, Inc.
[a]Michigan State University, East Lansing, Michigan 48824
[b]Oak Ridge Associated Universities, Oak Ridge, TN 37831
[c]Joint Institute for Heavy Ion Research, Oak Ridge, TN 37831
[d]University of Giessen, Giessen, Germany

Figure 1 shows the planned layout of the RIB facility after completion of this reconfiguration. In the past, ORIC served as an energy booster for stable heavy ions produced by the tandem accelerator. To produce RIBs, this process will simply be reversed: the tandem accelerator will be injected with radioactive heavy ions produced by ORIC. In this case, the two accelerators will be coupled by a new tandem injector consisting of an ISOLDE-type thick-target ion-source assembly,[2] mass separator, and charge-exchange canal, all mounted on a 300-kV high-voltage (HV) platform system in the existing shielded room C111. Light ions from ORIC, using an internal ion source, will produce negative radioactive heavy ions for tandem injection. Once accelerated by the tandem accelerator, the RIBs can be used for experiments with the existing beam line system and experimental apparatus. The RIB facility can be quickly and inexpensively constructed because both accelerators, the beam lines, and the experimental apparatus all exist. In addition, the original ORIC vault, room C109, and the experimental area to house the new RIB injector, room C111, were originally designed with shielding for a 75-MeV, 1-mA proton beam. No civil construction is required. Figure 1 also shows the new recoil mass separator[3] which has been ordered from DANFYSIK and the new "gammahall" addition to house the recoil mass separator. This major piece of experimental equipment will be an important part of the overall RIB capability at ORNL.

The process for producing RIBs with the HHIRF accelerator system is summarized quantitatively for a generic "very good case" in Fig. 2. The process starts with ORIC as the primary accelerator, for which it has been assumed that eventually 2.0 kW of H or He beam will be extracted. For the calculation of Fig. 2, 30-MeV protons are extracted, giving 67 μA or 4×10^{14} primary protons per second. The initial operation of ORIC for RIB production is scheduled for 0.5 kW of extracted beam power. These protons will be

accelerated onto the HV platform and stopped in a thick target. For a good case, with an isotopically pure elemental target, about one radioactive atom can be produced for each 1000 incident protons, giving 4×10^{11} radioactive atoms per second. This production rate assumes no decay, target release, or surface sticking losses. On average, these radioactive atoms can be positively ionized with a 30% efficiency, mass analyzed with a 50% efficiency, and charge exchanged with a 30% efficiency, giving 2×10^{10} of negative radioactive ions per second out of the RIB injector. Radioactive ions below mass 80 can be accelerated in the tandem accelerator on average with a 20% total efficiency, giving 4×10^{9} ions per second as beam-on-target for a good case under ideal conditions. To summarize, the loss in intensity between the ORIC beam and the RIB beam will be a factor of 100,000; a factor of 1000 to make radioactive atoms, and then, on average, another factor of 100 to deliver these radioactive atoms as beam-on-target. The remainder of this paper will discuss, in detail, the hardware and physics aspects of this process, starting with ORIC.

THE PRIMARY ACCELERATOR, ORIC

The k = 100 ORIC was designed for the acceleration of both light and heavy ions and was used initially for intense light-ion beam experiments in the first years after its completion in the early 1960s. In the early 1970s, the physics program changed and ORIC was used mostly for heavy ion acceleration. In the early 1980s, the facility changed and ORIC was used mostly as an energy booster for the tandem accelerator. ORIC was originally designed to accelerate 1 mA of 65-MeV protons. Thus, ORIC is an ideal driver for the intense light-ion primary beams needed to produce RIBs. Table 2 lists the main parameters of the cyclotron.

The present extraction efficiency from ORIC with the internal light-ion source is quite low and development work will be required to increase this efficiency so that 2.0 kW of beam can be extracted with acceptable activation levels in the present ES&H climate. The key to high extraction efficiency is intense, well-centered, separated orbits in the ORIC central region so that unextractable beam can be removed with slits at energies below the activation thresholds. This is not the case with the present central region configuration because ORIC was designed without the aid of computer codes to optimize central region design. Activation, in general, has not been an important issue with low-energy heavy-ion acceleration.

Figure 3 shows a new central region configuration for ORIC optimized to obtain intense well-centered separated orbits for a k = 80 H_2^+ beam. The major change from the present design is the decrease of the source distance to the puller face from 2.7 cm to 1.0 cm which will increase the electric field at the ion source slit, and hence beam intensity. Orbit studies have shown that a starting time of 20° in RF phase before peak voltage is the optimum choice to decrease orbit center spread and maximize intensity. A range of orbits ± 10° in RF phase around this central orbit will have good centering and good vertical focusing to give single-turn high-efficiency extraction. Over the next year, this central region design will be implemented with phase selection slits to decrease extraction losses.

Figure 4 shows the reconfigured beam line to transport high-intensity light-ion beams from ORIC to the new RIB injector. This line will be assembled from mostly existing components, including aluminum beam pipe, aluminum vacuum chambers, and carbon scrapers to minimize activation. The line will use existing cryopumps, quadrupoles, and a horizontal bending magnet. A new vertical bending magnet will bend the beam upwards

by 13° to change elevation from the ORIC beam line level of 48 inches to the RIB beam line level of 87 inches.

HIGH-VOLTAGE PLATFORM SYSTEM FOR THE RIB INJECTOR

The HV platform system for the RIB injector is rather complicated for two reasons. The first reason is illustrated with Figs. 5 and 6. Figure 5 shows the round beam, waist-to-waist beam transport system of the tandem accelerator.[4] The accelerating voltage of the existing injector was chosen to be rather high, operating between 150 and 500 kV, in order to obtain good beam bunching and good transit time factors for tandem beam injection into the 6° RF phase acceptance of ORIC. The subsequent optimization of the beam transport system into and through the low-energy acceleration tube was based on this high-injection voltage. In particular, the focal length of the effective entrance lens of the fringing electric field of the low-energy tube is four times the ratio of the injection voltage to the tube electric field gradient. This tube entrance lens is a strong effect, as shown in Fig. 5, and the design of the tandem accelerator requires a beam waist near the tube entrance. With a single lens positioned between the 90° injector mass analyzer magnet image and the tube entrance, this constraint imposes limits on the ratio of injector and terminal potential. To understand these limits, measurements of relative tandem transmission efficiency were made as a function of injector voltage for several different beams. The results are plotted in Fig. 6 for both gas and foil stripping cases. The tandem transmission efficiency remains relatively high with 200-keV injection. The RIB injector voltage will be specified at 300 kV and probably will operate at 250 kV.

The second reason for the complicated RIB-injector HV-platform system is illustrated with Fig. 7, taken from Ref. 5, which shows radiation damage to semiconductor devices as a function of both neutron fluence and total ionizing dose. The squares in Fig. 7

show the threshold level for damage and the assumed destruction level. The neutron fluence from the RIB target can be estimated from HETC[6] calculations which show that up to 0.07 fast neutrons can be produced from each 60-MeV proton stopping in a mass 70-region target. This neutron yield corresponds to an unshielded neutron fluence of about 1 x 10^{15} n/cm^2 one meter from the target-ion source for a 33 μA beam for 2000 hours. In addition, Fulmer et al.[7] directly measured the radiation level in room C111 as a function of energy for both proton and alpha beam stopping in various thick target materials. Extrapolation of these results indicates a total maximum dose of up to 1 x 10^7 rads per 2000 hours of operation one meter from the target-ion source. Clearly, all unshielded semiconductor devices near the target-ion source could be destroyed in one year, 2000 hours, of operation at full intensity.

The HV platform system for the RIB injector which solves these two problems is shown in Figs. 8, 9, and 10. The system is space constrained in room C111. Two platforms with a common power supply will be used. One platform, the source platform, will support most of the mechanical equipment, including the target-ion source and beam transport. The second platform, the instrumentation platform, will support most of the electrical apparatus, including all power supplie· The two platforms will be separated by a concrete shielding wall, but connected electrically by two HV conduits. The ORIC light-ion beam will enter the source platform through one 300-kV acceleration tube and RIBs will exit through a second 300-kV tube. On the source platform, the ORIC light-ion beam will enter the target-ion source at platform-plus-source voltage through a smaller 50-kV acceleration tube and RIBs will exit the target-ion source through a second 50-kV acceleration tube. Two motor-generator sets will provide power on the instrumentation platform at the two voltage levels; platform voltage and platform-plus-target-ion-source voltage. Cables at the two voltage levels will be run between the platforms in the two HV conduits.

Figure 10 gives an end view of the instrumentation platform showing the common high-voltage power supply for the system. The power supply hangs from the ceiling to conserve space and has two stacks: a voltage multiplier stack and a filter stack to reduce noise and ripple. Isobaric mass separation of ions in the negative ion injection line will be required and may be limited by the injector voltage stability. The power supply stability has been specified to be 1/25,000 for noise and ripple and 1/10,000 for drift over a one-hour period. The RIB injector and other new equipment, except for the ORIC beam line, will be operated by the tandem control system.

CALCULATED RADIOACTIVE ATOM YIELD ESTIMATES

The high-voltage platform system creates the environment for the production of RIBs with the target-ion source assembly. The first factor in this production process is the thick-target radioactive-atom yield per incident ORIC beam ion. To reduce the uncertainty in this factor, detailed production cross sections in the mass-70 region have been calculated with both the HETC code[6] for proton beams only, and with the PACE code[8] for both hydrogen and helium beams. Where possible, these results have been compared with measured values. The four main conclusions from this mass 70 production cross-section study are listed below:

1. PACE and HETC calculated cross sections usually agree within a factor of two.

2. PACE and HETC calculated cross sections usually agree with measured values within a factor of two or three.

3. A few calculated cross sections disagree strongly with measured values.

4. In most cases, the production cross section for an important specific beam should be measured.

The HETC code also gives yield estimates of all residual radioactive atoms from both compound and spallation processes. Figures 11 and 12 summarize the results of such calculations for ^{70}Ge, the most proton-rich Ge isotope, and ^{76}Ge, the most neutron-rich Ge isotope. Figure 11 gives yields per 1000 incident protons at 40, 50, and 60 MeV, stopping in a thick pure ^{70}Ge target. Many of these yields are near or above one radioactive atom per 1000 incident protons. In addition, some residual yields far from the target nucleus, such as ^{64}Ga, depend strongly on energy. These yields are for an isotopically and elementally pure ^{70}Ge target. The proposed Zr_5Ge_3 material for Ge targets would reduce these yields by about a factor of three. Less than 100% isotopically pure ^{70}Ge would also reduce these yields. In any case, at these proton energies, the highest yields for the most proton-rich nuclei seem to be produced with the simple (p, xn) reactions. Figure 11 shows that many radioactive beams can be made from a single target material. Figure 12 shows a similar HETC calculation for 60-MeV protons stopping in ^{76}Ge. The pattern of radioactive atom production is different because the path to the valley of beta stability is reached by neutron emission, not proton emission. Again, the (p, xn) yields are largest. It is possible, as shown in Fig. 12, that a few proton-rich RIBs can be made if a suitable target isotope is available.

The same HETC calculations give information on both the prompt and residual radioactivity from the target bombardment. For example, the calculation shown in Fig. 12 estimates 71 prompt neutrons per 1000 incident protons. Figure 13 shows the build up and decay of delayed-gamma radiation from a Zr_5 $^{70}Ge_3$ target bombarded with 2.0 kW of 43-MeV protons for five days. The target material is about 1 mm thick,

corresponding to a 7-MeV energy loss. During the time the beam is on the target, the prompt gammas and neutrons would produce a radiation field in the order of 10,000 rem/hour at one meter. After bombardment, the residual activity would be about 20 curies, corresponding to an unshielded radiation level of about 20 rem/hour one meter from the target. After about a week, the target radiation level would decay by about a factor of ten. This is an appreciable, but manageable, residual radiation level from the target material.

TARGET-ION SOURCE DEVELOPMENT

The tandem accelerator must be injected with negative ions. This fact both complicates and provides unique opportunities for the ORNL RIB project. Table 1 lists the beams for scheduled experiments from the HHIRF tandem accelerator over the last decade. At the present time, a tandem accelerator may be the only existing technology which can provide both focusing and acceleration for heavy beams at ion source energies with charge-to-mass ratios less than about 1/50.

Beams of negatively ionized atoms and molecules for tandem injection can be made with at least two different methods. All negative-ion beams can be produced by passing a low-energy positive-ion beam through a Li or Cs vapor charge-exchange canal. This is a two-step method. However, some atoms and molecules with high electron affinities can be made directly in a one-step process during emission from a low-work-function surface. Two target-ion sources based on these two methods are presently being pursued vigorously. The first of these, the "Mark-I" target-ion source, is shown in Figs. 14 and 15, and is similar to the ISOLDE FEBIAD target-ion source assembly. Figure 14 shows details of the target chamber and ionization chamber. The ORIC beam will stop in about one cubic centimeter of target material. The target material will be

refractory, probably in powder form, and may be heated up to 3000° K. Radioactive vapors will diffuse to the surface of the powder particles, desorb from these surfaces, and effuse into the ionization chamber. Surface sticking of radioactive atoms can be a major source of time delay, so the vapor transport tube will also be heated. The target temperature will be controlled independently of the heated cathode used for electron production. Positive ions from this FEBIAD source will be charge-exchanged on the source platform.

Figure 15 shows the assembly housing the target-ion source of Fig. 14. This assembly has been designed for remote installation. Both the electrical and water feedthroughs will be of a quick-disconnect type with an actuated bellows to disconnect the ORIC beam line. The assembly will be positioned on pins and will roll back on linear bearings with a quick vacuum disconnect to the RIB extraction insulator. Shutters will close remotely on both the ORIC input port and the RIB output port. The target-ion source assembly is then positioned to be lifted up remotely and placed in a shielding cask. Much of the engineering for this source has been completed and components are being fabricated.

The detailed design of the second target-ion source has just started. This source will be based on direct surface negative ionization, will be a multi-cusp-field plasma-sputter source, and will be similar in concept to the negative-ion sources presently used for stable heavy-ion tandem accelerator beams.[9] The concept is shown in Fig. 16. A Cs-rich plasma will be created in a multi-cusp magnetic-field chamber with hot walls. Radioactive vapors from the target will condense on a cooled cathode made of low sputtering material. The Cs-rich plasma incident on the cathode will both lower the surface work function, and directly sputter condensed atoms and molecules into

negative ions. Negative-ion beams of such elements as F, Cl, Br, O, S, and Se should be possible.

Using estimated efficiencies for negative-ion production for these two methods, the maximum overall efficiency for converting radioactive atoms in the target material to accelerated beam on target for experimental use is estimated in Table 3 and is a simple measure of the system merit. Both methods for negative ion formation are included. For this table, direct surface negative ionization efficiencies were estimated from the Langmuir-Saha relation for a LaB_6 surface ionizer operated at 1370 K, giving a 2.36-eV work function. Efficiencies using the charge-exchange method are the product of two factors: the efficiency for positive ionization and the efficiency for conversion of positive to negative ions. The positive ion efficiencies were estimated by scaling the probability for electron-impact ionization of the element in question to that of calcium which has a 30% measured efficiency.[10] The efficiencies for sequential charge exchange are based on measured results. In addition, a 50% loss factor has been included to account for transport losses. The transmission efficiency through the tandem accelerator is well understood and based on in-house experience. The average overall conversion efficiency from radioactive atoms to beam on target is about 1% and varies widely, depending on the element. Table 3 does not include any decay, target release, or surface sticking losses. These losses can be substantial.

UNISOR RELEASE MEASUREMENTS

Decay, target release, and surface sticking losses can be studied at ORNL independently of producing RIBs by using the UNISOR on-line isotope separator. In particular, for any radioactive isotope that will be accelerated as a RIB, there exists a stable isotope that can be accelerated with the tandem accelerator. Experiments have

started in which stable isotopes of the elements which are planned for future RIBs are implanted in thick target materials which could produce these RIBs. The chemistry and physics of the subsequent thermal diffusion, desorption, and ionization can be studied and optimized without actual production of RIBs. The UNISOR FEBIAD ion source and the Mark-I FEBIAD ion source are similar with similar origins.[11] The UNISOR and the RIB project ion sources have different arrangements of target material, but diffusion and surface desorption are common to both.

Figure 17 shows the results from implanting Br in a Zr_5Ge_3 cermet target which has a melting point near 2300°C. The target had a diameter of 9 mm, a thickness of 1 mm, and was mounted in the UNISOR FEBIAD target-ion source. After passing through a thin Ta window, the incident Br beam from the tandem had an energy of 183 MeV. This energy gives an implantation depth of 15.6 μm, which corresponds approximately to the average particle size of a Zr_5Ge_3 powder target. As shown in Fig. 17, there is no mass-79 output current above background from the UNISOR mass separator without an incident ^{79}Br beam. Immediately after the beam irradiates the target, mass-79 current is measured and reaches an equilibrium of 4.5×10^{-10} A. When the ^{79}Br beam is turned off, the mass-79 current decays to zero. This measured release profile gives information on both the total release time and total release efficiency. The release time is the total accumulated time for diffusion, desorption, effusion, ionization, and beam transport through the separator, and is defined to be the time required to release 50% of the steady-state beam intensity. For Br, this release time was measured to be seven seconds. The release efficiency is defined as the ratio of the ^{79}Br beam current out of the mass separator to the ^{79}Br beam current into the target normalized to the expected ^{79}Br output current, which was scaled to a measured Kr beam using a standard gas leak. If there were no decay, target release, or surface sticking losses, the release efficiency would be 100%. The release efficiency for ^{79}Br from Zr_3Ge_3 was 61%; that is

61% of the Br was released and was available for ionization in the UNISOR mass separator. Half of this Br was released within seven seconds of its production.

Table 4 summarizes some measured release results using this technique. For each line in the table, two measurements were made with the mass separator tuned at the listed beam mass. One measurement was with the beam of interest and the second measurement was with a different beam mass with identical power to measure beam-induced background. One problem with the UNISOR FEBIAD target-ion source is that the target temperature and electron ionizing current are both controlled with the same heating current. The UNISOR target operates at about 1700 K which is substantially lower than the expected Mark-I target temperature. The UNISOR mass separator system may be reconfigured to allow installation of the Mark-I target-ion source to overcome this limitation and to allow these measurements on the actual device that will be used for on-line RIB production.

MASS SELECTION AND RIB BEAM LINES

The target-ion source assembly will produce a positive-ion beam with many different elements, molecules, isotopes, and charge states. Some selection will occur because of physics and chemistry factors; however, in general, this beam needs to be filtered to produce an isotopically pure beam on target with a two- or three-stage magnetic-mass-separator system. The first stage of the mass-separation process will select a single isotopic mass chain and will occur before the charge-exchange cell on the source HV platform. Figure 18 shows the horizontal beam envelope and stretched vertical beam envelope calculated for the Mark-I target-ion source emittance through the first-stage mass separator. Four quadrupole singlet lenses and a multipole correction element will focus a round beam ($x = y + 0.2$ mm, $x' = y' = 20$ mrad) from the target-ion source into a

horizontal waist with a total width of 0.05 mm at the object slit of a 155° symmetric split pole dipole magnet with a 5-cm gap, 56-cm radius, and 21° edge angles. In the horizontal plane in the center of this dipole magnet, the beam will be parallel, whereas in the vertical plane, a waist will be formed. Assuming no aberrations, the object beam spot will be transported with unit magnification to the image slits with about 1.0-m dispersion, giving an expected mass resolution greater than 1/1000.

A single isobaric mass chain will be selected and refocused by an electrostatic quadrupole-triplet lens into a round beam for transport through a 12-cm-long, 8-mm-diameter, charge-exchange cell. The negative-ion output beam will be refocused by another quadrupole-triplet lens into the entrance of the 300-kV tube to accelerate the beam-to-ground potential.

The second stage of the mass separator will be part of the negative-ion injection line from the high-voltage source platform to the tandem accelerator. A horizontal view of this beam line is shown in Fig. 19 and a vertical view is shown in Fig. 1. Originally, this beam line was designed conceptually only to transport ions. The line is 23 m long with a 65° horizontal beam and a 90° vertical bend directly below the tandem accelerator. Injection will be accomplished by merging the RIB through the de-energized, existing mass-analyzer injector magnet. Looking down from the tandem injection line, there will be two injectors: the existing injector for stable heavy ion beams and a new injector for radioactive heavy-ion beams produced by ORIC. The negative-ion injection line will be optimized and reconfigured, as needed, to be a second-stage mass separator. Under certain conditions, the energy-analyzing system of the tandem accelerator will provide a second or perhaps third stage for mass separation.

THE HHIRF TANDEM AS A RIB ACCELERATOR

In many ways, tandem accelerators are ideal to produce RIBs for experimental use. Tandem accelerators combine simplicity and ease of operation with low beam energy spread and beam emittances of less than 1.0 π mm.mrad. Tandem accelerators are dc devices which provide the proper time matching to the target-ion source. More importantly, tandem accelerators are the only existing proven solution to accelerate low-charge-state, high-mass ions at low injection voltages. The HHIRF 25-MV tandem can accelerate all ions with masses up to 80 with single-foil or single-gas stripping to energies above the Coulomb barrier for nuclear structure studies. With double stripping, and the corresponding beam intensity loss, masses up to the rare earths can be accelerated over the Coulomb barrier. For very heavy beams, a postaccelerator would be required for nuclear structure physics; however, these very heavy beams would be available at lower energies for astrophysics and applied research.

With gas stripping, the beam-transport system of the tandem accelerator itself can be used as a second or perhaps third-stage mass separator. In particular, the beam energy-analyzer 90° magnet shown in Fig. 5 has a dispersion of 3.35 m. Figure 20 shows a direct beam profile measurement at the image plane of this magnet. The data on the left is the beam current measured on a single slit with a 63.3-MeV $^{16}O^{2+}$ beam. Subequilibrium gas stripping was used and the terminal potential was stabilized with a generating voltmeter. The function on the right is the derivative of a functional fit to the data on the left and is an approximation to the actual beam profile. The observed FWHM of the beam on the energy-analyzer magnet focal plane is 0.27 mm. This width corresponds to a mass-resolving power of one part in 12,400. This mass-resolving power could perhaps be increased by a factor of two by using more of the available aperture of the energy-analyzer magnet. This resolving power improvement would

require the addition of quadrupoles, and possibly multipole correctors, in both the entrance and exit lines of the energy-analyzer magnet. The measured emittance of this $^{16}O^{2+}$ beam is less than 0.5 π mm.mrad and the energy spread is small. The excellent beam quality from the HHIRF tandem accelerator, coupled with its fine beam transport system, may provide, with gas stripping, the necessary mass resolving power for isobar selection. With foil stripping, the beam energy spread may be too large to separate isobars.

CONCLUSIONS AND SCHEDULE

Almost all hardware required to reconfigure the HHIRF accelerator system to produce radioactive beams is now being designed and almost all physics factors for the process are being studied. It is hoped that about one year after this conference RIBs will be produced by ORIC with the new RIB injector and accelerated to 300 kV. These beams will be used to study and optimize RIB production and may be used for low-energy RIB experiments. About one and a half years later, in the first half of 1995, RIBs should be injected into the tandem, accelerated, and used for the first experiments requiring high beam energies.

REFERENCES

1. "A Proposal for Physics with Exotic Beams at the Holifield Heavy Ion Research Facility," eds. J. D. Garrett and D. K. Olsen (ORNL, February 1991).

2. H. L. Ravn and B. W. Allardyce, *Treatise on Heavy Ion Science*, ed. D. A. Bromley, Vol. **VIII**, *Nuclei Far From Stability* (Plenum Press, New York, 1989), p. 363.

3. J. D. Cole, T. M. Cormier, J. H. Hamilton, and A. V. Ramaypa, Nucl. Instr. and Meth. **B70**, 343 (1992).

4. W. T. Milner, G. D. Alton, D. C. Hensley, C. M. Jones, R. F. King, J. D. Larson, C. D. Moak, and R. O. Sayer, IEEE Trans. Nucl. Sci. **NS-22**, 1697 (1975).

5. J. P. Raymond, IEEE Trans. Nucl. Sci. **NS-34**, 1620 (1987).

6. R. G. Alsmiller, F. S. Alsmiller, and O. W. Hermann, Nucl. Instr. and Meth. **A295**, 337 (1990).

7. C. B. Fulmer, H. M. Butler, and K. M. Wallace, Particle Accelerators **4**, 63 (1972).

8. Some details on the approach of PACE can be found in A. Gavron, Phys. Rev. **C21**, 230 (1980).

9. G. D. Alton, Nucl. Instr. and Meth. **A244**, 133 (1986); G. D. Alton, Y. Mori, A. Takagi, A. Ueno, and S. Fukumoto, Nucl. Instr. and Meth. **A270**, 194 (1988).

10. J. G. Tracy, private communication (1990).

11. R. Kirchner, K. H. Burkard, W. Huller, and O. Klepper, Nucl. Instr. and Meth. **186**, 295 (1981).

Table 1. HHIRF beams provided for scheduled experiments.

BEAM	MAXIMUM ENERGY (MeV)	MODE*	BEAM	MAXIMUM ENERGY (MeV)	MODE*
^{1}H	25	T	^{52}Cr	230	T
^{6}Li**	70	T	^{56}Fe	890	T,C
^{7}Li	128	T,C	^{58}Ni	1010	T,C
^{9}Be	158	C	^{60}Ni	228	T
^{10}B	168	C	^{63}Cu	189	T
^{11}B	169	T,C	^{65}Cu	290	T
^{12}C	300	T,C	^{64}Ni**	290	T
^{13}C**	67	T	^{70}Ge	154	T
^{16}O	405	T,C	^{74}Ge	306	T
^{17}O**	381	C	^{76}Ge	305	T
^{18}O**	356	T,C	^{79}Br	1000	C
^{19}F	190	T	^{81}Br	604	C
^{23}Na	117	T	^{74}Se	164	T
^{24}Mg	200	T,C	^{76}Se	169	T
^{25}Mg	132	T	^{78}Se	320	T
^{26}Mg**	200	T	^{80}Se	285	T
^{27}Al	196	T	^{82}Se	315	T
^{28}Si	333	T,C	^{90}Zr	500	T
^{29}Si	150	T	^{93}Nb	276	T
^{30}Si	264	T	^{107}Ag	374	T
^{31}P	136	T	^{109}Ag	733	C
^{32}S	725	T,C	^{116}Cd**	499	C
^{34}S**	170	T	^{112}Sn**	570	C
^{36}S**	165	T	^{116}Sn**	684	T,C
^{35}Cl	703	T,C	^{117}Sn	645	T
^{37}Cl	187	T	^{120}Sn	240	T
^{40}Ca	601	C	^{127}I	399	T
^{44}Ca**	205	T	^{148}Nd**	700	C
^{48}Ca**	200	T	^{150}Nd**	760	C
^{45}Sc	200	T	^{150}Sm**	701	C
^{46}Ti**	280	T	^{156}Gd**	885	C
^{48}Ti	581	T,C	^{197}Au	591	T
^{49}Ti**	235	T	^{208}Pb	982	C
^{50}Ti**	250	T	^{238}U	119	T
^{51}V	216	T			

* T = Tandem alone; C = Coupled mode.
** Beam provided with separated isotope probe sample.

Table 2. Oak Ridge Isochronous Cyclotron (ORIC) parameters.

Bending Limit (ME/q2)	100
Focusing Limit (ME/q)	65
Magnet System	
Pole face diameter	193 cm
Number of compact sectors	3
Maximum spiral angle	30°
Minimum gap/maximum field	7.5 in/23.8 kG
Maximum gap/minimum field	28. in/13.2 kG
Main Coil Conductor	250 turns Al
Main Coil Power Supply	5000 A–350 V
Trim coils	10 pairs
Harmonic coils	4 pairs per valley
Weight	210 tons
RF System	
Configuration	Single 180° dee to ground
Maximum voltage per gap	70 kV
Maximum RF power	200 kW
Frequency range	6.7–20.1 MHz
Vacuum System	
Operating pressure	1×10^{-6} Torr
Pumps	Two 80-cm oil DP
	One 50-cm oil DP
	One 50-cm cryopump
Internal Ion Source	Cold cathode Penning
Extraction Channel	
One 60 cm long, 70 kV/cm, electrostatic deflector	
One 25 cm long, 3 kG, 5000 A, coaxial, septum magnet	
One 100 cm long, 6.5 kG, 3000 A-3000 A, compensated iron, magnetic channel	

Table 3. Estimated overall efficiency from atoms to accelerated beam.[a]

Element	Electron Affinity (eV)	Negative Ion Production Method[c]	Positive Ion Efficiency (%)[d]	Negative Ion Efficiency (%)[e]	Tandem Transport Efficiency (%)[f]	Overall Efficiency (%)[g]
He	0.08[b]	CE	2.4	1.5	80 G	0.01
Li	0.62	CE	14	9	80 G	0.50
Be	0.19[b]	CE	9.3	3	70 G	0.10
B	0.28	CE	11	12	60 G	0.40
C	1.27	CE	8.9	42	47 G	0.88
N	<0					
O	1.46	CE	8.5	45	35 G	0.67
F	3.40	SI		100	32 G	16.0
Ne	<0					
Na	0.55	CE	27	5	30 G	0.20
Mg	<0					
Al	0.46	CE	25	14	28 G	0.49
Si	1.39	CE	19	60	28 G	1.60
P	0.74	CE	15	70	26 G	1.37
S	2.08	SI		15.8	26 G	2.05
Cl	3.62	SI		100	25 G	12.5
Ar	<0					
K	0.50	CE	42	1.8	24 G	0.09
Ca	0.04	CE	30	0.4	23 G	0.01
Sc	<0					
Ti	0.2	CE	29	4	21 G	0.12
V	0.5	CE	31	10	21 G	0.33
Cr	0.66	CE	31	10	21 G	0.33
Mn	<0					
Fe	0.25	CE	27	6	11 F	0.09
Co	0.70	CE	28	12	10 F	0.17
Ni	1.15	CE	29	60	11 F	0.96
Cu	1.23	CE	30	60	9.5 F	0.86
Zn	<0					
Ga	0.3	CE	40	7	9.0 F	0.13
Ge	1.20	CE	31	62	8.6 F	0.83
As	0.80	CE	26	75	8.5 F	0.83
Se	2.02	CE	26	75	8.2 F	0.80
Br	3.36	SI		100	8.2 F	4.10
Kr	<0					
Rb	0.49	CE	64	0.8	8.0 F	0.02

[a]Excluding decay and target release losses.
[b]Metastable state.
[c]SI denotes direct surface ionization, CE denotes charge exchange.
[d]Scaled as discussed in the text.
[e]Measured efficiencies.
[f]F or G denotes gas or foil stripping in the tandem terminal.
[g]Includes an additional 50% reduction to account for transport losses to the tandem accelerator.

Table 4. Summary of release times $\tau_{1/2}$ and release efficiencies η.

Projectile	Implantation Energy (MeV)	Target Material	Range (μm)	τ (s)	η (%)
^{35}Cl	162	Zr_5Si_3	26.3	13	87
^{75}As	209	Zr_5Ge_3	18.3	39	24
^{79}Br	183	Zr_5Ge_3	15.6	7	61
^{78}Se	209	Zr_5Ge_3	18.0	40	5
^{78}Se	183	Zr_5Ge_3	15.0	25	27

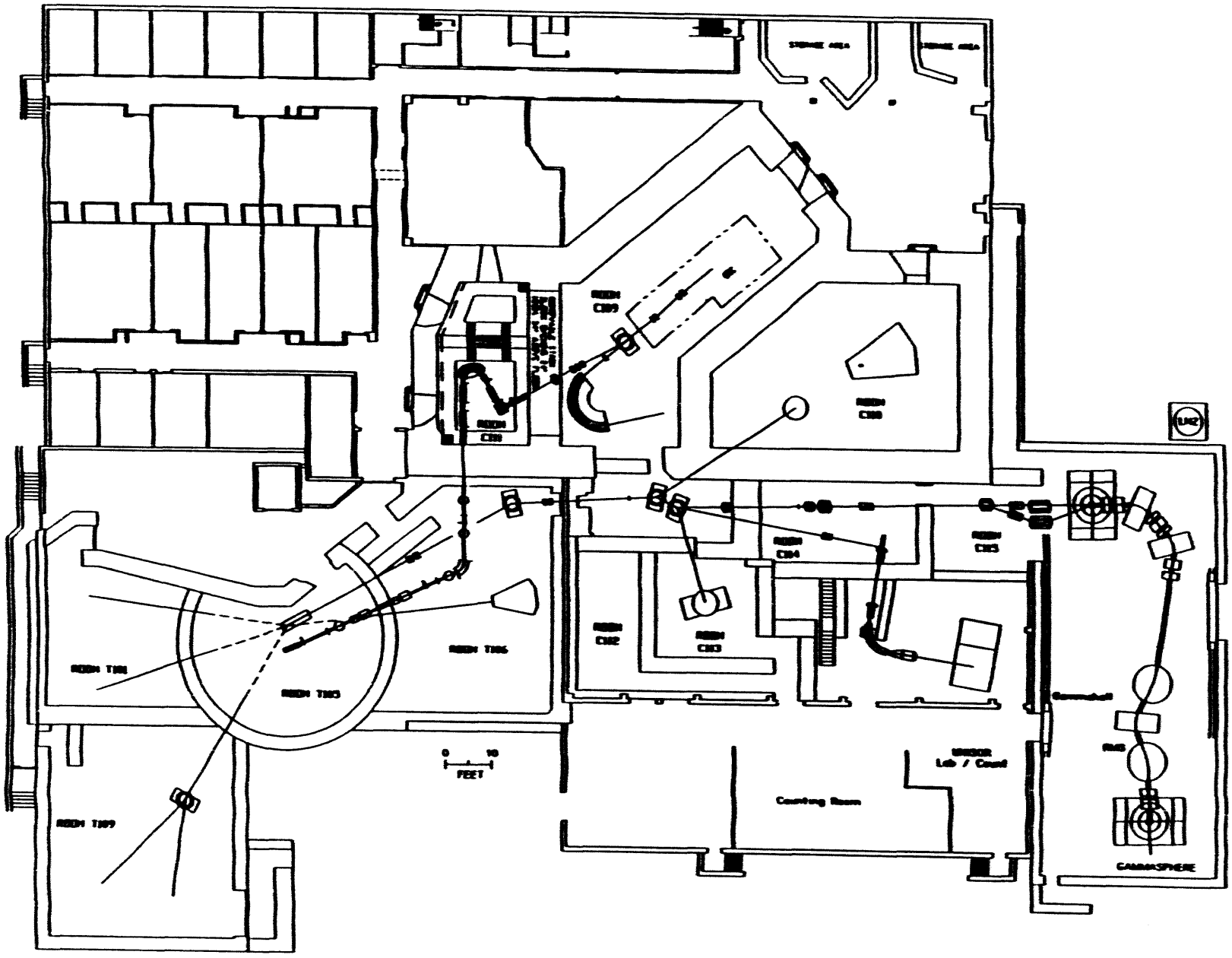

Fig. 1. First floor layout of the ORNL RIB facility.

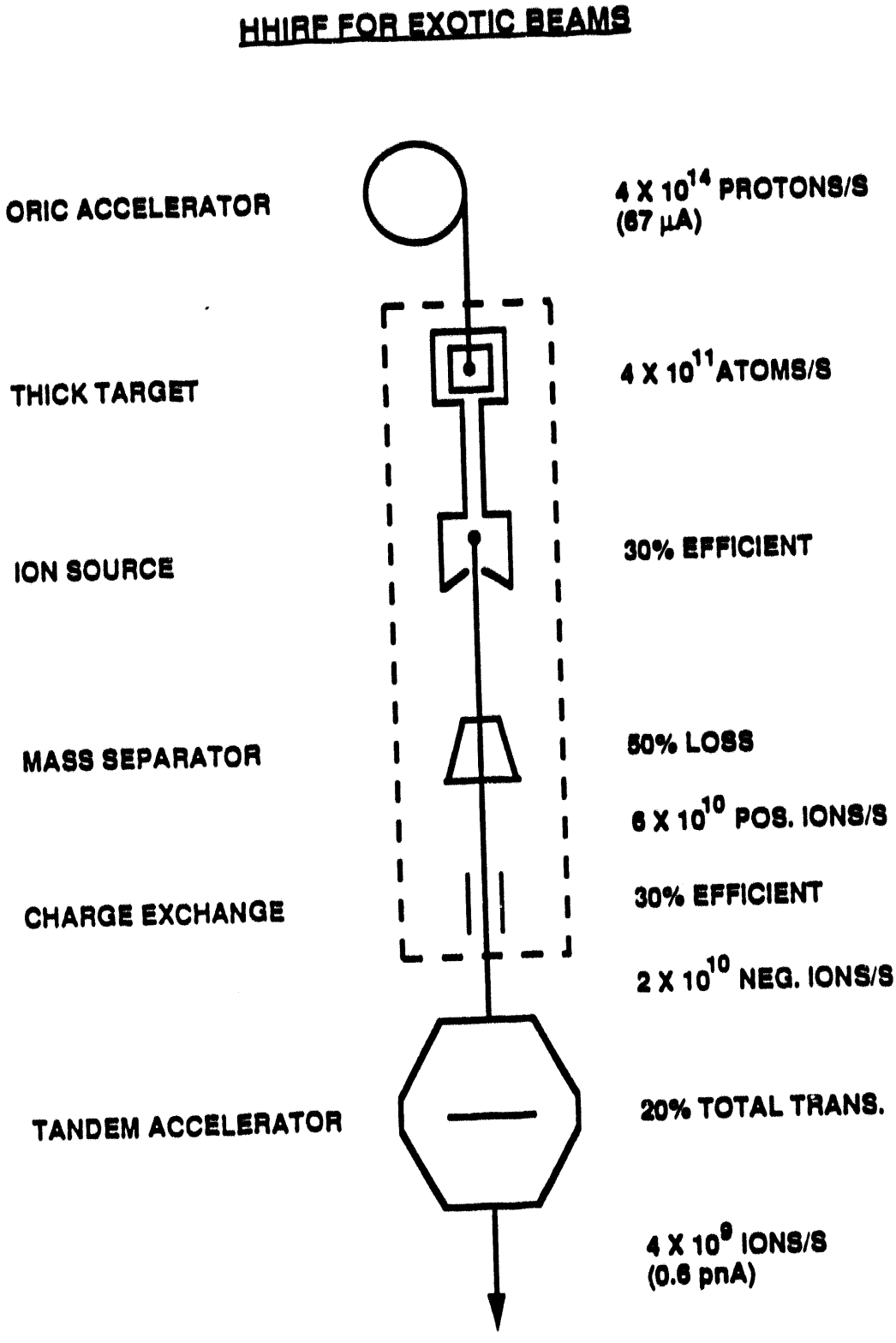

Fig. 2. Summary of the ORNL RIB concept with average efficiencies for a "very good case" RIB produced with 67 μA of 30-MeV protons. About 10^{-5} of the primary beam or 0.6 pnA of RIBs would be produced as beam on target under ideal conditions.

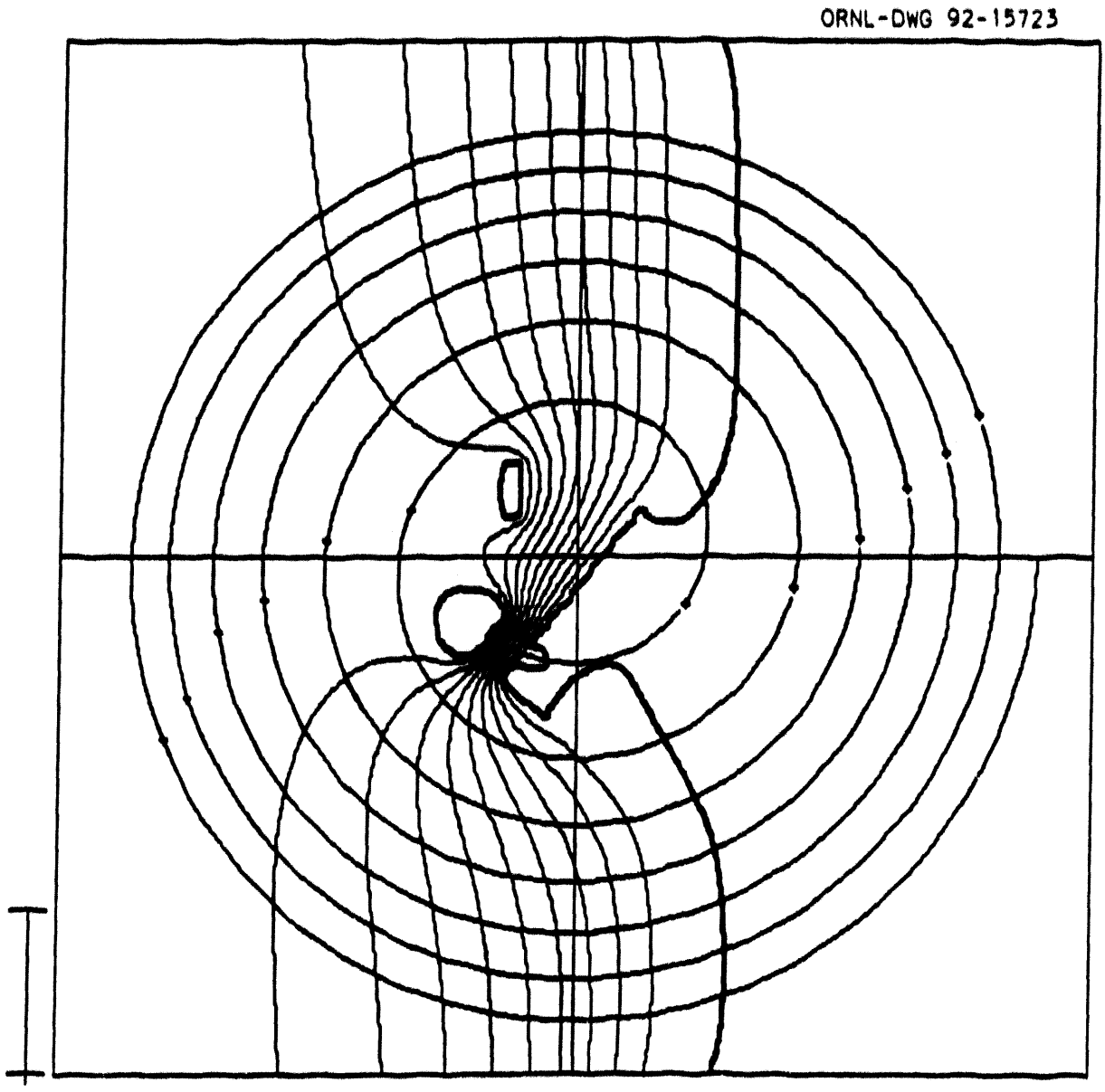

Fig. 3. The central ray trajectory for the first six turns superimposed on the electric field equipotential lines for an optimized ORIC central region for a K = 75 H_2^+ beam.

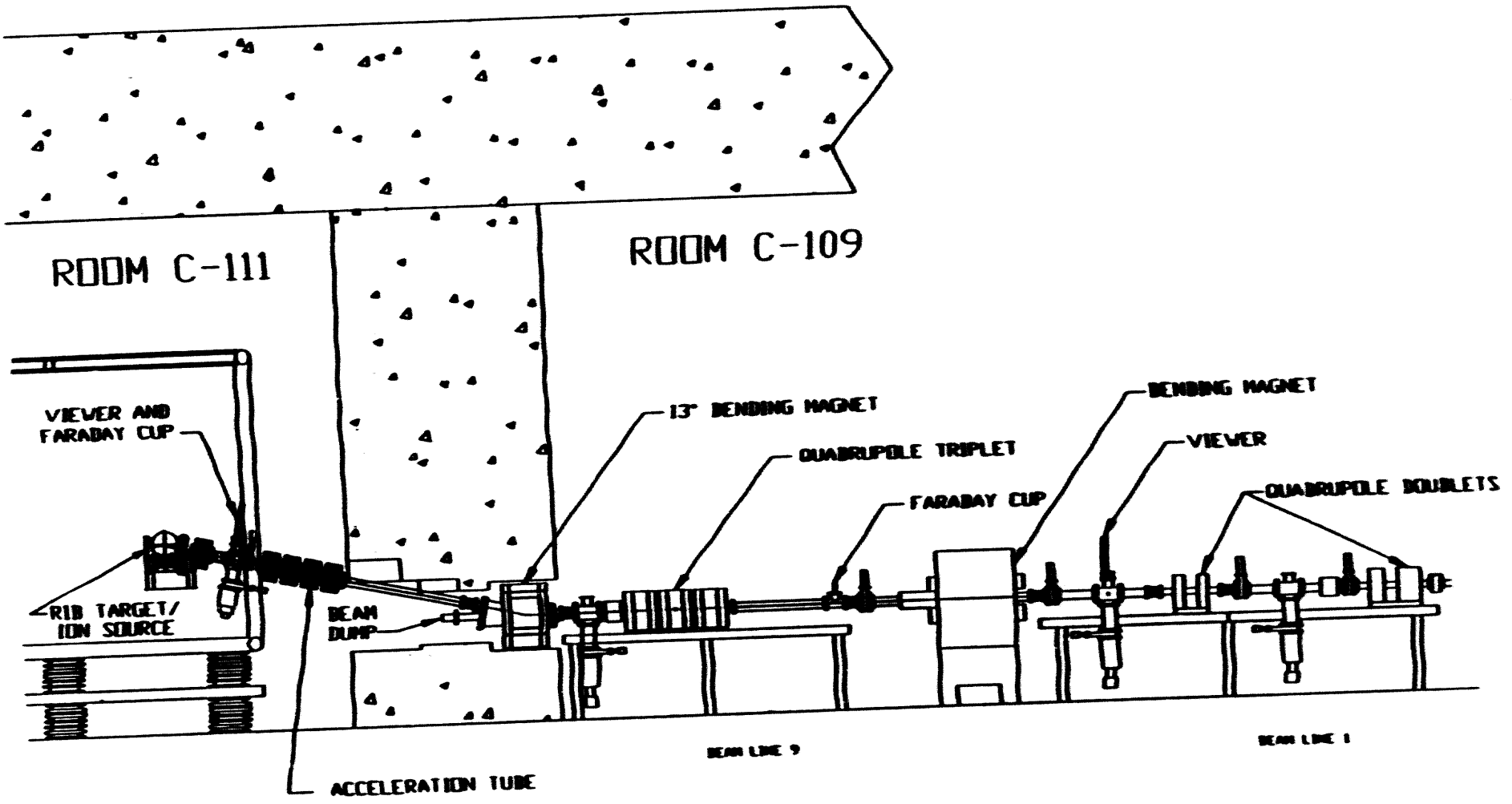

Fig. 4. Reconfigured light-ion all-aluminum beam line from ORIC to the RIB target-ion source on the HV platform.

ORNL-DWG 92-15734

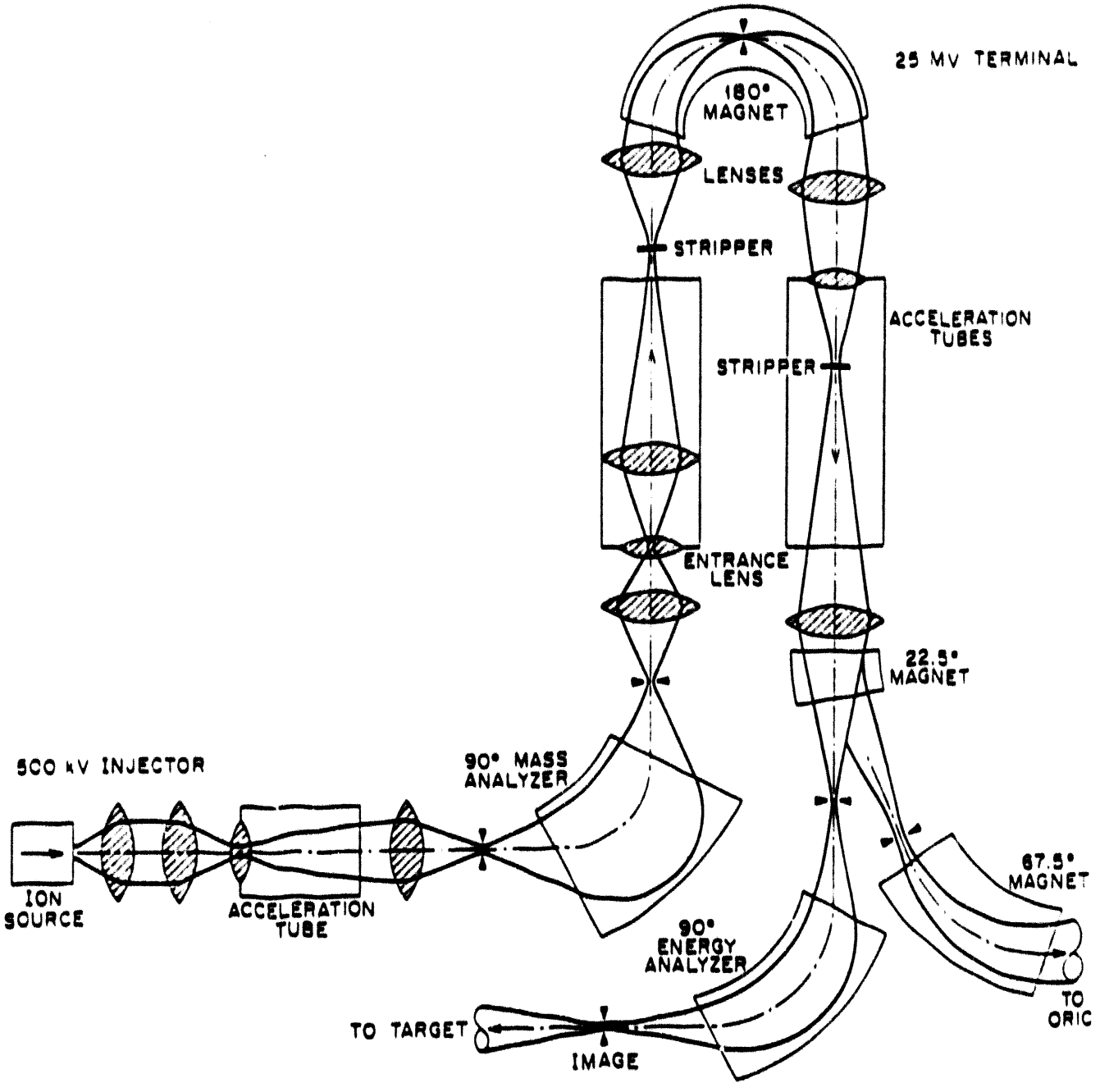

Fig. 5. Beam transport system of the HHIRF 25-MV folded tandem accelerator. The effective entrance lens of the low-energy and high-energy acceleration tubes are shown. With gas stripping, the 90° energy-analyzer magnet can be used to separate isobars.

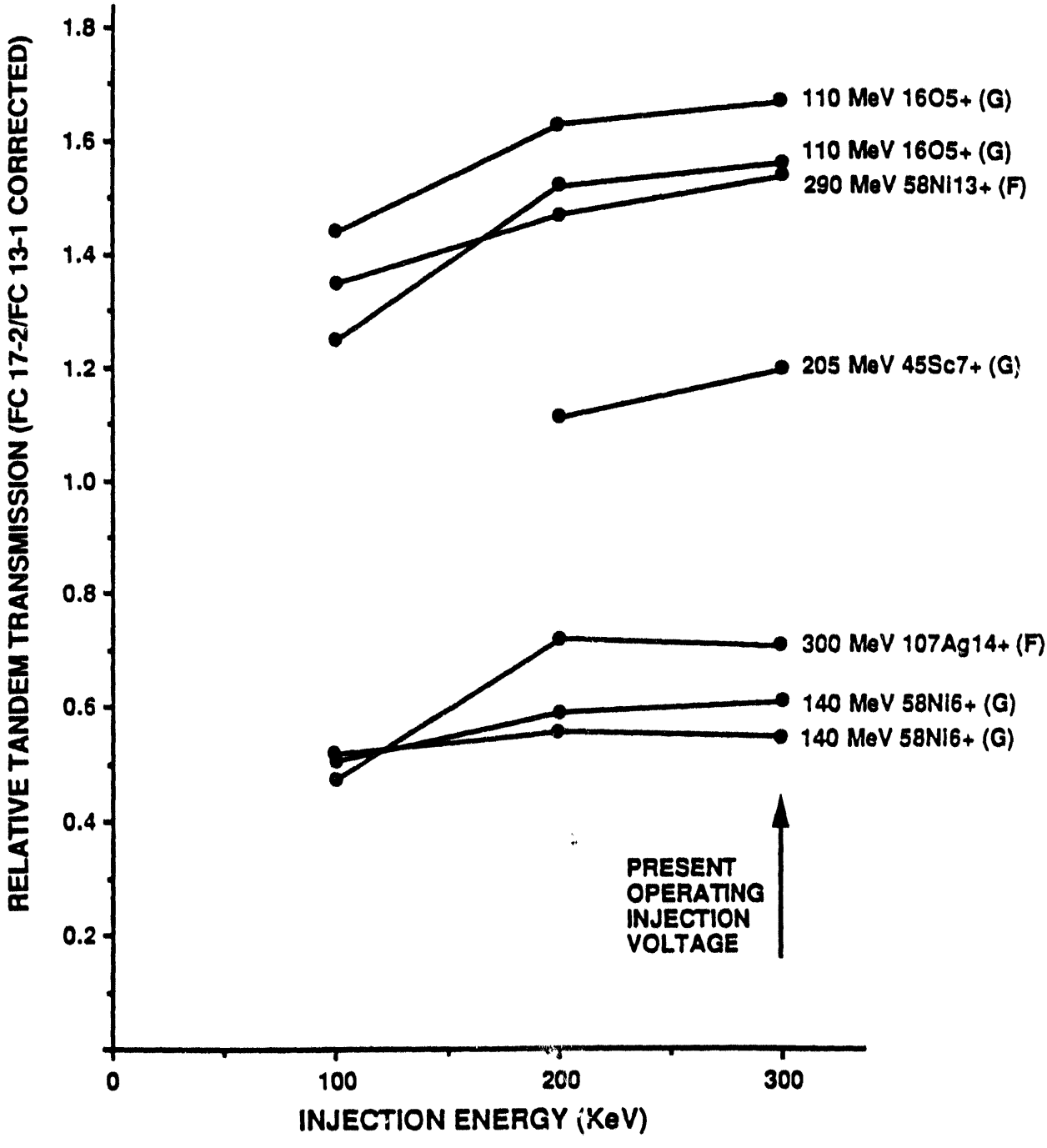

Fig. 6. Measured relative transmission efficiency through the tandem accelerator for various gas and foil stripped beams as a function of injection energy.

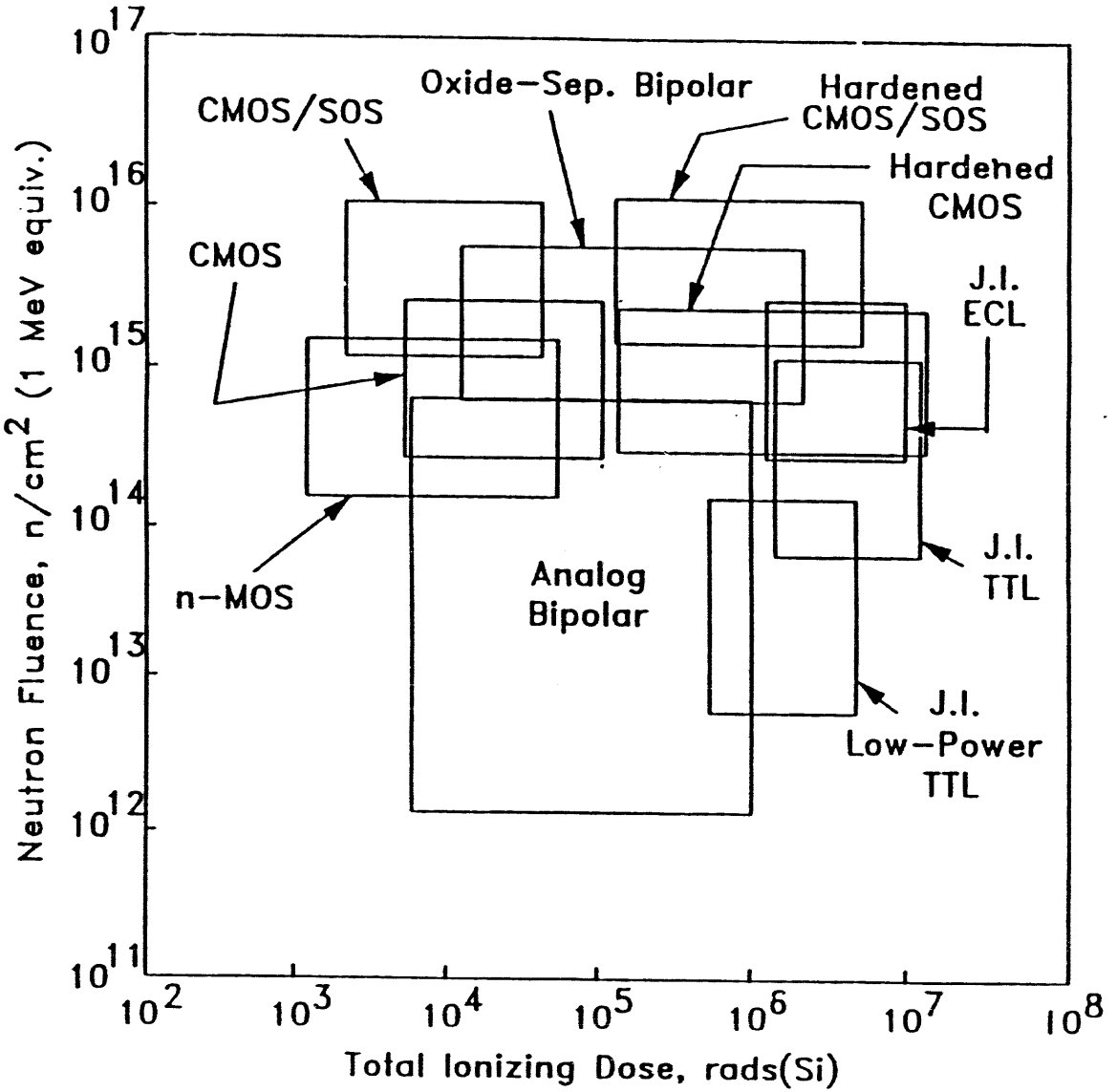

Fig. 7. Radiation damage to various semiconductor devices as a function both of total ionizing dose and neutron fluence. The squares outline the threshold and assumed levels of damage. Figure from J. P. Raymond, IEEE Trans. Nucl. Sci. **NS-22**, 1697 (1975).

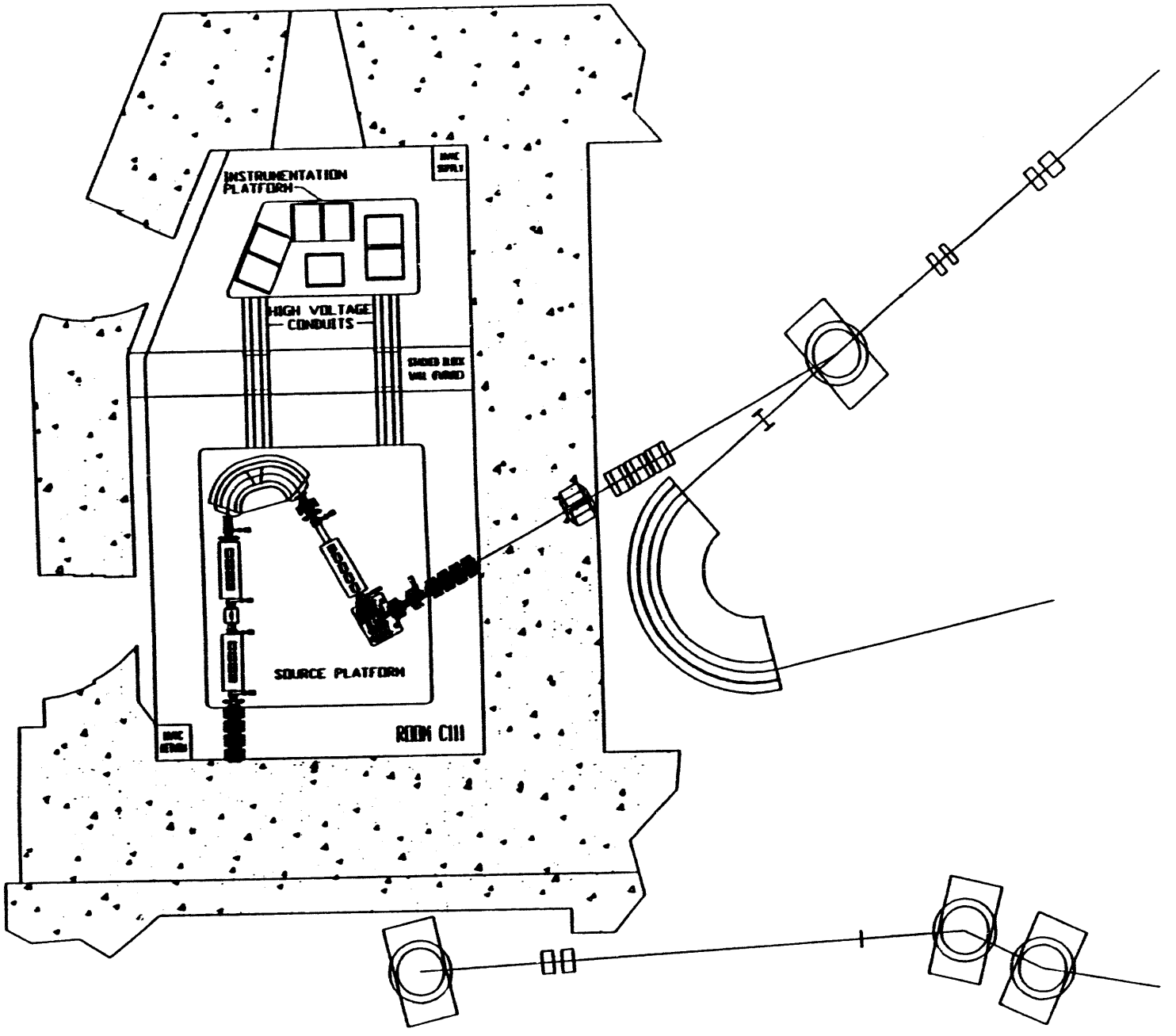

Fig. 8. High-voltage platform system floor plan showing the source platform, instrumentation platform, shielding wall, high-voltage conduits, MG sets, and instrumentation racks.

ORNL-DWG 92-15738

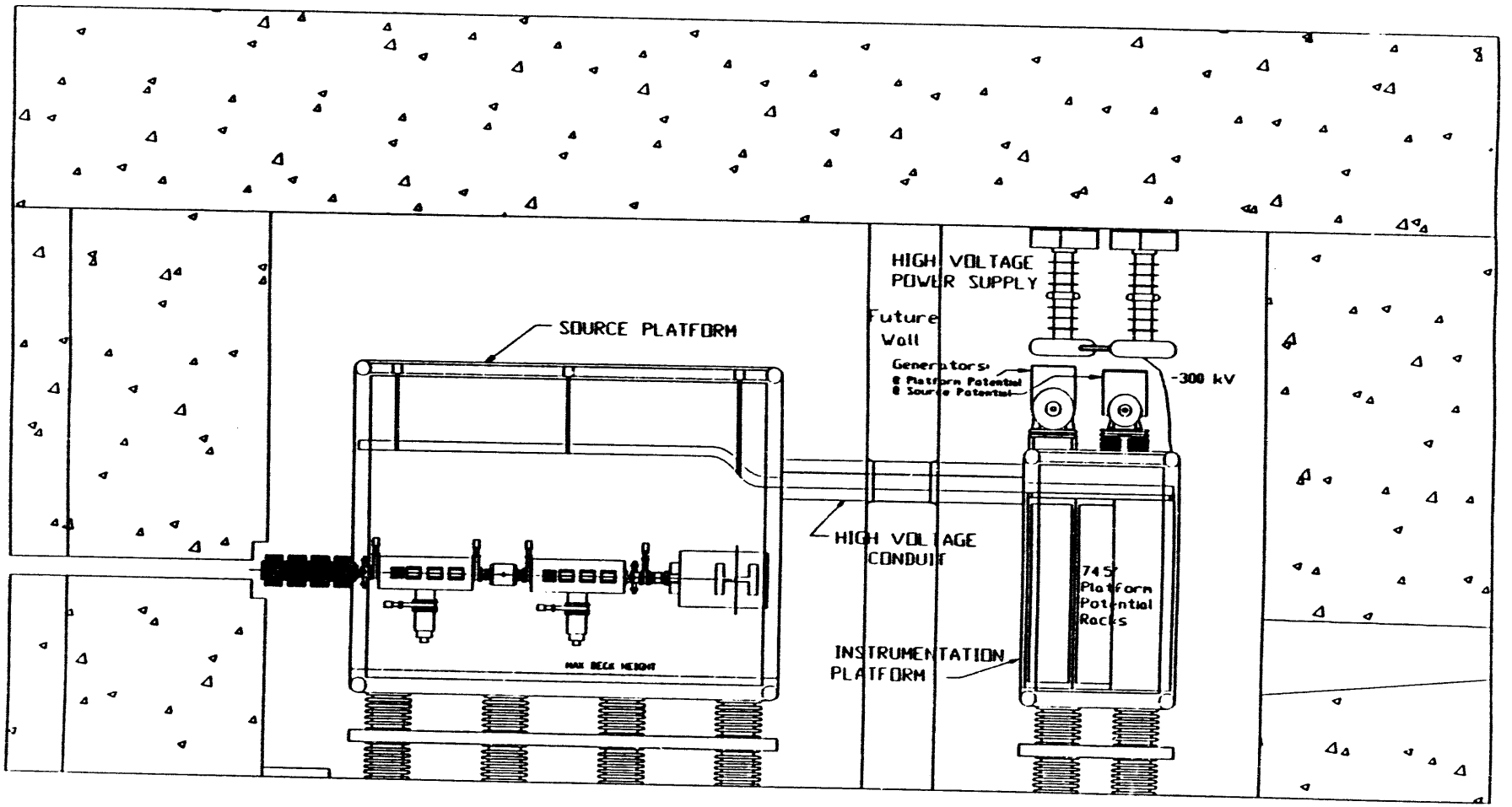

Fig. 9. High-voltage platform system elevation plan: west view showing platform components.

ORNL-DWG 92-15739

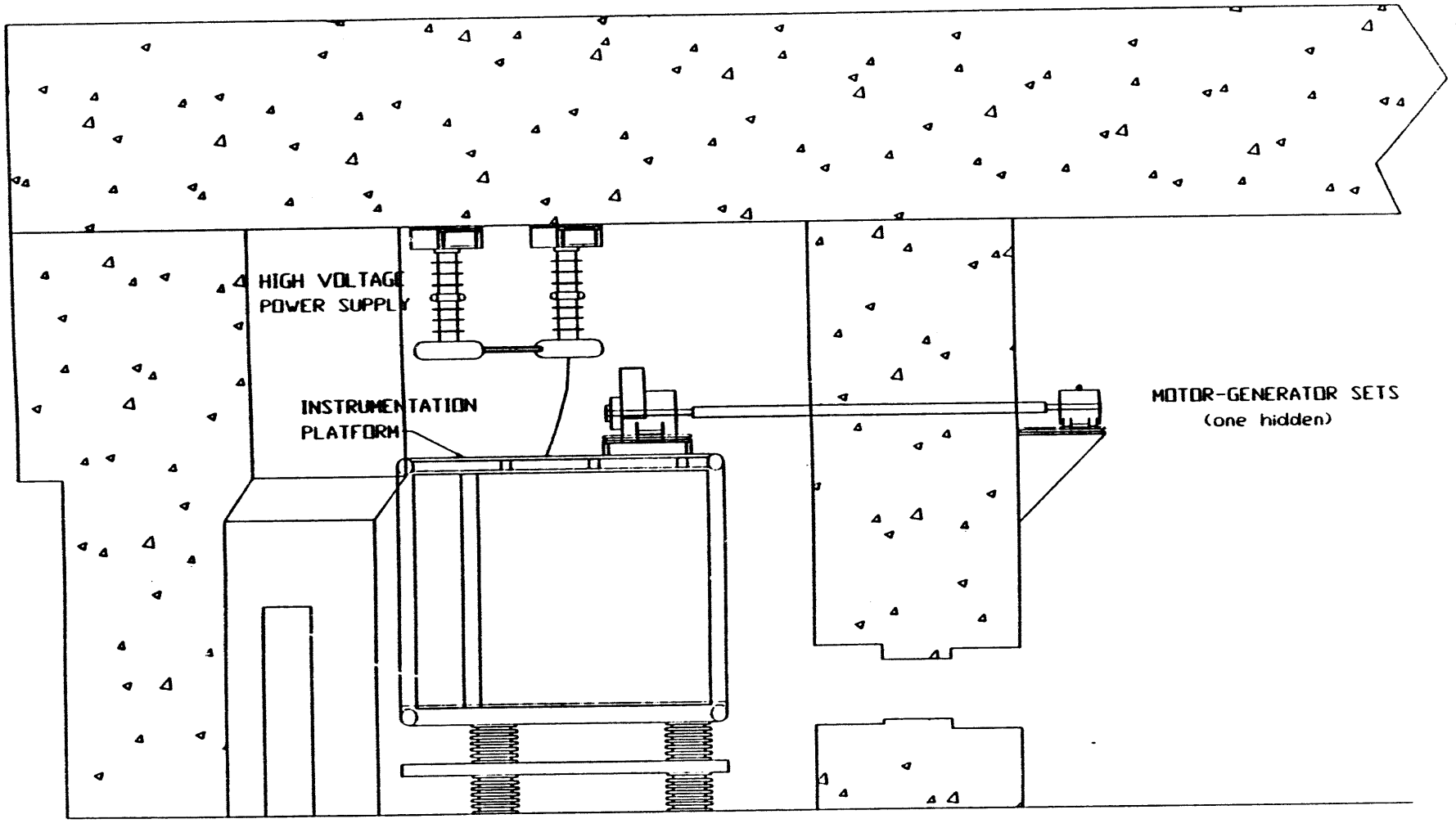

Fig. 10 High-voltage platform system elevation plan: north view of instrumentation platform.

HETC YIELD CALCULATION OF 40/50/60-MeV PROTONS STOPPING IN 70Ge32

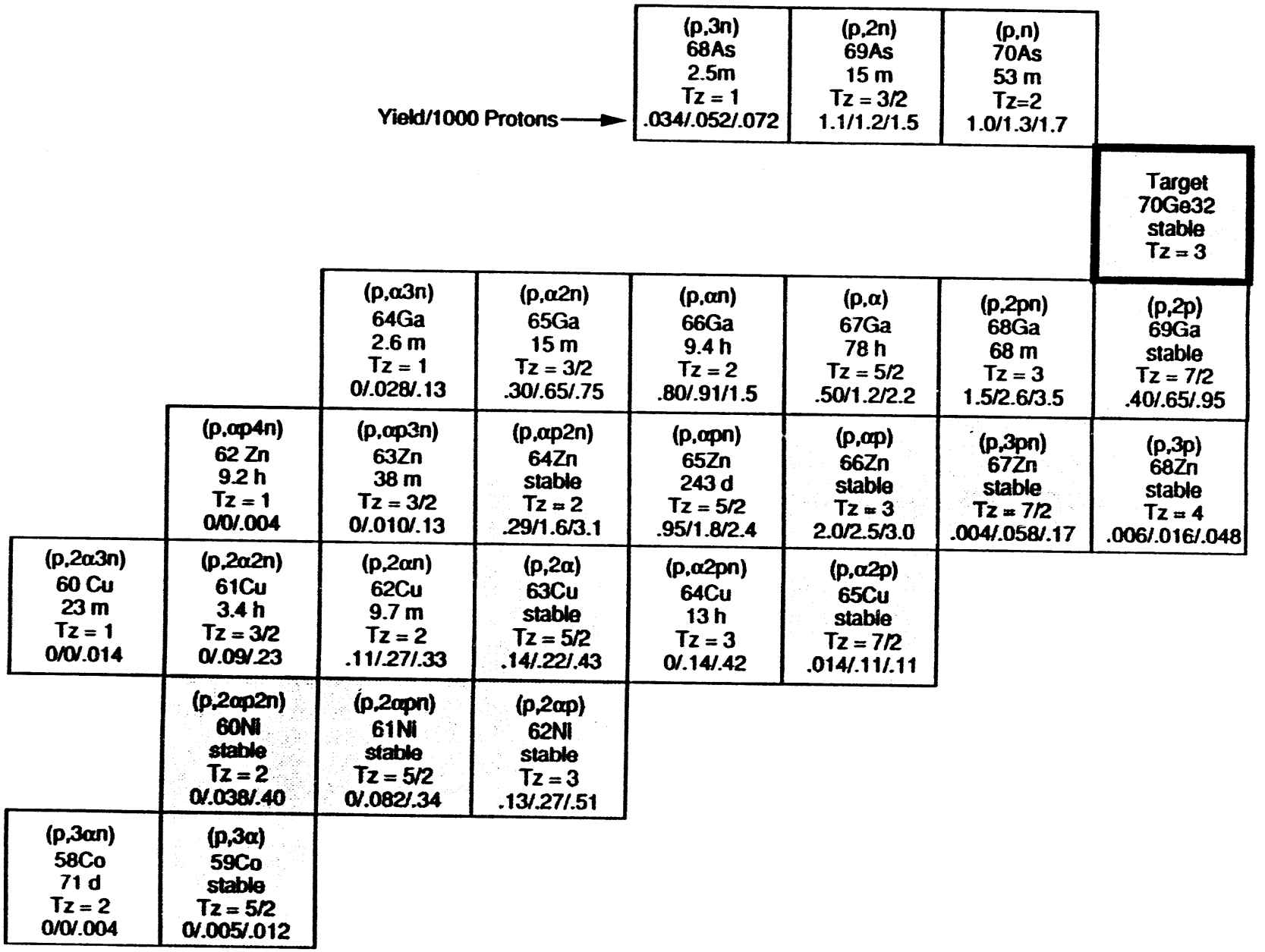

Fig. 11. HETC yield calculation of 40/50/60-MeV protons stopping in $^{70}Ge^{32}$.

HETC YIELD CALCULATION OF 60-MeV PROTONS STOPPING IN 76Ge32

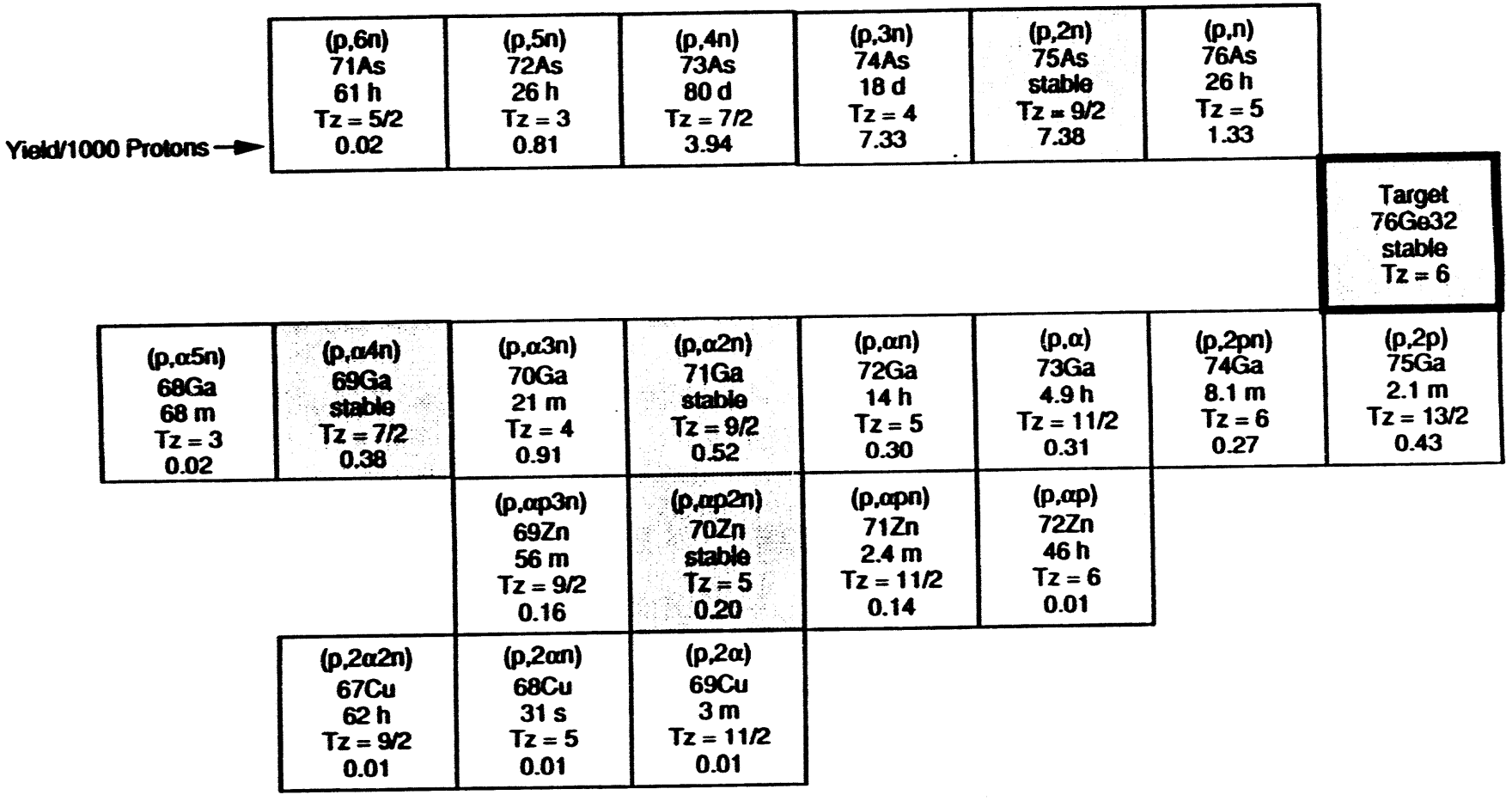

Fig. 12. HETC yield calculation of 60-MeV protons stopping in $^{76}Ge^{32}$.

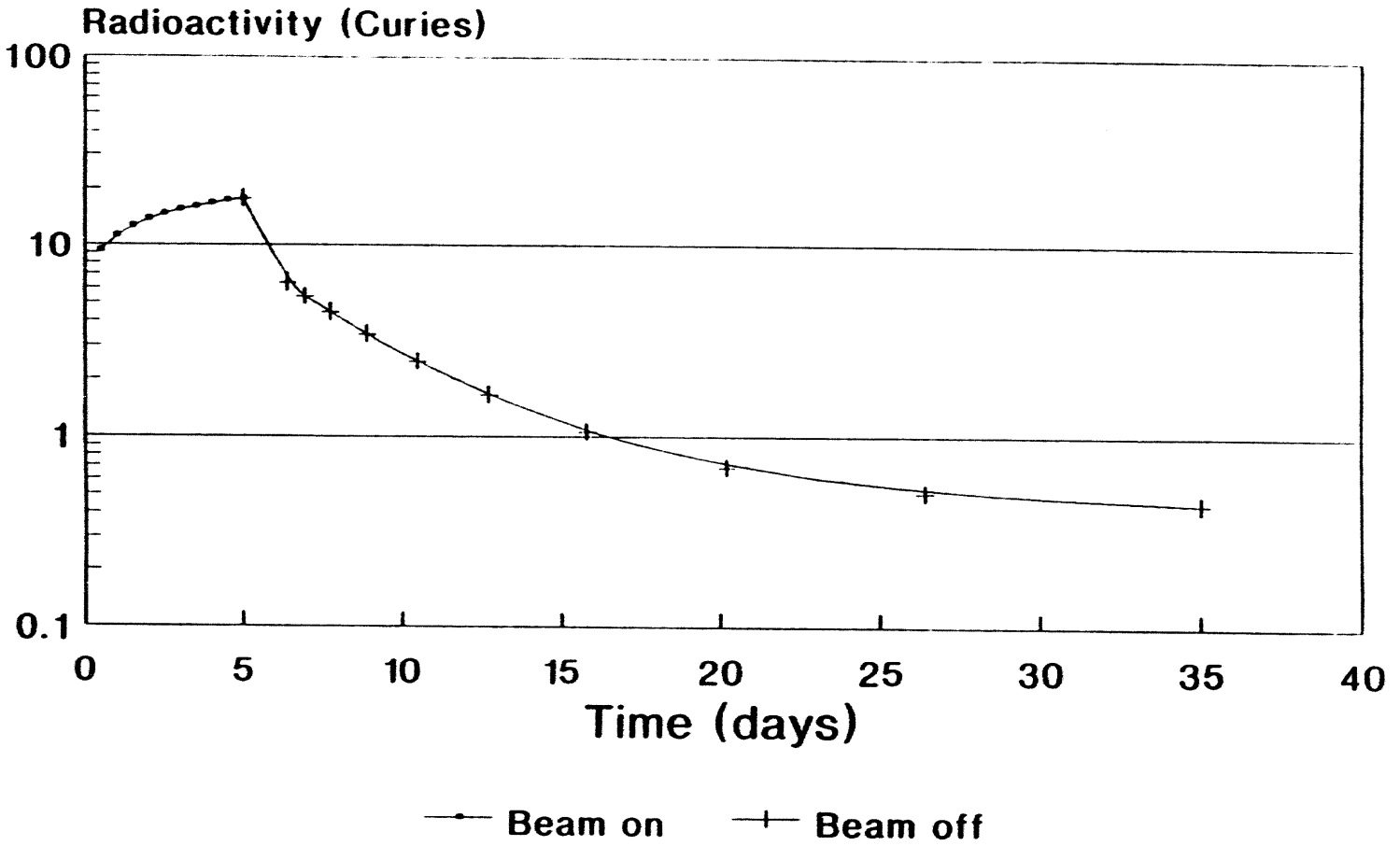

Fig. 13. Delayed gamma activity from a Zr(5)70Ge(3) target bombarded for five days with a 2.0 KW of 43-MeV proton beam. The target was about 1 mm thick, corresponding to a 7-MeV energy loss.

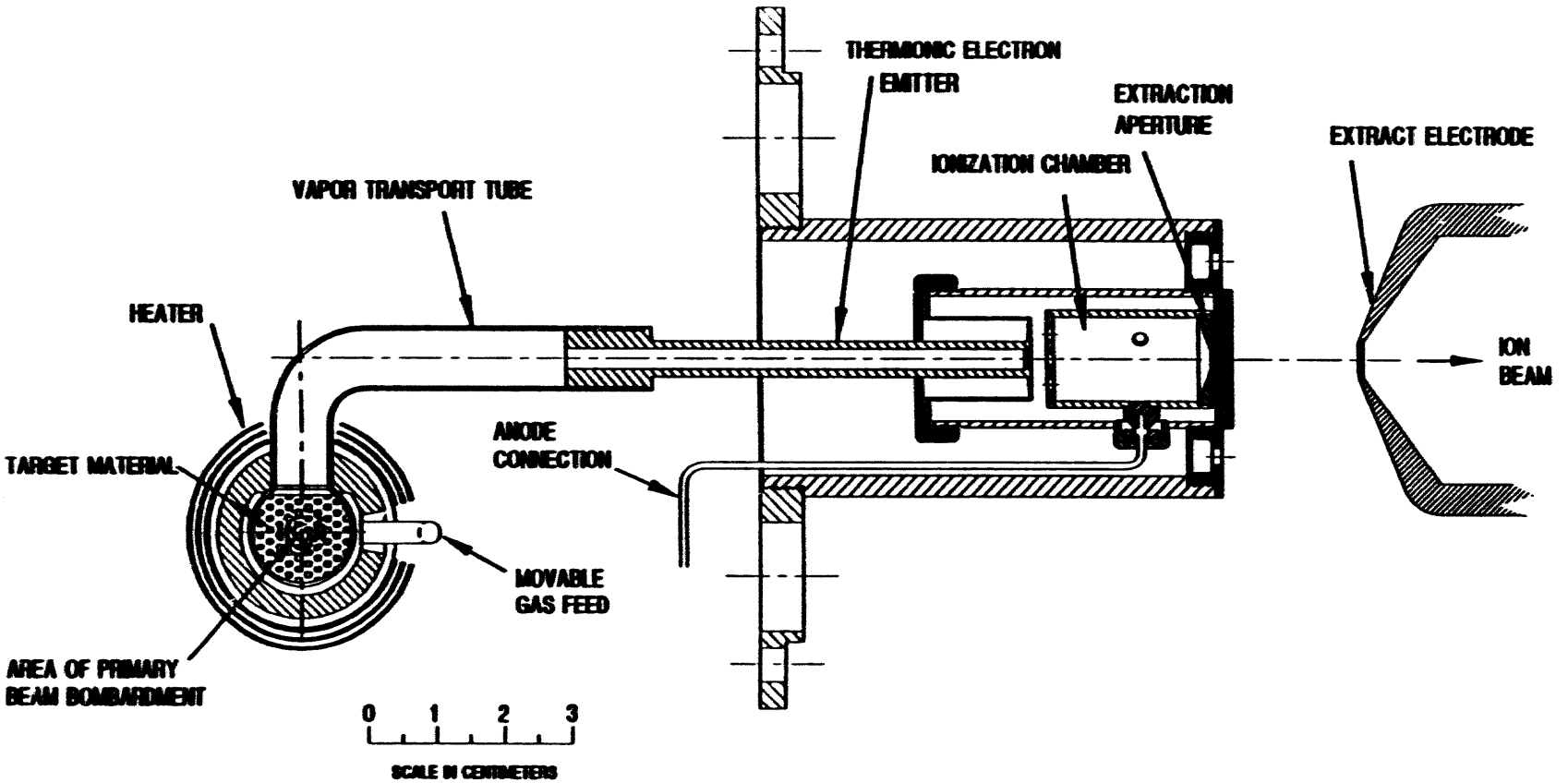

Fig. 14. ORNL Mark-I target-ion source based on the ISOLDE FEBIAD target-ion source design.

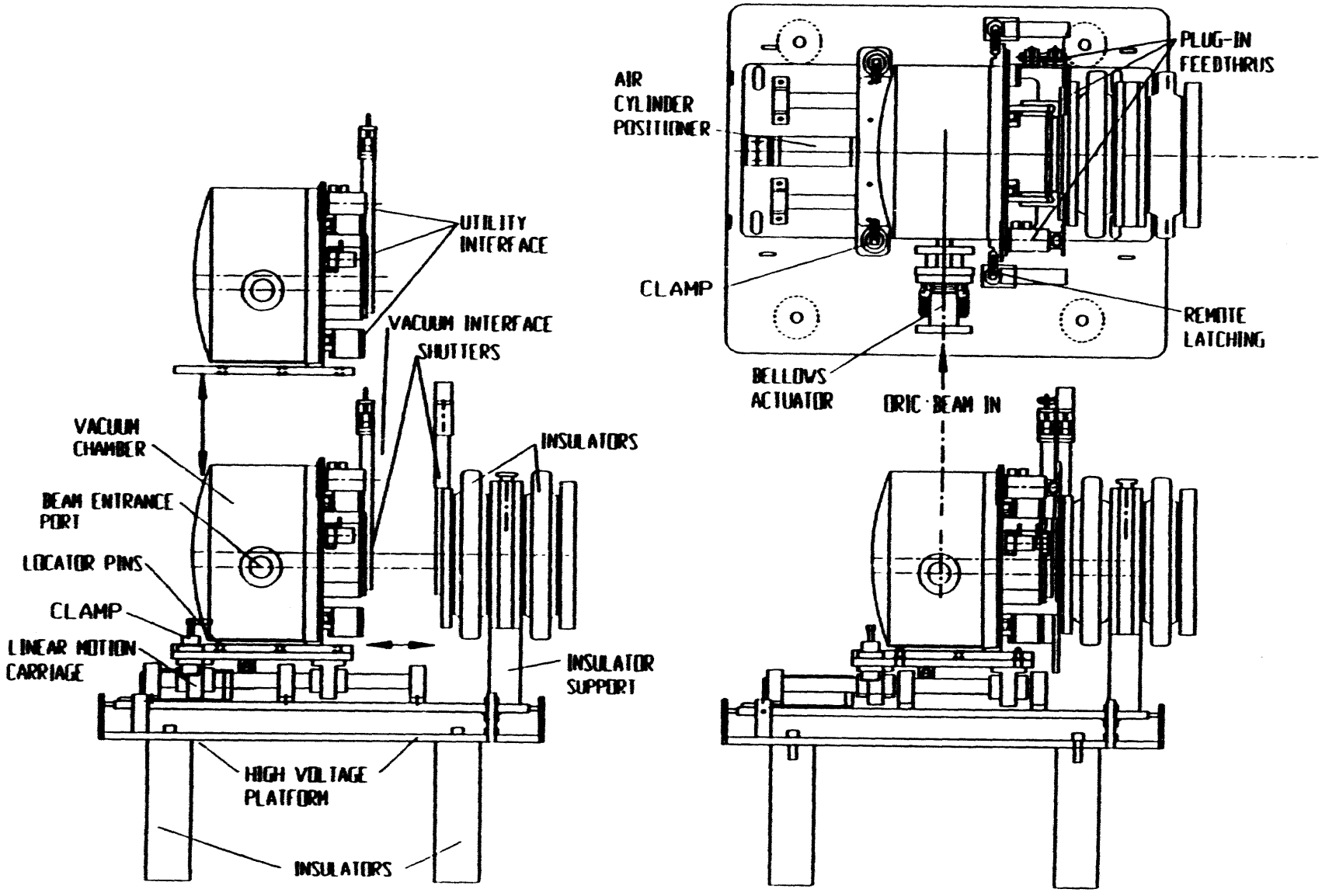

Fig. 15. ORNL RIB Mark-I target-ion source assembly which has been designed for remote installation and removal.

ORNL-DWG 92-15745

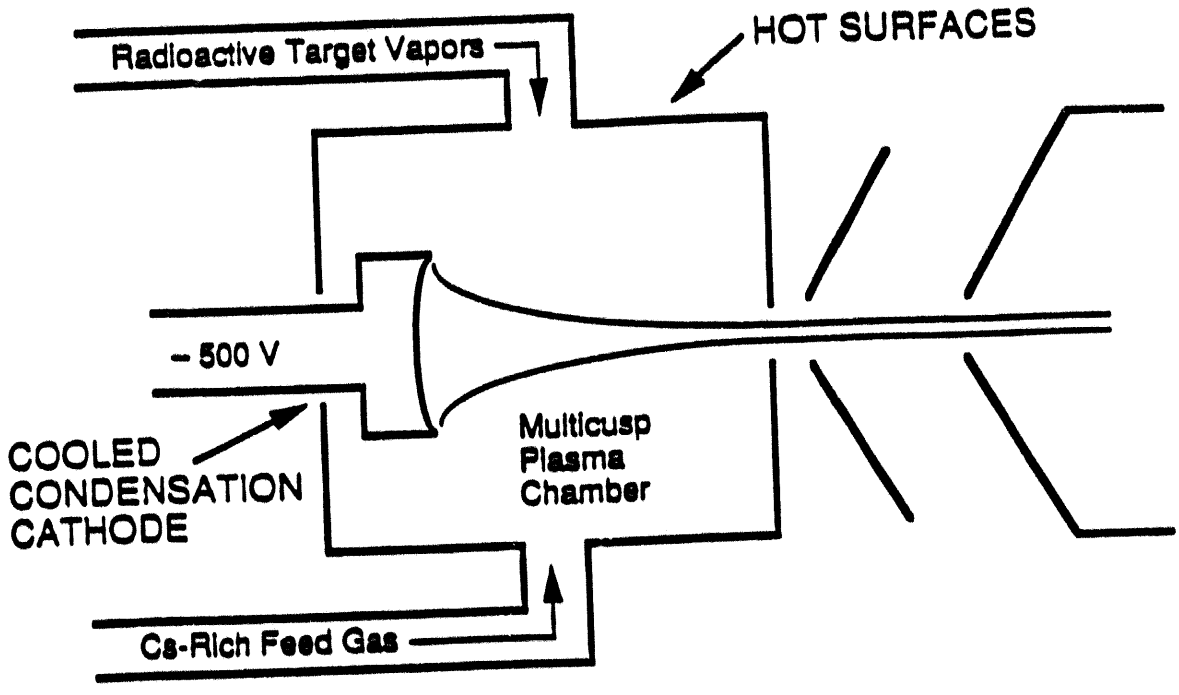

Fig. 16. Concept for the second ORNL RIB target-ion source. Negative ions will be made directly by plasma sputtering condensed radioactive vapors from a cold cathode. The plasma will be contained with a multi-cusp field in a chamber with hot walls.

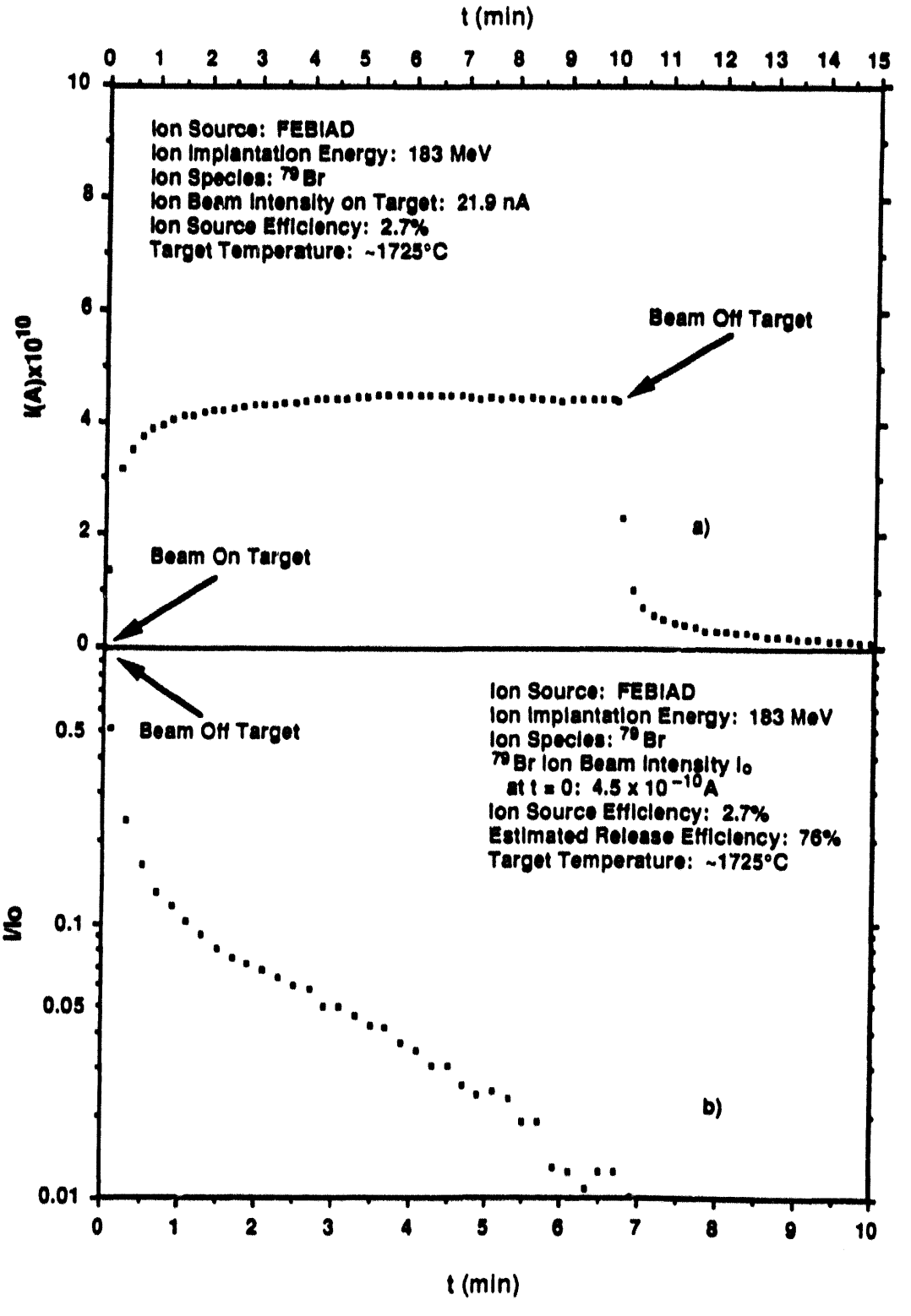

Fig. 17. Release profile using the UNISOR FEBIAD target-ion source and mass separator. A ^{79}Br beam was implanted in a Zr(5)Ge(3) target. About 76% of the ^{79}Br was available for ionization with a release time of seven seconds.

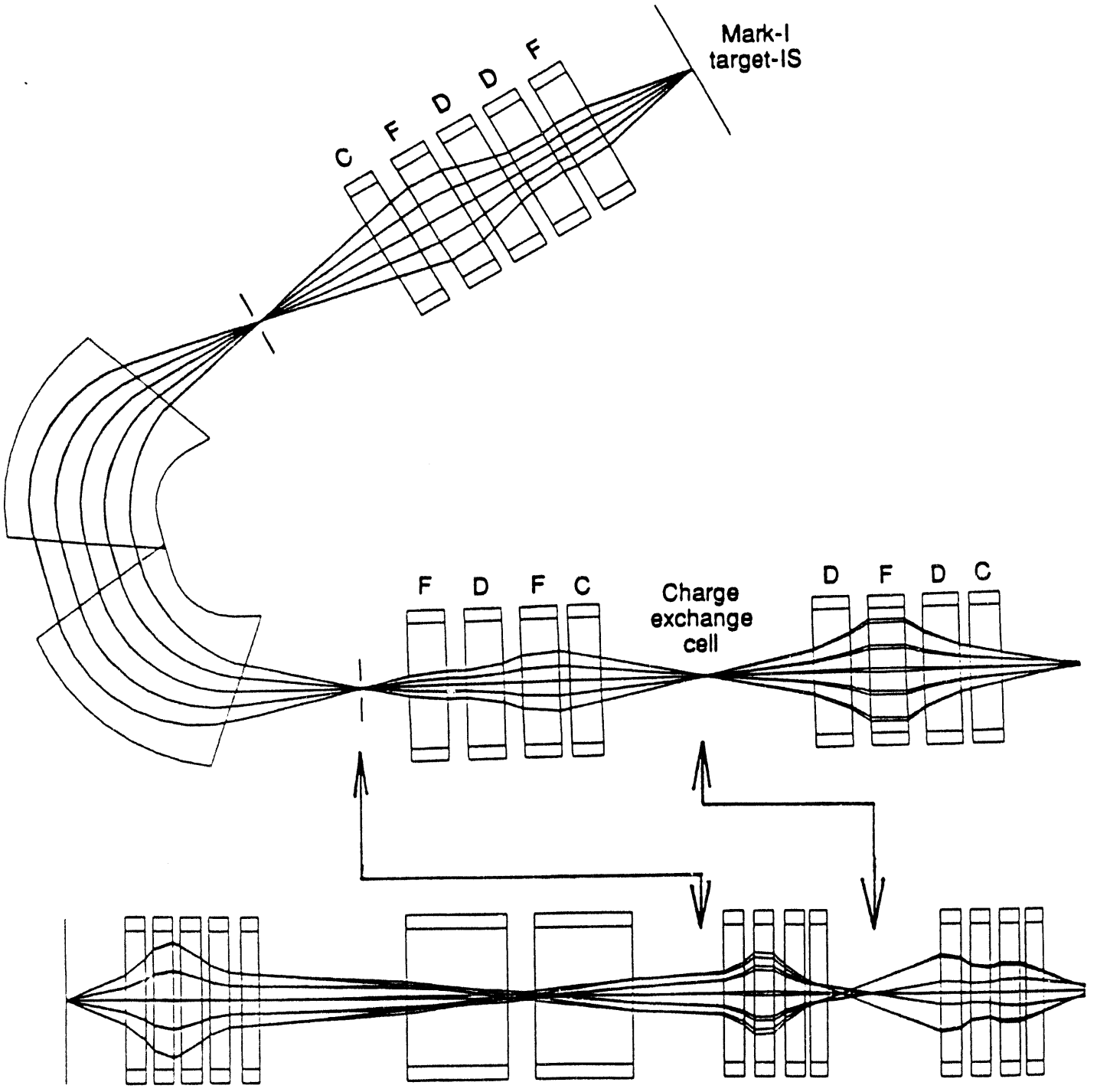

Fig. 18. Horizontal view and stretched vertical view of the beam envelope from the Mark-I target-ion source through the first-stage mass separator on the HV source platform. The envelopes were calculated to third order with the computer code GIOS.

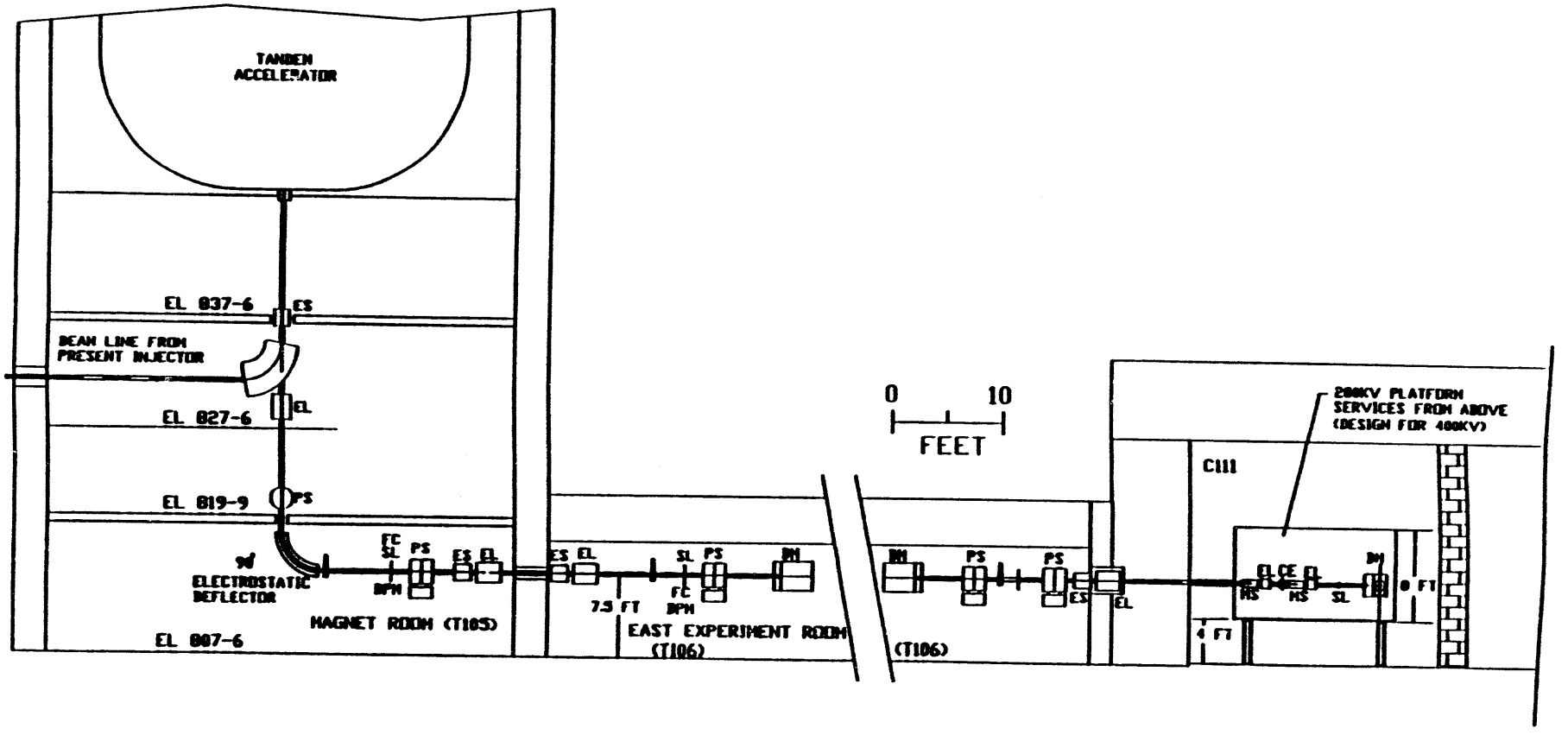

Fig. 19. Side view of the ORNL RIB facility showing the RIB HV injector and the negative ion transfer line to the tandem accelerator.

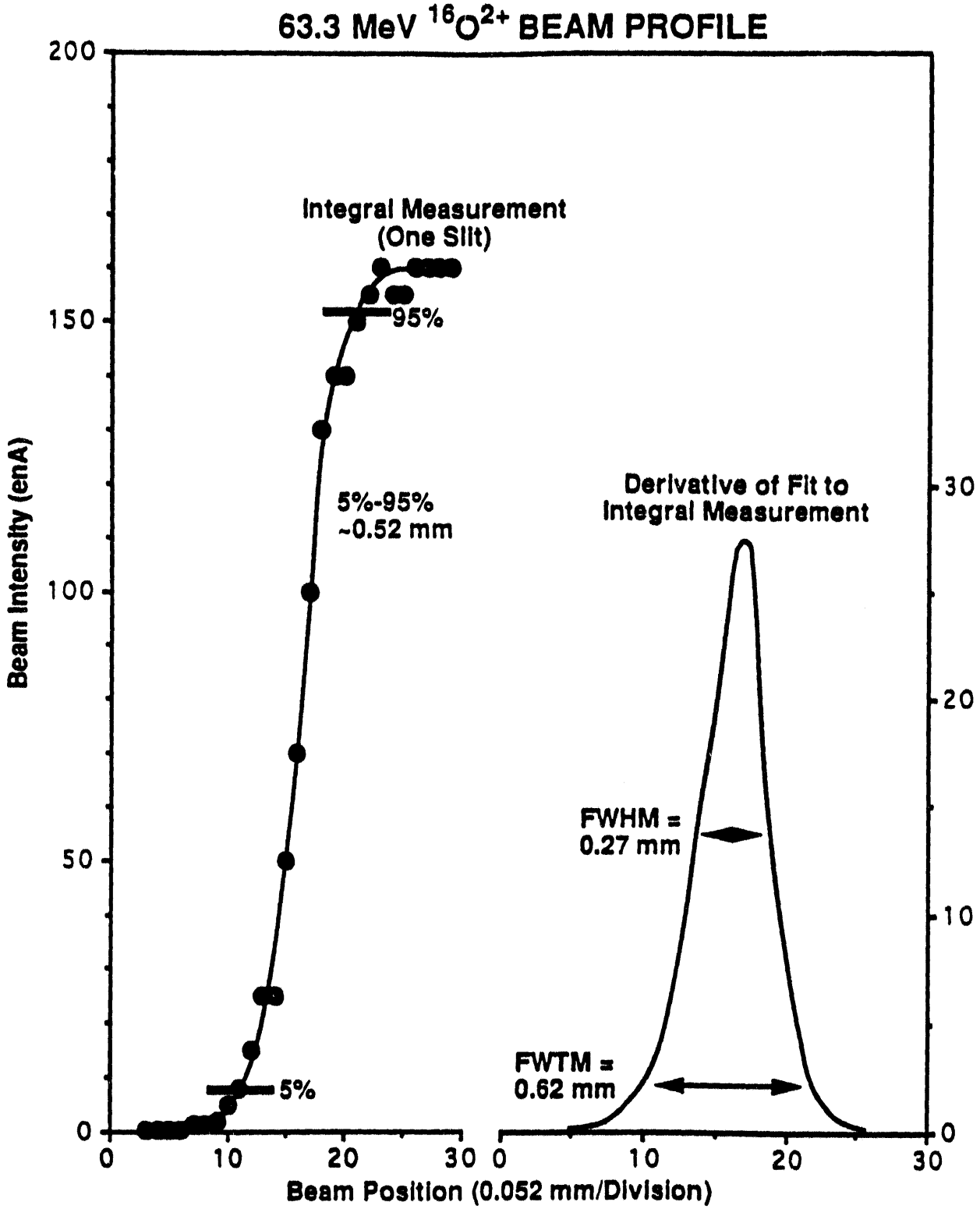

Fig. 20 Beam profile measurement at the image position of the energy-analyzing magnet of the 25-MV tandem accelerator. The function on the left was measured with a single slit for a 63.3-MeV $^{16}O^{2+}$ beam with the terminal potential stabilized with a generating voltmeter. The function on the right is the derivative of a functional fit to the measured data on the left and is an approximation to the actual beam profile. The observed FWHM of 0.27 mm corresponds to a mass resolving power of one part in 12,400.

Section V
Concluding Remarks

R. F. Casten, Chairman, ISL Steering Committee

Concluding Remarks*

R. F. Casten
Chairman, ISL Steering Committee

The following are some brief remarks and reflections on the Workshop and an indication of our plans and directions to continue the process that was begun in earnest here.

I would like to start by expressing my gratitude, on behalf of the ISL Steering Committee, to all the participants for coming but, more importantly, for your active role in the obvious success of the Workshop. This was, indeed, in the truest sense of the word, a real Workshop, a gathering that stressed communication, give-and-take, and exchange of ideas. I was very much impressed by the frank and open nature of both the formal and informal discussions. We were very fortunate to have an abundance of experts in many key areas related to RNBs--including primary and post-acceleration, targets and ion sources, front-end low energy ion beam acceleration, isotope/isobar separation, instrumentation for experiments, and so on. It is evident that you prepared in advance by relating your expertise to the needs and goals of the ISL. Early in the conference this was vividly clear in the invited talks. The speakers made extensive efforts to deal seriously with the ISL concept, as outlined in the White Paper, published in the Fall of 1991, without cringing from suggesting modifications to them. It was equally evident in the sessions of the three working groups in which an awesome amount of expert knowledge, experience, and forethought was brought to bear on the issues surrounding the production, extraction, and acceleration of RNBs and their use in a truly impressive array of experiments spanning many scientific disciplines ranging from atomic and materials science, through nuclear physics to astrophysics. Once again, we on the Steering Committee are very grateful for your efforts on behalf of the ISL.

*Based on concluding remarks at the close of the Workshop.

As a result of the talks and discussions, an imposing amount of information has been aired. It will need digesting and assimilating. Many new ideas were presented, many options debated, many difficulties studied. Some solutions to technical issues were achieved. In other cases, it is clear that solutions (sometimes multiple) exist and will not present serious problems. In other cases, there is a clear need for further work, for in-depth study of different scenarios, of the feasibility of various schemes, and, in some cases, such as target heating/ion source work, much room for innovative R&D. Indeed, some R&D is already underway, as witnessed by the ISL participation in the recently-approved RAL high-intensity target/ion source testbed facility which will provide 100 μA of proton beam on thick targets. R&D of a different sort is developing in earnest in the area of instrumentation for experiments, fostered and motivated in part by the need to prepare for experiments at the first-generation RIB facility under construction at Oak Ridge now.

One of the most important aspects of the Workshop, and one where many new realizations surfaced, was in understanding the relation between the science to be done and the output specifications of the ISL. It is clear that different science puts different demands on the facility. Moreover, this relationship of science to specifications is complex and multi-dimensional. Some experiments will require the highest RNB energies practical, but not for all masses. Others will require the heaviest nuclei but can tolerate lower beam energies. Different experiments, entailing different combinations of beam mass, energy and intensity, will have varying beam purity and/or emittance requirements. And, fortunately, there are also some experiments that are much less demanding in almost every specification.

Particularly important in this Workshop were the in-depth interactions between the machine experts and those interested in carrying out ISL experiments. It is through such interactions that impractical or overly grandiose schemes can be tempered with reality and the scope of current and foreseeable technology. These two groups have, sometimes, different approaches, needs, and philosophies: communication between them, which we tried to foster here, is critical, symbiotic, and effective.

This complex manifold of science and technical requirements needs to be well understood. This work will be greatly aided by the efforts of this Workshop, and the proceedings will be an invaluable resource. One of the summaries of this Workshop, by Dave Vieira, that appears elsewhere in these proceedings, attempts to address these issues, reflecting some of the viewpoints and consensus that began to emerge from this Workshop. By considering the needs of different classes of experiments, and groups of scientists, he develops a table that offers an updated summary of some of the "base" and "desired" output specifications for the ISL. In addition, the Steering Committee is preparing a new survey questionnaire, to be sent to the nearly 450 members of the ISL USERS Group, that will poll our community to get a more quantitative feeling for the interests and priorities of its members. We will publish the results of this survey in a subsequent ISL newsletter. In this way, it is hoped that a clearer picture will emerge of what science can be done with what beam characteristics and what is foreclosed by less ambitious specifications. Out of this process we hope will emerge a consensus on what the most exciting science possibilities are and what they require from the facility. We need to know and understand, as clearly and quantitatively as possible, our options and the long-term consequences of decisions that need to be made rather soon.

The establishment of embryonic working groups, in the areas of target/ion sources, acceleration, and detection and instrumentation, prior to the workshop, along with their intense work during it, provides a base to continue into the future. The momentum and communication achieved here needs to be maintained. To this end, the Steering Committee is establishing three working groups that will focus on the most critical areas where work, study, and R&D is most urgently required. Other areas will not be neglected, but these working groups reflect the perceived technical priorities. Each will be convened by a member of the Steering Committee but, following initial establishment, will be encouraged to develop themodes of operation and contact best suited to its charge, to select chairpersons, and to continue an active study of their areas.

The table below summarizes the working groups and lists their convenors. Anyone interested in working in particular areas should contact the appropriate convenor (or any other member of the Steering Committee) as soon as possible as the efforts of this Workshop will continue actively and in earnest so as not to lose the momentum that has clearly been established

Of course, the areas listed separately in the table are not truly independent and the working groups will maintain contact and collaboration. As appropriate, they will issue reports, some of which may be presented in subsequent ISL USERS Group news-

Table: ISL Technical Working Groups

Working Group	Convenor
Targets and Ion Sources	Dave Vieira (LAMPF) John D'Auria (TRIUMF)
Front-end RNB Acceleration Systems	Mike Nitschke (LBL)
Experimental Instrumentation & Detection Equipment	Cary Davids (ANL)

letters, and future workshops, either broadly-based as in the present case, or focused on specific areas, may be planned. We will also explore funding scenarios for the Working Groups and for other ISL R&D since it is clear that such work will require tangible resources.

. . . . . .

A workshop of this type entails extensive planning and preparation by many people, most significantly by the participants to whom I have already expressed our gratitude. Here I would like to express appreciation to a number of specific people and organizations who contributed in important ways.

First, we are grateful to the Local Organizing Committee, especially Ken Carter, Carrol Bingham, David Olsen, Gerald Alton, and I.-Y. Lee for helping with the detailed planning for a Workshop that ran very smoothly.

Secondly, as all the participants are keenly aware, we are greatly indebted to the expert secretarial and administrative help we received. I cite especially Jody Heath, the Workshop Secretary, as well as Jackie Smith and Carlene Stewart.

Of course, the Workshop had substantial financial support, and we are grateful to all the sponsoring organizations. In particular, we thank the Joint

Institute for Heavy Ion Research and the Oak Ridge Associated Universities for helping with the organization of the Workshop.

Lastly, the Workshop Organizing Committee, composed of members of the ISL Steering Committee, was responsible for the planning of topics, organizing the working groups, selecting the speakers, and arranging the mix of formal and informal discussions so as to optimize open, in-depth discussions of various options, scenarios, difficulties, and opportunities. They deserve great credit and gratitude. Thus, I close by thanking John D'Auria, Mike Nitschke, Dave Vieira, Michael Wiescher, and especially the Workshop Chairman, Jerry Garrett, for their truly excellent, successful, and dedicated efforts.

Appendices

Appendix A:

Program for the Workshop on the Production and Use of Intense Radioactive Beams at the Isospin Laboratory

Wednesday, October 7, 1992 (B. Sherrill, presiding morning)
(E. Zganjar, presiding afternoon)

8:30 **Welcome** - *Jim Ball*, Physics Division Director, ORNL
R.F. Casten, Chairman, ISL Steering Committee
8:50 **Production of High Intensity Radioactive Beams** - *H. Ravn*
9:50 **Isobaric Mass Separators** - *H. Wollnik*
10:40 **Coffee Break**
11:10 **Radiation Problems** - *I. Thorson*
12:00 **Lunch**
13:15 **Cyclic Accelerators** - *Y. Jongen*
14:05 **Linear Accelerators** - *K. Shepard*
14:55 **Coffee**
15:25 **The Oak Ridge RIB Facility** - *D. Olsen*
16:15 **Prototypical Expmnts.: Nuclear Astrophysics** - *A. Champagne*

Thursday, October 8, 1992 (C. Davids, presiding morning)

8:30 **Prototypical Expmnts.: High Spins** - *C. Baktash*
9:10 **Prototypical Expmnts.: Nuclear Reactions** - *F. Becchetti*
9:50 **Prototypical Expmnts.: Proton-Rich Nuclei** - *J. Hardy*
10:30 **Coffee Break**
10:50 **Prototypical Expmnts.: Neutron-Rich Nuclei** - *K.L. Kratz*
11:30 **Prototypical Expmnts.: Materials Science** - *H. Haas*
12:10 **Lunch**
13:30 **Working Groups** (See attached schedule.)
16:00 **Coffee Break**
16:30 **Short Report from Working Groups and General Discussion**
19:30 **ISL Users Meeting** (Garden Plaza Hotel) R. F. Casten, presiding

Friday, October 9, 1992

8:30 **Working Groups** (See attached schedule.)
10:30 **Coffee Break**
11:00 **Working Groups** (See attached schedule.)
12:00 **Lunch**
12:45 **Tour of Oak Ridge Facility** (for those interested)
13:30 **Working Groups** (See attached schedule.)
15:30 **Coffee Break**
16:00 **Working Groups** (See attached schedule.)

Saturday, October 10, 1992 (R. F. Casten, presiding)

8:30 **Report of Working Groups**
10:45 **Coffee Break**
11:00 **General Discussion**

DISCUSSION GROUPS

The aim of the discussion groups is to explore in depth the conceptual plan for the ISL Facility as outlined in the ISL White Paper and to consider the beam requirements and experimental equipment needed to properly utilize such a facility. The topics listed are only provided as starting points for these discussions, and the people listed have agreed to initiate the discussions. Others are encouraged to participate in these discussions.

Combined Session Discussion Groups A & B

Thursday, October 8 (Chair: D'Auria)

13:30

Ravn: **Expected Elements & Intensities**
Bricault: **Heavy Ions for RNB Production**
Talbert, Nitschke: **High Intensity Targets**

14:30

Thorsen, Borden, Donahue: **Radiation and Materials**
VanDuppen: **Ion Sources**

15:30

Shepard, Jongen, Schneider: Post-Acc: Cyclotrons vs. LINACs
Nitschke, et al.: Goal: 100%(?) Duty Cycle Post-Acc.
Goal: 100%(?) Transmission
Goal: Acceleration of A < 240 (?)
Stripping Schemes, q=1 vs. q>1

Friday, October 9 (Chair: Nitschke)

13:30

Group Leaders: **ISL Specifications: Revisions, Additions**

14:30

Ravn, VanDuppen, Moore: **Future Developments**

15:30

Ravn, VanDuppen, Moore: **Higher Energies, Identification of Problem Areas, Identification of R&D Topics**

Discussion Group A Target Ion Sources and Mass Separation

Friday, October 9 (Chair: D'Auria)

8:30

Steiner, Vincent, Ward: **Robotics & Remote Handling**

9:30

Wouters: **Thin Target & He-jet Approach**

Fairbanks: **Laser Ion Sources**

10:30

Wollnik, Ravn, D'Auria: **Operational Parameters for ISOL/Isobar Separator**

Discussion Group B Accelerators: Primary and Secondary

Friday, October 9 (Chair: Nitschke)

8:30

Clark: **A 600 MeV Primary Beam Cyclotron**
Discussion of LINACs for RNB Accel.

9:30

Paul: **SC Cavities at Stony Brook**
Discussion of Low-β, low-q/A Structures

10:30

Talbert: **Initial LINAC Acc. Stages for the ISL**

Tomizawa: **SC-RFQ & Interdigital H-Structures**

11:30

Schneider: **A LINAC Solution**

Lee/Young: **Storage Rings**

Löbner/Selph: **Charge State Enforcer**

Discussion Group C Experiments with Radioactive Beams

Thursday, October 8

13:30 - 16:30	**Experimental Problems Associated with RNB Experiments & Major Equipment Needed for the ISL** (Chair: Vieira)
Huyse:	**Special Experimental Problems Associated with RNBs**
Sarantites:	**Utility of Gamma, Charged-Particle, and Neutron 4π Arrays to RNB Experiments**
Davids:	**The Next Generation E x B Recoil Separators for RNB Experiments**
Sherrill:	**A Large Solid Angle Magnetic Spectrometer for Inverse Kinematic Reactions**
Moltz:	**A Storage Ring for Low-Energy RNB Experiments**
	Open Discussion

Friday, October 9

8:30 - 10:15	**Nuclear Astrophysics** (Chair: Wiescher)
Boyd:	**A Provocative R-Process Experiment Using the ISL**
Käppeler:	**S-Process Studies with Radioactive Targets and RNBs**
Goerres:	**Rp-Process Measurements with High-Intensity RNBs**
	Open Discussion
10:45 - 12:15	**High Spin and Prompt-Gamma Experiments** (Chair: Garrett)
Ahmad:	**High Spin Physics Experiments with the ISL**
Lee:	**High Spin - RNB Experiments in Neutron-Rich Nuclei**
Casten:	**BE2 Measurements via Coulomb Excitation with RNBs**
	Open Discussion
13:30 - 15:30	**Nuclear Structure** (Chair: Lee)
Wilhelmy:	**Experimental Search for New Regions of Shape Isomers Using RNBs**
Gregorich:	**Application of High-Intensity RNBs in the Heavy Element Region**
Sherrill:	**Reactions with Exotic RNBs Close to the Drip Lines**
	Open Discussion
16:00 - 17:40	**Weak Interaction and Materials Science Experiments** (Chair: Vieira)
Sprouse:	**The Next Generation of Atomic Parity Nonconservation Experiments Requiring High-Intensity (unaccelerated) RNBs**
Gai:	**Search for Weak Parity-Violating, Charged-Particle Decays Using High-Intensity RNBs**
Sawicki:	**Materials Science Experiments Using the ISL**
	Open Discussion

Appendix B:
Attendees

Irshad Ahmad
Argonne National Laboratory
9700 S. Cass Avenue
Argonne, IL 60439

Yurdanur A. Akovali
Oak Ridge National Laboratory
P.O. Box 2008
Oak Ridge, TN 37831-6371

Gerald D. Alton
Oak Ridge National Laboratory
P.O. Box 2008
Oak Ridge, TN 37831-6368

Timothy A. Antaya
Cyclotron Laboratory
Michigan State University
East Lansing, MI 48824-1321

Ronald L. Auble
Oak Ridge National Laboratory
P.O. Box 2008
Oak Ridge, TN 37831-6368

Ravi S. Babu
Department of Physics & Astronomy
Vanderbilt University
Nashville, TN 37235

Cyrus Baktash
Oak Ridge National Laboratory
P.O. Box 2008
Oak Ridge, TN 37831-6371

James B. Ball
Oak Ridge National Laboratory
P.O. Box 2008
Oak Ridge, TN 37831-6369

Marcel M. Barbier
Marcel M. Barbier, Inc.
3003 Rayjohn Lane
Herndon, VA 22071

Frederick D. Becchetti
Department of Physics
University of Michigan
Ann Arbor, MI 48109-1120

James R. Beene
Oak Ridge National Laboratory
P.O. Box 2008
Oak Ridge, TN 37831-6368

Fred E. Bertrand
Oak Ridge National Laboratory
P.O. Box 2008
Oak Ridge, TN 37831-6368

Carrol R. Bingham
Department of Physics
University of Tennessee
Knoxville, TN 37996-1200

Henry G. Blosser
Cyclotron Laboratory
Michigan State University
East Lansing, MI 48824-1321

Michael J. Borden
Los Alamos National Laboratory
P.O. Box 1663, MS H838
Los Alamos, NM 87545

Richard N. Boyd
Department of Astronomy
Ohio State University
Columbus, OH 43210

Daeg S. Brenner
Department of Chemistry
Clark University
Worcester, MA 01610

Pierre G. Bricault
GANIL, B.P. 5027
14021 Caen Cedex
France

H. K. Carter, UNISOR/ORISE
Oak Ridge National Laboratory
P.O. Box 2008
Oak Ridge, TN 37831-6374

Richard F. Casten
Physics Department
Brookhaven National Laboratory
Upton, NY 11973

Arthur E. Champagne
Department of Physics & Astronomy
University of North Carolina
CB# 3255, Phillips Hall
Chapel Hill, NC 27599-3255

Lakshman Chaturvedi
Department of Physics
Vanderbilt University
Nashville, TN 37315

Giovanni Ciavola
Instituto Nazionale Fisica Nucleare
Laboratorio Nazionale Del Sud
V.LE A. Doria, 95123 Catania
Italy

David J. Clark
Lawrence Berkeley Laboratory
Bldg. 88, 1 Cyclotron Road
Berkeley, CA 94720

Jerry D. Cole
INEL, MS 2114
2151 North Boulevard
Idaho Falls, ID 83402

David M. Cullen
Oak Ridge National Laboratory
P.O. Box 2008
Oak Ridge, TN 37831-6371

John M. D'Auria
Department of Chemistry
Simon Fraser University
Burnaby, B.C.
Canada V5A 136

Cary N. Davids
Argonne National Laboratory, 203
9700 S. Cass Avenue
Argonne, IL 60439

Joseph Dellwo
Oak Ridge National Laboratory
P.O. Box 2008
Oak Ridge, TN 37831-6368

Zdenek Dlouhy
Nuclear Physics Institute
CS-250 68 REZ
Czechoslovakia

Richard J. Donahue
Lawrence Berkeley Laboratory
1 Cyclotron Road
Berkeley, CA 94720

Darryl T. Dowling
Oak Ridge National Laboratory
P.O. Box 2008
Oak Ridge, TN 37831-6368

William M. Fairbank, Jr.
Physics Department
Colorado State University
Fort Collins, CO 80523

John D. Fox
Department of Physics B-159
Florida State University
Tallahassee, FL 32306

Moshe Gai
WNSL-Department of Physics
Yale University
New Haven, CT 06511

Jerry D. Garrett
Oak Ridge National Laboratory
P.O. Box 2008
Oak Ridge, TN 37831-6371

William Gelletly
Daresbury Laboratory
GB-Warrington WA4 4AD
United Kingdom

Ronald L. Gill
Department of Physics
Brookhaven National Laboratory
Upton, NY 11973

Joachim Goerres
Department of Physics
University of Notre Dame
Notre Dame, IN 46556

Kenneth E. Gregorich
Nuclear Science Division MS-88
Lawrence Berkeley Laboratory
70A-3307, 1 Cyclotron Road
Berkeley, CA 94720

Carl J. Gross
Oak Ridge National Laboratory
P.O. Box 2008
Oak Ridge, TN 37831-6371

Heinz Haas
CERN, PPE Division
CH 1211 Geneva-23
Switzerland

Melvyn L. Halbert
Oak Ridge National Laboratory
P.O. Box 2008
Oak Ridge, TN 37831-6368

Joseph H. Hamilton
Department of Physics
Vanderbilt University
Nashville, TN 37315

John C. Hardy
Chalk River Nuclear Laboratories
Chalk River, Ontario KOJ 1JO
Canada

David L. Haynes
Oak Ridge National Laboratory
P.O. Box 2008
Oak Ridge, TN 37831-6368

D. J. Horen
Oak Ridge National Laboratory
P.O. Box 2008
Oak Ridge, TN 37831-6368

Marc L. Huyse
University of Leuven
Celestijnenlaan 200D
B-3001 Leuven
Belgium

Holger Jensen
Niels Bohr Institute
RISØ
DK4000 Roskilde
Denmark

Noah R. Johnson
Oak Ridge National Laboratory
P.O. Box 2008
Oak Ridge, TN 37831-6371

Charles M. Jones
Oak Ridge National Laboratory
P.O. Box 2008
Oak Ridge, TN 37831-6368

Yves Jongen
IBA, Chemin du Cyclotron, 2
B-1348 Louvain-La-Neuve
Belgium

Paresh K. Joshi
Department of Physics & Astronomy
Louisiana State University
Baton Rouge, LA 70803

Alain R. Joubert
GANIL, BP 5027
F14000 Caen Cedex
France

R. C. Juras
Oak Ridge National Laboratory
P.O. Box 2008
Oak Ridge, TN 37831-6368

Dinakar Kanjilal
Nuclear Science Centre
J.N. University Campus
New Delhi-110067, India

Franz Käppeler
Institut für Kernphysik
University of Karlsruhe
W-7500 Karlsruhe, Germany

Paul E. Koehler
Los Alamos National Laboratory
MS-H803
Los alamos, NM 87545

Jan R. Kormicki
Department of Physics & Astronomy
Vanderbilt University
Nashville, TN 37325

Karl-Ludwig Kratz
Johannes Gutenberg-Universität
Institut für Kernchemie
Postfach 3980, D-6500 Mainz
Germany

S. Neil Lane
Oak Ridge National Laboratory
P.O. Box 2008
Oak Ridge, TN 37831-6368

Clifford T. LeCroy
Oak Ridge National Laboratory
P.O. Box 2008
Oak Ridge, TN 37831-6368

I-Yang Lee
Lawrence Berkeley Laboratory
1 Cyclotron Road, MS 70A-3307
Berkeley, CA 94720

Gunther K. E. Löbner
Sektion Physik
Universität München
Am Coulombwall1, 8046 Garching
Germany

Claude M. Lyneis, Director
88-Inch Cyclotron
Lawrence Berkeley Laboratory
1 Cyclotron Road, Bldg. 88
Berkeley, CA 94720

Paul V. Magnus
Nuclear Physics Lab. GL-10
University of Washington
Seattle, WA 98195

Paul F. Mantica, Jr.
Oak Ridge National Laboratory
P.O. Box 2008
Oak Ridge, TN 37831-6374

Felix Marti
Cyclotron Laboratory
Michigan State University
East Lansing, MI 48824

John B. McClelland
MP-10 MS H840
Los Alamos National Laboratory
Los alamos, NM 87545

Martha J. Meigs
Oak Ridge National Laboratory
P.O. Box 2008
Oak Ridge, TN 37831-6368

Gerald D. Mills
Oak Ridge National Laboratory
P.O. Box 2008
Oak Ridge, TN 37831-6368

Michael F. Mohar
Lawrence Berkeley Laboratory
MS 88, 1 Cyclotron Road
Berkeley, CA 94720

Dennis M. Moltz
Lawrence Berkeley Laboratory
MS 88, 1 Cyclotron Road
Berkeley, CA 94720

Robert B. Moore
Foster Radiation Lab., McGill Univ.
3610 University Street
Montreal, Quebec H3Z 2B2
Canada

David J. Morrissey
Cyclotron Laboratory
Michigan State University
East Lansing, MI 48824

S. W. Mosko
Oak Ridge National Laboratory
P.O. Box 2008
Oak Ridge, TN 37831-6368

Sydney N. Murray
Oak Ridge National Laboratory
P.O. Box 2008
Oak Ridge, TN 37831-6368

Witold Nazarewicz
JIHIR/ORNL
P.O. Box 2008
Oak Ridge, TN 37831-6374

J. Michael Nitschke
Lawrence Berkeley Laboratory
1 Cyclotron Road
Berkeley, CA 94720

Jerry A. Nolen, Jr.
Physics Division, Bldg. 203
Argonne National Laboratory
Argonne, IL 60439

David K. Olsen
Oak Ridge National Laboratory
P.O. Box 2008
Oak Ridge, TN 37831-6368

Peter D. M. Parker
Wright Nuclear Structure Laboratory
Yale University
P.O. Box 6666
New Haven, CT 06511

Peter Paul
Department of Physics
SUNY
Stony Brook, NY 11794-3800

Rodney B. Piercey
Department of Physics & Astronomy
Mississippi State University
Mississippi State, MS 39762

Antoni E. Piotrowski
Soltan Institute for Nuclear Studies
05-400 Otwock
Poland

Shaheen Rab
Oak Ridge National Laboratory
P.O. Box 2008
Oak Ridge, TN 37831-6371

Akunuri V. Ramayya
Department of Physics
Vanderbilt University
Nashville, TN 37235

Helge L. Ravn
Isolde Collaboration
CERN, CH-1211 Geneva 23
Switzerland

Louis A. Rayburn
UNISOR/ORISE
Oak Ridge National Laboratory
P.O. Box 2008
Oak Ridge, TN 37831-6374

Charles A. Reed
Oak Ridge National Laboratory
P.O. Box 2008
Oak Ridge, TN 37831-6368

L. L. Riedinger, Acting Associate
Vice-Chancellor of Research
University of Tennessee
404 Andy Holt Tower
Knoxville, TN 37996

Mark A. Riley
Department of Physics
Florida State University
Tallahassee, FL 32306

Russell L. Robinson
Oak Ridge National Laboratory
P.O. Box 2008
Oak Ridge, TN 37831-6368

James G. Ross
Department of Physics
University of Notre Dame
Notre Dame, IN 46556

Demetrios G. Sarantites
Department of Chemistry
Washington University
St. Louis, MO 63130

Jerzy A. Sawicki
Chalk River Nuclear Laboratories
Chalk River, Ontario KOJ 1JO
Canada

Harvey R. Schneider
TRIUMF, 4004 Wesbrook Mall
Vancouver, B.C. V6T 2A3
Canada

Frank Selph
Lawrence Berkeley Laboratory
1 Cyclotron Road
Berkeley, CA 94720

Paul B. Semmes
Tenn. Technological University
P.O. Box 5147
Cookeville, TN 38505

Kenneth W. Shepard
Argonne National Laboratory
9700 S. Cass Avenue
Argonne, IL 60439

Bradley M. Sherrill
Cyclotron Laboratory
Michigan State University
East Lansing, MI 48824

Michael S. Smith
Oak Ridge National Laboratory
P.O. Box 2008
Oak Ridge, TN 37831-6371

Gene D. Sprouse
Physics Department
State University of New York
Stony Brook, NY 11794-3800

Erich W. Steiner
Los Alamos National Laboratory
P.O. Box 1663, MS H847
Los Alamos, NM 87545

Michael R. Strayer
Oak Ridge National Laboratory
P.O. Box 2008
Oak Ridge, TN 37831-6373

Kruno M. Subotic
Institute of Nuclear Sciences Vinca
P.O. Box 522
11001 Beograd, Yugoslavia

Willard L. Talbert, Jr.
Group INC-11, MS J514
Los Alamos National Laboratory
Los Alamos, NM 87545

B. Alan Tatum
Oak Ridge National Laboratory
P.O. Box 2008
Oak Ridge, TN 37831-6368

Ian M. Thorson
TRIUMF, 4004 Wesbrook Mall
Vancouver, B.C.
Canada V6T-2A3

Masahito Tomizawa
Institute for Nuclear Study
University of Tokyo
3-2-1 Midori-cho
Tanashi, Tokyo 188, Japan

Kenneth S. Toth
Oak Ridge National Laboratory
P.O. Box 2008
Oak Ridge, TN 37831-6371

Piet Van Duppen
Inst. voor Kern-en Stralingsfysica
Dept. Natuurkunde-KU Leuven
Celestijnenlaan 200 D
B-3001 Heverlee, Leuven
Belgium

David J. Vieira
Los Alamos National Laboratory
INC-13, MS H824
Los Alamos, NM 87545

John Vincent
TRIUMF, 4004 Wesbrook Mall
Vancouver, B.C. V6T 2A3
Canada

William B. Walters
Department of Chemistry
University of Maryland
College Park, MD 20742

Thomas E. Ward
U.S. DOE-Office of Space
M.S. Ga-155, SC-1
1000 Independence Ave., SW
Washington, DC 20585

David D. Warner
Daresbury Laboratory
GB-Warrington WA4 4AD
United Kingdom

Michael C. F. Wiescher
Department of Physics
University of Notre Dame
Notre Dame, IN 46556

Jerry B. Wilhelmy
Los Alamos National Laboratory
MS J 514
Los Alamos, NM 87545

Hermann Wollnik
II. Physikalisches Institut
University of Giessen
Heinrich-Buff-Ring 16
D-6300 Giessen, Germany

John L. Wood
School of Physics
Georgia Tech
Atlanta, GA 30332-0430

Jan M. Wouters
Los Alamos National Laboratory
P.O. Box 1663
Los Alamos, NM 87545

Gordon J. Wozniak
Lawrence Berkeley Laboratory
MS 88
Berkeley, CA 94720

Edward F. Zganjar
Department of Physics & Astronomy
Louisiana State University
Baton Rouge, LA 70803

Brian E. Zimmerman
Department of Physics
University of Tennessee
401 Nielsen Physics Building
Knoxville, TN 37996-1200

Appendix C:
Committees and Sponsors

Workshop sponsored by:

Georgia Institute of Technology
Joint Institute for Heavy Ion Research
Lawrence Berkeley Laboratory
Los Alamos National Laboratory
Louisiana State University
Mississippi State University
Oak Ridge Institute for Science and Education
Oak Ridge National Laboratory
Simon Fraser University
Tennessee Technological University
University of Maryland
University of Notre Dame
University of Tennessee
Vanderbilt University

Organized on behalf of the ISL Steering Committee by:

John M. D'Auria, Simon Fraser University
Jerry D. Garrett, Chairman, Oak Ridge National Laboratory
J. Michael Nitschke, Lawrence Berkeley Laboratory
David J. Vieira, Los Alamos National Laboratory
Michael Wiescher, University of Notre Dame

Local Organizing Committee:

Gerald D. Alton, Oak Ridge National Laboratory
Cyrus Baktash, Oak Ridge National Laboratory
James B. Ball, Oak Ridge National Laboratory
Fred E. Bertrand, Oak Ridge National Laboratory
Carrol R. Bingham, University of Tennessee
H. Kenneth Carter, Oak Ridge Institute for Science and Education
Jerry D. Garrett, Chairman, Oak Ridge National Laboratory
Joseph H. Hamilton, Vanderbilt University
I-Yang Lee, Lawrence Berkeley Laboratory
David K. Olsen, Oak Ridge National Laboratory
Rodney B. Piercey, Mississippi State University
Russell L. Robinson, Oak Ridge National Laboratory

IsoSpin Laboratory Steering Committee:

Richard F. Casten, Chairman, Brookhaven National Laboratory
John M. D'Auria, Simon Fraser University
Cary N. Davids, Argonne National Laboratory
Jerry D. Garrett, Oak Ridge National Laboratory
J. Michael Nitschke, Lawrence Berkeley Laboratory
Bradley M. Sherrill, Michigan State University
David J. Vieira, Los Alamos National Laboratory
Michael Wiescher, University of Notre Dame
Edward F. Zganjar, Louisiana State University

Appendix D:
Author Index

END

DATE
FILMED
12/10/93